

Musculoskeletal Model of the Human Shoulder for Joint Force Estimation

THÈSE N° 6497 (2015)

PRÉSENTÉE LE 30 JANVIER 2015

À LA FACULTÉ DES SCIENCES ET TECHNIQUES DE L'INGÉNIEUR

LABORATOIRE D'AUTOMATIQUE - COMMUN

PROGRAMME DOCTORAL EN SYSTÈMES DE PRODUCTION ET ROBOTIQUE

ÉCOLE POLYTECHNIQUE FÉDÉRALE DE LAUSANNE

POUR L'OBTENTION DU GRADE DE DOCTEUR ÈS SCIENCES

PAR

David INGRAM

acceptée sur proposition du jury:

Dr A. Karimi, président du jury
Prof. R. Longchamp, Dr Ph. Müllhaupt, directeurs de thèse
Prof. R. Dumas, rapporteur
Prof. J. Rasmussen, rapporteur
Dr A. Terrier, rapporteur



ÉCOLE POLYTECHNIQUE
FÉDÉRALE DE LAUSANNE

Suisse
2015

The wheels on the bus go
round and round...
— Unknown

To my son Jonathan and my father Jim.

Acknowledgements

Writing a PhD dissertation is a voyage through the zone where normal things don't happen very often. Its a long personal journey that ends with a great uproar. However, the journey would not be possible without the help and support of so many others. I would therefore like to take this opportunity to express my thanks towards everyone who made this work possible.

First, I express my gratitude to my thesis directors, Prof. Roland Longchamp and Dr. Philippe Müllhaupt, without whom nothing would have been possible. The interactions with Dr. Müllhaupt kept my work focused and provided feedback for improvements. I would like to thank the external members of the jury, Prof. John Rasmussen and Prof. Raphael Dumas for their insight and constructive criticism. I would like to thank Dr. Alexandre Terrier for his participation in my research and for his presence on my jury. I also thank Dr. Alireza Karimi, the jury president. I thank Ehsan Sarshari for continuing my work and Christoph Engelhardt for overseeing the other side of things. The financial support from the Swiss National Science Foundation is gratefully acknowledged.

The Laboratoire d'Automatique provides a great atmosphere for work and for fun. As a great philosopher once said: "work before play". I would therefore like to thank the members of the lab direction for having granted me the possibility of carrying out a PhD. I would also like to thank those who facilitated administrative tasks. Ruth for making sure everything went smoothly. Francine for helping with the travel planning and financial tasks. As well as Petiot and Eva for making sure we pay our cafeteria fees on time. In no particular order, I want to thank all those who made my PhD a memorable experience; Philippe, for having aided in the creation of "Bouinopia", the capitol city of crazy ideas and wacky concepts. You are also the permanent boss of the "Empty Head Research Group" where people can study hyperlinearism and control everything of the future. Sandra, for her friendship and being a good colleague; Francine "La Migrue", for always keeping me focused on the important things in life. Francis for helping me test some of my more fundamental research ideas like: how to homogeneously roast a marshmallow. Dr. Christoph "Neo" Salzmann for your precious help with experiments; Dr. Gillet for being my mentor; Basile for being a really good office partner and a good friend, always ready for a good laugh. Willson for his friendship and help in putting my PhD on the right track from the start. Gorka for proving that Nutella is a food group. Andriana for creating the LA nail salon and her friendship. Evgeny for showing me how to cross-country ski properly. Timm for sharing my passion for downhill mountain biking. Sean for being Irish and a good friend and colleague. Greg; Jean-Hubert; Sriniketh. Thank you to all my other lab colleagues.

A lot of thanks goes to all friends in and around Lausanne as well as elsewhere. You always provided great moments.

I would like to thank my parents. Thanks to your love and support, I have had the great opportunity of doing a doctoral dissertation. Thanks also to my brothers, James, Michael and John.

I would like to thank my wife Sandy for all the love and support. It definitely was not easy, but you got me through the smooth and the rough times. You always knew what to say to keep me motivated. Thank you for making me who I am today.

Finally, I would like to thank my son Jonathan. Without your smiles and laughs, the final moments would not have been as enjoyable. This thesis is dedicated to you and to your grandfather.

Lausanne, 12 Janvier 2015

D. I.

Abstract

Human beings like all organisms, are subject to a variety of diseases. Musculoskeletal diseases such as arthritis, affecting our muscles and bones, are particularly debilitating because they considerably limit our ability to interact with our environment. The symptoms of arthritis are joint pain and loss of movement, caused by a deterioration of the cartilage in our articulations. The precise determination of the underlying cause of the deterioration is a challenging task. It is believed that it is caused by excessive force in the joints due to inappropriate muscle forces. Since only forces in muscles just beneath the skin can be measured, the force hypothesis remains unproven. Musculoskeletal models are essential in analysing musculoskeletal diseases because they address the lack of information on the forces involved. Such models are used to estimate muscle and joint reaction forces. Determining the key elements in a musculoskeletal model to assess its quality raises several challenges.

In this thesis, a musculoskeletal model of the shoulder is presented. The model is governed by the laws of rigid-body mechanics and is similar to a model of a cable-driven mechanism. Both the kinematic and dynamic aspects of the shoulder are contained in the model. Applying the theory of rigid body mechanics requires a certain level of rigour to ensure compatibility between the kinematic and dynamic parts of the model. Therefore, a considerable part of the thesis is devoted to presenting the details of the model's construction. The model is designed specifically for estimating muscle and joint-reaction forces in quasi-static and dynamic situations.

The muscle-force estimation problem is defined as a nonlinear program and solved in this thesis using a two-step approach. In a first step, the desired kinematics is constructed and inverse dynamics is used to estimate the associated joint torques. In a second step, the nonlinear program is solved using null-space optimisation. An initial solution to the estimation problem is obtained by taking a pseudo-inverse of the moment-arms matrix. The solution is then corrected using the matrix's null-space to satisfy the constraints. This approach redefines the estimation problem as a quadratic program and considerably reduces the time required to find a solution. Once the muscle-forces are estimated, the joint reaction forces are deduced from the dynamic model. Muscle and joint-reaction forces are compared to other results from the literature.

A key element of the first step is building the kinematics. The model's kinematics are analysed and a new method for describing them is presented. Indeed, obtaining compatible motion for the model's dynamics is a challenging task. The inverse kinematics technique is inappropriate and measured joint angle data is not always available. The

shoulder girdle is shown to be a parallel platform with three degrees of freedom. The kinematics are described by three coordinates obtained from a geometric interpretation of the scapulothoracic contact. The coordinates provide a direct, efficient method of planning the shoulder's motion, directly compatible with the dynamic model.

A key element of solving the nonlinear program, second step of the muscle-force estimation problem, is computing muscle moment-arms. A rigorous definition of muscle moment-arms is presented. The definition provides an alternative to the tendon excursion method that can lead to incorrect moment-arms if used inappropriately due to its dependency on the choice of joint coordinates. The proposed definition is independent of any kinematic coordinate choice. It is used to analyse the problem of the existence of a solution through the wrench- and torque-feasible sets. An analysis of the torque-feasible set is used to answer certain questions regarding the underestimation of certain muscle activities.

Lastly, the problem of how musculoskeletal systems are controlled through antagonistic muscle structures is addressed. A hypothesis for the cause of arthritis is a deterioration of neuromuscular coordination. Muscles are being badly coordinated by the neurological system. Given the similarities between musculoskeletal models and cable-driven systems, the problem is analysed using a cable-driven pendulum. The pendulum model constitutes a simplified model of the shoulder and is used to prove the stability of a human motor control mechanism called joint stiffness control through antagonistic muscle co-contraction. A control strategy is developed for the pendulum based on the mechanism of muscle co-contraction. Given a joint stiffness, the necessary muscle forces are obtained using the estimation method previously described. The strategy is applied to a physical cable-driven pendulum. Four cables, each controlled independently through a motor-driven pulley, drive the pendulum. The results are used to open the discussion on the possible neurological causes of neuromuscular dysfunctions.

Keywords: musculoskeletal modelling, shoulder mechanics, muscle-force estimation, joint-force estimation, moment-arms, cable-driven systems.

Version abrégée

Les êtres humains, comme tous les organismes vivants, sont exposés à une variété de maladies. Les maladies musculo-squelettiques comme l'arthrose, lequel affectent les muscles et les os, limitent considérablement notre capacité d'interagir avec notre environnement. Des douleurs articulaires et une perte de mouvement constituent les principaux symptômes de l'arthrose. Il s'agit d'une dégradation du cartilage articulaire. La détermination précise de la cause sous-jacente de la dégradation est une tâche difficile. On croit que cette dégradation est causée par une force excessive dans les articulations, en raison de l'application de forces musculaires inappropriées. Étant donné que seules les forces musculaires sous la peau peuvent être mesurées, l'hypothèse de la force reste à prouver. Les modèles musculo-squelettiques sont essentiels dans l'analyse de l'arthrose parce qu'ils fournissent des informations manquantes relatives aux forces impliquées. Ces modèles sont utilisés pour estimer les forces musculaires et les forces articulaires. La détermination des éléments clés d'un modèle musculo-squelettique, afin d'évaluer sa qualité, soulève plusieurs défis.

Dans cette thèse, un modèle musculo-squelettique de l'épaule est présenté. Le modèle est régi par les lois de la mécanique des corps rigides, et elle est similaire à un modèle d'un mécanisme actionné par câbles. Le modèle contient les deux aspects, cinématiques et dynamiques, de l'épaule. L'application de la théorie de la mécanique des corps rigides nécessite un certain niveau de rigueur pour assurer la compatibilité entre les parties cinématiques et dynamiques du modèle. Par conséquent, une grande partie de la thèse est consacrée à la présentation des détails de la construction du modèle. Le modèle est spécifiquement conçu pour estimer les forces musculaires et articulaires, dans des situations quasi - statiques et dynamiques.

L'estimation des forces musculaires est définie comme un programme non linéaire et résolue dans cette thèse en utilisant une approche en deux étapes. Dans une première étape, le modèle cinématique est construit, et la dynamique inverse est utilisée pour estimer les couples articulaires associés au mouvement de l'épaule. Dans une deuxième étape, le programme non linéaire est résolu en utilisant l'optimisation du nul espace. Une première solution au problème d'estimation est obtenue en prenant un pseudo-inverse de la matrice des bras de levier. La solution est ensuite corrigée en utilisant le nul espace de la matrice afin de satisfaire les contraintes. Cette approche redéfinit le problème d'estimation comme un programme quadratique et réduit considérablement le temps nécessaire pour trouver une solution. Une fois que les forces musculaires sont estimées, les forces articulaires sont déduites à partir du modèle dynamique. Les forces musculaires et articulaires estimées sont comparées à d'autres résultats de la littérature.

Un élément clé de la première étape est la construction de la cinématique. La cinématique du modèle est analysée et une nouvelle méthode pour les décrire est présentée. En effet, l'obtention de mouvement compatible pour la dynamique du modèle est une tâche laborieuse. La technique de cinématique inverse est inappropriée et les données des angles articulaires mesurés n'est pas toujours disponible. La ceinture scapulaire est indiquée comme étant une plate-forme parallèle à trois degrés de liberté. La cinématique est décrites par trois coordonnées obtenues à partir d'une interprétation géométrique du contact scapulo-thoracique. Les coordonnées constituent une méthode efficace de planification directe du mouvement de l'épaule, lequel est directement compatible avec le modèle dynamique de l'épaule.

Un élément clé de la résolution du programme non-linéaire, deuxième étape du problème d'estimation des forces musculaires, est le calcul des bras de levier musculaires. Une définition rigoureuse des bras de levier musculaires est présentée. La définition offre une alternative à la méthode d'excursion du tendon, laquelle pourrait induire des erreurs dans les bras de levier si utilisée de façon inappropriée, en raison de sa dépendance du choix des coordonnées des articulations. La définition proposée est indépendante de tout choix de coordonnées cinématique. Elle est utilisée afin d'analyser le problème de l'existence d'une solution à travers les espaces de réalisation cinématique et de couples. Une analyse de l'espace de couple réalisable est utilisée pour répondre à certaines questions concernant la sous-estimation de l'activité de certains muscles.

Pour finir, le contrôle des systèmes musculo-squelettique par des structures musculaires antagonistes est adressée. Une hypothèse expliquant l'origine de l'arthrose est une détérioration de la coordination neuro-musculaire. Les muscles sont mal coordonnés par le système neurologique. Étant donné les similarités entre les modèles musculo-squelettiques et les systèmes actionnés par câbles, le problème est analysée à travers un pendule actionné par câbles. Le pendule constitue un modèle simplifié de l'épaule et est utilisé pour prouver la stabilité d'un mécanisme de contrôle humain appelé le contrôle de la raideur articulaire par co-contraction des muscles antagonistes. Une stratégie de contrôle est proposée, basée sur la co-contraction musculaires. Etant donné une raideur articulaire, les forces musculaires nécessaire sont obtenue en utilisant la méthode d'estimation décrite précédemment. La stratégie de contrôle est appliquée à un pendule physique. Quatre câbles, chacun contrôlée de manière indépendante à travers des moteurs et poulies, actionnent le pendule. Les résultats sont utilisés pour ouvrir la discussion sur les causes possibles d'une détérioration de la coordination neuro-musculaire.

Mots-clés: modélisation musculo-squelettique, mécanique de l'épaule, estimation de forces musculaires, estimation de forces articulaires, bras de levier, systèmes actionnés par câbles.

Contents

Acknowledgements	i
List of figures	xi
List of tables	xv
List of Symbols	xvii
1 Introduction	1
1.1 Research Context	1
1.2 State of the Art	3
1.3 Contributions	6
1.4 Organisation of the Thesis	8
2 Anatomy, Physiology and Movement of the Human Shoulder	11
2.1 Shoulder Skeletal Anatomy and Physiology	11
2.2 Shoulder Muscle Anatomy and Physiology	14
2.3 Shoulder Movement	16
3 Multibody Systems Theory	21
3.1 Introduction	21
3.2 Preliminaries	22
3.2.1 Conventions	22
3.2.2 Geometric Configuration	23
3.2.3 Euclidean Displacements	24
3.2.4 Rotation Matrices	26
3.2.5 Angular Description of Rotations	27
3.2.6 Euler’s Rotation Theorem	29
3.3 Rigid-Body Kinematics	30
3.3.1 Instantaneous Angular velocity	30
3.3.2 Instantaneous Kinematics	32
3.3.3 Movement: Velocity and Acceleration	33
3.3.4 Chasles’ Theorem and the Instantaneous Screw Axis	35
3.4 Rigid-Body Dynamics	38
3.4.1 Newtonian Mechanics	38
3.4.2 Forces, Moments of Force and Poinsot’s Theorem	39
3.4.3 Inertia and Moment of Inertia	43

3.4.4	Equations of Motion	44
3.4.5	Mechanical Energy, Work and Power	48
3.5	Multibody Kinematics	52
3.5.1	Machines and Mechanisms	52
3.5.2	Kinematic Pairs and Kinematic Chains	53
3.5.3	Forward Kinematics and Mobility	57
3.5.4	Kinematic Constraints	60
3.5.5	Forward Kinematic Map	61
3.6	Multibody dynamics	62
3.6.1	Analytical Mechanics and Virtual Displacements	62
3.6.2	The Principles of Jourdain and d'Alembert	65
3.6.3	Principle of Virtual Power	66
3.6.4	The Euler-Lagrange Equation	67
3.6.5	The Principle of Virtual Work and Static Equilibrium	71
4	A Musculoskeletal Model of the Human Shoulder	73
4.1	Introduction	73
4.2	Kinematic Shoulder Model	74
4.2.1	Bony Landmarks and Reference Frames	75
4.2.2	Joint Angle Parameterisation of the Model's Kinematics	77
4.2.3	Scapulothoracic Contact Model	79
4.2.4	Forward Kinematic Map	81
4.3	Dynamic Shoulder Model	82
4.3.1	Equations of Motion	82
4.3.2	Muscle Forces	85
4.3.3	Muscle Cable Model	87
4.4	Remarks	89
4.5	Conclusions	91
5	Coordinated Redundancy	93
5.1	Introduction	93
5.2	Kinematic Redundancy	94
5.3	Overactuation	97
5.4	Tasks for Coordination Strategies	98
6	Shoulder Kinematic Redundancy Coordination	103
6.1	Introduction	103
6.2	Minimal Coordinates for Coordination	105
6.2.1	Shoulder Kinematic Redundancy Coordination	105
6.2.2	Manifolds and Coordinate Reduction	108
6.2.3	A Parallel Platform Kinematic Shoulder Model	114
6.2.4	Equivalent Kinematic Maps and Coordinates	117
6.2.5	The Coordinate Space	122
6.2.6	A Minimal Parameterisation	124
6.3	Remarks	130
6.3.1	Trammel of Archimedes	131

6.4	Conclusions	133
7	Shoulder Overactuation Coordination	135
7.1	Introduction	135
7.2	Moment-Arms for Coordination	137
7.2.1	Shoulder Overactuation Coordination	137
7.2.2	Constraint Gradient Projection	139
7.2.3	A Coordination Strategy to Shoulder Overactuation	142
7.3	Muscle Moment-Arms Theory	145
7.3.1	Fundamentals of Moment-Arms	146
7.3.2	A Geometric Method of Computing Moment-Arms	147
7.3.3	Tendon Excursion Method of Computing Moment-Arms	151
7.3.4	Computing Muscle Moment-Arms	153
7.4	The Solution Set and Wrench-Feasibility	155
7.5	Conclusions	159
8	Estimating Joint Force in the Human Shoulder	161
8.1	Introduction	161
8.2	Methods	162
8.2.1	A Musculoskeletal Model of the Human Shoulder	162
8.2.2	Kinematic Coordination	165
8.2.3	Muscle-Force Coordination	168
8.2.4	Implementation and Model Output	169
8.3	Results	172
8.3.1	Scapular Kinematics	172
8.3.2	Muscle Moment-Arms	172
8.3.3	Muscle Forces	174
8.3.4	Joint Reaction Force	176
8.4	Discussion	177
8.4.1	Wrench-Feasibility of a Shoulder Musculoskeletal Model	179
8.5	Conclusions	185
9	Introduction to Control Theory	187
9.1	Systems and Controllers	187
9.2	Open-Loop and Closed-Loop	189
9.3	Stability	191
9.4	Linear State Feedback Control	195
10	Musculoskeletal Stability through Joint Stiffness Control	199
10.1	Introduction	199
10.2	Stability by Antagonistic Muscle Co-contraction	201
10.2.1	Human Motor Control	201
10.2.2	Stability in Human Motor Control	204
10.2.3	Model of a Cable-Driven Pendulum	206
10.2.4	Stability by Antagonistic Cable Co-contraction	210
10.2.5	Joint Stiffness Control	213
10.2.6	Observability of Pendulum States	215

10.3 A Joint Stiffness Control Strategy	217
10.3.1 Control Algorithm	218
10.3.2 Implementation	221
10.3.3 Methods	224
10.4 Results	225
10.5 Discussion	226
10.6 Conclusions	229
11 Conclusions	231
11.1 Contributions	232
11.2 Future Research Directions	234
A Technical Details	237
A.1 Uniform Dilation of an Ellipsoid	237
A.2 Sphere-Ellipsoid Intersection	239
A.2.1 Quadric Surfaces	239
A.2.2 Ruled Surfaces	241
A.2.3 Quadric-Quadric Intersections	243
A.2.4 Sphere-Ellipsoid Intersection	244
B Shoulder Model Numerical Dataset	247
B.1 Bony Landmarks and Rotation Matrices	247
B.2 Mass, Intertia and Glendoid Stability	249
B.3 Muscle Geometry and Wrapping	250
Glossary	273
Curriculum Vitae	281

List of Figures

1.1	The shoulder's skeletal structure	3
1.2	The linkage model and joint sinus cones	4
1.3	Three musculoskeletal shoulder models from the literature	5
2.1	The shoulder's skeletal anatomy	12
2.2	The shoulder's articulations and ligaments	13
2.3	The glenoid cavity in the glenohumeral joint	13
2.4	The shoulder's muscle structure	14
2.5	Typical force-length behaviour of a skeletal muscle	16
2.6	The three body planes and the scapular plane	17
2.7	Schematic description of shoulder bone motion definitions	18
2.8	Three phase description of the scapulo-humeral rhythm	19
3.1	Coordinate system convention	22
3.2	A free rigid-body's geometric configuration	23
3.3	A Euclidean displacement	25
3.4	A coordinate transformation	25
3.5	Euler and Bryan angle rotation sequences	28
3.6	Illustration of Euler's Theorem	30
3.7	A screw encoding a helical vector field	36
3.8	Construction of the instantaneous screw axis	37
3.9	The moment of force created by a force	40
3.10	Duality between Chasles' theorem and Poincot's theorem	42
3.11	A rigid body as a collection of particles or a continuous mass distribution	44
3.12	Construction of the dynamics of a rigid body	46
3.13	A body moving along a path	48
3.14	Illustration of the energy conservation theorem	50
3.15	Machines and their corresponding mechanisms	53
3.16	The six lower kinematic pairs with their symbology	54
3.17	The higher kinematic pairs with their symbology	55
3.18	Kinematic relation between two bodies in a kinematic pair	56
3.19	Displacement of a kinematic pair in a mechanism	59
4.1	The shoulder's bony landmarks	76
4.2	Joint coordinates and reference systems	78
4.3	Scapulothoracic contact model	80
4.4	The shoulder mechanism	84

4.5	Centroid line approach to muscle modelling	87
4.6	3rd order spline parameterisation of muscle segments	88
4.7	The pectoralis major in the model	89
5.1	Coordinated redundancy in a milling machine	94
5.2	Machines and their corresponding mechanisms	95
5.3	Local manifolds in coordinated redundancy	99
6.1	Bony landmarks, reference frames and joint coordinates	105
6.2	Diagram of the shoulder's kinematic model	107
6.3	Examples of well known two-dimensional compact smooth manifolds . . .	109
6.4	Diagram of two charts of a C^∞ atlas on a differentiable (smooth) manifold	110
6.5	A two-dimensional analogue for the shoulder	111
6.6	Two-dimensional analogue shoulder model with the new kinematic chain	113
6.7	Mechanical description of a free body in space	116
6.8	Mechanism of a rigid body's motion on a two-dimensional surface	117
6.9	Equivalent parallel shoulder model	118
6.10	Three methods of parameterising the forward kinematic map	121
6.11	Coordinates in the coordinate submanifolds	123
6.12	The natural kinematic map charts	124
6.13	The submanifold decomposition	125
6.14	Polynomial description of the scapula's configuration	126
6.15	The minimal set of coordinates	128
6.16	The minimal coordinate charts onto the submanifolds	129
6.17	The driven Trammel of Archimedes	132
6.18	A use of the Trammel of Archimedes	133
7.1	Bony landmarks, reference frames and joint coordinates	138
7.2	Diagram of a manifold \mathcal{Q}_S in \mathbb{R}^3 of dimension 2: the two-torus T^2	140
7.3	Construction of the GH joint stability constraint	143
7.4	The classical mechanics definition of force moment-arm	146
7.5	A skeletal system with N joints and two muscles	148
7.6	Force isolation in moment-arm computations	149
7.7	Force cancellation and force transmission in a musculoskeletal model . . .	150
7.8	Inappropriate use of the tendon-excursion method	154
7.9	A two-dimensional toy musculoskeletal model	157
7.10	Range and image spaces of the torque-force map	157
7.11	Image space of the torque-force map in three different configurations . . .	158
7.12	The time-dependent behaviour of the image space polytope	159
8.1	Bony landmarks, reference frames and joint coordinates	163
8.2	Minimal coordinates used to coordinate the shoulder	166
8.3	The implemented musculoskeletal shoulder model	171
8.4	Comparison of model-predicted and measured kinematics	172
8.5	Comparison of mode-predicted and measured moment-arms	173
8.6	Muscle forces during abduction in the scapular plane	175
8.7	Comparisons of glenohumeral joint-reaction forces during abduction . . .	176

8.8	Comparisons of glenohumeral joint contact patterns	177
8.9	The glenohumeral image space polytope	183
8.10	The sternoclavicular image space polytope	183
8.11	The clavicle's actuation plane	184
9.1	Open-loop control	190
9.2	Closed-loop control	190
9.3	The multi-feedback loop strategy	191
9.4	Stability and instability	192
9.5	Lyapunov stability and instability	193
9.6	A Lyapunov function	194
10.1	The nervous system	202
10.2	Neuromuscular communication	203
10.3	The human motor control system	203
10.4	Pendulum metaphor for human postural control	205
10.5	Geometry of the cable-driven pendulum system	207
10.6	Two wrapping configurations	208
10.7	Cable moment-arms for $-60^\circ < \psi < 60^\circ$	209
10.8	Bounding of the moment-arm functions	212
10.9	Equilibrium point achieved my antagonistic cable co-contraction	214
10.10	The equilibrium stiffness	215
10.11	The physical cable-driven pendulum system	222
10.12	The reference signal	225
10.13	Measured behaviour for trajectory tracking	225
10.14	Observed pendulum states over one cycle of the path	226
10.15	Estimated cable tensions during one cycle of the path	227
10.16	Reaction force in the pendulum rotation axis	228
A.1	Error between the scapulothoracic contact models	239
A.2	A ruled surface: the hyperbolic paraboloid	242

List of Tables

3.1	Euclidean displacement characteristics of some kinematic pairs	58
8.1	Joint angle terminology	167
8.2	Muscle segment moment-arms for the shoulder	182
A.1	Real quadric surfaces in normalised canonical form	241
B.1	Bony landmarks for constructing the shoulder kinematic model	248
B.2	Inertial data to construct dynamic model	249
B.3	Glenoid stability model data	249
B.4	Muscle wrapping data for constructing the muscle geometric model . . .	251

List of Symbols

\mathbb{R}^n	The n -dimensional real Euclidean space,
S^n	Sphere in \mathbb{R}^n ,
\mathbb{RP}^n	Real projective space,
$O(3)$	The 3-dimensional orthogonal group
$SO(3)$	Special orthogonal group,
$SE(3)$	Special Euclidean group,
\mathcal{R}_0	Inertial reference frame,
O_0	Inertial frame centre,
$\mathbf{i}_0, \mathbf{j}_0, \mathbf{k}_0$	Inertial frame x -, y -, z -axis unit vectors,
P_0	Designates a geometric point in \mathbb{R}^3 with respect to \mathcal{R}_0 ,
\vec{p}_0	Vector representing a point in the inertial frame \mathcal{R}_0 ,
\mathbf{R}_0	Direct orthogonal rotation matrix in $SO(3)$,
\mathcal{B}_i	Designates a rigid-body i in \mathbb{R}^3 ,
\mathcal{R}_i	Reference frame of \mathcal{B}_i ,
O_i	Body frame centre,
$\mathbf{i}_i, \mathbf{j}_i, \mathbf{k}_i$	The x -, y -, z -axis unit vectors of a body frame \mathcal{R}_i ,
P_i	Designates a geometric point on \mathcal{B}_i with respect to \mathcal{R}_i ,
Γ	Muscle-force estimation cost function,
\vec{p}_i	Vector representing a point on \mathcal{B}_i with respect to \mathcal{R}_i ,
$p_{x,i}, p_{y,i}, p_{z,i}$	The x -, y -, z -coordinates of P_i in \mathcal{R}_i ,
$\mathcal{T}_{j,i}$	Transformation/Displacement on \mathbb{R}^3 from \mathcal{R}_j to \mathcal{R}_i ,
$\mathcal{TE}_{j,i}$	Euclidean displacement on \mathbb{R}^3 from \mathcal{R}_j to \mathcal{R}_i ,
$\vec{d}_{i,j}$	Translation of $\mathcal{TE}_{i,j}$, from O_i to O_j in \mathcal{R}_i ,
$\mathbf{R}_{j,i}$	Rotation matrix of $\mathcal{TE}_{i,j}$, from \mathcal{R}_j to \mathcal{R}_i ,
$\mathbf{D}_{j,i}$	Homogenous transformation matrix of $\mathcal{TE}_{i,j}$, from \mathcal{R}_j to \mathcal{R}_i ,
ψ, ϑ, φ	Euler or Bryan angles,
$\mathcal{C}_{j,i}$	Configuration of a body \mathcal{B}_i in the frame \mathcal{R}_j ,
\mathbf{P}	PCSA matrix,
$O_{j,i}$	Centre of the reference frame \mathcal{R}_i in frame \mathcal{R}_j ,
$\mathbf{i}_{j,i}, \mathbf{j}_{j,i}, \mathbf{k}_{j,i}$	The x -, y -, z -axis unit vectors of frame \mathcal{R}_i in frame \mathcal{R}_j ,
$P_{i,j}$	Designates a geometric point on \mathcal{B}_j with respect to \mathcal{R}_i ,
$\vec{p}_{i,j}$	Vector representing a point on \mathcal{B}_j in the frame \mathcal{R}_i ,

$\vec{p}_{i,j}^* = \mathbf{R}_{j,i}\vec{p}_i$	Abbreviates a vector being rotated from \mathcal{R}_j to \mathcal{R}_i ,
$Z_{j,i,k}$	Designates a point on \mathcal{B}_i with respect to \mathcal{R}_j , indexed by k ,
$\vec{z}_{j,i,k}$	Vector representing a point on \mathcal{B}_i with respect to \mathcal{R}_j , indexed by k ,
$\vec{x}_{0,i}, \dot{\vec{x}}_{0,i}, \ddot{\vec{x}}_{0,i}$	Position, velocity and acceleration of centre of gravity of \mathcal{B}_i in \mathcal{R}_0 ,
$x_{i,0}, y_{i,0}, z_{i,0}$	The x -, y -, z -coordinates of centre of gravity of \mathcal{B}_i in \mathcal{R}_0 ,
$\psi_i, \vartheta_i, \varphi_i$	Angular coordinates of \mathcal{B}_i with respect to \mathcal{R}_0 ,
\mathbf{N}	Null-space matrix,
\vec{q}_i	Vector of kinematic coordinates of \mathcal{B}_i with respect to \mathcal{R}_0 ,
$\vec{\Gamma}_i, \dot{\vec{\Gamma}}_i, \ddot{\vec{\Gamma}}_i$	Translational position, velocity and acceleration vectors of \mathcal{B}_i in \mathcal{R}_0 ,
$\vec{\Upsilon}_i, \dot{\vec{\Upsilon}}_i, \ddot{\vec{\Upsilon}}_i$	Angular position, velocity and acceleration vectors of \mathcal{B}_i in \mathcal{R}_0 ,
$\vec{\omega}_{0,i}, \Omega_{0,i}$	Instantaneous rotational velocity vector and matrix of \mathcal{B}_i in \mathcal{R}_0 ,
$\mathbf{W}_{0,i}$	Jacobian of $\vec{\omega}_{0,i}$ with respect to $\dot{\vec{\Gamma}}_i$,
$\angle(\vec{p}_i, \vec{q}_i)$	Angle between vectors \vec{p}_i and \vec{q}_i in \mathcal{R}_i ,
$\vec{m}_{0,i}, \vec{l}_{0,i}$	Linear and angular momentum vectors of \mathcal{B}_i in \mathcal{R}_0 ,
m_i, \mathcal{I}_i	Mass and inertia of \mathcal{B}_i ,
\vec{g}_e	Earth's gravitational field,
$\mathcal{I}_{0,i}$	Inertia of \mathcal{B}_i in \mathcal{R}_0 ,
$\mathbb{M}_{m \times n}(\mathbb{R})$	Space of real matrices,
$\rho(\vec{z}_i), \rho(\vec{z}_{0,i}^*)$	Density function of \mathcal{B}_i using vectors in \mathcal{R}_i , or in \mathcal{R}_0 ,
$\vec{f}_{0,i}$	Resulting force of a system of forces applied to \mathcal{B}_i in \mathcal{R}_0 ,
$\vec{f}_{0,i,k}$	Indexed force of a system of forces on \mathcal{B}_i in \mathcal{R}_0 ,
$\vec{b}_{0,i,k}$	Unit direction vector of a force $\vec{f}_{0,i,k}$ on \mathcal{B}_i in \mathcal{R}_0 ,
$\vec{t}_{0,i}$	Resulting moment of force of a system of forces applied to \mathcal{B}_i in \mathcal{R}_0 ,
$\vec{c}_{0,i,k}$	Moment-arm vector of a force $\vec{f}_{0,i,k}$ on \mathcal{B}_i around \mathcal{R}_i in \mathcal{R}_0 ,
$\mathbf{C}_{0,i}$	Moment-arm matrix of a system of forces on a body \mathcal{B}_i in \mathcal{R}_0 ,
\mathbf{C}_0	Moment-arm matrix of a system of forces on mechanism in \mathcal{R}_0 ,
$\mathcal{S}_{Y_i}, \mathcal{T}_{Y_i}, \mathcal{F}_{Y_i}$	Screw, twist or wrench at a point Y_i on \mathcal{B}_i in \mathcal{R}_i ,
p_s, p_t, p_f	Pitch of a screw, twist or wrench,
$\xi(\vec{x}_0, t)$	Free solution to an ordinary differential equation,
$\mathcal{W}_{0,i}, \mathcal{P}_{0,i}$	Total work and power of \mathcal{B}_i in \mathcal{R}_0
$\mathcal{E}_{K,i}, \mathcal{E}_{P,i}, \mathcal{E}_{M,i}$	Kinetic, potential or mechanical energy of \mathcal{B}_i in \mathcal{R}_0 ,
\mathcal{L}	Lagrange function of a mechanism,
\mathcal{L}_i	Lagrange function of a body \mathcal{B}_i in a mechanism,
$\tilde{\mathcal{L}}$	Lagrange function of a mechanism augmented by constraints,
$\vec{\kappa}$	Generalised coordinates,
Φ	Holonomic skleronomic constraint,
λ	Lagrangian multiplier of Φ ,
$\hat{\mathcal{L}}$	Lagrange function of a mechanism, augmented by holonomic constraint,
$\delta\vec{\kappa}$	Virtual displacement of generalised coordinates,
\Re	Real part of a number,

$\delta \vec{x}_{0,i}, \delta \dot{\vec{x}}_{0,i}$	Virtual displacement and velocity of centre of gravity in \mathcal{R}_0 ,
$\delta \vec{\omega}_{0,i}, \delta \dot{\vec{\omega}}_{0,i}$	Virtual angular velocity and acceleration of \mathcal{B}_i in \mathcal{R}_0 ,
IJ	Jugular incision (shoulder model inertial frame centre),
PX	Xyphoid process,
$C7$	7th cervical vertebrae,
$T8$	8th thoracic vertebrae,
SC	Sternoclavicular joint centre (clavicle frame centre),
AC	Acromioclavicular joint centre (scapula frame centre),
GH	Glenohumeral joint centre (humerus frame centre),
AA	Angulus Acromialis,
TS	Trigonum spinae,
AI	Angulus inferior,
HU	Humeroulnar joint centre (end-effector of kinematic model),
EL	Lateral Epicondyle,
EM	Medial Epicondyle,
\vec{e}_0	Scapulothoracic ellipsoid centre in inertial frame,
$\mathbf{E}_{TS}, \mathbf{E}_{AI}$	Scapulothoracic ellipsoid quadric matrices,
\mathcal{Q}_S	Forward kinematic map coordinate space,
\mathcal{W}_S	Forward kinematic map work space,
$\hat{\mathbf{C}}_0$	Muscle moment-arms matrix,
$\hat{\mathbf{C}}_{0,s}$	Scapulothoracic constraint moment-arms matrix,
\mathbf{D}_0	Muscle-force direction matrix,
$\vec{b}_{0,i,j}$	Muscle-force direction unit vector,
Ξ_S	Forward kinematic map,
\mathcal{M}	Differentiable manifold,
$T\mathcal{M}$	Differentiable manifold tangent space,
ϕ	Charts associated to a manifold,
ξ_S	Quadric-quadric intersection coordinate,
L, \dot{L}	Muscle length and rate of change,
\mathcal{F}	Muscle-force space,
\mathfrak{M}	Torque-force map,

Chapter 1

Introduction

1.1 Research Context

The human body is complex. It is made up of a number of interacting systems, including the musculoskeletal system that gives shape to our bodies and allows us to interact with our environment. It consists of bones, ligaments, cartilage, tendons and muscles. Like other systems in the human body, it is subject to a variety of debilitating diseases such as arthritis. Arthritis designates a family of musculoskeletal diseases characterised by an inflammation of one or more joint(s). There are more than 100 different types of arthritis, of which osteoarthritis is the most common.

Osteoarthritis, also known as degenerative joint disease, is defined as a progressive degradation of the mechanical elements in our articulations [206]. It occurs more frequently in elderly people and the main symptoms are joint pain and reduced mobility. In comparison to other diseases affecting the human body osteoarthritis is not as devastating as cancer. However, given its debilitating effect on everyday life and the number of people it affects, the development of a proper treatment for osteoarthritis is important. Indeed, the previous decade (2000-2010) was dubbed in 1999, the bone and joint decade for the treatment and prevention of musculoskeletal disorders by the UN secretary general Kofi-Annan [205].

The proper treatment of any disease requires a complete picture of the affected system, healthy and otherwise. This presents an issue for musculoskeletal diseases such as osteoarthritis because we do not have access to the affected areas consisting of the articulations. Indeed, the *observed* cause of osteoarthritis is either excessive mechanical stress in the articular cartilage or stress occurring in parts of the articulation that are not designed to be loaded [27]. Frequent excessive stress does not give the body enough time to repair the damage and the articulation progressively deteriorates. The *observed* cause of osteoarthritis can only be found after it has occurred through invasive surgery. We cannot observe the deterioration of the articulation as it occurs. We can measure the forces in certain muscles that are just beneath the skin but we cannot measure the mechanical loads occurring in the joints. Furthermore, the *underlying* cause of osteoarthritis remains poorly understood [30]. What causes the inappropriate loading of the joints

remains unknown. Deterioration of the joint is observed to occur even after complete arthroplasty [3]. It has been hypothesised that osteoarthritis is the result of a neuromuscular disfunction [16]. The nervous system is badly coordinating the muscles, which then produce excessive loading of the articulations. However, no conclusive evidence has been presented proving or disproving this statement due to a lack of information on the system. Thus, the development of effective treatments for musculoskeletal diseases such as osteoarthritis are impeded by a lack of information on the proper functioning of musculoskeletal systems.

To address the lack of information, we must rely on models of the musculoskeletal system. These models can represent the entire body [49] or just a specific part like the hip, knee or shoulder [144, 194]. Musculoskeletal models are essential in analysing musculoskeletal systems and their related diseases. Over the last twenty years, musculoskeletal modelling has improved immensely as a result of the advances in computer technology. Computers can handle larger, more complex models and can perform large computational procedures rapidly. Currently, there are two main techniques for constructing a musculoskeletal model. The first technique uses classical mechanics to construct a model where the bones are rigid bodies, the articulations are ideal mechanical joints and the muscles are cables wrapping over the bones. Such models are capable of estimating the force intensities in the muscles and joints during dynamic movements [76, 101, 144]. The second technique uses finite elements to construct a model that includes a constitutive model of the bones and muscles. Their internal behaviour is considered using models of their elementary material constituents. In comparison to the first type of musculoskeletal models, finite element models are most efficient in estimating the stress distributions in the muscles and the joints, in static or quasi-static situations [11, 88, 171]. Finite element models can be used in dynamic situations but are harder to build. These two types of models can be seen as complementary. For instance, a musculoskeletal model built using classical mechanics can be used to estimate the forces in the muscles during a motion. The estimated forces can then be used to estimate the stress distribution in the joints using a finite element model of the articular cartilage [121].

Although musculoskeletal modelling has greatly improved, there remains a substantial gap between the models and the real system. The reason for this gap is validation. A musculoskeletal model must be validated before it can be used for analysing the system it models [48]. Unlike models of other mechanical systems, validation of musculoskeletal models represents a challenging task. First, there is no perfect match between simulations of the model and experiments on the real system [182]. Second, there is no single test validating a model and validation is an open-ended process [135]. One must continuously assess a model's ability to reproduce the real system's behaviour.

To sum up, musculoskeletal diseases such as osteoarthritis are difficult to understand because of the un-observability of the affected area. Models of musculoskeletal systems help obtain the necessary information such as muscle forces and joint reaction forces, to develop proper treatments for musculoskeletal diseases. However, such models are challenging because there is no simple answer regarding their validity.

1.2 State of the Art

This thesis presents a musculoskeletal model of the human shoulder constructed from the framework of classical mechanics. The model was constructed for the purpose of studying osteoarthritis in the shoulder joint. To help set the context, the shoulder is comprised of the clavicle, the scapula and humerus bone. The clavicle is attached to the sternum (bone running down the centre of the chest) through the sternoclavicular articulation (SC). The scapula is attached to the clavicle through the acromioclavicular articulation (AC) and the humerus bone is attached to the scapula through the glenohumeral or shoulder articulation (GH). The contact between the scapula and ribcage is called the scapulothoracic contact (A more detailed presentation of shoulder anatomy and physiology can be found in chapter 2).

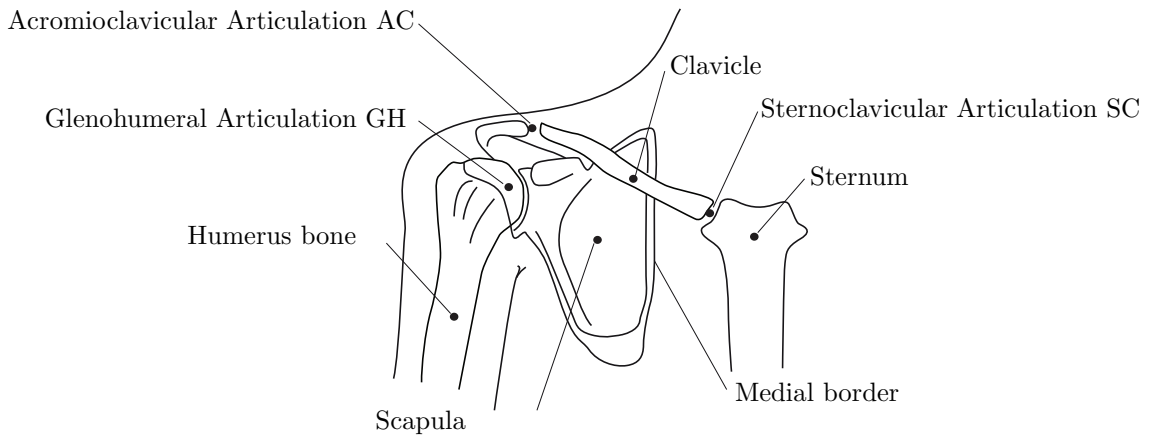


Figure 1.1: *Illustration of the shoulder skeletal structure with some basic terminology.*

The use of musculoskeletal models to help improve our understanding of the human body and its related musculoskeletal diseases is a relatively modern concept. Historically, human anatomy has been studied for a long time (~ 1600 B.C.). Leonardo da Vinci's drawings (~ 1500 A.D.) are the first recordings of human anatomy as we understand it today. It was not until the end of the 19th century and beginning of the 20th century that we started modelling the human body to better understand it. The first models of the shoulder appeared in the early years of the 20th century [152, 180]. These models were physical models using wooden structures to represent the bones and cables to represent the muscles. The cable model is still used today but in a virtual simulation context. Shoulder modelling as we understand it today was introduced in 1965 [53]. It was the first model to represent the bones as links in a mechanism. The clavicle was represented as a straight link from the articulation with the sternum, to the articulation with the scapula (Fig 1.1). The scapula was represented by a short link between the clavicle and the humerus bone. While the model introduced the idea of using linkages, it was mainly a descriptive model.

During the 1980's, a research program for building a more mathematical model of the shoulder for simulation purposes was carried out [65]. This research program introduced the idea of modelling the physical articulations as ideal mechanical joints [61, 62]. Each

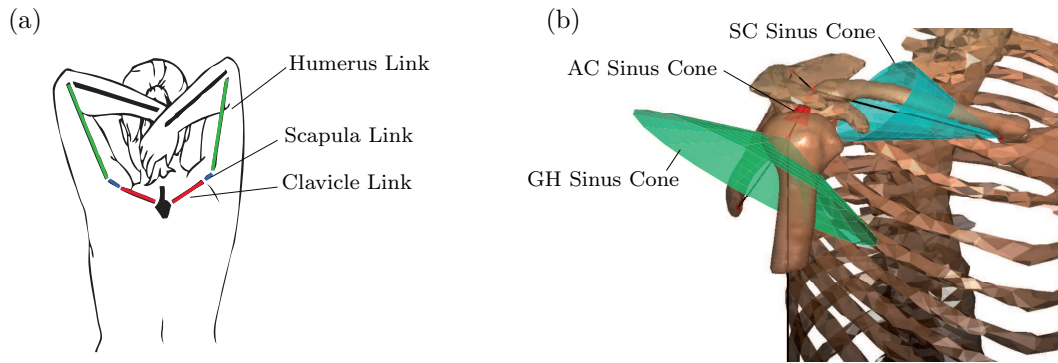


Figure 1.2: (a) *Illustration of the linkage model introduced by Dempster in 1965 [53].* (b) *Illustration of the joint sinus cone model introduced by Engin [65], Engin and Chen [61, 62] and Engin and Tumer [63, 64].*

joint was attributed a sinus cone, limiting its motion [63, 64]. The apex of the cone was set at the centre of the joint and the distal link was constrained to remain in the cone (Fig. 1.1). The model produced by this research program was mainly kinematic. In the late 80's, a specific set of coordinates for describing the configuration of the shoulder bones with respect to the sternum was published [103, 104]. The coordinates were used to construct a regression model for the kinematics of the clavicle and scapula. This model defined the kinematic coordinates of the clavicle and the scapula as functions of the coordinates of the humerus bone. This model is referred to as the swedish model and was initially kinematic. In 1992 and again in 1999, the swedish model was updated to include dynamics and a more accurate representation of the muscles [114, 138]. In 1994, the first high fidelity musculoskeletal model of the shoulder to include dynamics in the sense of classical mechanics, was constructed [194]. The model included a one-dimensional finite element model of the bones and muscles (Fig. 1.3). It included a model of the scapulothoracic contact, where two points on the scapula's medial border were constrained to remain at a constant distance from the surface of an ellipsoid representing the surface of the ribcage. The additional distance represented the layer of tissue in between. The model was also the first to investigate the most appropriate method of using the cable muscle model to represent muscles with large attachment sites [197].

The dynamic shoulder model with one-dimensional finite elements is now referred to as the Delft Elbow and Shoulder Model (DSEM). It can be seen as the first example of a modern musculoskeletal shoulder model. Indeed, many of its attributes are found in a number of more recent models. In 1998, a highly detailed musculoskeletal model for simulation of a virtual human being was published [142]. This model included all the bones and muscles as well as the skin. In 2001, a kinematic musculoskeletal model constructed from the Visible Human Project (VHP) dataset was developed [74, 76]. The model was designed for estimating the properties of a muscle model [77]. It also included a scapulothoracic contact model identical to the original model from [194]. Also in 2001, a dynamic musculoskeletal shoulder model was published [129]. This model has been progressively developed and is now included in the AnyBody® musculoskeletal modelling software [49]. The model was designed for multiple purposes. In 2005, a dynamic model of the shoulder was designed for studying the effects of musculoskeletal surgery [101].

This model is now one of many models available in the Simtk OpenSim musculoskeletal modelling software [52]. In 2006, a shoulder model was developed for estimating the force in the glenohumeral joint [37]. This model is sometimes referred to as the Newcastle shoulder model. In 2007, a musculoskeletal shoulder model was developed for analysing ergonomics [54]. In 2011, a model of the shoulder was developed for studying the stability of the glenohumeral joint [69]. Stability is understood here as keeping the articulation from dislocating. In 2012, the shoulder model constructed from the Visible Human Project was given a dynamic model [170]. More comprehensive reviews of musculoskeletal shoulder models can be found in the literature [168, 219].

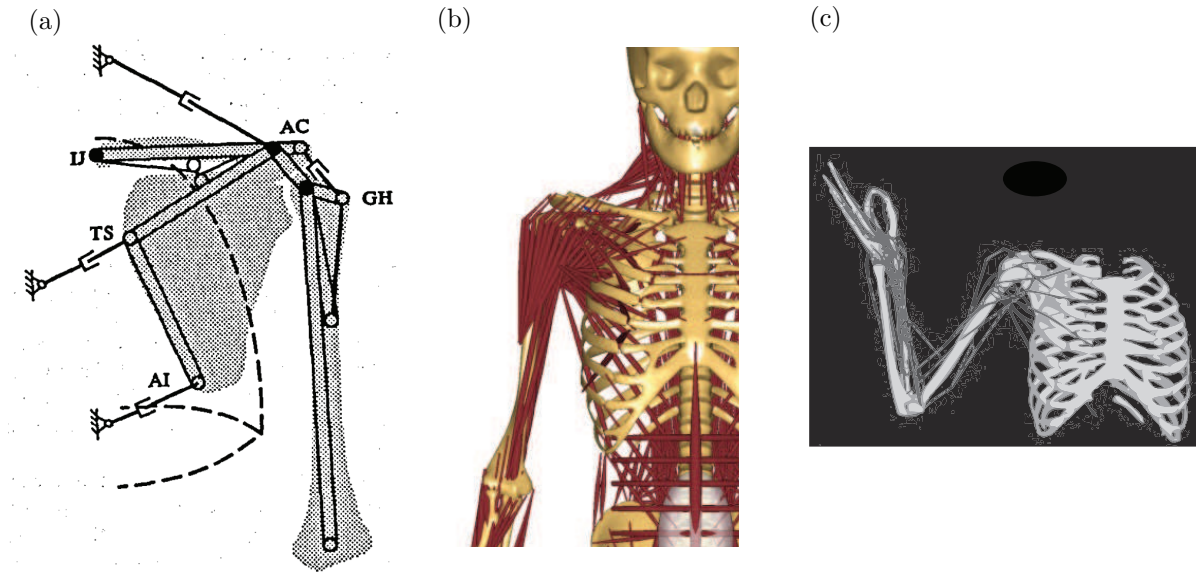


Figure 1.3: (a) Illustration of a diagram from the van der Helm musculoskeletal shoulder model [194]. (b) Illustration of the shoulder model from the AnyBody modelling software [129]. (c) Illustration of the shoulder model from the OpenSim modelling software [101].

A number of numerical methods have been developed in parallel, specifically for musculoskeletal models. These methods are designed either to deal with the different challenges arising from constructing a musculoskeletal model, or to simply use the model efficiently. This dissertation focuses on two families of numerical methods in particular; First, methods for motion planning of the model's kinematics, and second, methods for computing the necessary forces in the muscles to generate a specific motion.

The human shoulder is kinematically redundant. There are more internal degrees of freedom in the shoulder than degrees of freedom of the elbow's position. Therefore, planning the kinematics of shoulder models is not straightforward; A number of methods have been developed to deal with the kinematic redundancy such as regression models. As stated previously, the Swedish model was the first to introduce a coordinate system for describing the configuration of the bones [103, 104]. A set of three Tait-Bryan angles was defined for each bone and the coordinates were used to develop a regression model of shoulder kinematics. The kinematics of the clavicle and scapula were expressed as nonlinear functions of the kinematics of the humerus. Thus, reducing the number of coordinates to three. This regression model was adapted in 2009 to a Denavit-Hartenberg description of the kinematics [218]. There are other regression models using linear functions [50, 84, 215].

Inverse kinematics was also used in planning the kinematics of a shoulder model [142]. A third method consists of minimising the difference between the model's kinematics and measured kinematics [8, 156]. The development of kinematic motion planning strategies for the shoulder is still a very relevant research topic [211]. Indeed, recent developments in motion capture techniques have lead to more accurate descriptions of shoulder kinematics [58, 199]. Furthermore, a new direction in this research is to construct kinematic descriptions that are specific to an individual [20].

The human shoulder, like many other musculoskeletal systems, is overactuated. There is an infinite number of muscle activation patterns generating the same motion. A number of methods have been developed to estimate the forces in the muscles of a musculoskeletal system that generate a desired movement. The problem is also referred to as the force sharing problem. A comprehensive review can be found in the literature [66]. Solutions to this problem are called coordination strategies. A strategy commonly used for the shoulder is inverse dynamics coupled with static optimisation [70, 90, 195]. A kinematic motion of the model is planned over a time horizon. The motion is then given to an inverse dynamics model yielding the required torques or actuation at each joint. The temporal evolution of the joint torques is discretised and a static optimisation problem is defined at each instant, to find the muscle forces that generate the torques, while minimising a cost function. The problem is subject to a number of constraints representing the restrictions imposed by the physical system. The optimisation problem is generally formulated as a nonlinear program and solved using appropriate NLP algorithms. The optimisation problem has also been formulated as a quadratic program using the relation between joint torques and muscle forces [3, 190]. This method is called null-space optimisation. The most used cost function is the one minimising the mean square muscle stress [194]. This cost function is called the second-order polynomial cost function and is mathematically a quadratic sum of the forces, divided by their cross-sectional area. Another cost function has been introduced called the min/max criterion [6]. This cost function is shown to produce similar results to the polynomial cost function with higher orders [172]. More recently, energy-based cost functions involving oxygen consumption have been formulated [167].

The above presentation is not a comprehensive review of the literature. However, the references stated above are viewed as the most relevant to the current work.

1.3 Contributions

The present dissertation is part of a research program funded by the Swiss National Science Foundation (SNF)¹ to study osteoarthritis. The question driving the research program is the possibility of a neuromuscular dysfunction as the underlying cause of osteoarthritis. Osteoarthritis in the shoulder occurs mainly in the glenohumeral joint and it causes excessive loading of the joint. The humeral head is pressed into the glenoid. Therefore, the primary motivation behind the present dissertation, is the construction of a musculoskeletal shoulder model for estimating the intensity of the joint reaction force

¹Research grant reference number: K-32K1-122512

in the glenohumeral joint. The shoulder models presented in the previous section can also be used for such a study. However, given that the ultimate goal of the research program is to investigate neuromuscular interactions the model is being designed from scratch. Neuromuscular interactions are a control problem and therefore it is necessary to have full knowledge and access to the model's content. The model is capable of estimating the forces in the muscles and the contact force in the glenohumeral articulation. The dissertation focuses on the model's construction. The model is constructed from the laws of classical mechanics, considering the bones to be rigid bodies, the articulations to be idealised mechanical joints and the muscles to be ideal cables wrapping over the bones. The present model is based on the kinematic musculoskeletal shoulder model constructed from the Visible Human Project [74, 76]. The present model adds a dynamic layer in terms of equations of motion and uses a modified scapulothoracic contact model.

Using the modified contact model, a novel parameterisation of the shoulder's kinematics is proposed. The parameterisation uses a set of independent minimal coordinates that make kinematic computations related to the model, straightforward. The model formulates the muscle-force estimation problem as a quadratic program and solves it using null-space optimisation [3, 190]. The null-space optimisation, previously published [3, 190], was used in this dissertation to detect weaknesses in the model of the shoulder's muscle structure. The model was implemented and used to estimate the reaction forces in the glenohumeral joint during quasi-static and dynamic raising of the outstretched arm (abduction).

The present work addresses the topic of neuromuscular control through a brief analysis of a human motor control mechanism called joint stiffness control through antagonistic muscle co-contraction. This particular mechanism is analysed because it is related to muscle-force coordination and hence to the joint forces themselves. It is also a mechanism controlling a mechanical property of the joints, stiffness. The mechanism is analysed using a simple model of a cable-driven pendulum. The pendulum model is relevant to the analysis, given that it shares the same mathematical structure as models of musculoskeletal systems. The joint stiffness control mechanism is implemented on a physical system and the results are used to initiate the discussion of neuromuscular control as a possible cause to osteoarthritis.

A second contribution of this dissertation is to propose a formal and precise mathematical representation of musculoskeletal shoulder modelling. In general, musculoskeletal models are designed for clinical purposes such as analysing osteoarthritis. The models are constructed and used by both engineers and medical staff, which constitutes a challenge when presenting one's work. The message must be understandable for everyone working in the same interdisciplinary field. Therefore, many presentations of musculoskeletal models do not include the technical or mathematical details of the model. A point that makes it difficult for others to reconstruct the models.

Biomechanics and in particular biomechanics of the human shoulder involves research that can be classified into four categories. Experimental, theoretical, applied and fundamental research [47, 48]. Musculoskeletal modelling is situated between theoretical and fundamental research and is essentially applied physics. Physics describes our universe through a set of principles that are formally expressed as mathematical equations. These principles govern both the macroscopic and microscopic elements of the universe.

Given that musculoskeletal models are constructed from these principles, the equations they involve constitute the model's blueprint. Presenting the mathematical equations of a model allows others to reproduce the work and test it more thoroughly. Lastly, presenting the mathematics of a model favours dissemination of technical "know-how". Others can profit from a technical description of a model and thereby further improve research. Mathematics constitute an important foundation of musculoskeletal modelling and therefore a good portion of this dissertation tries to formalise the principles used to construct and work with the model. The work is presented such that technical details are given where they are required for others to reconstruct the work. The presentation is not however, entirely technical. A considerable effort has been made such that the presentations and discussions remain accessible to as wide an audience as possible.

1.4 Organisation of the Thesis

The dissertation, present chapter included, is composed of eleven chapters, organised as follows:

Chapter 2: Anatomy, physiology and movement of the human shoulder. The core of the thesis is modelling the human shoulder. Therefore, this chapter presents an overview of the human shoulder and introduces the system specific vocabulary.

Chapter 3: Multibody systems theory. This chapter gives an extended presentation of single-body and multibody mechanics and defines the notations used throughout the thesis. The purpose of this chapter is to construct the technical framework of the entire dissertation.

Chapter 4: A musculoskeletal model of the human shoulder. This chapter presents the musculoskeletal shoulder model that is being developed for estimating forces in the glenohumeral joint. The chapter focuses on the model's construction and mathematical structure. The chapter also presents the geometric muscle model linking the forces in the muscles to the dynamics of the skeletal system. The chapter concludes by introducing the idea that models of musculoskeletal systems and models of cable-driven robots have similar mathematical structures.

Chapter 5: Coordinated redundancy. This chapter defines the concept of coordinated redundancy and sets a specific framework for chapters 6 and 7. The chapter introduces the idea of using tasks for coordination and introduces the general coordination strategy used for the shoulder model.

Chapter 6: Shoulder kinematic redundancy coordination. This chapter presents a new method of solving the shoulder model's kinematic redundancy without requiring measured data. The method uses a minimal set of coordinates obtained through a parameterisation of the shoulder girdle as a parallel platform. The coordinates are independent from each other and significantly simplify the computational aspects of planning movements for the shoulder model. The coordinates are constructed from a detailed

analysis of the kinematic shoulder model's mathematical structure.

Chapter 7: Shoulder overactuation coordination. This chapter presents a coordination strategy for solving the shoulder's overactuation problem relying on muscle moment-arms. A classical definition of muscle moment-arms is given, followed by two methods of computing moment-arms. The first is a geometric method and the second is the well known tendon excursion method. The two methods are shown to not be strictly equivalent. This chapter defines the necessary conditions for the existence of a solution to the coordination problem and introduces the concept of wrench-feasibility.

Chapter 8: Estimating joint forces in the human shoulder. This chapter presents the implementation of the musculoskeletal shoulder model from chapter 4, using the methods described in chapters 6 and 7. The chapter briefly reviews the model and presents the results that were obtained, including model-estimated scapular kinematics, muscle moment-arms, muscle forces and most importantly the reaction force in the glenohumeral joint. The chapter discusses the model's current capabilities and uses wrench-feasibility to explain the results.

Chapter 9: Introduction to control theory. This chapter presents a brief overview of control theory, giving the essential concepts and definitions used in chapter 10.

Chapter 10: Joint stiffness control for musculoskeletal stability. This chapter investigates a mechanical stabilisation mechanism used in human motor control. The chapter demonstrates that the mechanism does achieve stability in the sense of modern control theory. A cable-driven pendulum is used as a tool to present and discuss the investigation. The chapter also presents a joint stiffness control strategy that was implemented on a physical cable-driven pendulum. The implementation results are used to initiate a discussion of the possible cause of osteoarthritis.

Chapter 11: Conclusions This chapter summarises the work, draws some more general conclusions and discusses future work.

Chapter 2

Anatomy, Physiology and Movement of the Human Shoulder

This chapter presents a brief, descriptive overview of the shoulder's anatomy and physiology. The shoulder's movement is also covered. All the elements described in the chapter can be found in closed-form in the literature [32, 53, 83].

The human musculoskeletal system allows us to move using our muscles and bones. It is what gives us form and supports our body. The system is comprised of bones, muscles, cartilage, tendons, ligaments, joints and connective tissue. These elements define its anatomy or structure. The role played by each element define its physiology or function. The purpose of this chapter is to introduce some of the terminology that will be used throughout the thesis.

2.1 Shoulder Skeletal Anatomy and Physiology

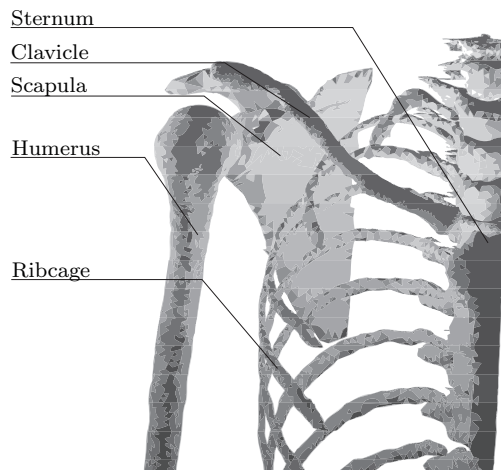
The human shoulder is comprised of three bones and the upper thorax. The thorax can be defined as the sternum, ribcage and spine (Fig. 2.1). The first bone is the clavicle, a small elongated bone connected to the sternum at one end and to the scapula at the other. The clavicle protects the neurovascular bundle (nerves and blood vessels) supplying the upper limb. It serves as a strut between the sternum and scapula, transmitting loads from the upper limb to the central skeletal axis of the body.

The second bone is the scapula, a concave triangular bone connected to the clavicle and the humerus. The scapula's inner edge is called the medial border. The bony ridge running outwards from the upper end of the medial border is called the scapula's spine. It finishes at the acromion, the bony protrusion connecting the scapula to the clavicle. Below the acromion is another bony protrusion called the coracoid process. This landmark is used as a muscle and ligament attachment site. Opposite the medial border is the lateral border running from the angulus inferior to the glenoid cavity. The clavicle and scapula together with the thorax define the shoulder girdle.

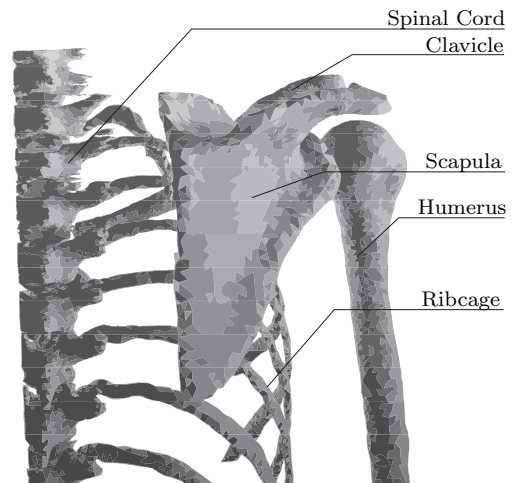
The third bone is the humerus, a long bone connected to the scapula, the radius and the

ulna. Its upper end is called the humeral head, having a spherical shape. Between the humeral head and elbow, the humerus has a cylindrical shape. Its lower end is triangular. The external points of this shape are the lateral epicondyle and medial epicondyle.

Anterior View



Posterior View



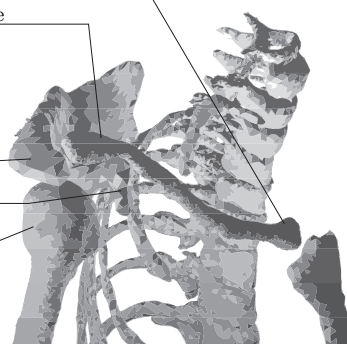
Sternal end of Clavicle

Distal end of Clavicle

Acromion

Coracoid Process

Humeral Head



Scapular Medial Border

Scapular Spine

Acromion

Glenoid

Humeral Head

Lateral Border

Angulus Inferior

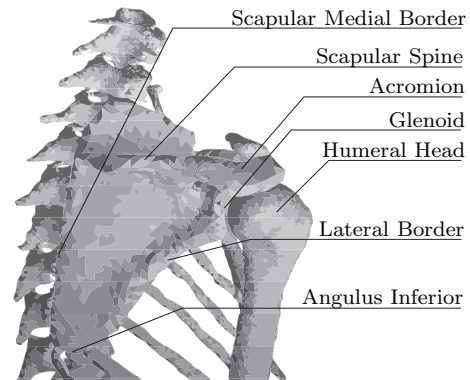


Figure 2.1: *Illustration of the shoulder's skeletal anatomy as described in section 2.1.*

The bones are joined together by three synovial articulations providing mobility. In synovial articulations, the bones are not directly connected and do not necessarily touch each other. There is a synovial cavity surrounding the part of the bones that are in contact. On the surface of each bone at the point of contact, there is layer of articular cartilage that is softer than bone and has less friction. The contact is held by dense tissue surrounding the bones called the articular capsules. The first articulation in the shoulder is called the sternoclavicular articulation (SC) between the sternum and clavicle (Fig. 2.2). The second articulation is called the acromioclavicular articulation (AC) between the clavicle and scapula. The third articulation is the glenohumeral articulation (GH) between the scapula and humerus. This articulation is commonly referred to as the "shoulder joint" and is the shoulder's primary articulation. When the joint is loaded, the round shape of the humeral head is pressed against the concave shape of the glenoid cavity on the scapula (Fig. 2.3). The glenoid has an elliptical shape with the long axis directed vertically. When the joint is relaxed, there is a cavity between the bones. Surrounding the glenoid is the glenoid labrum, a fibro-elastic element protecting the edges of the glenoid cavity. At the other end of the humerus is the elbow and humerolulnar articulation (HU).

Additional structures of the shoulder associated with articulations include ligaments which are viscoelastic elements having a passive role. They are used to stabilise the motion of the bones relative to each other. There are capsular ligaments mentioned previously stabilising the synovial articulations. Stability is understood as keeping the bones of an articulation in the correct configuration such that the load passing through the articulation is not excessive or misaligned with the contact surfaces. Other ligaments in the shoulder provide added strength to the shoulder. For instance, the conoid ligament and coracohumeral ligament stabilise the motion of the scapula relative to the clavicle and humerus. Lastly, the flat concave shape of the scapula allows it to glide over the ribcage. This contact is called the scapulothoracic joint or gliding plane (ST) and is not an articulation. Its role is mainly kinematic, guiding the scapula's movements.

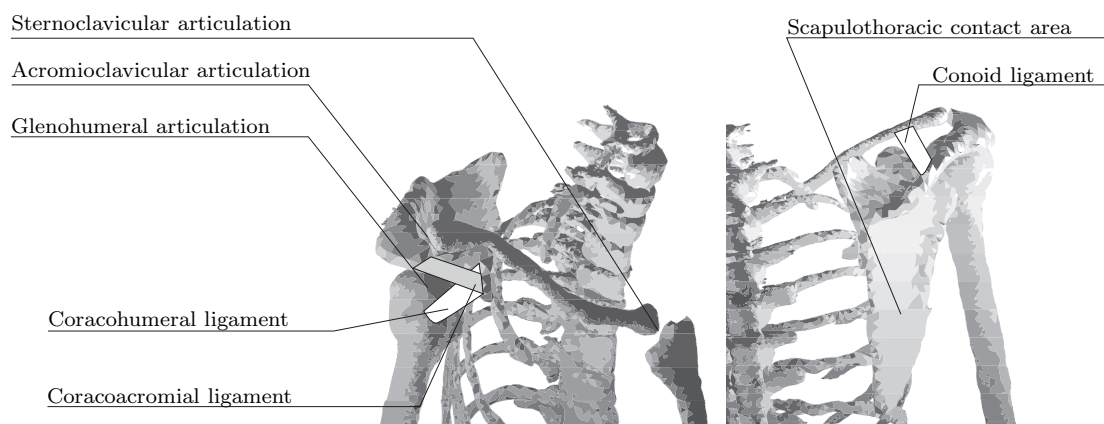


Figure 2.2: *Illustration of the shoulder's articulations and ligaments as described in section 2.1. The ligaments are not anatomically exact and were added to the illustration by the author.*

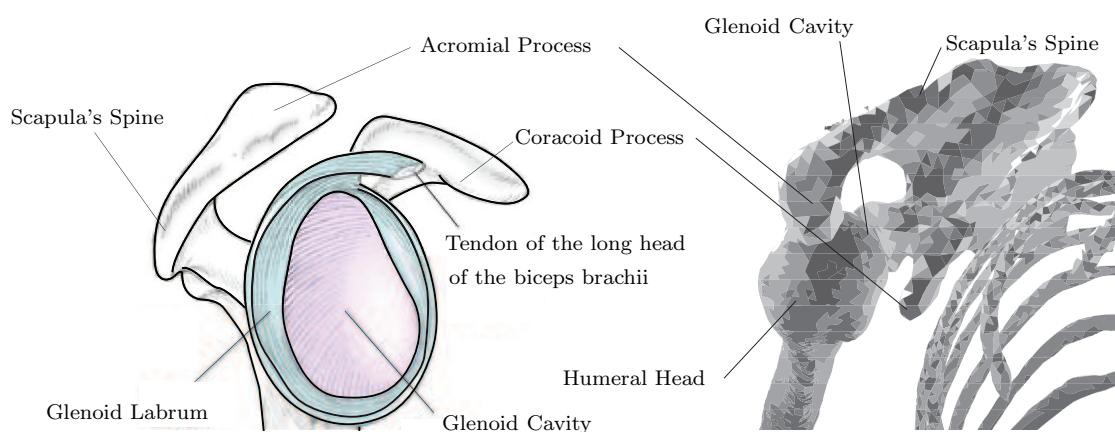


Figure 2.3: *Illustration of the glenoid cavity in the glenohumeral joint as described in section 2.1.*

2.2 Shoulder Muscle Anatomy and Physiology

There are 16 muscles actuating the shoulder. These muscles are called skeletal muscles and are comprised of large numbers of parallel fibres. At either end, there are tendons connecting the muscle fibres to the bone. The connection with the skeleton that is closest to the body's central axis (spine) is called the origin. The other connection is called the insertion. The names of each muscle and their anatomical locations are illustrated in figure 2.4.

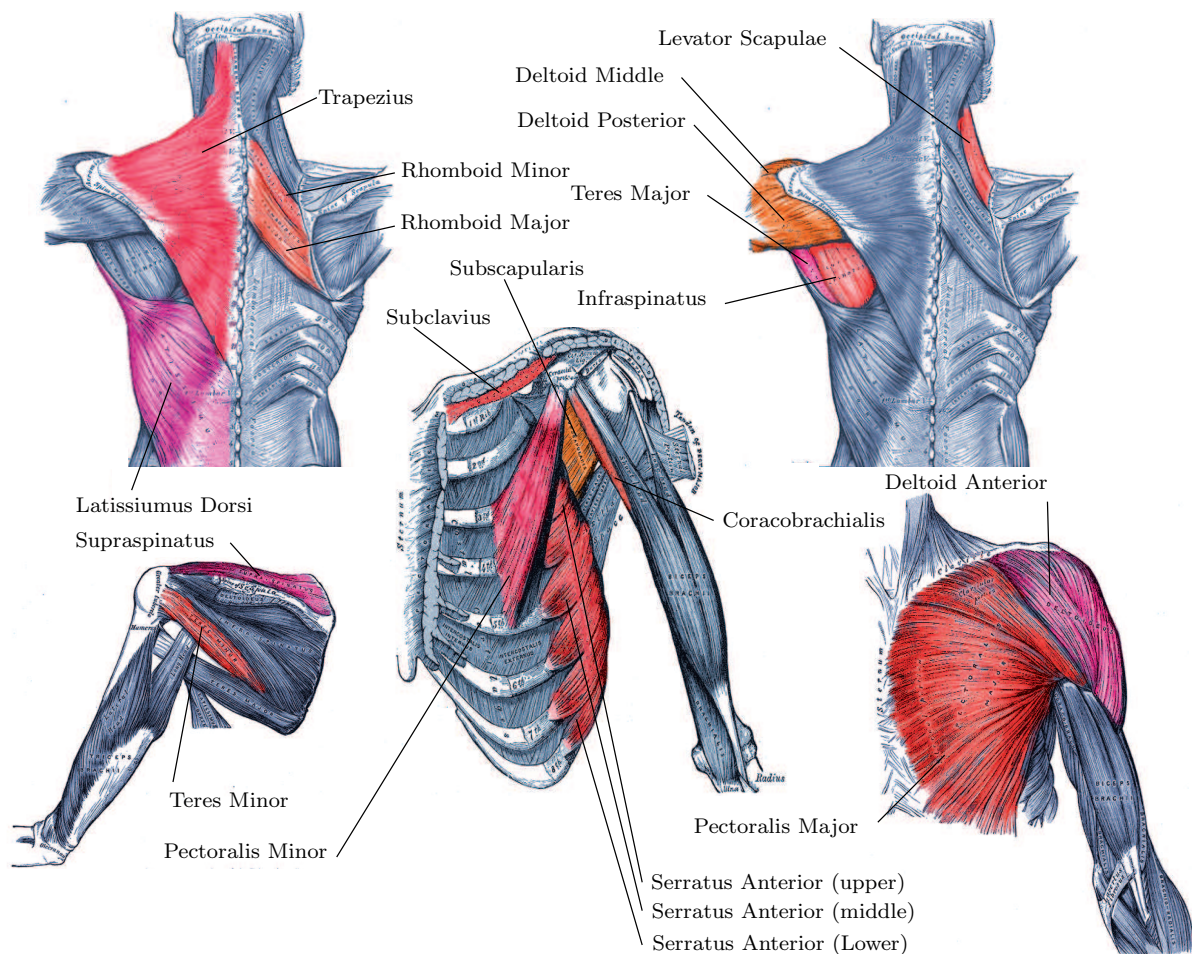


Figure 2.4: *Illustration of the shoulder's muscle structure. Illustrations taken from [83].*

The shoulder girdle is defined as the scapula, the clavicle and the upper left- or upper right-hand side of the thorax. The shoulder girdle is differentiated from the shoulder proper because it is the structure attaching the upper limb to the body. There are muscles actuating the shoulder girdle and muscles actuating the glenohumeral articulation or shoulder joint. The shoulder girdle muscles include:

- trapezius (TRP), serratus anterior (SRA), rhomboid minor (RMN), rhomboid major (RMJ), levator scapulae (LVS), pectoralis minor (PMN).

These muscles originate on the thorax and insert on the scapula. The superior part of the trapezius muscle inserts on the distal end of the clavicle. The trapezius and serratus anterior are the two major muscles of this group. The glenohumeral articulation muscles include:

- deltoid (DLT), infraspinatus (INFR), supraspinatus (SUPR), subscapularis (SBSC), teres minor (TMN), teres major (TMJ), coracobrachialis (CRCB).

The deltoid is the primary muscle of this group. The infraspinatus, supraspinatus, teres minor and subscapularis form a group of muscles collectively known as the rotator cuff muscles. The goal of these muscles is maintaining the stability of the glenohumeral articulation. Again, stability is understood as keeping the bones of an articulation in the correct configuration.

There are two additional muscles actuating the entire shoulder: the latissimus dorsi (LTD) and pectoralis major (PMJ). Both muscles originate on the thorax and insert on the humerus thereby influencing the motion of the entire shoulder. The subclavius (SBCL) muscle is of little importance in actuating the shoulder but rather plays a role of protecting certain arteries passing beneath the clavicle. If the clavicle breaks, this muscle protects the underlying arteries from puncture.

Skeletal muscles have a very specific structure. At either end there are tendons linking the muscle to the bone and in-between there is the muscle proper. The tendon attaches the muscle to the bone by dividing into many small fibres that insert into the bone. Internally, a skeletal muscle is made up of a collection of fibres called muscle bundles. Each bundle is made up of a collection of muscle fascicle. Each fascicle is a collection of muscle fibres or muscle cells. This structure is similar to steel cables that are made up of many thin wires of steel grouped together into larger cables forming the entire cable. Internally, each muscle fibre is made up of a number myofibrils, similar to the muscle fibre but much smaller. Each myofibril is a sequence of sacromeres linked end-to-end by Z-disks. Sacromeres and Z-disks are connected through a noncontracting filament called connectin. The connectin and Z-disks constitute the muscle's passive behaviour. A sacromere consists of two types of proteins, actin and myosin that can store and release energy by changing shape and constitute the muscles ability to produce force. There are two ways in which sacromeres are stacked: serial or parallel. Serial structures lead to muscles able to contract quickly while parallel structures lead to muscles producing more force because of the increased thickness.

There exist two types of fibres in a muscle; The first are called extrafusal muscle fibres and the second are called intrafusal muscle fibres. Extrafusal fibres represent the majority and constitute the muscle's strength. Intrafusal fibres are less numerous and act as length sensors for the nervous system. When myosin proteins in a muscle release energy, the result is either a change in length or the production of force without change in length. It will depend on the interaction of the muscle with the skeletal structure. For example, if the force generated by the muscle is insufficient to overcome inertia, there will be no movement. It is when muscles do not change length, that they produce the maximum force, this situation is known as isometric contraction. Given that muscle's have elastic

properties, they apply forces even when not active, this is called the force-length behaviour [95]. There is an optimal length at which a muscle can produce its overall maximum active force. The maximum amount of force a muscle can produce diminishes when the muscle's length is not optimal. The active force-length relationship is a bell curve (Fig. 2.5). The passive elements also produce force that steadily increases as the muscle's length increases. The total force produced by a muscle increases as the muscle's length increases until the optimal fibre length. Beyond the optimal fibre length, there is a slight decrease followed by a rapid increase. The muscle's passive resistance to being stretched dominates for high values of muscle length. During normal everyday activities, the muscle works in an area around the optimal fibre length. The muscle's total force also depends on the rate of change in muscle length. However, this behaviour is more complex and not covered here.

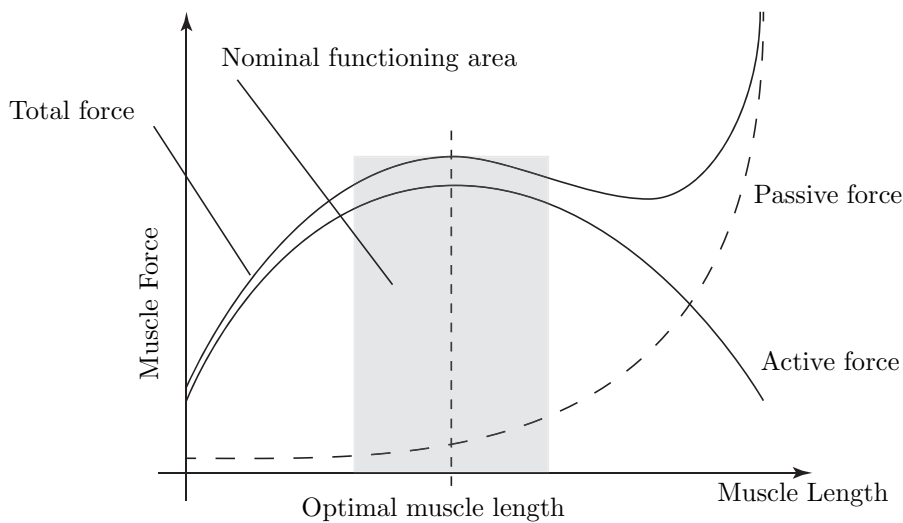


Figure 2.5: *Illustration of the typical force-length behaviour of a skeletal muscle as described in section 2.2.*

2.3 Shoulder Movement

Three orthogonal body planes are used to describe the human body and its motion. If the thorax is attributed a frame such that the x -axis and y -axis define the horizontal plane and the z -axis defines the vertical direction. The body planes are parallel to the planes defined by the thorax frame and are defined as (Fig. 2.6):

- X-Y plane: transverse plane,
- X-Z plane: coronal plane or frontal plane,
- Y-Z plane: sagittal plane.

The *scapular plane* represents a fourth plane that is necessary to define the shoulder's motion. It is a plane perpendicular to the transverse plane but rotated around the z -axes

by 30° . The scapular plane vertically cuts the glenohumeral joint in half.

Thoraco-clavicular motion is defined as the motion of the clavicle with respect to the thorax frame. *Scapulo-thoracic* motion is defined as the motion of the scapula over the thoracic cage with respect to the thorax frame. *Thoraco-humeral* motion is defined as the motion of the humerus around the glenohumeral joint with respect to the thorax. *Scapulo-humeral* motion is defined as the motion of the humerus around the glenohumeral joint with respect to the scapula.

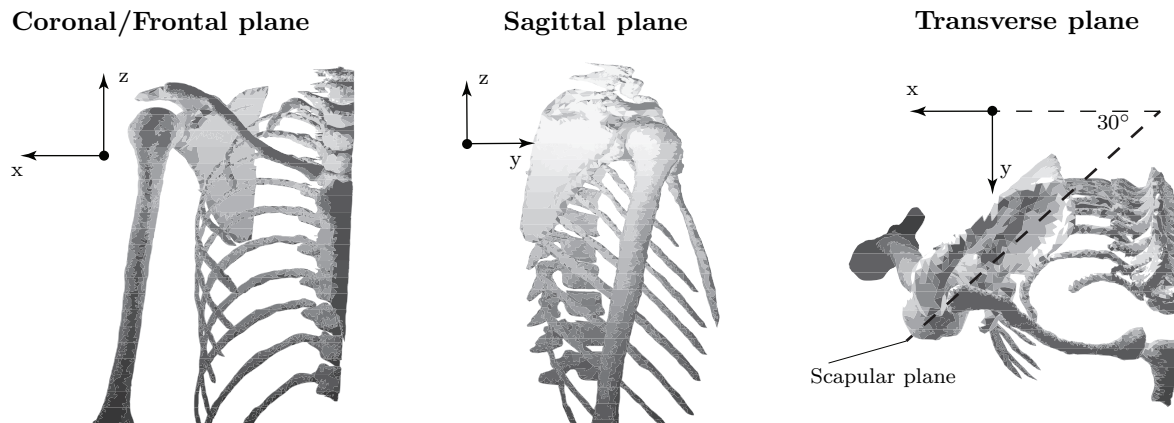


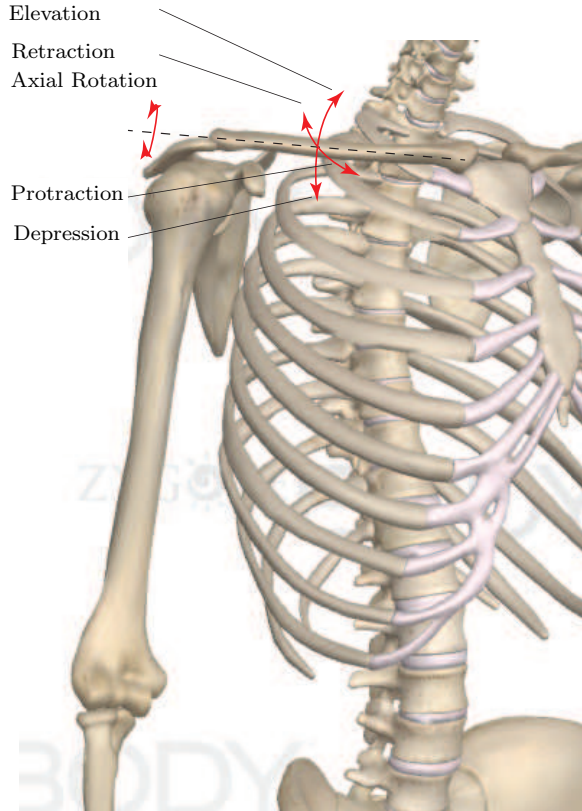
Figure 2.6: *Illustration of the three body planes and the scapular plane.*

Each bone has its own specific set of motions. These elementary motions are defined as follows (Fig. 2.7):

- Clavicle:
 - axial rotation: Rotation around the clavicle's longitudinal axes,
 - depression/elevation: rotation in the sagittal plane,
 - retraction (adduction of clavicle)/protraction (abduction of clavicle): rotation in the transverse plane.
- Scapula:
 - axial rotation: rotation around the scapula's spine,
 - depression/elevation: rotation around an axis normal to the scapular spine,
 - retraction (adduction of scapula)/protraction (abduction of scapula): rotation around the thoracic cage.
- Humerus:
 - axial rotation: rotation around the humerus's longitudinal axis,
 - flexion/extension: rotation in the sagittal plane,
 - abduction/adduction: rotation in the coronal plane.

The arm's large range of motion is primarily due to the scapulo-humeral rhythm. The scapulo-humeral rhythm is defined as the coordinated motion of the scapula and the humerus [43, 118]. If the scapula was to remain stationary during arm movement, the humerus/arm could at most abduct to 120° . Thus, the scapula's motion contributes up to 60° of the arm's total abduction angle [174]. Healthy scapulo-humeral rhythm is required to achieve full 180° abduction.

Clavicle Motions



Scapular Motions

Elevation
Retraction
Protraction
Depression
Spinal Tilt

Humeral Motions

Extension
Adduction
Flexion
Abduction
Axial Rotation

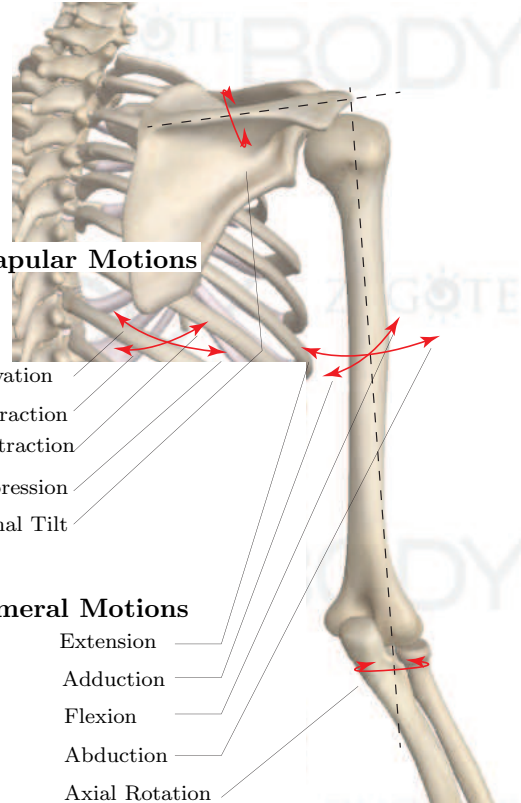


Figure 2.7: Schematic description of shoulder bone motion definitions. Image created using ZygoteBodyTM zygotebody.com.

There have been many studies of the scapulo-humeral rhythm to identify its characteristics [73, 105, 149]. The modern description decomposes the scapulo-humeral rhythm into three phases. In phase one, the humerus rotates upward to approximately 30° while the scapula remains motionless. This is called the settling phase (Fig. 2.8 I.). In phase two, the humerus has rotated up to 90° abduction. As the humerus rotates up to 90° , the scapula follows its rotation with a ratio of $1/2$. For every two degrees of scapulo-humeral rotation, there is one degree of scapulo-thoracic rotation. The humerus has rotated by 70° with respect to the scapula. The scapula has contributed 20° . This is called the 1-2 phase (Fig. 2.8 II.). The 1:2 ratio continues up to 150° abduction. There is 110° scapulo-humeral rotation and 40° scapulo-thoracic rotation. The third and last phase of abduction is characterised by a 1:1 ratio. At 180° abduction, there is a 120° scapulo-humeral rotation and 60° scapulo-thoracic rotation. This is called the 1-1 phase.

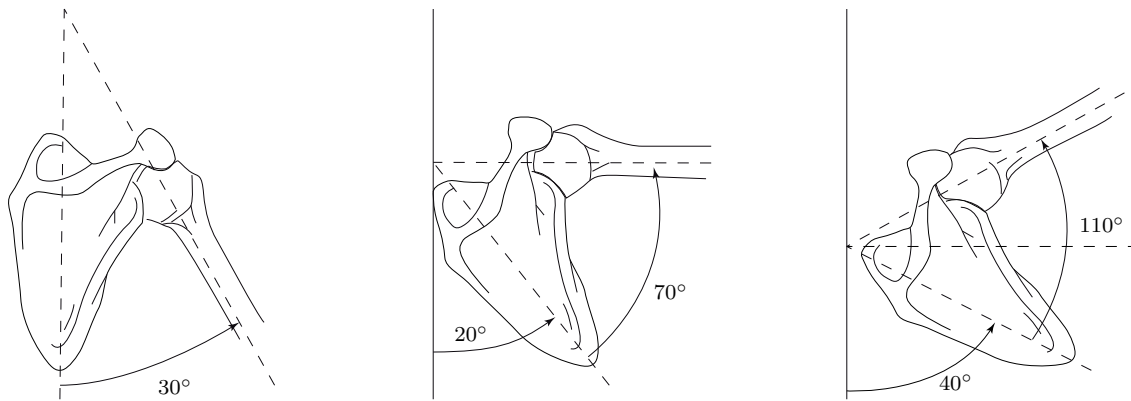


Figure 2.8: *Illustration of the three phase description of the scapulo-humeral rhythm.*

This chapter presented the anatomy, physiology and movement of the human shoulder. The remainder of this thesis deals with the construction of a model of this system and the associated computational methods. The model is built on the principles of general multibody mechanics. Therefore, the next chapter gives a presentation of multibody mechanics in order to set the framework and notations used throughout the remainder of the dissertation.

Chapter 3

Multibody Systems Theory

3.1 Introduction

Multibody systems theory is the study of the time-dependent behaviour or dynamics of interconnected bodies that can be either rigid or flexible. Multibody systems theory is governed by general mechanics and is therefore described by a formal mathematical framework. Thus, multibody systems modelling requires a the same rigour and formalism for the theory to be applied appropriately [18, 86, 157]. The goal of this chapter is to give a detailed overview of multibody systems and to introduce the notations and conventions that will be used throughout the thesis.

At the core of multibody systems theory is the construction of the nonlinear equations of motion which are derived from the expressions of a body's kinematics and mechanical energy. One of the principal methods of deriving a body's equations of motion is the Euler-Lagrange equation. However, the equations of motion alone are insufficient to completely analyse the dynamics of interconnected bodies. The equations of motion provide no information regarding the internal forces or interactions between the bodies. Thus, the Newtonian approach is also necessary to obtain a complete description of each body's dynamics.

This chapter is divided into two parts. Part one presents multibody systems theory for a single body beginning with the kinematics of a single rigid body. The kinematics are presented in the classical sense of position, velocity and acceleration. The equations of motion for a single rigid body are derived using the Newtonian approach. The same equations are used to express the body's mechanical energy. Part one also covers the duality between Chasles' theorem in kinematics and Poincot's theorem in dynamics.

Part two extends the presentation to the case of multiple bodies. The notions of kinematic pairs and kinematic chains are introduced and the interconnections between bodies are described in terms of constraints. This section also defines a system's forward kinematic map and the principle of mobility is introduced. The formalism of analytical mechanics is presented with a focus on virtual displacements and the principles of virtual power and work. The principle of virtual work is then used to derive the Euler-Lagrange equation.

Section 3.2 covers the fundamental concepts required to build the theory presented in the following sections. Sections 3.3 and 3.4 present the kinematics and dynamics of a single rigid body. Section 3.5 extends the presentation to systems of rigid bodies with a presentation of the formalism of analytical mechanics for building the equations of motion.

3.2 Preliminaries

3.2.1 Conventions

Space is the boundless three-dimensional extent, or three-dimensional Euclidean space, denoted \mathbb{R}^3 . A right-handed coordinate system \mathcal{R}_0 is used to describe space, defined by three, mutually perpendicular axes, referred to as x , y and z . The intersection point of the three axes is the origin O_0 of the reference system. To each axis is associated a unit vector \mathbf{i}_0 , \mathbf{j}_0 and \mathbf{k}_0 . A right-handed reference system is defined such that if one were to grab the z -axis with the right hand, such that the thumb points in the direction of the z -axis unit vector, the fingers would curl around the axis from the x -axis to the y -axis.

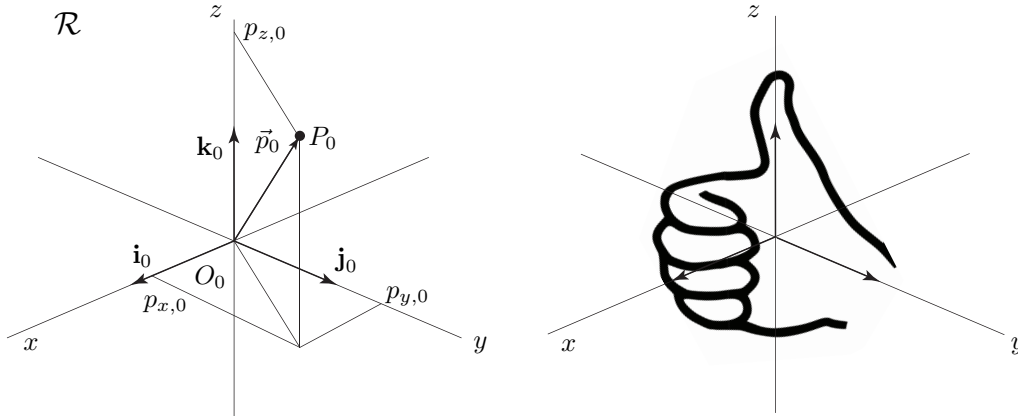


Figure 3.1: *Illustration of the right-handed coordinate system and the right hand thumb principle as described in section 3.2.1.*

The position of a point P_0 in space is defined by a vector emanating from the origin of the coordinate system to the point (Fig. 3.1). The components for this vector are $p_{x,0}$, $p_{y,0}$ and $p_{z,0}$. A component of a position vector is positive if the projection of the vector onto the corresponding coordinate axis points in the same direction as the unit vector otherwise it is negative.

$$P_0 : \vec{p}_0 = (p_{x,0} \ p_{y,0} \ p_{z,0})^T = p_{x,0}\mathbf{i} + p_{y,0}\mathbf{j} + p_{z,0}\mathbf{k}_0,$$

$$p_{x,0} = (\vec{p}_0 \cdot \mathbf{i}_0)\mathbf{i}_0, \quad p_{y,0} = (\vec{p}_0 \cdot \mathbf{j}_0)\mathbf{j}_0, \quad p_{z,0} = (\vec{p}_0 \cdot \mathbf{k}_0)\mathbf{k}_0.$$

The point O_0 is the only point in the reference system \mathcal{R}_0 with all three coordinates equal to zero. The coordinate system's unit vectors satisfy the orthonormality properties

in terms of the dot and cross products, defined in the usual manner.

$$\begin{aligned} \mathbf{i}_0 \cdot \mathbf{i}_0 = \mathbf{j}_0 \cdot \mathbf{j}_0 = \mathbf{k}_0 \cdot \mathbf{k}_0 &= 1, & \mathbf{i}_0 \times \mathbf{i}_0 = \mathbf{j}_0 \times \mathbf{j}_0 = \mathbf{k}_0 \times \mathbf{k}_0 &= 0, \\ \mathbf{j}_0 \cdot \mathbf{k}_0 = \mathbf{i}_0 \cdot \mathbf{k}_0 = \mathbf{i}_0 \cdot \mathbf{j}_0 &= 0, & \mathbf{i}_0 \times \mathbf{j}_0 = \mathbf{k}_0, \quad \mathbf{k}_0 \times \mathbf{i}_0 = \mathbf{j}_0, \quad \mathbf{j}_0 \times \mathbf{k}_0 &= \mathbf{i}_0. \end{aligned}$$

The reference frame which is fixed in space is referred to as the *inertial* reference frame and will be denoted \mathcal{R}_0 . The subindex will always indicate this frame. In the case of multiple reference systems, other reference systems will be denoted \mathcal{R}_i . The subindex $i = 1, 2, 3, \dots$ will always denote a particular frame. Vectors defined in a particular frame will have the associated subindex.

3.2.2 Geometric Configuration

The geometric configuration of a point P_0 in space with respect to the inertial frame \mathcal{R}_0 is simply the coordinates of the point. The geometric configuration $\mathcal{C}_{0,i}$ of a body \mathcal{B}_i in space is defined as the position of all its particles. A *rigid body* is an idealised solid, or collection of particles, that cannot be deformed. The distance between any two points on the body remains constant at all times. A *free* body is an unconstrained body that can move freely within \mathbb{R}^3 .

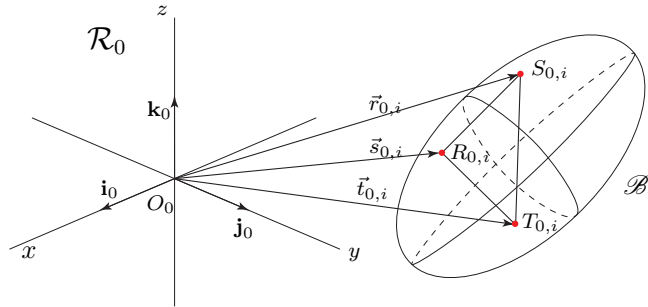


Figure 3.2: *Illustration of a free rigid-body's geometric configuration with respect to the inertial reference frame \mathcal{R}_0 as described in section 3.2.2.*

Under the rigid body hypothesis, it is sufficient to know the position of three non-colinear particles to know the geometric configuration of the body. The geometric configuration $\mathcal{C}_{0,i}$ of a free body \mathcal{B}_i is defined with respect to the inertial frame by three points subject to the rigid-body constraints (3.2).

$$\mathcal{C}_{0,i} : \begin{cases} R_{0,i} : \vec{r}_{0,i} = (r_{x,0} & r_{y,0} & r_{z,0})^T, \\ S_{0,i} : \vec{s}_{0,i} = (s_{x,0} & s_{y,0} & s_{z,0})^T, \\ T_{0,i} : \vec{t}_{0,i} = (t_{x,0} & t_{y,0} & t_{z,0})^T, \end{cases} \quad (3.1)$$

$$\|R_0 S_0\|_2 = cte, \quad \|R_0 T_0\|_2 = cte, \quad \|S_0 T_0\|_2 = cte. \quad (3.2)$$

There are nine coordinates subject to three equality constraints meaning that a *free rigid-body's geometric configuration is described by six independent coordinates.*

3.2.3 Euclidean Displacements

A transformation on \mathbb{R}^3 is a map $\mathcal{T}(P_0 \mapsto P'_0)$ defined by giving every point P_0 in \mathbb{R}^3 an image P'_0 in \mathbb{R}^3 . The map \mathcal{T} defines a one-to-one correspondence or bijection. Transformations on \mathbb{R}^3 have the following properties and form a group $\mathcal{G}(\mathbb{R}^3)$.

- Definition 1** (Transformations on \mathbb{R}^3). *1. For every transformation $\mathcal{T}(P_0 \mapsto P'_0)$, there is an inverse transformation $\mathcal{T}^{-1}(P'_0 \mapsto P_0)$.*
- 2. If $\mathcal{T}_A(P_0 \mapsto P'_0)$ and $\mathcal{T}_B(P'_0 \mapsto P''_0)$ are two transformations then $\mathcal{T}_B \mathcal{T}_A(P_0 \mapsto P''_0)$ is also a transformation called the product transformation.*
- 3. The product of a transformation and its inverse defines the unit or identity transformation $\mathcal{I} = \mathcal{T}^{-1} \mathcal{T}$.*
- 4. The product of transformations is associative: $\mathcal{T}_C(\mathcal{T}_B \mathcal{T}_A) = (\mathcal{T}_C \mathcal{T}_B) \mathcal{T}_A$.*

The rigid body hypothesis restricts the possible transformations to ones that do not deform space. The distances between points remains constant under the transformation. These transformations are called *Euclidean displacements*.

Definition 2 (Euclidean Displacement). *A Euclidean displacement is a transformation $\mathcal{T}(P_0 \mapsto P'_0)$ on \mathbb{R}^3 such that, the distance (in terms of the Euclidean norm) between any two points P_0 and Q_0 remains invariant under the transformation.*

$$\|P_0 Q_0\|_2 = \|P'_0 Q'_0\|_2.$$

Euclidean displacements preserve distances and angles and form a group $\mathcal{G}_E(\mathbb{R}^3)$ that is a subgroup of the group of transformations on \mathbb{R}^3 . In practice, Euclidean displacements are defined as either pure translations, pure rotations or both (Fig. 3.3). The equation for a general displacement is given by:

$$\begin{aligned} \mathcal{T} &: \mathbb{R}^3 \rightarrow \mathbb{R}^3, \\ P_0 &: \vec{p}_0 \mapsto \mathcal{T}(P) = P'_0 : \vec{p}'_0 = \vec{d}_0 + \mathbf{R}_0 \vec{p}_0, \end{aligned} \quad (3.3)$$

where \vec{d}_0 is the translation vector and \mathbf{R}_0 the rotation matrix.

A Euclidean displacement also describes a change of coordinates (Fig. 3.4). Consider two reference systems \mathcal{R}_i and \mathcal{R}_j for describing space, defined with respect to the inertial frame \mathcal{R}_0 , with two distinct origins $O_{0,i}$ and $O_{0,j}$. A vector \vec{p}_j defined in \mathcal{R}_j is defined in \mathcal{R}_i by:

$$P_i : \vec{p}_{i,j} = \vec{d}_{i,j} + \mathbf{R}_{j,i} \vec{p}_j, \quad P_j : \vec{p}_j, \quad (3.4)$$

Notations: The double index $\vec{p}_{i,j}$ indicates that it is a vector in the reference frame \mathcal{R}_i but is related to the reference frame \mathcal{R}_j . In this dissertation, the vector $\vec{d}_{i,j}$ will always designate the vector separating the origins of two reference systems \mathcal{R}_i and \mathcal{R}_j (The letter

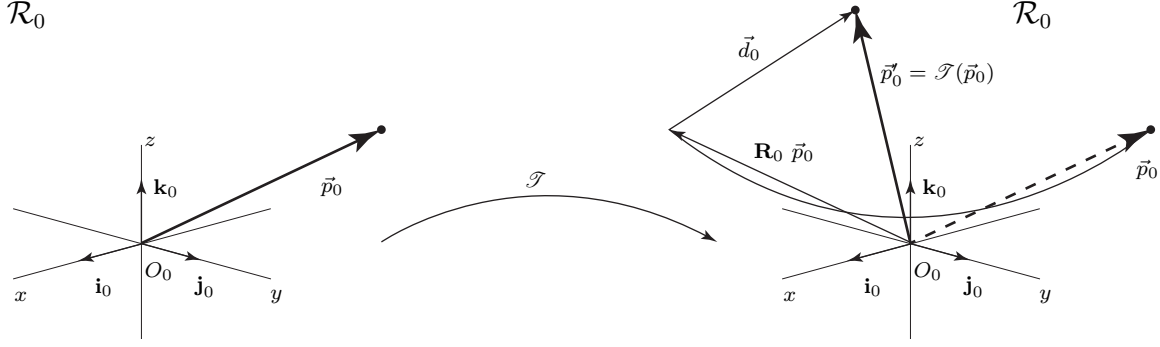


Figure 3.3: *Illustration of a Euclidean displacement as a translation and a rotation as described in section 3.2.3.*

d is specifically reserved for this). The first subindex will always designate the reference system in which the vector is explicitly defined. The matrix $\mathbf{R}_{j,i}$ is the rotation matrix, transforming a vector in frame \mathcal{R}_j into a vector in frame \mathcal{R}_i . For rotation matrices, the order of the subindexes will always indicate the direction of transformations. $\mathbf{R}_{j,i}$ indicates a transformation from \mathcal{R}_j to \mathcal{R}_i .

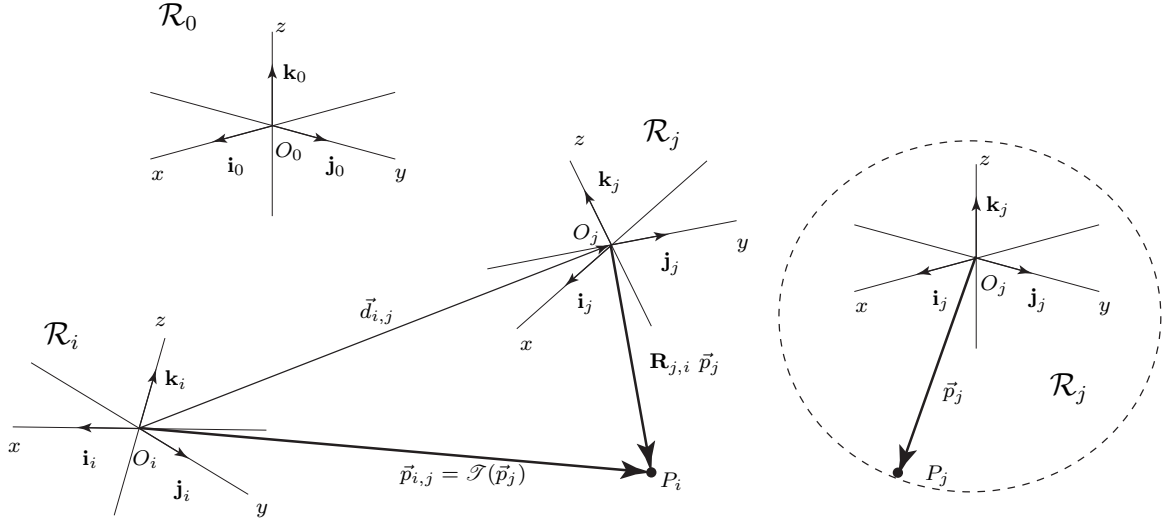


Figure 3.4: *Illustration of a Euclidean displacement as a coordinate transformation as described in section 3.2.3.*

Euclidean displacements can be expressed as linear applications using *homogeneous coordinates*. The entire transformation is grouped into a single matrix $\mathbf{H}_{j,i}$.

$$\begin{pmatrix} \vec{p}_{i,j} \\ 1 \end{pmatrix} = \begin{pmatrix} \mathbf{R}_{j,i} & | & \vec{d}_{i,j} \\ 0 & 0 & 0 & | & 1 \end{pmatrix} \begin{pmatrix} \vec{p}_j \\ 1 \end{pmatrix} = \mathbf{H}_{j,i} \begin{pmatrix} \vec{p}_j \\ 1 \end{pmatrix}, \quad \vec{p}_j \equiv \vec{p}_{j,i}. \quad (3.5)$$

The inverse transformation is defined by

$$\begin{pmatrix} \vec{p}_{j,i} \\ 1 \end{pmatrix} = \begin{pmatrix} \mathbf{R}_{i,j} & | & -\mathbf{R}_{i,j}\vec{d}_i \\ 0 & 0 & 0 & | & 1 \end{pmatrix} \begin{pmatrix} \vec{p}_i \\ 1 \end{pmatrix} = \mathbf{H}_{i,j} \begin{pmatrix} \vec{p}_i \\ 1 \end{pmatrix}, \quad \vec{p}_i \equiv \vec{p}_{i,j}. \quad (3.6)$$

The geometric description of a body's configuration is more appropriate for describing fixed configurations. Euclidean displacements are more appropriate for describing the change in configuration of a rigid body, i.e. a body's kinematics. The geometric and Euclidean displacement descriptions are related. Given the geometric description in terms of the points R_0 , S_0 and T_0 in a frame \mathcal{R}_i , the Euclidean displacement from \mathcal{R}_j to \mathcal{R}_i is defined by:

$$\vec{d}_{i,j} = \vec{r}_{i,j}, \quad \mathbf{R}_{j,i} = \begin{pmatrix} \frac{\vec{s}_{i,j} - \vec{r}_{i,j}}{\|\vec{s}_{i,j} - \vec{r}_{i,j}\|_2} & \frac{(\vec{t}_{i,j} - \vec{r}_{i,j}) \times (\vec{s}_{i,j} - \vec{r}_{i,j})}{\|(\vec{t}_{i,j} - \vec{r}_{i,j}) \times (\vec{s}_{i,j} - \vec{r}_{i,j})\|_2} & \frac{((\vec{s}_{i,j} - \vec{r}_{i,j}) \times (\vec{t}_{i,j} - \vec{r}_{i,j})) \times (\vec{s}_{i,j} - \vec{r}_{i,j})}{\|((\vec{s}_{i,j} - \vec{r}_{i,j}) \times (\vec{t}_{i,j} - \vec{r}_{i,j})) \times (\vec{s}_{i,j} - \vec{r}_{i,j})\|_2} \end{pmatrix}. \quad (3.7)$$

The columns of the matrix $\mathbf{R}_{j,i}$ are the base vectors \mathbf{i}_j , \mathbf{j}_j and \mathbf{k}_j described in the frame \mathcal{R}_i : $\mathbf{i}_{i,j}$, $\mathbf{j}_{i,j}$ and $\mathbf{k}_{i,j}$.

3.2.4 Rotation Matrices

A general 3×3 rotation matrix is a way of representing a rotation defining a transformation between two orthonormal representations of space. Rotation matrices satisfy the following properties.

Properties 1. (*Rotation matrices*)

1. For a rotation matrix \mathbf{R}_0 , there exists another matrix $\mathbf{R}_0^{-1} = \mathbf{R}_0^T$ such that $\mathbf{R}_0 \mathbf{R}_0^T = \mathbf{I}$ (*Identity matrix*).
2. For two rotation matrices \mathbf{R}_0 and \mathbf{R}'_0 , the product $\mathbf{R}_0 \mathbf{R}'_0 = \mathbf{R}''_0$ is also a rotation matrix.
3. The composition operation is not commutative $\mathbf{R}_0 \mathbf{R}'_0 \neq \mathbf{R}'_0 \mathbf{R}_0$.

Consider a rotation \mathbf{R}_i defined in a frame \mathcal{R}_i and a change of coordinates $\mathbf{R}_{i,j}$. The same rotation is defined in the frame \mathcal{R}_j by:

$$\mathbf{R}_{i,j} \mathbf{R}_i \mathbf{R}_{i,j}^T = \mathbf{R}_j. \quad (3.8)$$

This is valid for any frame two frames \mathcal{R}_i and \mathcal{R}_j and leads to the following statement. The rotation matrices \mathbf{R}_i and \mathbf{R}_j are said to be equivalent and are two representatives of a class of mutually orthogonal matrices. All the classes of such matrices under the composition operation form a non-commutative group $O(3)$ of dimension three. The elements of this group represent both proper and improper rotations. Proper rotations preserve orientation or right-handedness of the coordinate frame, improper rotations do not. In rigid-body mechanics, only proper rotations are used. The rotation matrices representing proper rotations satisfy the additional property.

$$\text{Proper Rotation: } \det(\mathbf{R}_i) = 1, \quad \text{Improper Rotation: } \det(\mathbf{R}_i) = -1. \quad (3.9)$$

All rotation matrices representing proper rotations form the subgroup $SO(3)$ of $O(3)$ called the special orthogonal group. This group will be discussed in section 3.2.5.

The components of a rotation matrix $\mathbf{R}_{j,i}$ are the direction cosines of the coordinate frame unit vectors. Direction cosines are the projections of the unit vectors of frame \mathcal{R}_j onto the unit vectors of \mathcal{R}_i . i.e. the cosines of the angles between the reference frame vectors.

$$\mathbf{i}_{i,j} \cdot \mathbf{j}_i = \cos(\angle(\mathbf{i}_{i,j}, \mathbf{j}_i)). \quad (3.10)$$

Notation: A reference frame unit vector with double subindex $\mathbf{i}_{i,j}$ means the vector is a unit vector of the frame j indicated by the second index but defined in the frame i indicated by the first index.

The columns of $\mathbf{R}_{j,i}$ are the unit vectors of \mathcal{R}_j , defined in \mathcal{R}_i .

$$\mathbf{R}_{j,i} = (\mathbf{i}_{i,j} \quad \mathbf{j}_{i,j} \quad \mathbf{k}_{i,j}), \quad \begin{aligned} \mathbf{i}_{i,j} &= (\mathbf{i}_{i,j} \cdot \mathbf{i}_i \quad \mathbf{i}_{i,j} \cdot \mathbf{j}_i \quad \mathbf{i}_{i,j} \cdot \mathbf{k}_i)^T, \\ \mathbf{j}_{i,j} &= (\mathbf{j}_{i,j} \cdot \mathbf{i}_i \quad \mathbf{j}_{i,j} \cdot \mathbf{j}_i \quad \mathbf{j}_{i,j} \cdot \mathbf{k}_i)^T, \\ \mathbf{k}_{i,j} &= (\mathbf{k}_{i,j} \cdot \mathbf{i}_i \quad \mathbf{k}_{i,j} \cdot \mathbf{j}_i \quad \mathbf{k}_{i,j} \cdot \mathbf{k}_i)^T. \end{aligned} \quad (3.11)$$

3.2.5 Angular Description of Rotations

As mentioned previously, rotations in multibody systems are elements of $SO(3)$. $SO(3)$ is a non-commutative group of dimension three, subgroup of $O(3)$. The group is a Lie group with a natural smooth manifold¹ structure, *diffeomorphic*² to the real projective space \mathbb{P}^3 [99, 100].³ This can be understood as there exist smooth, invertible maps or charts between subsets of \mathbb{R}^3 and $SO(3)$. Thus, three independent variables are needed to describe a rotation. There are many charts on $SO(3)$ defining coordinate systems. The most well known examples of charts on $SO(3)$ are *Euler angles* and *Tait-Bryan angles*. Both charts are based on the following statement:

A general rotation in \mathbb{R}^3 is built and determined by three successive planar rotations in three mutually orthogonal planes.

Leonard Euler, [67]

If the three rotations occur in the same frame, the rotation sequence is *extrinsic*. If the rotations occur in the intermediate frames, the rotation sequence is *intrinsic*. Euler angles and Tait-Bryan angles define charts mapping $[-\pi, \pi] \times [-\pi, \pi] \times [-\pi, \pi] \subset \mathbb{R}^3$ to $SO(3)$. The Euler and Bryan angle descriptions of rotations are the most prominent but define *local charts* on $SO(3)$. There is a one-to-one correspondence between a rotation matrix and its Euler or Bryan angles but this correspondence cannot be defined for every set of angles. Both charts become singular at certain points, a problem known as *gimbal lock*⁴. There exist multiple sets of rotation angles yielding the same rotation matrix.

¹A smooth manifold is a space of dimension n which locally looks like \mathbb{R}^n (cf. chapter 6).

²The term diffeomorphism designates that there is a smooth invertible map between $SO(3)$ and \mathbb{P}^3 .

³The real projective space \mathbb{P}^3 is comprised of all the lines in \mathbb{R}^4 passing through the origin.

⁴Gimbal lock: was coined because the mechanism used to measure the angles is called a gimbal.

The difference between the Euler and Bryan angle descriptions is the order of the rotation. Each planar rotation is defined by an angle: ψ , ϑ and φ . For Euler angles, the first and third rotation axes are the same. For Bryan angles, all three rotation axes are different. There are two sets of six rotation sequences.

- Euler sequences : $(x - y - x, \quad x - z - x, \quad y - x - y, \quad y - z - y, \quad z - x - z, \quad z - y - z),$
- Bryan sequences : $(x - y - x, \quad x - z - x, \quad y - x - y, \quad y - z - y, \quad z - x - z, \quad z - y - z).$

For Euler angles, independently of the sequence, the first angle is the *spin* angle, the second angle is *nutation* and the third angle is *precession*. For Bryan angles, the first angle is *roll*, the second *pitch* and the third *yaw* (Bryan angles are often used to describe an aircraft's configuration). In this presentation, only intrinsic sequences are considered. Intrinsic sequences define a change of coordinates between two reference frames \mathcal{R}_i and \mathcal{R}_j .

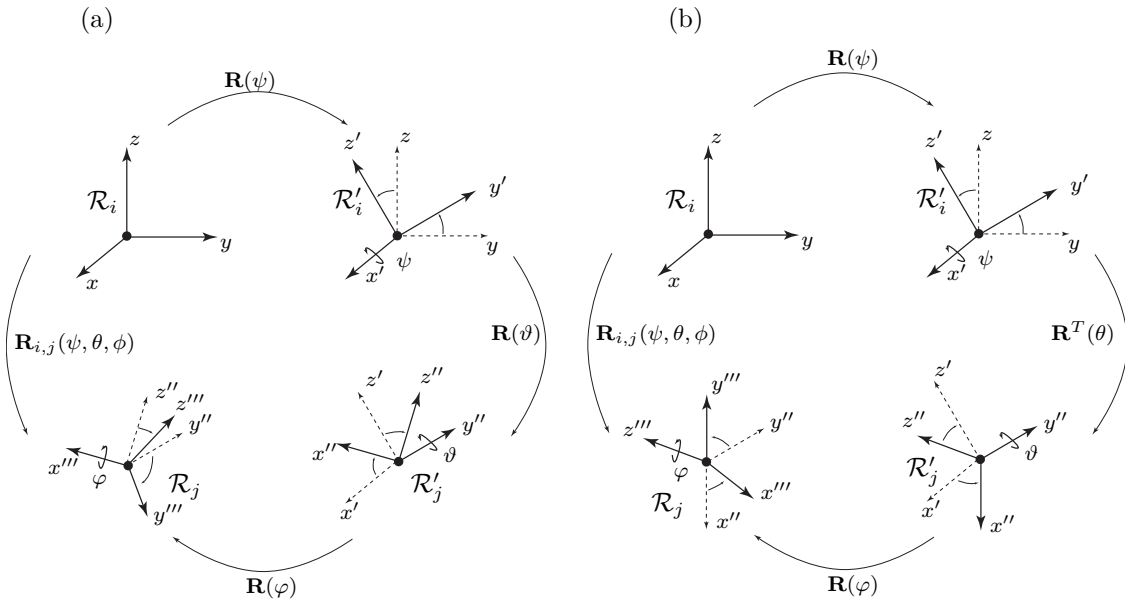


Figure 3.5: Illustration of (a) the $x - y - x$ Euler angle sequence and (b) the $x - y - z$ Bryan angle rotation sequence as described in section 3.2.5.

The intrinsic $x - y - x$ Euler angle sequence from \mathcal{R}_i to \mathcal{R}_j is defined as follows (Fig. 3.5 (a))

$$\mathbf{R}_{i,j}(\psi, \theta, \phi) = \mathbf{R}(\phi) \cdot \mathbf{R}^T(\theta) \cdot \mathbf{R}(\psi), \quad (3.12)$$

where

$$\mathbf{R}(\psi) = \begin{pmatrix} 1 & 0 & 0 \\ 0 & \cos(\psi) & -\sin(\psi) \\ 0 & \sin(\psi) & \cos(\psi) \end{pmatrix}, \quad \mathbf{R}(\vartheta) = \begin{pmatrix} \cos(\vartheta) & 0 & -\sin(\vartheta) \\ 0 & 1 & 0 \\ \sin(\vartheta) & 0 & \cos(\vartheta) \end{pmatrix}, \quad \mathbf{R}(\varphi) = \begin{pmatrix} 1 & 0 & 0 \\ 0 & \cos(\varphi) & -\sin(\varphi) \\ 0 & \sin(\varphi) & \cos(\varphi) \end{pmatrix}.$$

The first rotation $\mathbf{R}(\psi)$ can be viewed as a map from \mathcal{R}_i to \mathcal{R}'_i . The second rotation $\mathbf{R}(\vartheta)$ can be viewed as a map from \mathcal{R}'_i to \mathcal{R}'_j . The last rotation $\mathbf{R}(\varphi)$ maps \mathcal{R}'_j to \mathcal{R}_j . Euler sequences becomes singular if the nutation angle $\vartheta = n\pi$ ($n \in \mathbb{Z}$), then the first

and third rotation axes coincide. The intrinsic $x - y - z$ Bryan angle sequence from \mathcal{R}_i to \mathcal{R}_j is defined as (Fig. 3.5 (b))

$$\mathbf{R}_{i,j}(\psi, \theta, \phi) = \mathbf{R}(\phi) \cdot \mathbf{R}^T(\theta) \cdot \mathbf{R}(\psi), \quad (3.13)$$

where

$$\mathbf{R}(\psi) = \begin{pmatrix} 1 & 0 & 0 \\ 0 & \cos(\psi) & -\sin(\psi) \\ 0 & \sin(\psi) & \cos(\psi) \end{pmatrix}, \quad \mathbf{R}(\vartheta) = \begin{pmatrix} \cos(\vartheta) & 0 & -\sin(\vartheta) \\ 0 & 1 & 0 \\ \sin(\vartheta) & 0 & \cos(\vartheta) \end{pmatrix}, \quad \mathbf{R}(\varphi) = \begin{pmatrix} \cos(\varphi) & -\sin(\varphi) & 0 \\ \sin(\varphi) & \cos(\varphi) & 0 \\ 0 & 0 & 1 \end{pmatrix}.$$

The Tait-Bryan sequence can also be viewed as a sequential change of reference frames. Tait-Bryan sequences become singular when $\vartheta = n\frac{\pi}{2}$ ($n = 2m+1, m \in \mathbb{Z}$). The elementary rotation matrices are defined such that positive values of the angles yield counterclockwise rotations. Thus, both descriptions are valid for right-handed, orthonormal axes systems, according to the right-hand rule. There is no universal convention regarding the angular description of rotation matrices. Therefore, it becomes essential to always give the specific sequence and convention used. This will always be done throughout the presentation.

3.2.6 Euler's Rotation Theorem

The following theorem regarding rotations is of particular importance. Instead of considering each rotation as a sequence of three rotations around the reference frame axes, Euler considered a single rotation around a particular axis. This theorem is based on the property that all direct rotations have an eigenvalue of $+1$.

Theorem 1 (Euler's Theorem [67]). *For any rotation around a reference frame, there is a line passing through the reference frame origin such that, all points on this line are invariant under the rotation.*

Stated differently, a sequence of three planar rotations, is equivalent to a single rotation about an axis that runs through the centre of the frame by an angle γ . The direction \vec{n} of the rotation axis is the eigenvector of the rotation matrix associated to the eigenvalue $+1$.

$$\vec{n}_0 = \mathbf{R}_0 \vec{n}_0, \quad \cos(\gamma) = \frac{\text{tr} \mathbf{R}_0 - 1}{2}. \quad (3.14)$$

A vector \vec{p}_0 is related to its image \vec{p}'_0 by a rotation around an axis \vec{n}_0 of an angle γ , through the following relation (Fig. 3.6)

$$\vec{p}'_0 = \mathbf{R}_0 \vec{p}_0 = \vec{p}_0 + (1 - \cos(\gamma))\vec{n}_0 \times (\vec{n}_0 \times \vec{p}_0) + \sin(\gamma)\vec{n}_0 \times \vec{p}_0. \quad (3.15)$$

The rotation matrix can be expressed in terms of the coordinates of \vec{n} and the angle γ .

$$\mathbf{R}_0 = \begin{pmatrix} n_{x,0}^2 + (1 - n_{x,0}^2) \cos(\gamma), & n_{x,0}n_{y,0}(1 - \cos(\gamma)) + n_{z,0} \sin(\gamma), & n_{x,0}n_{z,0}(1 - \cos(\gamma)) - n_{y,0} \sin(\gamma) \\ n_{x,0}n_{y,0}(1 - \cos(\gamma)) - n_{z,0} \sin(\gamma), & n_{y,0}^2 + (1 - n_{y,0}^2) \cos(\gamma), & n_{y,0}n_{z,0}(1 - \cos(\gamma)) + n_{x,0} \sin(\gamma) \\ n_{x,0}n_{z,0}(1 - \cos(\gamma)) + n_{y,0} \sin(\gamma), & n_{y,0}n_{z,0}(1 - \cos(\gamma)) - n_{x,0} \sin(\gamma), & n_{z,0}^2 + (1 - n_{z,0}^2) \cos(\gamma) \end{pmatrix}. \quad (3.16)$$

Based on this description of the rotation matrix, the following quantities are called *Euler-Rodrigues parameters*.

$$\kappa_0 = \cos\left(\frac{\gamma}{2}\right), \quad \kappa_1 = n_{x,0} \sin\left(\frac{\gamma}{2}\right), \quad \kappa_2 = n_{y,0} \sin\left(\frac{\gamma}{2}\right), \quad \kappa_3 = n_{z,0} \sin\left(\frac{\gamma}{2}\right). \quad (3.17)$$

If grouped into a vector, these four variables constitute a *quaternion*.

The quaternion description of rotations is more suited to the structure of $SO(3)$. $SO(3)$ is a three-dimensional manifold embedded in a four dimensional space. A quaternion is a four dimensional vector subject to an equality constraint. The quaternion chart remains three-dimensional because of the unit length constraint. While quaternions avoid the problem of singularities, they are more difficult to use for analysing kinematics. Therefore, in many situations the angle description is used because only a portion of $SO(3)$ is considered.

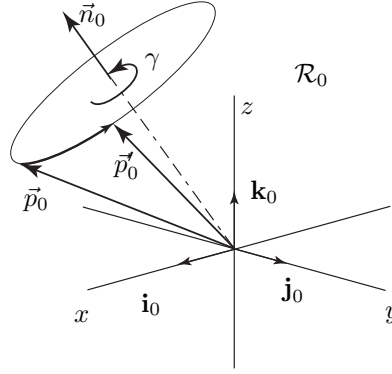


Figure 3.6: *Illustration of Euler's Theorem as described in section 3.2.6.*

3.3 Rigid-Body Kinematics

Kinematics studies the motion of points, bodies and systems of bodies in space without considering the possible causes. The study of the properties of motion not depending on time is called geometric kinematics. The study of time-dependent properties is called instantaneous kinematics. This section presents the instantaneous kinematics for a single rigid body. The classical description of a single-body's kinematics is also given in terms of position, velocity and acceleration. The Poisson formula for rotating vectors is given as well as the fundamental transport theorem. This section ends with Chasle's theorem from screw theory and the instantaneous screw axis.

3.3.1 Instantaneous Angular velocity

Consider a point $X_{0,i}$ fixed in \mathcal{R}_i but rotating around the inertial frame \mathcal{R}_0 . The location of the point at a given instant is defined by:

$$X_{0,i}(t) : \vec{x}_{0,i}(t) = \mathbf{R}_{i,0}(t)\vec{x}_i. \quad (3.18)$$

where \vec{x}_i is the location of the point in the frame \mathcal{R}_i . This point has an instantaneous linear velocity.

$$\dot{X}_{0,i}(t) : \dot{\vec{x}}_{0,i}(t) = \dot{\mathbf{R}}_{i,0}(t)\vec{x}_i = \dot{\mathbf{R}}_{i,0}\mathbf{R}_{i,0}^{-1}\vec{x}_{0,i}(t) = \Omega_{0,i}(t)\vec{x}_i(t). \quad (3.19)$$

The matrix $\Omega_{0,i}$ is called the instantaneous rotational velocity matrix. It is a skew-symmetric matrix. Rotational motion is instantaneously described by a single set of skew-symmetric matrices. Take the infinite Taylor expansion of the rotation matrix.

$$\mathbf{R}_{i,0}(t) = \mathbf{I} + \mathbf{R}_1 t + \frac{1}{2!}\mathbf{R}_2 t^2 + \frac{1}{3!}\mathbf{R}_3 t^3 + \dots \quad (3.20)$$

Each of the matrices \mathbf{R}_k can be written as the sum of a symmetric and skew symmetric matrix.

$$\mathbf{R}_{i,0}(t) = \mathbf{I} + (\mathbf{C}_1 + \mathbf{B}_1)t + \frac{1}{2!}(\mathbf{C}_2 + \mathbf{B}_2)t^2 + \frac{1}{3!}(\mathbf{C}_3 + \mathbf{B}_3)t^3 + \dots \quad (3.21)$$

The symmetric matrices \mathbf{C}_k can be expressed in terms of the matrices \mathbf{B}_k according to the recursion formula, given that $\mathbf{C}_1 = \mathbf{0}$.

$$\mathbf{C}_k = \frac{-1}{2} \sum_{j=1}^{k-1} \binom{k}{j} (\mathbf{C}_{k-j} + \mathbf{B}_{k-j})(\mathbf{C}_j - \mathbf{B}_j). \quad (3.22)$$

Following these relations, the instantaneous rotational velocity matrix is defined by:

$$\Omega_{0,i}(t) = \Omega_0 + \Omega_1 t + \frac{1}{2}\Omega_2 t^2 + \dots, \quad \Omega_k = \sum_{j=1}^{k+1} \binom{k}{j-1} (\mathbf{C}_j + \mathbf{B}_j)(\mathbf{C}_{k-j+1} - \mathbf{B}_{k-j+1}). \quad (3.23)$$

Using (3.22) leads to the following results:

$$\Omega_0 = \mathbf{B}_1, \quad \Omega_1 = \mathbf{B}_2, \quad \Omega_2 = -\mathbf{B}_1^3 + \frac{1}{2}(\mathbf{B}_1\mathbf{B}_2 - \mathbf{B}_2\mathbf{B}_1) + \mathbf{B}_3. \quad (3.24)$$

Thus, only the matrices \mathbf{B}_k describe rotational motion in and around a given instant ($t = 0$). Indeed, the matrices \mathbf{B}_k result from a temporal linearisation. The linearised rotation matrix describes the rotation from a moment shortly before the instant ($-\delta t$) to a moment shortly after (δt). The matrix $\Omega_{0,i}$ has three independent elements and always has the form:

$$\Omega_{0,i} = \begin{pmatrix} 0 & -\omega_z & \omega_y \\ \omega_z & 0 & -\omega_x \\ -\omega_y & \omega_x & 0 \end{pmatrix}. \quad (3.25)$$

Because the matrix has this form, the velocity of the point $X_{0,i}$ is also defined by

$$\dot{X}_{0,i}(t) : \dot{\vec{x}}_{0,i}(t) = \vec{\omega}_{0,i}(t) \times \vec{x}_{0,i}(t), \quad \vec{\omega}_{0,i} = (\omega_x \quad \omega_y \quad \omega_z)^T. \quad (3.26)$$

This is the fundamental formula defining the velocity for rotating vectors. This formula is sometimes referred to as the Poisson formula.

3.3.2 Instantaneous Kinematics

Given a rigid body \mathcal{B}_i , with a reference frame \mathcal{R}_i , moving in space with respect to the inertial frame \mathcal{R}_0 . The position of any point $X_{0,i}$ on the body in the inertial frame, at a given instant t is defined by a Euclidean displacement.

$$X_{0,i}(t) : \vec{x}_{0,i}(t) = \vec{d}_{0,i}(t) + \mathbf{R}_{i,0}(t) \vec{x}_i = \vec{d}_{0,i}(t) + \vec{x}_{0,i}^*(t). \quad (3.27)$$

This definition of Euclidean displacement is fundamental and will be continuously used in this presentation. A vector with a star indicates that it is a rotated vector. The position of the point X_0 is defined by a polynomial of time.

$$\begin{aligned} X_{0,i} : \vec{x}_{0,i} = & \vec{x}_1 + \vec{d}_0 + \left(\mathbf{B}_1 \vec{x}_1 + \vec{d}_1 \right) t + \\ & \frac{1}{2!} \left((\mathbf{C}_2 + \mathbf{B}_2) \vec{x}_1 + \vec{d}_2 \right) t^2 + \frac{1}{3!} \left((\mathbf{C}_3 + \mathbf{B}_3) \vec{x}_1 + \vec{d}_3 \right) t^3 + \dots \end{aligned} \quad (3.28)$$

Each coefficient of the polynomial is a itself a Euclidean displacement.

$$\vec{x}_k = \vec{d}_k + (\mathbf{C}_k + \mathbf{B}_k) \vec{x}_1. \quad (3.29)$$

The velocity and acceleration are defined by:

$$\dot{X}_{0,i} : \dot{\vec{x}}_{0,i} = \mathbf{B}_1 \vec{x}_1 + \vec{d}_1 + \left((\mathbf{C}_2 + \mathbf{B}_2) \vec{x}_1 + \vec{d}_2 \right) t + \frac{1}{2} \left((\mathbf{C}_3 + \mathbf{B}_3) \vec{x}_1 + \vec{d}_3 \right) t^2 + \dots, \quad (3.30)$$

$$\ddot{X}_{0,i} : \ddot{\vec{x}}_{0,i} = \left((\mathbf{C}_2 + \mathbf{B}_2) \vec{x}_1 + \vec{d}_2 \right) + \left((\mathbf{C}_3 + \mathbf{B}_3) \vec{x}_1 + \vec{d}_3 \right) t + \dots \quad (3.31)$$

All the matrices \mathbf{B}_k can be reduced to a set of vectors \vec{b}_k , using the definition of the instantaneous angular velocity matrix. The position, velocity and acceleration are therefore also defined by vectors.

$$\begin{aligned} X_{0,i} : \vec{x}_{0,i} = & \vec{x}_1 + \vec{d}_0 + \left(\vec{b}_1 \times \vec{x}_1 + \vec{d}_1 \right) t + \\ & \frac{1}{2} \left(-(\vec{b}_1 \cdot \vec{b}_1) \vec{x}_1 + (\vec{b}_1 \cdot \vec{x}_1) \vec{b}_1 + \vec{b}_2 \times \vec{x}_1 + \vec{d}_2 \right) t^2 + \dots \end{aligned} \quad (3.32)$$

$$\dot{X}_{0,i} : \dot{\vec{x}}_{0,i} = \vec{b}_1 \times \vec{x}_1 + \vec{d}_1 + \left(-(\vec{b}_1 \cdot \vec{b}_1) \vec{x}_1 + (\vec{b}_1 \cdot \vec{x}_1) \vec{b}_1 + \vec{b}_2 \times \vec{x}_1 + \vec{d}_2 \right) t + \dots \quad (3.33)$$

$$\begin{aligned} \ddot{X}_{0,i} : \ddot{\vec{x}}_{0,i} = & \left(-(\vec{b}_1 \cdot \vec{b}_1) \vec{x}_1 + (\vec{b}_1 \cdot \vec{x}_1) \vec{b}_1 + \vec{b}_2 \times \vec{x}_1 + \vec{d}_2 \right) + \\ & \left(\frac{3}{2} (\vec{b}_1 \cdot \vec{x}_1) \vec{b}_2 + \frac{3}{2} (\vec{b}_2 \cdot \vec{x}_1) \vec{b}_1 - 3(\vec{b}_1 \cdot \vec{b}_2) \vec{x}_1 + \vec{b}_3 \times \vec{x}_1 + \vec{d}_3 \right) t \dots \end{aligned} \quad (3.34)$$

Instantaneous kinematics studies the low order terms of these expansions. The vectors \vec{b}_1 and \vec{b}_2 are the instantaneous angular velocity and angular acceleration vectors at $t = 0$. These terms, along with \vec{b}_3 and \vec{b}_4 are used to construct the instantaneous kinematic invariants [23].

3.3.3 Movement: Velocity and Acceleration

As stated in section 3.2.2, six parameters are necessary to parameterise the geometric configuration of a free body \mathcal{B}_i in space. A euclidean displacement parameterises the position of a body as the linear position of the body frame's centre $O_{0,i}$ (in the inertial frame) and the orientation of a point $X_{0,i}$ (in the inertial frame) with respect to the centre of the body frame.

$$X_{0,i} : \vec{x}_{0,i} = \vec{d}_{0,i} + \mathbf{R}_{i,0}\vec{x}_i = \underbrace{\vec{d}_{0,i}}_{\text{linear position}} + \underbrace{\vec{x}_{0,i}^*}_{\text{orientation}}.$$

The asterisk symbol on a vector always is used to shorten the notation. It will always mean the following $\vec{x}_{j,i}^* = \mathbf{R}_{i,j}\vec{x}_i$. The six coordinates parameterising the body's geometric configuration are the three translational coordinates of the reference frame origin and the three rotation angles. The kinematics of a rigid body are parameterised in terms of the vector of kinematic coordinates and its derivatives.

$$\vec{q}_i = \left(\underbrace{x_i \ y_i \ z_i}_{\vec{\Gamma}_i^T} \ \underbrace{\psi_i \ \vartheta_i \ \varphi_i}_{\vec{\Upsilon}_i^T} \right)^T = (\vec{\Gamma}_i^T, \vec{\Upsilon}_i^T)^T \in SE(3). \quad (3.35)$$

The vector $\vec{\Gamma}_i$ is the translational coordinate vector and the vector $\vec{\Upsilon}_i$ is the rotational coordinate vector. The subindex i indicates that the coordinates parameterise the kinematics of body \mathcal{B}_i . The vector of kinematic coordinates belongs to the set $SE(3) = \mathbb{R}^3 \times SE(3)$ called the special Euclidean group. The group acts on elements of \mathbb{R}^3 through homogeneous transformations defined in section 3.2.3.

$$X_{0,i} : \begin{pmatrix} \vec{x}_{0,i} \\ 1 \end{pmatrix} = \mathbf{H}_{i,0} \begin{pmatrix} \vec{x}_i \\ 1 \end{pmatrix} = \left(\begin{array}{ccc|c} \mathbf{R}_{i,0} & & & \vec{d}_{0,i} \\ 0 & 0 & 0 & 1 \end{array} \right) \begin{pmatrix} \vec{x}_i \\ 1 \end{pmatrix}. \quad (3.36)$$

The matrix $\mathbf{H}_{i,0}$ is an element of $SE(3)$. Given that $SE(3)$ is composed of \mathbb{R}^3 and $SO(3)$, it is also a Lie group with a smooth manifold structure. The velocity of a point on the body in the inertial frame is defined by:

$$X_{0,i}(\vec{q}_i) : \dot{\vec{x}}_{0,i} = \dot{\vec{d}}_{0,i} + \mathbf{R}_{i,0}\dot{\vec{x}}_i, \quad (3.37)$$

$$\dot{X}_{0,i}(\vec{q}_i, \dot{\vec{q}}_i) : \dot{\vec{x}}_{0,i} = \dot{\vec{d}}_{0,i} + \vec{\omega}_{0,i} \times \vec{x}_{0,i}^*. \quad (3.38)$$

This is called the *fundamental transport theorem*. Using the Poisson formula again, the acceleration of the point $X_{0,i}$ is defined by the relation

$$\ddot{X}_{0,i}(\vec{q}_i, \dot{\vec{q}}_i, \ddot{\vec{q}}_i) : \ddot{\vec{x}}_{0,i} = \ddot{\vec{d}}_{0,i} + \dot{\vec{\omega}}_{0,i} \times \vec{x}_{0,i}^* + \vec{\omega}_{0,i} \times (\vec{\omega}_{0,i} \times \vec{x}_{0,i}^*), \quad (3.39)$$

Theorem 2 (Rigid-Body Kinematics (Classical Description)). *The spatial kinematics of a single free rigid-body \mathcal{B}_i , fixed in the body frame, are defined with respect to the inertial frame \mathcal{R}_0 , by the following set of equations:*

$$X_{0,i} : \vec{x}_{0,i} = \vec{d}_{0,i} + \mathbf{R}_{i,0}\vec{x}_i, \quad (3.40)$$

$$\dot{X}_{0,i} : \dot{\vec{x}}_{0,i} = \dot{\vec{d}}_{0,i} + \vec{\omega}_{0,i} \times \mathbf{R}_{i,0}\vec{x}_i, \quad (3.41)$$

$$\ddot{X}_{0,i} : \ddot{\vec{x}}_{0,i} = \ddot{\vec{d}}_{0,i} + \dot{\vec{\omega}}_{0,i} \times \mathbf{R}_{i,0}\vec{x}_i + \vec{\omega}_{0,i} \times (\vec{\omega}_{0,i} \times \mathbf{R}_{i,0}\vec{x}_i). \quad (3.42)$$

where $\vec{d}_{0,i}$ is the pure translational motion. $\mathbf{R}_{i,0}$ is the rotation matrix defining the rotational motion of the body and $\vec{\omega}_{0,i}$ is the instantaneous rotational velocity vector with respect to the inertial frame.

The instantaneous angular velocity vector is defined according to the rotation sequence. Consider the $x - y - z$ Tait-Bryan sequence defined previously in section 3.2.5. The velocity vector is parallel to the rotation axis and its direction gives the direction of rotation, according to the right-hand rule (clockwise (-) / counterclockwise (+)). The body is first rotated around the x -axis. Its first component is therefore defined by:

$$\mathbf{R}(\varphi_i)\mathbf{R}^T(\vartheta_i)\mathbf{R}(\psi_i) \begin{pmatrix} \dot{\psi}_i \\ 0 \\ 0 \end{pmatrix}.$$

The second rotation occurs around the y -axis of the first intermediate rotated frame \mathcal{R}'_i (cf. Fig. 3.5).

$$\mathbf{R}(\varphi_i)\mathbf{R}^T(\vartheta_i)\mathbf{R}(\psi_i) \begin{pmatrix} \dot{\psi}_i \\ 0 \\ 0 \end{pmatrix} + \mathbf{R}(\varphi_i)\mathbf{R}^T(\vartheta_i) \begin{pmatrix} 0 \\ \dot{\vartheta}_i \\ 0 \end{pmatrix}.$$

The third rotation occurs around the z -axis of the second intermediate rotated frame \mathcal{R}'_0 (cf. Fig. 3.5).

$$\vec{\omega}_{0,i}(\psi_i, \vartheta_i, \varphi_i) = \mathbf{R}(\varphi_i)\mathbf{R}^T(\vartheta_i)\mathbf{R}(\psi_i) \begin{pmatrix} \dot{\psi}_i \\ 0 \\ 0 \end{pmatrix} + \mathbf{R}(\varphi_i)\mathbf{R}^T(\vartheta_i) \begin{pmatrix} 0 \\ \dot{\vartheta}_i \\ 0 \end{pmatrix} + \mathbf{R}(\varphi_i) \begin{pmatrix} 0 \\ 0 \\ \dot{\varphi}_i \end{pmatrix}. \quad (3.43)$$

The instantaneous rotational velocity vector can also be expressed in the body frame. It defines the rotation of the inertial frame with respect to the body frame.

$$\vec{\omega}_i = \mathbf{R}_{0,i}\vec{\omega}_{0,i}. \quad (3.44)$$

The rotational velocity vector is a linear function of the angular velocities $\dot{\vec{\Upsilon}}_i$. The vector can be expressed in terms of its jacobian with respect to $\dot{\vec{\Upsilon}}_i$.

$$\vec{\omega}_{0,i} = \frac{\partial \vec{\omega}_{0,i}}{\partial \dot{\psi}_i} \dot{\psi}_i + \frac{\partial \vec{\omega}_{0,i}}{\partial \dot{\vartheta}_i} \dot{\vartheta}_i + \frac{\partial \vec{\omega}_{0,i}}{\partial \dot{\varphi}_i} \dot{\varphi}_i = \frac{\partial \vec{\omega}_{0,i}}{\partial \dot{\vec{\Upsilon}}_i} \dot{\vec{\Upsilon}}_i = \mathbf{W}_{0,i}(\vec{\Upsilon}_i) \dot{\vec{\Upsilon}}_i. \quad (3.45)$$

The matrix $\mathbf{W}_{0,i}$ is a 3×3 invertible matrix depending on the angle sequence and will be extensively used in rigid-body dynamics (Section 3.4). This matrix does become singular for certain values of Euler and Bryan angle sequences. A similar map is defined for the rotational velocities in the body frame.

Theorem 3 (Rigid-Body Kinematics (Parametric Description)). *The spatial kinematics of a single free rigid-body \mathcal{B}_i , fixed in the body frame, are parameterised with respect to the inertial frame \mathcal{R}_0 , in terms of the kinematic coordinates $\vec{q}_i = (\vec{\Gamma}_i^T, \vec{\Upsilon}_i^T)^T$, by the following set of equations:*

$$\vec{x}_{0,i}(\vec{\Gamma}_i, \vec{\Upsilon}_i) = \vec{\Gamma}_i + \mathbf{R}_{i,0}(\vec{\Upsilon}_i)\vec{x}_i = \vec{\Gamma}_i + \vec{x}_{0,i}^*(\vec{\Upsilon}_i), \quad (3.46)$$

$$\dot{\vec{x}}_{0,i}(\vec{\Gamma}_i, \vec{\Upsilon}_i, \dot{\vec{\Gamma}}_i, \dot{\vec{\Upsilon}}_i) = \dot{\vec{\Gamma}}_i + \mathbf{W}_{0,i}(\vec{\Upsilon}_i)\dot{\vec{\Upsilon}}_i \times \vec{x}_{0,i}^*(\vec{\Upsilon}_i), \quad (3.47)$$

$$\begin{aligned} \ddot{\vec{x}}_{0,i}(\vec{\Gamma}_i, \vec{\Upsilon}_i, \dot{\vec{\Gamma}}_i, \dot{\vec{\Upsilon}}_i, \ddot{\vec{\Gamma}}_i, \ddot{\vec{\Upsilon}}_i) = & \ddot{\vec{\Gamma}}_i + \left(\mathbf{W}_{0,i}(\vec{\Upsilon}_i)\ddot{\vec{\Upsilon}}_i + \dot{\mathbf{W}}_{0,i}(\vec{\Upsilon}_i)\dot{\vec{\Upsilon}}_i \right) \times \vec{x}_{0,i}^*(\vec{\Upsilon}_i) + \\ & \mathbf{W}_{0,i}(\vec{\Upsilon}_i)\dot{\vec{\Upsilon}}_i \times \left(\mathbf{W}_{0,i}(\vec{\Upsilon}_i)\dot{\vec{\Upsilon}}_i \times \vec{x}_{0,i}^*(\vec{\Upsilon}_i) \right). \end{aligned} \quad (3.48)$$

$\vec{\Gamma}_i = (x_i, y_i, z_i)^T$ is the vector of linear translational kinematic coordinates, $\vec{\Upsilon}_i = (\psi_i, \vartheta_i, \varphi_i)^T$ is the vector angular/rotational kinematic coordinates. $\mathbf{W}_{0,i}$ is the jacobian of the instantaneous rotational velocity vector with respect to $\dot{\vec{\Upsilon}}_i$.

3.3.4 Chasles' Theorem and the Instantaneous Screw Axis

Euler's theorem states that every rotation takes place about a single axis. A corollary to Euler's theorem is Chasles' theorem, obtained by allowing the rotation axis to translate in space.

Theorem 4 (Chasles' Theorem [39]). *General rigid body displacements can be reduced to a translation along a line followed by a rotation about that line.*

The motion described in Chasles' theorem is a screw motion. The translation axis is called the screw axis. Mathematically, a *screw* \mathcal{S} is a pair of three dimensional vectors [12]. Geometrically, the pair represents a line in space of direction \vec{n}_0 with an associated *pitch* p_s , ratio between linear and angular quantities. The screw encodes a helical vector field (Fig. 3.7). The screw of a point X_0 is defined by:

$$\mathcal{S}_{X_0} = \left(\vec{n}_0 \quad p_s \vec{n}_0 + \vec{n}_0 \times \vec{r}_0 \right), \quad \|\vec{n}\|_2 = 1. \quad (3.49)$$

\vec{r}_0 is the vector from X_0 to the screw axis, normal to the screw axis. In kinematics a screw encodes a velocity field. The Euclidean displacement associated to a screw motion is called a *twist* \mathcal{T} . A twist is a screw with a scalar called the *magnitude* equal to $\|\vec{\omega}_{0,i}\|_2$. The translation along the axis is equal to the magnitude times the pitch p_t .

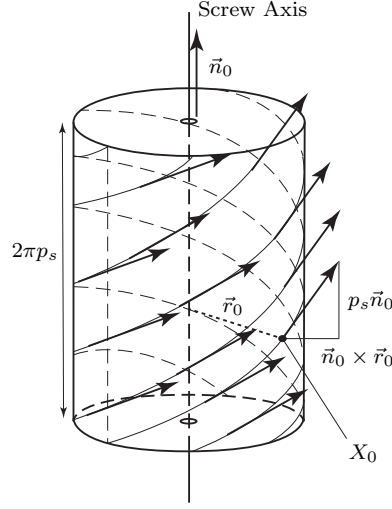


Figure 3.7: *Illustration of a screw encoding a helical vector field as described in section 3.3.4.*

To construct the screw axis for a body \mathcal{B}_i , consider a point $X_{0,i}$ on the screw axis.

$$X_{0,i} : \vec{x}_{0,i} = \vec{d}_{0,i} + \mathbf{R}_{i,0}\vec{x}_i = \vec{d}_{0,i} + \vec{x}_{0,i}^*, \quad \dot{X}_0 : \dot{\vec{x}}_{0,i} = \dot{\vec{d}}_{0,i} + \vec{\omega}_{0,i} \times \vec{x}_{0,i}^*.$$

The vector $\vec{x}_{0,i}^*$ is decomposed into a parallel and normal components to $\vec{\omega}_{0,i}$.

$$\vec{x}_{0,i}^* = \vec{x}_{0,i,\parallel}^* + \vec{x}_{0,i,\perp}^*, \quad \Rightarrow \quad \dot{\vec{x}}_{0,i} = \dot{\vec{d}}_{0,i} + \vec{\omega}_{0,i} \times \vec{x}_{0,i,\perp}^*, \quad \vec{\omega}_{0,i} \times \vec{x}_{0,i,\parallel}^* = \vec{0}$$

Instantaneously, all the points on the screw axis have the same velocity proportional to $\vec{\omega}_{0,i}$. The proportionality factor is the pitch p_t .

$$p_t \vec{\omega}_{0,i} = \dot{\vec{d}}_{0,i} + \vec{\omega}_{0,i} \times \vec{x}_{0,i,\perp}^*,$$

By dot- and cross-multiplying this relation by $\vec{\omega}_{0,i}$ and using the perpendicularity of $\vec{x}_{0,i,\perp}^*$ with respect to $\vec{\omega}_{0,i}$, yields the following relations [213]:

$$\vec{x}_{0,i,\perp}^* = \frac{\vec{\omega}_{0,i} \times \dot{\vec{d}}_{0,i}}{\vec{\omega}_{0,i} \cdot \vec{\omega}_{0,i}}, \quad p_t = \frac{\vec{\omega}_{0,i} \cdot \dot{\vec{d}}_{0,i}}{\vec{\omega}_{0,i} \cdot \vec{\omega}_{0,i}}. \quad (3.50)$$

If the body's reference frame is placed on the instantaneous screw axis, the position of any point $Y_{0,i}$ (not on the axis) is defined with respect to the inertial frame by:

$$Y_{0,i} : \vec{y}_{0,i} = \vec{d}_{0,i} + \vec{x}_{0,i,\perp}^* + \vec{y}_{0,i}^* = \vec{d}_{0,i} + \vec{y}_{0,i}^*, \quad (3.51)$$

and the velocity of the point $Y_{0,i}$ on the body is defined by:

$$\dot{Y}_{0,i} : \dot{\vec{y}}_{0,i} = p_s \vec{\omega}_{0,i} + \vec{\omega}_{0,i} \times \vec{y}_{0,i}^*, \quad (3.52)$$

where $\vec{y}_{0,i}^*$ is the vector from the screw axis to the point $Y_{0,i}$ normal to the screw axis. The point has a translational velocity parallel to the screw axis defined by $\vec{\omega}_{0,i}$ and proportional to the norm of the rotational velocity.

For rigid body motion, the twist is in general time variant and therefore one defines the *instantaneous screw axis* (ISA). The instantaneous twist is mathematically defined by its screw. This screw completely defines the body's motion.

$$\mathcal{T}_{Y_{0,i}}(t) = (\vec{\omega}_{0,i}(t) \quad p_s(t)\vec{\omega}_{0,i}(t) + \vec{\omega}_{0,i}(t) \times \vec{y}_{0,i,\perp}^*(t)) . \quad (3.53)$$

The norm of the instantaneous rotational velocity vector and the pitch of the screw are the first two instantaneous kinematic invariants mentioned in section 3.3.2. The instantaneous screw axis defines a *ruled surface*⁵ in the inertial frame and the body frame.

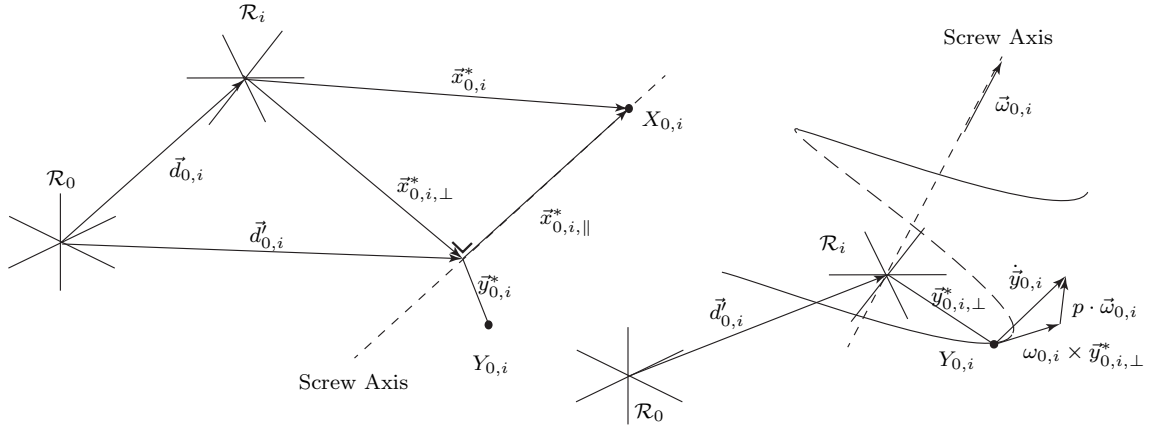


Figure 3.8: Illustration of the construction of the instantaneous screw axis as described in section 3.3.4.

⁵A ruled surface \mathcal{S} is such that at every point P on the surface, there is a line passing through the point which is also on the surface.

3.4 Rigid-Body Dynamics

Rigid-body dynamics relates motion to its cause, it expresses the time-dependent behaviour of rigid bodies under external influences. There are multiple aspects of rigid-body dynamics. The equations of motion describe how a body moves under the influence of forces. There is the energetic aspect defining how much energy a body has and how much energy is being given to it or taken away from it. This section describes both aspects and covers Newtonian mechanics for a single rigid body. The presentation begins with Newton's and Euler's laws of motion and the definitions of forces and moments of force. The inertia and moment of inertia of a body are also covered in this section. The equations of motion are derived and the presentation ends with considerations on the mechanical energy of a rigid body.

3.4.1 Newtonian Mechanics

The governing laws of rigid body dynamics are Newton's three laws which, completely define what causes translational motion.

Theorem 5. (Newton's laws of motion)

1. *When viewed in an inertial reference frame, a body \mathcal{B}_i either remains at rest or continues to move at a constant velocity, unless acted upon by an external force.*
2. *$\vec{f}_{0,i} = m_i \ddot{\vec{x}}_{0,i}$: the vector sum of the forces $\vec{f}_{0,i}$ on a body \mathcal{B}_i (in the inertial frame) is equal to the mass m_i of that body multiplied by the acceleration vector $\ddot{\vec{x}}_{0,i}$ of the body, in the inertial frame \mathcal{R}_0 .*
3. *When one body \mathcal{B}_i exerts a force on a second body \mathcal{B}_j , the second body \mathcal{B}_j simultaneously exerts a force equal in magnitude and opposite in direction on the first body \mathcal{B}_i .*

The first law states that any change in a rigid body's motion is caused by the action of an external force. It is the most fundamental law. *For there to be motion, there must be a force.* The second law states that the motion of a rigid body, defined by its acceleration, is related to the forces acting on it. Newton's second law provides a tool for computing the translational dynamics of a rigid body, described by the *equations of motion*. The third law defines the interactions between rigid bodies. When two bodies are in contact, they exert a force on each other. Thus, *forces are the underlying cause of any motion and will be discussed first.*

Newton's laws constitute only half the equations of motion of a rigid body. The second law governs the translational dynamics only. The rotational dynamics are governed by Euler's laws of motion. They are as important as Newton's laws of motion but are less well known because they were discovered later.

Theorem 6. (Euler's laws of motion)

1. *The linear momentum of a body $\vec{p}_{0,i}$, is equal to the product of the mass of the body m_i and the velocity of its centre of mass $\dot{x}_{0,i}$ in the inertial frame \mathcal{R}_0 : $\vec{p}_{0,i} = m_i \dot{x}_{0,i}$.*
2. *The rate of change of angular momentum $\vec{l}_{0,i}$ with respect to the centre of the inertial frame \mathcal{R}_0 , is equal to the sum of the external moments of force $\vec{t}_{0,i}$ about that point: $\dot{\vec{l}}_{0,i} = \vec{t}_{0,i}$.*

The first law is a restatement of Newton's second law, but is more general. Euler's formulation of the law is more general in that it incorporates the possibility of a time-dependent mass. This occurs in rockets where the mass drops as the fuel is spent. Euler's second law is the analogue of Newton's second law for rotational dynamics. It is used to obtain the rotational part of the equations of motion (if the body can rotate). The angular momentum $\vec{l}_{0,i}$ contains the angular acceleration vector $\ddot{\gamma}_i$.

3.4.2 Forces, Moments of Force and Poinsot's Theorem

A force is defined as any external action on a rigid body leading to a change in configuration or movement of the body. Physically, only the effect of forces can be measured and not the forces themselves. There are *internal* and *external* forces. Internal forces are for instance the interaction forces at the atomic level that depend on the material [22, 46]. Internal forces are eliminated by the rigid body hypothesis and are thus not considered in the remainder of this presentation. External forces are either the result of a contact with another body or the effect of a force field like gravity or electromagnetism. The first are called *contact forces*, the second are called *body forces*. There are *concentrated* forces, applied to a single point or *distributed* forces, applied along a line, over a surface or throughout a volume. All forces in the physical world are distributed. However, if the size of the surface is much smaller than the size of the body, the force can be viewed as a concentrated force. Furthermore, most distributed forces can be replaced by a resulting concentrated force. The point of application depends on the force distribution. The following presentation considers only concentrated forces.

Definition 3 (Force). A force (in the inertial frame) is characterised by a magnitude f_0 , a direction \vec{b}_0 and a line of action l_a . The line of action is the infinite line parallel to the force. The direction is the unit vector indicating in which direction the force is pointing along the line of action. Forces are therefore vector quantities and satisfy the rules of vector algebra.

The first two important points concerning force are the principle of transmissibility and the definition of moment of force about a point $Y_{0,i}$ on a body \mathcal{B}_i in the inertial frame.

Theorem 7 (Principle of Transmissibility). A force can be applied to a body at any point along its line of action without changing its overall effect on the body.

Definition 4 (Moment of Force). A force $\vec{f}_{0,i}$, applied at a point $Z_{0,i}$ on a body \mathcal{B}_i , creates a moment of force $\vec{t}_{0,i}$ at a point $Y_{0,i}$ of the body. The moment of force is defined as the cross product between the vector $\vec{r}_{0,i}$ from points $Y_{0,i}$ to $Z_{0,i}$ and the force.

$$\vec{t}_{0,i} = (\vec{z}_{0,i} - \vec{y}_{0,i}) \times \vec{f}_{0,i} = \vec{r}_{0,i} \times \vec{f}_{0,i}. \quad (3.54)$$

The double subindex of the force and moment of force vectors indicates the force vector is defined in the inertial frame but is applied to body i .

The vector from $Y_{0,i}$ to $Z_{0,i}$ is decomposed into a vector normal to the line of action and a vector parallel to the line of action. The moment of force is defined by

$$\vec{t}_{0,i} = \vec{r}_{0,i} \times \vec{f}_{0,i} = (\vec{r}_{0,i,\perp} + \vec{r}_{0,i,\parallel}) \times \vec{f}_{0,i} = \vec{r}_{0,i,\perp} \times \vec{f}_{0,i}, \quad (3.55)$$

where $\vec{r}_{0,i,\perp}$ is called the *lever arm* of the force with respect to the point $Y_{0,i}$.

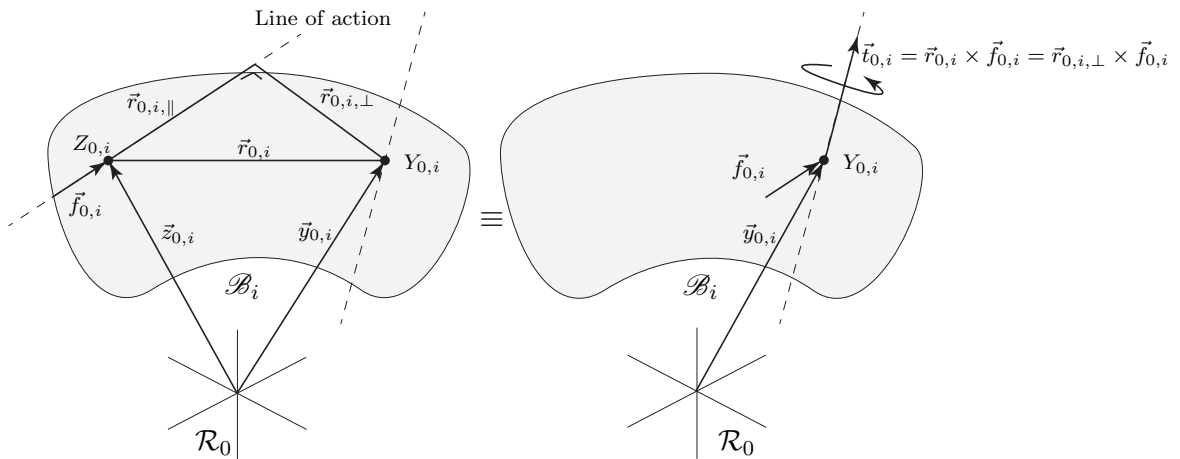


Figure 3.9: Illustration of the moment of force created by a force applied at a point $Z_{0,i}$ about a point $Y_{0,i}$ as described in section 3.4.2.

A force applied at a point $Z_{0,i}$ defines a moment of force at any other point $Y_{0,i}$ on the body. Thus, the overall effect of a force applied at a point $Z_{0,i}$ is equivalent to the

overall effect of an equal and parallel force applied at $Y_{0,i}$ plus a moment of force (Fig. 3.9). The force and its moment define a screw called a *wrench*, encoding a helical force field.

$$\mathcal{F}_{Y_{0,i}} = (\vec{f}_{0,i}, \vec{r}_{0,i} \times \vec{f}_{0,i}). \quad (3.56)$$

All the forces acting on a body define a *system of forces*. Every force $\vec{f}_{0,i,k}$ in a system of forces creates a moment of force at a point $Y_{0,i}$. Consider a body \mathcal{B}_i subject to a system of N forces. Each force is applied to a point $Z_{0,i,k}$. One defines the resulting force applied at $Y_{0,i}$ and moment of force about $Y_{0,i}$.

$$\vec{f}_{0,i} = \sum_k^N \vec{f}_{0,i,k}, \quad \vec{t}_{0,i} = \sum_k^N (\vec{z}_{0,i,k} - \vec{y}_{0,i}) \times \vec{f}_{0,i,k} = \sum_k^N \vec{r}_{0,i,k} \times \vec{f}_{0,i,k} = \sum_k^N \vec{r}_{0,i,k,\perp} \times \vec{f}_{0,i,k}. \quad (3.57)$$

Notation: The triple subindex on the forces indicates the following: $\vec{f}_{0,i,k}$ is the k^{th} force applied to body i in the inertial frame \mathcal{R}_0 . The triple indexes on the vectors $\vec{z}_{0,i,k}$ indicate the following: k^{th} vector associated to body i defined in the inertial frame. The first index always indicates the frame in which the vector is defined, the second subindex indicates to which body or frame the vector is related, and the third subindex is for indexing multiple instances of the vector. If the force is defined in the body's frame, there is a double subindex: $\vec{f}_{i,k}$.

Again, the vectors $\vec{r}_{0,i,k,\perp}$ are called the *lever arms* of the forces around the point $Y_{0,i}$. If the same system of forces is reduced to another point $V_{0,i}$ (different from $Y_{0,i}$) we have the following relation between the screws

$$\mathcal{F}_{V_{0,i}} = (\vec{f}_{0,i}, \vec{t}_{0,i}) + (0, (\vec{y}_{0,i} - \vec{v}_{0,i}) \times \vec{f}_{0,i}) = \mathcal{F}_{Y_{0,i}} + (0, (\vec{y}_{0,i} - \vec{v}_{0,i}) \times \vec{f}_{0,i}). \quad (3.58)$$

The difference between two resulting screws of the same force system at points $Y_{0,i}$ and $V_{0,i}$ is a screw with zero force.

Definition 5 (Couple of Force or Torque). *A couple or torque is a system of forces with a resulting force equal to zero. The moment of force defined by a couple of force is independent of any point of application.*

$$\mathcal{F} = (0, \vec{t}_{0,i}) \quad (3.59)$$

This definition is followed by the following theorem.

Theorem 8. *Every system of forces can be reduced to a single force applied at a point $Y_{0,i}$ and a couple of force.*

Consider a body \mathcal{B}_i with N forces acting on it at points $Z_{0,i,k}$. The screw at point $Y_{0,i}$ is defined by a screw at the origin of the inertial frame minus a couple of force.

$$\begin{aligned} \mathcal{F}_{Y_{0,i}} &= \left(\sum_{k=1}^N \vec{f}_{0,i,k}, \sum_{k=1}^N (\vec{z}_{0,i,k} - \vec{y}_{0,i}) \times \vec{f}_{0,i,k} \right) = \left(\vec{f}_{0,i}, \sum_{k=1}^N \vec{z}_{0,i,k} \times \vec{f}_{0,i,k} \right) - (0, \vec{y}_{0,i} \times \vec{f}_{0,i}), \\ &= (\vec{f}_{0,i}, \vec{t}_{0,i}) - (0, \vec{y}_{0,i} \times \vec{f}_{0,i}) = \mathcal{F}_{O_0} - (0, \vec{y}_{0,i} \times \vec{f}_{0,i}). \end{aligned} \quad (3.60)$$

The moment $\vec{t}_{0,i}$ is decomposed into moments parallel and normal to $\vec{f}_{0,i}$ (is the resulting force of the system of forces).

$$\mathcal{F}_{X_{0,i}} = (\vec{f}_{0,i}, \vec{t}_{0,i,\parallel} + \vec{t}_{0,i,\perp}) - (0, \vec{y}_{0,i} \times \vec{f}_{0,i}) = (\vec{f}_{0,i}, \vec{t}_{0,i,\parallel}) + (0, \vec{t}_{0,i,\perp}) - (0, \vec{y}_{0,i} \times \vec{f}_{0,i}). \quad (3.61)$$

If the point $Y_{0,i}$ is chosen appropriately, the two couples $(0, \vec{t}_{0,i,\perp})$ and $(0, \vec{y}_{0,i} \times \vec{f}_{0,i})$ cancel each other. Indeed, both couples are in a plane normal to $\vec{f}_{0,i}$. The result is a screw of force $\vec{f}_{0,i}$ and a couple parallel to the force.

The magnitude of a wrench is equal to $\|\vec{f}_{0,i}\|_2$. The pitch p_w is the ratio of moment to force. Thus, Chasles' theorem in kinematics has an analogue theorem in dynamics known as Poinso's theorem.

Theorem 9 (Poinso's Theorem [164]). *Every system of forces is equivalent to a single force and a couple of force with moment parallel to the force. The magnitude of the couple vector is proportional to the force's magnitude. The proportionality factor is called the pitch.*

The twist \mathcal{T} in kinematics and the wrench \mathcal{F} in dynamics are screws with magnitudes. They are *dual* (Fig. 3.10). The screw of a point $A_{0,i}$ not on the screw axis is defined by:

$$\mathcal{F}_{A_0} = (\vec{f}_{0,i}, \vec{t}_{0,i,\parallel}) - (0, \vec{r}_{0,i} \times \vec{f}_{0,i}) = (\vec{f}_{0,i}, p\vec{f}_{0,i} + \vec{f}_{0,i} \times \vec{r}_{0,i}). \quad (3.62)$$

The force will govern the change in translational velocity while the couple will govern the change in rotational velocity.

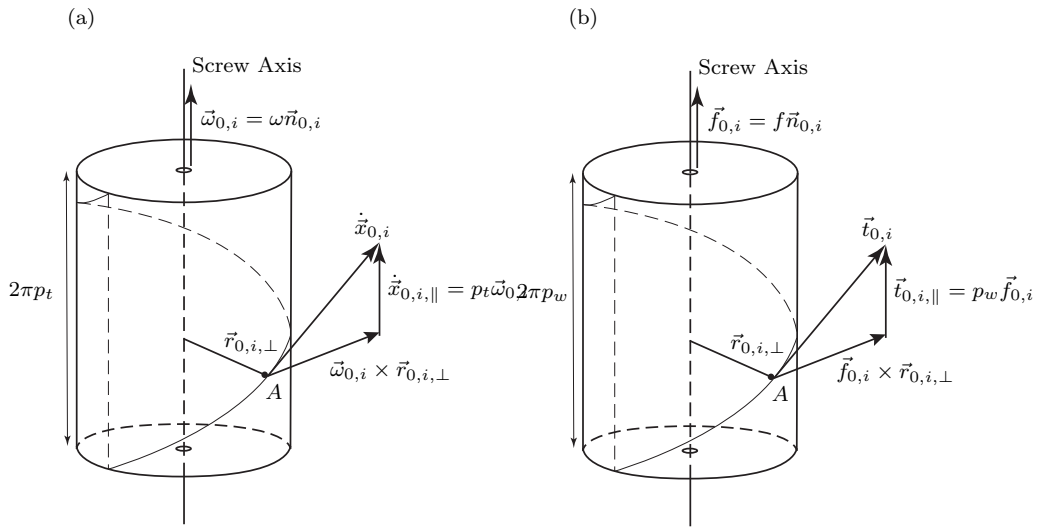


Figure 3.10: *Duality between Chasles' theorem (a) and Poinso's theorem (b) as described in sections 3.3.4 and 3.4.2.*

3.4.3 Inertia and Moment of Inertia

Newton's and Euler's second laws state that the forces and moments of force acting on a body are proportional to its linear acceleration and angular acceleration. From Chasle's theorem follows that a body will have a linear acceleration and a rotational acceleration. From Poincot's theorem follows that a body will have a force and couple. The proportionality factor between the linear acceleration and force is the inertia. The proportionality factor between the angular acceleration and couple is the *moment of inertia*. Both factors measure a bodies' resistance to linear and rotational motion.

For a rigid body \mathcal{B}_i made up of a discrete number of particles N . Each particle has a position $\vec{z}_{i,k}$ with respect to the body frame and an inertia or *mass* $m_{i,k}$. Mass is not to be confused with *weight* which is the mass multiplied by the earth's gravitational constant. The total inertia m of a rigid body is the sum of all particle masses.

$$m_i = \sum_{k=1}^N m_{i,k} \quad (3.63)$$

The total mass is viewed as concentrated at a point called the *centre of mass*. The location of the centre of mass is defined by:

$$\vec{x}_i = \sum_{k=1}^N \frac{m_{i,k} \vec{z}_{i,k}}{m_i}. \quad (3.64)$$

From now on, the notation \vec{x} will be reserved for the centre of mass. Mass is a single factor which describes the bodies' resistance to being translated in any direction. For rotations, three factors are required. For a body comprised of N particles, the moment of inertia matrix is computed in any frame using the following definition:

$$\mathcal{I}_i = \sum_{k=1}^N m_k \left((\vec{z}_{i,k} \cdot \vec{z}_{i,k}) \mathbf{I} - \vec{z}_{i,k} \vec{z}_{i,k}^T \right). \quad (3.65)$$

The matrix \mathbf{I} is the 3×3 identity matrix. If the body consists of an infinite number of particles which each occupy an infinitely small volume $(d\vec{z}_i)^3 \equiv dxdydz$ within the body. The total mass of the body is defined by the volume integral of the density $\rho(\vec{z}_i)$. The vector \vec{z}_i is now a continuous vector describing the entire body (in the body frame \mathcal{R}_i) that can be integrated.

$$m = \int \rho(\vec{z}_i) (d\vec{z}_i)^3. \quad (3.66)$$

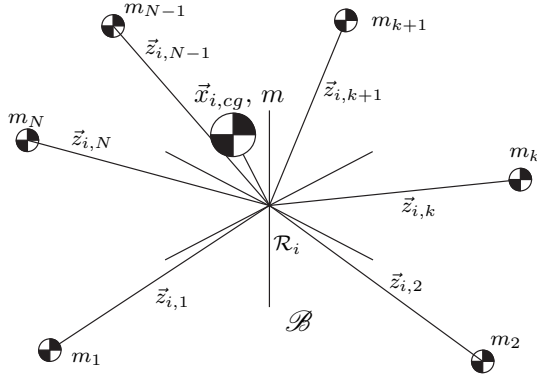
The centre of mass is defined by:

$$\vec{x}_i = \int \rho(\vec{z}_i) \vec{z}_i (d\vec{z}_i)^3, \quad (3.67)$$

and the moment of inertia is defined by:

$$\mathcal{I}_i = \int \rho(\vec{z}_i) \left((\vec{z}_i \cdot \vec{z}_i) \mathbf{I} - \vec{z}_i \vec{z}_i^T \right) (d\vec{z}_i)^3. \quad (3.68)$$

(a) Discrete Collection of Particles



(b) Continuous Distribution of Particles

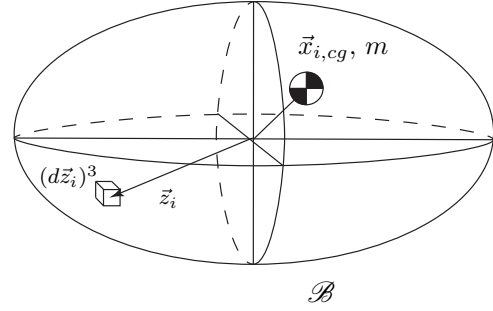


Figure 3.11: Illustration of a rigid body as (a) a collection of particles with mass m_k or as (b) a continuous mass distribution characterised by a density field $\rho(\vec{z}_k)$ as described in section 3.4.3.

In many problems, the body frame is located at the centre of mass and aligned with the principle axes of inertia. The units of mass and inertia are kilograms [kg] and [kgm²] respectively.

Any rotation is equivalent to three sequential rotations about three mutually perpendicular axes. Given a bodies' geometry, there is a unique definition of these axes such that the bodies' resistance to rotation around any axes is defined in terms of its resistance to rotation around the three axes. The moment's of inertia about these axes are called the principle moments of inertia. The axes are called the principle axes of inertia. If the body frame is aligned with these axes, the moment of inertia in the body frame is defined by a diagonal matrix.

$$\mathcal{I}_i = \begin{pmatrix} I_{xx,i} & 0 & 0 \\ 0 & I_{yy,i} & 0 \\ 0 & 0 & I_{zz,i} \end{pmatrix}. \quad (3.69)$$

In any other frame such as the inertial frame, the matrix is symmetric, positive definite but not diagonal.

$$\mathcal{I}_{0,i} = \begin{pmatrix} I_{xx,0} & I_{xy,0} & I_{xz,0} \\ I_{xy,0} & I_{yy,0} & I_{yz,0} \\ I_{xz,0} & I_{yz,0} & I_{zz,0} \end{pmatrix}. \quad (3.70)$$

3.4.4 Equations of Motion

The time-dependent behaviour of a rigid body, in terms of motion, is defined by the equations of motion. The equations of motion constitute a set of second order differential equations in terms of the kinematic coordinates. This section constructs the equations for a rigid body of constant mass, stationary in the body frame.

Definition 6 (Equations of motion). *The equations of motion for a rigid body \mathcal{B}_i are a set of second order differential equations (ODE) in terms of the vector of kinematic coordinates \vec{q}_i (3.35) and its first and second time derivatives with respect to time. The equations of motion are of the form*

$$\ddot{\vec{q}}_i = \mathcal{M}(t, \vec{q}_i, \dot{\vec{q}}_i), \quad \begin{cases} \vec{q}_i = (x_i, y_i, z_i, \psi_i, \vartheta_i, \varphi_i)^T = (\vec{\Gamma}_i^T, \vec{\Upsilon}_i^T)^T, \\ \dot{\vec{q}}_i = (\dot{x}_i, \dot{y}_i, \dot{z}_i, \dot{\psi}_i, \dot{\vartheta}_i, \dot{\varphi}_i)^T = (\dot{\vec{\Gamma}}_i^T, \dot{\vec{\Upsilon}}_i^T)^T, \end{cases} \quad (3.71)$$

with $\vec{q}_i(t_0)$, and $\dot{\vec{q}}_i(t_0)$ the initial conditions.

Consider the rigid body \mathcal{B}_i of the definition subject to N forces. The forces are applied at points $Z_{0,i,k}$ on the body. The body's centre of mass and the points of application of the forces are defined in the inertial frame \mathcal{R}_0 by (Fig. 3.12):

$$\vec{x}_{0,i} = \vec{d}_{0,i} + \mathbf{R}_{i,0}\vec{x}_i = \vec{d}_{0,i} + \vec{x}_{0,i}^*, \quad \vec{z}_{0,i,k} = \vec{d}_{0,i} + \mathbf{R}_{i,0}\vec{z}_{i,k} = \vec{d}_{0,i} + \vec{z}_{0,i,k}^*. \quad (3.72)$$

The centre of mass is assumed to be fixed in the body frame ($\vec{x}_i = c\vec{e}$). The system of forces is reduced to a single force $\vec{f}_{0,i}$ and couple $\vec{t}_{0,i}$ at the centre of the inertial frame.

$$\vec{f}_{0,i} = \sum_{k=1}^N \vec{f}_{0,i,k}, \quad \vec{t}_{0,i} = \vec{d}_{0,i} \times \vec{f}_{0,i} + \sum_{k=1}^N \vec{z}_{0,i,k}^* \times \vec{f}_{0,i,k}. \quad (3.73)$$

Newton's second law states that the vector sum of all the forces acting on the body is equal to the mass, multiplied by the acceleration of the centre of mass. The acceleration of the centre of mass is the acceleration of a point (3.53). Newton's second law for a three-dimensional rigid body is defined by:

$$m_i \ddot{\vec{x}}_{0,i} = m_i \left(\ddot{\vec{d}}_{0,i} + \dot{\vec{\omega}}_{0,i} \times \vec{x}_{0,i}^* + \vec{\omega}_{0,i} \times (\vec{\omega}_{0,i} \times \vec{x}_{0,i}^*) \right) = \sum_{k=1}^N \vec{f}_{0,i,k} = \vec{f}_{0,i}. \quad (3.74)$$

The term $m_i (\vec{\omega}_{0,i} \times (\vec{\omega}_{0,i} \times \vec{x}_{0,i}^*))$ is the centripetal force. If the centre of mass was not fixed in the body frame, there would be a Coriolis force equal to $m_i (2\vec{\omega}_{0,i} \times \mathbf{R}_{i,0}\dot{\vec{x}}_i)$. The linear acceleration is related to the forces by the equation.

$$\ddot{\vec{d}}_{0,i} = \ddot{\vec{\Gamma}}_i = \frac{1}{m_i} \vec{f}_{0,i} - \dot{\vec{\omega}}_{0,i} \times \vec{x}_{0,i}^* - \vec{\omega}_{0,i} \times (\vec{\omega}_{0,i} \times \vec{x}_{0,i}^*). \quad (3.75)$$

If the centre of mass is located at the centre of the body frame, this equation reduces to $\ddot{\vec{d}}_{0,i} = \frac{1}{m_i} \vec{f}_{0,i}$. This equation represents the translational part of the equations of motion.

The rotational part of the equations of motion is obtained by defining a quantity called angular momentum $\vec{l}_{0,i}$. Consider the rigid body \mathcal{B}_i to have a density distribution of $\rho(\vec{z}_{0,i})$ in the inertial frame \mathcal{R}_0 . The vector $\vec{z}_{0,i} = \vec{d}_{0,i} + \mathbf{R}_{i,0}\vec{z}_i = \vec{d}_{0,i} + \vec{z}_{0,i}^*$ is the location of elementary particles of mass with respect to the inertial frame (Fig. 3.12). The angular momentum of body \mathcal{B}_i in the inertial frame is defined by:

$$\vec{l}_{0,i} = \int \rho(\vec{z}_{0,i}^*) (\vec{z}_{0,i} \times \dot{\vec{z}}_{0,i}) (dz_{0,i}^*)^3. \quad (3.76)$$

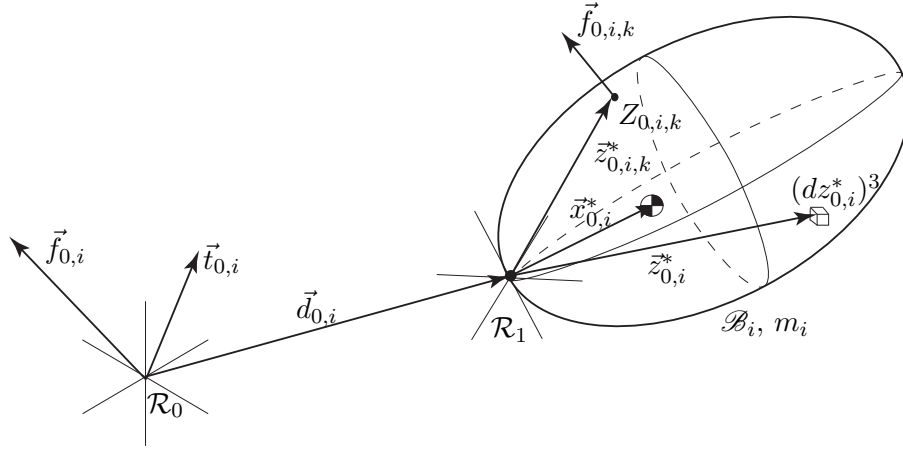


Figure 3.12: Illustration of the construction of the dynamics of a rigid body as described in section 3.4.4.

The relation is expanded using (3.63) and (3.67):

$$\begin{aligned} \vec{l}_{0,i} &= \int \rho(\vec{z}_{0,i}^*) \left((\vec{d}_{0,i} + \vec{z}_{0,i}^*) \times (\dot{\vec{d}}_{0,i} + \omega_{0,i} \times \vec{z}_{0,i}^*) \right) (dz_{0,i}^*)^3 \\ &= m_i \vec{d}_{0,i} \times (\dot{\vec{d}}_{0,i} + \omega_{0,i} \times \vec{x}_{0,i}^*) + m_i \vec{x}_{0,i}^* \times \dot{\vec{d}}_{0,i} + \int \rho(\vec{z}_{0,i}^*) (\vec{z}_{0,i}^* \times \omega_{0,i} \times \vec{z}_{0,i}^*) (dz_{0,i}^*)^3. \end{aligned} \quad (3.77)$$

The last term in this equation can be developed further.

$$\begin{aligned} \int \rho(\vec{z}_{0,i}^*) (\vec{z}_{0,i}^* \times (\vec{\omega}_{0,i} \times \vec{z}_{0,i}^*)) (dz_{0,i}^*)^3 &= \int \rho(\vec{z}_{0,i}^*) (\vec{\omega}_{0,i} (\vec{z}_{0,i}^{*T} \vec{z}_{0,i}^*) - \vec{z}_{0,i}^* (\vec{z}_{0,i}^{*T} \vec{\omega}_{0,i})) (dz_{0,i}^*)^3 \\ &= \int \rho(\vec{z}_{0,i}^*) (\vec{z}_{0,i}^{*T} \vec{z}_{0,i}^* \mathbf{I} - \vec{z}_{0,i}^* \vec{z}_{0,i}^{*T}) \vec{\omega}_{0,i} (dz_{0,i}^*)^3 = \mathcal{I}_{0,i} \vec{\omega}_{0,i}. \end{aligned} \quad (3.78)$$

Using the expression for inertia (3.65), the angular momentum vector is defined by:

$$\vec{l}_{0,i} = m_i \vec{d}_{0,i} \times \dot{\vec{x}}_{0,i} + m_i \vec{x}_{0,i}^* \times \dot{\vec{d}}_{0,i} + \mathcal{I}_{0,i} \vec{\omega}_{0,i}. \quad (3.79)$$

Given the expression of angular momentum for a rigid body \mathcal{B}_i , Euler's second law of motion can be expressed.

Theorem 10 (Euler's angular momentum theorem). *For a rigid body \mathcal{B}_i , the time derivative of the absolute angular momentum vector with respect to the inertial frame centre is equal to the sum of all the moments of force at the same point.*

$$\dot{\vec{l}}_{0,i} = \vec{t}_{0,i}. \quad (3.80)$$

The expression is expanded on both sides yielding the following relation:

$$\begin{aligned} m_i \dot{\vec{d}}_{0,i} \times \dot{\vec{x}}_{0,i} + m_i \vec{d}_{0,i} \times \ddot{\vec{x}}_{0,i} + m_i (\vec{\omega}_{0,i} \times \vec{x}_{0,i}^*) \times \dot{\vec{d}}_{0,i} + m_i \vec{x}_{0,i}^* \times \ddot{\vec{d}}_{0,i} + \mathcal{I}_{0,i} \dot{\vec{\omega}}_{0,i} + \vec{\omega}_{0,i} \times \mathcal{I}_{0,i} \vec{\omega}_{0,i} \\ = \vec{d}_{0,i} \times \vec{f}_{0,i} + \sum_{k=1}^N \vec{y}_{0,i,k}^* \times \vec{f}_{0,i,k}. \end{aligned} \quad (3.81)$$

Using (3.69) eliminates the second term on the left side with the first on the right. The first and third term on the left cancel each other. The resulting equation is

$$m_i \vec{x}_{0,i}^* \times \ddot{\vec{d}}_{0,i} + \mathcal{I}_{0,i} \dot{\vec{\omega}}_{0,i} + \vec{\omega}_{0,i} \times \mathcal{I}_{0,i} \vec{\omega}_{0,i} = \sum_{k=1}^N \vec{y}_{0,i,k}^* \times \vec{f}_{0,i,k}. \quad (3.82)$$

Theorem 11 (Equations of Motion (Classical Description)). *The equations of motion of a free rigid-body \mathcal{B}_i in the inertial frame, with constant mass, parameterised by the kinematic coordinates and their derivatives \vec{q}_i , $\dot{\vec{q}}_i$ and $\ddot{\vec{q}}_i$, with the centre of gravity located at the body frame's centre are defined by:*

$$m_i \ddot{\vec{d}}_{0,i} = \ddot{\vec{\Gamma}}_i = \frac{1}{m_i} \vec{f}_{0,i} - m_i \left(\dot{\vec{\omega}}_{0,i} \times \vec{x}_{0,i}^* + \vec{\omega}_{0,i} \times (\vec{\omega}_{0,i} \times \vec{x}_{0,i}^*) \right) \quad (3.83)$$

$$\mathcal{I}_{0,i} \dot{\vec{\omega}}_{0,i} = \sum_{k=1}^N \vec{y}_{0,i,k}^* \times \vec{f}_{0,i,k} - m_i \vec{x}_{0,i}^* \times \ddot{\vec{d}}_{0,i} - \vec{\omega}_{0,i} \times \mathcal{I}_{0,i} \vec{\omega}_{0,i}. \quad (3.84)$$

If the centre of mass is placed at the centre of the body frame, the angular momentum theorem takes its simplest form.

$$\mathcal{I}_{0,i} \dot{\vec{\omega}}_{0,i} + \vec{\omega}_{0,i} \times \mathcal{I}_{0,i} \vec{\omega}_{0,i} = \sum_{k=1}^N \vec{y}_{0,i,k}^* \times \vec{f}_{0,i,k}. \quad (3.85)$$

The vector $\vec{\omega}_{0,i} = \mathbf{W}_{0,i}(\vec{\Upsilon}_i) \dot{\vec{\Upsilon}}_i$ is used to express the equations of motion in terms of the kinematic coordinates for a rigid body with constant mass, fixed in the body frame.

Theorem 12 (Equations of Motion (Parametric Description)). *The equations of motion of a free rigid-body \mathcal{B}_i in the inertial frame, with constant mass, parameterised by the kinematic coordinates and their derivatives \vec{q}_i , $\dot{\vec{q}}_i$ and $\ddot{\vec{q}}_i$, with the centre of gravity located at the body frame's centre are defined by:*

$$\ddot{\vec{\Gamma}}_i = \frac{1}{m_i} \sum_{k=1}^N \vec{f}_{0,i,k} - \left(\mathbf{W}_{0,i}(\vec{\Upsilon}_i) \ddot{\vec{\Upsilon}}_i + \dot{\mathbf{W}}_{0,i}(\vec{\Upsilon}_i) \dot{\vec{\Upsilon}}_i \right) \times \vec{x}_{0,i}^*(\vec{\Upsilon}_i) - \mathbf{W}_{0,i}(\vec{\Upsilon}_i) \dot{\vec{\Upsilon}}_i \times \left(\mathbf{W}_{0,i}(\vec{\Upsilon}_i) \dot{\vec{\Upsilon}}_i \times \vec{x}_{0,i}^*(\vec{\Upsilon}_i) \right), \quad (3.86)$$

$$\dot{\vec{\omega}}_{0,i} = \mathbf{W}_{0,i}(\vec{\Upsilon}_i) \ddot{\vec{\Upsilon}}_i + \dot{\mathbf{W}}_{0,i}(\vec{\Upsilon}_i) \dot{\vec{\Upsilon}}_i = \mathcal{I}_{0,i}^{-1} \left(\sum_{k=1}^N \vec{y}_{0,i,k}^*(\vec{\Upsilon}_i) \times \vec{f}_{0,i,k} - \mathbf{W}_{0,i}(\vec{\Upsilon}_i) \dot{\vec{\Upsilon}}_i \times \mathcal{I}_0 \mathbf{W}_{0,i}(\vec{\Upsilon}_i) \dot{\vec{\Upsilon}}_i - m_i \vec{x}_{0,i}^*(\vec{\Upsilon}_i) \times \ddot{\vec{\Gamma}}_i \right). \quad (3.87)$$

If the body frame centre and centre of mass coincide, the equations simplify considerably. The forces $\vec{f}_{0,i,k}$ can also depend on the orientation if it is simpler to define them in the body frame. The equations of motion are in general non-linear and solutions are mostly found numerically.

3.4.5 Mechanical Energy, Work and Power

Because of the complexity of the equations of motion, the energy approach to rigid body mechanics provides insight without solving the equations. The energy of a rigid body has two sources: *kinetic energy* and *work*.

The kinetic energy of a rigid body with continuous mass distribution is defined by:

$$\mathcal{E}_{K,i} = \frac{1}{2} \int \rho(\vec{z}_{0,i}^*) \dot{\vec{z}}_0^T \dot{\vec{z}}_0 (dz_{0,i}^*)^3, \quad \vec{z}_{0,i} = \vec{d}_{0,i} + \vec{z}_{0,i}^*, \quad \dot{\vec{z}}_0 = \dot{\vec{d}}_0 + \vec{\omega}_{0,i} \times \vec{z}_{0,i}^*. \quad (3.88)$$

Expanding the expression yields:

$$\begin{aligned} \mathcal{E}_{K,i} &= \frac{1}{2} \int \rho(\vec{z}_{0,i}^*) (\dot{\vec{d}}_0 + \vec{\omega}_{0,i} \times \vec{z}_{0,i}^*)^T (\dot{\vec{d}}_0 + \vec{\omega}_{0,i} \times \vec{z}_{0,i}^*) (dz_{0,i}^*)^3, \\ &= \frac{1}{2} m_i \dot{\vec{d}}_0^T \dot{\vec{d}}_0 + m_i \dot{\vec{d}}_0^T (\vec{\omega}_{0,i} \times \vec{x}_{0,i}^*) + \frac{1}{2} \vec{\omega}_{0,i}^T \mathcal{I}_{0,i} \vec{\omega}_{0,i} = \frac{1}{2} m_i \dot{\vec{x}}_0^T \dot{\vec{x}}_0 + \frac{1}{2} \vec{\omega}_{0,i}^T \mathcal{I}_{0,i} \vec{\omega}_{0,i}. \end{aligned} \quad (3.89)$$

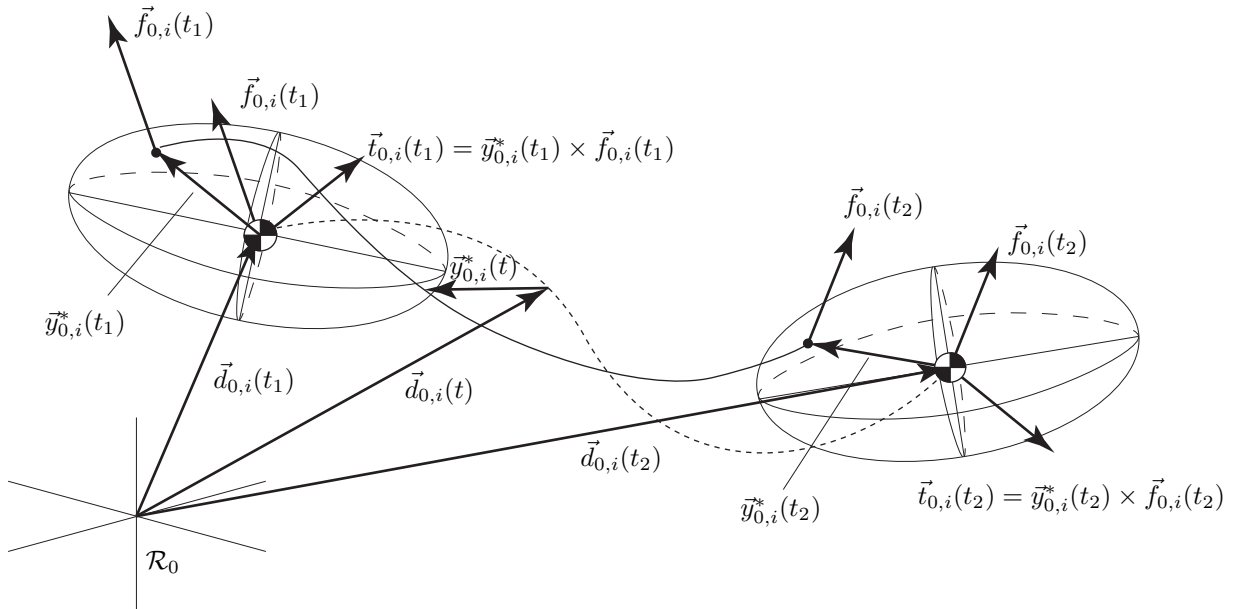


Figure 3.13: Construction for the mechanical work of a force on a rigid body along a path as described in section 3.4.5.

The energy given to a body by a force is called *work*. The body frame moves along a path $\vec{d}_{0,i}(t)$ with a single force $\vec{f}_{0,i}(t)$ applied at a point $Y_{0,i}$ ($\vec{y}_{0,i} = \vec{d}_{0,i} + \vec{y}_{0,i}^*$) (Fig. 3.13).

The total work \mathcal{W}_i of the force $\vec{f}_{0,i}$ between times t_1 and t_2 is defined in the inertial frame by:

$$\begin{aligned} (\mathcal{W}_i)_{t_1}^{t_2} &= \int_{t_1}^{t_2} \vec{f}_{0,i} \cdot \dot{\vec{y}}_0 dt = \int_{t_1}^{t_2} \vec{f}_{0,i} \cdot \left(\dot{\vec{d}}_{0,i} + \vec{\omega}_{0,i} \times \vec{y}_{0,i}^* \right) dt \\ &= \int_{t_1}^{t_2} \vec{f}_{0,i} \cdot \dot{\vec{d}}_{0,i} dt + \int_{t_1}^{t_2} \vec{\omega}_{0,i}^T \cdot (\vec{y}_{0,i}^* \times \vec{f}_{0,i}) dt. \end{aligned} \quad (3.90)$$

It is the integral of the power $\mathcal{P}_{i,f}(t) = \vec{f}_{0,i}(t) \cdot \dot{\vec{d}}_{0,i}(t)$ developed by the force along the path of the body frame plus the power $\mathcal{P}_{i,t}(t) = \vec{\omega}_{0,i}^T(t) \cdot (\vec{y}_{0,i}^*(t) \times \vec{f}_{0,i}(t))$ developed by the moment around the body frame over time. For an infinitesimal displacement of the body along the path, the infinitesimal amount of work is defined by:

$$\begin{aligned} \frac{d\mathcal{W}_i}{dt} &= \mathcal{P}_i(t) = \vec{f}_{0,i} \cdot \dot{\vec{d}}_{0,i} + \vec{\omega}_{0,i}^T \cdot (\vec{y}_{0,i}^* \times \vec{f}_{0,i}) = \vec{f}_{0,i} \cdot \frac{d(\vec{d}_{0,i})}{dt} + (\mathbf{W}_{0,i} \frac{d\vec{\Upsilon}_i}{dt})^T (\vec{y}_{0,i}^* \times \vec{f}_{0,i}) \\ d\mathcal{W}_i &= \mathcal{P}_i dt = \vec{f}_{0,i} \cdot d\vec{d}_{0,i} + (\mathbf{W}_{0,i} d\vec{\Upsilon}_i)^T (\vec{y}_{0,i}^* \times \vec{f}_{0,i}). \end{aligned} \quad (3.91)$$

The path is function of the kinematic coordinates \vec{q}_i . Thus, work can also be expressed as a path integral in terms of the coordinates $\vec{\Gamma}_i$ and $\vec{\Upsilon}_i$.

$$(\mathcal{W}_i)_{t_1}^{t_2} = \int_{\vec{\Gamma}_i(t_1)}^{\vec{\Gamma}_i(t_2)} \vec{f}_{0,i} \cdot d\vec{\Gamma}_i + \int_{\vec{\Upsilon}_i(t_1)}^{\vec{\Upsilon}_i(t_2)} \mathbf{W}_{0,i}^T(\vec{\Upsilon}_i) \cdot (\vec{y}_{0,i}^*(\vec{\Upsilon}_i) \times \vec{f}_{0,i}) d\vec{\Upsilon}_i. \quad (3.92)$$

A force producing work is said to be *active* otherwise it is *inactive*.

Force fields are of particular interest. They are forces dependent on the spatial position \vec{x}_0 . Given that forces act on bodies, the force field can be parameterised by the position of the body's centre of gravity that is function of the kinematic coordinates \vec{q}_i .

$$\vec{f}_{0,i}(\vec{x}_{0,i}) = \vec{f}_{0,i}(\vec{q}_i).$$

Examples of force fields include Newton's gravitational field around bodies, electromagnetic force fields and the force created by a elastic springs. There is a particular type of force field called a *conservative* force field.

Definition 7 (Conservative force field). *A force field $\vec{f}_{0,i}(\vec{q}_i)$ is conservative if the work it produces along a path is only dependent of the path's end points. The work is independent of the path. Such forces satisfy the following list of equivalent properties:*

- The work produced by a conservative force along a closed path is zero : $\oint dW_i = 0$.
- There exists a function $h(\vec{x}_{0,i}) = h(\vec{q}_i)$ such that $\vec{f}_{0,i}(\vec{q}_i) = -\nabla_{\vec{q}_i} h(\vec{q}_i)$.
- The rotational of a conservative force is zero. $\nabla_{\vec{q}_i} \times \vec{f}_{0,i} = \vec{0}$

Any force not satisfying these properties is called a *non-conservative* force field.

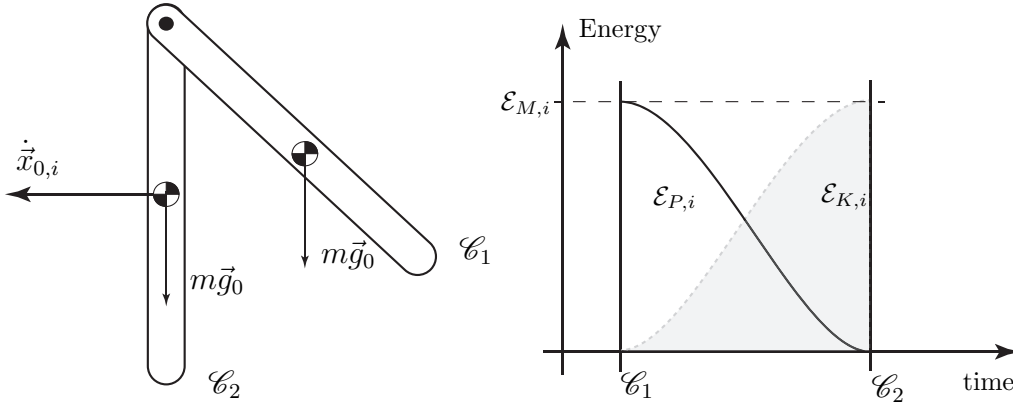


Figure 3.14: Illustration of the energy conservation theorem as described in section 3.4.5.

The energy produced by conservative force fields is called *potential energy* and the function $h(\vec{x}_{0,i})$ is called a *potential function*. More abstractly, a conservative force field is called an exact 1-form and is irrotational ($\nabla \times \vec{f}_{0,i}(\vec{q}_i) = 0$).

The total mechanical energy of a rigid-body is a scalar function. It is defined as the sum of the total kinetic energy due to the system's motion and the total potential energy due to conservative forces such as springs or gravity. The mechanical energy is a function of the kinematic coordinates and their first-order time derivatives.

$$\mathcal{E}_{M,i}(\vec{q}_i, \dot{\vec{q}}_i) = \mathcal{E}_{K,i}(\vec{q}_i, \dot{\vec{q}}_i) + \mathcal{E}_{P,i}(\vec{q}_i). \quad (3.93)$$

There are two important theorems involving a body's energy.

Theorem 13 (Energy Conservation theorem). *The total mechanical energy of a system not subject to any non-conservative forces is constant*

$$\mathcal{E}_{M,i} = cte, \quad \dot{\mathcal{E}}_{M,i} = 0. \quad (3.94)$$

Between two configurations, the variation in kinetic energy is equal to the opposite of the potential energy variation.

$$\Delta \mathcal{E}_{K,i}(t_1, t_2) = -\Delta \mathcal{E}_{P,i}(t_1, t_2). \quad (3.95)$$

This theorem is easy to understand when considering a frictionless pendulum subject only to the earth's gravitational force (Fig. 3.14). In a configuration \mathcal{C}_1 , the pendulum has no velocity and therefore no kinetic energy. However, the gravitational force is giving it energy that will cause it to rotate downwards. In configuration \mathcal{C}_2 , the pendulum can no longer drop any further and therefore has no potential energy. However, it does have a velocity. All the potential energy from configuration \mathcal{C}_1 is transformed into kinetic energy in configuration \mathcal{C}_2 .

Theorem 14 (Energy theorem). *The variation over time of a body's mechanical energy is equal to the power developed by all the non-conservative forces acting on it.*

$$\dot{\mathcal{E}}_{M,i} = \mathcal{P}_{nc,i}. \quad (3.96)$$

The energy theorems provide a method of verifying if the equations of motion are correct. If the solution obtained after numerical integration does not satisfy either theorem, depending on the type of forces acting on the body, the equations of motion contain errors. The energy approach provides a systematic method of constructing the equations of motion that will be discussed in the following section.

3.5 Multibody Kinematics

The previous sections presented the kinematics and dynamics of a single, free rigid body. This section extends the kinematics analysis to systems of rigid bodies where there are interactions between the bodies that are no longer free. The presentation's focus is mechanisms involving a specific type of interactions called joints. This section focuses on the interactions between the different bodies in terms of relative movement. The section begins by presenting the definitions of kinematic pairs and chains. The forward kinematics and mobility of a mechanism are also presented followed by a presentation of the constraints arising within mechanisms. Finally, a systematic method of constructing the forward kinematic map is described.

3.5.1 Machines and Mechanisms

One example of a system of bodies is a *machine*. A machine has multiple parts or links and uses energy to produce motion and therefore a force. In a machine there is always one fixed link called the *carrier link*. The links within a machine are connected through articulations or joints imposing a relative motion between two links. The motion produced by a machine is transmitted to a specific link in the machine called the *end-effector*. Machines are real systems where the link's are not necessarily perfectly rigid, the contacts have friction and there is play in the joints. Examples of machines include robot manipulators. A *mechanism* is defined in this chapter as an idealisation of a machine where the links are all rigid bodies and the contacts are perfect or ideal. There is no play or friction in the interactions between bodies. As such, mechanisms satisfy the rules of general mechanics. Each body's behaviour is governed by the kinematics and dynamics of a single rigid body under the influence of forces. The differences between each body in a mechanism are the constraints and forces restricting and influencing their motion.

Two families or types of mechanisms are differentiated by the configuration of the bodies between the carrier body and end-effector [126]. There are *serial* mechanisms where the bodies are connected in series between the carrier body and end-effector (Fig. 3.15). In a serial mechanism there is a single path passing through each body from carrier body to end-effector. An example of a serial mechanism is the SCARA pick and place robot used in assembly lines in industry [202]. The second type of mechanisms are *parallel* mechanisms where there are multiple serially connected groups of bodies between the carrier body and end-effector. In a parallel mechanism there are multiple paths between the carrier body and end-effector. The Gough-Stewart platform is a well known example of parallel mechanism [79, 184], initially designed for testing tires. There is a third type of mechanism, not considered here, called a hybrid mechanism with both serial and parallel configurations of its bodies.

Parallel mechanisms are more rigid than serial mechanisms because the play in the joints cancels itself through the parallel design. However, such mechanisms are more challenging to design. Serial mechanisms have a wider space in which the end-effector can

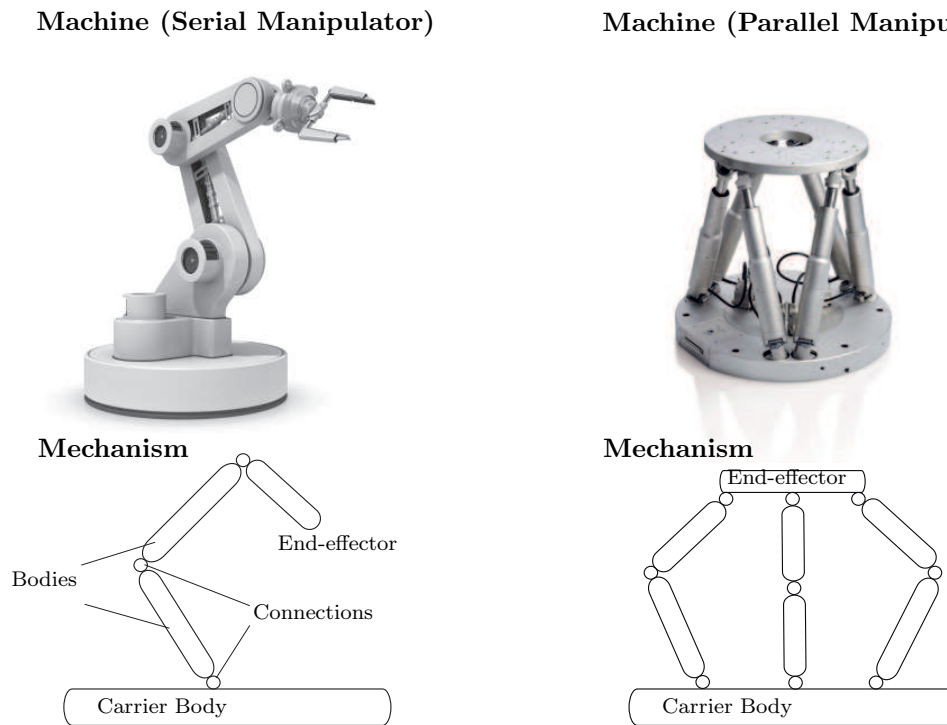


Figure 3.15: *Illustrations of machines and their corresponding mechanisms as described in section 3.5.1.*

move while parallel mechanisms have a smaller end-effector workspace. Parallel mechanisms can move at much greater speeds within their workspace than serial mechanisms. A human being standing on one foot can be seen as a serial mechanism. The ground is the carrier body and the body constitutes multiple serial elements. When the second foot touches the ground, the body becomes a parallel mechanism. The two legs constitute a parallel element of the mechanism between the ground and lower trunk. The upper trunk, upper limbs and head constitute serial elements of the mechanism. The standing human body is a hybrid mechanism.

3.5.2 Kinematic Pairs and Kinematic Chains

Mechanisms transmit motion and therefore forces. Forces are transmitted within a mechanism by the interactions between bodies called *connections*. Connections represent an idealised model of the interactions between two bodies. There is no friction or play in a connection. There are two types of connections, differentiated by the nature of the interaction forces. Force elements and kinematic pairs.

A *force element* creates a force on either body in a connection that is a function of their relative motion. For instance, a spring and damper creates a force that is a known function of the relative position and velocity of the two bodies. A force element produces a force that is *known*, given the mechanism's geometric configuration, but does not limit the kinematics of the mechanism.

A *kinematic pair* or joint defines a kinematic constraint between two bodies and limits their motion. The forces in a joint impose the constraint but are unknown a priori. This difference with force elements is essential. Kinematic constraints do impose forces on the bodies. These forces are dependent on the type of constraint but can only be resolved by solving the equations of motion.

One distinguishes between form- and force-closed joints. A *form-closed* joint is held together by the geometry of the joint. The kinematic constraint between the two bodies is always enforced. A *force-closed* joint requires the application of an external force to enforce the kinematic constraint. If there is no force, there is not necessarily a constraint and the bodies can move apart. In any connection, the interaction forces applied on either body are *always* equal and opposite according to Newton's third law.

A *kinematic chain* represents a kinematic model of a mechanism. It is a set of rigid bodies connected together by kinematic pairs. Because the model is kinematic, force elements are not considered. A serial mechanism defines an *open* kinematic chain. A parallel mechanism defines a *closed* kinematic chain. A kinematic chain is defined between the carrier body and the end-effector. Therefore, closed kinematic chains can be seen as multiple serial chains, joined together at the end-effector.

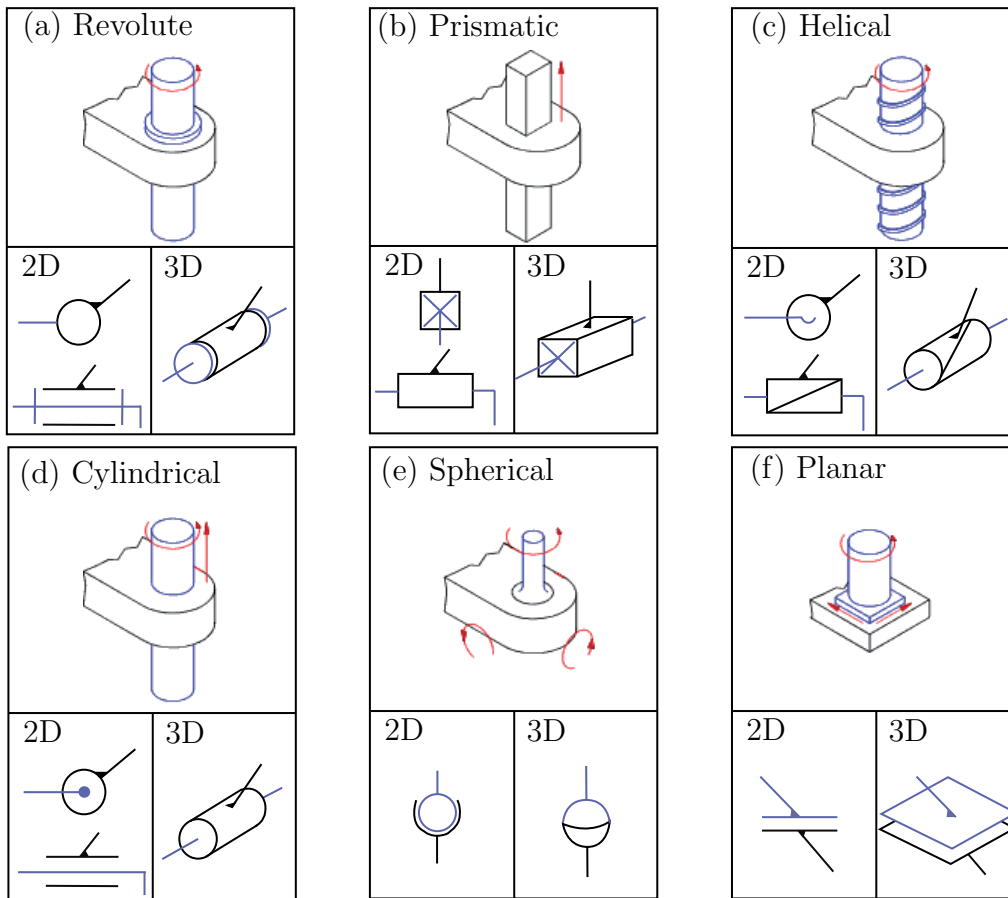


Figure 3.16: Illustration of the six lower kinematic pairs with their symbology. (a) Revolute (R) joint - 1 dof. (b) Prismatic (P) joint - 1 dof. (c) Helical (H) joint - 1 dof. (d) Cylindrical (C) joint - 2 dof. (e) Spherical (S) joint - 3 dof. (f) Planar (F) joint - 3 dof.

Kinematic pairs are characterised by the type of contact between the connecting bodies. They can be punctual, linear or over a surface. Surface contact pairs are called *lower kinematic pairs* while linear and punctual contact pairs are called *higher kinematic pairs* [91, 173]. Lower pairs are the most predominant kinematic pairs found in mechanisms. There are six different types of lower kinematic pairs (Fig. 3.16). The revolute pair (R), the prismatic pair (P), the cylindrical pair (C), the helical pair (H), the spherical pair (S) and the planar pair (F). The revolute and prismatic pairs are the most fundamental and can be used to construct all other pairs. Higher kinematic pairs include the universal pair (U) which is two serially connected revolute pairs (Fig. 3.16) and is for instance the cardan joint. The linear pair (L) which is for instance, a wheel rolling on the ground (linear contact). The spherical slider pair (E) which is a sphere that can slide and roll on a surface (punctual contact).

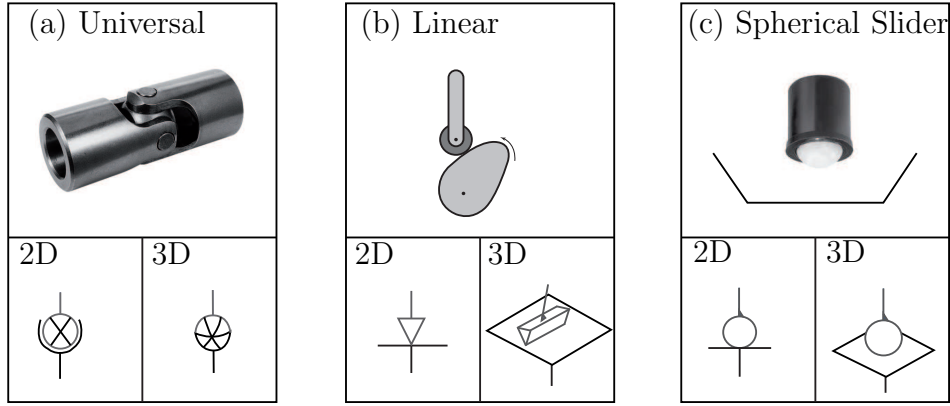


Figure 3.17: Illustration of the higher kinematic pairs with their symbology. (a) Universal joint (U) - 2 dof. (b) Linear joint (L) - 4 dof. (c) Spherical Slider joint (E) - 5 dof..

Kinematic pairs impose a specific kinematic relation between two bodies. The motion between two bodies \mathcal{B}_i and \mathcal{B}_j of a general kinematic pair is modelled by a Euclidean displacement. The displacement describes the position of a point $X_{0,j}$ on \mathcal{B}_j , for instance the centre of mass, with respect to the inertial frame \mathcal{R}_0 through the configuration $\mathcal{C}_{0,i}$ of the body \mathcal{B}_i .

$$X_{0,j} : \vec{x}_{0,j} = \vec{d}_{0,j} + \mathbf{R}_{j,0}\vec{x}_j = \vec{d}_{0,j} + \vec{x}_{0,j}^*. \quad (3.97)$$

The vector $\vec{d}_{0,j}$ defines the position of the reference frame \mathcal{R}_j . This vector can be defined as the position of the reference frame \mathcal{R}_i plus a vector.

$$\vec{d}_{0,j} = \vec{d}_{0,i} + \mathbf{R}_{i,0}\vec{y}_i \quad \text{and} \quad X_{i,j} : \vec{x}_{i,j} = \vec{y}_i + \mathbf{R}_{j,i}\vec{x}_j, \quad \mathbf{R}_{j,i} = \mathbf{R}_{j,0}\mathbf{R}_{i,0}^T. \quad (3.98)$$

where \vec{y}_i is the position of \mathcal{R}_j with respect to \mathcal{R}_i in the frame \mathcal{R}_i (Fig. 3.18). Thus, the configuration of a \mathcal{C}_j of a body \mathcal{B}_j is defined by:

$$\mathcal{C}_{0,j} = (\vec{d}_{0,j}, \mathbf{R}_{j,0}) = (\vec{d}_{0,i} + \mathbf{R}_{i,0}\vec{y}_i, \mathbf{R}_{j,i}\mathbf{R}_{i,0}).$$

The configuration of \mathcal{B}_j is parameterised by a vector of kinematic coordinates \vec{q}_j . If the coordinates are defined with respect to the inertial frame they are called absolute coordinates and the configuration of \mathcal{B}_j is the global configuration $\mathcal{C}_{0,j}$. If the coordinate

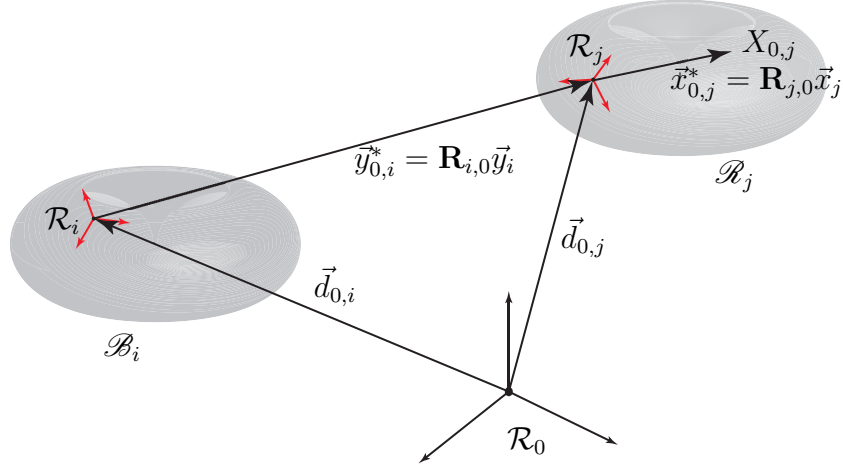


Figure 3.18: *Illustration of the kinematic relation between two bodies in a kinematic pair as described in section 3.5.2.*

are defined with respect to another body (\mathcal{B}_i) they are called local or relative coordinates and the configuration of \mathcal{B}_j is the local configuration $\mathcal{C}_{i,j}$. For a serial chain comprised of N_b bodies, any given body \mathcal{B}_j is connect to a body \mathcal{B}_{j-1} in the direction of the carrier body \mathcal{B}_0 , and connected to a body \mathcal{B}_{j+1} in the direction of the end-effector \mathcal{B}_e . In a serial chain, the kinematic coordinates \vec{q}_j parameterise the kinematic pair between \mathcal{B}_j and \mathcal{B}_{j-1} and the configuration of \mathcal{B}_j . Therefore, each kinematic pair has a specific set of kinematic coordinates (Table 3.1). The number of independent coordinates defines the degrees of freedom K_j of the kinematic pair. There are at most 6 degrees of freedom for a single kinematic pair. The kinematic coordinates of a kinematic pair are therefore elements of subsets of $SE(3)$. These subsets can for certain kinematic pairs be topologically equivalent or homeomorphic to other well known sets [31, 181].

- **Prismatic** pair is defined by one translational coordinate: $\vec{q}_i \in \mathbb{R}$,
- **Revolute** pair is defined by one rotational coordinate: $\vec{q}_i \in S^1 \equiv SO(2)$,
- **Cylindrical** pair is defined by one translational coordinate and one rotational coordinate: $\vec{q}_i \in \mathbb{R} \times S^1$,
- **Spherical** pair is defined by three rotational elements: $\vec{q}_i \in SO(3)$,
- **Planar** pair is defined by one rotational coordinate and two translational coordinate: $\vec{q}_i \in \mathbb{R}^2 \times S^1$,
- **Universal** pair is defined by two rotational coordinates: $\vec{q}_i \in S^2$,
- **Linear** pair is defined by two translational coordinates and two rotational coordinates: $\vec{q}_i \in \mathbb{R}^2 \times S^2$,
- **Spherical Slider** pair is defined by two translational coordinates and three rotational coordinates: $\vec{q}_i \in \mathbb{R}^2 \times SO(3)$.

Thus, the kinematics of any mechanism under the assumptions described in section 3.5.1 are governed by a well defined mathematical formalism. Each of the kinematic pairs

have kinematic coordinates belonging to smooth manifolds. Some of the manifolds are compact (closed and bounded): S^1 , S^2 , $SO(3)$. \mathbb{R}^n is not compact but a product of n intervals of \mathbb{R} is compact a compact subset of \mathbb{R}^n [31]. Remark: For the universal joint, $S^1 \times S^1 \neq S^2$. In a universal joint, the rotation axes always intersect and therefore the coordinates belong to S^2 . Two serial revolute joints with non intersecting rotation axes define coordinates belonging to $S^1 \times S^1$.

Consider the configuration of body \mathcal{B}_j to be defined with respect to \mathcal{B}_i using local coordinates of the kinematic pair between them. The kinematic pair's motion is characterised by a twist \mathcal{T} in terms of a local description of the kinematics. In a revolute joint, the second body \mathcal{B}_j rotates around the axis defined by $\vec{\omega}_{i,j}$ (Instantaneous rotational velocity of body \mathcal{B}_j in the frame \mathcal{R}_i). This axis is fixed with respect to the body \mathcal{B}_i . In a prismatic joint, \mathcal{B}_j translates along an axis defined by $\vec{d}_{i,j}$. This axis is also fixed with respect to the body \mathcal{B}_i . Using a local description of the kinematics, the twists of a revolute and prismatic pair are defined by:

$$\mathcal{T}_R = (\vec{\omega}_{i,j}, \vec{\omega}_{i,j} \times \vec{x}_{i,j}^*), \quad \mathcal{T}_P = (\vec{0}, \vec{d}_i). \quad (3.99)$$

A revolute joint is a twist with zero pitch, a prismatic joint is a twist with infinite pitch.

Although this section does not deal with forces, there is a final point concerning kinematic pairs. Given the duality between Chasles' theorem and Poincot's theorem, each kinematic pair has a wrench, dual to the twist. A kinematic pair's twist defines the permissible motion of body \mathcal{B}_j with respect to body \mathcal{B}_i . A kinematic pair's wrench defines the force and moment of force that body \mathcal{B}_i can apply to body \mathcal{B}_j . No force or moment of force can be transmitted in the direction of a permissible motion. For instance, in a prismatic pair, no force can be transmitted along the translation axis. This leads to the following statement: *the force and moment of force of a kinematic pair produce no work*. This point will become essential in building the equations of motion for a mechanism.

3.5.3 Forward Kinematics and Mobility

Forward kinematics analyses the motion of the end-effector, through the motion of the entire robot in terms of the kinematic coordinates of each body. Therefore, a description of the entire mechanism's kinematics is required. A systematic approach is to define the configuration $\mathcal{C}_{0,i}$ of each body in the mechanism with respect to the inertial frame \mathcal{R}_0 . The reference frame of body \mathcal{B}_i is placed at a point directly involved in the kinematic pair with \mathcal{B}_{i-1} . For instance, at the centre of a spherical pair or on the axis of a prismatic or revolute pair. The Euclidean displacement is defined with respect to the body's centre of gravity (Fig. 3.19):

$$\begin{pmatrix} \vec{x}_{0,i} \\ 1 \end{pmatrix} = \begin{pmatrix} \mathbf{R}_{i,0} & \vec{d}_{0,i} \\ \vec{0}^T & 1 \end{pmatrix} \begin{pmatrix} \vec{x}_i \\ 1 \end{pmatrix} = \mathbf{H}_{i,0} \begin{pmatrix} \vec{x}_i \\ 1 \end{pmatrix}. \quad (3.100)$$

The configuration $\mathcal{C}_{0,i}$ of every body in the mechanism is defined in the same way. As stated in section 3.5.2, the vector $\vec{d}_{0,i}$ can be expressed with respect to the displacement

Table 3.1: *Euclidean displacement characteristics of some kinematic pairs [181]. The displacements are described for body \mathcal{B}_j (with frame \mathcal{R}_j) with respect to body \mathcal{B}_i with frame \mathcal{R}_i .*

Kinematic Pair	Rotation Matrix $\vec{R}_{j,0}$	Vector $\vec{d}_{0,j}$	Variables \vec{q}_j
Revolute Pair	$\begin{pmatrix} \cos(\psi_j) & 0 & -\sin(\psi_j) \\ 0 & 1 & 0 \\ \sin(\psi_j) & 0 & \cos(\psi_j) \end{pmatrix}$	$\begin{pmatrix} 0 \\ 0 \\ 0 \end{pmatrix}$	$(0 \ 0 \ 0 \ \psi_j \ 0 \ 0)^T$
Prismatic Pair	$\begin{pmatrix} 1 & 0 & 0 \\ 0 & 1 & 0 \\ 0 & 0 & 1 \end{pmatrix}$	$\begin{pmatrix} x_j \\ 0 \\ 0 \end{pmatrix}$	$(x_j \ 0 \ 0 \ 0 \ 0 \ 0)^T$
Cylindrical Pair	$\begin{pmatrix} \cos(\psi_j) & 0 & -\sin(\psi_j) \\ 0 & 1 & 0 \\ \sin(\psi_j) & 0 & \cos(\psi_j) \end{pmatrix}$	$\begin{pmatrix} 0 \\ y_j \\ 0 \end{pmatrix}$	$(0 \ y_j \ 0 \ 0 \ \vartheta_j \ 0)^T$
Spherical Pair	$\mathbf{R}(\psi_j)\mathbf{R}^T(\vartheta_j)\mathbf{R}(\varphi_j)$	$\begin{pmatrix} 0 \\ 0 \\ 0 \end{pmatrix}$	$(0 \ 0 \ 0 \ \psi_j \ \vartheta_j \ \varphi_j)^T$
Planar Pair	$\begin{pmatrix} \cos(\varphi_j) & -\sin(\varphi_j) & 0 \\ \sin(\varphi_j) & \cos(\varphi_j) & 0 \\ 0 & 0 & 1 \end{pmatrix}$	$\begin{pmatrix} x_j \\ y_j \\ 0 \end{pmatrix}$	$(x_j \ y_j \ 0 \ 0 \ 0 \ \varphi_j)^T$
Universal Pair	$\begin{pmatrix} \cos(\varphi_j)\cos(\vartheta_j) & -\sin(\varphi_j) & \cos(\varphi_j)\sin(\vartheta_j) \\ \cos(\vartheta_j)\sin(\varphi_j) & \cos(\varphi_j) & \sin(\varphi_j)\sin(\vartheta_j) \\ -\sin(\vartheta_j) & 0 & \cos(\vartheta_j) \end{pmatrix}$	$\begin{pmatrix} 0 \\ 0 \\ 0 \end{pmatrix}$	$(0 \ 0 \ 0 \ 0 \ \vartheta_j \ \varphi_j)^T$
Linear Pair	$\begin{pmatrix} \cos(\varphi_j)\cos(\vartheta_j) & -\sin(\varphi_j) & \cos(\varphi_j)\sin(\vartheta_j) \\ \cos(\vartheta_j)\sin(\varphi_j) & \cos(\varphi_j) & \sin(\varphi_j)\sin(\vartheta_j) \\ -\sin(\vartheta_j) & 0 & \cos(\vartheta_j) \end{pmatrix}$	$\begin{pmatrix} x_j \\ y_j \\ 0 \end{pmatrix}$	$(x_j \ y_j \ 0 \ 0 \ \vartheta_j \ \varphi_j)^T$
Spherical Slider Pair	$\mathbf{R}(\psi_j)\mathbf{R}^T(\vartheta_j)\mathbf{R}(\varphi_j)$	$\begin{pmatrix} x_j \\ y_j \\ 0 \end{pmatrix}$	$(x_j \ y_j \ 0 \ \psi_j \ \vartheta_j \ \varphi_j)^T$

of the body \mathcal{B}_{i-1} .

$$\vec{d}_{0,i} = \vec{d}_{0,i-1} + \mathbf{R}_{i-1,0}\vec{y}_{i-1}, \quad (3.101)$$

where \vec{y}_{i-1} is the vector between the reference frame \mathcal{R}_{i-1} and \mathcal{R}_i in the frame \mathcal{R}_{i-1} . Proceeding backwards until the first body, one defines the following:

$$\vec{d}_{0,i} = \vec{d}_{0,1} + \mathbf{R}_{1,0}\vec{y}_1 \cdots + \mathbf{R}_{i-2,0}\vec{y}_{i-2} + \mathbf{R}_{i-1,0}\vec{y}_{i-1}, \quad (3.102)$$

The result is a homogeneous transformation, function of the global kinematic coordinates, defined by:

$$\begin{pmatrix} \vec{x}_{0,i} \\ 1 \end{pmatrix} = \begin{pmatrix} \mathbf{R}_{i,0} & \vec{d}_{0,1} + \mathbf{R}_{1,0}\vec{y}_1 \cdots + \mathbf{R}_{i-2,0}\vec{y}_{i-2} + \mathbf{R}_{i-1,0}\vec{y}_{i-1} \\ \vec{0}^T & 1 \end{pmatrix} \begin{pmatrix} \vec{x}_i \\ 1 \end{pmatrix}. \quad (3.103)$$

An alternative method is to use local coordinates. The configuration $\mathcal{C}_{i-1,i}$ of each body \mathcal{B}_i is defined with respect to the previous body \mathcal{B}_{i-1} . The displacement of \mathcal{B}_i with respect to \mathcal{B}_{i-1} is defined by the homogeneous transformation:

$$\begin{pmatrix} \vec{x}_{i-1,i} \\ 1 \end{pmatrix} = \begin{pmatrix} \mathbf{R}_{i,i-1} & \vec{d}_{i-1,i} \\ \vec{0}^T & 1 \end{pmatrix} \begin{pmatrix} \vec{x}_i \\ 1 \end{pmatrix} = \mathbf{H}_{i,i-1} \begin{pmatrix} \vec{x}_i \\ 1 \end{pmatrix}. \quad (3.104)$$

The vector $\vec{d}_{i-1,i}$ is vector from \mathcal{R}_{i-1} to \mathcal{R}_i in the frame \mathcal{R}_{i-1} . The vector \vec{x}_i is the vector from \mathcal{R}_i to the centre of mass on \mathcal{B}_i . The displacements can be compiled such that any point Y_i on the mechanism is defined with respect to the inertial frame by the following displacement:

$$Y_{0,i} : \vec{y}_{0,i} = \mathbf{H}_{1,0}\mathbf{H}_{2,1} \cdots \mathbf{H}_{i-1,i-2}\mathbf{H}_{i,i-1} \begin{pmatrix} \vec{y}_i \\ 1 \end{pmatrix} = \mathbf{H}_{i,0} \begin{pmatrix} \vec{y}_i \\ 1 \end{pmatrix}, \quad (3.105)$$

In both cases ((3.103),(3.105)), the homogeneous transformation matrix $\mathbf{H}_{i,0}$ can be defined in terms of all the kinematic coordinates \vec{q}_i of each kinematic pair between body \mathcal{B}_i and the carrier body. The coordinates are either global coordinates or local coordinates. For kinematic chains with only revolute and prismatic pairs, there is a convention on the parameterisation of the homogeneous transformation, called the Denevit-Hartenberg parameterisation [126].

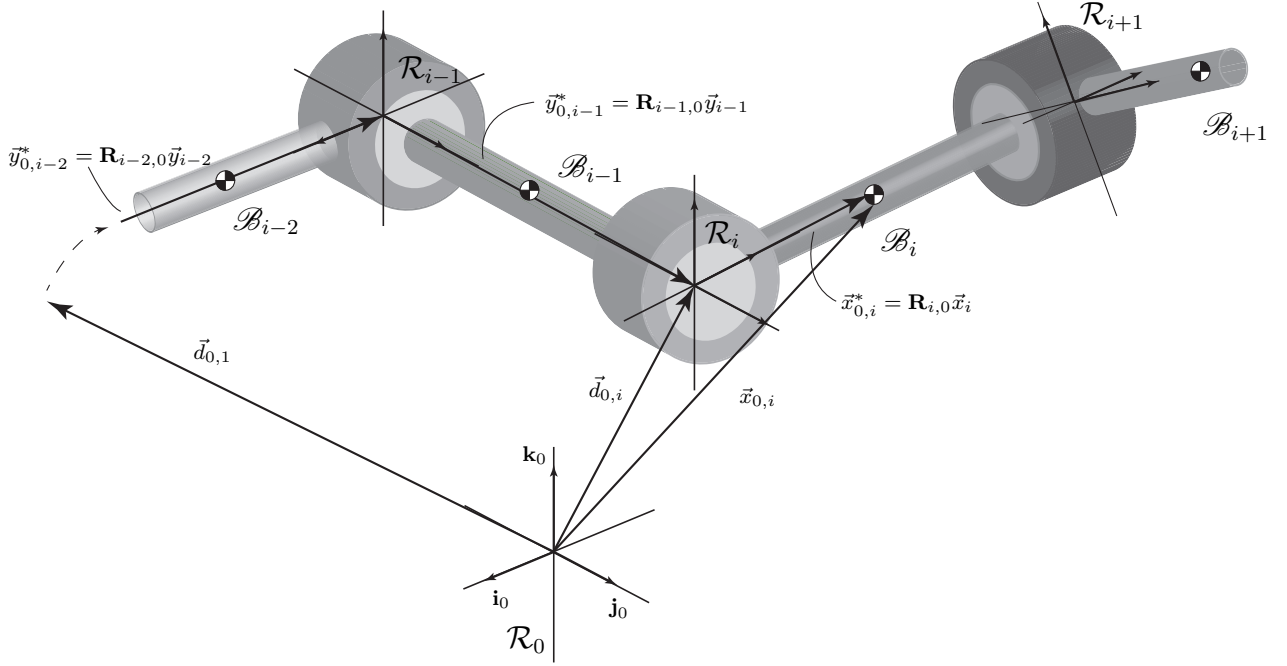


Figure 3.19: *Illustration of the displacement of a kinematic pair in a mechanism as described in section 3.5.3.*

Thus, the configuration ($\mathcal{C}_{0,i}$ or $\mathcal{C}_{0,i-1}$) of any body \mathcal{B}_i in a kinematic chain with N_b bodies and N_k kinematic pairs ($N_k \geq N_b$) is defined by a single homogeneous transformation. This transformation is function off all the kinematic coordinates of the mechanism \vec{q}_i , $i = 1, \dots, N_k$. The coordinates \vec{q}_i parameterise the kinematics of the kinematic pair between \mathcal{B}_{i-1} and \mathcal{B}_i and are either global or local coordinates. All the coordinates are grouped into a single vector:

$$\vec{q} = (\underbrace{\dots, \vec{q}_i^T, \dots}_{N_k \text{ vectors}})^T. \quad (3.106)$$

As stated previously, each kinematic pair has a certain number *degrees of freedom* $K_i \leq 6$ equal to the number of independent elements in \vec{q}_i . In general *degrees of freedom* designates the minimal number of independent coordinates need to parameterise the configuration of a joint, body or mechanism. Knowing K_i for each joint allows one to compute the number of degrees of freedom of the entire mechanism. The number of degrees of freedom or *mobility* D of a mechanism i with N_b bodies and N_k kinematic pairs is defined by the Chebychev–Grübler–Kutzbach or mobility formula [192].

$$D = 6(N_b - 1) - \sum_{i=1}^{N_k} (6 - K_i), \quad (3.107)$$

There are $(N_b - 1)$ rigid bodies without the carrier body. Each body has potentially six degrees of freedom. There are N_k joints with K_i degrees of freedom each. Each joint eliminates $6 - K_i$ degrees of freedom for body \mathcal{B}_i . The mobility D of the mechanism is equal to the number of independent elements of \vec{q} . A system is said to be *holonomic* with D degrees of freedom if all the coordinates are independent and there is no relation between \vec{q} and $\dot{\vec{q}}$. Otherwise, the system must have constraints limiting its motion. Theoretically, if the number of kinematic coordinates is always selected to match the number of degrees of freedom, there would never be constraints. This proposition is attractive in that analysing the kinematics using independent coordinates is straightforward. However, this is highly non-trivial for most mechanisms.

3.5.4 Kinematic Constraints

Any contact between two bodies restricts their relative motion and can be modelled as a kinematic constraint. All kinematic pairs can be defined as constraints. The constraint defines the restrictions on the motion as mathematical expressions. There are three types of kinematic constraints classified according their mathematical expression. The first type are called *holonomic* constraints and are expressed as algebraic functions of the kinematic coordinates and time.

$$\Phi(\vec{q}, t) = 0. \quad (3.108)$$

If time appears explicitly in the function Φ , the constraint is *holonomic-rheonomic*, otherwise it is *holonomic-skleronomic*. For instance, kinematic pairs define holonomic-skleronomic constraints. The second type of constraints are called *non-holonomic* constraints and are expressed as:

$$\Phi(\vec{q}, \dot{\vec{q}}, t) = 0. \quad (3.109)$$

An example of a non-holomic constraint is for instance the rolling wheel constraint. A wheel can only roll forwards and cannot translate sideways. The constraint states that the linear velocity must be equal to the wheel's rotation speed and orientation angle.

The last type of constraints are called *isoparametric* constraints. They are used for example to enforce the conservation of some quantity such as a length or energy. They are expressed as an integral with respect to time

$$\int_0^t \Phi(\vec{q}, \dot{\vec{q}}, \tau) d\tau = C = cte. \quad (3.110)$$

All the constraints stated above define equalities. This means that in the dynamic context a force will always be needed to enforce the constraint. All three types of constraints can also be defined as inequalities. In this situation, there is a force only when the system is on the edge of the inequality. However, this section will not discuss this possibility and will focus on holonomic-skleronomic constraints which are the most common type of constraints found in mechanisms. For instance, in parallel mechanisms where the geometry of the mechanism must be respected. Furthermore, the constraints will be assumed to be smooth functions of the coordinates.

3.5.5 Forward Kinematic Map

The *forward kinematic map* of a mechanism is a vector function defining the spatial configuration (linear position & orientation) $\mathcal{C}_{0,e}$ of the end-effector, in terms of the kinematic coordinates \vec{q} with respect to the inertial frame \mathcal{R}_0 . One method of constructing the map is to define a kinematic chain between the carrier body and end-effector. The associated homogeneous transformation is defined using the same approach as in section 3.5.4.

$$X_{0,e} : \begin{pmatrix} \vec{x}_{0,e} \\ 1 \end{pmatrix} = \mathbf{H}_{e,0}(\vec{q}) \begin{pmatrix} \vec{x}_e \\ 1 \end{pmatrix}. \quad (3.111)$$

The kinematic pairs used to construct this map are called the independent kinematic pairs. The sub-index e relates to the end-effector frame. If the mechanism is non-holonomic, additional coordinates are added until all the remaining kinematic pairs can be expressed in terms of the kinematic coordinates using constraints, function of the coordinates. Thus, the kinematics of the mechanism are defined by the map (3.111) subject to a certain number of constraints.

Definition 8 (Forward Kinematic Map). *For a mechanism with D degrees of freedom, Q kinematic coordinates and $N_c = Q - D$ smooth holonomic-skleronomic constraints, the forward kinematic map is defined by:*

$$\begin{aligned} \Xi : \mathcal{Q} &\rightarrow \mathcal{W}, \\ \vec{q} &\mapsto \Xi(\vec{q}) = \mathcal{C}_{0,e} = (\vec{x}_{0,e}^T, \Upsilon_e^T)^T, \end{aligned} \quad (3.112)$$

$$\begin{aligned} \Phi_1(\vec{q}) &= 0, \\ &\vdots \\ \Phi_{N_p}(\vec{q}) &= 0. \end{aligned} \quad (3.113)$$

The end-effector point $X_{0,e}$ moves within the work space \mathcal{W} . This space is at most parameterised by the six coordinates $(\vec{x}_{0,e}^T, \Upsilon_e^T)^T = (x_e, y_e, z_e, \psi_e, \vartheta_e, \varphi_e)^T$. The number of independent coordinates describing $\mathcal{C}_{0,e}$ is D_e , the number of degrees of freedom of the end-effector.

Definition 9 (Work Space). *The work space \mathcal{W} of a mechanism is the end-effector's accessibility area.*

The works space is in general a subspace of one of the following five possibilities

- \mathbb{R} : a linear manipulator ($D_e = 1$),
- \mathbb{R}^2 : a planar manipulator ($D_e = 2$),
- $\mathbb{R}^2 \times SO(2)$: a planar manipulator with orientation ($D_e = 3$),

- \mathbb{R}^3 : spatial manipulator ($D_e = 3$),
- $\mathbb{R}^3 \times SO(2)$: spatial manipulator ($D_e = 4$),
- $\mathbb{R}^3 \times S^2$: spatial manipulator ($D_e = 5$),
- $\mathbb{R}^3 \times SO(3)$: spatial manipulator with orientation ($D_e = 6$).

All possible joint configurations constitutes the configuration space \mathcal{Q} . The structure of this space is defined by the type of independent kinematic pairs and the constraints. The workspace of the unconstrained mechanism \mathcal{Q}_{uc} is defined as the cross product of all the coordinate spaces associated to the independent kinematic pairs (cf. section 3.5.2). The configuration space of the constrained mechanism is a subset: $\mathcal{Q} \subset \mathcal{Q}_{uc}$. For a mechanism with D degrees of freedom, Q kinematic coordinates and $N_c = Q - D$ smooth constraints, the space \mathcal{Q} can in general be defined as a smooth manifold of dimension D embedded in \mathbb{R}^Q . Depending on the type of kinematic pair, the manifold is compact or not. If \mathcal{Q} is compact, the workspace is also compact given that the map is a smooth invertible map.

3.6 Multibody dynamics

The following sections present a mathematical refinement of classical mechanics for rigid bodies called analytical mechanics. For system's of rigid bodies, the classical Newtonian method of constructing the equations of motion is complex and requires defining the velocity and acceleration of each body as well as all the forces acting on them. In analytical mechanics, the equations of motion are derived from a single scalar function. This is called Lagrangian formalism of multibody dynamics. The presentation begins with the definition of virtual displacements. The principles of virtual work and power are presented and used to derive the Euler-Lagrange equation. The equation is defined for a system of bodies subject to forces, moments of force and holonomic constraints. The Euler-Lagrange equation is used to define the equations of motion for a system of rigid bodies. The section concludes with a small discussion of the principle of virtual work in the context of static equilibrium.

3.6.1 Analytical Mechanics and Virtual Displacements

Analytical mechanics extends the theory of classical mechanics using mathematical formalism. There are two essentially equivalent formalisms: Lagrangian formalism and Hamiltonian formalism that construct the equations of motion using a set of *generalised coordinates* \vec{k} . In the previous sections, the equations of motion of a single body were described using cartesian coordinates and rotational coordinates that are linear coordinates. Indeed, the coordinates describe the configuration of a body in $SE(3)$. The first three coordinates belong to \mathbb{R}^3 which is a linear space and Euler or Bryan angles define

charts between a subset of \mathbb{R}^3 and $SO(3)$. Therefore, the configuration of a free rigid body is defined by a vector belonging to a subset of \mathbb{R}^6 . Newton's and Euler's laws of mechanics are built from a linear description of space.

Analytical mechanics uses a more general description of space. In the previous section, the parameterisation of a mechanism's configuration was defined using a set of coordinates that were all either cartesian coordinates or rotational coordinates. The result was a forward kinematic map between the coordinates and the configuration of the end-effector subject to holonomic constraints. As stated in section 3.5.5, the coordinate space $\vec{q} \in \mathcal{Q}$ is in general defined as a smooth manifold of dimension D embedded in \mathbb{R}^Q . There were more coordinates than necessary. The manifold can be viewed as a surface in \mathbb{R}^Q in the same way a sphere is a surface in \mathbb{R}^3 . Just like the sphere, the manifold is a curved surface. Analytical mechanics allows one to use a set of coordinates that is more suited to the curved nature of the manifold. These coordinates are called generalised coordinates $\vec{\kappa}$. Thus, instead of using Q coordinates subject to $N_c = Q - D$ constraints, one can use $D \leq \hat{Q} \leq Q$ coordinates, directly incorporating all or part of the constraints into the parameterisation. The generalised coordinates are a curved description of space. However, the generalised coordinates must be consistent with the original description using Q coordinates. This consistency is defined through the concept of virtual displacement that will be presented subsequently.

The following discussion supposes that there are $D \leq \hat{Q} \leq Q$ generalised coordinates parameterising the configuration of a mechanism. The centre of gravity $X_{0,i}$ of a body \mathcal{B}_i in the mechanism is defined with respect to the inertial frame by a position vector, function of the generalised coordinates $\vec{x}_{0,i}(\vec{q})$.

$$X_{0,i} : \vec{x}_{0,i}(\vec{\kappa}) = \vec{d}_{0,i}(\vec{\kappa}) + \mathbf{R}_{i,0}(\vec{\kappa})\vec{x}_i, \quad \text{or} \quad \begin{pmatrix} \vec{x}_{0,i} \\ 1 \end{pmatrix} = \mathbf{H}_{0,i}(\vec{\kappa}) \begin{pmatrix} \vec{x}_i \\ 1 \end{pmatrix}. \quad (3.114)$$

The generalised coordinates are function of time and the total derivative of the position with respect to time is defined by:

$$\frac{D\vec{x}_{0,i}}{Dt} = \dot{\vec{x}}_{0,i} = \sum_{k=1}^{\hat{Q}} \frac{\partial \vec{x}_{0,i}}{\partial \kappa_k} \dot{\kappa}_k, \quad \vec{\kappa} = (\kappa_1, \dots, \kappa_k, \dots, \kappa_Q)^T. \quad (3.115)$$

The relation is multiplied by dt , the infinitesimal change in time, yielding the real infinitesimal change in position of the point.

$$d\vec{x}_{0,i} = \sum_{k=1}^{\hat{Q}} \frac{\partial \vec{x}_{0,i}}{\partial \kappa_k} d\kappa_k. \quad (3.116)$$

A virtual change in position or virtual displacement, is an infinitesimal change in position without an infinitesimal change in time.

$$\delta\vec{x}_{0,i} = \sum_{k=1}^{\hat{Q}} \frac{\partial \vec{x}_{0,i}}{\partial \kappa_k} \delta\kappa_k. \quad (3.117)$$

One of the main differences between a real infinitesimal displacement and a virtual one is that $d\vec{x}_{0,i}$ can be integrated along a path, $\delta\vec{x}_{0,i}$ cannot. Otherwise they are mathematically similar. One can also define the infinitesimal change in velocity.

$$\delta\dot{\vec{x}}_{0,i} = \sum_{k=1}^{\hat{Q}} \frac{\partial \dot{\vec{x}}_{0,i}}{\partial \kappa_k} \delta\kappa_k. \quad (3.118)$$

If the mechanism has constraints, both the real and virtual displacements must be compatible with them. This yields the following definition of virtual displacements.

Definition 10 (Virtual displacement). *A virtual displacement $\delta\vec{x}_{0,i}$ compatible with the kinematic coordinates $\vec{\kappa} = (\kappa_1, \dots, \kappa_k, \dots, \kappa_{\hat{Q}})^T$ is any displacement which can be imposed on the system satisfying the following*

$$\delta\vec{x}_{0,i} = \sum_{k=1}^{\hat{Q}} \frac{\partial \vec{x}_{0,i}}{\partial \kappa_k} \delta\kappa_k. \quad (3.119)$$

This equation is called the compatibility equation. The δq_k are solutions to the equations

$$\begin{aligned} \sum_{k=1}^{\hat{Q}} \frac{\partial \Phi_1}{\partial \kappa_k} \delta\kappa_k &= 0, \\ \vdots \\ \sum_{k=1}^{\hat{Q}} \frac{\partial \Phi_p}{\partial \kappa_k} \delta\kappa_k &= 0. \end{aligned} \quad (3.120)$$

The virtual displacements $\delta\vec{\kappa}$ are part of the null space of the matrix $[\frac{\partial \Phi_1}{\partial \vec{\kappa}}, \dots, \frac{\partial \Phi_p}{\partial \vec{\kappa}}]$.

The set of equations (3.120) will be referred to as the *consistency equations* and must be satisfied.

The virtual velocities are also solutions of (3.120). Given that the position of any point is defined by a displacement in terms of the kinematic coordinates, the velocity of any point on the mechanism is defined by:

$$\dot{\vec{x}}_{0,i} = \dot{\vec{d}}_{0,i} + \vec{\omega}_{0,i} \times \vec{x}_{0,i}^* = \frac{\partial \vec{d}_{0,i}}{\partial \vec{\kappa}} \dot{\vec{\kappa}} + \frac{\partial \vec{\omega}_{0,i}}{\partial \dot{\vec{\kappa}}} \dot{\vec{\kappa}} \times \vec{x}_{0,i}^*. \quad (3.121)$$

Thus, the virtual displacement is fully expressed by:

$$\delta\vec{x}_{0,i} = \delta\vec{d}_{0,i} + \frac{\partial \vec{\omega}_{0,i}}{\partial \dot{\vec{\kappa}}} \delta\dot{\vec{\kappa}} \times \vec{x}_{0,i}^* = \frac{\partial \vec{d}_{0,i}}{\partial \vec{\kappa}} \delta\vec{\kappa} + \frac{\partial \vec{\omega}_{0,i}}{\partial \dot{\vec{\kappa}}} \delta\dot{\vec{\kappa}} \times \vec{x}_{0,i}^* = \delta\vec{d}_{0,i} + \delta\vec{\omega}_{0,i} \times \vec{x}_{0,i}^*. \quad (3.122)$$

The virtual velocity is defined by:

$$\delta\dot{\vec{x}}_{0,i} = \frac{\partial \dot{\vec{x}}_{0,i}}{\partial \dot{\vec{\kappa}}} \delta\dot{\vec{\kappa}} = \frac{\partial \dot{\vec{d}}_{0,i}}{\partial \dot{\vec{\kappa}}} \delta\dot{\vec{\kappa}} + \frac{\partial \dot{\vec{\omega}}_{0,i}}{\partial \dot{\vec{\kappa}}} \delta\dot{\vec{\kappa}} \times \vec{x}_{0,i}^* = \delta\dot{\vec{d}}_{0,i} + \delta\dot{\vec{\omega}}_{0,i} \times \vec{x}_{0,i}^*, \quad (3.123)$$

Not the difference between $\delta_\kappa \vec{\omega}_{0,i}$ and $\delta \vec{\omega}_{0,i}$.

$$\delta \vec{\omega}_{0,i} = \frac{\partial \vec{\omega}_{0,i}}{\partial \dot{\vec{\kappa}}} \delta \dot{\vec{\kappa}}, \quad \delta_\kappa \vec{\omega}_{0,i} = \frac{\partial \vec{\omega}_{0,i}}{\partial \vec{\kappa}} \delta \vec{\kappa}. \quad (3.124)$$

There is also a virtual change in rotational acceleration

$$\delta \dot{\vec{\omega}}_{0,i} = \frac{\partial \dot{\vec{\omega}}_{0,i}}{\partial \dot{\vec{\kappa}}} \delta \dot{\vec{\kappa}}. \quad (3.125)$$

There are two important relations associated to the virtual displacements

$$\frac{\partial \vec{x}_{0,i}}{\partial \vec{\kappa}} = \frac{\partial \dot{\vec{x}}_{0,i}}{\partial \dot{\vec{\kappa}}}, \quad \frac{\partial \vec{\omega}_{0,i}}{\partial \vec{\kappa}} = \frac{\partial \dot{\vec{\omega}}_{0,i}}{\partial \dot{\vec{\kappa}}}. \quad (3.126)$$

It is also to be remarked that the virtual displacements $\delta \vec{d}_{0,i}$ and $\delta \vec{\omega}_{0,i}$ are independent. The same can be said for $\delta \dot{\vec{d}}_{0,i}$ and $\delta_\kappa \vec{\omega}_{0,i}$. Their dot product is always zero. Finally, the generalised coordinates $\vec{\kappa}$ are in many situations equivalent to the kinematic coordinates \vec{q} .

3.6.2 The Principles of Jourdain and d'Alembert

Analytical mechanics uses an energy based approach for constructing the equations of motion. There are three central theorems that are closely related. The first is Jourdain's principle of virtual power containing the classical equations of motion obtained in section 3.4.4 ((3.83), (3.84)). The second is d'Alembert's principle of virtual work on which the Lagrangian approach is founded. The third is Gauss's principle of least action used in the Hamiltonian approach. Like Euler's second law of motion, Gauss's principle is the most general theorem and allows for a system with time-varying energy. The following sections and paragraphs will present the first two theorems. Gauss's principle is beyond the scope of this presentation.

Theorem 15 (Jourdain's Principle of Virtual Power). *For a system of N_b rigid bodies, each with continuous mass distributions $\rho(\vec{z}_{0,i}^*)$, and where each body is subject to a system of N_f forces. The sum of the virtual powers produced by each system of forces is equal to the virtual power produced by the motion of each body*

$$\begin{aligned} & \sum_{i=1}^{N_b} \left(\delta \mathcal{P}_i - \int \rho(\vec{z}_{0,i}^*) \ddot{\vec{z}}_{0,i} \cdot \delta \vec{z}_{0,i} (d\vec{z}_{0,i}^*)^3 \right) = \\ & \sum_{i=1}^{N_b} \left(\sum_{j=1}^{N_f} \vec{f}_{0,j} \cdot \delta \dot{\vec{y}}_{0,i,j} - \int \rho(\vec{r}_{0,i}^*) \ddot{\vec{z}}_{0,i} \cdot \delta \vec{z}_{0,i} (d\vec{z}_{0,i}^*)^3 \right) = 0. \end{aligned} \quad (3.127)$$

where $\vec{z}_{0,i} = \vec{d}_{0,i} + \mathbf{R}_{0,i} \vec{z}_i = \vec{d}_{0,i} + \vec{z}_{0,i}^*$.

d'Alembert's principle of virtual work is very similar to Jourdain's principle but does not involve any integrals.

Theorem 16 (d'Alembert's Principle of Virtual Work). *For a system of N_b rigid bodies with constant mass, and where each body is subject to a system of N_f forces. The sum of the virtual works produced by each system of forces is equal to the sum of the virtual works produced by the motion of each body.*

$$\begin{aligned} & \sum_{i=1}^{N_b} \left(\delta \mathcal{W}_i - m_i \ddot{\vec{x}}_{0,i} \cdot \delta \vec{x}_{0,i} - (\mathcal{I}_{0,i} \dot{\vec{\omega}}_{0,i})^T \delta \vec{\omega}_{0,i} \right) = \\ & \sum_{i=1}^{N_b} \left(\sum_{j=1}^{N_f} \vec{f}_{0,j} \cdot \delta \vec{y}_{0,i,j} - m_i \ddot{\vec{x}}_{0,i} \cdot \delta \vec{x}_{0,i} - (\mathcal{I}_{0,i} \dot{\vec{\omega}}_{0,i})^T \delta \vec{\omega}_{0,i} \right) = 0. \end{aligned} \quad (3.128)$$

3.6.3 Principle of Virtual Power

Given Jourdain's principle of virtual power, the following equation holds for one of the bodies \mathcal{B}_i in a mechanism with N_b bodies subject to a system of N_f forces.

$$\sum_{k=1}^{N_f} \vec{f}_{0,i,k} \cdot \delta \dot{\vec{y}}_{0,i,k} - \int \rho(\vec{z}_{0,i}^*) \ddot{\vec{z}}_{0,i} \cdot \delta \dot{\vec{z}}_{0,i} (d\vec{z}_{0,i}^*)^3 = 0. \quad (3.129)$$

where $\vec{z}_{0,i} = \vec{d}_{0,i} + \mathbf{R}_{i,0} \vec{z}_i = \vec{d}_{0,i} + \vec{z}_{0,i}^*$ and $\delta \dot{\vec{y}}_{0,i,k}$ is the virtual displacement of the point of application of the force $\vec{f}_{0,i,k}$. The second term of this equation is expanded.

$$\begin{aligned} & \int \rho(\vec{z}_{0,i}^*) \ddot{\vec{z}}_{0,i} \cdot \delta \dot{\vec{z}}_{0,i} (d\vec{z}_{0,i}^*)^3 \\ &= \int \rho(\vec{z}_{0,i}^*) \ddot{\vec{z}}_{0,i} \cdot \left(\delta \dot{\vec{d}}_{0,i} + \delta_\kappa \vec{\omega}_{0,i} \times \vec{z}_{0,i}^* \right) (d\vec{z}_{0,i}^*)^3 =, \\ &= \int \rho(\vec{z}_{0,i}^*) \ddot{\vec{z}}_{0,i} \cdot \delta \dot{\vec{d}}_{0,i} (d\vec{z}_{0,i}^*)^3 + \int \rho(\vec{r}_{0,i}^*) \left(\vec{z}_{0,i}^* \times \ddot{\vec{z}}_{0,i} \right) \cdot \delta_\kappa \vec{\omega}_{0,i} (d\vec{z}_{0,i}^*)^3. \end{aligned} \quad (3.130)$$

Using the same development as in section 3.4.4 for the angular momentum yields the following expression.

$$\int \rho(\vec{z}_{0,i}^*) \ddot{\vec{z}}_{0,i} \cdot \delta \dot{\vec{z}}_{0,i} (d\vec{z}_{0,i}^*)^3 = m_i \ddot{\vec{x}}_{0,i} \cdot \delta \dot{\vec{d}}_{0,i} + \vec{l}_{0,i} \cdot \delta_\kappa \vec{\omega}_{0,i}. \quad (3.131)$$

As stated in section 3.6.1, the virtual displacements $\delta \dot{\vec{d}}_{0,i}$ and $\delta_\kappa \vec{\omega}_{0,i}$ are independent and therefore the equation can be separated into two parts. Jourdain's theorem for a

mechanism with N_b bodies subject to N_f forces is expressed by the following equation.

$$\sum_{i=1}^{N_b} \left(\sum_{k=1}^{N_f} \vec{f}_{0,j} \cdot \delta \dot{\vec{d}}_{0,i} + \sum_{k=1}^{N_f} \vec{y}_{0,i,k} \times \vec{f}_{0,i,k} \cdot \delta_\kappa \vec{\omega}_{0,i} - \int \rho(\vec{z}_{0,i}^*) \ddot{\vec{r}}_{0,i} \cdot \delta \dot{\vec{z}}_{0,i} (d\vec{z}_{0,i}^*)^3 \right) = \sum_{i=1}^{N_b} \left(\left(\sum_{k=1}^{N_f} \vec{f}_{0,i,k} - m_i \ddot{\vec{x}}_{0,i} \right) \cdot \delta \dot{\vec{d}}_{0,i} + \left(\sum_{k=1}^{N_f} \vec{y}_{0,i,k} \times \vec{f}_{0,i,k} - \dot{\vec{l}}_{0,i} \right) \cdot \delta_\kappa \vec{\omega}_{0,i} \right) = 0. \quad (3.132)$$

Given the independence of $\delta \dot{\vec{d}}_{0,i}$ and $\delta_\kappa \vec{\omega}_{0,i}$ yields.

$$\sum_{i=1}^{N_b} \left(\sum_{k=1}^{N_f} \vec{f}_{0,i,k} - m_i \ddot{\vec{x}}_{0,i} \right) \cdot \delta \dot{\vec{d}}_{0,i} = 0, \quad (3.133)$$

$$\sum_{i=1}^{N_b} \left(\sum_{k=1}^{N_f} \vec{y}_{0,i,k} \times \vec{f}_{0,i,k} - \dot{\vec{l}}_{0,i} \right) \cdot \delta_\kappa \vec{\omega}_{0,i} = 0. \quad (3.134)$$

The first equation is Newton's second law of motion for every body in the mechanism and the second equation is Euler's second law. Thus, the complete set of equations of motion of a rigid body or system of rigid bodies is contained within Jourdain's principle of virtual power.

3.6.4 The Euler-Lagrange Equation

The Euler-Lagrange equation defines the equations of motion of a rigid body or system of rigid bodies with respect to the generalised coordinates. It is constructed from d'Alembert's principle of virtual work. d'Alembert's principle of virtual work for one of the bodies \mathcal{B}_i in a mechanism with N_b bodies is stated by:

$$\delta \mathcal{W}_i - m_i \ddot{\vec{x}}_{0,i} \cdot \delta \vec{x}_{0,i} - (\mathcal{I}_{0,i} \dot{\vec{\omega}}_{0,i})^T \cdot \delta \vec{\omega}_{0,i} = 0, \quad (3.135)$$

where $\vec{x}_{0,i} = \vec{d}_{0,i} + \mathbf{R}_{i,0} \vec{x}_i = \vec{d}_{0,i} + \vec{x}_{0,i}^*$ is the position of the body's centre of gravity. The second and third terms of (3.135) are also expressed by:

$$m_i \dot{\vec{x}}_{0,i} \cdot \delta \vec{x}_{0,i} = \frac{d}{dt} \left(m_i \dot{\vec{x}}_{0,i} \delta \vec{x}_{0,i} \right) - m_i \dot{\vec{x}}_{0,i} \frac{d}{dt} (\delta \vec{x}_{0,i}) = \frac{d}{dt} \left(m_i \dot{\vec{x}}_{0,i} \delta \vec{x}_{0,i} \right) - m_i \dot{\vec{x}}_{0,i} \delta \dot{\vec{x}}_{0,i}, \quad (3.136)$$

$$(\mathcal{I}_{0,i} \dot{\vec{\omega}}_{0,i})^T \cdot \delta \vec{\omega}_{0,i} = \frac{d}{dt} \left(\vec{\omega}_{0,i}^T \mathcal{I}_{0,i} \delta \vec{\omega}_{0,i} \right) - \vec{\omega}_{0,i}^T \mathcal{I}_{0,i} \frac{d}{dt} (\delta \vec{\omega}_{0,i}) = \frac{d}{dt} \left(\vec{\omega}_{0,i}^T \mathcal{I}_{0,i} \delta \vec{\omega}_{0,i} \right) - \vec{\omega}_{0,i}^T \mathcal{I}_{0,i} \delta \dot{\vec{\omega}}_{0,i}, \quad (3.137)$$

The kinetic energy of the body is defined by:

$$\mathcal{E}_{K,i}(\vec{q}, \dot{\vec{q}}) = \frac{1}{2} m_i \dot{\vec{x}}_{0,i}^T \dot{\vec{x}}_{0,i} + \frac{1}{2} \vec{\omega}_{0,i}^T \mathcal{I}_{0,i} \vec{\omega}_{0,i}. \quad (3.138)$$

The two partial derivatives of the kinetic energy with respect to $\vec{\kappa}$ and $\dot{\vec{\kappa}}$ are defined by:

$$\frac{\partial \mathcal{E}_{K,i}}{\partial \vec{\kappa}} = m_i \dot{\vec{x}}_{0,i}^T \frac{\partial \dot{\vec{x}}_{0,i}}{\partial \vec{\kappa}} + \vec{\omega}_{0,i}^T \mathcal{I}_{0,i} \frac{\partial \vec{\omega}_{0,i}}{\partial \vec{\kappa}} = m_i \dot{\vec{x}}_{0,i}^T \frac{\partial \dot{\vec{x}}_{0,i}}{\partial \vec{\kappa}} + \vec{\omega}_{0,i}^T \mathcal{I}_{0,i} \frac{\partial \dot{\vec{\omega}}_{0,i}}{\partial \dot{\vec{\kappa}}}. \quad (3.139)$$

$$\frac{\partial \mathcal{E}_{K,i}}{\partial \dot{\vec{\kappa}}} = m_i \dot{\vec{x}}_{0,i}^T \frac{\partial \dot{\vec{x}}_{0,i}}{\partial \dot{\vec{\kappa}}} + \vec{\omega}_{0,i}^T \mathcal{I}_{0,i} \frac{\partial \vec{\omega}_{0,i}}{\partial \dot{\vec{\kappa}}} = m_i \dot{\vec{x}}_{0,i}^T \frac{\partial \vec{x}_{0,i}}{\partial \dot{\vec{\kappa}}} + \vec{\omega}_{0,i}^T \mathcal{I}_{0,i} \frac{\partial \vec{\omega}_{0,i}}{\partial \dot{\vec{\kappa}}}. \quad (3.140)$$

Using the relations between the virtual displacements stated in section 3.6.1 (3.126), d'Alembert's principle is expressed in terms of these two partial derivatives.

$$\sum_{i=1}^{N_b} \left(\delta \mathcal{W}_i - \frac{d}{dt} \left(\frac{\partial \mathcal{E}_{K,i}}{\partial \dot{\vec{\kappa}}} \cdot \delta \vec{\kappa} \right) - \frac{\partial \mathcal{E}_{K,i}}{\partial \vec{\kappa}} \cdot \delta \vec{\kappa} \right) = 0. \quad (3.141)$$

There are N_p non-conservative forces acting on the body and N_s conservative forces. The virtual work is defined with respect to the generalised coordinates by:

$$\begin{aligned} \delta \mathcal{W}_i &= \sum_{k=1}^{N_p} \vec{f}_{0,i,k} \cdot \delta \vec{y}_{0,i,k} - \sum_{k=1}^{N_s} \left(\frac{\partial h_{i,k}(\vec{x}_{0,i})}{\partial \vec{x}_{0,i}} \right)^T \cdot \delta \vec{x}_{0,i} \\ &= \sum_{k=1}^{N_p} \vec{f}_{0,i,k} \cdot \delta \vec{y}_{0,i,k} - \sum_{k=1}^{N_s} \left(\frac{\partial h_{i,k}(\vec{\kappa})}{\partial \vec{\kappa}} \right)^T \cdot \delta \vec{\kappa}. \end{aligned} \quad (3.142)$$

The second term is the partial derivative of the potential energy $\mathcal{E}_{P,i}$ of the body with respect to the generalised coordinates.

$$\delta \mathcal{W}_i = \sum_{j=k}^{N_p} \vec{f}_{0,i,k} \cdot \delta \vec{y}_{0,i,k} - \frac{\partial \mathcal{E}_{P,i}}{\partial \vec{\kappa}} \cdot \delta \vec{\kappa}. \quad (3.143)$$

The partial derivative of the potential energy with respect to $\dot{\vec{\kappa}}$ is equal to zero. Thus, the following statement holds for d'Alembert's principle.

$$\begin{aligned} &\sum_{i=1}^{N_b} \left(\delta \mathcal{W}_i - \frac{d}{dt} \left(\frac{\partial \mathcal{E}_{K,i}}{\partial \dot{\vec{\kappa}}} \right) \delta \vec{\kappa} - \frac{\partial \mathcal{E}_{K,i}}{\partial \vec{\kappa}} \delta \vec{\kappa} \right) =, \\ &\sum_{i=1}^{N_b} \left(\sum_{k=1}^{N_p} \vec{f}_{0,i,k} \cdot \delta \vec{y}_{0,i,k} - \frac{\partial \mathcal{E}_{P,i}}{\partial \vec{\kappa}} \cdot \delta \vec{\kappa} - \frac{d}{dt} \left(\frac{\partial \mathcal{E}_{K,i}}{\partial \dot{\vec{\kappa}}} - \underbrace{\frac{\partial \mathcal{E}_{P,i}}{\partial \dot{\vec{\kappa}}}}_{=0} \right) \cdot \delta \vec{\kappa} - \frac{\partial \mathcal{E}_{K,i}}{\partial \vec{\kappa}} \cdot \delta \vec{\kappa} \right) = 0. \end{aligned} \quad (3.144)$$

This last expression can be written using partial derivatives of a single scalar function called the Lagrangian. The Lagrangian function of a mechanism with N rigid bodies is defined by:

$$\mathcal{L}(\vec{\kappa}, \dot{\vec{\kappa}}) = \sum_{i=1}^{N_b} \left(\mathcal{E}_{K,i}(\vec{\kappa}, \dot{\vec{\kappa}}) - \mathcal{E}_{P,i}(\vec{\kappa}) \right). \quad (3.145)$$

The virtual displacement $\delta \vec{y}_{0,i,k}$ is expressed differently using the same approach as (3.136).

$$\delta \vec{y}_{0,i,k} = \delta \vec{d}_{0,i} + \delta \vec{\omega}_{0,i} \times \vec{y}_{0,i,k}^* = \frac{\partial \vec{d}_{0,i}}{\partial \vec{\kappa}} \cdot \delta \vec{\kappa} + \frac{\partial \vec{\omega}_{0,i}}{\partial \dot{\vec{\kappa}}} \cdot \delta \dot{\vec{\kappa}} \times \vec{y}_{0,i,k}^*. \quad (3.146)$$

Using this expression in (3.144) yields the Euler-Lagrange equation of a mechanism with N_b bodies and N_p non-conservative forces without any constraints.

$$\frac{d}{dt} \left(\frac{\partial \mathcal{L}}{\partial \dot{\vec{\kappa}}} \right) - \frac{\partial \mathcal{L}}{\partial \vec{\kappa}} = \sum_{i=1}^{N_b} \left(\sum_{k=1}^{N_p} \left(\frac{\partial \vec{d}_{0,i}}{\partial \vec{\kappa}} \right)^T \cdot \vec{f}_{0,i,k} + \left(\frac{\partial \vec{\omega}_{0,i}}{\partial \dot{\vec{\kappa}}} \right)^T \cdot \left(\vec{y}_{0,i,k}^* \times \vec{f}_{0,i,k} \right) \right). \quad (3.147)$$

The first term of the left hand side of this equation is expanded yielding the equations of motion in terms of $\vec{\kappa}$, $\dot{\vec{\kappa}}$ and $\ddot{\vec{\kappa}}$.

Definition 11. (*Euler-Lagrange Equation*) For a system of N_b bodies parameterised by a vector of \hat{Q} generalised coordinates $\vec{\kappa}$, subject to N_p conservative forces and no constraints, the Euler-Lagrange equation is defined by:

$$\frac{\partial^2 \mathcal{L}}{\partial \dot{\vec{\kappa}}^2} \ddot{\vec{\kappa}} + \frac{\partial^2 \mathcal{L}}{\partial \vec{\kappa} \partial \dot{\vec{\kappa}}} \dot{\vec{\kappa}} - \frac{\partial \mathcal{L}}{\partial \vec{\kappa}} = \sum_{i=1}^{N_b} \left(\sum_{k=1}^{N_p} \left(\frac{\partial \vec{d}_{0,i}}{\partial \vec{\kappa}} \right)^T \cdot \vec{f}_{0,i,k} + \left(\frac{\partial \vec{\omega}_{0,i}}{\partial \dot{\vec{\kappa}}} \right)^T \cdot \left(\vec{y}_{0,i,k}^* \times \vec{f}_{0,i,k} \right) \right). \quad (3.148)$$

In this definition of the Euler-Lagrange equation, the matrices $\left(\frac{\partial \vec{d}_{0,i}}{\partial \vec{\kappa}} \right)^T$ and $\left(\frac{\partial \vec{\omega}_{0,i}}{\partial \dot{\vec{\kappa}}} \right)^T$ require further explanation. The vector $\vec{d}_{0,i}$ is the linear translation vector of the centre of the reference frame \mathcal{R}_i with respect to the inertial frame. The vector $\vec{\omega}_{0,i}$ is the instantaneous rotational velocity vector of the reference frame \mathcal{R}_i with respect to the inertial frame. Taking the partial derivatives with respect to the generalised coordinates and their first derivatives generates two matrix. Both are $\hat{Q} \times 3$ matrices. If the rotational coordinates are global coordinates, the second matrix $\left(\frac{\partial \vec{\omega}_{0,i}}{\partial \dot{\vec{\kappa}}} \right)^T$ has a very particular structure. Recall in section 3.3.3 that the instantaneous rotational velocity of a body can be expressed in the following form:

$$\vec{\omega}_{0,i} = \frac{\partial \vec{\omega}_{0,i}}{\partial \dot{\vec{\Upsilon}}_i} \dot{\vec{\Upsilon}}_i = \mathbf{W}_{0,i} \dot{\vec{\Upsilon}}_i, \quad \text{where} \quad \vec{\Upsilon}_i = (\psi_i \quad \vartheta_i \quad \varphi_i)^T. \quad (3.149)$$

The rotational coordinate vector $\vec{\Upsilon}_i$ uses global coordinates. If the same coordinates are used to define the generalised coordinates, the partial derivative takes the following form:

$$\left(\frac{\partial \vec{\omega}_{0,i}}{\partial \dot{\vec{\kappa}}} \right)^T = \begin{pmatrix} \vec{0} \\ \mathbf{W}_{0,i}^T \\ \vec{0} \end{pmatrix}. \quad (3.150)$$

The only part that is not zero is the 3×3 matrix $\mathbf{W}_{0,i}^T$. If all the rotational coordinates are global the following expression holds. The moment of force component of the generalised forces can be expressed in matrix form.

$$\sum_{i=1}^{N_b} \left(\sum_{k=1}^{N_p} \left(\frac{\partial \vec{\omega}_{0,i}}{\partial \dot{\vec{\kappa}}} \right)^T \cdot \left(\vec{y}_{0,i,k}^* \times \vec{f}_{0,i,k} \right) \right) = \underbrace{\begin{pmatrix} \mathbf{W}_{0,1}^T & \vec{0} & \dots & \vec{0} \\ \vec{0} & \ddots & & \vdots \\ \vdots & & \ddots & \vec{0} \\ \vec{0} & \dots & \vec{0} & \mathbf{W}_{0,N_b}^T \end{pmatrix}}_{\tilde{\mathbf{W}}_0} \left(\sum_{k=1}^{N_p} \left(\vec{y}_{0,1,k}^* \times \vec{f}_{0,1,k} \right) \quad \dots \quad \sum_{k=1}^{N_p} \left(\vec{y}_{0,N_b,k}^* \times \vec{f}_{0,N_b,k} \right) \right). \quad (3.151)$$

If the mechanism is subject to holonomic constraints, they must be added to the equations. Consider a mechanism with N_c holonomic constraints. The constraints are defined by:

$$\Phi_j(\vec{\kappa}) = 0. \quad j = 1, \dots, N_c \quad (3.152)$$

In this situation, the equations of motion are constructed from the augmented lagrange function [89].

$$\tilde{\mathcal{L}} = \mathcal{L} + \sum_{j=1}^{N_c} \lambda_j \Phi_j(\vec{\kappa}) = \mathcal{L} + \vec{\Phi}^T(\vec{\kappa}) \cdot \vec{\lambda}. \quad (3.153)$$

The scalars λ_j are called the lagrangian multipliers. This result originates from the following reasoning. A holonomic-skleronomic constraint $\Phi_j(\vec{\kappa})$ is a smooth function of the \hat{Q} generalised coordinates $\vec{\kappa}$. In most cases, the equality (3.156) defines a smooth manifold of dimension $\hat{Q} - 1$ embedded in $\mathbb{R}^{\hat{Q}}$. As stated previously in section 3.6.1, such a manifold can be viewed as a surface. Inserting the augmented lagrangian into the Euler-Lagrange equation yields the following:

$$\frac{d}{dt} \left(\frac{\partial \tilde{\mathcal{L}}}{\partial \dot{\vec{\kappa}}} \right) - \frac{\partial \tilde{\mathcal{L}}}{\partial \vec{\kappa}} = \frac{d}{dt} \left(\frac{\partial \mathcal{L}}{\partial \dot{\vec{\kappa}}} \right) - \frac{\partial \mathcal{L}}{\partial \vec{\kappa}} - \left(\frac{\partial \vec{\Phi}}{\partial \vec{\kappa}} \right). \quad (3.154)$$

The partial derivative $\nabla_{\vec{\kappa}} \vec{\Phi}$ can be viewed as the force vectors which are normal to the manifold surfaces of each constraint. Just like a bead on wire, constraints apply forces on the system to keep the system on the constraint manifold surface. The lagrangian multiplier is thus an intensity factor of sorts. Thus, the equations of motion for a mechanism with N_b bodies, N_p non conservative forces and N_c constraints are defined by:

$$\frac{\partial^2 \mathcal{L}}{\partial \dot{\vec{\kappa}}^2} \ddot{\vec{\kappa}} + \frac{\partial^2 \mathcal{L}}{\partial \vec{\kappa} \partial \dot{\vec{\kappa}}} \dot{\vec{\kappa}} - \frac{\partial \mathcal{L}}{\partial \vec{\kappa}} = \sum_{i=1}^{N_b} \left(\sum_{k=1}^{N_p} \left(\frac{\partial \vec{d}_{0,i}}{\partial \dot{\vec{\kappa}}} \right)^T \cdot \vec{f}_{0,i,k} + \left(\frac{\partial \vec{\omega}_{0,i}}{\partial \dot{\vec{\kappa}}} \right)^T \cdot \left(\vec{y}_{0,i,k}^* \times \vec{f}_{0,i,k} \right) \right) + \sum_{j=1}^{N_c} \lambda_j \left(\frac{\partial \Phi_j}{\partial \vec{\kappa}} \right)^T. \quad (3.155)$$

The Lagrange approach to rigid body dynamics is very systematic and efficient. In comparison to the Newtonian approach, this method yields only information on the dynamics of the system. The contact forces in the joints are unknown because the principle of virtual work has directly incorporated them into the Lagrangian. Thus, the Newtonian and Lagrange approaches to rigid body dynamics can be seen as complementary.

3.6.5 The Principle of Virtual Work and Static Equilibrium

Static equilibrium represents a special case of rigid body dynamics. A body is in *static equilibrium* when the left hand sides of (3.83) and (3.84) are zero. The body is either stationary or moving at a constant velocity. For a system of N_b rigid bodies, the following conditions are both necessary and sufficient.

$$\sum_{i=1}^{N_b} \vec{f}_{0,i} = \vec{0}, \quad \sum_{i=1}^N \vec{y}_{0,i} \times \vec{f}_{0,i} = \vec{0}. \quad (3.156)$$

Although trivial in the case of a single rigid body, these equations are essential in analysing the forces within a mechanism in static equilibrium. Both these equations provide the means of computing the forces applied to a single rigid body or to a system of rigid bodies at equilibrium. Given a mechanism, each body is in turn isolated from the others and all the forces acting on it are modelled and the body's equilibrium is expressed in terms of eq. (3.156). This procedure requires the modelling of forces acting on the body in question due to its interaction with the other bodies. This method analyses the equilibrium of a mechanical system in terms of forces and moments of forces. Therefore the equilibrium position must be known a priori.

In many mechanical systems, there can be multiple equilibrium points and the approach described above does not apply directly. The principle of virtual work provides an alternate method of analysing static equilibrium. At equilibrium, the principle is reduced to

Theorem 17 (Principle of virtual work for Static Equilibrium). *At equilibrium the sum of all the virtual works produced by external forces on a rigid body is zero.*

$$\delta \mathcal{W} = \sum_{i=1}^{N_p} \vec{f}_{0,i} \cdot \delta \vec{y}_{0,i} - \frac{\partial \mathcal{E}_P}{\partial \vec{\kappa}} \cdot \delta \vec{\kappa} = 0. \quad (3.157)$$

If the system is only subject to conservative forces, the principle of virtual work means that any virtual change in potential energy is zero. Thus, we have the following statements. An equilibrium exists if

$$\frac{\partial \mathcal{E}_P}{\partial \vec{\kappa}} = 0. \quad (3.158)$$

The equilibrium is stable if

$$\frac{\partial^2 \mathcal{E}_P}{\partial \vec{\kappa}^2} > 0, \quad (3.159)$$

otherwise it is unstable. For conservative systems, the principle of virtual work helps identify the stable equilibrium points. Once identified, the force analysis can be applied for each equilibrium point.

Chapter 4

A Musculoskeletal Model of the Human Shoulder

4.1 Introduction

The shoulder is the most complex joint in the human body with the widest range of motion (Guinness World Records 2006). It is therefore a challenging system to model. Several models of the shoulder have been developed over the years with varying degrees of complexity depending on their purpose. The Delft shoulder and elbow model (DSEM), developed for clinical purposes such as muscle and joint force estimation [156, 194]. The Swedish model developed for muscle and joint force estimation [114, 138]. The model is based on a previous model [103, 104]. The CHARM model, designed for virtual reality purposes [142]. The kinematic Visible Human Project (VHP) model constructed for analysing forces and joint torques in the upper limb [74, 76]. The dynamic Visible Human Project model constructed for force estimation through inverse dynamics [170]. The human body model of the AnyBody software also contains a shoulder model [49, 129]. The Stanford model, available in opensim¹ and developed for simulating musculoskeletal surgery [101, 200] and the Newcastle model developed for estimating glenohumeral joint forces [37]. There are a number of other models which have been reviewed in the literature [168, 219].

Although all the models listed above are different, they are all constructed using the same three principles. The first principle is that the bones in the skeletal system behave like rigid bodies in a mechanism [53]. The second principle is that articulations behave like ideal mechanical joints without play or friction. The joints in the shoulder behave like spherical joints [61, 62]. The third principle is that muscles are ideal cables, modelled by one or more massless, frictionless cable(s), spanning from origin to insertion like a pulley [108, 197]. As the skeletal system moves, the cables change length and remain perfectly taut. The cable's overall effect is represented by a system of forces [166]. The muscle

¹Opensim is the free version of the SIMM musculoskeletal modelling software.

cables are either straight lines or they wrap over regular surfaces, such as spheres and cylinders, representing the muscle's anatomical constraints. Under these three principles, shoulder models fall into the domain of multibody systems and are governed by the laws of general mechanics. A musculoskeletal model is a mechanism according to the definition given in chapter 3.

Many of the musculoskeletal models listed in the first paragraph are developed and designed for clinical applications such as estimating muscle and joint forces. As such, they are in general presented in the context of their clinical application. The presentation focuses on the model's ability to represent reality by comparing certain model estimated quantities with measured quantities such as moment-arms and muscle forces. Clinical validation of musculoskeletal models is essential [135]. A musculoskeletal model must be able to predict the behaviour of the real healthy system before it can be used to study its dysfunctions. However, clinical validation of a musculoskeletal model can only be achieved once the model has been mathematically validated. A presentation in the context of multibody systems is deemed to be as important for such models to be accurately reconstructed and validated by others. Therefore, the goal of this chapter is to present a musculoskeletal model of the human shoulder in the context of multibody systems, giving each element of the model a detailed mathematical description. Its ability to predict real shoulder behaviour will be discussed in chapter 8.

The model contains kinematic and dynamic sub-models, includes all 16 muscles of the shoulder divided into 28 parts and a model of the scapulothoracic contact. The model was built using the same framework as the VHP model [74, 76] but does not contain a model of the entire upper limb. The upper limb is considered to remain outstretched. The model's kinematics are parameterised in terms of Euler and Bryan angles using the spherical model of anatomical articulations [214]. The dynamic model is constructed using rigid-body mechanics. The muscles are modelled as one or more ideal cables, wrapping over the skeletal structure. The muscle model considers the effect of each cable on the dynamic model but does not consider the muscle's internal behaviour. The chapter ends with a discussion of the model's mathematical structure, showing it to be similar to models of cable-driven robots.

This chapter is structured as follows. Section 4.2 describes the kinematic model including the scapulothoracic contact model and forward kinematic map. Section 4.3 describes the dynamic model and defines the equations of motion. The muscle cable model and its contribution to the dynamic model is also presented. Section 4.4 reviews the model's structure and section 4.4 concludes the chapter.

4.2 Kinematic Shoulder Model

This section describes a musculoskeletal model of an adult male's right shoulder [60]. The bones are considered to be rigid bodies. The articulations are considered to be ideal mechanical joints. The muscles are considered to be massless, frictionless, elastic cables, wrapping over the bones. The model is presented in four parts. The first part describes

the model's kinematic parameterisation. The second part describes the model's dynamics in terms of the equations of motion. The third and fourth parts describe the muscle cable model in terms of its contribution to the dynamic model and in terms of its geometric characteristics. The model is constructed using the kinematic VHP shoulder model as a canvas [74, 76]. The model presented in this chapter and the VHP model share the same muscle wrapping geometry but with different numerical implementations.

4.2.1 Bony Landmarks and Reference Frames

The kinematic model parameterises the movement of each of the three bones in the shoulder relative to the thorax which is fixed. Movement is understood as the change of a body's spatial configuration over time. A rigid body's configuration is defined as the location of a point on the body and its orientation in space. At least three points are needed to define a body's spatial configuration (cf. chapter 3). Therefore, the kinematic model is constructed by reducing each bone to a set of three geometric points. The kinematic model parameterises the movement of these points which are the nine points defined in the following list (Fig. 4.1):

1. CR : Clavicle reference point (Clavicle configuration: point 1),
2. SC : Center of Sternoclavicular articulation (Clavicle configuration: point 2),
3. AC : Center of Acromioclavicular articulation (Clavicle configuration: point 3),
4. AA : Angulus acromialis (Scapula configuration: point 1),
5. TS : Trigonum Spinae (Scapula configuration: point 2),
6. AI : Angulus Inferior (Scapula configuration: point 3),
7. GH : Center of Glenohumeral articulation (Humerus configuration: point 1),
8. EL : Lateral epicondyle of the humerus (Humerus configuration: point 2),
9. EM : Medial epicondyle (Humerus configuration: point 3).

The first point is a fictional point located directly above the centre of the sternoclavicular articulation. This is necessary to complete the description of the clavicle's configuration with respect to the axial rotation around the $SC - AC$ axis. The eight other points represent the geometric location of bony landmarks. The fixed reference frame is constructed using four bony landmarks on the thorax. The first landmark defines the origin of the fixed reference frame.

1. IJ : Jugular Incision at the top of the sternum,
2. PX : Xyphoid process at the bottom of the sternum,
3. T8 : Eighth thoracic vertebrae,
4. C7 : Seventh cervical vertebrae.

To construct this model, the geometric position of all these points is needed for a given position of the bones. This data was collected using MRI scans of a human male's shoulder and constitutes the skeletal model's geometric dataset [60]. The same MRI scans were also used to obtain the muscle geometry discussed subsequently.

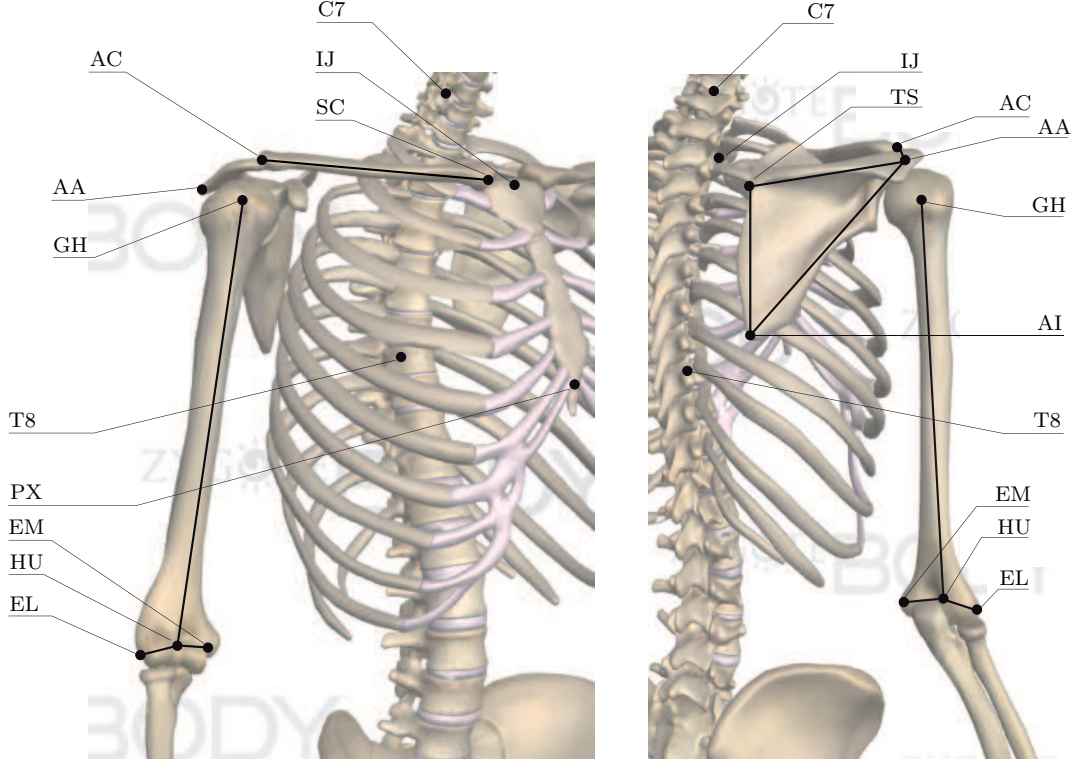


Figure 4.1: *Illustration of the bony landmarks used to construct the geometric model as described in section 4.2.1. Image created using ZygoteBody™ zygotebody.com.*

A set of four reference systems are used to define the orientation of each bone. These reference systems are constructed following the guide lines set by the International Society of Biomechanics (ISB) [214]. As defined in chapter 3, a subindex is attributed to each reference frame² ($\mathbf{i}_i, \mathbf{j}_i, \mathbf{k}_i, i = 0, 1, 2, 3$) (Fig. 4.2). The thorax is defined as the carrier body and is attributed the subindex 0.

• **Thorax Reference System \mathcal{R}_0 ($\mathbf{i}_0, \mathbf{j}_0, \mathbf{k}_0$):**

- Centre: $IJ \equiv O_0$,
- x -axis (\mathbf{i}_0): normal to the plane defined by $IJ, C7, \frac{1}{2}(T8 + PX) - IJ$, pointing to the right,
- y -axis (\mathbf{j}_0): normal to the x and z axes, pointing forwards,

²Notation: Geometric points are defined by plane upper case lettres. Their vector position with respect to the centre of a reference frame is defined by a plane lower case lettre with an arrow and the subindex associated with the reference frame. A matrix is defined by a bold upper case letter. Plane lower case letters with subindexes x, y or z define a vector's coordinates. The three bold lower case lettres $\mathbf{i}_i, \mathbf{j}_i, \mathbf{k}_i$ are the unit vectors of a reference frame.

- z -axis (\mathbf{k}_0): parallel to the line between the points $P_1 = \frac{1}{2}(PX + C7)$ and $P_2 = \frac{1}{2}(T8 + IJ)$.
- **Clavicle Reference System \mathcal{R}_1 ($\mathbf{i}_1, \mathbf{j}_1, \mathbf{k}_1$):**
 - Centre: $SC \equiv O_1$,
 - x -axis (\mathbf{i}_1): parallel to the line defined by SC and AC , pointing to the right,
 - y -axis (\mathbf{j}_1): normal to the plane defined by \mathbf{i}_1 and \mathbf{k}_0 , pointing forwards,
 - z -axis (\mathbf{k}_1): normal to the x and y axes, pointing upwards.
- **Scapula Reference System \mathcal{R}_2 ($\mathbf{i}_2, \mathbf{j}_2, \mathbf{k}_2$):**
 - Centre: $AC \equiv O_2$,
 - x -axis (\mathbf{i}_2): parallel to the line defined by TS and AA , pointing to the right.
 - y -axis (\mathbf{j}_2): normal to the plane defined by \mathbf{i}_2 and $AI - TS$ axes, pointing forwards,
 - z -axis (\mathbf{k}_2): normal to the x and y axes, pointing upwards.
- **Humerus Reference System \mathcal{R}_3 ($\mathbf{i}_3, \mathbf{j}_3, \mathbf{k}_3$):**
 - Centre: $GH \equiv O_3$,
 - x -axis (\mathbf{i}_3): normal to the y and z axes, pointing to the right,
 - y -axis (\mathbf{j}_3): normal to the plane defined by GH , EL and EM , pointing forwards,
 - z -axis (\mathbf{k}_3): parallel to the line between the points $P_1 = \frac{1}{2}(EL + EM)$ and $P_2 = GH$.

The orientations of the reference frames are equivalent to the recommendations set by the ISB but with a 90° clockwise rotation around the x -axis. In the model presented in this chapter, the x -axis of the inertial frame \mathcal{R}_0 points laterally to the right, the y -axis points forwards and the z -axis points upwards. In the ISB recommendations, the x -axis points lateral to the right, the y -axis points upwards and the z -axis points backwards. Both descriptions are consistent with each other. Two reference systems are consistent if their axes are parallel. They are identical if the unit vectors have same direction. The direction of the unit vectors used in this model are a more natural description of space. The plane is defined by the $x - y$ axes and the vertical direction is parameterised by the z axis. Lastly, the scapula's reference frame is placed at the acromioclavicular joint centre and not the point AA . In the dynamic model, the moments of force are defined with respect to the reference frame centre. Therefore, it is better to place the reference frames at the joint centres.

4.2.2 Joint Angle Parameterisation of the Model's Kinematics

In real musculoskeletal systems, each bone's movement is mostly defined by its articulations with other bones. Therefore, parameterisation of each articulation's motion is a natural choice to parameterise a musculoskeletal model's motion. In the shoulder model, the three articulations are modelled as ideal ball and socket joints. A ball and socket joint

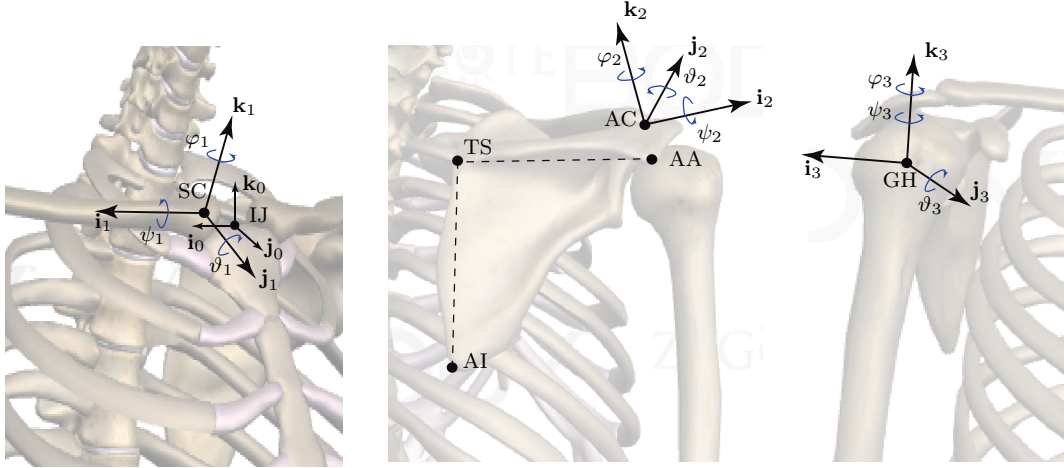


Figure 4.2: Illustration of joint coordinates and reference systems as described in sections 4.2.1 and 4.2.2. Left to right, thorax, clavicle, scapula and humerus reference frames. Image created using ZygoteBodyTM zygotebody.com.

is the mechanical equivalent of the spherical kinematic pair. Possible parameterisations of the spherical pair include Euler or Bryan angles (cf. chapter 3.5.2). The sternoclavicular and acromioclavicular spherical pairs are parameterised using Bryan angles. The rotation sequences are defined as X-Y-Z. The glenohumeral spherical pair is parameterised using Euler angles. The rotation sequence is defined as Z-Y-Z. These angles and sequences are based on the ISB guide lines [214]. Thus, each articulation is modelled as a spherical kinematic pair, parameterised by a set of three coordinates angular coordinates.

$$\vec{\Upsilon}_i = (\psi_i \quad \vartheta_i \quad \varphi_i)^T, \quad i = 1, 2, 3. \quad (4.1)$$

As stated in chapter 3, these angles also parameterise each bone's orientation. Using the definitions from chapter 3, the sternoclavicular coordinates $\vec{\Upsilon}_1$ are thoraco-clavicular angles and parameterise the clavicle's orientation. The acromioclavicular coordinates $\vec{\Upsilon}_2$ are scapulo-thoracic angles and parameterise the scapula's orientation. The glenohumeral coordinates $\vec{\Upsilon}_3$ are thoraco-humeral angles and parameterise the humerus's orientation. The three angular coordinates of $\vec{\Upsilon}_i$ are all equal to zero when the reference frame \mathcal{R}_i is aligned with the thorax or inertial frame \mathcal{R}_0 .

The Euclidean displacements which transform points defined in a bone's reference frame \mathcal{R}_i into a points defined in the thorax reference frame \mathcal{R}_0 are defined by:

$$P_{0,1} : \vec{p}_{0,1} = \vec{d}_{0,1} + \mathbf{R}_{1,0}\vec{p}_1, \quad (4.2)$$

$$P_{0,2} : \vec{p}_{0,2} = \vec{d}_{0,2} + \mathbf{R}_{2,0}\vec{x}_2 = \vec{d}_{0,1} + \mathbf{R}_{1,0}\vec{z}_1 + \mathbf{R}_{2,0}\vec{p}_2, \quad (4.3)$$

$$P_{0,3} : \vec{p}_{0,3} = \vec{d}_{0,3} + \mathbf{R}_{3,0}\vec{x}_3 = \vec{d}_{0,1} + \mathbf{R}_{1,0}\vec{z}_1 + \mathbf{R}_{2,0}\vec{z}_2 + \mathbf{R}_{3,0}\vec{p}_3. \quad (4.4)$$

The vectors $\vec{d}_{0,i}$, \vec{z}_1 , \vec{z}_2 and \vec{w}_2 parameterise the following geometric elements of the model.

- $\vec{d}_{0,1}$ Vector from IJ to SC in \mathcal{R}_0 .
- $\vec{d}_{0,2}$ Vector from IJ to AC in \mathcal{R}_0 . Also expressed by $\vec{d}_{0,2} = \vec{d}_{0,1} + \mathbf{R}_{1,0}\vec{z}_1$.

- $\vec{d}_{0,3}$ Vector from IJ to GH in \mathcal{R}_0 . Also expressed by $\vec{d}_{0,3} = \vec{d}_{0,1} + \mathbf{R}_{1,0}\vec{z}_1 + \mathbf{R}_{2,0}\vec{z}_2$.
- \vec{z}_1 Vector from SC to AC in \mathcal{R}_1 .
- \vec{z}_2 Vector from AC to GH in \mathcal{R}_2 .

The rotation matrices are defined by:

$$\text{Clavicle: } \mathbf{R}_{1,0} = \mathbf{R}_{z,1}\mathbf{R}_{y,1}^T\mathbf{R}_{x,1}, \quad (4.5)$$

$$\mathbf{R}_{x,1} = \begin{pmatrix} 1 & 0 & 0 \\ 0 & \cos(\psi_1) & -\sin(\psi_1) \\ 0 & \sin(\psi_1) & \cos(\psi_1) \end{pmatrix}, \quad \mathbf{R}_{y,1} = \begin{pmatrix} \cos(\vartheta_1) & 0 & -\sin(\vartheta_1) \\ 0 & 1 & 0 \\ \sin(\vartheta_1) & 0 & \cos(\vartheta_1) \end{pmatrix}, \quad \mathbf{R}_{z,1} = \begin{pmatrix} \cos(\varphi_1) & -\sin(\varphi_1) & 0 \\ \sin(\varphi_1) & \cos(\varphi_1) & 0 \\ 0 & 0 & 1 \end{pmatrix},$$

$$\text{Scapula: } \mathbf{R}_{2,0} = \mathbf{R}_{z,2}\mathbf{R}_{y,2}^T\mathbf{R}_{x,2}, \quad (4.6)$$

$$\mathbf{R}_{x,2} = \begin{pmatrix} 1 & 0 & 0 \\ 0 & \cos(\psi_2) & -\sin(\psi_2) \\ 0 & \sin(\psi_2) & \cos(\psi_2) \end{pmatrix}, \quad \mathbf{R}_{y,2} = \begin{pmatrix} \cos(\vartheta_2) & 0 & -\sin(\vartheta_2) \\ 0 & 1 & 0 \\ \sin(\vartheta_2) & 0 & \cos(\vartheta_2) \end{pmatrix}, \quad \mathbf{R}_{z,2} = \begin{pmatrix} \cos(\varphi_2) & -\sin(\varphi_2) & 0 \\ \sin(\varphi_2) & \cos(\varphi_2) & 0 \\ 0 & 0 & 1 \end{pmatrix},$$

$$\text{Humerus: } \mathbf{R}_{3,0} = \mathbf{R}_{z',3}\mathbf{R}_{y,1}^T\mathbf{R}_{z,3}, \quad (4.7)$$

$$\mathbf{R}_{z,3} = \begin{pmatrix} \cos(\psi_3) & -\sin(\psi_3) & 0 \\ \sin(\psi_3) & \cos(\psi_3) & 0 \\ 0 & 0 & 1 \end{pmatrix}, \quad \mathbf{R}_{y,3} = \begin{pmatrix} \cos(\vartheta_3) & 0 & -\sin(\vartheta_3) \\ 0 & 1 & 0 \\ \sin(\vartheta_3) & 0 & \cos(\vartheta_3) \end{pmatrix}, \quad \mathbf{R}_{z',3} = \begin{pmatrix} \cos(\varphi_3) & -\sin(\varphi_3) & 0 \\ \sin(\varphi_3) & \cos(\varphi_3) & 0 \\ 0 & 0 & 1 \end{pmatrix}.$$

4.2.3 Scapulothoracic Contact Model

The present model includes the scapulothoracic contact using an ellipsoid model. Other shoulder models which include the scapulothoracic contact constraint one or two points on the scapula to remain at a constant distance from the surface of a single ellipsoid. Single-point models use the mid point on the scapula's medial border $(TS + AI)/2$ [58, 142]. Double-point models use the points TS and AI [74, 194]. In single or double-point models, the ellipsoid represents the curved surface of the ribcage and the additional fixed distance represents the layer of muscle tissue between the ribcage and scapula (Fig. 4.3 (a)). The ellipsoid is constructed to best fit the ribcages's surface obtained from CT scans [74]. For example, in a double-point model, the points TS and AI are projected onto the ellipsoid along the normal to its surface, yielding two new points TS_p and AI_p . The distance constraint defines two holonomic scleronomic constraints. The points are defined in the ellipsoid frame (the subindex 4 indicates the ellipsoid frame \mathcal{R}_4).

$$\begin{aligned} \Phi_{TS}(\vec{\Upsilon}_1, \vec{\Upsilon}_2) &= \|\vec{u}_{4,2} - \vec{u}_{4,2,p}\|_2 - c_1 = 0, & TS_{4,2} : \vec{u}_{4,2} &= \mathbf{R}_{0,4}(\vec{d}_{0,2} + \mathbf{R}_{2,0}\vec{u}_2) \\ \Phi_{AI}(\vec{\Upsilon}_1, \vec{\Upsilon}_2) &= \|\vec{v}_{4,2} - \vec{v}_{4,2,p}\|_2 - c_2 = 0, & AI_{4,2} : \vec{v}_{4,2} &= \mathbf{R}_{0,4}(\vec{d}_{0,2} + \mathbf{R}_{2,0}\vec{v}_2). \end{aligned} \quad (4.8)$$

The double subindex $(4, 2)$ on TS and AI indicates the points are defined in the ellipsoid frame \mathcal{R}_4 but are related to the scapula and its frame \mathcal{R}_2 .

In the shoulder model presented in this chapter, the scapulothoracic contact is modelled as a double-point model but differs from other models in that the points TS and AI are constrained to remain on the surface of two separate ellipsoids (Fig. 4.3 (b)). The scapulothoracic contact model used in the musculoskeletal model of the shoulder presented in this chapter is different from other double-point models [74, 194] in that it uses two separate ellipsoids rather than a single ellipsoid. Both ellipsoids have the same

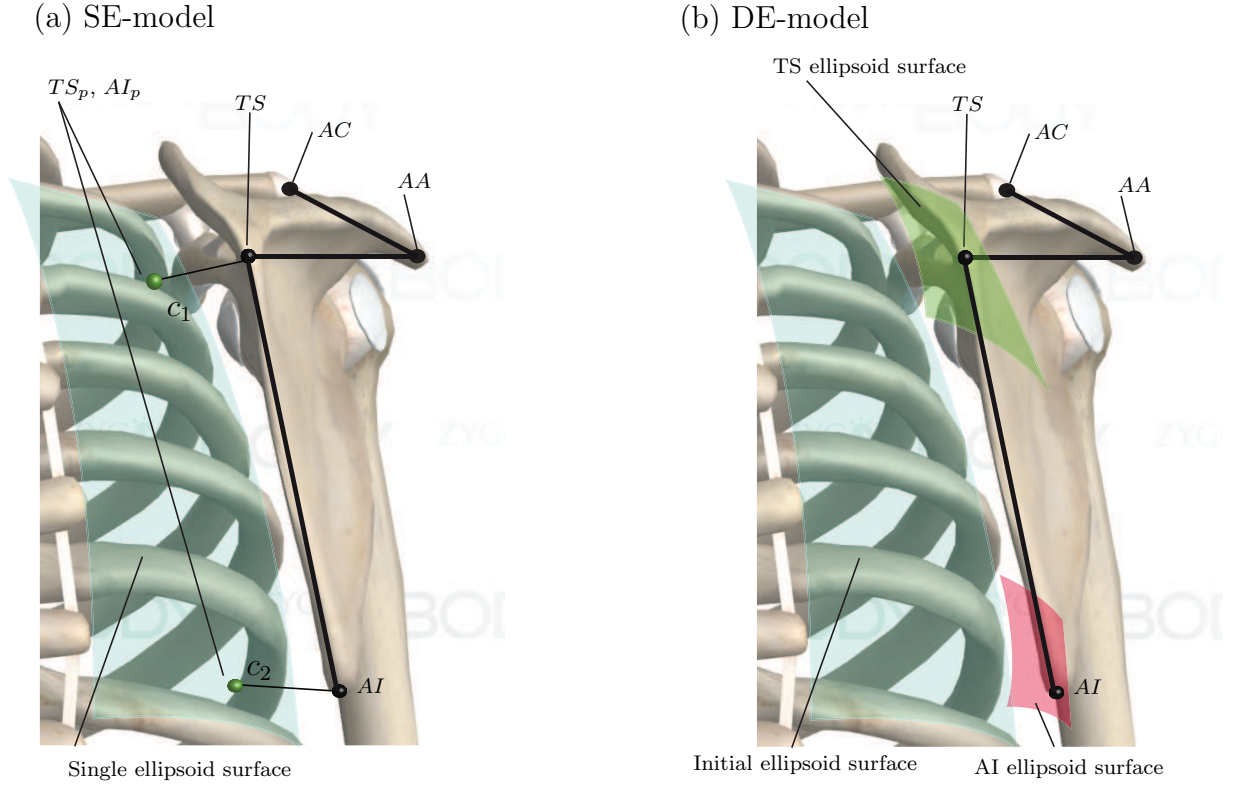


Figure 4.3: Illustrations of the scapulothoracic contact model. (a) single ellipsoid used by the DSEM model. (b) double ellipsoid model as described in section 4.2.3. Image created using ZygoteBodyTM zygotebody.com.

centre but different axial dimensions. They are constructed by fitting a single ellipsoid to the surface of the ribcage. This ellipsoid is then uniformly dilated twice (a constant is added to all three axial dimensions) such that two new ellipsoids are obtained. The dilation constants are defined such that the points TS and AI lie on the surface of their respective ellipsoids. The geometric data of the model collected using MRI scans is for a shoulder in the resting configuration. The subject was lying down with his arms down against his sides. The ellipsoid was fitted to the scanned ribcage and the dilation coefficients μ_{TS} and μ_{AI} were defined such that the scanned points TS and AI were on the dilated ellipsoids. The ellipsoid was fitted such that its reference system coincides with the thorax frame: $\mathcal{R}_4 \equiv \mathcal{R}_0$. This yields two holonomic scleronomic constraints of the form:

$$\Phi_{TS}(\vec{\Upsilon}_1, \vec{\Upsilon}_2) = (\vec{u}_{0,2} - \vec{e}_0)^T \mathbf{E}_{TS} (\vec{u}_{0,2} - \vec{e}_0) - 1 = 0, \quad TS_{0,2} : \vec{u}_{0,2} = \vec{d}_{0,2} + \mathbf{R}_{2,0} \vec{u}_2, \quad (4.9)$$

$$\Phi_{AI}(\vec{\Upsilon}_1, \vec{\Upsilon}_2) = (\vec{v}_{0,2} - \vec{e}_0)^T \mathbf{E}_{AI} (\vec{v}_{0,2} - \vec{e}_0) - 1 = 0, \quad AI_{0,2} : \vec{v}_{0,2} = \vec{d}_{0,2} + \mathbf{R}_{2,0} \vec{v}_2. \quad (4.10)$$

The matrices \mathbf{E}_{TS} and \mathbf{E}_{AI} are the quadric matrices associated to each ellipsoid and \vec{e}_0 is the ellipsoid's common centre in the inertial frame \mathcal{R}_0 .

$$\mathbf{E}_k = \begin{pmatrix} \frac{1}{a_k^2} & 0 & 0 \\ 0 & \frac{1}{b_k^2} & 0 \\ 0 & 0 & \frac{1}{c_k^2} \end{pmatrix}, \quad \begin{aligned} a_k &= a + \mu_k, & b_k &= b + \mu_k, & c_k &= c + \mu_k, \\ k &= TS, AI, & a, b, c &: \text{ellipsoid half-axis dimensions.} \end{aligned}$$

This model will be referred to as the double-ellipsoid model (DE-model). Other scapulothoracic contact models from the literature will be referred to as single-ellipsoid models (SE-model) [58, 74, 142, 194]. The reason for constructing the DE-model is to obtain a simpler description of the contact. The SE-models from the literature require computing the projection(s) of point(s) onto an ellipsoid's surface. This operation gives the SE-models added complexity. However, the difference between the models is small enough to be neglected, a point demonstrated in Appendix A. Indeed, the DE-model used in this shoulder model takes the original ellipsoid representing the thorax and uniformly expands it twice such that the points TS and AI lie on the surface of one of the expanded ellipsoids. A projection is therefore no longer needed.

4.2.4 Forward Kinematic Map

The forward kinematic map completely characterises a mechanism's kinematic model. It is defined as a map between the model's kinematic coordinates and the configuration of one of the bodies in the model called the end-effector (cf. chapter 3, section 3.5.4). The map also includes all the kinematic constraints. For the shoulder model, the kinematic coordinates vector is defined as the vector of nine joint angles $\vec{q} = (\vec{\Upsilon}_1^T, \vec{\Upsilon}_2^T, \vec{\Upsilon}_3^T)^T$. The end-effector is defined as the humerus. The kinematic map relates the vector \vec{q} to the position of the humeroulnar joint centre $HU_{0,3}$ in the inertial frame \mathcal{R}_0 and the glenohumeral joint configuration $\vec{\Upsilon}_3$. The scapulothoracic contact constraints are imposed on the map to constraint the coordinates.

$$\Xi_S : \mathcal{Q}_S \rightarrow \mathcal{W}_S,$$

$$\vec{q} \mapsto \Xi_S(\vec{q}) = \mathcal{C}_e = \left(\vec{\epsilon}_{0,3}^T, \vec{\Upsilon}_3^T \right)^T, \quad HU_{0,3} : \vec{\epsilon}_{0,3} = \vec{d}_{0,3} + \mathbf{R}_{3,0} \vec{\epsilon}_3, \quad (4.11)$$

$$s.t. \quad \Phi_{TS}(\vec{\Upsilon}_1, \vec{\Upsilon}_2) = (\vec{u}_{0,2} - \vec{e}_0)^T \mathbf{E}_{TS} (\vec{u}_{0,2} - \vec{e}_0) - 1 = 0, \quad (4.12)$$

$$\Phi_{AI}(\vec{\Upsilon}_1, \vec{\Upsilon}_2) = (\vec{v}_{0,2} - \vec{e}_0)^T \mathbf{E}_{AI} (\vec{v}_{0,2} - \vec{e}_0) - 1 = 0. \quad (4.13)$$

The vector position of the end-effector $\vec{\epsilon}_3$ is defined according to the Euclidean displacement (4.4).

The spaces \mathcal{Q}_S and \mathcal{W}_S are the shoulder's forward kinematic map range and image spaces called the coordinate and end-effector work spaces respectively [31]. The configuration space \mathcal{Q}_S is a subset of $SO(3) \times SO(3) \times SO(3)$. The work space is a subset of $SE(3) = \mathbb{R}^3 \times SO(3)$ (cf. chapter 3, sections 3.5.2 and 3.5.5).

The kinematic shoulder model is redundant [44]. The configuration of the humerus is defined by six degrees of freedom. There are nine kinematic coordinates which parameterise the model's kinematics subject to two holonomic scleronomic constraints. Using the Chebychev–Grübler–Kutzbach or mobility formula, the kinematic shoulder model has seven degrees of freedom [192]

$$M = 6n - \sum_{j=1}^m (6 - k_j) = 7, \quad (4.14)$$

where $n = 3$ is the number of links, $m = 5$ is the number of kinematic joints and k_j is their associated degrees of freedom. There are three spherical kinematic pairs with three degrees of freedom each and there are two constraints which define two spherical slider kinematic pairs with five degrees of freedom each. The model is redundant of degree one [181]. It is noteworthy that the conoid ligament is not considered in the model. This ligament constrains the clavicle's axial rotation to follow the scapula's motion. This ligament has been modelled in the DSEM model [156, 194] but is not considered here because the clavicle's axial rotation can be freely imposed using measured data, for instance [50].

4.3 Dynamic Shoulder Model

4.3.1 Equations of Motion

The dynamic shoulder model parameterises the behaviour of the skeletal structure under the mechanical action of the muscles. Mechanical action is defined as the action of a system of forces on a body or system of bodies. The dynamic model is built by attributing to each bone a mass m_i and an inertia \mathcal{I}_i ($i = 1, 2, 3$) [28]. These parameters are defined with respect to each bone's centre of gravity. The thorax is defined as the carrier body and its frame defines the inertial frame. The dynamic model considers the entire arm and includes its mass and inertia which are added to the humeral mass and inertia using the parallel axis theorem [111]. The centre of gravity positions in the thorax frame are listed below using the Euclidean displacement definitions from section 4.2.2 (Eq. (4.2)-(4.4)).

- Clavicle CG_1 : $\vec{x}_{0,1} = \vec{d}_{0,1} + \frac{1}{2}\mathbf{R}_{1,0}\vec{z}_1$,
- Scapula CG_2 : $\vec{x}_{0,2} = \vec{d}_{0,1} + \mathbf{R}_{1,0}\vec{z}_1 + \mathbf{R}_{2,0}(\frac{2}{3}\vec{z}_2 + \frac{1}{3}\vec{v}_2)$,
- Humerus CG_3 : $\vec{x}_{0,3} = \vec{d}_{0,1} + \mathbf{R}_{1,0}\vec{z}_1 + \mathbf{R}_{2,0}(\vec{w}_2 - \vec{z}_2) + \mathbf{R}_{3,0}\vec{e}_3$.

The shoulder model's dynamics are obtained from analytical mechanics using the Euler-Lagrange equation. The generalised coordinates are defined as the kinematic coordinates.

$$\begin{aligned} \vec{q} \equiv \vec{\kappa} &= (\psi_1 \quad \vartheta_1 \quad \varphi_1 \quad \psi_2 \quad \vartheta_2 \quad \varphi_2 \quad \psi_3 \quad \vartheta_3 \quad \varphi_3)^T = \\ &(\vec{\kappa}_1^T \quad \vec{\kappa}_2^T \quad \vec{\kappa}_3^T)^T = (\vec{\Upsilon}_1^T, \vec{\Upsilon}_2^T, \vec{\Upsilon}_3^T)^T. \end{aligned} \quad (4.15)$$

The action of the muscle's on the skeleton is modelled by a system of forces [166] which is reduced to a vector of generalised torques \vec{t}_m (cf. chapter 3, section 3.6.4), the Euler-Lagrange equation is expressed by

$$\frac{d}{dt} \left(\frac{\partial \mathcal{L}}{\partial \dot{\vec{\kappa}}} \right) - \frac{\partial \mathcal{L}}{\partial \vec{\kappa}} = \vec{t}_m \quad (4.16)$$

The right hand side of the Euler-Lagrange equation defines the generalised torques applied by each muscle on each bone. The left hand side contains each bone's acceleration and

the conservative forces to which it is subject, including gravity and Coriolis force. The shoulder's lagrangian is the sum of the clavicle's, scapula's and humerus's lagrangian augmented by the two scapulothoracic constraints (Chapter 3, section 3.6.4).

$$\mathcal{L} = \mathcal{L}_1 + \mathcal{L}_2 + \mathcal{L}_3 + \lambda_{TS}\Phi_{TS}(\vec{\kappa}) + \lambda_{AI}\Phi_{AI}(\vec{\kappa}) = \tilde{\mathcal{L}} + \lambda_{TS}\Phi_{TS}(\vec{\kappa}) + \lambda_{AI}\Phi_{AI}(\vec{\kappa}). \quad (4.17)$$

Each bone's lagrangian is defined by its kinetic and potential energies. The general expression is given by:

$$\mathcal{L}_i = \frac{1}{2} \left\{ M_i \dot{\vec{x}}_{0,i}^T \dot{\vec{x}}_{0,i} + \vec{\omega}_i^T \mathcal{I}_i \vec{\omega}_i \right\} - M_i g \begin{pmatrix} 0 & 0 & 1 \end{pmatrix} \cdot \vec{x}_{0,i}, \quad i = 1, 2, 3, \quad (4.18)$$

where, as stated previously, the vector $\vec{x}_{0,i}$ is the position of the centre of gravity of the bone i , described in the global reference frame. The vector $\dot{\vec{x}}_{0,i}$ is the translational velocity vector of the bone i 's centre of gravity defined in the global reference frame. The vector $\vec{\omega}_i$ is bone i 's instantaneous rotational velocity vector in the bone's reference frame.

$$\dot{\vec{x}}_{0,i} = \frac{\partial \vec{x}_{0,i}}{\partial \vec{\kappa}} \dot{\vec{\kappa}}, \quad (4.19)$$

$$\ddot{\vec{x}}_{0,i} = \frac{\partial \vec{x}_{0,i}}{\partial \vec{\kappa}} \ddot{\vec{\kappa}} + \frac{d}{dt} \left(\frac{\partial \vec{x}_{0,i}}{\partial \vec{q}} \right) \dot{\vec{\kappa}} \quad (4.20)$$

$$\vec{\omega}_i = \mathbf{R}_{x,i}^T \mathbf{R}_{y,i} \begin{pmatrix} 0 \\ 0 \\ \dot{\varphi}_i \end{pmatrix} + \mathbf{R}_{x,i}^T \begin{pmatrix} 0 \\ \dot{\vartheta}_i \\ 0 \end{pmatrix} + \begin{pmatrix} \dot{\psi}_i \\ 0 \\ 0 \end{pmatrix}, \quad i = 1, 2, \quad (4.21)$$

$$\vec{\omega}_3 = \mathbf{R}_{z,i}^T \mathbf{R}_{y,i} \begin{pmatrix} 0 \\ 0 \\ \dot{\varphi}_3 \end{pmatrix} + \mathbf{R}_{z,i}^T \begin{pmatrix} 0 \\ \dot{\vartheta}_1 \\ 0 \end{pmatrix} + \begin{pmatrix} 0 \\ 0 \\ \dot{\psi}_3 \end{pmatrix}, \quad (4.22)$$

$$\vec{\omega}_{0,i} = \mathbf{R}_{i,0} \vec{\omega}_i, \quad (4.23)$$

$$\mathcal{I}_i = \begin{pmatrix} I_{1,1} & 0 & 0 \\ 0 & I_{2,2} & 0 \\ 0 & 0 & I_{3,3} \end{pmatrix}. \quad (4.24)$$

Note that the inertia tensor \mathcal{I}_i is defined in the bone's reference frame making it diagonal. For the clavicle and scapula, $I_{1,1}$ is the longitudinal inertia and $I_{2,2} = I_{3,3}$ the transverse inertia. For the humerus, $I_{3,3}$ is the longitudinal inertia and $I_{1,1} = I_{2,2}$ the transverse inertia [28].

The equations of motion are defined by a set of differential algebraic equations (DAE):

$$\frac{\partial^2 \tilde{\mathcal{L}}}{\partial \dot{\vec{\kappa}}^2} \ddot{\vec{\kappa}} + \frac{\partial^2 \tilde{\mathcal{L}}}{\partial \vec{\kappa} \partial \dot{\vec{\kappa}}} \dot{\vec{\kappa}} - \frac{\partial \tilde{\mathcal{L}}}{\partial \vec{\kappa}} = \vec{t}_m + \lambda_{TS} \left(\frac{\partial \Phi_{TS}}{\partial \vec{\kappa}} \right)^T + \lambda_{AI} \left(\frac{\partial \Phi_{AI}}{\partial \vec{\kappa}} \right)^T, \quad (4.25)$$

$$s.t. \quad \Phi_{TS}(\vec{\kappa}) = (\vec{u}_{0,2} - \vec{e}_0)^T \mathbf{E}_{TS} (\vec{u}_{0,2} - \vec{e}_0) - 1 = 0, \quad (4.26)$$

$$\Phi_{AI}(\vec{\kappa}) = (\vec{v}_{0,2} - \vec{e}_0)^T \mathbf{E}_{AI} (\vec{v}_{0,2} - \vec{e}_0) - 1 = 0. \quad (4.27)$$

The constraint terms on the right hand side of the equations of motion (4.25) correspond to the torques created at the joints by the reaction forces at the scapulothoracic contact points TS and AI. Holonomic skleronomic constraints impose forces on the equations of motion to enforce the constraints like a bead on the wire of a necklace. The wire

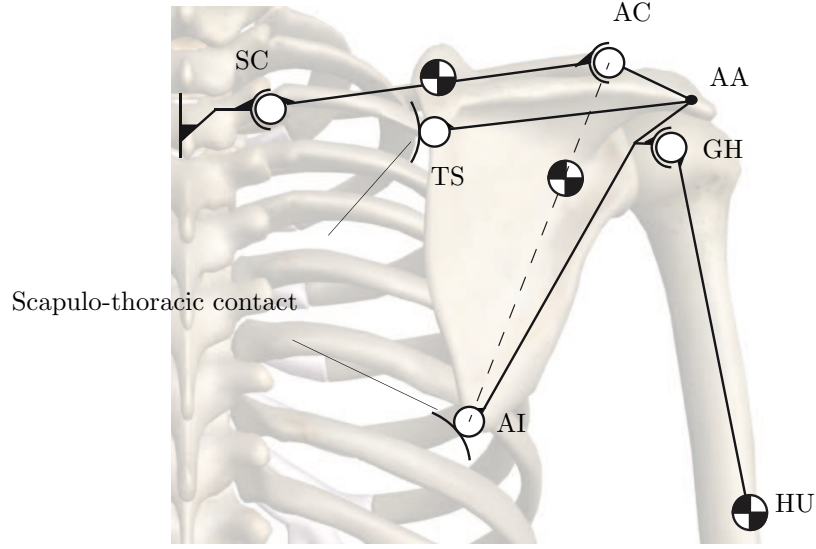


Figure 4.4: *Illustration of the shoulder mechanism and location of the bone centres of gravity as described in section 4.3.1. Illustration is done using the standard kinematic pair symbology from chapter 3, section 3.5.2. Image created using ZygoteBodyTM zygote-body.com.*

applies a force on the beed to keep it on the wire. In model of the beed, the wire becomes a constraint. The constraint's jacobian defines the force's direction and the lagrangian multiplier is proportional to its amplitude. If the model's geometry is simple enough, the constraint forces can explicitly be defined without using the constraints.

For the shoulder model, the constraints are defined by ellipsoid parametric equations (4.26)-(4.27). The jacobians of these constraints are the generalised torques created by the scapulothoracic contact forces around the SC and AC joints. The scapulothoracic contact forces create no torque at the glenohumeral joint. Knowing that the contact forces are parallel to the ellipsoid surfaces, leads to the following equalities.

$$\begin{aligned} \lambda_{TS} \left(\frac{\partial \Phi_{TS}}{\partial \vec{\kappa}} \right)^T &= \begin{pmatrix} \mathbf{W}_{0,1}^T (\vec{z}_{0,1} - \vec{d}_{0,1}) \times \vec{f}_{0,2,TS} \\ \mathbf{W}_{0,2} (\vec{u}_{0,2} - \vec{z}_{0,1}) \times \vec{f}_{0,2,TS} \\ \vec{0} \end{pmatrix}, \\ \lambda_{0,AI} \left(\frac{\partial \Phi_{AI}}{\partial \vec{\kappa}} \right)^T &= \begin{pmatrix} \mathbf{W}_{0,1} (\vec{z}_{0,1} - \vec{d}_{0,1}) \times \vec{f}_{0,2,AI} \\ \mathbf{W}_{0,2} (\vec{v}_{0,2} - \vec{z}_{0,1}) \times \vec{f}_{0,2,AI} \\ \vec{0} \end{pmatrix}. \end{aligned} \quad (4.28)$$

The matrices $\mathbf{W}_{0,1}$ and $\mathbf{W}_{0,2}$ are the jacobians of $\vec{\omega}_{0,1}$ and $\vec{\omega}_{0,2}$ respectively with respect to $\dot{\vec{\kappa}}$ (cf. principle of virtual work, chapter 3, section 3.6.4). The vectors $\vec{f}_{0,2,TS}$ and $\vec{f}_{0,2,AI}$ are the reaction forces in the inertial frame. The lagrangian multiplier multiplied by the constraint jacobian is equal to the contact force torque projected into the generalised

coordinate space, using $\mathbf{W}_{0,i}$. The reaction force intensities are extracted.

$$\begin{aligned} \lambda_{TS} \left(\frac{\partial \Phi_{TS}}{\partial \vec{\kappa}} \right)^T &= f_{TS} \begin{pmatrix} \mathbf{W}_{0,1}^T ((\vec{z}_{0,1} - \vec{d}_{0,1}) \times \vec{b}_{0,2,TS}) \\ \mathbf{W}_{0,1}^T ((\vec{u}_{0,1} - \vec{z}_{0,1}) \times \vec{b}_{0,2,AI}) \\ \vec{0} \end{pmatrix} = f_{TS} \begin{pmatrix} \mathbf{W}_{0,1}^T \vec{c}_{0,1,TS} \\ \mathbf{W}_{0,2}^T \vec{c}_{0,2,TS} \\ \vec{0} \end{pmatrix}, \\ \lambda_{AI} \left(\frac{\partial \Phi_{AI}}{\partial \vec{\kappa}} \right)^T &= f_{AI} \begin{pmatrix} \mathbf{W}_{0,1}^T ((\vec{z}_{0,1} - \vec{d}_{0,1}) \times \vec{b}_{0,2,AI}) \\ \mathbf{W}_{0,1}^T ((\vec{v}_{0,1} - \vec{z}_{0,1}) \times \vec{b}_{0,2,AI}) \\ \vec{0} \end{pmatrix} = f_{AI} \begin{pmatrix} \mathbf{W}_{0,1}^T \vec{c}_{0,1,AI} \\ \mathbf{W}_{0,2}^T \vec{c}_{0,2,AI} \\ \vec{0} \end{pmatrix}, \end{aligned} \quad (4.29)$$

The vectors $\vec{c}_{0,i,TS}$ and $\vec{c}_{0,i,AI}$ are the moment-arm vectors around the sternoclavicular and acromioclavicular joints respectively. The vectors $\vec{b}_{0,i,TS}$ and $\vec{b}_{0,i,AI}$ are the ellipsoid reaction force unit vectors. They are normal to the surface of the ellipsoids and depend on the generalised coordinates, defined in the thorax frame.

$$\begin{aligned} \vec{b}_{0,2,TS}(\vec{q}) &= \frac{\begin{pmatrix} \frac{2p_x}{a_{TS}^2} & \frac{2p_y}{b_{TS}^2} & \frac{2p_z}{c_{TS}^2} \end{pmatrix}^T}{\left\| \begin{pmatrix} \frac{2p_x}{a_{TS}^2} & \frac{2p_y}{b_{TS}^2} & \frac{2p_z}{c_{TS}^2} \end{pmatrix}^T \right\|_2}, \quad \begin{pmatrix} p_x \\ p_y \\ p_z \end{pmatrix} = \vec{u}_{0,2}(\vec{\kappa}) - \vec{e}_0, \\ \vec{b}_{0,2,AI}(\vec{q}) &= \frac{\begin{pmatrix} \frac{2p_x}{a_{AI}^2} & \frac{2p_y}{b_{AI}^2} & \frac{2p_z}{c_{AI}^2} \end{pmatrix}^T}{\left\| \begin{pmatrix} \frac{2p_x}{a_{AI}^2} & \frac{2p_y}{b_{AI}^2} & \frac{2p_z}{c_{AI}^2} \end{pmatrix}^T \right\|_2}, \quad \begin{pmatrix} p_x \\ p_y \\ p_z \end{pmatrix} = \vec{v}_{0,2}(\vec{\kappa}) - \vec{e}_0, \end{aligned} \quad (4.30)$$

The constraint terms in the equations of motion are grouped into matrix form:

$$\begin{aligned} \lambda_{TS} \left(\frac{\partial \Phi_{TS}}{\partial \vec{\kappa}} \right)^T + \lambda_{AI} \left(\frac{\partial \Phi_{AI}}{\partial \vec{\kappa}} \right)^T &= \\ \begin{pmatrix} \mathbf{W}_{0,1}^T & \mathbf{0} & \mathbf{0} \\ \mathbf{0} & \mathbf{W}_{0,2}^T & \mathbf{0} \\ \mathbf{0} & \mathbf{0} & \mathbf{W}_{0,3}^T \end{pmatrix} \begin{pmatrix} \vec{c}_{0,1,TS} & \vec{c}_{0,1,AI} \\ \vec{c}_{0,2,TS} & \vec{c}_{0,2,AI} \\ \vec{0} & \vec{0} \end{pmatrix} \begin{pmatrix} f_{TS} \\ f_{AI} \end{pmatrix} &= \hat{\mathbf{W}}_0 \hat{\mathbf{C}}_{0,s} \vec{f}_s. \end{aligned} \quad (4.31)$$

The matrix $\hat{\mathbf{C}}_{0,s}$ is the moment-arms matrix of the scapulo-thoracic contact model in the inertial frame. The vector \vec{f}_s is the vector of force intensities of the scapulothoracic contact model.

4.3.2 Muscle Forces

This section describes the muscle actuation model and its contribution to the dynamic model's equations of motion (\vec{t}_m in equation (4.25)). The principle hypothesis of the muscle model, is that a muscle applies a system of forces on the skeletal structure [166]. Muscles are modelled using the ideal cable model. The shoulder's musculature is modelled by N_p massless, frictionless, elastic cables. The geometry of the cable model will be discussed in the following section. Each cable applies a system of forces on the skeletal structure. All the forces applied by a single cable on the same bone are reduced to a single force at a point and a moment of force about that point. Thus, each cable applies a single force at each joint and moment of force around each joint. All the forces applied by a given cable on the skeletal structure have the same amplitude or intensity f_k . The

forces and moments of force can be zero depending on the muscle. For instance, muscles which do not span the GH joint create no force and no moment of force about that joint. Forces applied to the clavicle are reduced to the centre of the SC joint. Forces applied to the scapula are reduced to the centre of the AC joint. Forces applied to the humerus are reduced to the centre of the GH joint.

For a model with N_p muscle segments, the total force and moment of force at each joint in the inertial reference frame \mathcal{R}_0 is defined by:

$$\vec{f}_{0,i} = \sum_{k=1}^{N_p} \vec{f}_{0,i,k}, \quad i = 1, 2, 3, \quad (4.32)$$

$$\vec{t}_{0,i} = \sum_{k=1}^{N_p} \vec{y}_{0,i,k} \times \vec{f}_{0,i,k} = \sum_{j=1}^{N_p} \left(\vec{y}_{0,i,k} \times \vec{b}_{0,i,k} \right) f_k = \sum_{j=1}^{N_p} \vec{c}_{0,i,k} f_k = \mathbf{C}_{0,i} \vec{f}. \quad (4.33)$$

where the terms in these expressions are defined as:

- $\vec{f}_{0,i,k}$: resulting force of muscle k applied to body \mathcal{B}_i in \mathcal{R}_0 ,
- $\vec{y}_{0,i,k}$: force system reduction vector for muscle k and body i in \mathcal{R}_0 ,
- $\vec{c}_{0,i,k} = \vec{y}_{0,i,k} \times \vec{b}_{0,i,k}$: moment-arms of cable k and joint i in \mathcal{R}_0 .
- $\mathbf{C}_{0,i}$: matrix of moment-arms of joint i in \mathcal{R}_0 .
- \vec{f} : $N_p \times 1$ total vector of muscle force intensities.

The equations of motion are in terms of rotational coordinates. Therefore, the muscle contribution to the equations of motion is from the resulting moments of force. The resulting moment of force vectors $\vec{t}_{0,i}$ are transformed to obtain the generalised moment of force vector \vec{t}_m , using the method described in chapter 3 section 3.6.4. The generalised moment of force is defined by

$$\vec{t}_m = \begin{pmatrix} \mathbf{W}_{0,1}^T & \mathbf{0} & \mathbf{0} \\ \mathbf{0} & \mathbf{W}_{0,2}^T & \mathbf{0} \\ \mathbf{0} & \mathbf{0} & \mathbf{W}_{0,3}^T \end{pmatrix} \begin{pmatrix} \vec{t}_{0,1} \\ \vec{t}_{0,2} \\ \vec{t}_{0,3} \end{pmatrix} = \hat{\mathbf{W}}_0 \begin{pmatrix} \mathbf{C}_{0,1} \vec{f} \\ \mathbf{C}_{0,2} \vec{f} \\ \mathbf{C}_{0,3} \vec{f} \end{pmatrix} = \hat{\mathbf{W}}_0 \hat{\mathbf{C}}_0 \vec{f}. \quad (4.34)$$

$\hat{\mathbf{C}}_0$ is the $9 \times N_p$ matrix of moment-arms dependent on the configuration of the model. Its computation will be discussed in detail in chapter 7. The expression (4.34) defines a map between the muscle force intensities and the generalised moments of force will be referred to as the torque-force map.

The muscle-force contribution to the dynamic model's equations of motion (4.25)-(4.27) is defined in terms of the force intensities using the torque-force map.

$$\frac{\partial^2 \tilde{\mathcal{L}}}{\partial \vec{\kappa}^2} \ddot{\vec{\kappa}} + \frac{\partial^2 \tilde{\mathcal{L}}}{\partial \vec{\kappa} \partial \dot{\vec{\kappa}}} \dot{\vec{\kappa}} - \frac{\partial \tilde{\mathcal{L}}}{\partial \vec{\kappa}} = \hat{\mathbf{W}}_0 \hat{\mathbf{C}}_0 \vec{f} + \hat{\mathbf{W}}_0 \hat{\mathbf{C}}_{0,s} \vec{f}_s. \quad (4.35)$$

Muscles can only pull the skeletal structure. As they contract, they pull on the bones to which they are attached. This effect is included in the muscle force model by imposing bounds on the muscle-force intensities. A muscle's force must be positive or zero with an upper limit given by the muscle's maximum isometric strength (cf. chapter 2, section 2.2).

$$\vec{0} \leq \vec{f} \leq \vec{f}_{\max}. \quad (4.36)$$

The values used to implement these bounds were taken from VHP kinematic shoulder model [76].

4.3.3 Muscle Cable Model

Geometrically, a muscle is an elongated volume between two points, the origin and insertion. The volume is filled with parallel fibres which go from origin to insertion. The cable model represents a particular fibre called the centroid line. The centroid line represents the fibre which passes through the centre of the volume and therefore the centre of the volume's cross-sections.

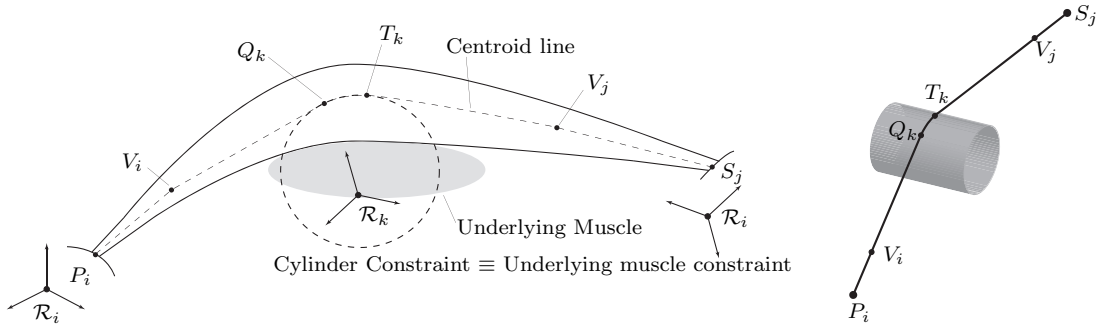


Figure 4.5: *Illustration of the centroid line approach to muscle modelling as described in section 4.3.3. The underlying muscle is represented by a cylinder.*

Once the centroid line is defined for the anatomical muscle, using MRI scans of the musculature, the geometric cable model is defined. The model is defined such that the cable follows the centroid line as closely as possible. To start, the cable is attached at two points representing the origin P_i and insertion S_j which are fixed in the bone reference frames \mathcal{R}_i and \mathcal{R}_j respectively (Fig. 4.5). The centroid line of the anatomical muscle curves as the muscle passes over other anatomical structures. In the model, smooth geometric surfaces are inserted into the model to force the cable to curve as the anatomical centroid line does. The surfaces are spheres, cylinders, or cylinders with half spheres at one end. For certain muscles, up to two extra fixed via points V_i and V_j are added to force the cable to always pass through the point. These points are near the origin and insertion points and are defined in the same reference frame. As the cable passes over the surface, two points are defined which are the initial contact point Q_k and final contact point T_k with the surface. The points are defined in the same frame as the surface itself \mathcal{R}_k . This construction of the cable model is called the *obstacle*

set method and was initially developed for the VHP kinematic shoulder model [75]. The approach of modelling the muscle's centroid line was first used in a model of the hip [108].

For the shoulder model, there are 16 anatomical muscles actuating the shoulder divided into 28 parts using the guide lines set fourth in [197] (cf. Appendix C for details). Thus, the shoulder model presented in this chapter uses at least 28 cables to model the musculature. A method of adding more cables is defined by parameterising the muscle's centroid plane. A muscle's centroid line passes through the centre of the muscle's volume. The muscle's centroid plane cuts the muscle in half longitudinally and contains the centroid line. The centroid plane defines a line at the muscle's origin and insertion. The number of cables is modulated by parameterising these two lines using a third order spline. The splines are constructed using three anchor points. The middle points are the centroid line origins and insertions (Fig. 4.6).

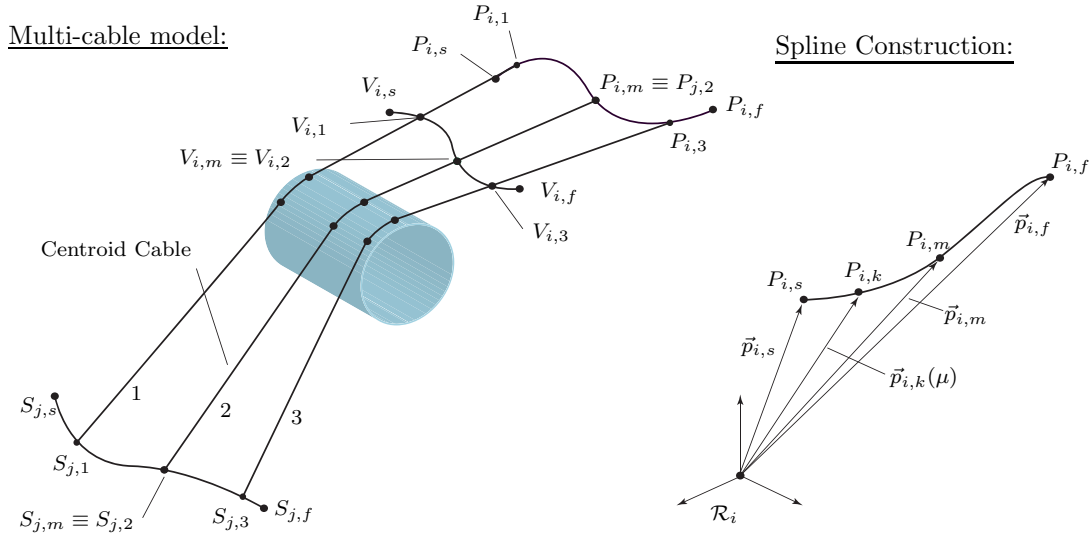


Figure 4.6: (a) Illustration of a muscle's centroid represented by three cables. (b) Illustration of the 3rd order spline parameterisation as described in section 4.3.3.

To illustrate the spline construction, consider the origin of a muscle which has been identified by a curved line. In the model, this line is parameterised using a 3rd order spline with three anchor points $P_{i,s}$, $P_{i,m}$ and $P_{i,f}$ (Fig. 4.7). The spline is defined in the reference frame of the bone on which the muscle originates \mathcal{R}_i . The location of any point $P_{i,k}$ on the spline is defined using a single variable $\mu \in [0, 1]$. The parameterisation is defined by:

$$P_{i,k}(\mu) : \vec{p}_{i,k}(\mu) = \begin{cases} (\mu^3 \ \mu^2 \ \mu \ 1) \mathbf{S} \begin{pmatrix} \vec{p}_{i,s} \\ \vec{p}_{i,m} \\ \vec{p}_{i,f} \end{pmatrix} & \text{if } 0 \leq \mu < 0.5 \\ (\mu^3 \ \mu^2 \ \mu \ 1) \mathbf{S} \begin{pmatrix} \vec{p}_{i,s} \\ \vec{p}_{i,m} \\ \vec{p}_{i,f} \end{pmatrix} & \text{if } 0.5 \leq \mu \leq 1 \end{cases}, \mathbf{S} = \begin{pmatrix} -\frac{1}{2} & \frac{3}{2} & -\frac{3}{2} & \frac{1}{2} \\ 1 & \frac{5}{2} & 2 & -\frac{1}{2} \\ -\frac{1}{2} & 0 & \frac{1}{2} & 0 \\ 0 & 1 & 0 & 0 \end{pmatrix}. \quad (4.37)$$

The vectors $\vec{p}_{i,s}$, $\vec{p}_{i,m}$ and $\vec{p}_{i,f}$ are the points vectors of the points $P_{i,s}$, $P_{i,m}$ and $P_{i,f}$ in the local frame \mathcal{R}_i . The matrix \mathbf{S} is the spline coefficient matrix and is the same for every spline. For muscle parts with multiple cables, the origin and insertion points of each cable are evenly distributed along the spline: $\mu = 1/(2 \cdot \text{Nb cables})$. This parameterisation is also applied to the fixed via points (Fig. 4.6). If the number of cables is odd, there is a cable which represents the muscle's centroid line. All the data necessary to construct the geometry of the cable model was obtained through MRI scans of an adult male (cf. Appendix B).

The cable model defines the geometry of each cable. Once the geometry is known, pulley mechanics can be used to obtain the forces applied by each cable on the skeletal system. This information can then be used to compute the moment-arms and related the forces in the cables to the torques around the joints. This model does not state how much force is applied. The model simply gives the relation between the muscle force intensities and the joint torques. If there is force, this model transforms the force into torques at the three joints.

4.4 Remarks

The musculoskeletal shoulder model presented in this chapter was developed for estimating the forces within the muscles and in the glenohumeral joint. This is the model's purpose that will be analysed in chapter 8. There are two other aspects to a model; its structure and numerical implementation. Many musculoskeletal models of the shoulder are presented in the context of their clinical application with a focus on the model's clinical validity. While clinical validation is essential, the model's mathematical structure and validity is also important. However, it seems there are few model oriented presentations of musculoskeletal shoulder models, making their accurate reconstruction a challenging task.

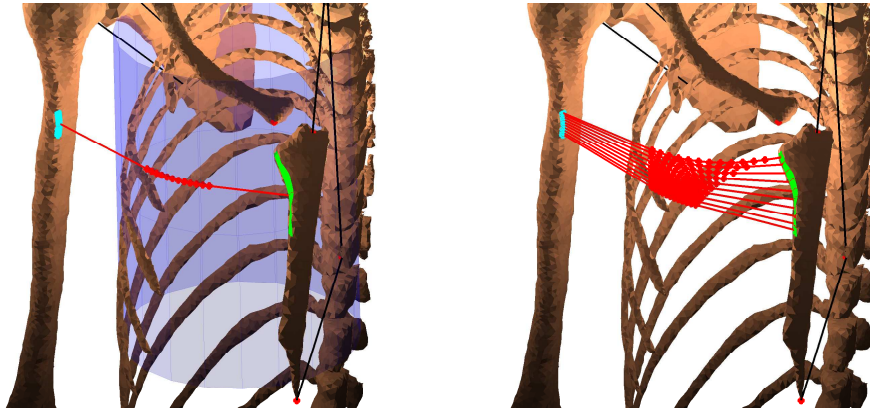


Figure 4.7: *Pectoralis major (sternal muscle part, PMJs) modelled using one (left) and ten segments (right). Single cylinder wrapping constraint. The green and blue lines represent the muscle origin and insertion spline parameterisation.*

The musculoskeletal shoulder model presented in this chapter contains a kinematic model of the skeletal structure. The bones are considered to be rigid bodies and the synovial joints are modelled as ideal ball and socket joints parameterised by spherical kinematic pairs. The model also considers the scapulothoracic contact, modelled by constraining two points (TS , AI) to remain on the surface of two ellipsoids. The ellipsoids represent the surface of the ribcage with an additional layer of muscle. The model's kinematics are completely characterised by the forward kinematic map.

$$\Xi_S : \mathcal{Q}_S \rightarrow \mathcal{W}_S \subset SE(3),$$

$$\vec{q} \mapsto \Xi(\vec{q}) = (\vec{e}_{0,3}(\vec{q}), \vec{\Upsilon}_3), \quad \text{with} \quad \vec{q} = (\vec{\Upsilon}_1^T, \vec{\Upsilon}_2^T, \vec{\Upsilon}_3^T)^T \quad (4.38)$$

$$s.t. \quad \Phi_{TS}(\vec{\Upsilon}_1, \vec{\Upsilon}_2) = (\vec{u}_{0,2} - \vec{e}_0)^T \mathbf{E}_{TS} (\vec{u}_{0,2} - \vec{e}_0) - 1 = 0, \quad (4.39)$$

$$\Phi_{AI}(\vec{\Upsilon}_1, \vec{\Upsilon}_2) = (\vec{v}_{0,2} - \vec{e}_0)^T \mathbf{E}_{AI} (\vec{v}_{0,2} - \vec{e}_0) - 1 = 0. \quad (4.40)$$

The kinematic coordinates are the Euler and Bryan angles of the spherical kinematic pairs. There are nine coordinates total and the model has seven degrees of freedom given the two scapul-thoracic constraints.

The dynamic model is constructed from the Euler-Lagrange equation. The kinematic coordinates are defined as the generalised coordinates $\vec{\kappa} \equiv \vec{q}$. The dynamics are subject to the scapulothoracic contact constraints (Eq. (4.39)-(4.40)). The muscles are modelled as massless, frictionless, perfectly elastic cables wrapping over the skeletal structure. Each cable applies a system of forces to the skeletal structure modelled by a single matrix called the moment-arm matrix $\hat{\mathbf{C}}_0$. The cable forces are also limited. Cables can only pull and therefore the forces must be positive. Each cable's ability to pull is limited by the muscle's maximum isometric strength. This is the maximum force the muscle can produce when it is at its optimal length (cf. chapter 3).

$$\frac{\partial^2 \tilde{\mathcal{L}}}{\partial \dot{\vec{\kappa}}^2} \ddot{\vec{\kappa}} + \frac{\partial^2 \tilde{\mathcal{L}}}{\partial \dot{\vec{\kappa}} \partial \vec{\kappa}} \dot{\vec{\kappa}} - \frac{\partial \tilde{\mathcal{L}}}{\partial \vec{\kappa}} = \hat{\mathbf{W}}_0 \hat{\mathbf{C}}_0 \vec{f} + \hat{\mathbf{W}}_0 \hat{\mathbf{C}}_{0,s} \vec{f}_s, \quad (4.41)$$

$$s.t. \quad \Phi_{TS}(\vec{\kappa}) = (\vec{u}_{0,2} - \vec{e}_0)^T \mathbf{E}_{TS} (\vec{u}_{0,2} - \vec{e}_0) - 1 = 0, \quad (4.42)$$

$$\Phi_{AI}(\vec{\kappa}) = (\vec{v}_{0,2} - \vec{e}_0)^T \mathbf{E}_{AI} (\vec{v}_{0,2} - \vec{e}_0) - 1 = 0, \quad (4.43)$$

$$\vec{0} \leq \vec{f} \leq \vec{f}_{\max}. \quad (4.44)$$

The musculoskeletal shoulder model presented in this chapter is most similar to the dynamic shoulder model constructed from the Visible Human Project (VHP) [76, 170]. Both models differ mainly on the numerical data used to implement them and on the scapulothoracic contact model. The present model uses two ellipsoids while the VHP model uses a single ellipsoid. The model does not contain the entire upper limb or the conoid ligament constraint. The upper limb is considered to be outstretched.

From a different perspective, the model presented in this chapter shares many similarities with models of cable-driven robots [29]. A cable-driven robot is a mechanism or system of rigid bodies actuated by a network of cables [21, 80, 92, 178, 217, 220]. Models of such systems use the same hypothesis used to construct the musculoskeletal model presented in this chapter. That is rigid bodies, ideal joints and ideal cables. This point is of interest because it means that theory developed for cable-driven robots can be applied to models of musculoskeletal systems. This will be used in chapter 7 to introduce a new concept related to the muscle model.

4.5 Conclusions

This chapter presented a musculoskeletal model of the human shoulder constructed for the purpose of estimating forces in the muscles and in the glenohumeral joint. The model is constructed from three hypothesis. i. the bones are rigid bodies. ii. the synovial articulations are ideal ball and socket joints. iii. the muscles are massless, frictionless cables wrapping over the skeletal structure. The model also includes an ellipsoid model of the scapulothoracic contact. In comparison to other shoulder models, the present model is most similar to the models constructed from the Visible Human Project. Furthermore, the model is shown to share similarities with models of cable-driven robots. Therefore, the outlook of this thesis on musculoskeletal modelling in general is that the mathematical structure of musculoskeletal models is as important as their clinical validation. This chapter presented many of the models mathematical details. The following chapters will continue to discuss the different aspects of the shoulder model using the formalism introduced in this chapter.

Chapter 5

Coordinated Redundancy

5.1 Introduction

The human shoulder is a system that is kinematically redundant and overactuated [36]. The shoulder (humerus included) can move without moving the position of the elbow (tip of humerus) and multiple muscle activation patterns yield the same movement [66]. To function properly, the shoulder uses coordination strategies to ensure that all parts work together harmoniously. Without the two characteristics of kinematic redundancy and overactuation, the shoulder would not be nearly as performant as it is. The coordinated motion of the scapula and humerus, called the scapulo-humeral rhythm is an example of this coordination. As stated in chapter 2, the arm's reachable space would be severely reduced without the scapulo-humeral rhythm.

The general philosophy behind kinematic redundancy and overactuation is the duplication of certain elements such that the tasks they perform are divided amongst them to enhance the system's performance and flexibility [148]. This is called *coordinated redundancy* and is different from the usual definition of redundancy implying the duplication of elements to increase reliability and not necessarily performance. Coordinated redundancy is used in systems design and robotics to increase performance and reduce costs. For example, in a milling machine multiple motors are used to drive the same positioning axis (Fig. 5.1). One motor does the rough positioning of the part. Once the rough positioning of the part is achieved, a second motor is used to precisely position the part. The first motor drives the axis over its entire range of positions. The second motor drives the axis around the rough position and has a small range of motion. This design enhances the milling machine's precision and is cheaper. A single motor with higher performance characteristics is more expensive than two less performant motors. This is also an example of overactuation. Two motors are used when one could theoretically do the job.

Models of real systems that are kinematically redundant or overactuated or both, involve mathematical problems that are underdetermined. The primary characteristic of underdetermined mathematical problems is that there is an infinite number of solutions

[96]. Thus, a method of differentiating between the solutions is required, such that a solution can be selected that is best suited to the physics of the real system. There exist many methods of differentiating between solutions. Some consider the specifics of the system and others are more general and can be used for different systems sharing the same mathematical structure. In general, a good solution is one taking advantage of the model's mathematics while considering the physics of the real system.

The goal of this chapter is to present kinematic redundancy and overactuation in an abstract mathematical context and to introduce possible coordination strategies without considering the specifics of the system. The notions of objective and task are also given formal definitions. Kinematic redundancy is presented in section 5.2 with a formal definition of a kinematically redundant mechanism. Overactuation is presented in section 5.3 for a system where the equations of motion are described by the Euler-Lagrange equation. Section 5.4 concludes the chapter with a presentation of using tasks for coordinating redundancy.

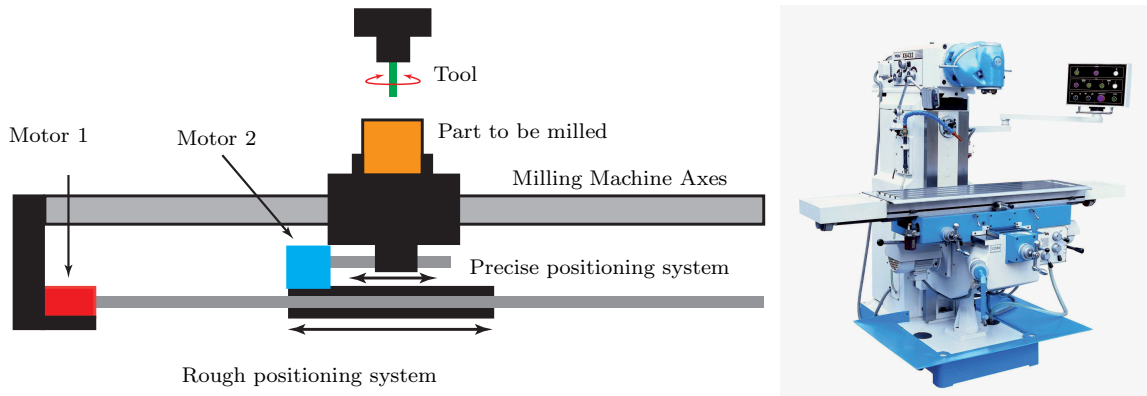


Figure 5.1: *Illustration of coordinated redundancy in a milling machine as described in section 5.1.*

5.2 Kinematic Redundancy

A kinematically redundant mechanism is informally defined as a mechanism with a number of internal degrees of freedom that exceeds the number of degrees of freedom of the end-effector [148]. As stated in chapter 3, a *mechanism* is a rigid body model of a machine where one body is fixed in the inertial frame. This body is called the *carrier body*. The purpose of a machine is to transmit motion and therefore force to a specific part of the machine called the *end-effector*. Motion is transmitted within a machine by the interactions between bodies. Joints represent idealised mechanical models of the interactions and *kinematic pairs* represent mathematical parameterisations of the interactions. Kinematic pairs also impose holonomic skleronomic constraints on the bodies forming the joint. This discussion is limited to systems subject to holonomic skleronomic constraints. Thus, a mechanism is a set of rigid bodies connected by kinematic pairs and subject to a certain number of constraints.

A *kinematic chain* is a set of rigid bodies connected together by kinematic pairs. If all the bodies are connected in series from carrier body to end-effector, the kinematic chain is *open*. An example is a serial robot manipulator (Fig. 5.2). A kinematic chain is *closed* if there are two serial chains with same initial and final bodies. The simplest closed kinematic chain is two serial chains, joined together (not necessarily at the carrier body and end-effector). A mechanism with more than two kinematic chains between two bodies is called a parallel mechanism. An example of a parallel mechanism is the Gough-Stewart platform. An important remark is that redundancy is not related to whether a kinematic chain is open or closed. Kinematic redundancy is defined by the number of bodies and the number and types of connections. A Gough-Stewart platform is not kinematically redundant.

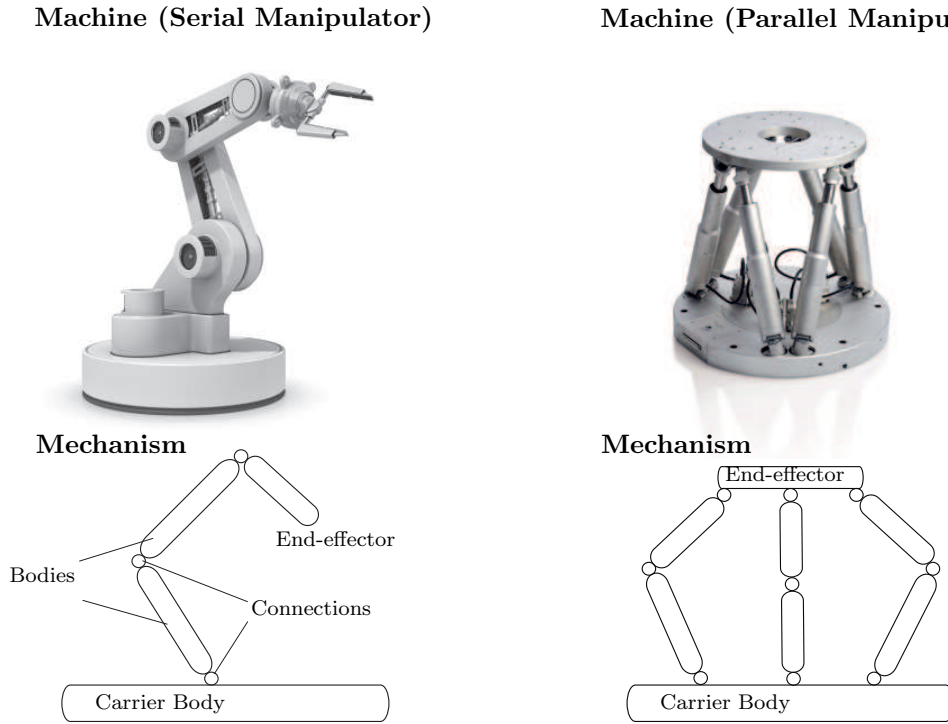


Figure 5.2: Illustrations of machines and their corresponding mechanisms as described in section 5.2 and chapter 3.

A kinematic model is a parameterisation of a mechanism's geometric configuration and how it can change over time. Kinematics analyses the possible effects in terms of motion without considering the cause. The parameterisation is obtained by constructing a set of coordinates \vec{q} completely defining the mechanism's geometric configuration \mathcal{C} at any given instant. Geometric configuration is understood as the position and orientation of each body \mathcal{B}_i in the mechanism, defined by a Euclidean displacement with respect to the inertial frame (cf. chapter 3).

$$X_{0,i} \in \mathcal{B}_i : \vec{x}_{0,i} = \underbrace{\vec{d}_{0,i}}_{\text{Position}} + \underbrace{\mathbf{R}_{i,0}\vec{x}_i}_{\text{Orientation}} . \quad (5.1)$$

A possible method of constructing the set of coordinates is to define coordinates for every kinematic pair along one of the kinematic chains between the carrier body and end-effector. If the set is incomplete, additional coordinates are defined until the remaining

kinematic pairs can be expressed as holonomic skleronomic constraints in terms of the complete set of kinematic coordinates. The selected kinematic chain between the carrier body and end-effector is used to define the forward kinematic map which is then subject to the constraints. The forward kinematic map of a mechanism with N_b bodies and N_k kinematic pairs parameterised by Q coordinates and subject to N_c holonomic skleronomic constraints is defined by:

$$\begin{aligned} \Xi : \mathcal{Q} &\rightarrow \mathcal{W}, \\ \vec{q} &\mapsto \Xi(\vec{q}) = \mathcal{C}_e = (\vec{\epsilon}_{0,e}^T, \vec{\gamma}_e^T)^T, \quad \text{with} \quad \begin{pmatrix} \vec{\epsilon}_{0,e} \\ 1 \end{pmatrix} = \mathbf{H}_{e,0} \begin{pmatrix} \vec{\epsilon}_e \\ 1 \end{pmatrix} \\ \Phi_1(\vec{q}) &= 0, \\ \text{s.t.} \quad &\vdots \\ \Phi_{N_c}(\vec{q}) &= 0. \end{aligned} \tag{5.2}$$

$$\tag{5.3}$$

The vector $\vec{\epsilon}_{0,e}$ is the end-effector's position with respect to the carrier body and $\mathbf{H}_{e,0}$ is the 4×4 homogeneous transformation matrix. \mathcal{Q} defines the coordinate or configuration space and \mathcal{W} defines the workspace. The workspace defines in what space the end-effector can move. The nature of the work space is dependent on the type of manipulator. Given that a rigid body has at most six degrees of freedom (dof), the work space is a subset of one of the following possibilities.

- $\mathcal{W} \subseteq \mathbb{R}$: a linear manipulator (End-effector dof: $D_e = 1$)
- $\mathcal{W} \subseteq \mathbb{R}^2$: a planar manipulator (dof: $D_e = 2$)
- $\mathcal{W} \subseteq \mathbb{R}^2 \times SO(2)$: a planar manipulator with orientation (dof: $D_e = 3$)
- $\mathcal{W} \subseteq \mathbb{R}^3$: spatial manipulator (dof: $D_e = 3$)
- $\mathcal{W} \subseteq \mathbb{R}^3 \times SO(2)$: spatial manipulator with partial orientation (dof: $D_e = 4$)
- $\mathcal{W} \subseteq \mathbb{R}^3 \times S^2$: spatial manipulator with partial orientation (dof: $D_e = 5$)
- $\mathcal{W} \subseteq (\mathbb{R}^3 \times SO(3)) \equiv SE(3)$: spatial manipulator with orientation (dof: $D_e = 6$)

The number of internal degrees of freedom of a mechanism is defined as $D_i = Q - N_c$. Thus, a mechanism is kinematically redundant when $D_i > D_e$. The number $D_r = D_i - D_e$ is called the degree of redundancy. An equivalent formal definition is stated as follows.

Definition 12 (Kinematically Redundant Mechanism [148]). *A mechanism consisting of N_b rigid bodies and N_k kinematic pairs, parameterised by Q coordinates subject to N_c holonomic skleronomic constraints is kinematically redundant, when, for a fixed configuration $\bar{\mathcal{C}}_e \in \mathcal{W}$ of the end-effector, there exists an infinite number of joint configurations $\vec{q} \in \mathcal{Q}$.*

Given this definition of kinematic redundancy, a coordination strategy consists of finding for any fixed configuration $\bar{\mathcal{C}}_e \in \mathcal{W}$ of the end-effector, a solution $\vec{q} \in \mathcal{Q}$ of the joint

coordinates that satisfies the constraints. Furthermore, given the infinite number of solutions one can find a solution satisfying additional requirements. The greater the degree of redundancy, the more additional requirements the solution can satisfy simultaneously.

The concepts discussed above are very machine inspired concepts. The notion of end-effector is a robotics oriented term. However, this discussion does have its meaning in the context of biomechanics and musculoskeletal modelling. Indeed, the model presented in chapter 4 is built as a multibody systems model. This type of model can be abstractly seen as machine. Furthermore, the hand is a manipulator that we continuously use to interact with our environment. Our hand is an end-effector in the same way a mechanical gripper is the end-effector of a robotic machine.

5.3 Overactuation

Actuation is defined as to put into action. In a machine, the external forces make the different links move. However, the term actuation is limited to the forces that can be controlled. The torque generated by an electric motor is an actuation, the earth's gravitational pull is not. A machine can be fully actuated, underactuated or overactuated. A machine can also be simultaneously under and overactuated. Although this situation is not common, it is possible. Overactuation is to use more controlled forces than necessary. An overactuated mechanism has a number of controlled actuators that exceeds the number of internal degrees of freedom [159]. Fully actuated and underactuated machines have respectively an equal number or less controlled actuators than internal degrees of freedom.

An actuator is a controlled element of a mechanism that applies a force and/or moment of force to the mechanism. The force and moment of force are function of a single variable u_i allowing the actuation to be controlled over time. The force in a muscle is controlled by its activation level. The force depends on other variables but is actively controlled by its neural activation level. Given that actuators generate forces in a machine, they appear in the dynamic model of a mechanism relating the mechanism's movement to the forces and moments of force that are applied to it. Consider the dynamic model of a mechanism parameterised by a vector of Q generalised coordinates $\vec{\kappa}$ and subject to N_c holonomic skleronomic constraints. The model is constructed using the Euler-Lagrange equation. The generalised coordinates are defined as the kinematic coordinates from the previous section: $\vec{\kappa} = \vec{q}$. The system has N_a actuators. The Euler-Lagrange equation, with the lagrangian augmented by the constraints is defined according to chapter 3 by:

$$\frac{d}{dt} \left(\frac{\partial \tilde{\mathcal{L}}}{\partial \dot{\vec{\kappa}}} \right) - \frac{\partial \tilde{\mathcal{L}}}{\partial \vec{\kappa}} = \sum_{i=1}^{N_a} \vec{t}_i(u_i), \quad \tilde{\mathcal{L}} = \mathcal{L} + \vec{\Phi}(\vec{\kappa})^T \cdot \vec{\lambda}. \quad (5.4)$$

$$s.t. \quad \vec{\Phi}(\vec{\kappa}) = \vec{0}, \quad N_c \text{ constraints.} \quad (5.5)$$

where $\vec{t}_i(u_i)$ is the generalised force associated to an actuator, parameterised by the variable u_i . The generalised actuator force is either a real force or a moment of force.

The right-hand side of (5.4) is parameterised by the position, velocity and accelerations of the mechanism's generalised coordinates. The set $\{\vec{\kappa}, \dot{\vec{\kappa}}, \ddot{\vec{\kappa}}\}$ defines the mechanism's dynamic state. The vector $\vec{u} = (u_1, \dots, u_{N_a})^T \in \mathbb{R}^{N_a}$ defines the mechanism's actuator state or input state. The degree of actuation of a mechanism is defined by the number of actuator variables N_a . A mechanism is overactuated when $N_a > D = \hat{Q} - N_c$. An equivalent formal definition is stated below.

Definition 13 (Overactuated Mechanism [148]). *A mechanism consisting of a number of bodies and kinematic pairs, parameterised by n coordinates subject to p holonomic skleronomic constraints is overactuated, when, for a fixed dynamic state $\{\vec{\kappa}, \dot{\vec{\kappa}}, \ddot{\vec{\kappa}}\}$ of the mechanism, there exists an infinite number actuator states $\vec{u} \in \mathbb{R}^k$.*

Given this definition of overactuation, a coordination strategy consists of finding a solution $\vec{u} \in \mathbb{R}^k$ of the input states for any dynamic state $\{\vec{\kappa}, \dot{\vec{\kappa}}, \ddot{\vec{\kappa}}\}$ of the mechanism. Just like kinematic redundancy, if the mechanism is highly overactuated a solution can be found satisfying multiple criteria.

5.4 Tasks for Coordination Strategies

In both kinematic redundancy and overactuation, a coordination strategy consists of finding a solution to a mathematically underdetermined problem. In this presentation, a mathematically underdetermined problem is defined by a set of N_e smooth scalar equations, function of $N_q > N_e$ variables. The equations are grouped to define a map.

$$\chi(\vec{v}) : \mathcal{R}_q \subset \mathbb{R}^{N_q} \rightarrow \mathcal{R}_e \subset \mathbb{R}^{N_e},$$

$$\vec{v} \mapsto \left. \begin{array}{l} \chi_1(\vec{v}) = \varepsilon_1 \\ \vdots \\ \chi_{N_e}(\vec{v}) = \varepsilon_{N_e} \end{array} \right\} \chi(\vec{v}) = \vec{\varepsilon}, \quad (5.6)$$

The map is surjective. There are more equations than variables and therefore there is an infinite number of vectors \vec{v} for a given vector $\vec{\varepsilon}$. A coordination strategy for such a problem is to find a parameterisation of the variables v_j in terms of the parameters ε_i .

$$\vec{v} = \vec{v}(\vec{\varepsilon}). \quad (5.7)$$

The problem can be solved for a continuous time-dependent parameterisation of $\vec{\varepsilon}(t)$, $t \in [t_0, t_f]$. For every point $\vec{\varepsilon}(t_i)$ along the path, there are an infinite number of solutions $\vec{v}_a(t_i), \vec{v}_b(t_i), \vec{v}_c(t_i), \dots$ (Fig. 5.3). Thus, for every path $\vec{\varepsilon}(t)$ there are an infinite number of paths $\vec{v}_a(t), \vec{v}_b(t), \vec{v}_c(t), \dots$, defined by the collection of points for all $t \in [t_0, t_f]$.

All the solutions $\vec{v}_a(t_i), \vec{v}_b(t_i), \vec{v}_c(t_i), \dots$ for a given point $\vec{\varepsilon}(t_i)$ define a local manifold $\Omega_{\vec{\varepsilon}(t_i)}$ within \mathcal{R}_q . For a given path $\vec{\varepsilon}(t)$, all the paths $\vec{v}_a(t), \vec{v}_b(t), \vec{v}_c(t), \dots$ pass through the local manifolds $\Omega_{\vec{\varepsilon}(t)}$ at a point, respectively $\vec{v}_a(t_i), \vec{v}_b(t_i), \vec{v}_c(t_i), \dots$. This is important, the local manifolds $\Omega_{\vec{\varepsilon}(t_i)}$ are normal to each other and do not intersect.

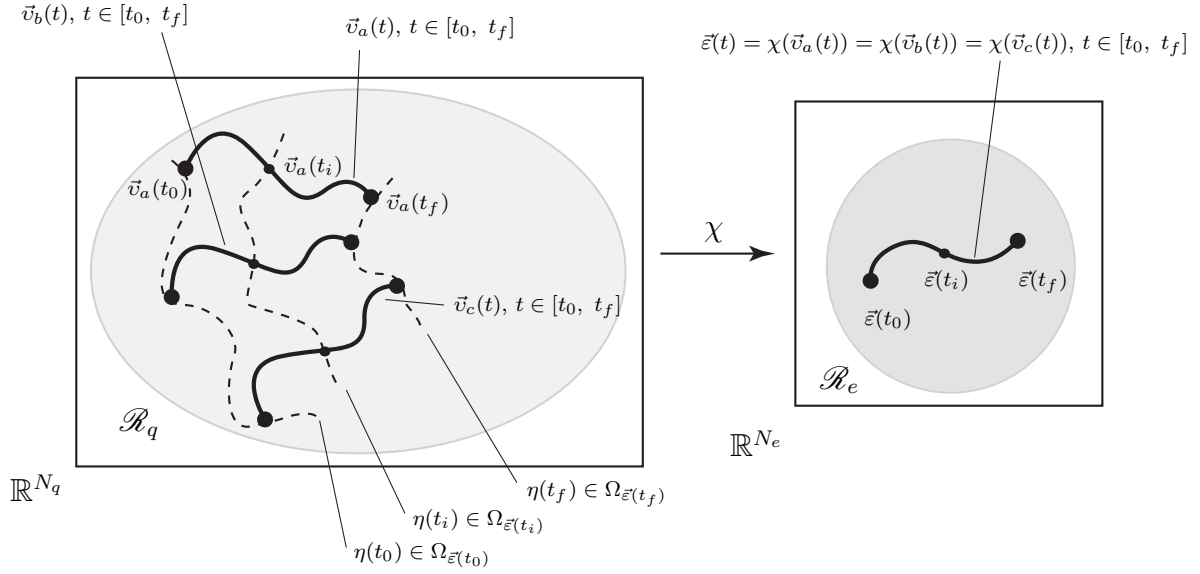


Figure 5.3: Illustrations of local manifolds $\Omega_{\vec{v}(t_i)}$ in coordinated redundancy as described in section 5.4.

The collection of local manifolds defines the redundant manifold $\Omega_{\vec{v}(t)}$. A coordination strategy is to find a path $\vec{v}(t)$ on the redundant manifold, given $\vec{e}(t)$.

The solutions are obtained by differentiation of the solution set \mathcal{R}_q using a task [148]. The primary task is $\vec{e}(t)$ because it differentiates the redundant manifold from within \mathcal{R}_q . The redundant manifold is a subset of \mathcal{R}_q and contains all possible solutions given the primary task. The primary task reduces the search for a solution to a subset of \mathcal{R}_q but does not define a specific solution. Multiple tasks can be used to obtain a finer differentiation of the solution set. The resulting solution will be a compromise between the individual task specific solutions. This is defined as constructive coordination [148].

There are multiple methods of finding a specific solution. A first method which applies to almost all underdetermined problems is to use static optimisation. A secondary task is defined using a cost function of the variables \vec{v} . The primary task is discretised into N_t points: $\vec{e}(t)$, $t \in \{t_0, t_1, \dots, t_{N_t} = t_f\}$. A static optimisation problem or nonlinear program (NLP) is defined for each point, where the underdetermined map defines an equality constraint. The solution must also belong to the coordinate set \mathcal{R}_q .

$$\min_{\vec{v}(t_k)} \Gamma(\vec{v}(t_k)), \quad \vec{v}(t_k) \in \mathcal{R}_q, \quad (5.8)$$

$$s.t. \quad \chi(\vec{v}(t_k)) = \vec{e}(t_k), \quad (5.9)$$

A second method is to use an extension of the map χ . Extra equations are added such as to reduce the degree of underdeterminacy and thereby extend the map. Underdeterminacy cannot be fully eliminated because there is no guarantee a solution will exist. However, by adding additional equations, the search for a solution can be made easier. An optimisation

problem is defined using the extended map. The extension defines additional tasks.

$$\min_{\vec{v}(t_k)} \Gamma(\vec{v}(t_k)), \quad \vec{v}(t_k) \in \mathcal{R}_q, \quad (5.10)$$

$$s.t. \quad \chi(\vec{v}(t_k)) = \vec{\varepsilon}(t_k), \quad (5.11)$$

$$\vec{\Phi}(\vec{v}(t_k)) = \vec{0}, \quad (5.12)$$

A third method is to define a reduced set of coordinates $\hat{\vec{v}}$ that is better suited to the mathematical structure of the problem. This method is similar to the idea of using generalised coordinates in analytical mechanics (cf. chapter 3). In analytical mechanics, generalised coordinates are defined that are better suited to the mathematics of the dynamic model. These coordinates are constructed from equality constraints that are thereby eliminated. In the context of underdetermined problems, the idea is the same. A reduced set of coordinates is constructed using the mathematical structure of the redundant manifold $\Omega_{\vec{\varepsilon}(t)}$. If the number of coordinates still exceeds the number of equations, some form of optimisation will be needed. However, the problem will be easier, given that there are less optimisation variables.

These three methods are not the only solutions to solving underdeterminacy. There exist a number of other methods not discussed here. The following paragraphs redefine the problems of kinematic redundancy and overactuation using the definitions of task and redundancy manifold.

In kinematic redundancy, the primary task is a specific trajectory of the end-effector $\mathcal{C}_e(t)$, $t \in [0, T]$, defined with respect to the internal reference frame. The problem is to find the kinematic coordinates $\vec{q} \equiv \vec{v}$. If the static optimisation method is used, the cost function could be for instance, the error between the kinematic coordinates of the model and a set of measured coordinates obtained from the real system $\vec{q}_m(t_k)$, $t_k \in [0, T]$. The coordination problem is solved at each time step t_k for which a measurement was taken.

$$\min_{\vec{q}(t_k)} \Gamma(\vec{q}(t_k)) = \|\vec{q}_m(t_k) - \vec{q}(t_k)\|^2, \quad \vec{q}(t_k) \in \mathcal{Q}, \quad (5.13)$$

$$s.t. \quad \Xi(\vec{q}(t_k)) = \mathcal{C}_e(t_k) = \Xi(\vec{q}_m(t_k)), \quad (5.14)$$

$$\begin{aligned} \Phi_1(\vec{q}) &= 0, \\ \vdots & \\ \Phi_{N_c}(\vec{q}) &= 0 \end{aligned} \quad (5.15)$$

The redundant manifold $\Omega_{\mathcal{C}_e(t)}$ is comprised of all the local manifolds $\Omega_{\mathcal{C}_e(t_i)}$. The local manifolds are called self motions. The mechanism moves without changing the configuration of the end-effector.

In overactuation, the primary task is a dynamic behaviour defined by a time-dependent parameterisation of the dynamic state: $\vec{\kappa}(t), \dot{\vec{\kappa}}(t), \ddot{\vec{\kappa}}(t)$, $t \in [0, T]$. The problem is to find the input variables $\vec{u} \equiv \vec{v}$. If the static optimisation method is used, the cost function could be for instance, the inputs using the least amount of energy. A static optimisation is defined for every discrete instant of the primary task and the input variables are further

constrained by the real systems physical limitations.

$$\min_{\vec{u}(t_k)} \Gamma(\vec{u}(t_k)) = \frac{1}{2} \sum_{j=1}^{N_a} u_j(t_k), \quad \vec{u}(t_k) \in \mathbb{R}^{N_a}, \quad (5.16)$$

$$s.t. \quad \left(\frac{d}{dt} \left(\frac{\partial \tilde{\mathcal{L}}}{\partial \dot{\vec{\kappa}}} \right) - \frac{\partial \tilde{\mathcal{L}}}{\partial \vec{\kappa}} \right)_{\vec{\kappa}(t_k), \dot{\vec{\kappa}}(t_k), \ddot{\vec{\kappa}}(t_k)} = \sum_{j=1}^{N_a} \vec{t}_j(u_j(t_k)), \quad (5.17)$$

$$\vec{u}_{\min} \leq \vec{u}(t_k) \leq \vec{u}_{\max}. \quad (5.18)$$

The redundant manifold Ω_u is the set of inputs that can be applied to the system without changing the dynamic state.

As stated in the introduction, the human shoulder is a system that is both kinematically redundant and overactuated. There are seven degrees of freedom while the humerus has six and there are $p > 28$ muscle forces. Overactuation coordination strategies require the dynamic state of the model. If a system is both kinematically redundant and overactuated, one must choose to either use two independent coordination strategies or to use a combined strategy. Combined strategies are in general more complex. An example of a combined strategy is optimal control [66, 165]. Therefore, this thesis proposes to use two strategies that are solved successively. Chapter 6 discusses the coordination strategy for the kinematic redundancy problem and chapter 7 discusses the coordination strategy for the overactuation problem.

Chapter 6

Shoulder Kinematic Redundancy Coordination

6.1 Introduction

Human motion or kinematics is defined as the combined motion of all the bones in the skeletal system. Its synthesis for the purpose of simulation in a model is a challenging task because the skeletal system is covered by a layer of skin and muscle. Human kinematics are not directly observable [42]. One can only estimate human motion and a possible technique is the palpation of markers on the skin [211].

The synthesis of human movement is composed of two parts: measurement based description and model based parameterisation. The description of human motion is the description based on measurements of each bone's individual movement relative to the other and with respect to a fixed frame [113, 143, 147]. The parameterisation of human motion is the use of mathematical models called kinematic pairs and chains to reproduce the description [50, 61, 104]. The models are constructed under the hypothesis that physiological articulations behave like ideal mechanical joints [61, 62]. The use of kinematic pairs to model joints provides a natural parameterisation of joint motion using joint coordinates. This chapter focuses on the parametrisation of shoulder motion that has an additional challenge. The skeletal structure of the human shoulder is a kinematically redundant system. Multiple sets of joint coordinates produce the same elbow position.

Given the hypothesis of ideal mechanical joints, constructing kinematic shoulder models is straightforward. Many different models have been developed that can be divided into two types. The first type includes the three anatomical joints and model the system as an open kinematic chain [54, 63, 101, 103, 114]. The second type of kinematic shoulder model includes the three joints and a model of the scapulothoracic contact, defining the system as a closed kinematic chain [74, 194]. Open kinematic chain models are easier to use because all the coordinates are independent but are less accurate because they do not consider the scapula being held against the thoracic cage by the muscles [58]. Closed kinematic chain models are more accurate but more difficult to use because the coordi-

nates are not independent, there are constraints. The constraints impose a kinematic relation between the thoracic cage and scapula. For any kinematic shoulder model the challenge is motion planning, given that the system is redundant. Closed kinematic chain models are more challenging due to constraints related to scapular kinematics.

There are three strategies of planning motion for a kinematic model of the shoulder. The first strategy is data-driven, minimising the difference between measured joint coordinates and the model's joint coordinates [20, 156]. The second strategy is model-based, using regression models of the shoulder's kinematics [54, 101, 114]. The third strategy of planning shoulder motion is to use inverse kinematics [142]. Data-driven methods are the most effective, but require measured data, not easily obtainable [199]. Regression models are constructed from measured data. However, once constructed they can be used without data [33]. The primary disadvantage of regression models is they cannot be used on models with constraints. Inverse kinematics does not require measured data but is the least effective method because there is no guarantee that the joint coordinate motion will reflect the description of the anatomical shoulder's motion [142]. Thus it seems, there does not exist an effective method of planning motion for a kinematic shoulder model including constraints, without measured data.

The goal of this chapter is to present a new parameterisation of a kinematic shoulder model including constraints that facilitates motion planning without measured data. The parameterisation satisfies the constraints but does not explicitly include them and renders all computations related to the kinematic model very straightforward. The chapter begins with a summary of the model presented in chapter 4 and the kinematic redundancy problem. The model considers the synovial articulations to be ball and socket joints, parameterised by spherical kinematic pairs. The scapulothoracic contact is included in the model and represented by two constraints. The end-points of the scapula's medial border are constrained to remain on the surfaces of two ellipsoids with common centre. The concept of coordinate reduction is introduced and illustrated with a two-dimensional model. The scapulothoracic contact model is replaced by two kinematic chains that are used to analyse the model's kinematics. The model is shown to be analogous to a parallel mechanism similar to a Stewart platform. A minimal number of coordinates are defined using the parallel description of the shoulder. The coordinates are minimal in the sense of chapter 3. The number of coordinates equals the number of internal degrees of freedom. Independent from one another, they uniquely parameterise the shoulder model's kinematics. The minimal coordinates parametrisation is compared to other parameterisations from the literature and shown to have potential in developing a general description of kinematic shoulder models which include the scapulothoracic contact.

6.2 Minimal Coordinates for Coordination

6.2.1 Shoulder Kinematic Redundancy Coordination

In chapter 4, a kinematic model of the shoulder's skeletal structure is presented. The model is constructed on the hypotheses that all bones are rigid bodies and that all the synovial articulations behave like ideal ball and socket joints. The joints are parameterised using spherical kinematic pairs. The scapulothoracic contact is modelled using two holonomic skleronomic constraints that keep the points TS and AI on the surface of two ellipsoids with identical centres E (cf. chapter 2 for anatomical references). The ellipsoids represent the thoracic cage with the additional layer of muscle between the ribs and the under side of the scapula. The constraints are equivalent to two spherical slider kinematic pairs between the scapula and ribcage. A body gliding on a surface through a punctual contact is a spherical slider kinematic pair (cf. chapter 3).

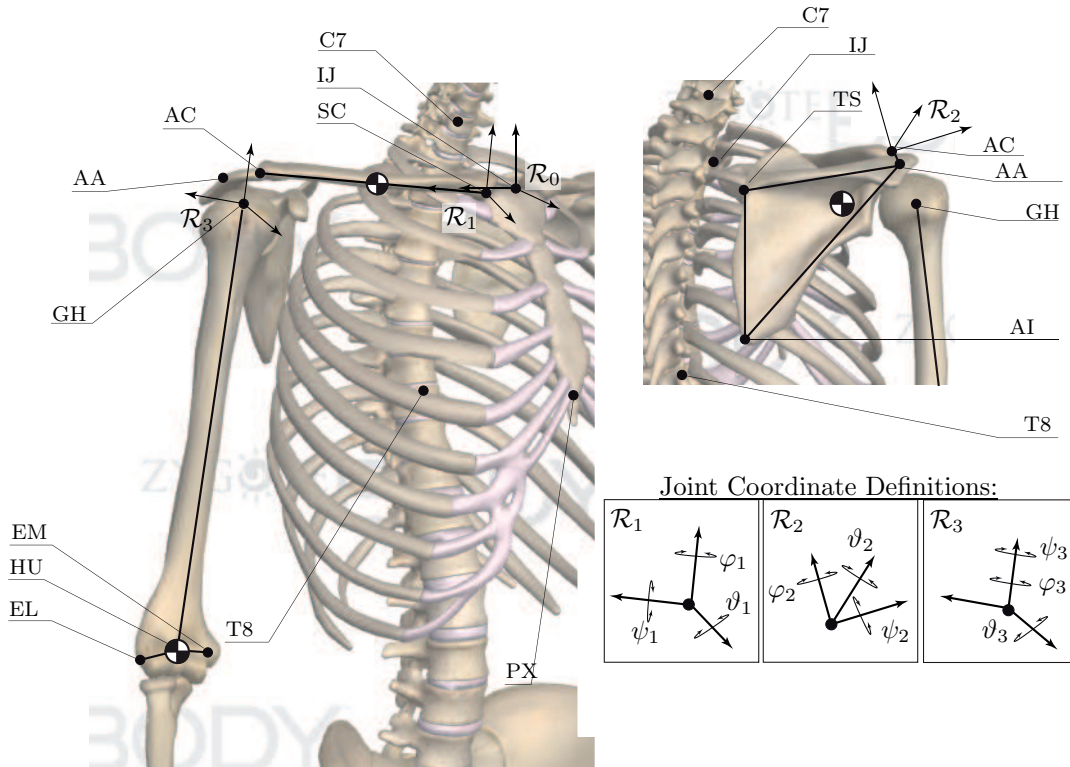


Figure 6.1: *Illustration of the bony landmarks, reference frames and joint coordinates as defined in section 6.2.1. Image created using ZygoteBodyTM zygotebody.com.*

Each bone is attributed a reference system located at the centre of a joint. The bone reference frames are defined according to the ISB guide lines [214]. The thorax is the carrier body and its reference frame is defined as the inertial frame \mathcal{R}_0 (cf. chapter 4). The frame is located at the point IJ (Fig. 6.1). The clavicle's reference frame \mathcal{R}_1 is located as the centre of the sternoclavicular joint SC . The scapula's reference frame \mathcal{R}_2 is located at the centre of the acromioclavicular joint AC . The humeral reference frame \mathcal{R}_3 is located at the centre of the glenohumeral joint \mathcal{R}_3 . The reference frames are

differentiated using subindexes. 0: thorax frame, 1: clavicle frame, 2: scapula frame, 3: humerus frame.

The model's configuration is parameterised by a set of nine angular coordinates grouped into subsets of three. The first three coordinates $\vec{\Upsilon}_1 = (\psi_1, \vartheta_1, \varphi_1)^T$ are Bryan angles parameterising the configuration of the sternoclavicular joint (SC) and thereby the clavicle's configuration with respect to the thorax frame. The next three coordinates $\vec{\Upsilon}_2 = (\psi_2, \vartheta_2, \varphi_2)^T$ are Bryan angles parameterising the configuration of the acromioclavicular joint (AC) and scapula with respect to the thorax. The Bryan angle rotation sequence is defined as XYZ. The last three coordinates $\vec{\Upsilon}_3 = (\psi_3, \vartheta_3, \varphi_3)^T$ are Euler angles parameterising the configuration of the glenohumeral joint (GH) and humerus with respect to the thorax. The Euler angle rotation sequence is ZYZ. Thus, the vector of kinematic coordinates is defined by:

$$\vec{q} = (\vec{\Upsilon}_1^T \quad \vec{\Upsilon}_2^T \quad \vec{\Upsilon}_3^T)^T = (\psi_1 \quad \vartheta_1 \quad \varphi_1 \quad \psi_2 \quad \vartheta_2 \quad \varphi_2 \quad \psi_3 \quad \vartheta_3 \quad \varphi_3)^T. \quad (6.1)$$

The end-effector is defined as the humerus. Its configuration \mathcal{C}_e is defined as the position of the humeroulnar joint $HU_{0,3}$ and the orientation of the humerus with respect to the thorax frame (cf. chapter 2 for conventions on notation).

$$\mathcal{C}_e = (\vec{\epsilon}_{0,3}^T, \vec{\Upsilon}_3^T)^T, \quad (6.2)$$

$$HU_{0,3} : \vec{\epsilon}_{0,3} = \vec{d}_{0,1} + \mathbf{R}_{1,0}\vec{z}_1 + \mathbf{R}_{2,0}\vec{z}_2 + \mathbf{R}_{3,0}\vec{\epsilon}_3. \quad (6.3)$$

$\vec{d}_{0,1}$: vector from IJ to SC in \mathcal{R}_0 . \vec{z}_1 : vector from SC to AC in \mathcal{R}_1 . \vec{z}_2 : vector from AC to GH in \mathcal{R}_2 . $\vec{\epsilon}_3$: vector from GH to HU in \mathcal{R}_3 . The conventions on the rotation matrices are defined in chapter 4.

The forward kinematic map is defined as the function which maps the joint coordinates to the spatial configuration of the humerus (position and orientation). The map is subject to the constraints modelling the scapulothoracic contact.

$$\Xi_S : \mathcal{Q}_S \rightarrow \mathcal{W}_S, \quad \vec{q} \mapsto \Xi_S(\vec{q}) = \mathcal{C}_e = (\vec{\epsilon}_{0,3}^T, \vec{\Upsilon}_3^T)^T, \quad (6.4)$$

$$s.t. \quad \Phi_{TS}(\vec{q}) = (\vec{u}_{0,2} - \vec{e}_0)^T \mathbf{E}_{TS} (\vec{u}_{0,2} - \vec{e}_0) - 1 = 0, \quad (6.5)$$

$$\Phi_{AI}(\vec{q}) = (\vec{v}_{0,2} - \vec{e}_0)^T \mathbf{E}_{AI} (\vec{v}_{0,2} - \vec{e}_0) - 1 = 0. \quad (6.6)$$

The matrices \mathbf{E}_{TS} and \mathbf{E}_{AI} are the ellipsoid quadric matrices. The vectors $\vec{u}_{0,2}$ and $\vec{v}_{0,2}$ are the point vectors of TS and AI respectively, in the inertial frame \mathcal{R}_0 . The vector \vec{e}_0 is the point vector of the common centre of the ellipsoids.

As stated in chapter 5, this kinematic shoulder model is kinematically redundant and the map is underdetermined. For a fixed configuration of the humerus $\mathcal{C}_e \in \mathcal{W}_S$, there is an infinite number of kinematic coordinates sets $\vec{q} \in \mathcal{Q}_S$. Furthermore, it was also stated in chapter 5 that a possible solution to the problem is to minimise the error between the model's coordinates $\vec{q}(t_k)$ and the measured values of the coordinates $\vec{q}_m(t_k)$ at discrete instances of a motion $t_k \in [0, T]$ (the subindex m indicates measured).

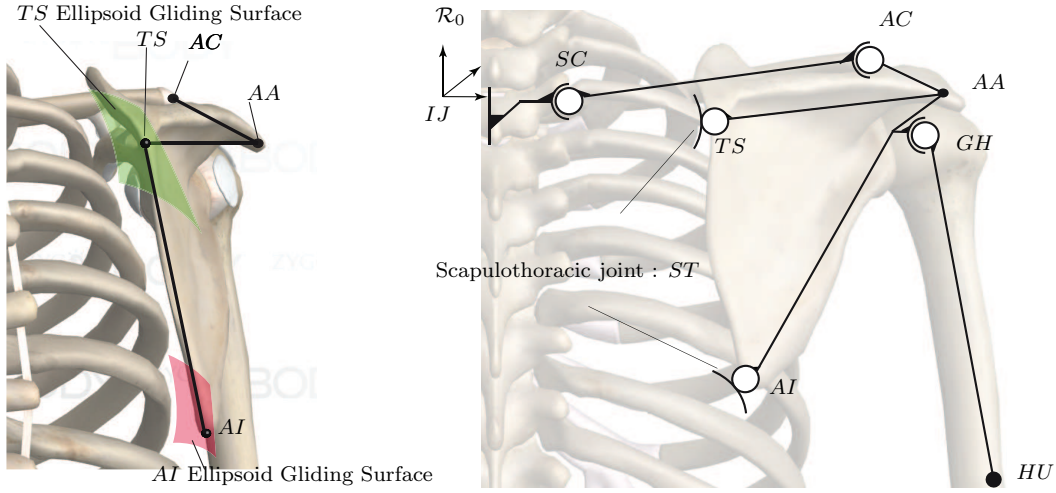


Figure 6.2: *Diagram of the shoulder's kinematic model, as defined in chapter 4. Image created using ZygoteBodyTM zygotebody.com.*

Consider a movement was measured on a real shoulder, for instance abduction in the scapular plane (cf. chapter 2). Markers were placed on the body of a subject at the locations of bony landmarks and measurements of the marker locations were taken at N different instants $t_k \in \{t_0, \dots, t_N\}$ during the motion. The palpated marker positions were then used to estimate the position of the bony landmarks [56]. The estimated bony landmark positions were used to reconstruct the bone reference frames and the Euler and Bryan angles were extracted [56, 58, 199]. The result is a set of measured coordinate vectors: $\{\vec{q}_m(t_0), \vec{q}_m(t_1), \dots, \vec{q}_m(t_k), \dots, \vec{q}_m(t_N)\}$. As defined in chapter 5, a set of model coordinate vectors $\{\vec{q}(t_0), \vec{q}(t_1), \dots, \vec{q}(t_k), \dots, \vec{q}(t_N)\}$ can be found by solving the following static optimisation problem at every instant t_k of the motion.

$$\min_{\vec{q}(t_k)} \Gamma(\vec{q}(t_k)) = \frac{1}{2} \|\vec{q}_m(t_k) - \vec{q}(t_k)\|^2 = \frac{1}{2} \sum_{i=1}^9 (q_{m,i}(t_k) - q_i(t_k))^2, \quad \vec{q}(t_k) \in \mathcal{Q}_S, \quad (6.7)$$

$$s.t. \quad \Xi_S(\vec{q}(t_k)) - \Xi_S(\vec{q}_m(t_k)) = \vec{0}, \quad (6.8)$$

$$\Phi_{TS}(\vec{q}(t_k)) = 0, \quad (6.9)$$

$$\Phi_{AI}(\vec{q}(t_k)) = 0. \quad (6.10)$$

This problem defines a kinematic coordination strategy as presented in chapter 5. The approach is straightforward but requires the availability of measured data. If the problem is unconstrained, an optimisation problem is unnecessary. One could directly impose the equality between the model's coordinates and the measured coordinates.

6.2.2 Manifolds and Coordinate Reduction

This section introduces the idea that a different parameterisation of the coordinate space \mathcal{Q}_S can eliminate the constraints in the kinematic coordination strategy. Furthermore, the parameterisation makes all computational operations related to the model's kinematic coordination straightforward. The parameterisation is constructed by taking advantage of the mathematical structure of the coordinate space \mathcal{Q}_S .

The forward kinematic map and the two scapulothoracic constraints are assumed to be smooth or C^∞ functions of the joint coordinates. Under these assumptions, the coordinate space is a compact smooth manifold. Indeed, the nine kinematic coordinates define charts $\phi_{i,S}$ from subsets of \mathbb{R}^3 to $SO(3)$ in sets of three.

$$\begin{aligned} \phi_{i,S} : [-\pi, \pi] \times [-\pi, \pi] \times [-\pi, \pi] &\rightarrow SO(3), \quad i = 1, 2, 3, \\ (\psi_i, \vartheta_i, \varphi_i) &\mapsto \phi_{i,S}(\psi_i, \vartheta_i, \varphi_i) = \mathbf{R}_{i,0}. \end{aligned} \quad (6.11)$$

The coordinate space \mathcal{Q}_S is a subset of the space $(SO(3))^3 = SO(3) \times SO(3) \times SO(3)$. The elements of the coordinate space are the rotation matrices $(\mathbf{R}_{1,0}, \mathbf{R}_{2,0}, \mathbf{R}_{3,0}) \in \mathcal{Q}_S \subset (SO(3))^3$. For a given task of the end-effector, the redundant manifold $\Omega_{\vec{c}(t)}$ is a subspace of \mathcal{Q}_S (cf. chapter 5). The redundant manifold contains all the self motions associated to the task.

The group $SO(3)$ is isomorphic or identical to the space of rotations in \mathbb{R}^3 . It is a Lie group (group with a natural manifold structure), diffeomorphic to the real projective space \mathbb{RP}^3 , a compact smooth or C^∞ -manifold. This implies that $SO(3)$ is a compact C^∞ -manifold which implies that $(SO(3))^3$ is also a compact C^∞ -manifold. *The coordinate space of the kinematic shoulder model presented in chapter 4 and summarised in section 6.2.1 is a compact C^∞ -manifold of dimension seven.* There are nine coordinates subject to smooth equality constraints.

The image space or work space \mathcal{W}_S is a subset of $SE(3) = \mathbb{R}^3 \times SO(3)$. $SE(3)$ is not compact (\mathbb{R}^3 is not compact) but is a smooth manifold. However, given that \mathcal{Q}_S is compact and that Ξ_S is smooth, the work space is also compact. The image of a compact space through a smooth map is also compact. The humerus works in a compact subset of \mathbb{R}^3 . Thus, the coordinate space \mathcal{Q}_S and work space \mathcal{W}_S of the shoulder's forward kinematic maps are compact C^∞ -manifolds of dimensions seven and six respectively, having the particular mathematical structure of locally looking like subsets of the Euclidean space of the same respective dimension.

A smooth or C^∞ -manifold is a particular type of differentiable manifold. Differentiable manifolds are found in numerous engineering problems and involve C^k functions with $k \geq 1$. The constraints of an optimisation problem can define a differentiable manifold, under certain assumptions on the type of constraints. The domain space and image space of the kinematic map of a robot manipulator can involve differentiable manifolds as illustrated previously. Dynamic systems can evolve on differentiable manifolds. Thus, differentiable manifolds are important from an engineering point of view but are not always apparent. A simple definition of a differentiable manifold is that it is a subset of \mathbb{R}^n of dimension k that locally "looks" exactly like \mathbb{R}^k . This can also be understood as

a surface in \mathbb{R}^n for which any parameterisation requires at least k coordinates. A formal definition is stated as follows.

Definition 14 (Differentiable Manifold [55]). *A subset \mathcal{M} of \mathbb{R}^n is a k -dimensional manifold if for each $\vec{x} \in \mathcal{M}$ there are: open subsets \mathcal{U} and \mathcal{V} of \mathbb{R}^n with $\vec{x} \in \mathcal{U}$, and a differentiable (bijective C^k function) f from \mathcal{U} to \mathcal{V} such that*

$$f(\mathcal{U} \cap \mathcal{M}) = \{\vec{y} = (y_1, \dots, y_n)^T \in \mathcal{V} : y_{k+1} = \dots = y_n = 0\}. \quad (6.12)$$

Thus, the point \vec{y} in the image of f has a representation like:

$$\vec{y} = (y_1(\vec{x}), \dots, y_k(\vec{x}), 0, \dots, 0)^T. \quad (6.13)$$

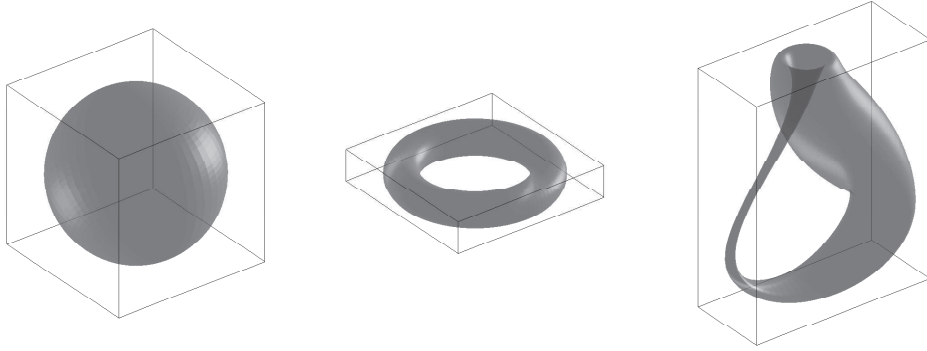


Figure 6.3: Examples of well known two-dimensional compact smooth manifolds. From left to right, a sphere, a torus and a Klein bottle.

A smooth manifold is a differentiable manifold where all the maps f are smooth or C^∞ . The most well known examples are two-dimensional compact smooth manifolds in \mathbb{R}^3 such as the sphere, the torus or the Klein bottle (Fig. 6.3). It is noteworthy that compact manifolds of lower dimension are in general easier to work with and are therefore better documented. All the two-dimensional compact manifolds in \mathbb{R}^3 have been catalogued. The step from two-dimensional compact manifolds to three-dimensional compact manifolds is already a very large step in complexity and is the reason why the Poincaré conjecture remained unproven for such a long period of time [137, 185]. The two most important definitions related to a differentiable manifold are the definitions of charts and atlas providing a basis for working with manifolds.

Definition 15 (Charts and Atlas for a Smooth Manifold [55]). *A chart in \mathcal{M} is a pair (\mathcal{V}, ϕ_v) with \mathcal{V} an open set of \mathcal{M} and ϕ_v a C^∞ function onto an open set in \mathbb{R}^k and having a C^∞ inverse. A C^∞ atlas is a set of such charts $\{(\mathcal{V}_i, \phi_i)\} = \mathcal{A}$, with the following properties.*

- $\mathcal{M} = \cup \mathcal{V}_i$: the manifold is equal to the union of all the sets \mathcal{V}_i ,

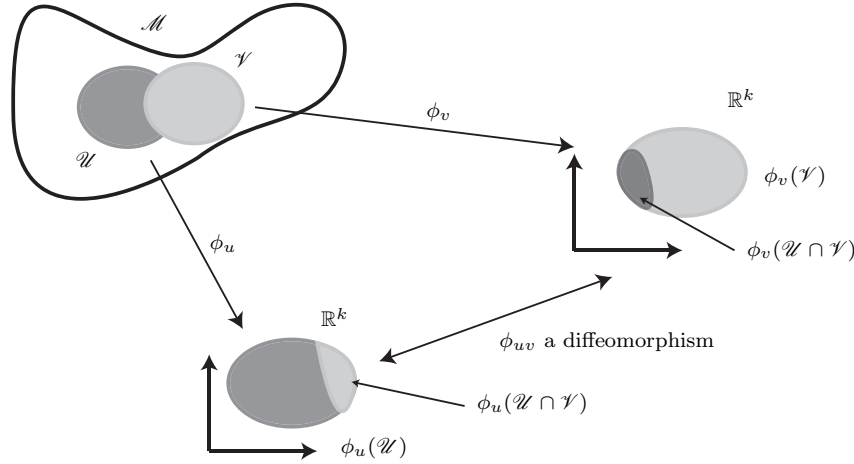


Figure 6.4: *Diagram of two charts of a C^∞ atlas on a differentiable (smooth) manifold \mathcal{M} in \mathbb{R}^n of dimension \mathbb{R}^k as described in section 6.2.2, definition 4.*

- If (\mathcal{V}_u, ϕ_u) and (\mathcal{V}_v, ϕ_v) are in \mathcal{A} and $\mathcal{V}_v \cap \mathcal{V}_u \neq \emptyset$, then

$$\phi_{vu} = \phi_u \circ \phi_v^{-1} : \phi_v(\mathcal{V}_v \cap \mathcal{V}_u) \rightarrow \phi_u(\mathcal{V}_v \cap \mathcal{V}_u)$$

is a C^∞ diffeomorphism (bijective C^∞ function)

An intuitive example of charts and atlases on a smooth manifold, is the maps of the Earth that are flat. They are parameterised in \mathbb{R}^2 but they map at part of the Earth which is a sphere in \mathbb{R}^3 . Each map defines a chart and all the maps form an atlas of the Earth's spherical manifold. Just like maps of the Earth, charts and atlases are not unique.

A k -dimensional, differentiable manifold in \mathbb{R}^n can be parameterised by $k \leq \hat{Q} \leq n$ coordinates. In general, each coordinate belongs to a subset of \mathbb{R} and the vector of coordinates belongs to a subset of $\mathbb{R}^{\hat{Q}}$. The most attractive description is to use k coordinates because they are all independent. Furthermore, the Euclidean space \mathbb{R}^k is a vector space that is very easy to work with for any finite k . Given that the charts from the previous definition are all C^k and invertible, all operations related to the manifold can be carried out in \mathbb{R}^k and then mapped onto the manifold using the inverse chart. The independent directions related to each variable are orthogonal and straight. It is the charts that curve the representation. If k coordinates parameterise a k -dimensional, differentiable manifold in \mathbb{R}^n , the coordinates are said to be minimal. The difficulty lies in the construction of charts and an atlas.

If the number of coordinates is greater than k , the coordinates are interdependent and describe the curved space. Although, they belong to $\mathbb{R}^{\hat{Q}}$, the independent direction are not not orthogonal and not straight. A sphere can be described by interdependent cartesian coordinates x , y and z . The interdependency is defined by $x^2 + y^2 + z^2 - r^2 = 0$, describing the curved surface of the sphere. This example is fairly simple and straightforward. However, the interdependency is in general not straightforward and the use of such coordinates becomes difficult.

Given a k -dimensional, differentiable manifold in \mathbb{R}^n , parameterised by $\hat{Q} > k$ coordinates, the construction of charts and an atlas is a coordinate reduction. The number of coordinates is reduced from \hat{Q} to k , through the construction of the charts.

To illustrate the concept of coordinate reduction applied to kinematics, consider a two-dimensional analogue model of the shoulder (Fig. 6.5). The model considers the clavicle rotating around the sternoclavicular joint (SC) through a revolute joint. The joint is parameterised by the coordinate φ_1 . The model considers the scapula (TS , AC and GH) rotating around the acromioclavicular joint (AC) through a revolute joint. The joint is parameterised by the coordinate φ_2 . The point TS on the scapula is constrained to remain on an ellipse of axial dimensions a_e , b_e centred at E . The scapula is not attached to the ellipse, the point TS glides over the surface. The humerus is modelled as a body rotating around the glenohumeral joint (GH) through a revolute joint. The joint is parameterised by the coordinate φ_3 .

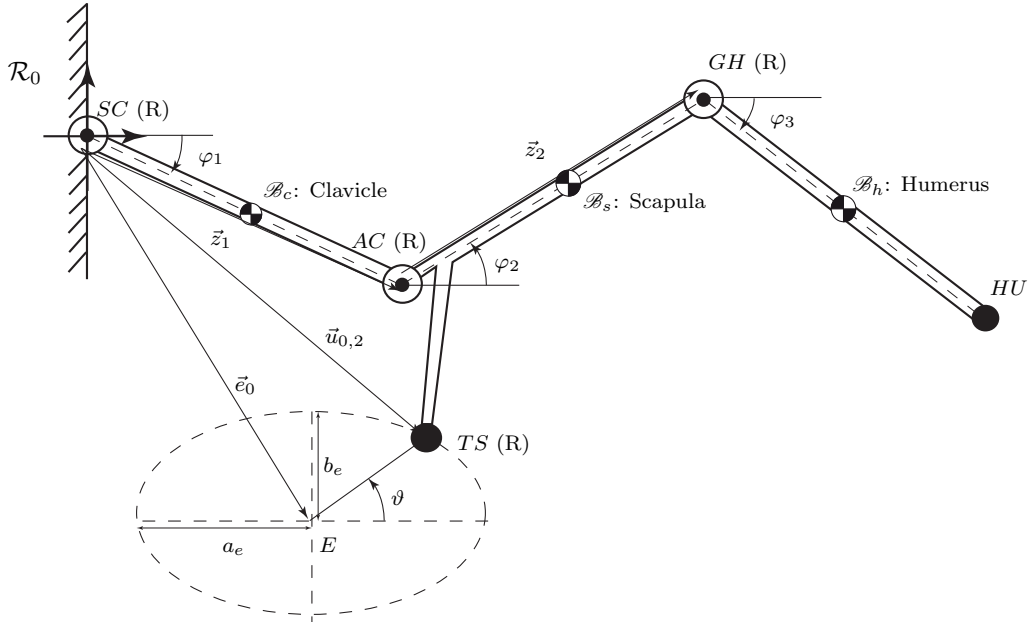


Figure 6.5: *Illustration of a two-dimensional analogue for the shoulder discussed in section 6.2.2.*

The most natural kinematic model of this system is to use the three joint coordinates φ_i subject to the circular constraint. The end-effector is defined as the humerus and its configuration is simply defined as the position of $HU_{0,3}$. The forward kinematic map is defined by

$$\Xi : \mathcal{Q} \rightarrow \mathcal{W},$$

$$(\varphi_1, \varphi_2, \varphi_3) \mapsto \mathcal{C}_e = \vec{e}_{0,3} = \mathbf{R}_{1,0}(\varphi_1)\vec{z}_1 + \mathbf{R}_{2,0}(\varphi_2)\vec{z}_2 + \mathbf{R}_{3,0}(\varphi_3)\vec{e}_3, \quad (6.14)$$

$$s.t. \quad \Phi_{TS}(\varphi_1, \varphi_2, \varphi_3) = (\vec{u}_{0,2} - \vec{e}_0)^T \mathbf{E}_{TS}(\vec{u}_{0,2} - \vec{e}_0) - 1 = 0. \quad (6.15)$$

where $\mathbf{R}_{i,0}(\varphi_i)$ are the rotation matrices from local to inertial frame. The model has two degrees of freedom and is not redundant. There are three coordinates subject to a single constraint. The coordinate space of a revolute joint is S^1 , a compact smooth manifold (cf.

chapter 3). Thus, the coordinate space is a compact subset of $\mathcal{Q} \subset (S^1)^3 = S^1 \times S^1 \times S^1$. The map Ξ is smooth and the work space \mathcal{W} is a compact subset of \mathbb{R}^2 . To each coordinate is associated a map ϕ_i from $[-\pi, \pi] \subset \mathbb{R}$ to $SO(2) \equiv S^1$. These three maps define the inverse charts of $(S^1)^3$ but not the coordinate manifold \mathcal{Q} .

$$\begin{aligned}\phi_i &: [-\pi, \pi] \rightarrow S^1, \\ \psi_i &\mapsto \phi_i(\psi) = \mathbf{R}_{i,0}(\psi_i).\end{aligned}\tag{6.16}$$

The constraint (6.15), defines an interdependency between ψ_1 and ψ_2 . The coordinate reduction will be defined by using the constraint directly.

The point TS is constrained to remain on an ellipse that is homeomorphic or topologically equivalent to a circle. Like the shoulder kinematic model where the scapulothoracic constraints define spherical slider kinematic pairs, the circular constraint also defines a two dimensional spherical slider kinematic pair. The scapula can rotate around the points TS if not connected to anything else and the point TS can translate along the edge of the ellipse. The position of TS can be parameterised by a polar coordinate ϑ . This coordinate defines a chart from $[-\pi, \pi] \subset \mathbb{R}$ to $S^1 = \{\vec{x} \in \mathbb{R}^2 \mid \|\vec{x}\|_2 = 1\}$. The ellipse is a deformed circle. Given the ellipse constraint, the radial polar coordinate ρ will also be function of ϑ .

$$\begin{aligned}\phi_\vartheta &: [-\pi, \pi] \rightarrow S^1, \\ \vartheta &\mapsto \phi_\vartheta(\vartheta) = \vec{u}_{0,2} = \begin{pmatrix} \rho(\vartheta) \cos(\vartheta) + x_e \\ \rho(\vartheta) \sin(\vartheta) + y_e \end{pmatrix},\end{aligned}\tag{6.17}$$

where x_e and y_e are the cartesian coordinates with respect to the inertial frame located at SC . This parameterisation must satisfy the ellipse constraint. This is imposed by defining the following relation between the parameterisation and the parameterisation of an ellipse, using a different angular coordinate ψ .

$$\begin{pmatrix} \rho(\vartheta) \cos(\vartheta) \\ \rho(\vartheta) \sin(\vartheta) \end{pmatrix} = \begin{pmatrix} a_e \cos(\psi) \\ b_e \sin(\psi) \end{pmatrix} \Rightarrow \begin{cases} \tan(\vartheta) = (b_e/a_e) \tan(\psi), \\ \rho(\vartheta) = \sqrt{(a_e \cos(\psi))^2 + (b_e \sin(\psi))^2}. \end{cases}\tag{6.18}$$

The parameterisation (6.16) is now be expressed in terms of the single elliptical coordinate ψ .

$$\vec{u}_{0,2}(\vartheta(\psi)) = \begin{pmatrix} \rho(\vartheta) \cos(\vartheta) + x_e \\ \rho(\vartheta) \sin(\vartheta) + y_e \end{pmatrix} = \begin{pmatrix} \cos(\vartheta(\psi)) & -\sin(\vartheta(\psi)) \\ \sin(\vartheta(\psi)) & \cos(\vartheta(\psi)) \end{pmatrix} \begin{pmatrix} \rho(\vartheta(\psi)) \\ 0 \end{pmatrix} + \begin{pmatrix} x_e \\ y_e \end{pmatrix}.\tag{6.19}$$

This parameterisation mathematically represents a linear prismatic joint parameterised by $\rho(\vartheta(\psi))$. The prismatic joint is dependent on the elliptical coordinate ψ which is attached to a point E through a revolute joint parameterised by the elliptical coordinate. Effectively, the spherical slider kinematic pair has been replaced a revolute joint at E , a revolute joint at TS and a dependent or passive linear prismatic joint in-between (Fig. 6.6). A second kinematic chain has been constructed between the carrier body and end-effector. A coordinate reduction will use this parameterisation of TS to parameterise the mechanism's kinematics instead of using the two joint angles φ_1 and φ_2 .

If the position of TS is known, using the elliptical coordinate ψ , the configuration of the scapula and clavicle are known. The point SC is fixed and the point TS is known. Under the rigid body hypothesis, the distance between SC and AC is constant and the distance between TS and AC is constant. The point AC lies on the intersection of two circles, centred at SC and TS (Fig. 6.5). The intersection has a single solution with two branches. The two branches meet when the distance between SC and TS is equal to the sum of the radii. The mechanism's initial configuration defines AC to be on one of the two branches. When the mechanism moves, it suffices to guarantee that AC is always on the same branch. Depending on the mechanism's geometry in terms of length, the branches meet or not. Furthermore, it is not guaranteed that the point TS can travel around the entire ellipse. Thus, ϑ is a map between $[\vartheta_-, \vartheta_+] \subset \mathbb{R}$ and $\mathcal{Q}_\vartheta \subset S^1$.

The kinematics of the entire mechanism can be parameterised using two coordinates (ϑ, φ_3) in stead of three $(\varphi_1, \varphi_2, \varphi_3)$. The first two joint angles are defined as functions of the coordinate ϑ . The corresponding kinematic map is now defined without constraints.

$$\begin{aligned} \Xi : \mathcal{Q} \subset (S^1)^3 &\rightarrow \mathcal{W} \subset \mathbb{R}^2, \\ (\vartheta, \varphi_3) &\mapsto \mathcal{C}_3 = \vec{e}_{0,3} = \vec{u}_{0,2}(\vartheta) + \mathbf{R}_{2,0}(\varphi_2(\vartheta))\vec{z}_2 + \mathbf{R}_{3,0}(\varphi_3)\vec{e}_3, \end{aligned} \quad (6.20)$$

The two coordinates (ϑ, φ_3) and the two maps ϕ_ϑ and ϕ_3 define the charts on the coordinate manifold \mathcal{Q} . This parameterisation of the kinematics makes all kinematic computations very straightforward given that there are no constraints. However, the parameterisation using the joint angles will be kept for constructing the dynamic model. The following section extends this example to the entire shoulder model.

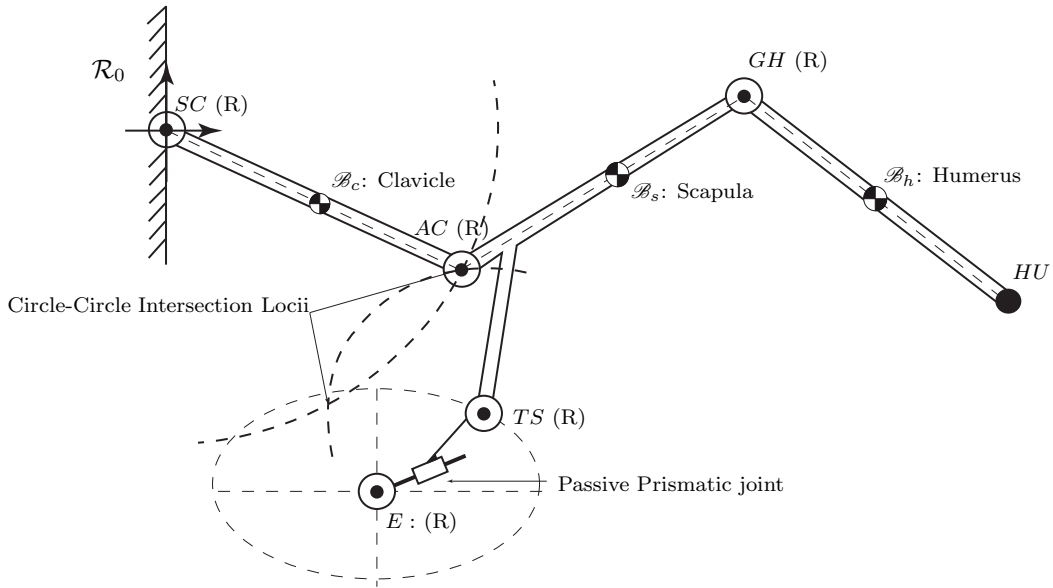


Figure 6.6: *Illustration of a two-dimensional analogue shoulder model with the new kinematic chain as discussed in section 6.2.2.*

6.2.3 A Parallel Platform Kinematic Shoulder Model

The shoulder kinematic model presented in chapter 4 and briefly reviewed in section 6.2.1 parameterises the skeletal system's motion using the joint coordinates. The forward kinematic map between the coordinates and the configuration of the humerus is subject to two holonomic skleronomic constraints modelling the scapulothoracic contact. In the previous section a method of constructing a coordinate reduction was presented. The underlying idea of the method is to redefine the constraints as kinematic chains between the body that is constrained and the carrier body. Once the constraint is redefined, its corresponding kinematic chain is used to parameterise the kinematics using less coordinates.

The scapulothoracic contact is modelled using two holonomic skleronomic constraints. The points TS and AI are constrained to remain on the surface of ellipsoids. It is stated in section 6.2.1, that these constraints can be viewed as spherical slider kinematic pairs. A single spherical slider kinematic pair as described in chapter 3 is a body gliding over a two-dimensional surface in \mathbb{R}^3 . The contact between the body and the surface is punctual. The following paragraphs present a mechanical description of this kinematic pair using other pairs.

The configuration $\mathcal{C}_{0,i}$ of a three dimensional rigid body \mathcal{B}_i in $SE(3)$, is defined by a Euclidean displacement with respect to the inertial reference frame. Any point $P_{0,i}$ on the body is defined in the inertial frame by:

$$P_{0,i} : \vec{p}_{0,i} = \vec{d}_{0,i} + \mathbf{R}_{i,0} \vec{p}_i, \quad (6.21)$$

If the body is free, the displacement is parameterised by six independent coordinates. The three cartesian coordinates of the centre of the body's frame with respect to the inertial frame: $\vec{d}_{0,i}$. The three rotation angles (Bryan angles) of the body frame about the inertial frame: $\mathbf{R}_{i,0}(\psi, \vartheta, \varphi)$.

A spherical kinematic pair parameterises the body's rotation and is a mathematical description of a ball and socket joint. A ball and socket joint is an idealised mechanical description of a freely rotating body. An ideal ball and socket joint is a mechanical implementation of $SO(3)$.

An alternate parameterisation of the linear translation $\vec{d}_{0,i}$ uses spherical coordinates. Spherical coordinates (ρ, α, β) are an alternate way of charting \mathbb{R}^3 . The cartesian coordinates of the displacement (6.21) are replaced by spherical coordinates.

$$\vec{d}_{0,i} = \begin{pmatrix} x_{0,i} \\ y_{0,i} \\ z_{0,i} \end{pmatrix} = \begin{pmatrix} \rho_d \cos(\alpha_d) \sin(\beta_d) \\ \rho_d \sin(\alpha_d) \sin(\beta_d) \\ \rho_d \cos(\beta_d) \end{pmatrix}. \quad (6.22)$$

In the Euclidean displacement (6.21), the rotation is mechanically described by a ball and socket joint. The mechanical description of the linear translation is defined by the following theorem.

Theorem 18 (Mechanical Description of \mathbb{R}^3). *The three-dimensional Euclidean space \mathbb{R}^3 is mechanically described using a linear prismatic joint connected to a fixed point through a universal joint (cf. chapter 3).*

Proof. Any point P in \mathbb{R}^3 is described with respect to a fixed point in a fixed frame by three coordinates. Cartesian coordinates are the standard coordinates and define an atlas with one chart, the identity chart. Each point is identified with itself and this atlas defines the standard smooth structure of \mathbb{R}^3 . Another possible parameterisation is spherical coordinates. The usual spherical coordinates define the following chart:

$$\phi : \mathbb{R}_+ \times [0, 2\pi[\times [0, \pi] \rightarrow \mathcal{U} \subset \mathbb{R}^3,$$

$$(\rho, \alpha, \beta) \mapsto \phi(\rho, \alpha, \beta) = \vec{p} = \begin{pmatrix} x \\ y \\ z \end{pmatrix} = \begin{pmatrix} \rho \cos(\alpha) \sin(\beta) \\ \rho \sin(\alpha) \sin(\beta) \\ \rho \cos(\beta) \end{pmatrix}. \quad (6.23)$$

The inverse chart is defined by

$$\phi^{-1} : \mathcal{U} \subset \mathbb{R}^3 \rightarrow \mathbb{R}_+ \times [0, 2\pi[\times [0, \pi],$$

$$(x, y, z) \mapsto \phi^{-1}(x, y, z) = \begin{pmatrix} \rho \\ \alpha \\ \beta \end{pmatrix} = \begin{pmatrix} \sqrt{x^2 + y^2 + z^2} \\ \arctan\left(\frac{y}{x}\right) \\ \arctan\left(\frac{\sqrt{x^2 + y^2}}{z}\right) \end{pmatrix}. \quad (6.24)$$

These charts are local charts. A single set of spherical coordinates does not uniquely cover \mathbb{R}^3 . For a fixed value of ρ , the two coordinates α and β chart S^2 requiring at least two charts. For instance, the north and south pole stereographic projections. The spherical parameterisation states that \mathbb{R}^3 is locally equivalent to $\mathbb{R}_+ \times S^2$. The chart ϕ is smooth but not global. Thus, spherical coordinates do chart \mathbb{R}^3 .

The chart (6.23) can be written in the following form:

$$P_0 : \vec{p}_{0,i} = \begin{pmatrix} \cos(\alpha) & -\sin(\alpha) & 0 \\ \sin(\alpha) & \cos(\alpha) & 0 \\ 0 & 0 & 1 \end{pmatrix} \begin{pmatrix} \cos(\beta) & 0 & \sin(\beta) \\ 0 & 1 & 0 \\ \sin(\beta) & 0 & \cos(\beta) \end{pmatrix} \begin{pmatrix} 0 \\ 0 \\ \rho \end{pmatrix}. \quad (6.25)$$

The vector $(0 \ 0 \ \rho)^T$, with $\rho \in \mathbb{R}_+$, parameterises an infinite linear prismatic kinematic pair. There is one coordinate parameterising a one-dimensional axes [23].

The two successive rotations are rotations around intersecting axes. As stated in chapter 3, the universal or cardan joint is a mechanical description of a two-dimensional rotation in three-dimensional space. In a universal joint, the rotations occur around intersecting. This differentiates the universal joint from two serially connected revolute joints with non intersecting rotation axes. Thus, the spherical description of space is a mathematical parameterisation of a mechanical description of space. The mechanical description uses a linear prismatic joint connected to a fixed point through a universal joint. \square

The special Euclidean group $SE(3)$ has a mechanical implementation. The mechanism has a universal joint fixed to a point in the inertial frame. An infinite prismatic joint is attached, at one end, to the universal joint and allowed to freely rotate around the fixed point. On the other end, there is a ball and socket joint connecting the body to the prismatic joint (Fig: 6.7).

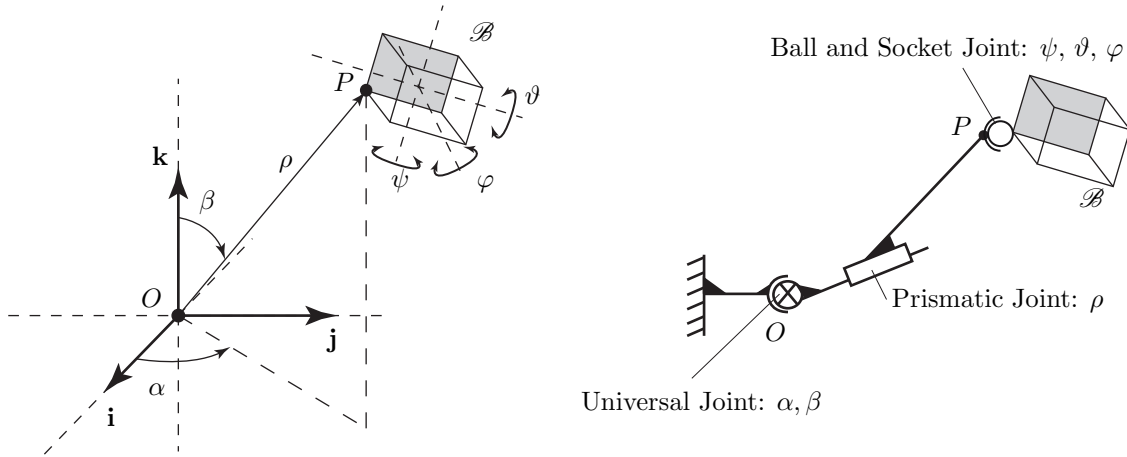


Figure 6.7: Illustration of the mechanical description of a free body in space defined by spherical coordinates and a spherical joint as described in Theorem 18, section 6.2.3.

The scapulothoracic contact is modelled using two spherical slider joints on surfaces that are ellipsoids. A spherical slider kinematic pair has five degrees of freedom (cf. chapter 2). In the mechanical description of a body gliding on a surface, one of the coordinates becomes function of the other two. The point P on the body is now constrained to glide on a two-dimensional algebraic surface \mathcal{S} defined by a smooth function of the coordinates of P .

$$\mathcal{S} : f(x, y, z) = f(\rho, \alpha, \beta) = 0. \quad (6.26)$$

Constraining P to remain on an algebraic surface \mathcal{S} , is to enforce a dependency between the coordinates. One of them is function of the others. For instance, $\rho = \rho(\alpha_s, \beta_s)$. The subindex s indicates that (α_s, β_s) parameterise the surface. The three Bryan angles $(\psi, \vartheta, \varphi)$ remain independent. Mechanically, the prismatic joint's length is now function of both of the universal joint's angles. The prismatic joint is said to be passive, and cannot be actuated independently from the motion of the universal joint (Fig. 6.5). In the shoulder model, the surface is an ellipsoid imposing the following relation on the spherical coordinates:

$$\begin{pmatrix} \rho \cos(\alpha) \sin(\beta) \\ \rho \sin(\alpha) \sin(\beta) \\ \rho \cos(\beta) \end{pmatrix} = \begin{pmatrix} a_e \cos(\alpha_e) \sin(\beta_e) \\ b_e \sin(\alpha_e) \sin(\beta_e) \\ c_e \cos(\beta_e) \end{pmatrix}, \quad \begin{array}{l} (\alpha, \beta) : \text{Universal joint coordinates,} \\ (\alpha_e, \beta_e) : \text{Ellipsoid coordinates.} \end{array} \quad (6.27)$$

The prismatic and universal joint coordinates are now expressed in terms of the ellipsoid coordinates (α_e, β_e) .

$$\begin{aligned} \rho &= \sqrt{(a_e \cos(\alpha_e) \sin(\beta_e))^2 + (b_e \sin(\alpha_e) \sin(\beta_e))^2 + (c_e \cos(\beta_e))^2}, \\ \alpha &= \arctan \left(\frac{b_e}{a_e} \tan(\alpha_e) \right), \\ \beta &= \arctan \left(\frac{\sqrt{(a_e \cos(\alpha_e))^2 + (b_e \sin(\alpha_e))^2}}{c_e} \tan(\beta_e) \right). \end{aligned} \quad (6.28)$$

The mechanism is a universal joint with coordinates (α_e, β_e) and a passive prismatic joint with coordinate $\rho(\alpha_e, \beta_e)$. This illustrates the following point. Kinematic pairs with

more degrees of freedom can be described using lower kinematic pairs. The spherical slider kinematic pair is described by a universal pair, a prismatic pair and a spherical pair [123].

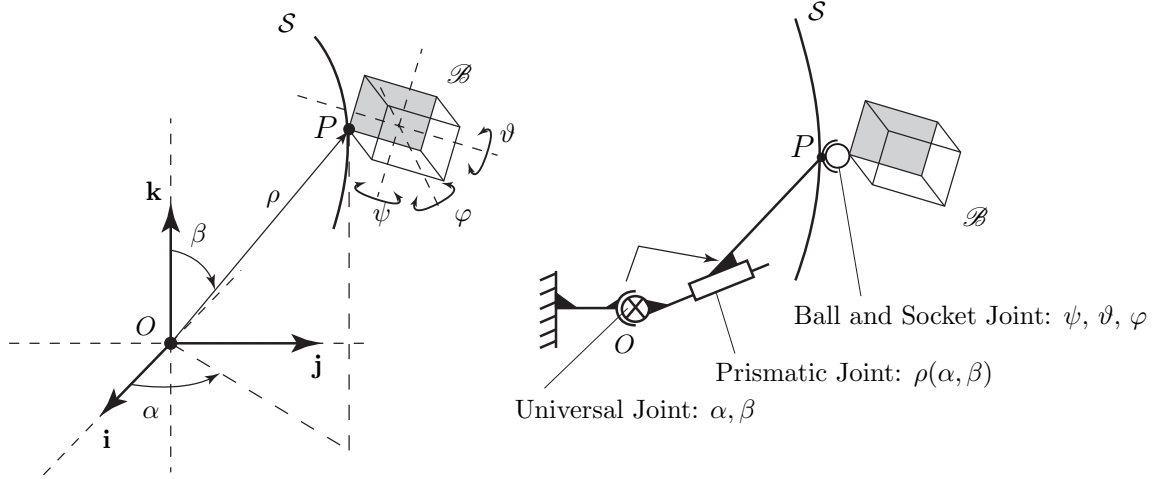


Figure 6.8: *Illustration of the mechanical equivalent of a rigid body's motion on a two-dimensional, algebraic surface as described in section 6.2.3.*

The kinematic shoulder model described in chapter 3 contains two spherical slider pairs. The algebraic surfaces are ellipsoids with identical centres. Applying the principles described in the previous paragraphs yields a kinematic model of the shoulder where the scapula is a 2-3 parallel platform. The synovial articulations are modelled as ball and socket joints (Fig.6.9). There are two additional ball and socket joints at the points TS and AI . There are two universal joints located at the centre of the ellipsoids E . Between the point E and TS there is a prismatic joint and between the point E and the point AI there is a another. The lengths of both prismatic joints are function of the universal joint coordinates (α_{TS} , β_{TS}) and (α_{AI} , β_{AI}) according to (6.27).

$$\rho_{TS} = \rho_{TS}(\alpha_{TS}, \beta_{TS}), \quad \rho_{AI} = \rho_{AI}(\alpha_{AI}, \beta_{AI}). \quad (6.29)$$

The kinematic model described in chapter 3 and the parallel model described in this chapter are equivalent. The change in representation of the scapulothoracic contact does not change the kinematic model. However, two additional kinematic chains have been added between the carrier body (thorax) and scapula. These kinematic chains will be used to find a reduced set of coordinates.

6.2.4 Equivalent Kinematic Maps and Coordinates

Section 6.2.1 summarised the kinematic shoulder model presented in chapter 4. The model is characterised by its forward kinematic map. This map is defined as the natural kinematic map between the spherical joint coordinates and the configuration of the humerus. The natural kinematic model is now given a formal definition.

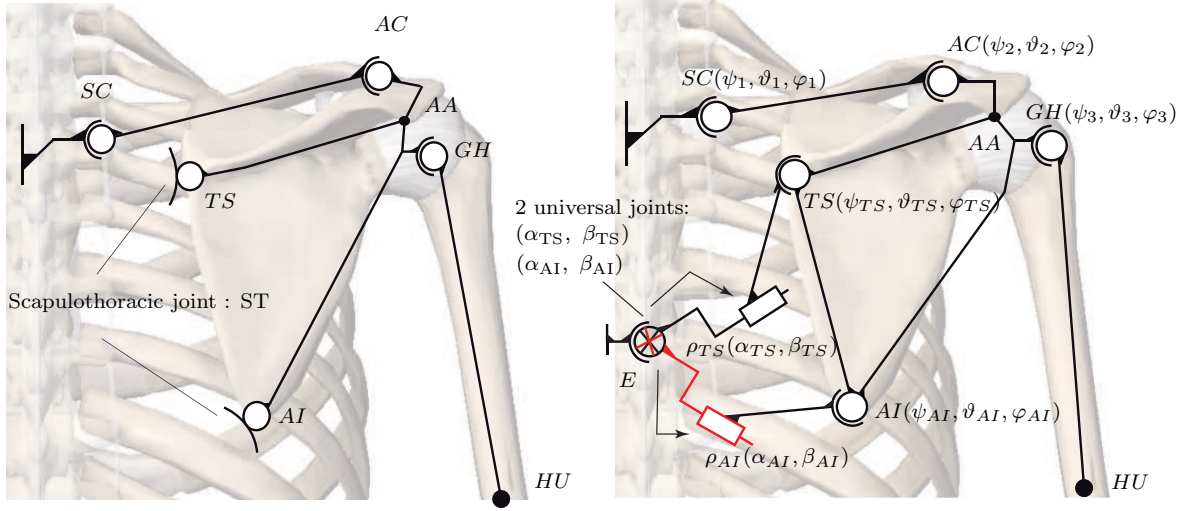


Figure 6.9: Illustration of the equivalent parallel shoulder model as described in section 6.2.3. Image courtesy of Visible Body (www.visiblebody.com).

Definition 16 (The Shoulder's Natural Kinematic Map). *The natural kinematic model of the shoulder defines the bones as rigid bodies, the synovial articulations as ball and socket joints, parameterised by spherical kinematic pairs. The scapulothoracic contact is modelled using two spherical slider kinematic pairs with respect to two ellipsoids with identical centres. The kinematic coordinates are defined by:*

$$\mathcal{Q}_{S,\mathcal{N}} := \left\{ \vec{q} = \begin{pmatrix} \vec{q}_1 \\ \vec{q}_2 \\ \vec{q}_3 \end{pmatrix} \mid \vec{q}_i = \begin{pmatrix} \psi_i \\ \vartheta_i \\ \varphi_i \end{pmatrix} \in \mathcal{Q}_{i,S} \subset [-\pi, \pi]^3, \phi_{i,S}(\mathcal{Q}_{i,S}) \subset SO(3), i = 1, 2, 3 \right\},$$

$$\Rightarrow \mathcal{Q}_{S,\mathcal{N}} = \mathcal{Q}_{1,S} \times \mathcal{Q}_{2,S} \times \mathcal{Q}_{3,S} \subset (SO(3))^3 \equiv (SO(3) \times SO(3) \times SO(3)). \quad (6.30)$$

The end-effector is defined as the humerus and its configuration \mathcal{C}_e is defined as the position of the humeroulnar joint HU and orientation of the humerus with respect to the inertial frame \mathcal{R}_0 . Under these assumptions, such a kinematic model of the shoulder has a the following forward kinematic map, called the natural kinematic map.

$$\Xi_{S,\mathcal{N}} : \mathcal{Q}_{S,\mathcal{N}} \rightarrow \mathcal{W}_{S,\mathcal{N}},$$

$$\vec{q} \mapsto \Xi_{S,\mathcal{N}}(\vec{q}) = \mathcal{C}_e, \quad \vec{e}_{0,3} = \vec{d}_{0,1} + \mathbf{R}_{1,0}(\vec{q}_1)\vec{z}_1 + \mathbf{R}_{2,0}(\vec{q}_2)\vec{z}_2 + \mathbf{R}_{3,0}(\vec{q}_3)\vec{e}_3, \quad (6.31)$$

$$s.t. \quad \Phi_{TS}(\vec{q}) = (\vec{u}_{0,2} - \vec{e}_0)^T \mathbf{E}_{TS} (\vec{u}_{0,2} - \vec{e}_0) - 1 = 0, \quad (6.32)$$

$$\Phi_{AI}(\vec{q}) = (\vec{v}_{0,2} - \vec{e}_0)^T \mathbf{E}_{AI} (\vec{v}_{0,2} - \vec{e}_0) - 1 = 0. \quad (6.33)$$

where $\vec{e}_0 = (x_e, y_e, z_e)^T$ is the point vector of the common ellipsoid centre E_0 in the inertial frame. The map parameterises the kinematic shoulder model using nine coordinates and has seven degrees of freedom. The coordinate space $\mathcal{Q}_{S,\mathcal{N}}$ is a compact C^∞ -manifold of dimension seven. The work space $\mathcal{W}_{S,\mathcal{N}}$ is a compact C^∞ -manifold of dimension six.

$$\mathcal{W}_{S,\mathcal{N}} := \left\{ \mathcal{C}_e = \begin{pmatrix} \vec{e}_{0,3} \\ \vec{q}_3 \end{pmatrix} \in SE(3) \mid \vec{e}_{0,3} \in \mathbb{R}^3, \vec{q}_3 \in \mathcal{Q}_{3,S}, \mathcal{C}_e = \Xi_{S,\mathcal{N}}(\vec{q}) \right\} \subset SE(3). \quad (6.34)$$

The equivalent parallel model of the shoulder presented in section 6.2.3 replaces the scapulothoracic contact constraints by two kinematic chains. This equivalency provides two alternate parameterisations of the shoulder model's kinematics, using the method described in chapter 3, section 3.5.5. Two sets of three Bryan angles are defined for the two spherical kinematic pairs at TS and AI : $(\psi_{TS}, \vartheta_{TS}, \varphi_{TS})$, $(\psi_{AI}, \vartheta_{AI}, \varphi_{AI})$ (Fig. 6.9). Two sets of spherical angles are defined for the two superimposed universal joints located at the point E : $(\alpha_{TS}, \beta_{TS})$, $(\alpha_{AI}, \beta_{AI})$. The method is to define a forward kinematic map with the necessary constraints, using either of these two kinematic chains.

The position of the humeroulnar joint centre HU is defined by one of the following two expressions (cf. chapter 4).

$$\text{TS map: } \vec{e}_{0,3} = \vec{u}_{0,2}(\alpha_{TS}, \beta_{TS}) - \mathbf{R}_{2,0}(\vec{q}_2)\vec{u}_2 + \mathbf{R}_{2,0}(\vec{q}_2)\vec{z}_2 + \mathbf{R}_{3,0}(\vec{q}_3)\vec{e}_3, \quad (6.35)$$

$$\text{AI map: } \vec{e}_{0,3} = \vec{v}_{0,2}(\alpha_{AI}, \beta_{AI}) - \mathbf{R}_{2,0}(\vec{q}_2)\vec{v}_2 + \mathbf{R}_{2,0}(\vec{q}_2)\vec{z}_2 + \mathbf{R}_{3,0}(\vec{q}_3)\vec{e}_3, \quad (6.36)$$

where the vectors $TS_0 : \vec{u}_{0,2}(\alpha_{TS}, \beta_{TS})$ and $AI_0 : \vec{v}_{0,2}(\alpha_{AI}, \beta_{AI})$ are defined by:

$$\vec{u}_{0,2} = \begin{pmatrix} a_{TS} \cos(\alpha_{TS}) \sin(\beta_{TS}) + x_e \\ b_{TS} \sin(\alpha_{TS}) \sin(\beta_{TS}) + y_e \\ c_{TS} \cos(\beta_{TS}) + z_e \end{pmatrix}, \quad \vec{v}_{0,2} = \begin{pmatrix} a_{AI} \cos(\alpha_{AI}) \sin(\beta_{AI}) + x_e \\ b_{AI} \sin(\alpha_{AI}) \sin(\beta_{AI}) + y_e \\ c_{AI} \cos(\beta_{AI}) + z_e \end{pmatrix} \quad (6.37)$$

The two definitions imply the following relation defining an interdependency between $(\alpha_{TS}, \beta_{TS})$ and $(\alpha_{AI}, \beta_{AI})$.

$$\vec{u}_{0,2}(\alpha_{TS}, \beta_{TS}) - \mathbf{R}_{2,0}(\vec{q}_2)\vec{u}_2 - \vec{v}_{0,2}(\alpha_{AI}, \beta_{AI}) + \mathbf{R}_{2,0}(\vec{q}_2)\vec{v}_2 = \vec{0}. \quad (6.38)$$

The two alternate definitions of HU are parameterised by the following sets of coordinates

$$\begin{aligned} \hat{\vec{q}}_{TS} &= (\psi_1 \quad \alpha_{TS} \quad \beta_{TS} \quad \psi_2 \quad \theta_2 \quad \phi_2 \quad \psi_3 \quad \theta_3 \quad \phi_3)^T, \\ \hat{\vec{q}}_{AI} &= (\psi_1 \quad \alpha_{AI} \quad \beta_{AI} \quad \psi_2 \quad \theta_2 \quad \phi_2 \quad \psi_3 \quad \theta_3 \quad \phi_3)^T. \end{aligned} \quad (6.39)$$

The coordinate ψ_1 is added to the list of coordinates because the clavicle can rotate around its longitudinal axes ($SC - AC$ axes) without disturbing the scapula. The coordinate is not in either map (6.35) or (6.36) but is included in the coordinate set to be complete.

The two alternate parameterisations are used to define two alternate forward kinematic maps. They are called the upper and lower scapulothoracic kinematic maps. Although different from the natural kinematic map, they parameterise the same kinematic structure.

Definition 17 (The Shoulder's Upper Scapulothoracic Kinematic Map). *The upper scapulothoracic kinematic model of the shoulder defined the bones as rigid bodies, the synovial articulations as ball and socket joints, parameterised by spherical kinematic pairs. The scapulothoracic contact is modelled, using two spherical slider kinematic pairs with respect to two ellipsoids with identical centres. The kinematic coordinates are defined by:*

$$\begin{aligned} \mathcal{Q}_{S,\mathcal{U}} &:= \left\{ \hat{\vec{q}}_{TS} \text{ (eq. (6.39))} \mid \psi_1 \in \hat{\mathcal{Q}}_{1,S} \subset S^1, (\alpha_{TS}, \beta_{TS}) \in \hat{\mathcal{Q}}_{2,S} \subset S^2, \vec{q}_2 \in \mathcal{Q}_{2,S}, \vec{q}_3 \in \mathcal{Q}_{3,S} \right\}, \\ \Rightarrow \mathcal{Q}_{S,\mathcal{U}} &\subset (S^1 \times S^2 \times SO(3) \times SO(3)). \end{aligned} \quad (6.40)$$

The end-effector is defined as the humerus and its configuration \mathcal{C}_e is defined as the position of the humeroulnar joint HU and orientation of the humerus with respect to the inertial frame \mathcal{R}_0 . Under these assumptions, such a kinematic model of the shoulder has the following forward kinematic map, called the upper scapulothoracic kinematic map.

$$\Xi_{S,\mathcal{U}} : \mathcal{Q}_{S,\mathcal{U}} \rightarrow \mathcal{W}_{S,\mathcal{U}},$$

$$\hat{q}_{TS} \mapsto \Xi_{S,\mathcal{U}}(\hat{q}_{TS}) = \mathcal{C}_e, \quad \vec{e}_{0,3} = eq. \quad (6.35), \quad (6.41)$$

$$s.t. \quad \Phi_{AC}(\hat{q}_{TS}) = \left(\vec{d}_{0,1} - \vec{d}_{0,2} \right)^T \left(\vec{d}_{0,1} - \vec{d}_{0,2} \right) - \|SC - AC\|_2^2 = 0, \quad (6.42)$$

$$\Phi_{AI}(\hat{q}_{TS}) = (\vec{v}_{0,2} - \vec{e}_0)^T \mathbf{E}_{AI} (\vec{v}_{0,2} - \vec{e}_0) - 1 = 0. \quad (6.43)$$

where $\vec{d}_{0,1}$ and $\vec{d}_{0,2}$ are the point vectors of SC and AC respectively in the inertial frame. The map parameterises the kinematic shoulder model using nine coordinates and has seven degrees of freedom. The coordinate space $\mathcal{Q}_{S,\mathcal{U}}$ is compact C^∞ -manifold of dimension seven. The work space $\mathcal{W}_{S,\mathcal{U}}$ is a compact C^∞ -manifold of dimension six.

$$\mathcal{W}_{S,\mathcal{U}} := \left\{ \mathcal{C}_e = \begin{pmatrix} \vec{e}_{0,3} \\ \vec{q}_3 \end{pmatrix} \in SE(3) \mid \vec{e}_{0,3} \in \mathbb{R}^3, \vec{q}_3 \in \mathcal{Q}_{3,S}, \mathcal{C}_e = \Xi_{S,\mathcal{U}}(\vec{q}) \right\} \subset SE(3). \quad (6.44)$$

The lower scapulothoracic kinematic map is defined in a similar way.

Definition 18 (The Shoulder's Lower Scapulothoracic Kinematic Map). *The upper scapulothoracic kinematic model of the shoulder models the bones as rigid bodies, the synovial articulations as ball and socket joints, parameterised by spherical kinematic pairs. The scapulothoracic contact is modelled, using two spherical slider kinematic pairs with respect to two ellipsoids with identical centres. The kinematic coordinates are defined by:*

$$\mathcal{Q}_{S,\mathcal{L}} := \left\{ \hat{q}_{TS} \text{ (eq. (6.39))} \mid \psi_1 \in \hat{\mathcal{Q}}_{1,S} \subset S^1, (\alpha_{AI}, \beta_{AI}) \in \hat{\mathcal{Q}}_{2,S} \subset S^2, \vec{q}_2 \in \mathcal{Q}_{2,S}, \vec{q}_3 \in \mathcal{Q}_{3,S} \right\},$$

$$\Rightarrow \mathcal{Q}_{S,\mathcal{L}} \subset (S^1 \times S^2 \times SO(3) \times SO(3)). \quad (6.45)$$

The end-effector is defined as the humerus and its configuration \mathcal{C}_e is defined as the position of the humeroulnar joint HU and orientation of the humerus with respect to the inertial frame \mathcal{R}_0 . Under these assumptions, such a kinematic model of the shoulder has the following forward kinematic map, called the lower scapulothoracic kinematic map.

$$\Xi_{S,\mathcal{L}} : \mathcal{Q}_{S,\mathcal{L}} \rightarrow \mathcal{W}_{S,\mathcal{L}},$$

$$\hat{q}_{AI} \mapsto \Xi_{S,\mathcal{L}}(\hat{q}_{AI}) = \mathcal{C}_e, \quad \vec{e}_{0,3} = eq. \quad (6.36), \quad (6.46)$$

$$s.t. \quad \Phi_{AC}(\hat{q}_{AI}) = \left(\vec{d}_{0,1} - \vec{d}_{0,2} \right)^T \left(\vec{d}_{0,1} - \vec{d}_{0,2} \right) - \|SC - AC\|_2^2 = 0, \quad (6.47)$$

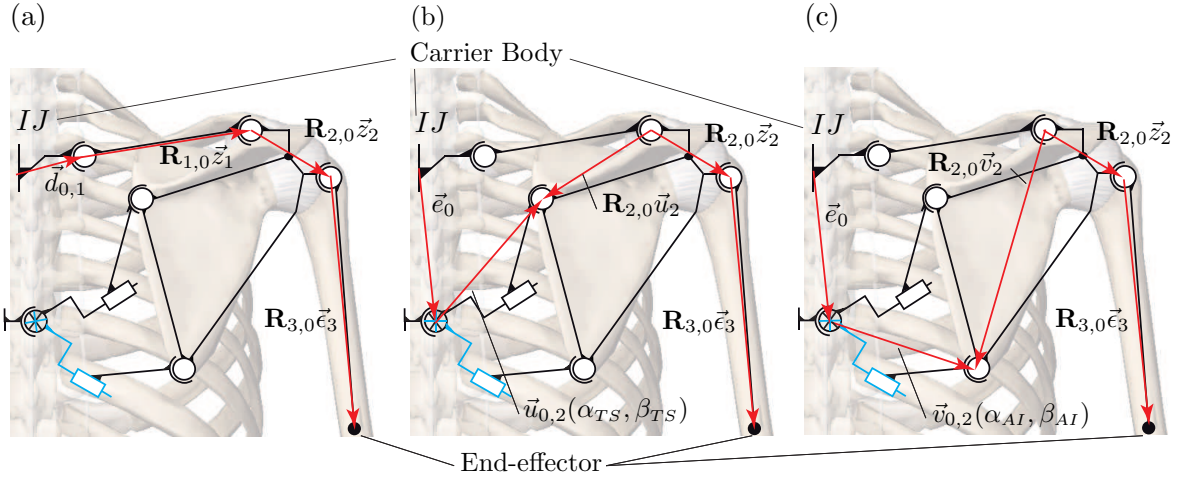
$$\Phi_{TS}(\hat{q}_{AI}) = (\vec{u}_{0,2} - \vec{e}_0)^T \mathbf{E}_{TS} (\vec{u}_{0,2} - \vec{e}_0) - 1 = 0. \quad (6.48)$$

where $\vec{d}_{0,1}$ and $\vec{d}_{0,2}$ are the point vectors of SC and AC respectively in the inertial frame. The map parameterises the kinematic shoulder model using nine coordinates and has seven degrees of freedom. The coordinate space $\mathcal{Q}_{S,\mathcal{L}}$ is compact C^∞ -manifold of dimension seven. The work space $\mathcal{W}_{S,\mathcal{L}}$ is a compact C^∞ -manifold of dimension six.

$$\mathcal{W}_{S,\mathcal{L}} := \left\{ \mathcal{C}_e = \begin{pmatrix} \vec{e}_{0,3} \\ \vec{q}_3 \end{pmatrix} \in SE(3) \mid \vec{e}_{0,3} \in \mathbb{R}^3, \vec{q}_3 \in \mathcal{Q}_{3,S}, \mathcal{C}_e = \Xi_{S,\mathcal{L}}(\vec{q}) \right\} \subset SE(3). \quad (6.49)$$

The parallel model of the shoulder defines the shoulder girdle as a 2-3 parallel platform. A platform with three legs. Each leg defines a kinematic chain between the carrier body (thorax) and end-effector (humerus). The natural kinematic map, the upper scapulothoracic kinematic map and the lower scapulothoracic kinematic map, each define a map between a vector of nine kinematic coordinates and the configuration of the end-effector. The maps are each subject to two smooth equality constraints (Fig. 6.10).

The three forward kinematic maps define coordinate spaces that are different representations of the same kinematic structure. Given that the maps all use nine coordinates, there are interdependencies between them. The following section analyses the three coordinates spaces to identify the interdependencies. It will be shown that the interdependencies are between specific coordinates. Once the interdependencies have been identified, the coordinate reduction will be presented.



The three forward kinematic maps:

$$(a) \quad \vec{e}_{0,3} = \vec{d}_{0,1} + \mathbf{R}_{1,0}(\vec{q}_1)\vec{z}_1 + \mathbf{R}_{2,0}(\vec{q}_2)\vec{z}_2 + \mathbf{R}_{3,0}(\vec{q}_3)\vec{e}_3$$

$$(b) \quad \vec{e}_{0,3} = \vec{u}_{0,2}(\alpha_{TS}, \beta_{TS}) - \mathbf{R}_{2,0}(\vec{q}_2)\vec{u}_2 + \mathbf{R}_{2,0}(\vec{q}_2)\vec{z}_2 + \mathbf{R}_{3,0}(\vec{q}_3)\vec{e}_3$$

$$(c) \quad \vec{e}_{0,3} = \vec{v}_{0,2}(\alpha_{AI}, \beta_{AI}) - \mathbf{R}_{2,0}(\vec{q}_2)\vec{v}_2 + \mathbf{R}_{2,0}(\vec{q}_2)\vec{z}_2 + \mathbf{R}_{3,0}(\vec{q}_3)\vec{e}_3$$

Figure 6.10: *Illustration of the three different methods of parameterising the forward kinematic map. (a) The natural forward kinematic map. (b) The upper scapulothoracic kinematic map. (c) The lower scapulothoracic kinematic map as described in section 6.2.4. Image courtesy of Visible Body (www.visiblebody.com).*

6.2.5 The Coordinate Space

The coordinate spaces of the natural kinematic map $\mathcal{Q}_{S,\mathcal{N}}$, the upper scapulothoracic kinematic map $\mathcal{Q}_{S,\mathcal{U}}$ and the lower scapulothoracic kinematic map $\mathcal{Q}_{S,\mathcal{L}}$ are defined as subsets of a product of C^∞ -manifolds. Each of the coordinate spaces are parameterised by nine coordinates subject to two smooth constraints. They are all C^∞ -manifolds in \mathbb{R}^9 of dimension 7. The coordinate spaces are defined by:

$$\vec{q} \in \mathcal{Q}_{S,\mathcal{N}} \subset \left(\underbrace{SO(3)}_{\psi_1, \vartheta_1, \varphi_1} \times \underbrace{SO(3)}_{\psi_2, \vartheta_2, \varphi_2} \times \underbrace{SO(3)}_{\psi_3, \vartheta_3, \varphi_3} \right), \quad (6.50)$$

$$\hat{q}_{TS} \in \mathcal{Q}_{S,\mathcal{U}} \subset \left(\underbrace{S^1}_{\psi_1} \times \underbrace{S^2}_{\alpha_{TS}, \beta_{TS}} \times \underbrace{SO(3)}_{\psi_2, \vartheta_2, \varphi_2} \times \underbrace{SO(3)}_{\psi_3, \vartheta_3, \varphi_3} \right), \quad (6.51)$$

$$\hat{q}_{AI} \in \mathcal{Q}_{S,\mathcal{L}} \subset \left(\underbrace{S^1}_{\psi_1} \times \underbrace{S^2}_{\alpha_{AI}, \beta_{AI}} \times \underbrace{SO(3)}_{\psi_2, \vartheta_2, \varphi_2} \times \underbrace{SO(3)}_{\psi_3, \vartheta_3, \varphi_3} \right). \quad (6.52)$$

The three sets are equivalent in the sense that they each parameterises the configuration of three bodies in space. They all parameterise the same kinematic structure. Independently of the coordinates, the kinematic shoulder model defines a smooth manifold of dimension 7 in \mathbb{R}^9 . The bodies are connected by spherical kinematic pairs and therefore, the kinematic coordinate set can always be seen as a subset of $(SO(3))^3$.

$$\mathcal{Q}_{S,\mathcal{N}} \equiv \mathcal{Q}_{S,\mathcal{U}} \equiv \mathcal{Q}_{S,\mathcal{L}} \equiv \mathcal{Q}_S \subset (SO(3))^3 = (SO(3) \times SO(3) \times SO(3)). \quad (6.53)$$

The three kinematic maps presented in the previous section define charts from subsets of \mathbb{R}^9 to the same subset \mathcal{Q}_S of $(SO(3))^3$.

A coordinate reduction for the kinematic shoulder model is to define charts from subsets of \mathbb{R}^7 to any of the three submanifolds. To define such charts, it is first necessary to define the charts from the subsets \mathbb{R}^9 to the same subset \mathcal{Q}_S of $(SO(3))^3$ for each kinematic map.

The natural kinematic map defines the space \mathcal{Q}_S . It uses three sets of Euler/Bryan angles belonging to three subsets $\mathcal{Q}_{i,S}$ of $SO(3)$. The natural parameterisation uses three identical charts from $[-\pi, \pi]^3$ to $SO(3)$. In section 6.2.2, it was stated that Euler and Bryan angles define maps from subsets of \mathbb{R}^3 to $SO(3)$ (6.11). The three maps define the charts from \mathbb{R}^9 to the compact smooth manifold $(SO(3))^3$.

$$\begin{aligned} \phi_{i,S} : [-\pi, \pi]^3 \subset \mathbb{R}^3 &\rightarrow SO(3), \\ (\psi_i, \vartheta_i, \varphi_i) &\mapsto \phi_{i,S}(\psi_i, \vartheta_i, \varphi_i) = \mathbf{R}_{i,0}. \end{aligned} \quad (6.54)$$

Given the constraints in the natural kinematic map, the domain spaces of the three charts $\phi_{i,S}$ are restricted to subsets $\mathcal{Q}_{i,S} \subset [-\pi, \pi]^3 \subset \mathbb{R}^3$ and the image spaces are three subsets $\phi_{i,S}(\mathcal{Q}_{i,S}) \subset SO(3)$ (Fig. 6.11). The subsets $\mathcal{Q}_{i,S}$ are defined by the constraints. Without constraints $\mathcal{Q}_{i,S} \equiv [-\pi, \pi]^3$ and $\phi_{i,S}(\mathcal{Q}_{i,S}) \equiv SO(3)$ for $i = 1, 2, 3$.

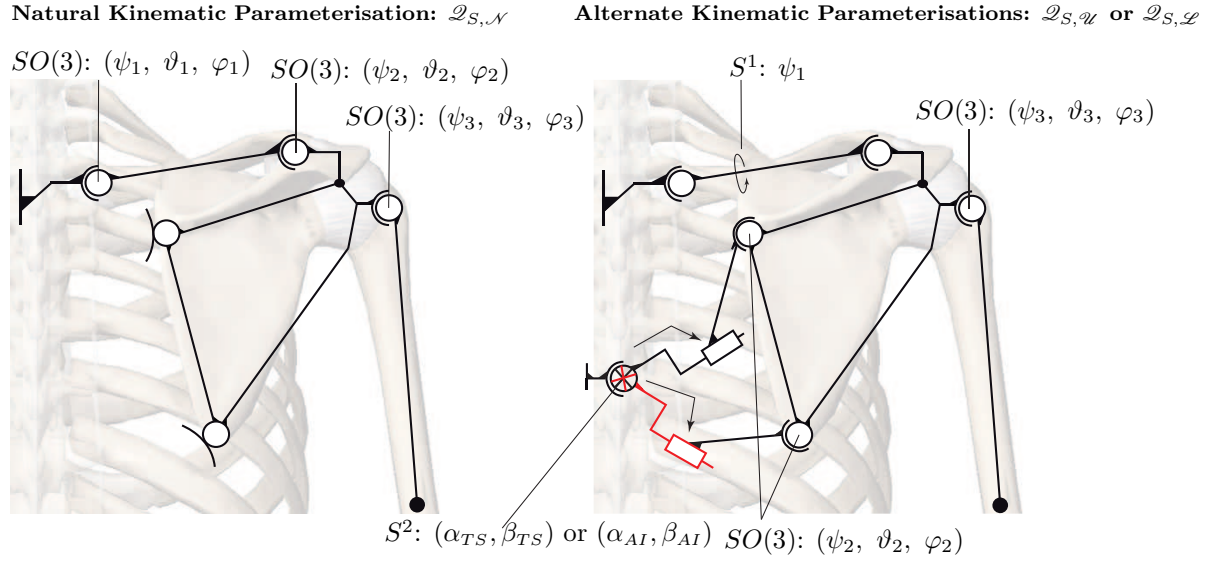


Figure 6.11: *Illustration of the coordinates in the coordinate submanifolds as defined in section 6.2.5, eq. (6.50)-(6.52). Image courtesy of Visible Body (www.visiblebody.com).*

The constraints are function of the clavicular coordinates and scapular coordinates only. The humeral coordinates are independent of any constraint $\mathcal{Q}_{3,S} \equiv [-\pi, \pi]^3$. There is an interdependency of the clavicular and scapular coordinates, not directly apparent in the natural kinematic description of the shoulder.

The upper and lower scapulothoracic forward kinematic maps use four maps. Two maps $\phi_{2,S}$ and $\phi_{3,S}$ from $[-\pi, \pi]^3$ to $SO(3)$, one map $\hat{\phi}_{1,S}$ from $[-\pi, \pi]$ to $S^1 \equiv SO(2)$ and one map $\hat{\phi}_{2,S}$ from $[-\pi, \pi] \times [-\frac{\pi}{2}, \frac{\pi}{2}]$ to S^2 . The two maps $\phi_{2,S}$ and $\phi_{3,S}$ are the same as the natural parameterisation discussed previously.

$$\begin{aligned} \hat{\phi}_{1,S} : [-\pi, \pi] \subset \mathbb{R} &\rightarrow S^1, \\ \psi_1 &\mapsto \hat{\phi}_{1,S}(\psi_1) = \mathbf{R}_x(\psi_1). \end{aligned} \quad (6.55)$$

$$\begin{aligned} \hat{\phi}_{2,S} : [-\pi, \pi] \times [-\frac{\pi}{2}, \frac{\pi}{2}] &\subset \mathbb{R}^2 \rightarrow S^2, \\ (\alpha_{TS}, \beta_{TS}) \text{ or } (\alpha_{AI}, \beta_{AI}) &\mapsto \hat{\phi}_{2,S}(\alpha_*, \beta_*) = \mathbf{R}(\alpha_*, \beta_*). \end{aligned} \quad (6.56)$$

The domain space of $\hat{\phi}_{1,S}$ is $\hat{\mathcal{Q}}_{1,S} \equiv [-\pi, \pi]$ and the image space is $\hat{\phi}_{1,S}(\hat{\mathcal{Q}}_{1,S}) \equiv S^1 \equiv SO(2)$. The clavicle can rotate around its longitudinal axes independently of all the other coordinates. The domain space of $\hat{\phi}_{2,S}$ is a subset of the full domain space $\hat{\mathcal{Q}}_{2,S} \subset [-\pi, \pi] \times [-\frac{\pi}{2}, \frac{\pi}{2}]$ and the image space is a subset $\hat{\phi}_{2,S}(\hat{\mathcal{Q}}_{2,S}) \subset S^2$.

This analysis shows that four of the nine kinematic coordinates are independent of any constraints and of each other: $(\psi_1, \psi_3, \vartheta_3, \varphi_3)$. They define the clavicle's axial rotation and the orientation of the humerus. Furthermore, the five remaining coordinates parameterise the scapula's Euclidean displacement, a point that was not directly apparent in the natural kinematic map. Two of the three clavicle coordinates (ϑ_1, φ_1) parameterise the linear position of the scapula and the three scapular coordinates $(\psi_2, \vartheta_2, \varphi_2)$ parameterise the orientation about the linear position.

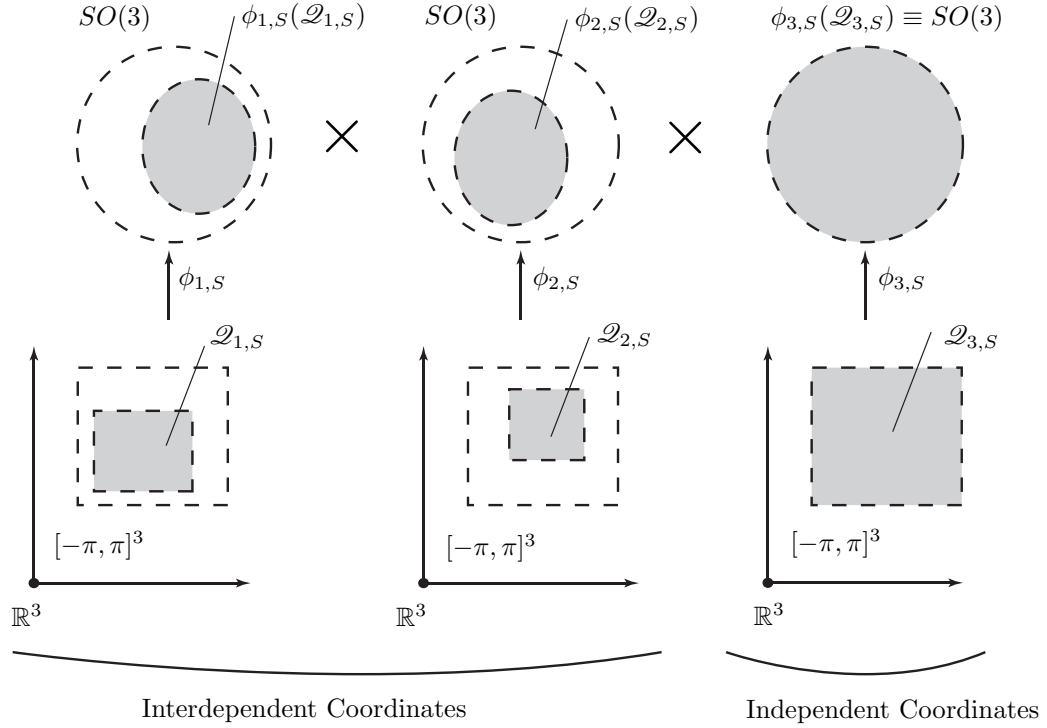


Figure 6.12: *Illustration of the natural kinematic map charts from three subsets of $\mathcal{Q}_{i,S} \subset [-\pi, \pi]^3$ to three subsets of $SO(3)$ as described in 6.2.5.*

The upper and lower scapulothoracic kinematic maps model the scapula as a 2-3 parallel platform. The platform includes six independent kinematic pairs without including the passive prismatic pairs. The mobility formula applied to the shoulder girdle (clavicle and scapula) states that there are four degrees of freedom.

$$D_S = 6 \cdot 4 - \sum_{i=1}^6 (6 - k_i) = 6 \cdot 4 - \underbrace{4 \cdot 3}_{\text{Spherical Joints}} - \underbrace{2 \cdot 4}_{\text{Universal Joints}} = 4. \quad (6.57)$$

Without the clavicle's self rotation, the scapula has three degrees of freedom. In the kinematic maps defined thus far, the scapula's three degrees of freedom are parameterised by five coordinates: $(\alpha_{TS}, \beta_{TS}, \psi_2, \vartheta_2, \varphi_2)$ or $(\alpha_{AI}, \beta_{AI}, \psi_2, \vartheta_2, \varphi_2)$. The following section presents how the five coordinates are reduced to three, using two coordinates to parameterise the scapula's linear position and one coordinate to parameterise the orientation.

6.2.6 A Minimal Parameterisation

Finding a minimal parameterisation of the shoulder model's kinematics is to find a set of seven coordinates. Four coordinates have already been found through the analysis of the coordinate manifold, associated to three different but equivalent kinematic maps. The four coordinates are the clavicle's axial rotation and the glenohumeral Euler angles: $(\psi_1, \psi_3, \vartheta_3, \varphi_3)$. The three missing coordinates parameterise the scapula's configuration.

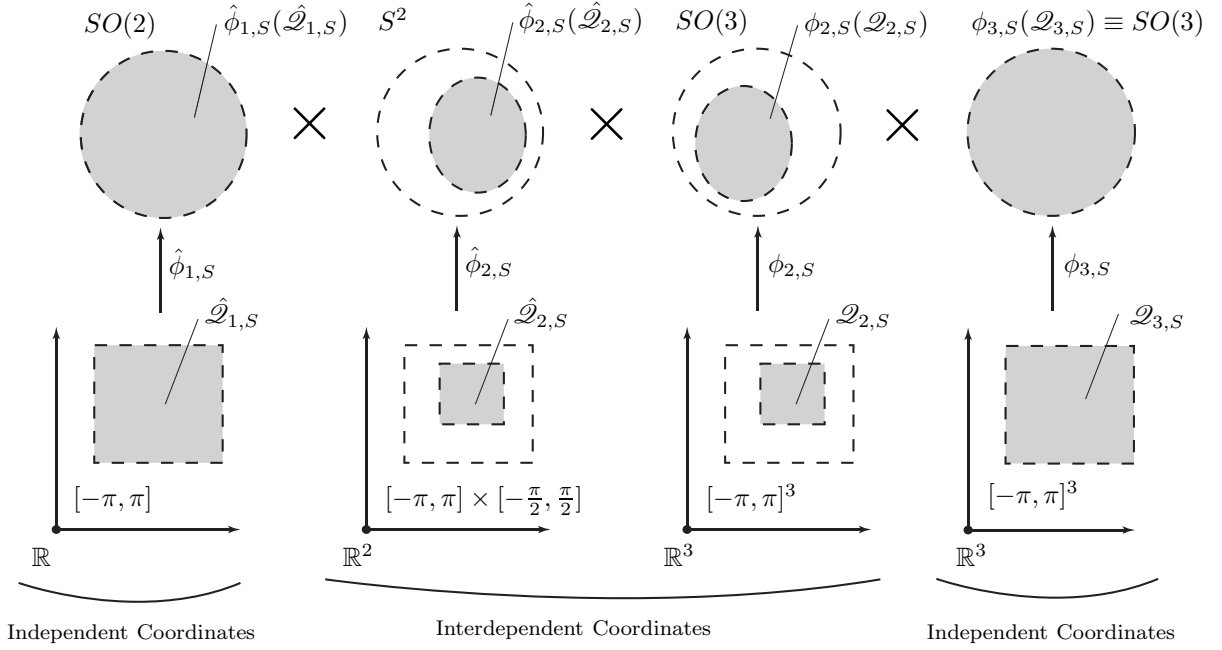


Figure 6.13: *Illustration of the submanifold decomposition as defined in section 6.2.5.*

In the parallel platform description of the shoulder girdle (thorax, clavicle and scapula), the scapula is a platform resting on three legs. The points TS and AI are defined in the model as articulations. Using this perspective, its configuration is defined using six polynomial equations. The polynomials are defined in terms of the cartesian coordinates of the three articulation points AC, TS, AI .

$$\text{TS ellipsoid:} \quad (\vec{u}_{0,2} - \vec{e}_0)^T \mathbf{E}_{TS} (\vec{u}_{0,2} - \vec{e}_0) = 1, \quad (6.58)$$

$$\text{AI ellipsoid:} \quad (\vec{v}_{0,2} - \vec{e}_0)^T \mathbf{E}_{AI} (\vec{v}_{0,2} - \vec{e}_0) = 1, \quad (6.59)$$

$$\text{AC is on a sphere around SC:} \quad (\vec{d}_{0,2} - \vec{d}_{0,1})^T (\vec{d}_{0,2} - \vec{d}_{0,1}) = \rho_{AC}^2, \quad (6.60)$$

$$\text{TS is on a sphere around AC:} \quad (\vec{d}_{0,2} - \vec{u}_{0,2})^T (\vec{d}_{0,2} - \vec{u}_{0,2}) = \mu_1^2, \quad (6.61)$$

$$\text{AI is on a sphere around AC:} \quad (\vec{d}_{0,2} - \vec{v}_{0,2})^T (\vec{d}_{0,2} - \vec{v}_{0,2}) = \mu_2^2, \quad (6.62)$$

$$\text{TS is on a sphere around AI:} \quad (\vec{u}_{0,2} - \vec{v}_{0,2})^T (\vec{u}_{0,2} - \vec{v}_{0,2}) = \mu_3^2. \quad (6.63)$$

The first three equations define the location of the three points with respect to the thorax and the remaining equations define their position with respect to each other (Fig. 6.14). The scapula's configuration is defined by a Euclidean displacement. Any point on the scapula, for instance $GH_{0,2}$, is defined by:

$$GH_{0,2} : \vec{z}_{2,0} = \vec{d}_{0,2} + \mathbf{R}_{2,0} \vec{z}_2. \quad (6.64)$$

The minimal set of coordinates can be obtained through either of the three kinematic maps. In the three kinematic maps, there are two coordinates defining the position of one of the three points on the scapula.

- AC: ϑ_1, φ_1 , the y - and z -axis Bryan angles,
- TS: α_{TS}, β_{TS} , the two spherical coordinates of the TS ellipsoid,
- AI: α_{AI}, β_{AI} , the two spherical coordinates of the AI ellipsoid.

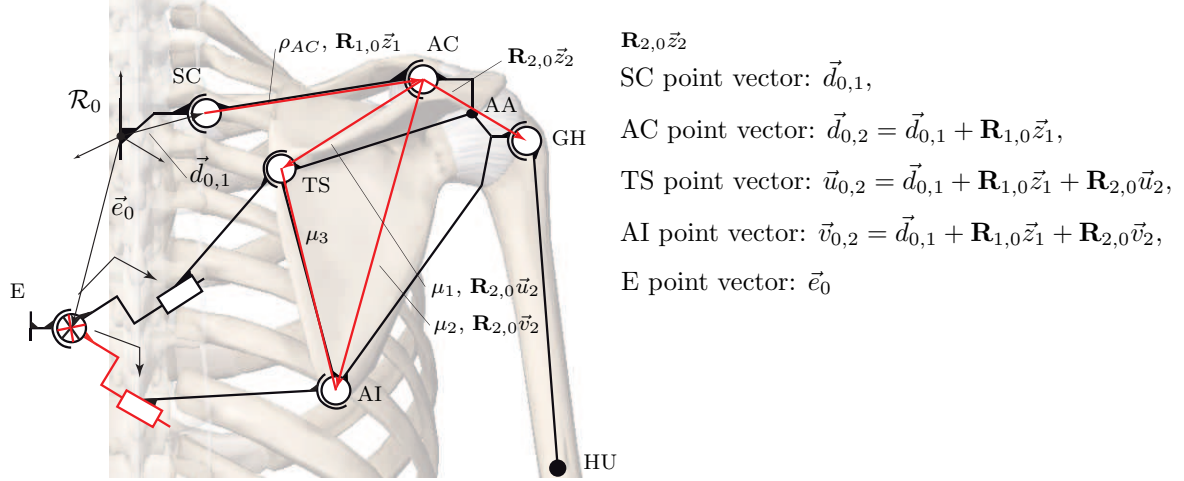


Figure 6.14: Diagram illustrating the vectors and constants defined in the polynomial description of the scapula's configuration (6.58)-(6.63). Image courtesy of Visible Body (www.visiblebody.com)

Once either of these points is fixed, the scapula has a single degree of freedom ξ_S . The coordinate defines the motion of one of the other two points with respect to the one that is known, using the two coordinates. The point lies on the intersection of two quadrics. All six polynomial equations stated previously define quadrics. The parameterisation of the intersection between two quadrics is well defined and is extensively used in computer aided design software (CAD). The locus can be parameterised using a single coordinate ξ_S [127, 128].

Definition 19 (Natural Minimal Coordinates). *The natural kinematic map defines the following vector of minimal coordinates:*

$$\vec{q}^* = (\psi_1, \vartheta_1, \varphi_1, \xi_S, \psi_3, \vartheta_3, \varphi_3)^T \in \mathcal{Q}_{S,\mathcal{N}}^* \subset (SO(3) \times S^1 \times SO(3)). \quad (6.65)$$

Construction: *The natural kinematic map defines the position of AC through the configuration of the sternoclavicular joint angles: $\psi_1, \vartheta_1, \varphi_1$. The point TS lies on the intersection of two quadrics. A sphere centred at AC of radius μ_1 and an ellipsoid centred at E (eq. 6.60, 6.57). This intersection is homeomorphic (topologically equivalent) to a circle [127]. It can be described using a single coordinate ξ_S . Once the position of TS is known, the position of AI is known by trilateration (Intersection of three spheres). AI belongs to the common intersection between a sphere centred at*

AC, a sphere centred at TS and an ellipsoid centred at E (eq. 6.61, 6.62, 6.58). Once the scapula's configuration is known, the humerus configuration is defined through the glenohumeral joint angles $\psi_3, \vartheta_3, \varphi_3$.

Definition 20 (Upper Scapulothoracic Minimal Coordinates). *The upper scapulothoracic kinematic map defines the following vector of minimal coordinates:*

$$\bar{q}^* = (\psi_1, \alpha_{TS}, \beta_{TS}, \xi_S, \psi_3, \vartheta_3, \varphi_3)^T \in \mathcal{Q}_{S, \mathcal{U}}^* \subset (S^1 \times S^2 \times S^1 \times SO(3)). \quad (6.66)$$

Construction: *The upper scapulothoracic kinematic map defines the position of the point TS through the spherical coordinates $(\alpha_{TS}, \beta_{TS})$. The point AI lies on the intersection of two quadrics. A sphere centred at TS of radius μ_3 and an ellipsoid centred at E eq. 6.62, 6.58). This intersection is also homeomorphic to a circle and parameterised by a single coordinate ξ_S . Once the position of AI is known, the position of AC is known by trilateration. AC belongs to the common intersection between a sphere centred at AI, a sphere centred at TS and a sphere centred at SC. The same works for the lower kinematic map by replacing TS with AI. (eq. 6.59, 6.60, 6.61). Once the scapula's configuration is known, the humerus configuration is defined through the glenohumeral joint angles $\psi_3, \vartheta_3, \varphi_3$. The clavicle's self rotation is also defined through ψ_1 .*

Definition 21 (Lower Scapulothoracic Minimal Coordinates). *The lower scapulothoracic kinematic map defines the following vector of minimal coordinates:*

$$\bar{q}^* = (\psi_1, \alpha_{AI}, \beta_{AI}, \xi_S, \psi_3, \vartheta_3, \varphi_3)^T \in \mathcal{Q}_{S, \mathcal{L}}^* \subset (S^1 \times S^2 \times S^1 \times SO(3)). \quad (6.67)$$

Construction: *The lower scapulothoracic kinematic map defines the position of the point AI through the spherical coordinates $(\alpha_{AI}, \beta_{AI})$. The point TS lies on the intersection of two quadrics. A sphere centred at AI of radius μ_3 and an ellipsoid centred at E eq. 6.62, 6.59). This intersection is also homeomorphic to a circle and parameterised by a single coordinate ξ_S . Once the position of TS is known, the position of AC is known by trilateration. AC belongs to the common intersection between a sphere centred at AI, a sphere centred at TS and a sphere centred at SC. The same works for the upper kinematic map by replacing AI with TS. (eq. 6.59, 6.60, 6.61). Once the scapula's configuration is known, the humerus configuration is defined through the glenohumeral joint angles $\psi_3, \vartheta_3, \varphi_3$. The clavicle's self rotation is also defined through ψ_1 .*

In all three definitions, coordinate ξ_S parameterises the intersection between a sphere and an ellipsoid. The technical details of defining ξ_S are found in Appendix A. The intersection locus is homeomorphic to a circle. Thus, the coordinate ξ_S has an associated chart between $[0, 1] \subset \mathbb{R}$ and S^1 . The coordinate is not an angular coordinate and therefore the domain space is defined as the unit interval. The chart is defined by:

$$\begin{aligned} \phi_{2,S}^* : [0, 1] \subset \mathbb{R} &\rightarrow S^1, \\ \xi_S &\mapsto \phi_{2,S}^*(\xi_S) = \mathbf{R}_{2,0}(\xi_S). \end{aligned} \quad (6.68)$$

The domain space is restricted to $\mathcal{Q}_{2,S}^* \subset [0, 1]$ because, the triple sphere intersection must exist. Given the location of two of the three points, the third point must lie on the intersection of three spheres. This constraint limits the actual domain space and the image space is therefore also a subset $\phi_{2,S}^*(\mathcal{Q}_{2,S}^*) \subset S^1$ (Fig. 6.15). This condition also restricts the domain space of the chart associated to (ϑ_1, φ_1) , $(\alpha_{TS}, \beta_{TS})$ or $(\alpha_{AI}, \beta_{AI})$, depending on the set of minimal coordinates

The coordinate space \mathcal{Q}_S of the shoulder model is defined by a set of seven coordinates ((6.65), (6.66) or (6.67)). The set of seven coordinates is said to be a minimal set of coordinates in the sense that the number of coordinates is equal to the number of degrees of freedom. There are three possible choices of coordinates depending on which kinematic chain is used. The coordinates define maps from subsets of \mathbb{R}^7 to the kinematic coordinate manifold which is a submanifold of $(SO(3))^3$.

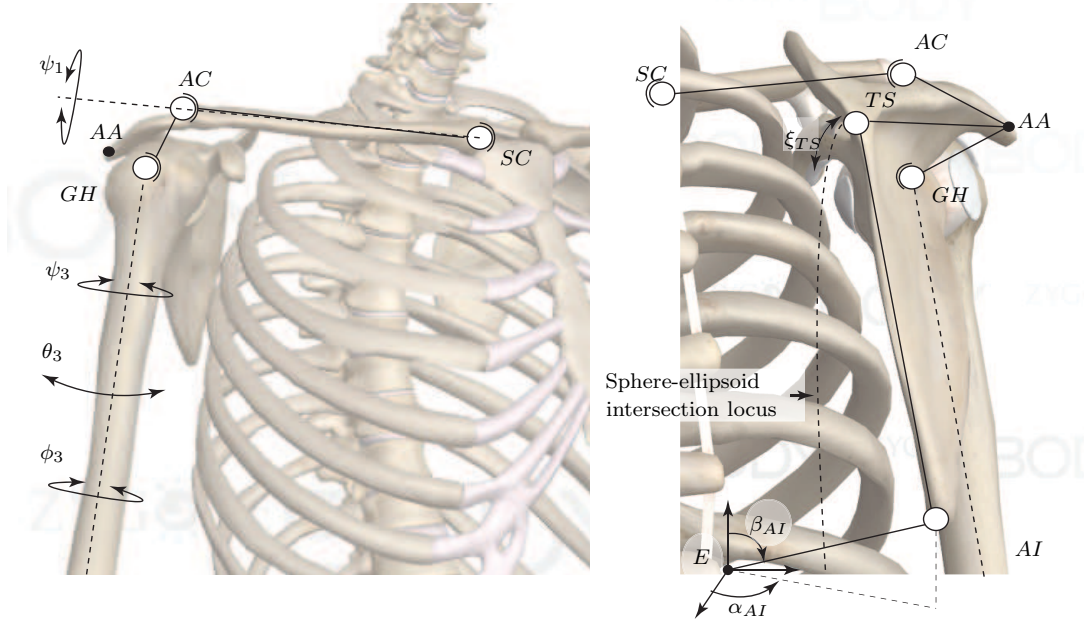


Figure 6.15: *Illustration of the minimal set of coordinates, using the lower scapulothoracic kinematic map as described in section 6.2.5 (Definition 21). Image created using ZygoteBodyTM zygotebody.com.*

The chart associated to the minimal coordinates, from a subset of \mathbb{R}^7 onto the coordinate manifold \mathcal{Q}_S , using the natural kinematic map, is defined by:

$$\begin{aligned} \phi_{S,\mathcal{N}} : \mathcal{Q}_{1,S} \times \mathcal{Q}_{2,S}^* \times \mathcal{Q}_{3,S} &\rightarrow \mathcal{Q}_S, \\ \bar{q}^* = (\psi_1, \vartheta_1, \varphi_1, \xi_S, \psi_3, \vartheta_3, \varphi_3) &\mapsto \phi_{S,\mathcal{N}}(\bar{q}^*) = (\phi_{1,S}(\psi_1, \vartheta_1, \varphi_1), \phi_{2,S}^*(\xi_S), \phi_{3,S}(\psi_3, \vartheta_3, \varphi_3)), \\ &= (\mathbf{R}_{1,0}, \mathbf{R}_{2,0}, \mathbf{R}_{3,0}). \end{aligned} \quad (6.69)$$

The chart associated to the minimal coordinates, constructed from the upper scapulothoracic kinematic map, is defined by:

$$\begin{aligned} \phi_{S,\mathcal{U}} : \hat{\mathcal{Q}}_{1,S} \times \hat{\mathcal{Q}}_{2,S} \times \mathcal{Q}_{2,S}^* \times \mathcal{Q}_{3,S} &\rightarrow \mathcal{Q}_S, \\ \bar{q}^* = (\psi_1, \alpha_{TS}, \beta_{TS}, \xi_S, \psi_3, \vartheta_3, \varphi_3) &\mapsto \phi_{S,\mathcal{U}}(\bar{q}^*) = (\hat{\phi}_{1,S}(\psi_1), \hat{\phi}_{2,S}(\alpha_{TS}, \beta_{TS}), \phi_{2,S}^*(\xi_S), \phi_{3,S}(\psi_3, \vartheta_3, \varphi_3)), \\ &= (\mathbf{R}_{1,0}, \mathbf{R}_{2,0}, \mathbf{R}_{3,0}). \end{aligned} \quad (6.70)$$

The chart associated to the minimal coordinates, constructed from the lower scapulothoracic kinematic map, is defined by:

$$\begin{aligned} \phi_{S,\mathcal{L}} : \hat{\mathcal{Q}}_{1,S} \times \hat{\mathcal{Q}}_{2,S} \times \mathcal{Q}_{2,S}^* \times \mathcal{Q}_{3,S} &\rightarrow \mathcal{Q}_S, \\ \bar{q}^* = (\psi_1, \alpha_{AI}, \beta_{AI}, \xi_S, \psi_3, \vartheta_3, \varphi_3) &\mapsto \phi_{S,\mathcal{L}}(\bar{q}^*) = (\hat{\phi}_{1,S}(\psi_1), \hat{\phi}_{2,S}(\alpha_{AI}, \beta_{AI}), \phi_{2,S}^*(\xi_S), \phi_{3,S}(\psi_3, \vartheta_3, \varphi_3)), \\ &= (\mathbf{R}_{1,0}, \mathbf{R}_{2,0}, \mathbf{R}_{3,0}). \end{aligned} \quad (6.71)$$

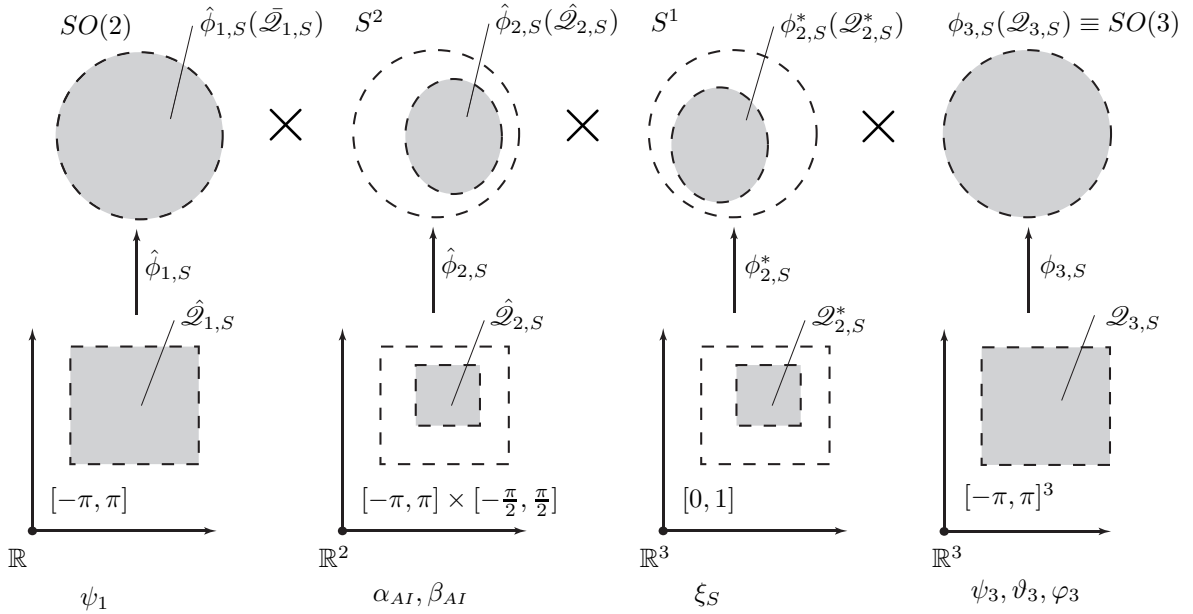


Figure 6.16: *Illustration of the minimal coordinate charts onto the submanifolds as defined in section 6.2.6.*

The coordinates parameterise the three rotation matrices of the clavicle, scapula and humerus. The Euler and Bryan angle or natural parameterisation can be obtained, once the three matrices are defined. The natural parameterisation is needed to define the

dynamic model. The minimal coordinates are suited for describing the shoulder's kinematics but not its dynamics.

In comparison to each other, the three possible sets of minimal coordinate parameterise the same kinematic structure. Given this point, it is natural to ask if they are exactly equivalent. The short answer is no. They are similar but not identical. There are four coordinates that are found in all three sets of minimal coordinates. The differences between the sets lies in the three coordinates parameterising the scapula's configuration. For instance, if the natural set of minimal coordinates is used, the third point on the scapula (TS or AI) is obtained by computing the intersection between two spheres and an ellipsoid. For the other two sets of minimal coordinates, the third point is AC, lying on the common intersection is between three spheres. Finally, an important difference between the coordinate sets is in their implementation. The numerical range of each coordinate will differ. Furthermore, this chapter presented the definition of the three coordinate sets without discussing the numerical values. The specifics of the domain space of the kinematic maps will depend on the numerical values of the shoulder model. It could be that when implemented, a coordinate set could lead to difficulties because of the numerics. The most likely source of trouble is the definition of the ellipsoids. Their orientation and dimensions will have an impact on the implementation.

6.3 Remarks

This chapter began by presenting the usual parameterisation of a kinematic shoulder model that includes the three synovial articulations and the scapulothoracic contact (cf. chapter 4). This parameterisation defines a natural forward kinematic map using the natural joint coordinates as kinematic coordinates. The chapter then presented an alternate description of a kinematic model of the shoulder by replacing the scapulothoracic contact model with two kinematic chains between the carrier body (thorax) and scapula. The kinematic chains were used to construct two alternate forward kinematic maps and to analyse the shoulder model's kinematic structure. The result is a minimal set of seven coordinates. A set of four charts are defined to map the minimal coordinates onto the shoulder model's coordinate manifold, defined as a subset of $(SO(3))^3$ and parameterised by the three rotation matrices. The minimal coordinates considerably simplify any computational procedure associated with the kinematic model such as motion planning. The following paragraphs compare the use of minimal coordinates for shoulder motion planning to other solutions from the literature.

Most kinematic models of the shoulder use the natural joint angle parameterisation [58, 61, 74, 101, 114, 129, 194]. For models that contain constraints [58, 74, 194], the most appropriate method of planning motion has been to use data-driven optimisation [8, 66, 156]. The motion is planned by minimising, at discrete instances during the motion, the error between the model's kinematic coordinates and measured values of the kinematic coordinates. The measured values can be obtained for instance, from palpated skin marker locations, using a model of the soft tissue effect [42, 56]. The variables of the optimisation problem are the model's coordinates for every discrete configuration.

The philosophy behind this approach is to obtain motion that satisfies the constraints and reflects the real shoulder's motion. Without the constraints, the model's coordinates are equal to the measured coordinates and motion planning is straightforward. With constraints, the problem is considerably more difficult because the coordinates are interdependent. Thus, constraints constitute one of the main challenges in planning the motion of shoulder models including constraints.

The solution presented in this chapter eliminates the constraints by constructing coordinates directly parameterising the constraints. The coordinates are independent from each other. If motion of the real shoulder is described directly in terms of these coordinates, the motion planning problem is mathematically trivial in that the model coordinates are equal to the measured coordinates. The minimal coordinates are specific to kinematic models of the shoulder where the scapulothoracic contact is modelled using two points constrained on the surface of an ellipsoid [74, 194]. The coordinates are not specific to a numerical implementation, but are specific to shoulder model's with the structure described above. This observation leads to the following remarks.

The minimal coordinate parameterisation of a kinematic shoulder model has potential beyond the kinematic model presented in this chapter. In the literature, there are a number of regression models that define thoraco-clavicular and scapulo-thoracic motion in terms of thoraco-humeral motion [50, 84, 101, 104]. The sternoclavicular and acromioclavicular joint angles are defined as functions of the glenohumeral joint angles. These models are highly appealing because they can be used to build clavicular and scapular motion using only the motion of the humerus which is very straightforward to define. The disadvantage with these models is that they produce motion that is generally incompatible with any of the model's kinematic constraints. Furthermore, most of these models are linear. The coordinate manifolds associated to kinematic shoulder models are in general nonlinear [215]. Linear regression models are local models of shoulder kinematics. The primary drawback of regression models is that they do not respect the scapulothoracic kinematic constraints. Therefore, the minimal coordinate parameterisation does present an attractive alternative. Furthermore, given that the minimal coordinates presented in this chapter directly incorporate the scapulothoracic constraints, they could be used to construct a regression model. The model would respect the constraints and be nonlinear and could be used to build general shoulder movements. Also, the minimal coordinates parameterise the movement of bony landmarks and are seemingly suited for skin marker palpation techniques. The possibility of building a constraint compatible regression model requires further investigation but is an attractive prospect.

6.3.1 Trammel of Archimedes

Before concluding this chapter, it is of interest to return to the two-dimensional mechanism presented in section 6.2.2. Recall that in the mechanism, the point TS glides on an ellipse. A coordinate was defined directly parameterising the ellipse. This section proposes a method of enforcing and actuating the constraint using a very old mechanism: The Trammel of Archimedes. Kempe's Universality theorem states that any portion of a smooth curve in \mathbb{R}^2 can be constructed using a linkage mechanism with only prismatic

and revolute joints [116]. The Trammel of Archimedes is a particular example of such a mechanism.

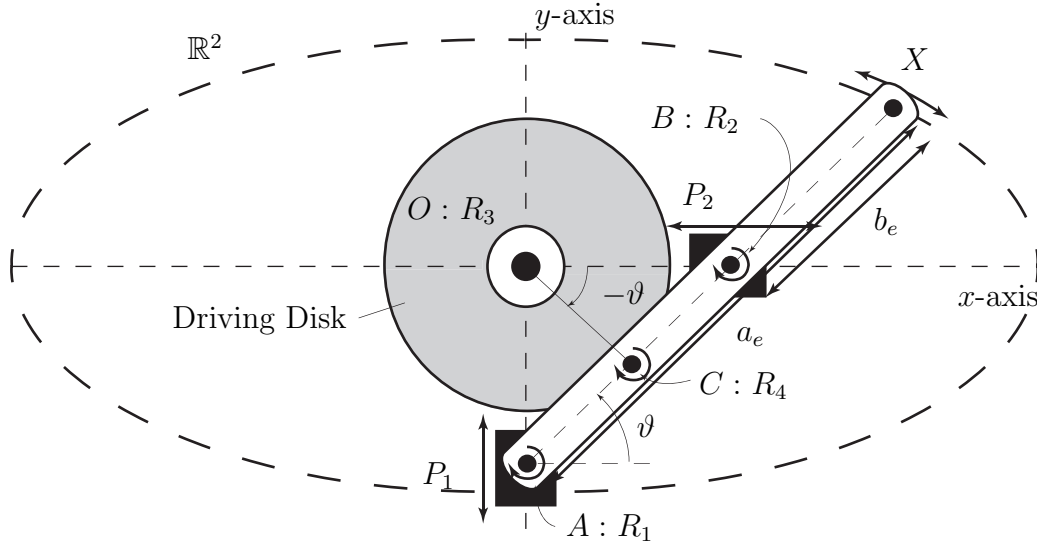


Figure 6.17: *Illustration of the driven Trammel of Archimedes as described in section 6.3.1.*

In the mechanism from section 6.2.2, the point TS must follow an ellipse of dimensions a_e and b_e . An ellipse can be constructed using a number of different mechanisms. The most notable mechanism is the Trammel of Archimedes, using two blocks which move along the two axes of the ellipse through two prismatic joints P_1 and P_2 (Fig. 6.17). A straight link of length a_e is connected to the two blocks through two revolute joints R_1 and R_2 . The first revolute joint is connected at the tip of the link and the other revolute joint is connected at a distance $a_e - b_e$. As the two blocks move, the opposite tip of the link X follows the edge of the ellipse. If the point TS on the two-dimensional mechanism is attached at this point to the link through a revolute joint, it will follow the ellipse.

It was further explained in section 6.2.2 that the ellipse coordinate ϑ kinematically defines part of the mechanism. The Trammel of Archimedes can be driven through a revolute joint parameterised by ϑ . There is a point on the link which is always at a distance $\frac{a_e - b_e}{2}$ from the centre of the ellipse. If a disk of radius $\frac{a_e - b_e}{2}$ is set at the centre and connected to the link, the mechanism can be driven through the rotation of the disk. This mechanism would be a mechanically more robust solution because there is a single driven joint. The initial solution using a single revolute joint and a single prismatic joint would not be a good solution because the prismatic joint would need to be driven although its length is dependent on ϑ . The point TS would not follow a perfect ellipse. The Trammel of Archimedes on the other hand would guarantee that TS remain on a perfect ellipse.

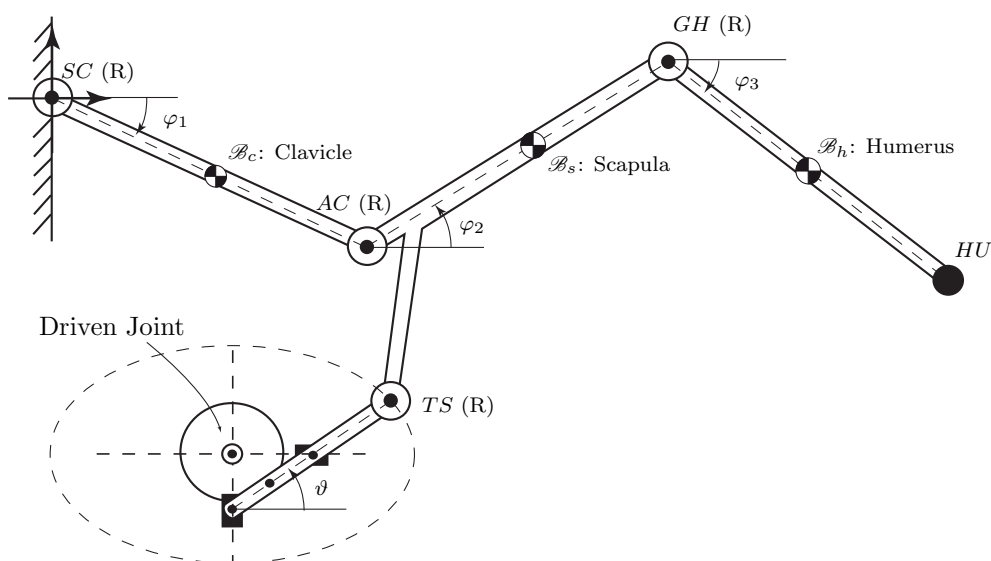


Figure 6.18: *Illustration of the use of the Trammel of Archimedes in driving the two-dimensional analogue for the shoulder discussed in section 6.2.2.*

6.4 Conclusions

The goal of this chapter was to present a novel parameterisation of a kinematic shoulder model with constraints, facilitating motion planning without measured data. The main idea of the parameterisation is minimal coordinates. Instead of using more coordinates subject to constraints, the parameterisation uses a number of coordinates equal to the number of internal degrees of freedom. The coordinates were defined for the musculoskeletal shoulder model presented in chapter 4. The model considers the synovial articulations to be ball and socket joints, parameterised by spherical kinematic pairs. The scapulothoracic contact is modelled by constraining the end points of the scapula's medial border to remain on the surface of two ellipsoids. The parameterisation in terms of the minimal coordinates was derived by replacing the contact model with two equivalent kinematic chains. There are three possible sets of minimal coordinates. Within each set, the coordinates are independent from one another. The coordinates are shown to be a highly efficient solution of parameterising the model's kinematics. Finally, the parameterisation shows potential in constructing a regression model of the shoulder kinematics. Such a regression model would be compatible with the kinematic constraints present in the model.

Chapter 7

Shoulder Overactuation Coordination

7.1 Introduction

Musculoskeletal systems such as the shoulder, the hip or the knee, consist mainly of bones, articulations and muscles. The bones and articulations define the skeletal system with a number of degrees of freedom and the muscles act as external force generators actuating the system. Musculoskeletal systems are overactuated. The number of muscles exceeds the number of degrees of freedom. Overactuation is necessary given that muscles can only pull and is a desirable characteristic to increase flexibility. This leads to what chapter 5 defines as coordinated redundancy. The additional actuators are redundant, providing additional flexibility. However, the redundant actuators must be coordinated to use the redundancy efficiently. The human body does this very well using neuromuscular control.

In models of musculoskeletal systems, the bones and articulations are modelled as ideal rigid bodies and joints, yielding a dynamical system. The muscles are modelled as massless, frictionless cables wrapping over the bones, applying forces on the skeletal system. The models are also highly overactuated. For a given state of the dynamical skeletal system, there are an infinite number of muscle-force patterns. Therefore, coordination strategies for working with musculoskeletal models are also required.

There exist many different types of coordination strategies [66]. Such strategies are often referred to in the literature as the force sharing problem [191], the muscle recruitment problem [172] or muscle-force estimation problem [90]. There are three main families of strategies. The first is called the inverse dynamics, static optimisation strategy [26, 94, 190]. The dynamical model of the skeletal system is inverted. A kinematic movement is imposed and the muscle forces are obtained by static optimisation (an optimisation problem is solved at discrete instances in time). The second family is called forward dynamics assisted data tracking [145, 154]. Muscle forces are found, minimising

the error between the skeletal model's kinematics and measured kinematics. EMG¹ measurements have also been used for this type of method. The third family of coordination strategies is optimal control [163]. These methods use a forward dynamics approach but the cost function includes muscle forces and kinematics without measured data.

The development of coordination strategies presents a challenge. The coordination strategies must reproduce similar activation patterns as the ones observed in the real system. Therefore, research related to muscle-force coordination has focused on the cost functions and results which they produce [66]. For instance, it has been shown that minimising mean square muscle stress yields muscle forces that agree with measured data [194]. This particular cost function is referred to as the polynomial cost function. Another cost function is the min/max function that is shown to produce similar results to the polynomial cost function with higher orders [6]. More recently energy based cost functions have been proposed [167]. These results are fundamental but analyse the problem from a practical application perspective.

There has been little research into the theoretical aspect of the muscle-force estimation problem. The problem represents an example of a family of mathematically underdetermined problems. These problems consist of finding a single solution within an infinite set of solutions. Another example of this type of problem is found in cable-driven robotics [57, 92, 178]. The forces in the cables actuating the system must be found to produce a desired movement. In fact, the coordination problems found in cable-driven robotics and the coordination problems found in biomechanics share a number of similarities. The approach taken in this chapter is therefore relatively novel in that it uses a concept from cable-driven robots to analyse the muscle-force coordination problem. The concept is called wrench-feasibility and involves muscle moment-arms. Muscle moment-arms are of fundamental importance and require further development. At present most presentations related to moment-arms are experimental. They present the measured moment-arms of certain muscles using cadaveric studies [2, 102, 130, 161]. It seems that the main theoretical developments concerning muscle moment-arms are, the tendon-excursion method for computing moment-arms [7, 51, 179] and the minimum number of muscle segments required to model muscles with large attachment sites [197].

The goal of this chapter, is to extend the theory of moment-arms using the concept of wrench-feasibility. The presentation begins by giving a general definition of the muscle-force coordination problem that applies to most musculoskeletal models. The musculoskeletal shoulder model presented in chapter 4 is used to present the definition. A strategy for solving the muscle-force coordination problem for the shoulder model is presented that uses the moment-arm map directly [3, 60, 190]. This particular method is selected because it highlights the importance of moment-arms. The general theory behind muscle moment-arms is reviewed. Two definitions of muscle moment-arm are presented. The first is geometric and based on the cross-product of two vectors and the second is the tendon excursion method. This review also includes a presentation of the main problems related to computing muscle moment-arms. Finally, the concept of wrench feasibility is introduced. Its implications are analysed using a two-dimensional musculoskeletal model where it is possible to visualise the mathematical structures involved in wrench-feasibility.

¹Electromyography (EMG) is a technique for evaluating and recording the electrical activity produced by skeletal muscles.

7.2 Moment-Arms for Coordination

7.2.1 Shoulder Overactuation Coordination

In chapter 4, a musculoskeletal model of the shoulder is presented. The synovial articulations are modelled as ball and socket joints and parameterised using spherical kinematic pairs. The model is parameterised by nine generalised coordinates representing the joint angles, defined with respect to the inertial frame located on the thorax at the point IJ . The reference frame axes are defined according the ISB guide lines [214]. Subindexes are used to refer to each reference frame. 0: thorax (inertial), 1: clavicle, 2: scapula, 3: humerus. Mass and inertia is attributed to each bone, defined with respect to the bone's centre of gravity [28] (cf. chapter 4 for details).

$$\vec{\kappa} = (\psi_1 \ \vartheta_1 \ \varphi_1 \ \psi_2 \ \vartheta_2 \ \varphi_2 \ \psi_3 \ \vartheta_3 \ \varphi_3)^T. \quad (7.1)$$

The model considers the scapulothoracic contact. The contact is modelled by constraining the points TS and AI on the scapula's medial border to remain in contact with the surface of two ellipsoids. The ellipsoids have common centre and model the surface of the thoracic cage with an additional layer of muscle tissue. The muscles are modelled as one or more massless, frictionless, perfectly elastic cables from origin to insertion. The cables wrap over the skeletal structure, modelled using constraints in the form of smooth surfaces such as spheres and cylinders. Each cable creates a moment-arm around the joints and the maximum amount of force a muscle can apply is limited. Muscles can only pull and therefore the force must be positive and the upper bound is the muscle's maximum isometric strength (cf. chapter 2). The model is defined in terms of the skeletal structure's equations of motion. These equations are obtained using the Euler-Lagrange equation (cf. chapter 4). The dynamic model is defined by a set of differential algebraic equations (DAE):

$$\frac{\partial^2 \tilde{\mathcal{L}}}{\partial \dot{\vec{\kappa}}^2} \ddot{\vec{\kappa}} + \frac{\partial^2 \tilde{\mathcal{L}}}{\partial \vec{\kappa} \partial \dot{\vec{\kappa}}} \dot{\vec{\kappa}} - \frac{\partial \tilde{\mathcal{L}}}{\partial \vec{\kappa}} = \hat{\mathbf{W}}_0 \hat{\mathbf{C}}_0 \vec{f} + \hat{\mathbf{W}}_0 \hat{\mathbf{C}}_{0,s} \vec{f}_s, \quad (7.2)$$

$$s.t. \quad \vec{\Phi}(\vec{\kappa}) = (\Phi_{TS}(\vec{\kappa}) \ \Phi_{AI}(\vec{\kappa}))^T = \vec{0}, \quad (7.3)$$

$$\vec{0} \leq \vec{f} \leq \vec{f}_{\max}. \quad (7.4)$$

$\tilde{\mathcal{L}}$ defines the total lagrangian, sum of the three bone lagrangians. $\hat{\mathbf{W}}_0$ is the matrix containing the jacobians of the instantaneous rotational velocity vectors. $\hat{\mathbf{C}}_0$ is the matrix containing the muscle moment-arms. $\hat{\mathbf{C}}_{0,s}$ is the matrix containing the constraint moment-arms. \vec{f} is the vector of muscle-force intensities. The vector \vec{f}_s is the constraint force intensities. For the constraint forces, the following equivalency holds (cf. chapter 4):

$$\hat{\mathbf{W}}_0 \hat{\mathbf{C}}_{0,s} \vec{f}_s = \left(\frac{\partial \vec{\Phi}}{\partial \vec{\kappa}} \right)^T \cdot \vec{\lambda}, \quad \hat{\mathbf{W}}_0 \hat{\mathbf{C}}_{0,s} \propto \left(\frac{\partial \vec{\Phi}}{\partial \vec{\kappa}} \right)^T. \quad (7.5)$$

The vector $\vec{\lambda}$ is the vector of lagrangian multipliers. The projected constraint moment-arms $\hat{\mathbf{W}}_0 \hat{\mathbf{C}}_{0,s}$ are proportional to the constraint gradients. The columns of both matrices are collinear.

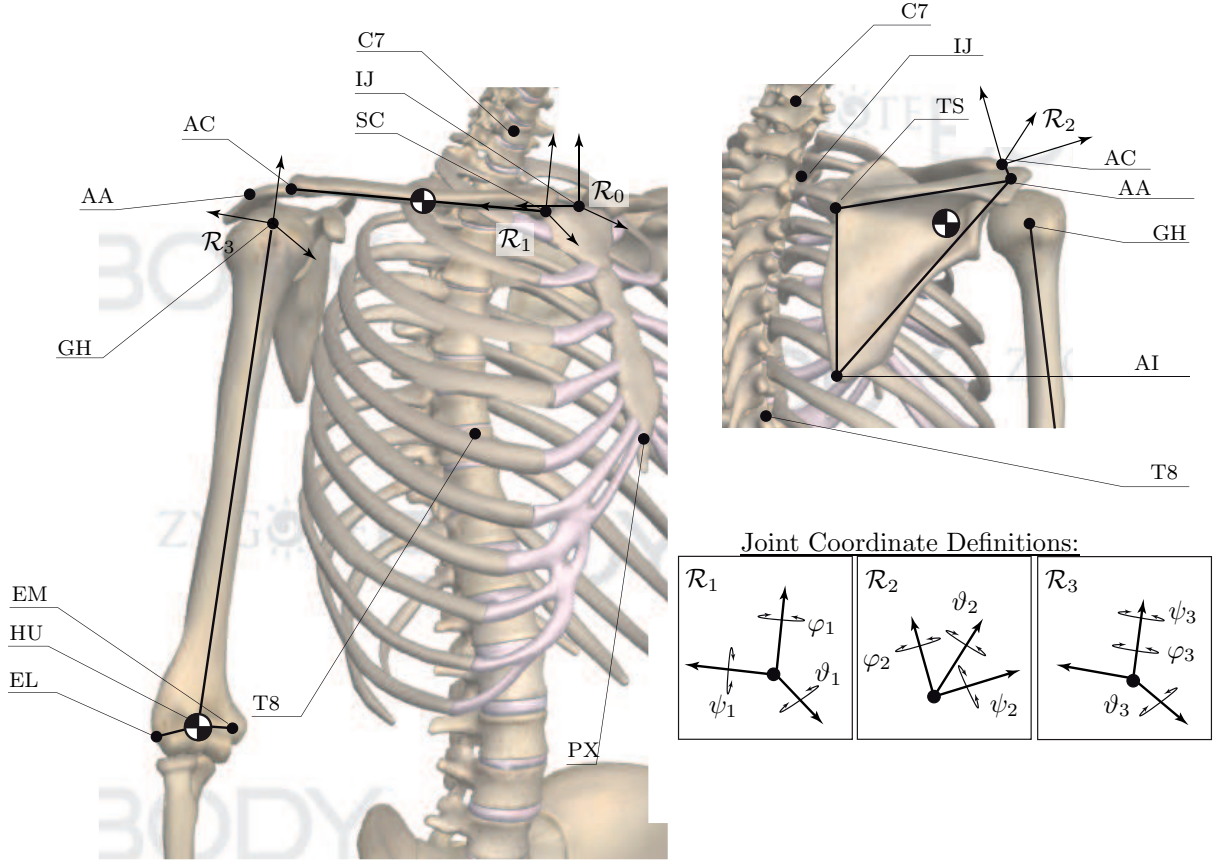


Figure 7.1: *Illustration of the bony landmarks, reference frame and the locations of the bone centres of gravity. Image created using ZygoteBody™ zygotebody.com.*

The model is actuated by the muscle forces. The muscle-force intensities multiplied by the moment-arms yield the actuation vector \vec{t}_a of the dynamic model. The actuation vector is also defined by inverting the dynamic model. The actuation is function of the dynamic state and the intensity of the constraint forces.

$$\frac{\partial^2 \tilde{\mathcal{L}}}{\partial \vec{\kappa}^2} \ddot{\vec{\kappa}} + \frac{\partial^2 \tilde{\mathcal{L}}}{\partial \vec{\kappa} \partial \dot{\vec{\kappa}}} \dot{\vec{\kappa}} - \frac{\partial \tilde{\mathcal{L}}}{\partial \vec{\kappa}} - \hat{\mathbf{W}}_0 \hat{\mathbf{C}}_{0,s} \vec{f}_s = \vec{t}_a(\vec{\kappa}, \dot{\vec{\kappa}}, \ddot{\vec{\kappa}}, \vec{f}_s) = \hat{\mathbf{W}}_0 \hat{\mathbf{C}}_0 \vec{f}. \quad (7.6)$$

The dynamic musculoskeletal model is overactuated. The number of muscle-force intensities is much larger than the number of generalised coordinates. For a given dynamic state $(\vec{\kappa}, \dot{\vec{\kappa}}, \ddot{\vec{\kappa}})$, there are an infinite number of muscle-force intensities producing this state. Finding a solution requires a coordination strategy. In chapter 5, it is stated that a solution can be found using a task. The primary task of the muscle forces is to produce motion. Therefore, a solution can be found by imposing a motion defined in terms of the dynamic state $(\vec{\kappa}(t), \dot{\vec{\kappa}}(t), \ddot{\vec{\kappa}}(t))$. An appropriate solution that agrees with measured muscle forces, is found by minimising the amount of stress in each muscle [194]. Stress is defined as the force in the muscle divided by the physiological cross-sectional area (PCSA).

To construct such a solution, consider a dynamic movement of the skeletal structure defined as a discrete sequence of dynamic states $(\vec{\kappa}(t_k), \dot{\vec{\kappa}}(t_k), \ddot{\vec{\kappa}}(t_k)), \forall t_k \in \{t_0, \dots, t_N\}$. The dynamic states all satisfy the constraints: $\vec{\Phi}(\vec{\kappa}(t_k)) = \vec{0} \forall t_k \in \{t_0, \dots, t_N\}$. The model

has N_p cables representing the musculature. A set of muscle-force intensities \vec{f}_k can be found for each dynamic state by solving the following static optimisation problem.

$$\min_{\vec{f}_k} \Gamma(\vec{f}_k) = \frac{1}{2} \sum_{j=1}^p \frac{(f_j^2)_k}{PCSA_j^2} = \frac{1}{2} \vec{f}_k^T \mathbf{P} \vec{f}_k, \quad (\mathbf{P})_{i,j} = \frac{\delta_{i,j}}{PCSA_j^2}. \quad (7.7)$$

$$\text{s.t. } \vec{t}_a(\vec{\kappa}(t_k), \dot{\vec{\kappa}}(t_k), \ddot{\vec{\kappa}}(t_k), \vec{f}_s(t_k)) = \hat{\mathbf{W}}_0 \hat{\mathbf{C}}_0 \vec{f}_k, \quad \text{Torque-force constraint,} \quad (7.8)$$

$$\vec{0} \leq \vec{f}_k \leq \vec{f}_{\max}, \quad \text{Min/max force bounds.} \quad (7.9)$$

This problem is referred to as the muscle-force estimation problem and represents a particular coordination strategy. The first constraint imposes the primary task, the cost function defines a secondary task and the second constraint imposes the limitations of the physical system. A comprehensive review of implementations of this problem can be found in [66].

7.2.2 Constraint Gradient Projection

The muscle-force coordination problem presented in the previous section has constraints which is not the case with all musculoskeletal models. The particular musculoskeletal model of the shoulder presented in chapter 4 considers the scapulothoracic contact using two holonomic skleronomic constraints. The forces \vec{f}_s representing the contact of the scapula on the thorax ellipsoids are unknown a priori. This section presents two possible methods of dealing with the vector \vec{f}_s . The first method uses the mathematical structure of the constraints and the second method incorporates the vector into the force coordination problem.

The first method is called the *constraint gradient projective method* [13]. As stated in chapter 6, the coordinates $\vec{\kappa}$ chart the space $(SO(3))^3$ that is a compact smooth manifold. They are mapped onto the manifold by:

$$\begin{aligned} \phi_S : [-\pi, \pi]^3 \times [-\pi, \pi]^3 \times [-\pi, \pi]^3 &\rightarrow (SO(3))^3, \\ \vec{\kappa} &\mapsto \phi_S(\vec{\kappa}) = (\mathbf{R}_{1,0}, \mathbf{R}_{2,0}, \mathbf{R}_{3,0}). \end{aligned} \quad (7.10)$$

The manifold $(SO(3))^3$ locally looks like \mathbb{R}^9 . Given the presence of smooth holonomic skleronomic constraints, the coordinate space \mathcal{Q}_S is defined as a compact smooth sub-manifold of $(SO(3))^3$.

$$\mathcal{Q}_S := \left\{ \vec{\kappa} \in [-\pi, \pi]^9 \subset \mathbb{R}^9, \phi_S(\vec{\kappa}) \in (SO(3))^3, \Phi(\vec{\kappa}) = \vec{0} \right\}. \quad (7.11)$$

There are two constraints and the dimension of the manifold is seven. This can be understood in the sense that the coordinates $\vec{\kappa}$ belong to a closed and bounded smooth surface in \mathbb{R}^9 of dimension seven.

At every point $\vec{\kappa} \in \mathcal{Q}_S$ there is a tangent space $T_{\vec{\kappa}}\mathcal{Q}_S$ of dimension seven. This can be understood as the linear surface or plane that is tangent to the manifold surface at $\vec{\kappa}$. In dynamics, the vector $\dot{\vec{\kappa}} \in \mathbb{R}^9$ belongs to the tangent space. It is a vector of dimension 9

restricted to a subspace of dimension 7. The tangent bundle $T\mathcal{Q}_S$ is defined as the union of the manifold and all the associated tangent spaces for all the points on the manifold.

$$T\mathcal{Q}_S = \bigcup_{\vec{\kappa} \in \mathcal{Q}_S} T_{\vec{\kappa}}\mathcal{Q}_S := \left\{ (\vec{\kappa}, \dot{\vec{\kappa}}), \vec{\kappa} \in \mathcal{Q}_S, \dot{\vec{\kappa}} \in T_{\vec{\kappa}}\mathcal{Q}_S \right\}. \quad (7.12)$$

The tangent bundle is locally equivalent to $\mathbb{R}^7 \times \mathbb{R}^7$, a Euclidean vector space of dimension 14. Given an initial condition $(\vec{\kappa}_0, \dot{\vec{\kappa}}_0)$, a solution $\mathcal{K}(\vec{\kappa}_0, \dot{\vec{\kappa}}_0, t)$ to the equations of motion is defined as a path on the manifold \mathcal{Q}_S . At every instant along the path, the vector $\dot{\vec{\kappa}}$ belongs to the tangent space and is tangent to the path.

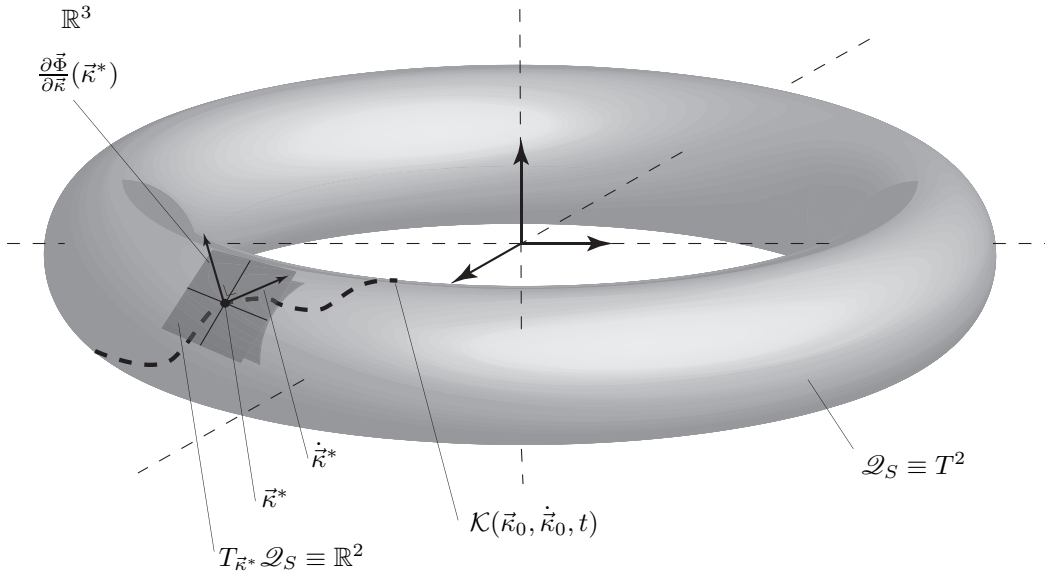


Figure 7.2: Diagram of a manifold \mathcal{Q}_S in \mathbb{R}^3 of dimension 2: the two-torus T^2 . The tangent space $T_{\vec{\kappa}}\mathcal{Q}_S$ at a point $\vec{\kappa}^*$ is locally equivalent to \mathbb{R}^2 and the orthogonal space is locally equivalent to \mathbb{R} as described in section 7.2.2.

The constraints are defined by two functions of the generalised coordinates that are equal to zero. In the tangent space at a given point $\vec{\kappa}^*$, these functions define the following relation.

$$\forall \vec{\kappa}^* \in \mathcal{Q}_S, \quad \vec{\Phi}(\vec{\kappa}^*) = \vec{0}, \quad \Rightarrow \quad \frac{\partial \vec{\Phi}}{\partial \vec{\kappa}}(\vec{\kappa}^*) \dot{\vec{\kappa}}^* = 0. \quad (7.13)$$

The velocity and the constraint jacobian are orthogonal at every point on the manifold \mathcal{Q}_S . Furthermore, the column vectors of the constraint jacobian or constraint gradient are always orthogonal to the tangent space of every point $\vec{\kappa}^*$. Thus, the null-space of the constrain jacobian parameterises the tangent space.

The constraint gradient projective method projects the dynamics onto the tangent space. The dynamics are defined using nine coordinates. Thus, nine equations of motion are needed to describe the dynamics. Projecting the initial set of equations onto the tangent space yields seven equations. The constraint gradients provide the missing equations and define a dynamic extension.

The dynamics are projected onto the tangent space, using the constraint gradient null-space. The null-space is parameterised by a matrix \mathbf{N}_Φ that annihilates the jacobian of the constraints for any configuration $\vec{\kappa} \in \mathcal{Q}_S$.

$$\forall \vec{\kappa} \in \mathcal{Q}_S \text{ and } \vec{\Phi}(\vec{\kappa}) = 0, \quad \exists \mathbf{N}_\Phi(\vec{\kappa}), \quad s.t. \quad \mathbf{N}_\Phi(\vec{\kappa}) \left(\frac{\partial \vec{\Phi}}{\partial \vec{\kappa}} \right)^T = 0. \quad (7.14)$$

The projected dynamics are defined by:

$$\mathbf{N}_\Phi(\vec{\kappa}) \vec{t}_a(\vec{\kappa}, \dot{\vec{\kappa}}, \ddot{\vec{\kappa}}, \vec{\lambda}) = \tilde{t}_a(\vec{\kappa}, \dot{\vec{\kappa}}, \ddot{\vec{\kappa}}) = \mathbf{N}_\Phi \frac{\partial^2 \tilde{\mathcal{L}}}{\partial \vec{\kappa}^2} \ddot{\vec{\kappa}} + \mathbf{N}_\Phi \frac{\partial^2 \tilde{\mathcal{L}}}{\partial \vec{\kappa} \partial \dot{\vec{\kappa}}} \dot{\vec{\kappa}} - \mathbf{N}_\Phi \frac{\partial \tilde{\mathcal{L}}}{\partial \vec{\kappa}} = \mathbf{N}_\Phi \hat{\mathbf{W}}_0 \hat{\mathbf{C}}_0 \vec{f}. \quad (7.15)$$

There are now seven dynamic equations and the constraints have been eliminated from the equations. To dynamics are extended using the second order derivative of the constraints with respect to time. The constraints must always be equal to zero and therefore so must their derivatives.

$$\vec{\Phi}(\vec{\kappa}) = \vec{0}, \quad \dot{\vec{\Phi}}(\vec{\kappa}) = \frac{\partial \vec{\Phi}}{\partial \vec{\kappa}} \dot{\vec{\kappa}} = \vec{0}, \quad \ddot{\vec{\Phi}}(\vec{\kappa}) = \frac{\partial \vec{\Phi}}{\partial \vec{\kappa}} \ddot{\vec{\kappa}} + \frac{d}{dt} \left(\frac{\partial \vec{\Phi}}{\partial \dot{\vec{\kappa}}} \right) \dot{\vec{\kappa}} = \vec{0}. \quad (7.16)$$

The constraint gradient projective method leads to the equations of motion without the constraints, defined by:

$$\begin{pmatrix} \mathbf{N}_\Phi \frac{\partial^2 \tilde{\mathcal{L}}}{\partial \vec{\kappa}^2} \\ \frac{\partial \vec{\Phi}}{\partial \vec{\kappa}} \end{pmatrix} \ddot{\vec{\kappa}} + \begin{pmatrix} \mathbf{N}_\Phi \frac{\partial^2 \tilde{\mathcal{L}}}{\partial \vec{\kappa} \partial \dot{\vec{\kappa}}} \\ -\frac{d}{dt} \left(\frac{\partial \vec{\Phi}}{\partial \dot{\vec{\kappa}}} \right) \end{pmatrix} \dot{\vec{\kappa}} - \begin{pmatrix} \mathbf{N}_\Phi \frac{\partial \tilde{\mathcal{L}}}{\partial \vec{\kappa}} \\ \vec{0} \end{pmatrix} = \begin{pmatrix} \mathbf{N}_\Phi \hat{\mathbf{W}}_0 \hat{\mathbf{C}}_0 \vec{f} \\ \vec{0} \end{pmatrix}. \quad (7.17)$$

This method is used most often in forward dynamics simulation but is presented here to be complete.

The second method, used in this chapter, is to include the vector of lagrangian multipliers in the vector of muscle forces. In chapter 4, the constraint terms in the dynamic equations (7.2) are shown to be equivalent to the moments of force created by the scapulo-thoracic contact model around the joints. Thus, the constraint force intensities can be included in the muscle-force coordination problem. The constraint forces are found simultaneously with the muscle forces.

$$\frac{\partial^2 \tilde{\mathcal{L}}}{\partial \vec{\kappa}^2} \ddot{\vec{\kappa}} + \frac{\partial^2 \tilde{\mathcal{L}}}{\partial \vec{\kappa} \partial \dot{\vec{\kappa}}} \dot{\vec{\kappa}} - \frac{\partial \tilde{\mathcal{L}}}{\partial \vec{\kappa}} = (\hat{\mathbf{W}}_0 \hat{\mathbf{C}}_0 \quad \hat{\mathbf{W}}_0 \hat{\mathbf{C}}_{0,s}) \begin{pmatrix} \vec{f} \\ \vec{f}_s \end{pmatrix} = \tilde{\mathbf{W}}_0 \tilde{\vec{f}}. \quad (7.18)$$

The vector $\tilde{\vec{f}}$ is called the augmented muscle-force vector and the matrix $\tilde{\mathbf{W}}_0$ is the augmented generalised moment-arms matrix. This matrix is function of the generalised coordinates only. The drawback of this approach is that the constraint forces are an effect of the muscle forces. The muscles apply a force that pushes the scapula onto the thorax resulting in a contact. The second method includes them into the coordination strategy and defines them as additional parameters which is not entirely correct.

7.2.3 A Coordination Strategy to Shoulder Overactuation

This section presents a particular coordination strategy for solving the muscle-force estimation problem. The problem is initially defined as in section 7.2.1. An additional constraint is added to ensure glenohumeral joint stability. This is understood as constraining the glenohumeral reaction force to always be directed at the surface of the glenoid.

$$\min_{\tilde{f}_k} \Gamma(\tilde{f}_k) = \frac{1}{2} \sum_{j=1}^p \frac{(\tilde{f}_j^2)_k}{PCSA_j^2} = \frac{1}{2} \tilde{f}_k^T \tilde{\mathbf{P}} \tilde{f}_k, \quad (\tilde{\mathbf{P}})_{i,j} = \frac{\delta_{i,j}}{PCSA_j^2}. \quad (7.19)$$

$$\text{s.t. } \vec{t}_a(\vec{\kappa}(t_k), \dot{\vec{\kappa}}(t_k), \ddot{\vec{\kappa}}(t_k)) = \tilde{\mathbf{W}}_0(\vec{\kappa}(t_k)) \tilde{f}_k, \quad \text{Torque-force constraint,} \quad (7.20)$$

$$\vec{0} \leq \tilde{f}_k \leq \tilde{f}_{\max}, \quad \text{Min/max force bounds,} \quad (7.21)$$

$$\vec{\Psi}(\vec{\kappa}(t_k), \dot{\vec{\kappa}}(t_k), \ddot{\vec{\kappa}}(t_k), \vec{f}_k) \leq \vec{0}, \quad \text{GH stability constraint.} \quad (7.22)$$

The scapulothoracic contact forces \vec{f}_s are compressive forces, the reaction forces are always pointed away from the surface of the ellipsoids. Thus, the contact force intensities must be positive. An upper bound is selected according to the observations from [88, 195]. The PSCA values for the constraint forces are selected at 1.

Glenohumeral joint stability is imposed in this model by constraining the GH joint reaction force \vec{f}_r to remain within a cone representing the glenoid fossa's orientation. The reaction force in the glenohumeral joint satisfies the following relation:

$$M_3 \ddot{\vec{x}}_{0,3} = M_3 \vec{g}_e + \mathbf{D}_0 \vec{f} + \vec{f}_r, \quad (7.23)$$

where $\ddot{\vec{x}}_{0,3}$ is the linear acceleration of the humerus's centre of gravity with respect to the inertial frame \mathcal{R}_0 . The vector \vec{g}_e is the Earth's gravitational field vector. \mathbf{D}_0 is the matrix containing the muscle-force direction vectors. For a model with N_p muscle segments, the total force and moment of force at each joint in the inertial frame \mathcal{R}_0 is defined by:

$$\vec{f}_{0,i} = \sum_{k=1}^{N_p} \vec{f}_{0,i,k} = \mathbf{D}_0 \vec{f}, \quad i = 1, 2, 3, \quad (7.24)$$

$$\vec{t}_{0,i} = \sum_{k=1}^{N_p} \vec{y}_{0,i,k} \times \vec{f}_{0,i,k} = \sum_{j=1}^{N_p} \left(\vec{y}_{0,i,k} \times \vec{b}_{0,i,k} \right) f_k = \sum_{j=1}^{N_p} \vec{c}_{0,i,k} f_k = \mathbf{C}_{0,i} \vec{f}. \quad (7.25)$$

The reaction force with respect to the humerus points away from the glenoid fossa into the humeral head. The reaction force with respect to the scapula points in the opposite direction. Glenohumeral joint stability is imposed by constraining the reaction force with respect to the scapula to remain within a cone. The cone's apex is centred on the glenohumeral joint centre (near the centre of the humeral head) and its basis is an ellipse that fits the glenoid (Fig. 7.3). Mathematically, the constraint is defined by the scalar product between the reaction force and the normal vectors to the cone's surface around the cone's base. The scalar products must remain positive. N_K points evenly distributed around the cone define N_K normal vectors and therefore N_K inequality constraints, which

together define the joint stability constraint. The cone is given its own reference system situated at its apex (subindex 5). The x -axis is parallel to the line passing through the base ellipse centre and the GH joint centre, pointing away from the base. The constraints are grouped into matrix form and defined by:

$$0 \leq \mathbf{B}_{0,5} \left(M_3(\vec{g} - \ddot{\vec{x}}_{0,3}) + \mathbf{D}_0 \vec{f} \right) = \mathbf{B}_{0,5} \left(\mathbf{D}_0 \vec{f} - \vec{f}_{dyn} \right). \quad (7.26)$$

$\mathbf{B}_{0,5}$ contains the N_K vectors normal to the cone's surface around the edge of the glenoid in the inertial frame.

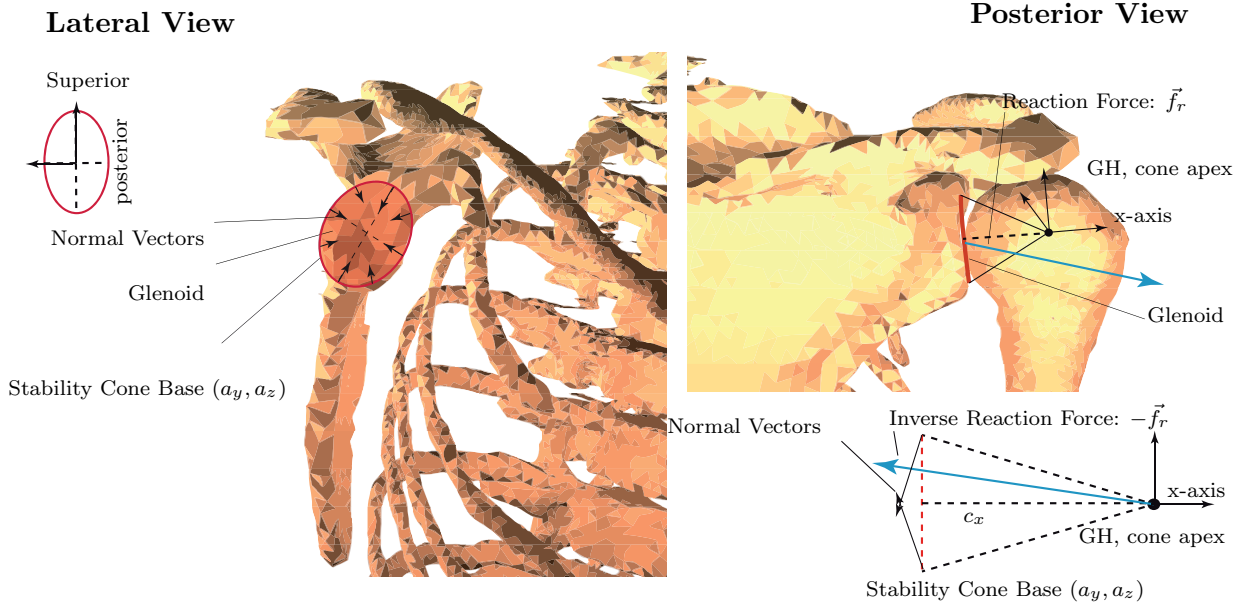


Figure 7.3: Construction of the GH joint stability constraint as presented in section 7.2.3. The reaction force is attached to the glenoid but in the model, it is attached to the glenohumeral joint centre.

A point on the edge of the glenoid in the cone's frame \mathcal{R}_5 is defined by:

$$P_5 : \vec{p}_5 = (c_x \quad a_y \cos(\vartheta) \quad a_z \sin(\vartheta))^T, \quad (7.27)$$

where a_y and a_z are the ellipse half axis representing the glenoid and c_x is the cone height. The vector normal to the cone's surface at this point is defined by:

$$\vec{n}_5 = \left(-1 \quad -\frac{c_x \cos(\vartheta)}{a_y} \quad -\frac{c_x \sin(\vartheta)}{a_z} \right)^T. \quad (7.28)$$

The cone's reference frame is defined with respect to the scapular frame \mathcal{R}_2 . Thus, all the normal vectors are rotated into the absolute frame using the following transformation:

$$\vec{n}_{0,5} = \mathbf{R}_{2,0} \mathbf{R}_{5,2} \vec{n}_5, \quad \Rightarrow \quad \mathbf{B}_{0,5}^T = (\vec{n}_{0,5,1} \quad \dots \quad \vec{n}_{0,5,N_K}). \quad (7.29)$$

The matrix $\mathbf{R}_{5,2}$ is constructed by defining the cone frame unit vectors in the scapular frame. The matrix $\mathbf{R}_{5,2}$ is the scapula to thorax rotation matrix. This constraint models

the edge of the glenoid as an ellipse. This is not strictly the shape of the anatomical glenoid but is necessary to obtain an analytical form of the cone and define a constraint.

The muscle-force coordination strategy defined at the beginning of this section (7.19)-(7.22) is generally solved using a conventional optimisation solver. The idea of the following method is to use the torque-force constraint directly. The constraint is an equality constraint and can be used directly to find an initial solution to the problem. Given an actuation vector $\vec{t}_a(\vec{\kappa}(t_k), \dot{\vec{\kappa}}(t_k), \ddot{\vec{\kappa}}(t_k))$, a vector of muscle-force intensities is found by taking the Moore-Penrose pseudo-inverse of the augmented generalised moment-arms matrix [3].

$$\tilde{f}_k^* = \tilde{\mathbf{W}}_{0,k}^T \left(\tilde{\mathbf{W}}_{0,k} \tilde{\mathbf{W}}_{0,k}^T \right)^{-1} \vec{t}_a(\vec{\kappa}(t_k), \dot{\vec{\kappa}}(t_k), \ddot{\vec{\kappa}}(t_k)). \quad (7.30)$$

This solution is shown to minimise the mean square muscle forces [203]. Inserting the PCSA matrix \mathbf{P} yields a solution that minimises the mean square muscle stress.

$$\tilde{f}_k^* = \tilde{\mathbf{P}} \tilde{\mathbf{W}}_{0,k}^T \left(\tilde{\mathbf{W}}_{0,k} \tilde{\mathbf{P}} \tilde{\mathbf{W}}_{0,k}^T \right)^{-1} \vec{t}_a(\vec{\kappa}(t_k), \dot{\vec{\kappa}}(t_k), \ddot{\vec{\kappa}}(t_k)). \quad (7.31)$$

This solution satisfies the first constraint (7.20) but not the others. The remaining constraints (7.21) and (7.22) are satisfied by making use of the moment-arms matrix null-space. Any vector within the moment-arm matrix's null-space can be added to this solution and the resulting solution will still respect the constraint (7.20). The solution satisfying all three constraints is parameterised by:

$$\tilde{f}_k = \tilde{f}_k^* + \tilde{\mathbf{N}}_{W,k} \vec{v}, \quad \tilde{\mathbf{W}}_{0,k} \tilde{\mathbf{N}}_{W,k} = 0. \quad (7.32)$$

The vector \vec{v} is used to search for a solution, that respects all the constraints, but does not violate the torque-force constraint. Using the re-parameterisation, the matrix form of the cost function is defined by:

$$\Gamma_k(\vec{v}) = \frac{1}{2} \tilde{f}_k^T \tilde{\mathbf{P}} \tilde{f}_k = \frac{1}{2} \vec{v}^T \tilde{\mathbf{N}}_{W,k}^T \tilde{\mathbf{P}} \tilde{\mathbf{N}}_{W,k} \vec{v} + (\tilde{f}_k^*)^T \tilde{\mathbf{P}} \tilde{\mathbf{N}}_{W,k} \vec{v} + \frac{1}{2} (\tilde{f}_k^*)^T \tilde{\mathbf{P}} \tilde{f}_k^*. \quad (7.33)$$

The maximum force constraint becomes:

$$\begin{aligned} 0 &\leq \tilde{f}_k \leq \tilde{f}_{max}, \\ \Rightarrow 0 &\leq \tilde{f}_k^* + \tilde{\mathbf{N}}_{W,k} \vec{v} \leq \tilde{f}_{max}, \\ \Rightarrow -\tilde{f}_k^* &\leq \tilde{\mathbf{N}}_{W,k} \vec{v} \leq \tilde{f}_{max} - \tilde{f}_k^*. \end{aligned} \quad (7.34)$$

The joint stability constraint becomes:

$$0 \leq \mathbf{B}_{0,5} \left(\mathbf{D}_{0,k} \vec{f}_k - \vec{f}_{dyn,k} \right), \quad \Rightarrow -\mathbf{B}_{0,5,k} \mathbf{D}_{0,k} \tilde{\mathbf{N}}_{W,k} \vec{v} \leq \mathbf{B}_{0,5,k} \left(\mathbf{D}_{0,k} \tilde{f}_k^* - \vec{f}_{dyn,k} \right). \quad (7.35)$$

The matrix $\mathbf{N}_{W,k}$ is the null space of the generalised moment-arms matrix without the scapulothoracic contact forces. Thus, the nonlinear program is now defined as a quadratic program with the constraints grouped together into a single linear inequality constraint [3, 190].

$$\min_{\vec{v}} \quad \Gamma_k(\vec{v}) = \frac{1}{2} \vec{v}^T \tilde{\mathbf{N}}_{W,k}^T \tilde{\mathbf{P}} \tilde{\mathbf{N}}_{W,k} \vec{v} + (\tilde{f}_k^*)^T \tilde{\mathbf{P}} \tilde{\mathbf{N}}_{W,k} \vec{v}, \quad (7.36)$$

$$\text{s.t.} \quad \mathbf{A}_k \vec{v} - \vec{b}_k \leq \vec{0}, \quad (7.37)$$

The constraint matrix \mathbf{A}_k and vector \vec{b}_k are defined by:

$$\mathbf{A}_k = \begin{pmatrix} \tilde{\mathbf{N}}_{W,k} \\ -\tilde{\mathbf{N}}_{W,k} \\ -\mathbf{B}_{0,5,k}\mathbf{D}_{0,k}\mathbf{N}_{W,k} \end{pmatrix}, \quad \vec{b}_k = \begin{pmatrix} \tilde{f}_{max} - \tilde{f}_k^* \\ \tilde{f}_k^* \\ \mathbf{B}_{0,5,k}(\mathbf{D}_{0,k}\tilde{f}_k^* - \vec{f}_{dyn}) \end{pmatrix}. \quad (7.38)$$

Once a solution to the muscle-force estimation problem is found, the results are used in combination with (7.23) to obtain the joint reaction force.

7.3 Muscle Moment-Arms Theory

As stated in the introduction to this chapter, moment-arms play a central role in determining if a solution to the muscle-force estimation problem exists. In the previous section, a coordination strategy was presented and solved using the moment-arms matrix directly. The moment-arms matrix was used to parameterise the solution. Muscle moment-arms are the key element in any coordination strategy. Given this fact, muscle moment-arms require a formal presentation..

Physically a muscle's moment-arm characterises its ability to actuate the skeletal system. It characterises the muscle's ability to change the configuration of the joints in the skeletal system. The muscle moment-arms relate the forces in the muscles to the primary task of movement. They map the muscle-force vector to the actuation vector and appear in the equations of motion. Muscle moment-arms were initially defined experimentally in cadaveric studies, by relating the change in muscle length to the change in joint angle [2, 5, 25, 130, 161]. This experimental definition was formalised using the principle of virtual work, leading to the tendon excursion definition, where the moment-arm is defined as partial derivative of the muscle length with respect to the joint angle [7, 51]. This formalisation was done on the basis of a number of assumptions. First, the muscles are represented by one or more massless, frictionless cable(s). The path taken by the cable is the minimum distance between the two points passing over the bones modelled using constraints. The constraints define smooth surfaces. A second assumption is that the cable's length depends only on the configuration of the skeletal structure. It is a kinematic quantity. The third assumption is that there is a uniform tension in the cable.

The tendon excursion method is not the only method of computing muscle moment-arms. Other methods have been proposed using velocities [179]. However, moment-arms have a more fundamental interpretation that was introduced to biomechanics previously to the tendon excursion method. If the notion of muscle is removed, the concept of moment-arm has a more fundamental geometric interpretation. A moment-arm can be defined for any system of forces. The notion of muscle length and coordinates is not required to define moment-arms. Previous to the formalisation of the tendon excursion method, muscles were initially considered to apply a system of forces on the skeletal system [166]. Furthermore, all the forces in the system of forces are assumed to have the same intensity. This assumption can therefore be seen as the fundamental assumption behind muscle moment-arms.

This section completely reviews the concept of moment-arm starting with the fundamental concept of moment-arm without muscles. A method of computing a muscle's moment-arm is presented based on the geometric interpretation. This method is related to the tendon excursion definition of moment-arms. Finally, a some practical issues related to moment-arms are presented.

7.3.1 Fundamentals of Moment-Arms

In classical mechanics, a force $\vec{f}_{0,i}$, applied on a rigid body \mathcal{B}_i at a point A , creates a moment of force at any other point B of the body (Fig. 7.4). The moment of force $\vec{t}_{0,i}$ is defined as the cross product between the vector $\vec{r}_{0,i}$ from points B to A and the force. The force and its moment, if grouped together in an ordered pair, define a wrench with respect to the point B [12, 86, 204]. The wrench is defined by:

$$\mathcal{F}_{B0,i} = \left(\vec{f}_{0,i}, \vec{r}_{0,i} \times \vec{f}_{0,i} \right)_{B0,i} = |f_{0,i}| \left(\vec{b}_{0,i}, \vec{r}_{0,i} \times \vec{b}_{0,i} \right)_B = |f_{0,i}| \left(\vec{b}_{0,i}, \vec{c}_{0,i} \right)_{B0,i}. \quad (7.39)$$

All the vectors are defined in the inertial frame \mathcal{R}_0 . The associated moment-arm $\vec{c}_{0,i}$ is defined by the same cross product but with a normalised force vector $\vec{b}_{0,i}$. This definition of moment-arm applies to a single body subject to a single force, and has a geometric interpretation. The norm of the moment-arm represents the distance from point B to the line defined by the vector $\vec{b}_{0,i}$ passing through A , a quantity called the lever-arm. The moment-arm is therefore a purely geometric quantity associated to a given point on the body, depending only on the direction of the force and its point of application.

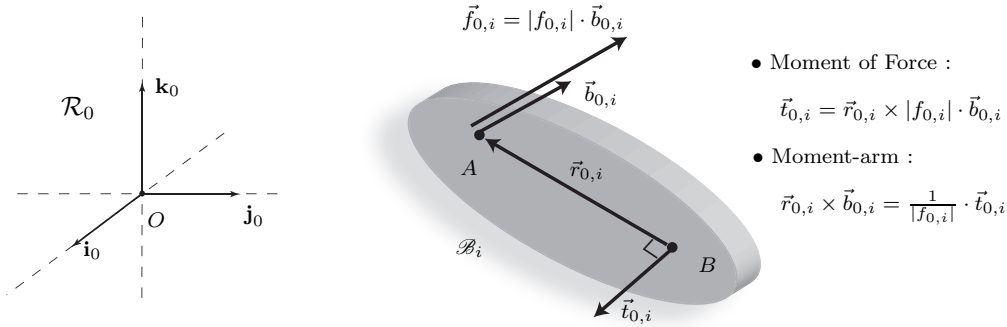


Figure 7.4: *Illustration of the classical mechanics definition of force moment-arm as described in section 7.3.1.*

There is another interpretation of the moment-arm. If the body is attached to a fixed point through a spherical kinematic pair at the point B , and no other force is applied to the body, then the moment-arm vector defines the instantaneous axis of rotation of the body around the joint. This is a direct result of the duality between Chasle's theorem in kinematics and Poinot's theorem in dynamics (cf. chapter 3).

A system of N_f forces applied to a body can always be reduced to a single force and moment of force at a given point. The resulting force is the sum of all the forces applied

to the body and the resulting moment of force is the sum of all the individual moments of force.

$$\vec{f}_{0,i} = \sum_{j=1}^{N_f} \vec{f}_{0,i,j}, \quad \vec{t}_{0,i} = \sum_{j=1}^{N_f} \vec{r}_{0,i,j} \times \vec{f}_{0,i,j}. \quad (7.40)$$

Assuming that all the forces have the same intensity, a total moment-arm is defined by:

$$\vec{c}_{0,i} = \sum_{j=1}^{N_f} \vec{r}_{0,i,j} \times \frac{1}{\|\vec{f}_{0,i,j}\|} \vec{f}_{0,i,j} = \sum_{j=1}^{N_f} \vec{r}_{0,i,j} \times \vec{b}_{0,i,j}. \quad (7.41)$$

Without the assumption on the intensity, the resulting torque cannot be expressed by a single scalar multiplied by a single moment-arm.

$$\vec{t}_{0,i} = \|\vec{f}_{0,i,j}\| \vec{c}_{0,i}. \quad (7.42)$$

The uniform intensity assumption is what allows one to represent the action of a muscle by a single moment-arm for each body.

7.3.2 A Geometric Method of Computing Moment-Arms

The previous definition only considered a single body. A musculoskeletal system is defined by a number of bones and muscles apply multiple forces on the bones. Each muscle is defined as a massless, frictionless cable with a certain geometry. Given this assumption, pulley mechanics are used to compute the points of application and direction of the forces applied by the muscles on the bones.

A cable applies forces at its origin and insertion points parallel to and directed along the cable. At every point in between, the muscle applies two forces parallel to the cable with opposite directions. If the muscle wraps over a bone, it applies two forces on the bone at the initial and final points of contact parallel to the cable but in opposite directions. All the forces applied by a single muscle on the bone are of equal magnitude. In accordance with this description, a muscle applies multiple forces $\vec{f}_{0,i,j}$ to the bodies and creates moment-arms for every body to which it applies a force. These forces include the forces applied at the origin and insertion as well as the forces applied on the wrapping objects attached to the bones. Like the moment-arm of a force, muscle moment-arms are defined with respect to a specific point, usually one of the joints attached to the body. In this manner, a muscle's moment-arms define its ability to change the configuration of the joints.

To illustrate the application of the geometric definition, consider a serial skeletal system with N_b bones \mathcal{B}_i and N_b joints J_i (Fig. 7.5). The bones are considered to be rigid bodies and the joints are ideal ball and socket joints parameterised by spherical kinematic pairs. A reference system \mathcal{R}_i is attached to each joint J_i (subindex i) describing the configuration of the bone \mathcal{B}_i with respect to the carrier body reference frame \mathcal{R}_0 . A first muscle \mathcal{M}_1 spans the last joint J_{N_b} and is attached to the bones \mathcal{B}_{N_b} and \mathcal{B}_{N_b-1} . A second muscle inserts on the bone \mathcal{B}_{N_b-1} and originates on the carrier body.

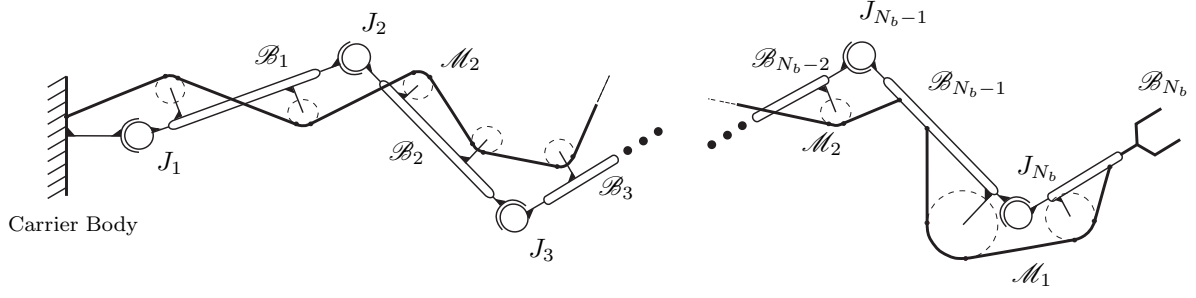


Figure 7.5: Illustration of a skeletal system with n joints and two muscles. Muscle \mathcal{M}_1 spans a single joint. Muscle \mathcal{M}_2 spans multiple joints with m via points including origin and insertion as described in section 7.3.2.

The muscle \mathcal{M}_1 spans the joint J_{N_b} , originates on the bone \mathcal{B}_{N_b-1} and inserts on the bone \mathcal{B}_{N_b} . In between it wraps over two surfaces \mathcal{W}_{N_b-1} and \mathcal{W}_{N_b} , modelling the bones. Given the location of the muscle's origin and insertion points, the muscle creates moment-arms at the joints J_{N_b} and J_{N_b-1} . To define the moment-arms around the joints J_{N_b} and J_{N_b-1} , the two bodies are isolated (Fig. 7.6). There are three contact points with body \mathcal{B}_{N_b} : $P_{N_b,1}$, $P_{N_b,2}$, $P_{N_b,3}$. There are three forces. The two contact points associated to the wrapping surface and the insertion force. The total screw at the joint J_{N_b} in the fixed frame (subindex 0) is defined by

$$\begin{aligned} \mathcal{F}_{J_{N_b}} &= \left(\vec{f}_{0,N_b,1}, \vec{y}_{0,N_b,1} \times \vec{f}_{0,N_b,1} \right)_{J_{N_b}} + \left(\vec{f}_{0,N_b,2}, \vec{y}_{0,N_b,2} \times \vec{f}_{0,N_b,2} \right)_{J_{N_b}} + \left(\vec{f}_{0,N_b,3}, \vec{y}_{0,N_b,3} \times \vec{f}_{0,N_b,3} \right)_{J_{N_b}}, \\ &= \left(\vec{f}_{0,N_b,1}, \vec{y}_{0,N_b,1} \times \vec{f}_{0,n,1} \right)_{J_{N_b}} - \left(\vec{f}_{0,N_b,1}, \vec{y}_{0,N_b,2} \times \vec{f}_{0,N_b,1} \right)_{J_{N_b}} + \left(\vec{f}_{0,N_b,3}, \vec{y}_{0,N_b,3} \times \vec{f}_{0,N_b,3} \right)_{J_{N_b}}, \\ &= \left(\vec{f}_{0,N_b,3}, \vec{y}_{0,N_b,3} \times \vec{f}_{0,N_b,3} \right)_{J_{N_b}}. \end{aligned} \quad (7.43)$$

The forces applied at the points $P_{N_b,1}$ and $P_{N_b,2}$ completely cancel each other out. The moment-arm of the muscle around the joint J_{N_b} is thus equal to:

$$\vec{c}_{0,N_b} = \vec{y}_{0,N_b,3} \times \frac{1}{|f|} \vec{f}_{0,N_b,3} = \vec{y}_{0,N_b,3} \times \vec{b}_{0,N_b}. \quad (7.44)$$

There are three contact points with body \mathcal{B}_{N_b-1} : $P_{N_b-1,1}$, $P_{N_b-1,2}$, $P_{N_b-1,3}$. The joint J_{N_b} is a ball and socket joint. It therefore transmits only forces and no moments of force. There are three forces associated to the contact points and the reaction force transmitted by the joint. This force is equal to the resulting force in the screw at the joint J_{N_b} . The screw at the joint J_{N_b-1} is defined by

$$\begin{aligned} \mathcal{F}_{J_{N_b-1}} &= \left(\vec{f}_{0,N_b-1,1}, \vec{y}_{0,N_b-1,1} \times \vec{f}_{0,N_b-1,1} \right)_{J_{N_b-1}} + \left(\vec{f}_{0,N_b-1,2}, \vec{y}_{0,N_b-1,2} \times \vec{f}_{0,N_b-1,2} \right)_{J_{N_b-1}} + \\ &\quad \left(\vec{f}_{0,N_b-1,3}, \vec{y}_{0,N_b-1,3} \times \vec{f}_{0,N_b-1,3} \right)_{J_{N_b-1}} + \left(\vec{f}_{0,N_b-1,4}, \vec{y}_{0,N_b-1,4} \times \vec{f}_{0,N_b-1,4} \right)_{J_{N_b-1}}. \end{aligned} \quad (7.45)$$

The vector $\vec{y}_{0,N_b-1,4}$ is the vector between the joints, from J_{N_b-1} to J_{N_b} . The force $\vec{f}_{0,N_b-1,4}$ is equal to $\vec{f}_{0,N_b,3}$ and is the inverse of $\vec{f}_{0,N_b-1,1}$. The forces at the points $P_{N_b-1,2}$ and $P_{N_b-1,3}$

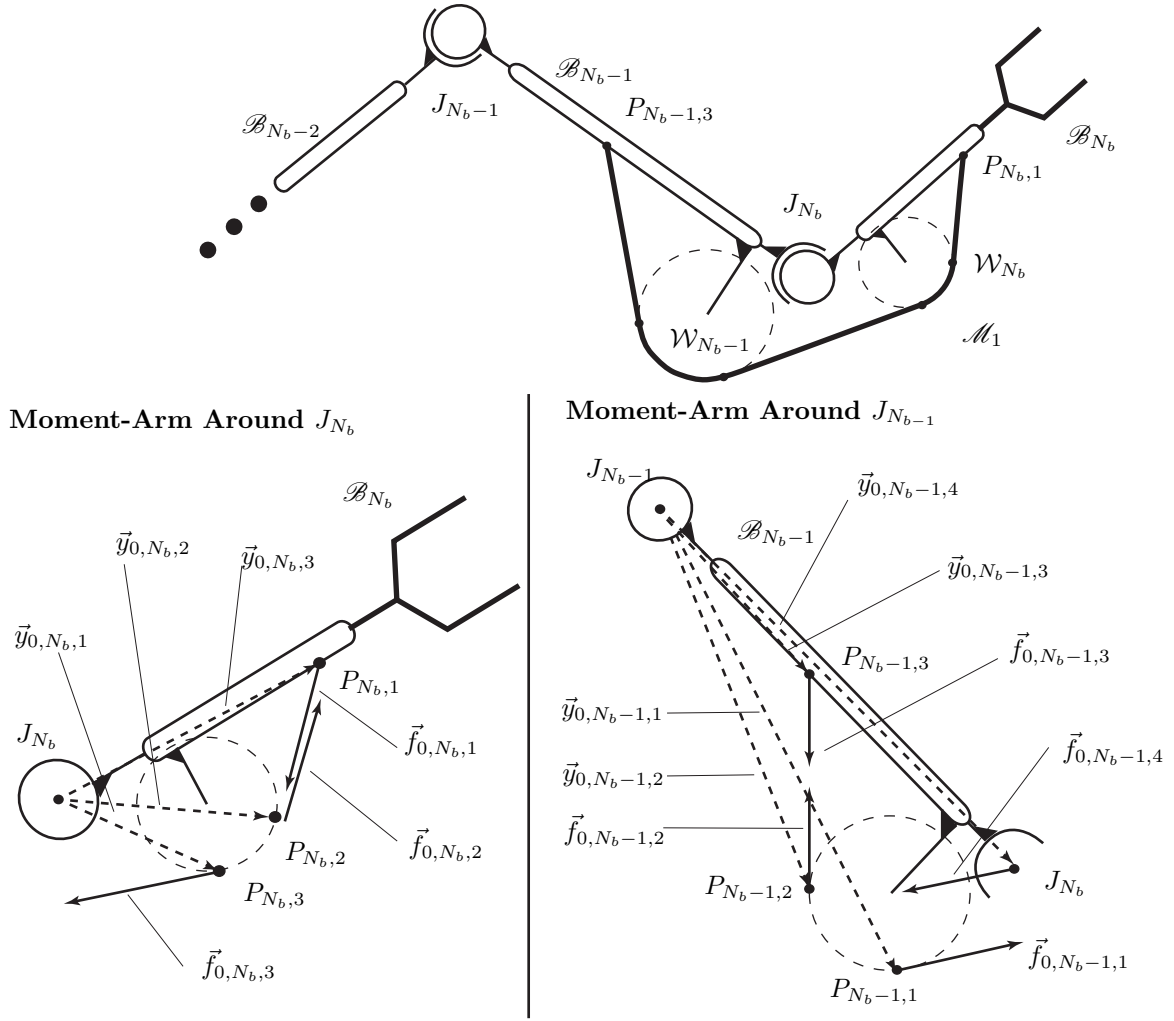


Figure 7.6: Isolation of the bones that the muscle \mathcal{M}_1 contacts and identification of all forces and points of application as described in section 7.3.2.

cancel each other out. The screw at joint J_{N_b-1} reduces to the following expression

$$\begin{aligned} \mathcal{F}_{J_{N_b-1}} &= - \left(\vec{f}_{0,n,3}, \vec{y}_{0,N_b-1,1} \times \vec{f}_{0,N_b,3} \right)_{J_{N_b-1}} + \left(\vec{f}_{0,N_b,3}, \vec{y}_{0,N_b-1,4} \times \vec{f}_{0,N_b,3} \right)_{J_{N_b-1}}, \\ &= \left(0, (\vec{y}_{0,N_b-1,4} - \vec{y}_{0,N_b-1,1}) \times \vec{f}_{0,N_b,3} \right)_{J_{N_b-1}}. \end{aligned} \quad (7.46)$$

The resulting force at the joint J_{N_b-1} is zero but the moment of force is not, and therefore the moment arm is also not zero.

$$\vec{c}_{0,N_b-1} = (\vec{y}_{0,N_b-1,4} - \vec{y}_{0,N_b-1,1}) \times \frac{1}{|\vec{f}|} \vec{f}_{0,N_b,3} = (\vec{y}_{0,N_b-1,4} - \vec{y}_{0,N_b-1,1}) \times \vec{b}_{0,N_b-1}. \quad (7.47)$$

The location of all the contact points can be computed using any one of a number of wrapping algorithms [38, 75, 139]. Given these points, the force direction vectors \vec{b}_{0,N_b} and \vec{b}_{0,N_b-1} can be computed.

In the more general situation, a muscle's moment-arm vector around a joint is computed by isolating the body associated to the joint and identifying all the forces which

apply to it. Consider the muscle \mathcal{M}_2 from the illustration which applies forces to the body \mathcal{B}_i (Fig. 7.7). There are m points where forces are applied $P_{i,k}$, $k = 1, 2, \dots, m$. The first observation is that the only forces which are of importance are the forces being applied at the end points in the direction of the other bodies and the reaction force at the joint J_{i+1} . All the other forces cancel each other. This leads to the second observation, the force transmitted to the next body through the joint J_i along the chain in the direction of the carrier body is equal to the force being applied at the last point $P_{i,m}$. Thus, the screw of the muscle at the joint J_i is defined by

$$\begin{aligned} \mathcal{F}_{J_i} &= \left(\vec{f}_{0,i,m}, \vec{y}_{0,i,m} \times \vec{f}_{0,i,m} \right)_{J_i} + \left(\vec{f}_{0,i,1}, \vec{y}_{0,i,1} \times \vec{f}_{0,i,1} \right)_{J_i} - \left(\vec{f}_{0,i,1}, \vec{y}_{0,i,m+1} \times \vec{f}_{0,i,1} \right)_{J_i}, \\ &= \left(\vec{f}_{0,i,m}, \vec{y}_{0,i,m} \times \vec{f}_{0,i,m} \right)_{J_i} + \left(0, (\vec{y}_{0,i,1} - \vec{y}_{0,i,m-1}) \times \vec{f}_{0,i,1} \right)_{J_i}. \end{aligned} \quad (7.48)$$

The muscle moment-arm around the joint J_k is defined by

$$\begin{aligned} \vec{c}_{0,i} &= \vec{y}_{0,i,m} \times \frac{1}{|\vec{f}|} \vec{f}_{0,i,m} + (\vec{y}_{0,i,1} - \vec{y}_{0,i,m-1}) \times \frac{1}{|\vec{f}|} \vec{f}_{0,i,1}, \\ &\vec{y}_{0,i,m} \times \vec{b}_{0,i,m} + (\vec{y}_{0,i,1} - \vec{y}_{0,i,m-1}) \times \vec{b}_{0,i,1}. \end{aligned} \quad (7.49)$$

This method of computing moment-arms is valid under the hypothesis that the bones are rigid bodies, the muscles are ideal cables and that the joints are parameterised by spherical pairs. If the type of kinematic pairs within the musculoskeletal model are different than spherical pairs, the method of computing the moment-arms would need to be adapted. Different types of kinematic pairs transfer different types of forces and moments of force. However, the philosophy remains the same. Each body is isolated and analysed in terms of muscle forces and joint reaction forces.

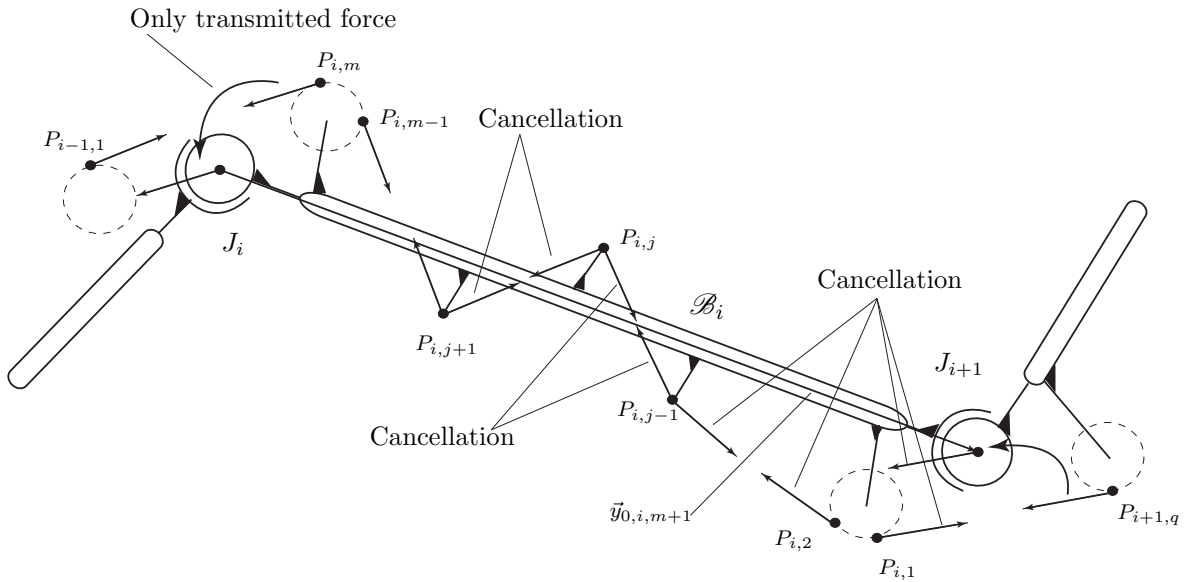


Figure 7.7: *Illustration of force cancellations and force transmissions in a general musculoskeletal model as described in section 7.3.2.*

7.3.3 Tendon Excursion Method of Computing Moment-Arms

The second method of computing muscle moment-arms is the tendon excursion method. This method depends on the generalised coordinates used to define the model. This method is derived from the principle of virtual work. Given its simplicity and relation to the experimental definition, the tendon excursion method has been widely used to compute and validate model-based moment-arms [38, 76, 101]. However, it is a definition that requires caution and a certain amount of rigour. The tendon excursion method is defined using the principle of virtual work, a concept from analytical mechanics, and must be applied according to the same framework and hypothesis.

Consider a rigid body \mathcal{B}_i in space that is part of a mechanism. Its configuration with respect to a fixed frame \mathcal{R}_0 is parameterised by a Euclidean displacement function of the mechanism's generalised coordinates $\vec{\kappa} = (\kappa_1, \dots, \kappa_{\hat{Q}})^T$.

$$\vec{x}_{0,i} = \vec{d}_{0,i} + \mathbf{R}_{i,0}\vec{x}_i = \vec{d}_{0,i} + \vec{x}_{0,i}^*, \quad \vec{x}_{0,i}^* = \mathbf{R}_{i,0}\vec{x}_i. \quad (7.50)$$

The velocity of the point is defined by:

$$\dot{\vec{x}}_{0,i} = \dot{\vec{d}}_{0,i} + \vec{\omega}_{0,i} \times \vec{x}_{0,i}^* = \frac{\partial \vec{d}_{0,i}}{\partial \vec{\kappa}} \dot{\vec{\kappa}} + \frac{\partial \vec{\omega}_{0,i}}{\partial \vec{\kappa}} \dot{\vec{\kappa}} \times \vec{x}_{0,i}^* = \sum_{k=1}^{\hat{Q}} \frac{\partial \vec{x}_{0,i}}{\partial \kappa_k} \dot{\kappa}_k. \quad (7.51)$$

where $\vec{\omega}_{0,i}$ is the instantaneous rotational velocity of the body in the fixed frame. Given this definition of velocity, the real infinitesimal change in configuration or real infinitesimal displacement of the body is defined by (cf. chapter 3 for details):

$$d\vec{x}_{0,i} = \sum_{k=1}^{\hat{Q}} \frac{\partial \vec{x}_{0,i}}{\partial \kappa_k} d\kappa_k = \frac{\partial \vec{d}_{0,i}}{\partial \vec{\kappa}} d\vec{\kappa} + \frac{\partial \vec{\omega}_{0,i}}{\partial \vec{\kappa}} d\vec{\kappa} \times \vec{x}_{0,i}^*. \quad (7.52)$$

A virtual displacement, is an infinitesimal displacement without an infinitesimal change in time.

$$\delta\vec{x}_{0,i} = \sum_{k=1}^{\hat{Q}} \frac{\partial \vec{x}_{0,i}}{\partial \kappa_k} \delta\kappa_k = \frac{\partial \vec{d}_{0,i}}{\partial \vec{\kappa}} \delta\vec{\kappa} + \frac{\partial \vec{\omega}_{0,i}}{\partial \vec{\kappa}} \delta\vec{\kappa} \times \vec{x}_{0,i}^*. \quad (7.53)$$

One of the primary differences between real and virtual displacements is that real displacements $d\vec{x}_{0,i}$ can be integrated along a path and virtual displacements $\delta\vec{x}_{0,i}$ cannot. If the mechanism's kinematic parameterisation contains holonomic skleronomic constraints of the form $\vec{\Phi}(\vec{\kappa}) = (\Phi_1(\vec{\kappa}), \dots, \Phi_p(\vec{\kappa}))^T = \vec{0}$, both real and virtual displacements must be compatible with the constraints. The formal definition is as follows.

Definition 22 (Virtual displacement [86]). *A virtual displacement $\delta\vec{x}_{0,i}$ compatible with the kinematic coordinates $\vec{\kappa} = (\kappa_1, \dots, \kappa_k, \dots, \kappa_{\hat{Q}})^T$ is any displacement that can be imposed on the system satisfying the following relation:*

$$\delta\vec{x}_{0,i} = \sum_{k=1}^{\hat{Q}} \frac{\partial \vec{x}_{0,i}}{\partial \kappa_k} \delta\kappa_k. \quad (7.54)$$

This equation is called the compatibility equation. The δq_k are solutions to the equations

$$\begin{aligned} \sum_{k=1}^{\hat{Q}} \frac{\partial \Phi_1}{\partial \kappa_k} \delta \kappa_k &= 0, \\ \vdots \\ \sum_{k=1}^{\hat{Q}} \frac{\partial \Phi_p}{\partial \kappa_k} \delta \kappa_k &= 0. \end{aligned} \quad (7.55)$$

The virtual displacement $\delta \vec{\kappa}$ vector is part of the null-space of the matrix $[\frac{\partial \Phi_1}{\partial \vec{\kappa}}, \dots, \frac{\partial \Phi_p}{\partial \vec{\kappa}}]$.

This definition states that if there are constraints, the real and virtual displacements are in the constraint manifold's tangent space, orthogonal to the space defined by the constraint jacobians (cf. section 7.2.2).

There is a muscle inserting on the body \mathcal{B}_i . This muscle applies a force $\vec{f}_{0,i}$, defined in the fixed frame at a point P ($\vec{y}_{0,i}$). The virtual work created by the force, due to a virtual displacement, is defined by:

$$\delta W = \vec{f}_{0,i}^T \cdot \delta \vec{y}_{0,i} = \vec{f}_{0,i}^T \cdot \frac{\partial \vec{d}_{0,i}}{\partial \vec{\kappa}} \delta \vec{\kappa} + \vec{f}_{0,i}^T \cdot \frac{\partial \vec{\omega}_{0,i}}{\partial \vec{\kappa}} \delta \vec{\kappa} \times \vec{y}_{0,i}. \quad (7.56)$$

The same force also shortens the muscle's length by δL . The virtual work associated to the muscle's change in length is defined by:

$$\delta W = -f_{0,i} \cdot \delta L = -f_{0,i}^T \cdot \frac{\partial L}{\partial \vec{\kappa}} \delta \vec{\kappa}. \quad (7.57)$$

The work in one-dimensional and function of the force intensity. The tendon excursion method is based on the hypothesis that both virtual works are equal.

$$\delta W = -f_{0,i}^T \cdot \delta L = \vec{f}_{0,i}^T \cdot \delta \vec{y}_{0,i}, \Rightarrow -f_{0,i}^T \cdot \frac{\partial L}{\partial \vec{\kappa}} \delta \vec{\kappa} = \vec{f}_{0,i}^T \cdot \frac{\partial \vec{d}_{0,i}}{\partial \vec{\kappa}} \delta \vec{\kappa} + \vec{f}_{0,i}^T \cdot \frac{\partial \vec{\omega}_{0,i}}{\partial \vec{\kappa}} \delta \vec{\kappa} \times \vec{y}_{0,i}. \quad (7.58)$$

The virtual change in generalised coordinates can be eliminated from the problem by rearranging the dot and cross products leading to:

$$-\left(\frac{\partial L}{\partial \vec{\kappa}}\right)^T f_{0,i} = \left(\frac{\partial \vec{d}_{0,i}}{\partial \vec{\kappa}}\right)^T \vec{f}_{0,i} + \left(\frac{\partial \vec{\omega}_{0,i}}{\partial \vec{\kappa}}\right)^T (\vec{y}_{0,i} \times \vec{f}_{0,i}). \quad (7.59)$$

The force intensity can also be removed from the expression yielding the following equivalence

$$-\left(\frac{\partial L}{\partial \vec{\kappa}}\right)^T \cdot 1 = \left(\frac{\partial \vec{d}_{0,i}}{\partial \vec{\kappa}}\right)^T \vec{b}_{0,i} + \left(\frac{\partial \vec{\omega}_{0,i}}{\partial \vec{\kappa}}\right)^T (\vec{y}_{0,i} \times \vec{b}_{0,i}). \quad (7.60)$$

This expression states that the partial derivative of the muscle length with respect to the generalised coordinates is equal to the generalised muscle moment-arms. This point is fundamentally important. The tendon excursion method does not yield the moment-arms proper but the generalised moment-arms associated to the generalised coordinates. The

following equality is true for models with revolute joints that all have parallel rotation axes (one-dimensional moment-arms)

$$-\left(\frac{\partial L}{\partial \vec{\kappa}}\right)^T = \left(\vec{y}_{0,i} \times \vec{b}_{0,i}\right)_{3^{rd} \text{ coordinate}}. \quad (7.61)$$

Thus, the coordinates used to construct the definition are not just any joint coordinates, but the generalised coordinates used to describe the musculoskeletal model. This last point is key: the tendon excursion method is dependent on the choice of generalised coordinates and must be used accordingly. Furthermore, it is based on the principle of virtual displacements and therefore it must satisfy all the conditions of the definition of virtual displacement. The importance of this point will be illustrated in the following section.

7.3.4 Computing Muscle Moment-Arms

In the previous sections two definitions of moment-arms were presented. The first is geometric and defined moment-arms using the cross-product. The second definition is the well known tendon-excursion definition. The two definitions were shown not to be strictly equivalent. The geometric definition yields the moment-arms proper in the inertial frame. The tendon excursion definition yields the moment-arms in the generalised coordinate space. The definitions of moment-arms for a muscle \mathcal{M}_j around joint J_i are given by:

$$\text{Geometric definition : } \left(\vec{y}_{0,i,j} \times \vec{b}_{0,i,j}\right), \quad \vec{f}_{0,i,j} = f_{0,i,j} \vec{b}_{0,i,j} \quad (7.62)$$

$$\text{Tendon excursion definition : } -\left(\frac{\partial L_j}{\partial \vec{\kappa}_i}\right)^T, \quad (7.63)$$

where L_j is the length of muscle \mathcal{M}_j . The vector $\vec{\kappa}_i$ is the vector of generalised coordinates parameterising joint J_i . The other coordinates are not considered. The vector $\vec{y}_{0,i,j}$ is the vector between the joint J_i and the point where muscle \mathcal{M}_j applies a force. $\vec{f}_{0,i,j}$ is the force itself of amplitude $f_{0,i,j}$. The two definitions are related by the following expression.

$$-\left(\frac{\partial L_j}{\partial \vec{\kappa}_i}\right)^T = \left(\frac{\partial \vec{d}_{0,i}}{\partial \vec{\kappa}_i}\right)^T \vec{b}_{0,i} + \left(\frac{\partial \vec{\omega}_{0,i}}{\partial \dot{\vec{\kappa}}_i}\right)^T \left(\vec{y}_{0,i} \times \vec{b}_{0,i}\right). \quad (7.64)$$

where $\vec{d}_{0,i}$ is the displacement vector of joint i in the inertial frame. The vector $\vec{\omega}_{0,i}$ is the instantaneous rotational velocity vector of the joint i in the inertial frame.

As stated in section 7.3.3, the tendon excursion method is defined from the principle of virtual work and must satisfy the conditions of the definition of virtual displacement. Given a configuration of the skeletal structure defined by the vector of generalised coordinates $\vec{\kappa}^*$, the moment-arms of a muscle are computed using the tendon excursion method. The muscle's length is computed for the configuration $L_j(\vec{\kappa}^*)$. The muscle's length is then computed again after adding a small displacement δq_k to each coordinate

κ_k^* in turn. Each generalised coordinate κ_k is displaced and the muscle length is computed $L_j(\vec{\kappa}^* + \delta\kappa_k^*)$. The moment-arm associated to each coordinate is thus defined by:

$$c(\kappa_k^*) = -\frac{L_j(\vec{\kappa}^* + \delta\kappa_k^*) - L_j(\vec{\kappa}^*)}{\delta\kappa_k}. \quad (7.65)$$

The displacement $\delta\kappa_k$ is a virtual displacement and therefore must respect the conditions of the definition of virtual displacement. These conditions are restated here.

$$\begin{aligned} \sum_{k=1}^{\hat{Q}} \frac{\partial \Phi_1}{\partial \kappa_k} \delta\kappa_k &= 0, \\ \vdots \\ \sum_{k=1}^{\hat{Q}} \frac{\partial \Phi_p}{\partial \kappa_k} \delta\kappa_k &= 0. \end{aligned} \quad (7.66)$$

The virtual displacements must respect the holonomic constraints. This point is fundamental and can lead to issues during practical implementation. The musculoskeletal shoulder model presented in chapter 4 contains two holonomic constraints defining the scapulothoracic contact and a number N_w of holonomic constraints defining the wrapping surfaces. Under the assumption that the muscle's length is a purely kinematic quantity, the wrapping constraints for each muscle are constraints that must be respected by each virtual displacement. Therefore, if a fixed point of a muscle lies on the wrapping constraint, the small displacements must be defined such that the point does not violate the constraint. This point concerning constraints is essential and makes the tendon excursion method difficult to use appropriately if there are many muscles with many constraints.

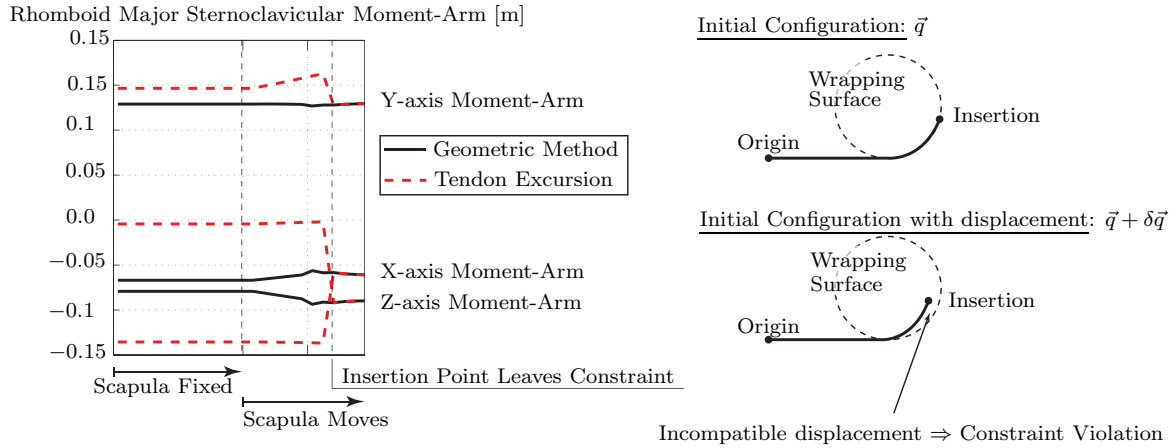


Figure 7.8: *Illustration of how the tendon-excursion method can lead to incorrect moment-arms because the virtual displacement used to compute the moment-arm does not respect the constraints.*

To illustrate the difficulty of using the tendon excursion method appropriately, consider the rhomboid major muscle that originates on the thorax and inserts on the scapula. There is a wrapping constraint for this muscle that is cylinder (Fig. 7.8). The muscle segment representing the rhomboid major must pass over the surface of this cylinder. For this particular muscle, the insertion point of the segment lies on the surface of the cylinder in the initial configuration of the skeletal structure. If the tendon excursion method is applied inappropriately the moment-arms differ greatly from the moment-arms computed

using the geometric method. When the insertion point leaves the wrapping constraint, the tendon excursion method moment-arms coincide with the geometric moment-arms. However, there is a significant discontinuity of the tendon-excursion moment-arms.

By comparison, the geometric method does not rely on the principle of virtual displacements. Furthermore, the method does not rely on a particular choice of coordinates. It simply depends on the definition of the body frames and carrier body frames. However, the geometric method cannot easily be generalised to an algorithm. It can require a case by case analysis of the muscles and is therefore more difficult to work with. The tendon excursion method can be generalised more easily and is therefore favoured as a method of computing moment-arms.

7.4 The Solution Set and Wrench-Feasibility

The previous sections showed that moment-arms are key in estimating muscle forces and reviewed the theory of moment-arms. This section re-introduces the concept of wrench feasibility. The concept has been extensively used in cable-driven robots [81] and has been used in neuromuscular control [183]. However, it seems that it is a concept that is rarely found in presentations of musculoskeletal models. The concept is related to the existence of a solution to the muscle-force estimation problem.

In chapter 4 it is stated that models of musculoskeletal systems and models of cable-driven robots are constructed from the same hypothesis. These hypothesis include rigid body mechanics, ideal mechanical joints and massless, frictionless, perfectly elastic muscles/cables. A cable-driven robot is a mechanism that is actuated by a network of cables. There are two types of cable-driven robots: suspended and articulated. In suspended robots there is only one body connected to a frame through a network of cables [21, 80, 178]. In articulated robots there is a mechanical skeleton composed of multiple bodies with joints between them and a network of cables [92, 217, 220]. In any cable-driven robot, each cable applies a system of forces to the bodies comprising the mechanism and the tension in each cable is uniform. The system of forces is reduced to a single force and moment of force about one point for each body. This reduction yields the body's actuation as defined in section 7.3.1. Each cable has a motor and pulley at one end generating a tractive force within the cable by winding the cable around the pulley. The cable can only pull and its tractive strength is limited by the motor's power. The first constraint of the cable-force coordination problem is the torque-force map. The cables must apply the necessary actuation. The second constraint is the limitation of the cable's strength. Thus, the first two constraints of the cable-force coordination problem are identical to the first two constraints of the muscle-force coordination problem ((7.8)-(7.9)).

$$\vec{t}_a(\vec{\kappa}(t_k), \dot{\vec{\kappa}}(t_k), \ddot{\vec{\kappa}}(t_k)) = \mathbf{W}_0(\vec{\kappa}(t_k)) \vec{f}_k, \quad \text{Torque-force constraint,} \quad (7.67)$$

$$\vec{0} \leq \vec{f}_k \leq \vec{f}_{\max}, \quad \text{Min/max force bounds.} \quad (7.68)$$

As described in chapter 5, cost functions provide a means of differentiating the solutions

within the feasible set. The solution set itself is defined by the constraints and the space of the decision variables (forces within the muscles/cables). Additional constraints further restrict the solution set defined by the first two constraints (7.8)-(7.9). Therefore, the muscle-force coordination problem defined in section 7.2.1 is mathematically almost identical to the cable-force coordination problem of cable-driven robots. Both coordination problems are defined by nonlinear programs. Their purpose being to compute the required forces in the muscles/cables to drive the system (skeleton/mechanism) along a pre-defined kinematic path. Therefore, theory regarding the force coordination problem that has been developed for models of cable-driven robots can be applied to models of musculoskeletal systems such as the shoulder.

For both coordination problems, solving the NLP is straightforward [14, 24, 35]. There exist numerous NLP solvers. However, the question of the existence of a solution is not. In cable-driven robotics, this question is called wrench feasibility [21, 81, 146]. At the core of the analysis is the torque-force map (7.75) governing the solutions to the NLP. At a given instant t_k , the relation between the forces in the cables and the actuation applied to the system, defines a linear map between two vector spaces. The force intensity space \mathcal{F} which is a subset of \mathbb{R}^{N_p} and the tangent space of the coordinate manifold $T_{\vec{\kappa}(t_k)}\mathcal{Q}_S \subset \mathbb{R}^D$, where D is the number of degrees of freedom.

$$\begin{aligned} \mathfrak{M}_k : \mathcal{F} &\rightarrow T_{\vec{\kappa}(t_k)}\mathcal{Q}_S, \\ \vec{f}_k &\mapsto \mathfrak{M}_k(\vec{f}_k) = \vec{t}_a(\vec{\kappa}(t_k), \dot{\vec{\kappa}}(t_k), \ddot{\vec{\kappa}}(t_k)) = \mathbf{W}_0(\vec{\kappa}(t_k))\vec{f}_k. \end{aligned} \quad (7.69)$$

For a system with N_p forces, the upper and lower bounds (7.68) on the forces (without additional constraints) define the map's domain space \mathcal{F} as a convex polytope² in \mathbb{R}^{N_p} . The geometry of the domain space polytope is defined by the values of \vec{f}_{\max} . The image of a convex polytope under linear transformation is a convex polytope [87]. The image space $\mathfrak{M}_k(\mathcal{F})$ is therefore also a convex polytope in $T_{\vec{\kappa}(t_k)}\mathcal{Q}_S$. The geometry of the image space polytope is defined by $\mathfrak{M}_k(\vec{f}_{\max})$.

Definition 23 (Torque Set $\mathcal{W}_{req}(\vec{\kappa})$). *The torque set $\mathcal{W}_{req}(\vec{\kappa})$ is the set of actuation vectors that the cables must be able to produce for a given kinematic configuration $(\vec{\kappa}, \dot{\vec{\kappa}}, \ddot{\vec{\kappa}})$.*

$$\mathcal{W}_{req}(\vec{\kappa}) = \{\vec{t}_a \in T_{\vec{\kappa}}\mathcal{Q}_S \subset \mathbb{R}^D\}. \quad (7.70)$$

Definition 24 (Wrench-Feasible Workspace and Torque-Feasible Space). *The wrench-feasible workspace is the set of kinematic configurations $(\vec{\kappa}, \dot{\vec{\kappa}}, \ddot{\vec{\kappa}})$ such that for any actuation vector $\vec{t}_a \in \mathcal{W}_{req}(\vec{\kappa})$, there is a vector of cable forces $\vec{f} \in \mathcal{F}$ satisfying*

$$\vec{t}_a = \mathbf{W}_0(\vec{\kappa})\vec{f}. \quad (7.71)$$

The actuation vectors belong to the torque-feasible space.

Given this definition of wrench-feasible workspace, a system is said to be wrench-feasible if the following condition holds [21, 57]:

$$\mathcal{W}_{req}(\vec{\kappa}) \subset \mathfrak{M}_k(\mathcal{F}), \quad \forall (\vec{\kappa}, \dot{\vec{\kappa}}, \ddot{\vec{\kappa}}) \in T\mathcal{Q}_S. \quad (7.72)$$

²A polytope is a geometric object with flat sides. Examples include polygons in 2-dimensions and polyhedrons in 3-dimensions.

The torque set must be a subset of the image set of the force intensity space. This condition guarantees the existence of a solution to force coordination problem.

In cable-driven robotics, wrench-feasibility is a design criterion. In musculoskeletal systems, although the real system is already wrench-feasible, the model must be well defined such that wrench-feasibility naturally occurs. Design of the cable/muscle structure is the design of the moment-arms matrix. Thus, again the moment-arms matrix is the key element in muscle-force estimation.

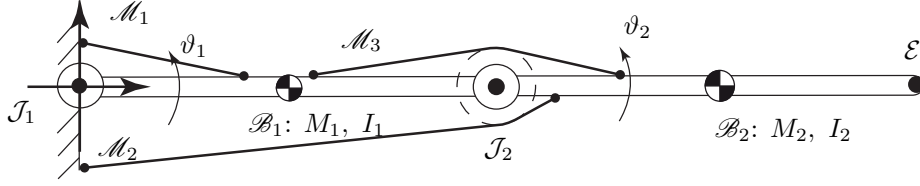


Figure 7.9: A two-dimensional toy musculoskeletal model used to illustrate the discussion of section 7.4.

To illustrate wrench feasibility, consider a musculoskeletal model with two bones \mathcal{B}_1 and \mathcal{B}_2 (Fig. 7.9). The bones are connected through a revolute joint \mathcal{J}_2 and the first bone is connected to a carrier body through a second revolute joint \mathcal{J}_1 . There are three muscles actuating the skeletal structure. The first muscle \mathcal{M}_1 spans the revolute joint \mathcal{J}_1 . The second muscle \mathcal{M}_1 spans both joints. There is a cylinder aligned with the second joint's rotation axis to constrain the muscle paths. The third muscle \mathcal{M}_3 spans the revolute joint \mathcal{J}_2 . The configuration of the skeletal structure is defined by the configurations of the revolute joints which are parameterised by the angles $\vec{\kappa} = (\vartheta_1, \vartheta_2)^T$. The coordinate manifold \mathcal{Q}_S is $S^1 \times S^1$.

$$\mathcal{F} = [0, 125] \times [0, 75] \times [0, 200] \subset \mathbb{R}^3$$

$$\mathfrak{M}_k(\mathcal{F}) \subset T_{\vec{\kappa}(t_k)}\mathcal{Q}_S \subset \mathbb{R}^2$$

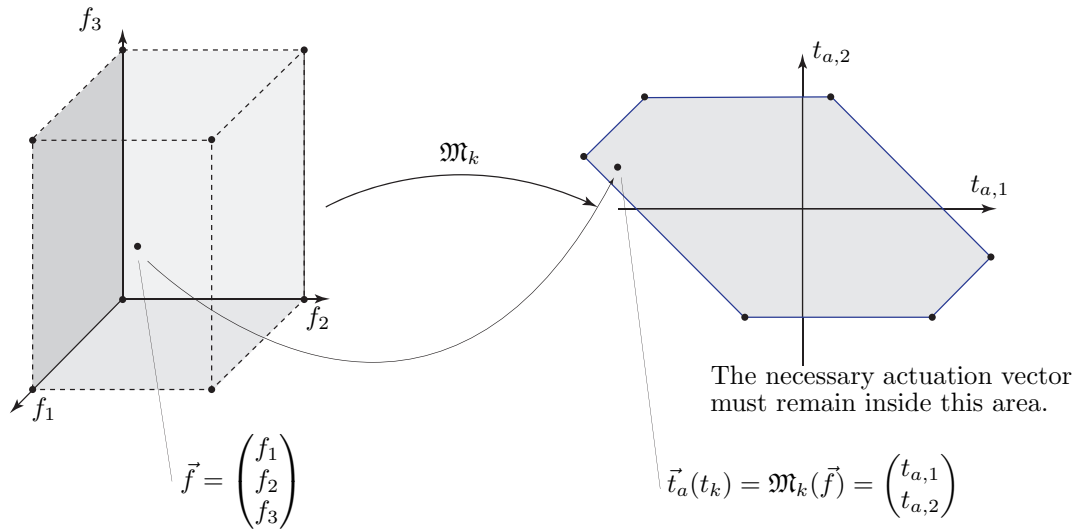


Figure 7.10: Range and image spaces of the torque-force map for the musculoskeletal model presented in section 7.4 and illustrated in figure 7.9.

The dynamics of the system are the dynamics of a double pendulum with distributed

mass [209]. There are two equations of motion and the actuation vector is defined by:

$$\vec{t}_a = \begin{pmatrix} t_{a,1} \\ t_{a,2} \end{pmatrix} = \mathbf{M}(\vartheta_1, \vartheta_2) \ddot{\vec{\kappa}} - \vec{h}(\vec{\kappa}, \dot{\vec{\kappa}}) = \mathbf{W}_0(\vec{\kappa}) \vec{f}. \quad (7.73)$$

There are three cable-force intensities. The torque-force map is defined by:

$$\begin{aligned} \mathfrak{M}_k : \mathcal{F} \subset \mathbb{R}^3 &\rightarrow T_{\vec{\kappa}(t_k)} \mathcal{Q}_S \subset \mathbb{R}^2, \\ \vec{f}_k &\mapsto \mathfrak{M}_k(\vec{f}_k) = \vec{t}_a(t_k) = \mathbf{W}_0(\vec{\kappa}(t_k)) \vec{f}_k. \end{aligned} \quad (7.74)$$

The first muscle always creates a moment-arm around the joint \mathcal{J}_1 . The second and third muscles define moment-arms around both joints. The moment-arm matrix has the following structure:

$$\vec{t}_a = \begin{pmatrix} t_{a,1} \\ t_{a,2} \end{pmatrix} = \mathcal{M}(\vec{t}_g) = \mathbf{W}_0(\vec{\kappa}) \vec{f} = \begin{pmatrix} w_{1,1}(\vartheta_1) & w_{1,2}(\vartheta_1, \vartheta_2) & w_{1,3}(\vartheta_1, \vartheta_2) \\ 0 & w_{2,2}(\vartheta_2) & w_{2,3}(\vartheta_2) \end{pmatrix} \begin{pmatrix} f_1 \\ f_2 \\ f_3 \end{pmatrix}. \quad (7.75)$$

The muscles are attributed different maximum forces: $f_{1,\max} = 125[N]$, $f_{1,\max} = 75[N]$, $f_{3,\max} = 200[N]$. All the physical constants are set to 1, including the lengths of the pendulum's links.

As the configuration of the mechanism changes, the image space polytope $\mathfrak{M}_k(\mathcal{F})$ changes shape (Fig. 7.11). The mechanism is wrench feasible as long as the necessary actuation \vec{t}_a remains inside the image space polytope, and this for any configuration $\vec{\kappa} = (\vartheta_1, \vartheta_2)^T$.

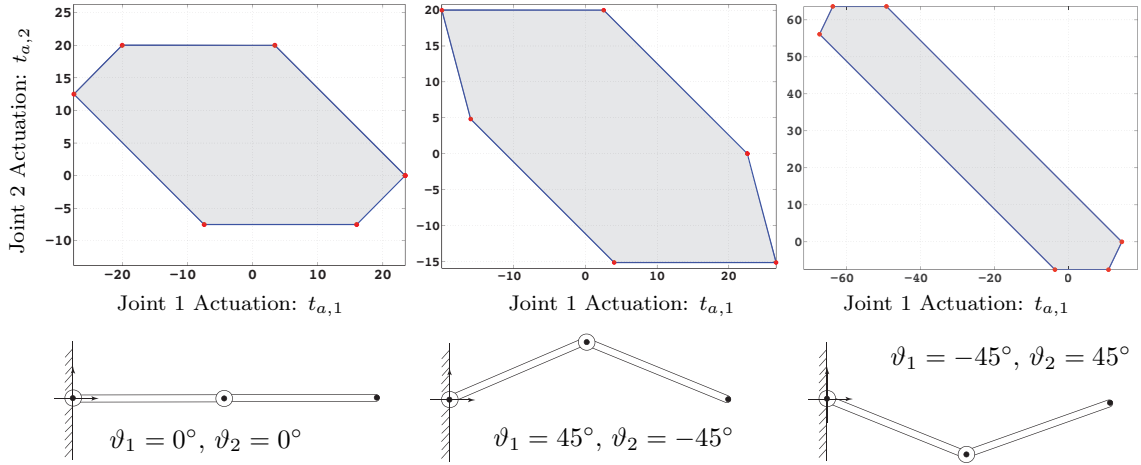


Figure 7.11: Image space of the torque-force map in three different configurations for the musculoskeletal model presented in section 7.4 and illustrated in figure 7.9.

For a path $\vec{\kappa}(t)$ in the configuration space, the set $\mathfrak{M}_t(\mathcal{F})$ defines the time-dependent behaviour of the image space polytope. The image space depends only on the set of configurations $\vec{\kappa}(t)$ that the path passes through. The system remains wrench-feasible as long as the necessary actuation to perform the motion remains within the image space polytope for the entire motion. The wrench-feasibility condition will limit how fast the motion can be performed. At slower speeds, the required actuation is smaller and more likely to be inside $\mathfrak{M}_t(\mathcal{F})$, whereas at higher speed, the actuation vector increases and can leave $\mathfrak{M}_t(\mathcal{F})$.

The concept of wrench-feasibility allows one to design the musculature as a collective [183]. This result complements the result regarding the modelling of large muscles [197]. The previous result states how best to model each muscle individually. Wrench-feasibility uses that result as a basis for improving the muscle model as a collective. Therefore, both results combined provide a tool for developing improved geometric muscle models. The use of wrench feasibility will be illustrated in the following chapter.

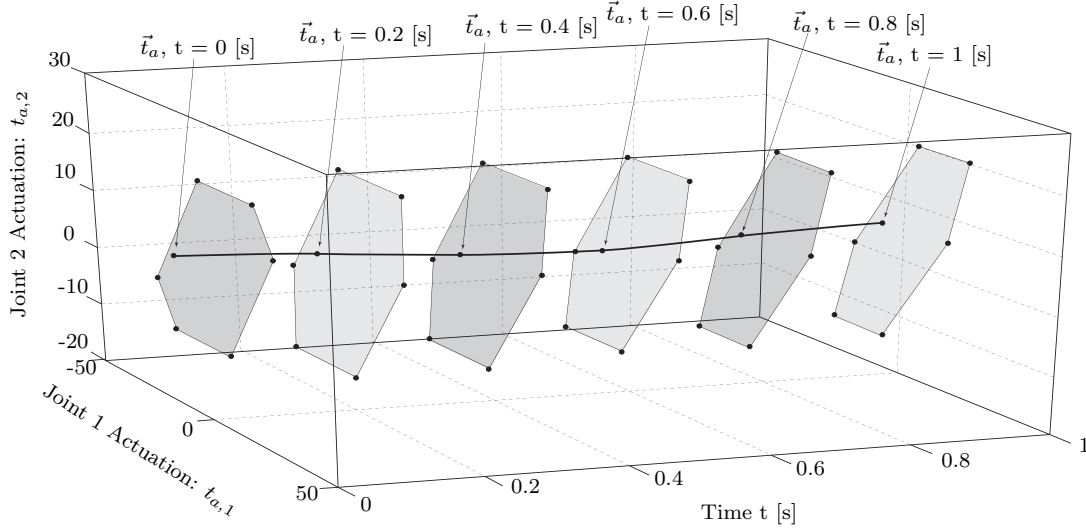


Figure 7.12: *Illustration of the time-dependent behaviour of the image space polytope for the musculoskeletal model presented in section 7.4 and illustrated in figure 7.9.*

7.5 Conclusions

The goal of this chapter was to present the muscle-force coordination strategy used to estimate the forces in the musculoskeletal shoulder model presented in chapter 4. Based on this presentation, moment-arms were shown to be the key element governing muscle-force estimation. Therefore, this chapter reviewed the theory of moment-arms by discussing the fundamental geometric concepts behind moment-arms and presenting the tendon-excursion method of computing moment-arms. This chapter showed that the tendon excursion method does not yield the muscle moment-arms in the geometric sense. The tendon excursion method and geometric definition of moment-arms are related through a projection matrix from analytical mechanics. Finally, this chapter re-introduced a relatively new concept with respect to musculoskeletal modelling called wrench-feasibility. The concept complements the already existing results concerning muscle-force estimation by providing information regarding the possible movements, the system can perform. The limitations on the muscle forces defines limitations on the possible movements that the model can realise. These limitations can be pre-analysed without solving the muscle-force estimation problem by computing the torque-feasible set. The torque-feasible set can be used to improve the model of the musculature.

Chapter 8

Estimating Joint Force in the Human Shoulder

8.1 Introduction

Osteoarthritis or degenerative arthritis is the most common form of arthritis and is just one of the many dysfunctions affecting the human musculoskeletal system. In the shoulder, it causes premature degradation of the glenohumeral or shoulder joint and is quite painful. The degradation is the result of frequent inappropriate mechanical loading of the articular cartilage [27] (cf. chapter 2 for anatomical references). To help understand osteoarthritis of the shoulder, it is necessary to have an estimate of how the articular cartilage is being loaded in healthy and dysfunctional shoulders. This information is critical in the development of treatments of osteoarthritis.

In general, the stress occurring in the articular cartilage cannot be measured. In recent years a prosthesis of the humeral bone has been developed containing a load sensor [201]. The measurements obtained from such a device are a good indicator of the stress but are not a completely accurate representation of the loading given that part of the shoulder has been replaced with a prosthesis. We must therefore continue to rely on musculoskeletal models to estimate the stress occurring in the articular cartilage of joints affected by osteoarthritis.

There are a number of musculoskeletal models of the shoulder that have been developed for the purpose of studying the forces in the glenohumeral joint. There is the Delft shoulder and elbow model (DSEM). Constructed in 1994 [194], the model has been recently validated as a model for measuring the force in the glenohumeral joint [155]. The validation process was done using data collected by the shoulder prosthesis mentioned previously [156]. There is the AnyBody® shoulder model. Developed for multiple purposes [49], the model has been used to specifically estimate the force in the glenohumeral joint [158]. There is the model developed at the ETH Zurich Switzerland. Developed for analysing the stability of the glenohumeral articulation [71], the model uses an algorithm designed specifically for computing the force in the glenohumeral joint [70]. Finally there

is the Newcastle model. The model was initially developed for analysing the forces in the glenohumeral joint during activities of daily living [37] and has since been used to study the effects of surgery on the joint force [120].

Although these models are high fidelity models and are successful in estimating glenohumeral joint forces, the consensus of the International Shoulder Group (ISG)¹ is that there still remains a considerably large gap between models and reality [47, 48]. Given that there is no perfect match between simulations and experiments [182], future research should focus on clinical validation. A musculoskeletal model must be validated before it can be used to make conclusions regarding musculoskeletal systems. Validation constitutes the most challenging task of musculoskeletal modelling once a model has been constructed [135].

The goal of this chapter is to present the implementation of the musculoskeletal shoulder model discussed in chapter 4. The model is being designed specifically for the purpose of estimating the force in the glenohumeral joint. The model is to be used in parallel with a finite element model of the glenohumeral joint [59]. The chapter begins by reviewing the model's characteristics and the methods from chapters 6 and 7 to solve its kinematic redundancy and overactuation. The chapter then introduces the computational procedure used to compute the models outputs that are muscle forces and the joint reaction force in the glenohumeral joint. The model is used to estimate the forces during fast and slow abduction in the scapular plane. The results are presented in terms of scapular kinematics, muscle moment-arms, muscle forces, joint reaction forces (intensity and orientation). The results are discussed and compared to results from the literature. The chapter concludes with a brief discussion regarding the models current most important weakness and suggestions on how to improve it.

8.2 Methods

8.2.1 A Musculoskeletal Model of the Human Shoulder

This section presents a brief review of the musculoskeletal shoulder model from chapter 4. The model is a right shoulder of an adult male. It includes the thorax, clavicle, scapula and humerus. The thorax is the carrier body to which the inertial reference frame is attached \mathcal{R}_0 . A reference frame \mathcal{R}_i is also defined for the clavicle, scapula and humerus (Fig. 8.1). The reference frames are defined according the guide lines set by the International Society of Biomechanics (ISB) [214] (cf. chapter 4). Subindexes are used to identify each frame: thorax: 0, clavicle: 1, scapula: 2, humerus: 3.

The three synovial articulations (sternoclavicular SC , acromioclavicular AC and glenohumeral GH) are modelled as ideal ball and socket joints and parameterised using spherical kinematic pairs. The configurations of the sternoclavicular and acromioclavic-

¹The ISG is a collaboration of biomechanics research groups who's main focus is the shoulder. It is also one of the many technical groups of the International Society of Biomechanics (ISB).

ular spherical pairs are described using two sets of Bryan angles: $\vec{\Upsilon}_1^T = (\psi_1, \vartheta_1, \varphi_1)^T$ and $\vec{\Upsilon}_2^T = (\psi_2, \vartheta_2, \varphi_2)^T$. The rotation sequence is XYZ. The configuration of the glenohumeral spherical pair is described using Euler angles: $\vec{\Upsilon}_3^T = (\psi_3, \vartheta_3, \varphi_3)^T$. The rotation sequence is ZYZ. The shoulder's configuration is parameterised by a vector of nine joint angles.

$$\vec{q} = (\vec{\Upsilon}_1^T \quad \vec{\Upsilon}_2^T \quad \vec{\Upsilon}_3^T)^T = (\psi_1 \quad \vartheta_1 \quad \varphi_1 \quad \psi_2 \quad \vartheta_2 \quad \varphi_2 \quad \psi_3 \quad \vartheta_3 \quad \varphi_3)^T. \quad (8.1)$$

Three Euclidean displacements are defined that map vectors in a local frame to vectors in the inertial frame. The displacements are parameterised by the vector of coordinates \vec{q} using the standard charts on $SO(3)$ to build the rotation matrices (cf. chapters 4 and 6 for details on constructing the rotation sequences).

$$P_{0,i} : \vec{p}_{0,i} = \vec{d}_{0,i} + \mathbf{R}_{i,0}(\psi_i, \vartheta_i, \varphi_i) \vec{p}_i. \quad (8.2)$$

The vector $\vec{d}_{0,i}$ is the translation vector from the centre of the inertial frame to the centre of the local frame, defined in the inertial frame (cf. chapter 3 for notations regarding Euclidean displacements). The matrix $\mathbf{R}_{i,0}$ is the rotation matrix from the local frame \mathcal{R}_i to the inertial frame \mathcal{R}_0 .

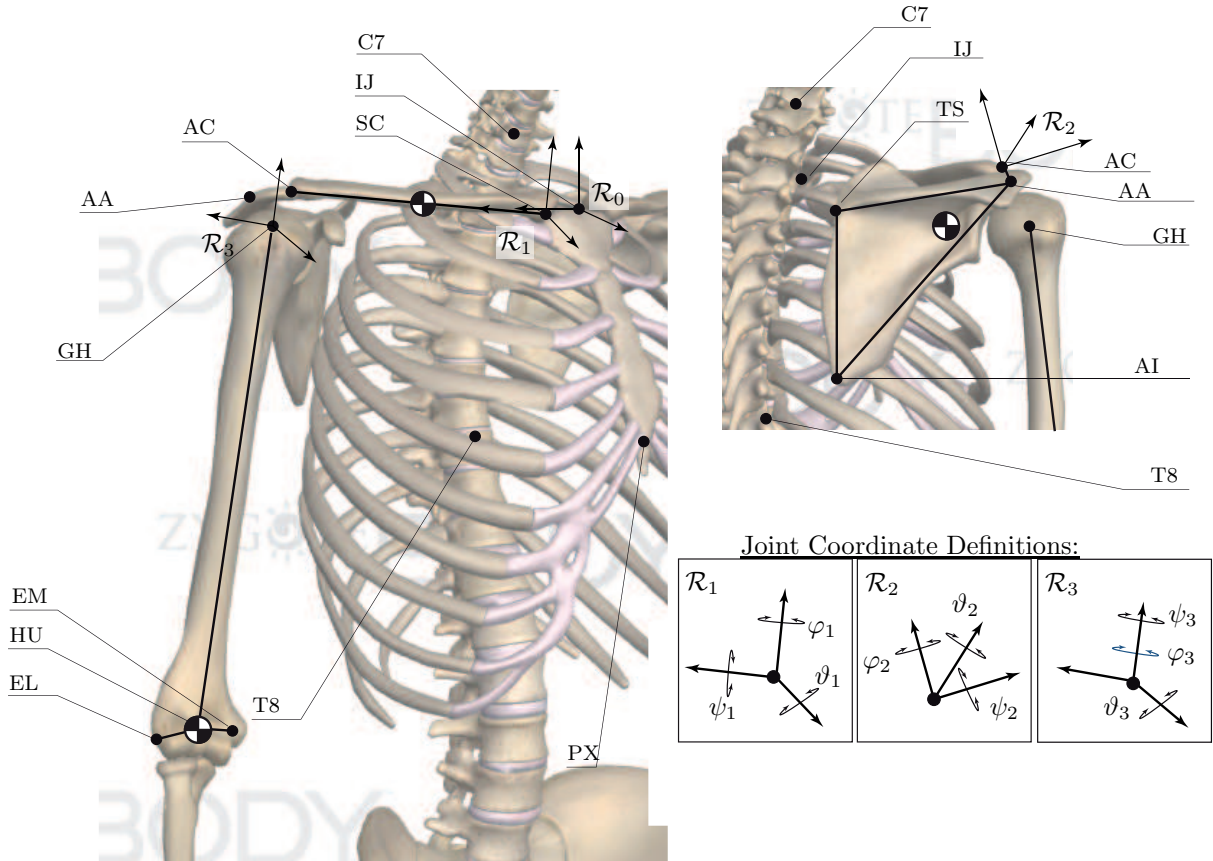


Figure 8.1: *Illustration of the bony landmarks, reference frame and the locations of the bone centres of gravity. Image created using ZygoteBodyTM zygotebody.com.*

The scapulothoracic contact is modelled by constraining two points on the scapula's medial border to remain on the surface of two ellipsoids. The ellipsoids have identical

centres but different dimensions and are aligned with the inertial frame. The ellipsoids model the surface of the ribcage with an additional layer of muscle. The points defining the constraints are the trigonum spinae (TS) and the angulus inferior (AI). They are the end-points of the scapula's medial border. The ellipsoids are defined in the thorax frame yielding the following two holonomic skleronomic constraints.

$$\Phi_{TS}(\vec{\Upsilon}_1, \vec{\Upsilon}_2) = (\vec{u}_{0,2} - \vec{e}_0)^T \mathbf{E}_{TS} (\vec{u}_{0,2} - \vec{e}_0) - 1 = 0, \quad TS_{0,2} : \vec{u}_{0,2} = \vec{d}_{0,2} + \mathbf{R}_{2,0} \vec{u}_2, \quad (8.3)$$

$$\Phi_{AI}(\vec{\Upsilon}_1, \vec{\Upsilon}_2) = (\vec{v}_{0,2} - \vec{e}_0)^T \mathbf{E}_{AI} (\vec{v}_{0,2} - \vec{e}_0) - 1 = 0, \quad AI_{0,2} : \vec{v}_{0,2} = \vec{d}_{0,2} + \mathbf{R}_{2,0} \vec{v}_2. \quad (8.4)$$

where \vec{e}_0 is the point vector of the centre of the ellipsoid E common to both constraints, in the inertial frame. The matrices \mathbf{E}_{TS} and \mathbf{E}_{AI} are the quadric matrices of each ellipsoid (cf. appendix A).

The forward kinematic map defines the map from the joint coordinates to the spatial configuration of the end-effector. The end-effector is defined as the centre of the humeroulnar joint (HU). Its spatial configuration is defined as the position of the humeroulnar joint centre HU and the orientation of the humerus.

$$\Xi_S : \mathcal{Q}_S \rightarrow \mathcal{W}_S,$$

$$\vec{q} \mapsto \Xi_S(\vec{q}) = \mathcal{C}_e = \left(\vec{e}_{0,3}^T, \vec{\Upsilon}_3^T \right)^T, \quad HU_{0,3} : \vec{e}_{0,3} = \vec{d}_{0,3} + \mathbf{R}_{3,0} \vec{e}_3, \quad (8.5)$$

$$s.t. \quad \Phi_{TS}(\vec{\Upsilon}_1, \vec{\Upsilon}_2) = (\vec{u}_{0,2} - \vec{e}_0)^T \mathbf{E}_{TS} (\vec{u}_{0,2} - \vec{e}_0) - 1 = 0, \quad (8.6)$$

$$\Phi_{AI}(\vec{\Upsilon}_1, \vec{\Upsilon}_2) = (\vec{v}_{0,2} - \vec{e}_0)^T \mathbf{E}_{AI} (\vec{v}_{0,2} - \vec{e}_0) - 1 = 0. \quad (8.7)$$

The kinematic model has seven degrees of freedom. The map is parameterised by the nine kinematic coordinates (8.1) and subject to the two scapulothoracic constraints.

Each body is given a mass M_i and an inertia \mathcal{I}_i defined with respect to the centre of gravity [28]. The clavicle's centre of gravity is located at the mid-point along the axis between the SC and AC joints. The scapula's centre of gravity is located one third of the way along the axis between the AC and AI points, starting from the AC point. The humerus centre of gravity also defining the arm's centre of gravity, is located at the point HU. The arm is considered to always be outstretched. The equations of motion are obtained using the Euler-Lagrange equation. The generalised coordinates are defined as the kinematic coordinates: $\vec{\kappa} = \vec{q}$. The total lagrangian is the sum of the bone lagrangians augmented by the constraints (cf. chapter 3 and 4). The dynamic model is defined by:

$$\frac{\partial^2 \tilde{\mathcal{L}}}{\partial \dot{\vec{\kappa}}^2} \ddot{\vec{\kappa}} + \frac{\partial^2 \tilde{\mathcal{L}}}{\partial \vec{\kappa} \partial \dot{\vec{\kappa}}} \dot{\vec{\kappa}} - \frac{\partial \tilde{\mathcal{L}}}{\partial \vec{\kappa}} = \tilde{\mathbf{W}}_0(\vec{\kappa}) \tilde{\vec{f}}, \quad (8.8)$$

$$s.t. \quad \Phi_{TS}(\vec{\kappa}) = (\vec{u}_{0,2} - \vec{e}_0)^T \mathbf{E}_{TS} (\vec{u}_{0,2} - \vec{e}_0) - 1 = 0, \quad (8.9)$$

$$\Phi_{AI}(\vec{\kappa}) = (\vec{v}_{0,2} - \vec{e}_0)^T \mathbf{E}_{AI} (\vec{v}_{0,2} - \vec{e}_0) - 1 = 0, \quad (8.10)$$

where $\tilde{\mathcal{L}}$ is the sum of the bone lagrangians. As presented in chapter 7, the constraint forces (scapulothoracic contact forces) and muscle forces are grouped into a single vector $\tilde{\vec{f}}$. The matrix $\tilde{\mathbf{W}}_0$ is the generalised moment-arm matrix defined with respect to the inertial frame. The muscles can only pull and the scapulothoracic contact forces are

only compressive forces. They cannot pull the scapula onto the surface of the ellipsoid. Furthermore, the muscles have a maximum isometric strength [76] and the contact forces are limited using the observations from [88, 195]

$$\vec{0} \leq \vec{f} \leq \vec{f}_{max}. \quad (8.11)$$

The geometric muscle model was constructed using the framework set in [76]. The 16 anatomical muscles are divided into 28 segments and wrapping constraints are defined for each segment using the algorithms from [75]. Thus, the wrapping constraints and topology of the geometric muscle model are identical to the model defined in [76] but the numerical values are different. Furthermore, in chapter 4 it is stated that each muscle segment can be parameterised by one or more cable(s). The musculature in the present model is represented by $N_p \geq 28$ cables.

8.2.2 Kinematic Coordination

The forward kinematic map (8.5)-(8.7) is parameterised by nine angular coordinates subject to two holonomic skleronomic constraints. This map is the structure for the dynamic model. In chapter 6, a method of planning the model's kinematics is presented. The method proposes an alternate set of coordinates $\vec{\zeta}$ that can be used to construct a time-dependent parameterisation of the joint angles \vec{q} . The coordinates are called minimal coordinates because their number is equal to the number of degrees of freedom. They are independent and make kinematic computations more straightforward. Optimisation can be used but is no longer required.

The minimal coordinates are defined using the lower scapulothoracic kinematic map. In chapter 6, the scapula is shown to be equivalent to a rigid body constrained to glide over three surfaces through punctual contacts AC , TS and AI . The surfaces are a sphere centred at SC , an ellipsoid centred at E and a second ellipsoid centred at E of different dimensions. According to this description, the minimal coordinates are defined as follows. The first coordinate ζ_1 parameterises the clavicle's axial rotation and is equivalent to the angular coordinate ψ_1 . The last three coordinates ζ_5 , ζ_6 and ζ_7 parameterise the glenohumeral motion and are equivalent the glenohumeral joint Euler angles $(\psi_3, \vartheta_3, \varphi_3)$. The three remaining coordinates ζ_2 , ζ_3 and ζ_4 parameterise the configuration of the scapula. The point AI is located by the two spherical coordinates $(\alpha_{AI}, \beta_{AI}) \equiv (\zeta_2, \zeta_3)$ parameterising the ellipsoid on which it glides.

$$AI = \begin{cases} x_e + a_{AI} \cos(\alpha_{AI}) \sin(\beta_{AI}), \\ y_e + b_{AI} \sin(\alpha_{AI}) \sin(\beta_{AI}), \\ z_e + c_{AI} \cos(\beta_{AI}). \end{cases} \quad \vec{e}_0 = \begin{pmatrix} x_e \\ y_e \\ z_e \end{pmatrix} \quad (8.12)$$

where a_{AI} , b_{AI} , c_{AI} are the ellipsoid axial dimensions. The point TS is constrained on the ellipsoid Φ_{TS} (8.10) and is at a fixed distance from AI . The point is located by the intersection of a sphere centred at AI and the ellipsoid Φ_{TS} . The intersection between two such quadrics is well defined and is homeomorphic to a circle. The coordinate ζ_4 parameterises the intersection. Once the locations of the points AI and TS are known,

the point AC is known by trilateration [125]. It lies on the intersection of three spheres. The coordinates ζ_2 , ζ_3 and ζ_4 parameterise thoraco-scapular motion and are equivalent to the five joint angles $(\vartheta_1, \varphi_1, \psi_2, \vartheta_2, \varphi_2)$. The relation between the joint angle coordinates \vec{q} and the minimal coordinates is summarised by:

$$\begin{array}{lll} \zeta_1 & \equiv & \psi_1, & \text{Clavicle axial rotation,} \\ \zeta_2 \ \zeta_3 \ \zeta_4 & \equiv & \vartheta_1 \ \varphi_1 \ \psi_2 \ \vartheta_2 \ \varphi_2, & \text{Thoraco-Scapular motion,} \\ \zeta_5 \ \zeta_6 \ \zeta_7 & \equiv & \psi_3 \ \vartheta_3 \ \varphi_3. & \text{Glenohumeral motion rotation.} \end{array}$$

Given the set of minimal coordinate, kinematic coordination of the shoulder model is achieved by first planning the motion in terms of the minimal coordinates $\vec{\zeta}$. Once a motion is constructed in terms of $\vec{\zeta}(t)$, it is mapped to a motion in terms of $\vec{q}(t)$. For coordinates ζ_1 , ζ_5 , ζ_6 and ζ_7 the mapping is the identity map. For the coordinates ζ_2 , ζ_3 and ζ_4 , the five angular coordinates $(\vartheta_1, \varphi_1, \psi_2, \vartheta_2, \varphi_2)$ are obtained by constructing the rotation matrices $\mathbf{R}_{1,0}$ and $\mathbf{R}_{2,0}$, using the geometric location of the points AC , AA , TS and AI with respect to the inertial frame. Once the rotations are known the angles are extracted using the inverse trigonometric functions. The joint angles $\vec{q}(t)$ are equivalent to the generalised coordinates $\vec{\kappa}(t)$.

The parameterisation is defined over the interval $t \in [0, 1]$. The first and second derivatives are obtained numerically. The dynamic behaviour is further defined by setting the time horizon T . As T increases, the behaviour becomes more quasi-static. Oppositely, as T decreases, the behaviour becomes more dynamic.

$$\dot{\vec{\kappa}}(t_k) = \frac{\vec{\kappa}(t_{k+1}) - \vec{\kappa}(t_k)}{T(t_{k+1} - t_k)}, \quad \ddot{\vec{\kappa}}(t_k) = \frac{\vec{\kappa}(t_{k+2}) - 2\vec{\kappa}(t_{k+1}) + \vec{\kappa}(t_k)}{T^2(t_{k+2} - t_{k+1})(t_{k+1} - t_k)}, \quad \forall t_k \in [0, 1]. \quad (8.13)$$

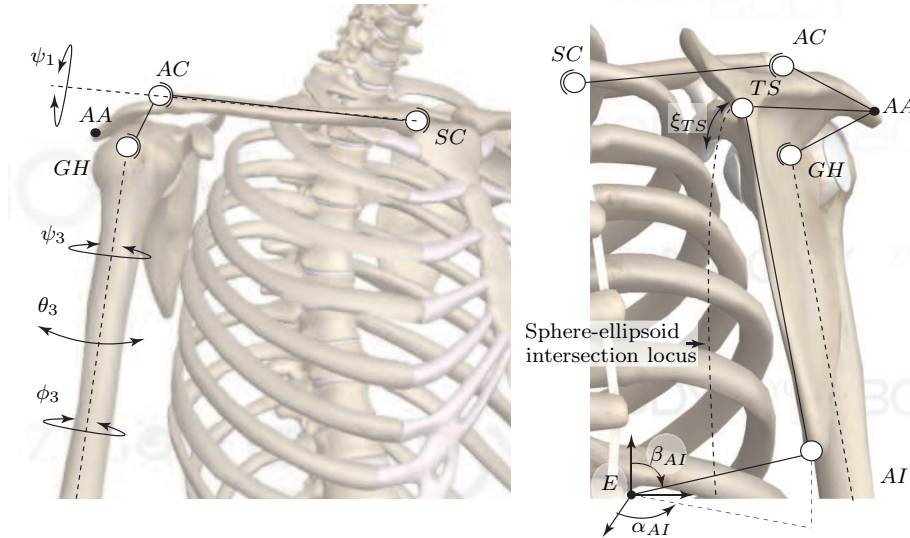


Figure 8.2: Illustration of the minimal coordinates used to coordinate the shoulder as defined in section 8.2.2. Image created using ZygoteBodyTM zygotebody.com.

The model has thus far been used for humeral abduction in the scapular plane. The time-dependent parameterisation of the minimal coordinates was defined using a dataset

from the literature [58]². This particular dataset was chosen because it was specifically constructed to obtain measured shoulder kinematics. The data contains the location of all the bony landmarks necessary to implement the kinematic model. The bony landmarks were obtained by transformation of their corresponding measured skin markers [56]. The dataset also contains a single ellipsoid that was used to construct the two ellipsoids necessary for the model described in this thesis. The single ellipsoid was rotated such that its axes coincide with the inertial frame axes. The ellipsoid was then uniformly dilated twice to produce two ellipsoids with identical centres. The dilation coefficient was obtained such that *TS* and *AI* lie on their respective ellipsoids. Finally, the dataset contains measured values of the three scapular angles ψ_2 , ϑ_2 and φ_2 during humeral abduction in the scapular plane for six subjects. The measurements were taken at 0°, 45°, 90°, 120°, 140° and 160° humeral abduction. The minimal coordinates were planned to match these values as closely as possible.

Table 8.1: *Joint angle terminology. The joint angles are defined in chapter 4.*

$\psi_1 \equiv \zeta_1$	Axial Rotation	ψ_2	Anterior/Posterior Tilt	$\psi_3 \equiv \zeta_5$	Axial Rotation
ϑ_1	Depression/Elevation	ϑ_2	Depression/Elevation	$\vartheta_3 \equiv \zeta_6$	Elevation
φ_1	Protraction/Retraction	φ_2	Protraction/Retraction	$\varphi_3 \equiv \zeta_7$	Elevation Plane

Using the dataset, each coordinate $\zeta_i(t)$ was planned according to the description of humeral abduction presented in chapter 3. Between 0° and 30° abduction, the scapular coordinates ζ_2 , ζ_3 and ζ_4 were held constant at their initial values. Between 30° and 160° abduction, the scapular coordinates were planned using a linear function of time. The clavicle's axial rotation coordinate ζ_1 was held constant during the first 30° humeral abduction and then rotated posteriorly by 40° using a linear function of time. The glenohumeral coordinates ζ_5 and ζ_7 were held constant at 0° and 30° to obtain abduction in the scapular plane with no internal rotation. The third glenohumeral coordinate ζ_6 was planned using a linear function of time.

$$\zeta_1(t) = \begin{cases} 0^\circ, & t \in [0, 30/160] \\ 0^\circ + 40^\circ t, & t \in [30/160, 1] \end{cases} \quad (8.14)$$

$$\zeta_2(t) = \begin{cases} \zeta_2(0), & t \in [0, 30/160] \\ \zeta_2(0) + (\zeta_2(1) - \zeta_2(0))t, & t \in [30/160, 1] \end{cases} \quad (8.15)$$

$$\zeta_3(t) = \begin{cases} \zeta_3(0), & t \in [0, 30/160] \\ \zeta_3(0) + (\zeta_3(1) - \zeta_3(0))t, & t \in [30/160, 1] \end{cases} \quad (8.16)$$

$$\zeta_4(t) = \begin{cases} \zeta_4(0), & t \in [0, 30/160] \\ \zeta_4(0) + (\zeta_4(1) - \zeta_4(0))t, & t \in [30/160, 1] \end{cases} \quad (8.17)$$

$$\zeta_5(t) = 0^\circ, \quad t \in [0, 1] \quad (8.18)$$

$$\zeta_6(t) = 0^\circ + 160^\circ t, \quad t \in [0, 1] \quad (8.19)$$

$$\zeta_7(t) = 30^\circ, \quad t \in [0, 1] \quad (8.20)$$

The initial values $\zeta_2(0)$, $\zeta_3(0)$ and $\zeta_4(0)$ are obtained from the location of the bony landmarks at 0° abduction. The values $\zeta_2(1)$, $\zeta_3(1)$ and $\zeta_4(1)$ are selected appropriately to

²The dataset was provided courtesy of the Laboratoire de Biomécanique et Mécanique des Chocs, Université de Lyon

obtain a configuration of the scapula which is consistent with the measured configurations at 160° abduction. The values were set by hand, but an optimisation method could also be used.

8.2.3 Muscle-Force Coordination

In chapter 7, the proposed muscle-force coordination strategy is to impose a desired motion and use the model's inverse dynamics (8.8)-(8.10) to obtain the required actuation torque for each joint. The desired kinematics reduce to a single vector $\vec{t}_a(\vec{\kappa}, \dot{\vec{\kappa}}, \ddot{\vec{\kappa}})$ called the actuation vector. Given this torque, the muscle forces are computed by solving a non-linear program. As stated in chapter 7, the central equation of muscle-force coordination is the relation between the kinematics and the muscle forces.

$$\frac{\partial^2 \tilde{\mathcal{L}}}{\partial \dot{\vec{\kappa}}^2} \ddot{\vec{\kappa}} + \frac{\partial^2 \tilde{\mathcal{L}}}{\partial \vec{\kappa} \partial \dot{\vec{\kappa}}} \dot{\vec{\kappa}} - \frac{\partial \tilde{\mathcal{L}}}{\partial \vec{\kappa}} = \vec{t}_a(\vec{\kappa}, \dot{\vec{\kappa}}, \ddot{\vec{\kappa}}) = \tilde{\mathbf{W}}_0(\vec{\kappa}) \tilde{\vec{f}}. \quad (8.21)$$

This relation defines the inverse dynamic model used to coordinate the muscle forces. Using the same terminology as chapter 5, the primary task is the kinematics. By imposing this task, a set of solutions has already been differentiated from the complete set of solutions for any kinematics. The muscle forces must generate the desired kinematics. The next phase is to use a secondary task to differentiate a *single* solution from within the subset.

Given the desired kinematics $(\vec{\kappa}(t), \dot{\vec{\kappa}}(t), \ddot{\vec{\kappa}}(t))$, a single solution to (8.21) is differentiated from the subset using a static optimisation problem for a finite number of instances t_k . The set of solutions is further differentiated by imposing the bounds on the muscle forces (8.11) and the glenohumeral stability constraint (cf. chapter 7). The secondary task is the cost function of the optimisation problem. It has been shown that minimising the mean square muscle stress yields solutions that agree with measured muscle forces [195]. This cost function has been selected, although others are possible [167, 172].

Muscle stress is defined as the muscle's force divided by the physiological cross-sectional area (PCSA). The optimisation problem uses the primary task as a constraint. This constraint is called the torque-force constraint.

$$\min_{\tilde{\vec{f}}_k} \Gamma(\tilde{\vec{f}}_k) = \frac{1}{2} \sum_{j=1}^p \frac{(\tilde{f}_j^2)_k}{PCSA_j^2} = \frac{1}{2} \tilde{\vec{f}}_k^T \tilde{\mathbf{P}} \tilde{\vec{f}}_k, \quad (\tilde{\mathbf{P}})_{i,j} = \frac{\delta_{i,j}}{PCSA_j^2}. \quad (8.22)$$

$$\text{s.t. } \vec{t}_a(\vec{\kappa}(t_k), \dot{\vec{\kappa}}(t_k), \ddot{\vec{\kappa}}(t_k)) = \tilde{\mathbf{W}}_0(\vec{\kappa}(t_k)) \tilde{\vec{f}}_k, \quad \text{Torque-force constraint,} \quad (8.23)$$

$$\vec{0} \leq \tilde{\vec{f}} \leq \tilde{\vec{f}}_{max}, \quad \text{Min/max force bounds,} \quad (8.24)$$

$$\vec{g}(\vec{\kappa}(t_k), \dot{\vec{\kappa}}(t_k), \ddot{\vec{\kappa}}(t_k), \tilde{\vec{f}}_k) \leq \vec{0}, \quad \text{GH stability constraint.} \quad (8.25)$$

A solution to this problem is found using null-space optimisation. The muscle-force vector is parameterised directly in terms of the primary task or torque-force constraint. The solution is defined by:

$$\tilde{\vec{f}}_k = \tilde{\vec{f}}_k^* + \tilde{\mathbf{N}}_k \vec{v}_k, \quad \tilde{\vec{f}}_k^* = \tilde{\mathbf{W}}_0^+(\vec{\kappa}(t_k)) \vec{t}_a(\vec{\kappa}(t_k), \dot{\vec{\kappa}}(t_k), \ddot{\vec{\kappa}}(t_k)) \quad \tilde{\mathbf{W}}_0(\vec{\kappa}(t_k)) \tilde{\mathbf{N}}_k = \vec{0}. \quad (8.26)$$

where $\tilde{\vec{f}}_k^*$ is an initial solution obtained by taking the Moore-Penrose pseudo-inverse of the generalised moment-arms matrix $\tilde{\mathbf{W}}_0(\vec{\kappa}(t_k))$. This particular pseudo-inverse minimises the mean-square muscle stress if it is weighted by the PCSAs [203]. The initial solution does not however satisfy the other two constraints. The vector \vec{v}_k parameterises the null-space \mathbf{N}_k of the generalised moment-arms matrix. This parameterisation is inserted into the cost function (8.22) yielding a quadratic optimisation problem (c.f. chapter 7 for details).

$$\min_{\vec{v}_k} \Gamma(\vec{v}_k) = \frac{1}{2} \vec{v}_k^T \tilde{\mathbf{N}}_k^T \tilde{\mathbf{P}} \tilde{\mathbf{N}}_k \vec{v}_k + (\tilde{\vec{f}}_k^*)^T \tilde{\mathbf{P}} \tilde{\mathbf{N}}_k \vec{v}_k, \quad (8.27)$$

$$\text{s.t. } \mathbf{A}_k \vec{v}_k - \vec{b}_k \leq \vec{0}, \quad (8.28)$$

The null-space of the moment-arms matrix is used to change the initial solution without violating the primary task while realising the secondary task and satisfying the addition constraints.

Once the solution to the muscle-force coordination problem is found, the glenohumeral joint reaction force is computed. The constraint forces are removed from the solution yielding \vec{f} , containing just the muscle forces. As stated previously in section 8.2.2, the scapulothoracic contact forces are included in the vector $\tilde{\vec{f}}$ and must be removed before compute the joint reaction force. The glenohumeral reaction force \vec{f}_r is computed from the expression of the arm's translational dynamics (Newton's second law of motion).

$$M_3 \ddot{\vec{x}}_{0,3} = M_3 \vec{g}_0 + \mathbf{D}_0 \vec{f} + \vec{f}_r, \quad (8.29)$$

where M_3 is the arm's mass. The vector $\ddot{\vec{x}}_{0,3}$ is the arms translational acceleration defined in the inertial frame. The vector \vec{g}_0 is the earth's gravitational vector field defined in the inertial frame. The matrix \mathbf{D}_0 is the force direction matrix defined in the inertial frame.

8.2.4 Implementation and Model Output

The musculoskeletal model of the human shoulder presented in chapter 4 and briefly reviewed in section 8.2.1 was implemented into the Mathworks computing environment: MATLAB (Version 2014a for Mac) (Fig. 8.3). The necessary physical data (bony landmarks, muscle insertions and origins, etc.) to construct the model was collected from MRI scans of an adult male [60]. All the data required to reconstruct and implement the model can be found in appendix B.

The model is being designed to estimate the force in the glenohumeral joint. As stated previously the general methodology is to define a kinematic motion. The inverse dynamics model is used to compute the associated actuation vector. The muscle-forces that generate the actuation vector are found through a static optimisation program. Once the muscle-forces are found, the joint reaction force is obtained using the arm's translational dynamics. The computational procedure for obtaining the glenohumeral joint reaction force for a given movement is defined as follows:

Glenohumeral Joint-Force Estimation Computational Procedure:

1. A motion of the skeletal system is planned using the minimal coordinates $\vec{\zeta}(t)$. The motion is planned over the time horizon $t \in [0, 1]$ for N evenly distributed discrete instances.
2. The same motion is computed in terms of the generalised kinematics $\vec{\kappa}(t)$, $\dot{\vec{\kappa}}(t)$ and $\ddot{\vec{\kappa}}(t)$. The dynamic behaviour is defined by setting the time horizon T (8.13).
3. The necessary actuation vector $\vec{t}_a(\vec{\kappa}(t), \dot{\vec{\kappa}}(t), \ddot{\vec{\kappa}}(t))$ is computed using the inverse dynamic model (8.21). The lagrangians are computed using the method presented in chapter 3.
4. For each time step $t_k \in \{t_0, t_1, \dots, t_N = T\}$ the muscle-force coordination problem is solved using the quadratic optimisation problem (8.27), (8.28). The moment-arms matrix is computed using the geometric method from chapter 7. The problem is numerically solved using MATLAB's `quadprog` function. The upper bounds on the muscle forces are taken from [76].
5. The scapulothoracic contact forces are removed from the solution to yield the muscle forces $\vec{f}(t_k)$. The glenohumeral joint reaction force $\vec{f}_r(t)$ is computed using the arms translational dynamics (8.29). These dynamics are computed using the method presented in chapter 3.

The model's performance is evaluated with respect to four points that cover the important aspects of muscle and joint-force estimation. The results will be presented in terms of these points.

- **Scapular kinematics:** The most challenging point of kinematic shoulder modelling is the description of scapular kinematics due to the scapulothoracic constraints. The model-predicted scapular kinematics are compared to the measured scapular kinematics from [58].
- **Muscle moment-arms:** The muscle-force coordination strategy is centred around the moment-arms matrix. The moment-arms are compared to measured moment-arms from cadaveric studies [2, 102, 130, 161]. In cadaveric studies, the rotator cuff muscle moment-arms are measured for humeral abduction in the scapular plane. the scapula remains fixed and the humerus is abducted up to 90° in the scapular plane. The moment-arm of each muscle in the rotator cuff is measured in terms of its component around the y -axis normal to the scapular plane. The model's moment-arms were also compared to the moment-arms from the Visible Human Project (VHP) kinematic model [76]. This comparison is well founded, given that the two models share the same muscle topology. The present model's geometric muscle model was constructed using the same framework.

- **Muscle-forces:** The model is designed to estimate muscle forces. The muscle forces are presented for quasi-static ($T = 20$ [s]) and dynamic ($T = 2$ [s]) abduction in the scapular plane. The computation was done for 100 points evenly distributed between 0° and 140° abduction. The computation was stopped at 140° because the model's validity is questionable for high abduction angles. The estimation was performed using 28 muscle segments (one segment per muscle).
- **Joint reaction force intensity and orientation:** Is the primary objective of the model. The joint reaction force intensity for quasi-static abduction is compared to results reported in [10, 71, 155]. The joint force orientation with respect to the glenoid is compared to results reported in [59, 195].

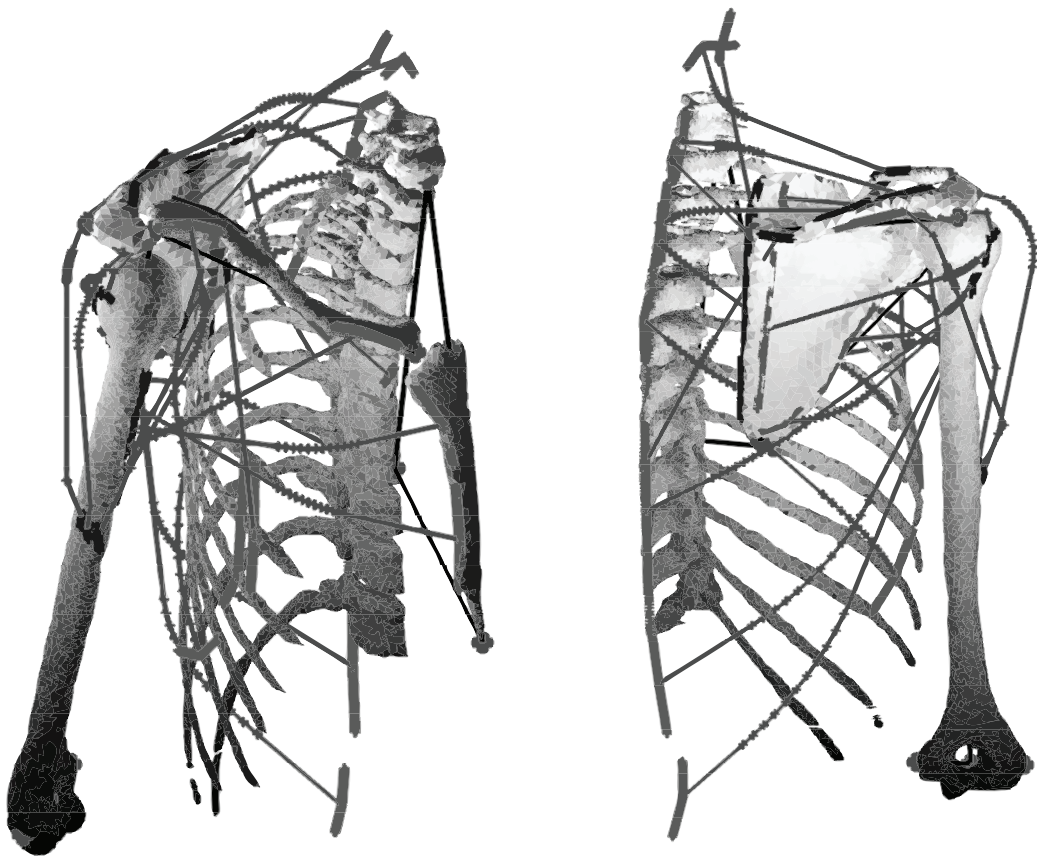


Figure 8.3: *Illustration of the musculoskeletal shoulder model implemented into the Mathworks computing environment: MATLAB (Version 2014a for Mac).*

8.3 Results

8.3.1 Scapular Kinematics

For humeral abduction in the scapular plane, the model predicted scapular kinematics show protraction, depression and posterior tilt (Fig. 8.4). The scapula protracts forwards around the ribcage and depresses. The movement of the lowest point on the scapula (angelus inferior AI) creates posterior tilt. The elevation/depression angle shows the largest variation between initial and final values.

For all three angles, the minimal coordinate-constructed scapular kinematics remain within the variability of the measured behaviour during the entire motion (Fig. 8.4). The tilt angle is the one that agrees best with the mean measured behaviour. The minimal coordinate-constructed kinematics show less overall depression and protraction. The scapula is observed to depress quicker than the measured kinematics but finishes with less depression than the mean measured value. The minimal coordinate-constructed protraction initially has the same slope but slightly diverges after 120° abduction. Lastly, holding the scapula fixed in its initial configuration for the first 30° of abduction agrees with the mean measured kinematics. The mean measured kinematics for all angles are observed to remain nearly constant during the first 45° abduction.

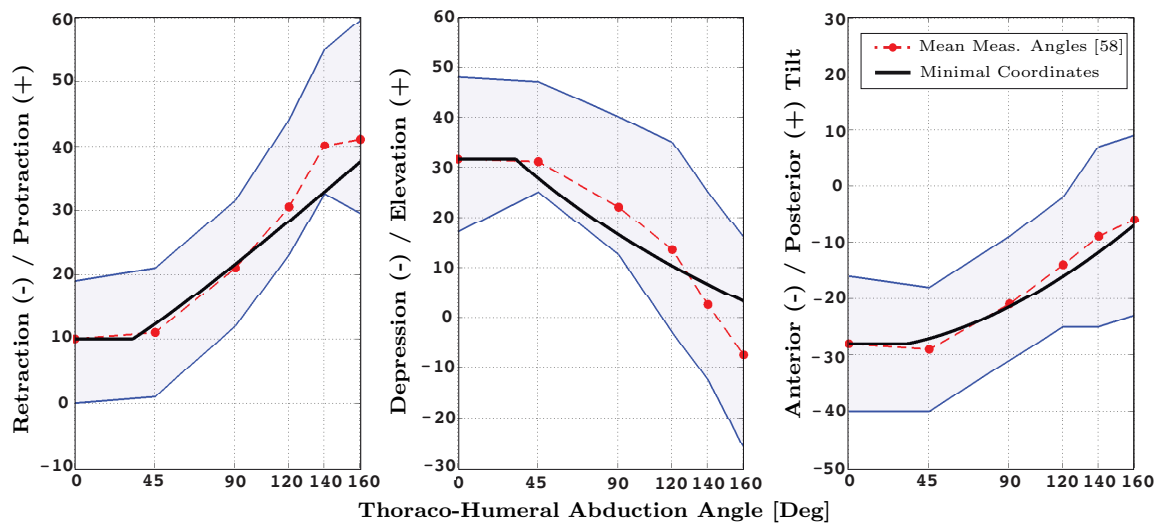


Figure 8.4: Comparison of model-predicted (black) scapular kinematics and measured scapular kinematics (red). The shaded area represents the measured data variability as described in section 8.3.1.

8.3.2 Muscle Moment-Arms

The muscle moment-arms are presented for the anterior deltoid, middle deltoid, posterior deltoid, supraspinatus, infraspinatus and subscapularis (Fig. 8.5). The moment-arms of all six muscles are of the same order of magnitude as the moment arms reported in the

literature. The moment-arm of the **anterior deltoid** is slightly larger than the moment-arm reported in [2] but has the same tendency to increase as the humerus abducts. The observed discontinuity is the segment leaving the wrapping surface. The moment-arm of the **middle deltoid** is initially larger than the values reported in the literature but decreases as the humerus abducts. The **posterior deltoid** moment-arm is positive and increasing where as the moment-arms reported in the literature are negative and increasing. The trends are similar but with an offset. The **supraspinatus** moment-arm shows the best correspondence with the measured moment-arms [102, 130]. The **infraspinatus** moment-arm shows an overall similar trend as the moment-arms from [2, 102]. The **subscapularis** exhibits an inverse trend to the moment-arms reported in [2, 102, 130].

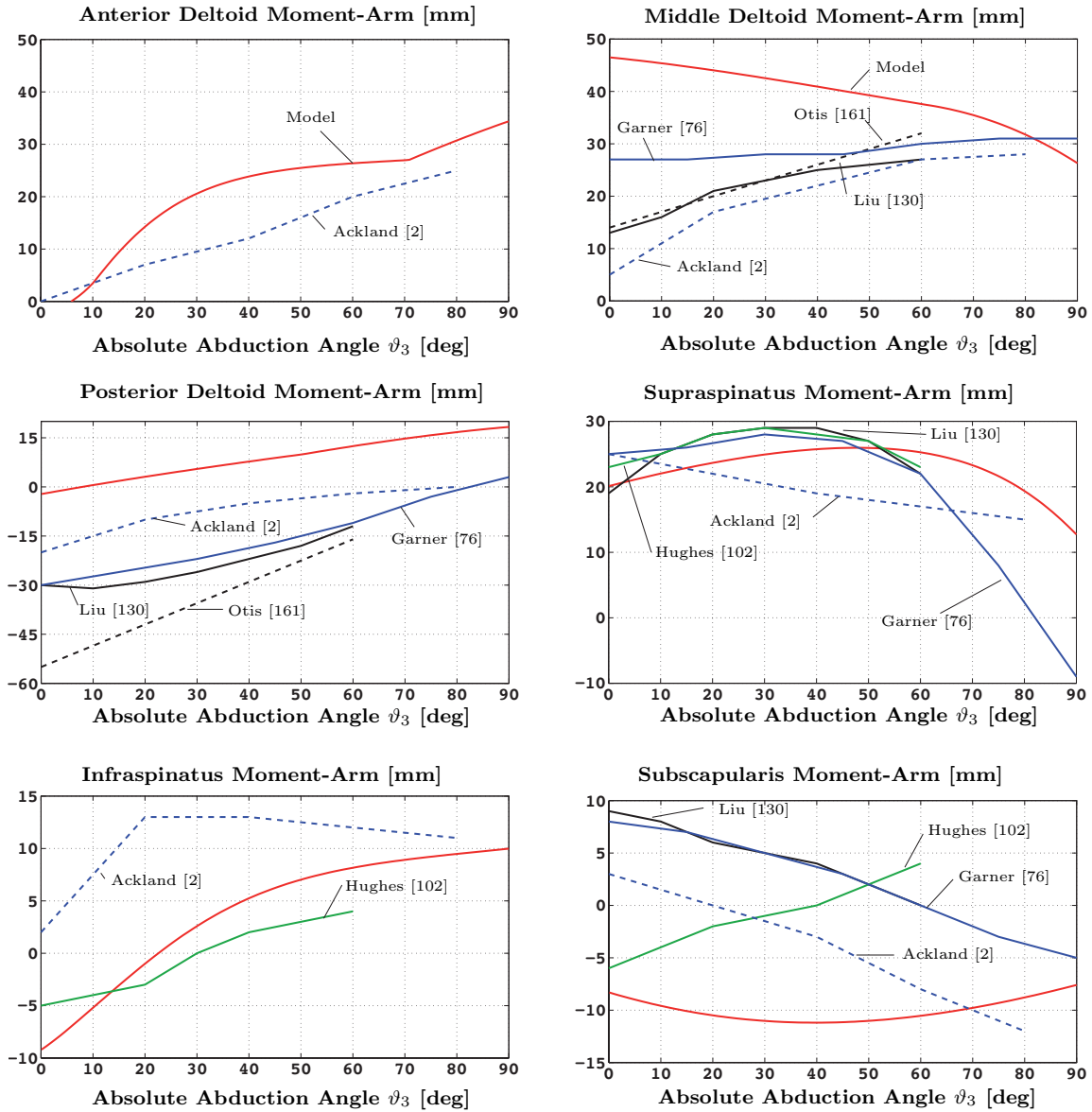


Figure 8.5: Comparison of model-predicted (red) and measured moment-arms [2, 76, 102, 130, 161] for abduction in the scapular plane as described in section 8.3.2.

Compared to the moment arms predicted by the Visible Human Project (VHP) kinematic shoulder model [76], the moment-arms of the middle deltoid, posterior deltoid, supraspinatus and subscapularis of the present model differ more significantly from measured values than do the moment-arms from the VHP model.

8.3.3 Muscle Forces

The model predicted muscle-forces are presented in % of the maximum isometric muscle force (Fig. 8.6). The muscle-forces are presented for all the muscles spanning the glenohumeral joint, not including the latissimus dorsi and pectoralis major muscles. All the muscles are active during part or all the motion. The only muscle not showing activity is the anterior part of the deltoid. The middle deltoid, teres minor and coracobrachialis are the muscles showing the most activity with activation levels above 50%, and are the only muscles to remain active throughout the motion.

During quasi-static abduction, all active muscles except the middle deltoid, show an increase followed by a decrease in muscle force. The curves are all more or less bell-shaped. In contrast, the middle deltoid shows a steady increase in muscle force throughout the entire motion.

The **middle deltoid** shows a maximum activation level of almost 60% at 140° abduction. The **posterior deltoid** shows a maximum activation level of 17% at 110° abduction. The muscle becomes inactive above 130° abduction. The supraspinatus and infraspinatus show a small amount of activity during the initiation of the movement. The **supraspinatus** remains active to around 125° abduction with a maximum value of 6%. The **infraspinatus** remains active up to 30° abduction with a maximum value of 4%. The **subscapularis** muscle shows a peak activation level of 20% at 120° abduction after which it becomes inactive. The **teres minor** muscle shows a monotonous rise towards its peak activation level of 57% at 105° abduction, followed by a rapid decrease. The **teres major** muscle shows a behaviour similar to the posterior deltoid. The force initially decreases and then increases to a peak value of 21% at 125° abduction. The **coracobrachialis** shows a monotonous increase to its peak value of 28% at 70° abduction, followed by a decrease to near inactivity. The peak activation levels of the posterior deltoid, subscapularis, teres minor and teres major occurs after 90° abduction.

During dynamic abduction, the behaviour is consistently a sharp rise at the initiation of the movement, followed by a steady decrease in muscle force. Furthermore, a number of muscles show a notch at 30° abduction corresponding to the scapula beginning to move. The middle deltoid, teres minor, teres major and coracobrachialis show a sharp increase at the end of the dynamic motion.

The **middle deltoid** has a peak value of 55% at 140° abduction. The **posterior deltoid** exhibits a similar behaviour as in quasi-static but with a peak value of 8% at 100° abduction. The **supraspinatus** as a peak value of 17% at 10° abduction. After 45° abduction it shows the same trend as in quasi-static. The **infraspinatus** has a peak value of 10% at 10° abduction and also exhibits the same behaviour as in quasi-static

after 30° abduction. The **subscapularis** has a peak value of 18% at 10° abduction. The force then decreases progressively. The **teres minor** has a peak value of 44% at 45° abduction. Its final value at 140° is almost identical to its final value in quasi-static. The **teres major** has a peak value of 8% at 140° abduction and follows the same trend as in quasi-static but with less amplitude at the end. The **coracobrachialis** shows a peak value of 56% at 140° abduction.

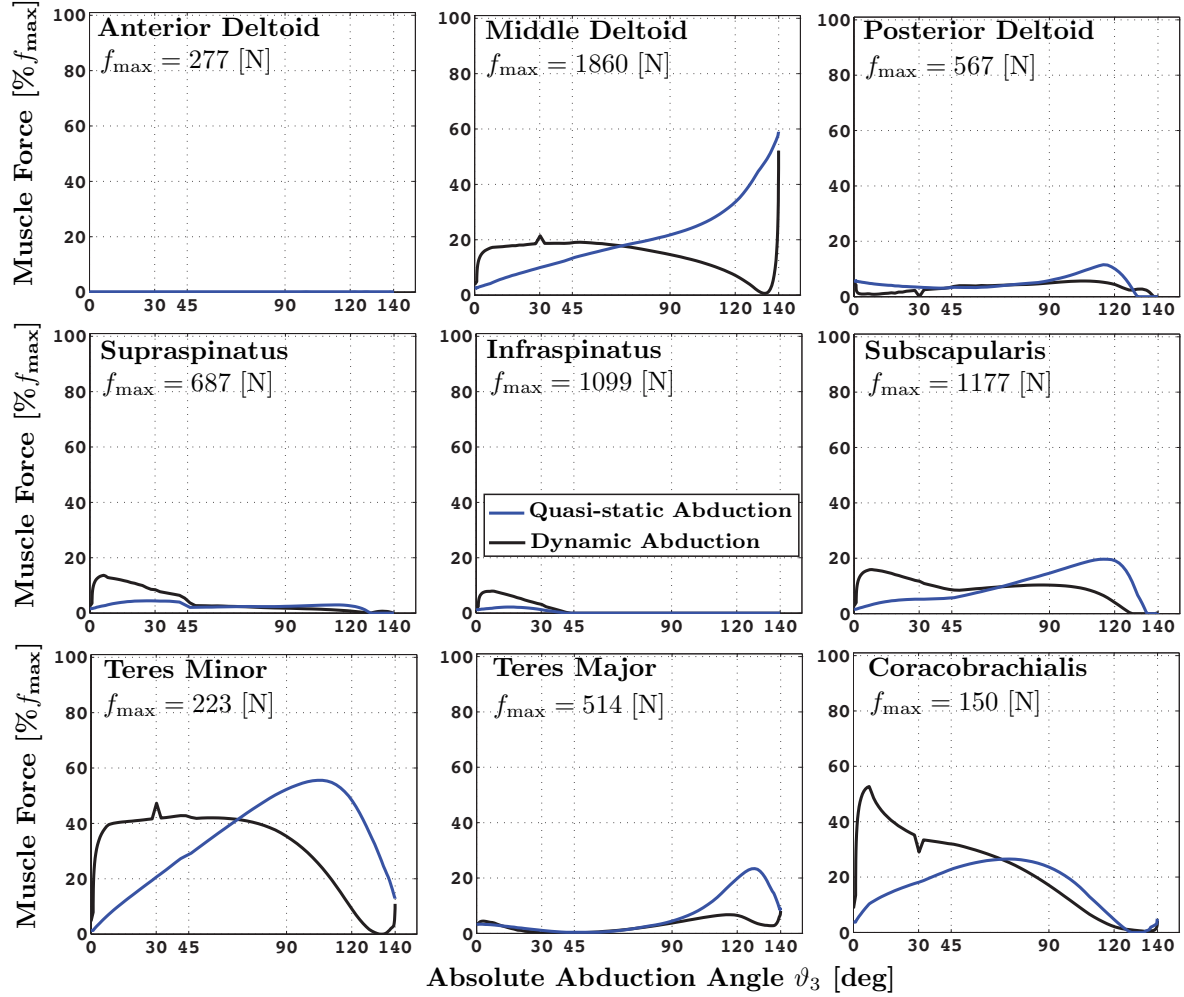


Figure 8.6: Muscle forces in the muscles spanning the glenohumeral joint during quasi-static and dynamic abduction in the scapular plane (plane rotated 30° anteriorly with respect to the frontal plane) as described in section 8.3.3.

8.3.4 Joint Reaction Force

The glenohumeral joint reaction force is presented in terms of the force intensity in Newtons (Fig. 8.7). The stereographic projection of the reaction force vector onto the glenoid is also presented (Fig. 8.8).

During quasi-static abduction, the force intensity rises steadily from 140 [N] at 0° abduction to a peak value of 1200 [N] at 140° abduction. Between 120° and 140° abduction, the force intensity slightly drops. The initial behaviour is consistent with other behaviours reported in the literature [10, 71, 155]. The joint force direction is initially on the superior-anterior edge (quadrant I) of the glenoid (Fig. 8.8). From 0° to 45° abduction. The force initially moves posteriorly and then moves anteriorly between 0° and 45° abduction. After 45° abduction the force moves downwards almost vertically. At 90° abduction, the force is close to the middle axes in the anterior region (quadrant I). The force then continues to drop until 140° abduction. The predicted behaviour is most similar to the behaviour from [195].

During dynamic abduction, the joint reaction force shows a rapid increase from 100 [N] at 0° to 550 [N] at 10° abduction. The reaction force intensity then shows a slightly decreasing behaviour. Like the muscle forces, there is a notch at 30° abduction. Between 100° and 140° abduction, the force shows a rapid decrease follow by a sharp increase to its peak value of 1100 [N] at 140° abduction. This behaviour is consistent with having to stop the arm's abduction. The contact pattern in dynamic abduction is similar to the quasi-static situation. The force is observed to drop all the way to the bottom anterior edge of the glenoid (quadrant II). The final directions for both quasi-static and dynamic abduction are similar.

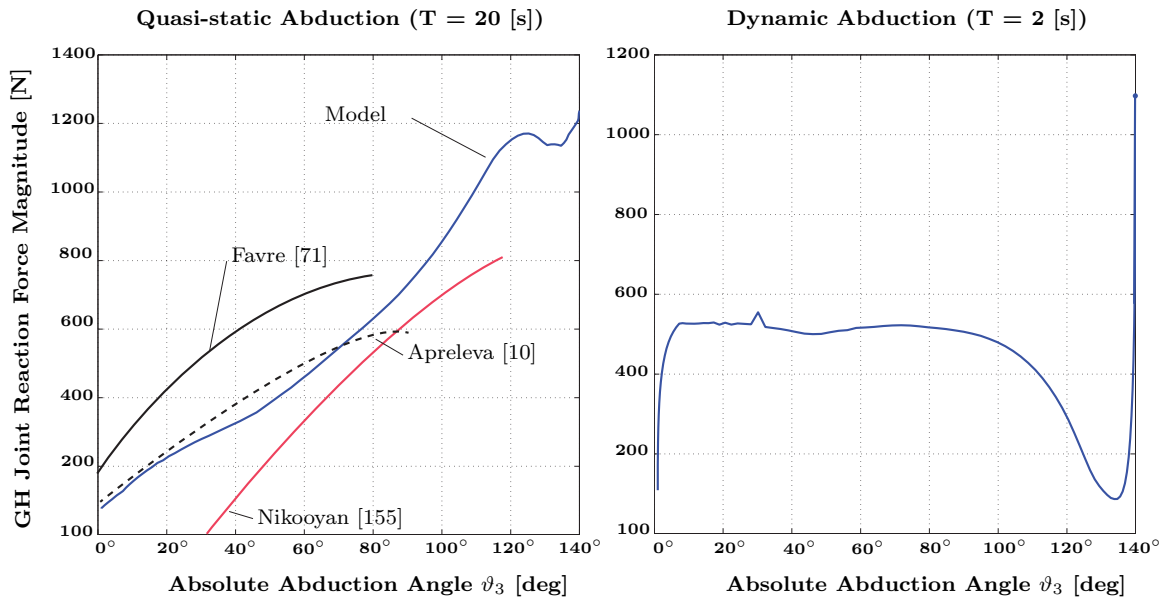


Figure 8.7: Reaction force in the glenohumeral joint during quasi-static and dynamic abduction in the scapular plane as described in section 8.3.4.

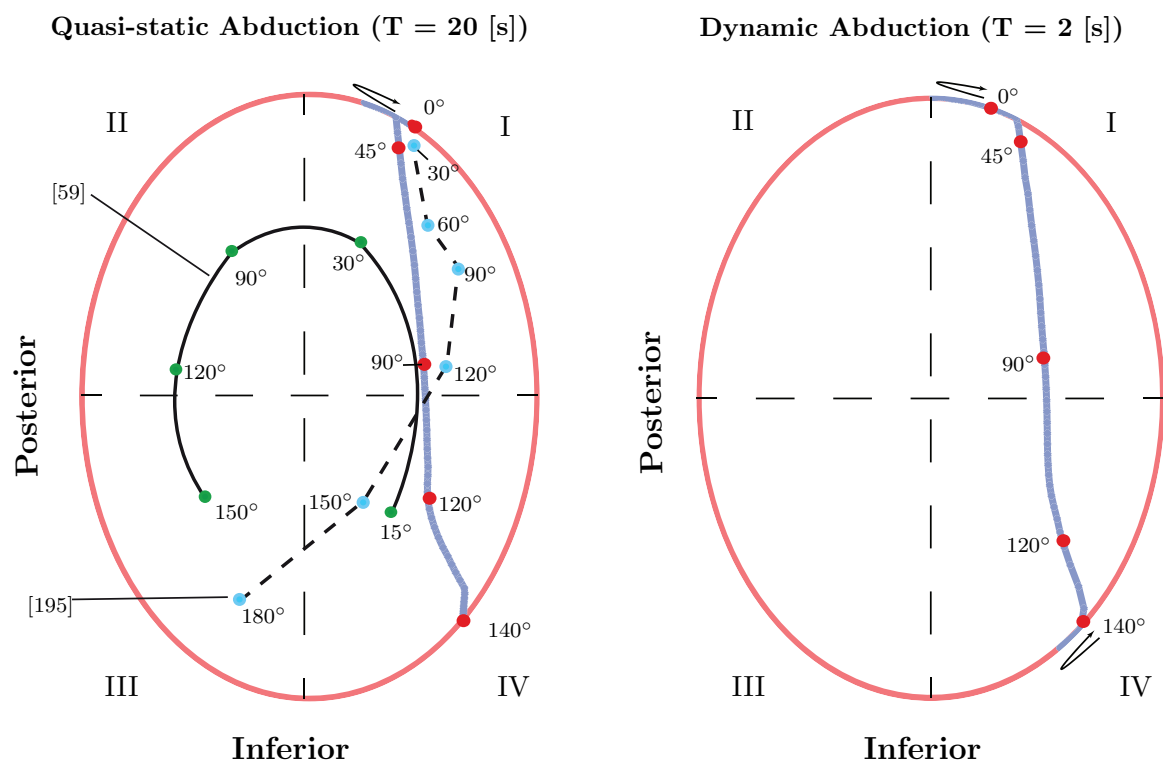


Figure 8.8: *Visualisation of the model predicted glenohumeral joint contact patterns for quasi-static and dynamic optimisation as described in section 8.3.4.*

8.4 Discussion

The goal of this chapter was to assess and review the ability of a musculoskeletal shoulder model at estimating the reaction force in the glenohumeral joint. The model assumes the bones to be rigid bodies, the articulations to be ideal mechanical joints and the muscles to be massless frictionless cables wrapping over the bones. The model has been tested for the simple movement of abduction in the scapular plane and shown to perform moderately well. The results presented in this chapter constitute the first step of a lengthy validation process.

To fully review the model's performance, it is necessary to review the computational procedure and extract the key points. The computational procedure that is currently being used to estimate the glenohumeral contact force involves two stages. The first stage imposes the primary task of movement. A movement of the entire shoulder is defined that provides through inverse dynamics, the required joint torques that the muscles must generate. The secondary task computes the required muscle-force activation patterns. The joint reaction force is deduced from the activation pattern. The two important elements of the computational procedure are kinematics and muscle geometry. The kinematics define the required torque through the inverse dynamics model. Physical parameters such as length, mass and inertia do influence the torque but the kinematics are the key element of inverse dynamics. The kinematics also contribute directly to the joint

reaction force through the translational dynamics, along with the muscle-force activation patterns.

A muscle's geometry defines its contribution to the actuation of the skeletal system. For the shoulder model, the contribution is summarised by a vector of moment-arms that define the relation between joint torques and muscle forces. The moment-arms matrix in the torque-force relation (8.21) drives the muscle-force activation patterns. The moment-arm matrix is what relates the muscle-force intensities to the primary task of movement.

The model is currently able to produce shoulder kinematics that are in very good agreement with the literature. The kinematics were planned using a new method with respect to the shoulder. Minimal coordinates have been used in other contexts [106], but to the authors knowledge, this is the first time minimal coordinates have been used to plan a shoulder model's kinematics. There are seven coordinates, four of which are equivalent to joint angles. The three remaining coordinates uniquely parameterise the scapula's kinematics and are new. The minimal coordinates have been used to plan abduction in the scapular plane and produce scapular kinematics that are very similar to the findings from [58].

In comparison to the joint angle-description of shoulder kinematics [214], the minimal coordinates have the advantage of being independent. The traditional description is redundant and subject to constraints. The coordinates are dependent. The available solutions for constructing shoulder movement using the redundant description are, minimisation with respect to measured kinematics [156] or regression models of scapular kinematics with respect to humeral kinematics [33]. The first solution requires measured data that is not easily obtainable. Measuring scapular kinematics is a lengthy, challenging task and therefore regression models of scapular kinematics have been developed [50, 84, 104, 215, 218]. These models define scapular kinematics in terms of Euler or Bryan angles as functions of the glenohumeral joint angles. There are linear [50, 84] and non-linear models [104, 215, 218]. The attractiveness of regression models is the ease with which movements can be defined once the model is constructed. The downside to this point is that regression models do not satisfy the kinematic constraints such as the scapulothoracic constraints. Regression models can only be used with shoulder models exempt of kinematic constraints. Minimal coordinates present a method of correcting this characteristic of regression models. If a regression model were to be constructed using the minimal coordinate description of a shoulder model with scapulothoracic contact constraints, it would be usable on other shoulder models that have the same constraints. Thus, minimal coordinates represent a promising new solution to planning shoulder kinematics that merits further development.

The model is currently able to produce consistent kinematics but is unable to produce muscle activation patterns that are consistent with activation patterns from the literature. Although the intensity of the force in the glenohumeral joint does agree with results reported in the literature up to 90° [10, 71, 155], it over estimates the force intensity for higher abduction values. A number of studies have reported that after 90° abduction, the reaction force decreases [189, 195]. However, more recently the force has been estimated through simulation and measured in-vivo to steadily increase throughout the entire abduction movement [17, 68]. The predicted contact pattern is similar to the

contact pattern initially reported by the DSEM model [195] but lies partially on the edge of the glenoid. These inconsistencies come from the muscle activation patterns that are not in complete agreement with the literature and as explained previously, the muscle activation patterns are primarily governed by the geometric muscle model. A poor geometric muscle model explains all these inconsistencies.

The current geometric muscle model is constructed on the same framework as the kinematic shoulder model constructed from the Visible Human Project (VHP) [74, 76]. Both models share the same wrapping topology but have different numerical implementations. Furthermore, the VHP dataset was the result of an optimisation to follow the centroid line of the muscles. The dataset used to construct the current model has not been optimised. A careful review of the wrapping topology defined in the presentation of the VHP model, revealed a number of inaccuracies. For instance, the superior part of the trapezius is defined in the VHP model to insert on the scapula while anatomically it inserts on the clavicle. This point is an inaccuracy because after implementation of the VHP model, the superior part of the trapezius visually inserts on the clavicle. A second example concerns the definition of the wrapping objects for the deltoid and rotator cuff muscles. The objects are used to represent the humeral head but are defined as being part of the scapula. While these inaccuracies explain part of the inconsistencies in the muscle activation patterns, they do not explain the inactive anterior deltoid muscle segment. This point has a source related to the fundamental approach of modelling the musculature using cables that will be expanded subsequently in section 8.4.1.

The results presented in this chapter show that the model is currently capable of generating consistent shoulder kinematics but does not completely fulfil its primary purpose of estimating the force in the glenohumeral joint. There are a number of points with the estimated muscle forces that must be sorted out before testing can continue. In comparison to other models from the literature [71, 155, 158], the present model requires further development. The glenohumeral joint is now modelled as a fixed centre ball and socket joint while in reality the humeral head moves with respect to the glenoid. The model has been insufficiently validated and tested. To illustrate this point, the DSEM model underwent its most thorough round of validation in 2011 while its initial development was presented in 1994. Although in its initial development phase, the model does show promise at being a competitive model for studying the shoulder and more specifically the force in the glenohumeral joint.

8.4.1 Wrench-Feasibility of a Shoulder Musculoskeletal Model

The previous discussion stated that the source of the inconsistent muscle activation patterns comes from a poor definition of the geometric muscle model. The best example of the inconsistent behaviour is the inactivity of the anterior deltoid muscle segment. The source of the anterior deltoid's inactivity is moment-arms and the torque-feasible workspace defined in chapter 7. This section analyses the shoulder model's wrench-feasible workspace and proposes a solution to the problem.

The presentation begins with a more complete description of the model's geometric

muscle model. The shoulder musculature is modelled in this thesis using the same framework as the Visible Human Project (VHP) kinematic model [74, 76]. Both models share the same topological structure of the geometric muscle model but use different numerical implementations. Both models use 28 cables or segments to represent the musculature. In both models, there are three joints parameterised by nine coordinates and both models consider two points on the scapula's medial border to define the scapulothoracic contact. Therefore, the size of the moment-arm matrix without the scapula-thoracic constraints is 9×28 . Each column of the matrix corresponds to the moment-arms of a muscle segment around all three joints. The moment-arm matrix is defined by:

$$\mathbf{W}_0 \in \mathbb{M}_{9 \times 28}(\mathbb{R}), \quad (\mathbf{W}_0)_{*,i} = \begin{pmatrix} \vec{w}_{1,i} \\ \vec{w}_{2,i} \\ \vec{w}_{3,i} \end{pmatrix}, \quad \begin{array}{l} \vec{w}_{1,i} : \text{SC moment-arms for muscle } i, \\ \vec{w}_{2,i} : \text{AC moment-arms for muscle } i, \\ \vec{w}_{3,i} : \text{GH moment-arms for muscle } i. \end{array} \quad (8.30)$$

The relation between the columns and muscle segments is defined as follows:

- Column 1: The first muscle is the **subclavius**, defining three moment-arms around each of the three SC joint axes.
- Columns 2-4: The three **serratus anterior** muscle segments originate on the thorax and insert on the scapula. They all define six moment arms. Three moment-arms around the SC joint axes and three moment-arms around the AC joint axes.
- Columns 5-8: The four **trapezius** muscle segments. All segments originate on the thorax. The first segment corresponds to the superior part and inserts on the clavicle. The three remaining segments insert on the scapula.
- Column 9: The **levator scapulae** muscle segment. Originates on the thorax and insert on the scapula.
- Columns 10-12: The **rhomboid minor and major** muscle segments. Originate on the thorax and insert on the scapula.
- Column 13: The **pectoralis minor** muscle segment. Originates on the thorax and insert on the scapula.
- Columns 14-16: The three **pectoralis major** muscle segments. The first segment originates on the scapula and inserts on the humerus. The other two segments originate on the sternum and insert on the humerus.
- Columns 17-19: The three **latissimus dorsi** muscle segments. All the segments originate on the thorax and insert on the humerus.
- Columns 20-22: The three **deltoid** muscle segments. The first segment represents the anterior deltoid, originating on the clavicle and inserting on the humerus. The other two segments represent the middle and posterior parts of the deltoid. Both originate on the scapula and insert on the humerus.
- Columns 23-24: The **supraspinatus and infraspinatus** muscle segments. Both originates on the scapula and insert on humerus.

- Columns 25: The **subscapularis** muscle segment. Originates on the scapula and inserts on humerus.
- Columns 26-27: The **teres minor and major** muscle segments. Both originate on the scapula and insert on humerus.
- Column 28: The **coracobrachialis** muscle segment. Originates on the scapula and inserts on humerus.

In chapter 7 a geometric method of computing moment-arms is defined. The method shows that each muscle defines non-zero moment-arms around the joints it spans and around the proximal joint along the kinematic chain that it does not span. For instance, the middle deltoid spans the glenohumeral joint only but creates moment-arms around the glenohumeral and acromioclavicular joints. Thus, the non-zero elements of the moment-arm matrix can be defined using only the knowledge of each muscles origin and insertion (Table 8.2). The moment-arm around a joint that the muscle does not span is called the *coupling moment-arm*. The coupling moment-arms of the shoulder model explain the inconsistent muscle activation patterns.

The moment-arms of a muscle segment relate the intensity of the force in the segment to the torque or actuation around the joints. This relation is defined for the entire model by the torque-force map (8.21). The moment-arm matrix \mathbf{W}_0 defines the torque-force map for a given configuration $\vec{\kappa}$.

$$\begin{aligned}\mathfrak{M}_{\vec{\kappa}} : \mathcal{F} &\rightarrow T_{\vec{\kappa}}\mathcal{Q}_S, \\ \vec{f} &\mapsto \mathfrak{M}_{\vec{\kappa}}(\vec{f}) = \vec{t}_a = \mathbf{W}_0(\vec{\kappa})\vec{f}.\end{aligned}\tag{8.31}$$

As presented in chapter 7, the domain of the map \mathcal{F} is defined by the upper and lower bounds on the muscle forces. These bounds are simple inequalities that define the domain as being a polytope in \mathbb{R}^{28} . This polytope is referred to as the muscle-force polytope. For the shoulder model specifically, the image of the muscle-force polytope through the torque-force map is three polytopes. Each image polytope corresponds to the range of possible actuations that the musculature can produce at a each joint in a given configuration $\vec{\kappa}$. Given the presence of the coupling moment-arms, the image polytopes are not independent. To illustrate the concept, the image polytopes of the shoulder model have been computed in the resting configuration for the glenohumeral and sternoclavicular joints (Figs. 8.9, 8.10).

There is a striking difference between the glenohumeral and sternoclavicular joint image polytopes. The sternoclavicular image polytope is almost flat. There is a direction in which it has almost no thickness. This results is explained by the following reasoning: The sternoclavicular polytope is defined by the first 20 muscles (Table 8.2). There are four muscles originating or inserting directly on the clavicle (marked by a star in table 8.2). The remaining 16 muscles originate on the thorax and insert on the scapula. These muscles do not attach to the clavicle that has the following consequence. The moment-arms created by the 16 muscles not attached to the clavicle define moment-arms

Table 8.2: *Muscle segment moment-arms. This table describes where the muscle segments define moment-arms given their origin and insertion.*

Muscle Name	Origin	Insertion	SC	AC	GH	
Subclavius	Sternum	Clavicle	$\vec{w}_{1,1}$	$\vec{0}$	$\vec{0}$	*
Serratus Anterior 1	Thorax	Scapula	$\vec{w}_{1,2}$	$\vec{w}_{2,2}$	$\vec{0}$	
Serratus Anterior 2	Thorax	Scapula	$\vec{w}_{1,3}$	$\vec{w}_{2,3}$	$\vec{0}$	
Serratus Anterior 3	Thorax	Scapula	$\vec{w}_{1,4}$	$\vec{w}_{2,4}$	$\vec{0}$	
Trapezius 1	Thorax	Clavicle	$\vec{w}_{1,5}$	$\vec{0}$	$\vec{0}$	*
Trapezius 2	Thorax	Scapula	$\vec{w}_{1,6}$	$\vec{w}_{2,6}$	$\vec{0}$	
Trapezius 3	Thorax	Scapula	$\vec{w}_{1,7}$	$\vec{w}_{2,7}$	$\vec{0}$	
Trapezius 4	Thorax	Scapula	$\vec{w}_{1,8}$	$\vec{w}_{2,8}$	$\vec{0}$	
Levator scapulae	Thorax	Scapula	$\vec{w}_{1,9}$	$\vec{w}_{2,9}$	$\vec{0}$	
Rhomboid minor	Thorax	Scapula	$\vec{w}_{1,10}$	$\vec{w}_{2,10}$	$\vec{0}$	
Rhomboid major 1	Thorax	Scapula	$\vec{w}_{1,11}$	$\vec{w}_{2,11}$	$\vec{0}$	
Rhomboid major 2	Thorax	Scapula	$\vec{w}_{1,12}$	$\vec{w}_{2,12}$	$\vec{0}$	
Pectoralis minor	Thorax	Scapula	$\vec{w}_{1,13}$	$\vec{w}_{2,8}$	$\vec{0}$	
Pectoralis major 1	Clavicle	Humerus	$\vec{w}_{1,14}$	$\vec{w}_{2,14}$	$\vec{w}_{3,14}$	*
Pectoralis major 2	Thorax	Humerus	$\vec{w}_{1,15}$	$\vec{w}_{2,15}$	$\vec{w}_{3,15}$	
Pectoralis major 3	Thorax	Humerus	$\vec{w}_{1,16}$	$\vec{w}_{2,16}$	$\vec{w}_{3,16}$	
Latissimus dorsi 1	Thorax	Humerus	$\vec{w}_{1,17}$	$\vec{w}_{2,17}$	$\vec{w}_{3,17}$	
Latissimus dorsi 2	Thorax	Humerus	$\vec{w}_{1,18}$	$\vec{w}_{2,18}$	$\vec{w}_{3,18}$	
Latissimus dorsi 3	Thorax	Humerus	$\vec{w}_{1,19}$	$\vec{w}_{2,19}$	$\vec{w}_{3,19}$	
Anterior Deltoid	Clavicle	Humerus	$\vec{w}_{1,20}$	$\vec{w}_{2,20}$	$\vec{w}_{3,20}$	*
Middle Deltoid	Scapula	Humerus	$\vec{0}$	$\vec{w}_{2,21}$	$\vec{w}_{3,21}$	
Posterior Deltoid	Scapula	Humerus	$\vec{0}$	$\vec{w}_{2,22}$	$\vec{w}_{3,22}$	
Supraspinatus	Scapula	Humerus	$\vec{0}$	$\vec{w}_{2,23}$	$\vec{w}_{3,23}$	
Infraspinatus	Scapula	Humerus	$\vec{0}$	$\vec{w}_{2,24}$	$\vec{w}_{3,24}$	
Subscapularis	Scapula	Humerus	$\vec{0}$	$\vec{w}_{2,25}$	$\vec{w}_{3,25}$	
Teres minor	Scapula	Humerus	$\vec{0}$	$\vec{w}_{2,26}$	$\vec{w}_{3,26}$	
Teres major	Scapula	Humerus	$\vec{0}$	$\vec{w}_{2,27}$	$\vec{w}_{3,27}$	
Coracobrachialis	Scapula	Humerus	$\vec{0}$	$\vec{w}_{2,28}$	$\vec{w}_{3,28}$	

around the sternoclavicular joint through the force they transmit across the acromioclavicular joint. These muscles apply a force on the scapula that is transmitted across the acromioclavicular joint. Therefore, the moment-arm of the transmitted force is always perpendicular to the vector between the two joints. Out of the 20 muscles creating a moment-arm around the sternoclavicular joint, 16 muscles create moment-arms that are co-planar. The plane in which they lie is normal the SC-AC axis (Fig. 8.11).

The flat shape of the sternoclavicular image polytope explains the inactivity of the anterior deltoid. If the anterior deltoid is activated, it creates a torque around the sternoclavicular joint that cannot be compensated for. The anterior deltoid is one of the four muscles creating a moment-arm around the sternoclavicular joint not in the plane normal to the SC-AC axis. The model's current geometry is such that the moment-arms

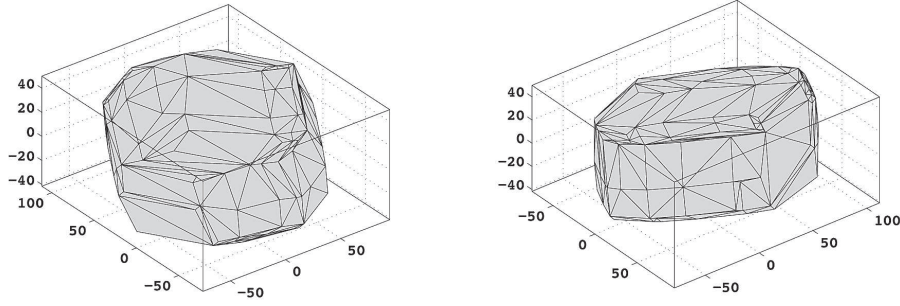


Figure 8.9: *Visualisation of the glenohumeral image space polytope $\mathfrak{M}_{\vec{\kappa},GH}(\mathcal{F})$ through the torque-force map $\mathfrak{M}_{\vec{\kappa}}$ as defined in section 8.4.1. The polytope is computed for the shoulder in the resting position and visualised from two different stand points.*

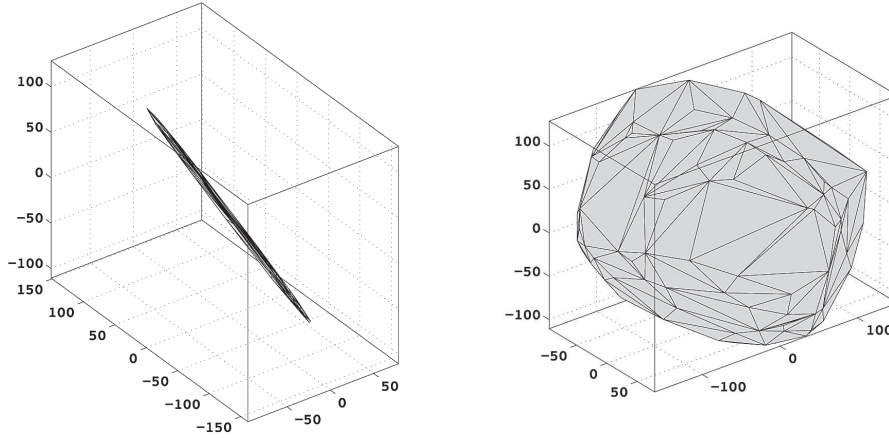


Figure 8.10: *Visualisation of the sternoclavicular image space polytope $\mathfrak{M}_{\vec{\kappa},SC}(\mathcal{F})$ through the torque-force map $\mathfrak{M}_{\vec{\kappa}}$ as defined in section 8.4.1. The polytope is computed for the shoulder in the resting position and visualised from two different stand points.*

of the other three muscles cannot compensate for an active anterior deltoid. This analysis of the torque-force map is called wrench-feasibility analysis, and is extensively used in cable-driven robotics to assess the geometry of the cable network [80, 81].

This preliminary analysis leads to a more fundamental remark concerning muscle modelling in general. At present, the theory of modelling muscles using cables has not been fully developed. To the authors knowledge, there is a single theoretical result regarding the use of cables to model muscles with large attachment sites [197]. The result gives the minimum number of cables to accurately and efficiently represent the mechanical effect of muscles. The result is of fundamental importance but is incomplete in that it does not consider the collective effect of the musculature. To illustrate this point, consider the following. The geometric muscle model of the musculoskeletal shoulder model presented in this thesis is based on the framework from the VHP model. The geometric muscle model of the VHP shoulder model was constructed using the guide lines to model muscles with

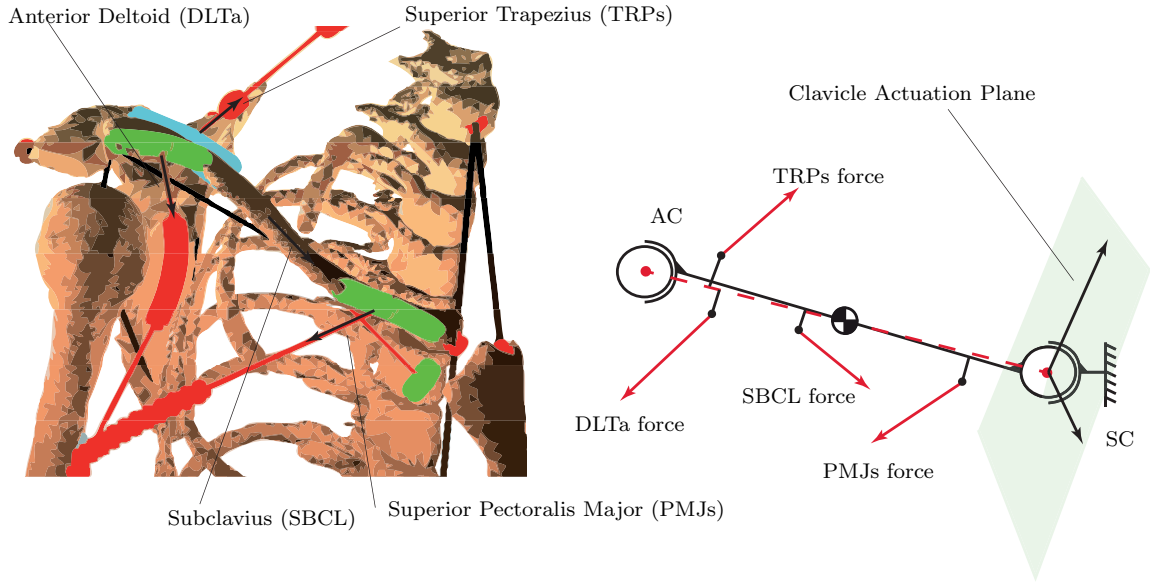


Figure 8.11: *Visualisation of the clavicle's actuation plane and the four forces not creating moment-arms in this plane as described in section 8.4.1.*

large attachment sites [197]. Before the implementation presented in this chapter, the VHP model was implemented. The results were no activation of the anterior deltoid and no solution to the muscle-force coordination problem in certain configurations of the model during simple movements such as abduction and elevation.

These observations were not made during the presentation of the VHP model, because the torque-force map was not inverted. The VHP model found the muscle forces by minimising the error between the model's joint torques and desired joint torques. The torque-force map was not imposed as an equality constraint. Therefore, a solution to the optimisation problem could always be found. Imposing the torque-force map as an equality constraint restricts the possible actuations to the image polytopes of the torque-force map. This leads to the final remark. The theoretical result regarding muscles with large attachment sites defines a necessary condition of the muscle cable model. The moment-arm matrix must be full column rank. This result is necessary to invert the torque-force map when it is used as an equality constraint but is not sufficient to guarantee the existence of a solution to the muscle-force coordination problem. The imposed actuation vector must be inside the wrench feasibility space.

8.5 Conclusions

This chapter presented the implementation of the musculoskeletal shoulder model described in chapter 4. The model is being designed to estimate the force in the glenohumeral articulation for the study of osteoarthritis. The implementation used the minimal coordinates from chapter 6 to plan the kinematics and the null-space optimisation method from chapter 7 to estimate the muscle forces. The joint reaction force was determined from the muscle forces using Newton's second law of motion. The model was tested for abduction in the scapular plane and is currently capable of estimating the force in the glenohumeral articulation. However, the force is overestimated for high abduction values and the model predicts a contact pattern outside the glenoid during part of the movement. Furthermore, the estimated muscle forces are shown to exhibit abnormal behaviours. The anterior part of the deltoid never activates.

The muscle-force abnormalities have been investigated and are shown to come from the geometric muscle model. The coupling terms in the moment-arm matrix are such that an active anterior deltoid creates torque that cannot be compensated for by the other muscles. The present model's muscle geometry was constructed using the same framework as another model from the literature [76] but with different numerical values. The model from the literature constructed the muscle geometry using a method to determine the number of cables required for each muscle [197]. The method defines the minimum number of cables for each muscle individually. The final conclusion of this chapter is that this method requires updating. The muscle geometry should be designed as a collective to maximise wrench feasibility. Each muscle must be represented accurately and the complete musculature should be represented. Future developments should therefore completely remodel the muscle geometry and continue the validation process.

Chapter 9

Introduction to Control Theory

This chapter presents a brief introduction to control theory that is necessary for chapter 10 where the theory is used to investigate human motor control. Complete presentations can be found in closed-form in the literature [117, 131, 153].

Control theory is a field of engineering that analyses how the behaviour of dynamic systems with inputs can be manipulated by feedback using one or more controller(s). It is a theory that can be applied to a large number of systems. Examples include, the cruise control in motor vehicles, the current flow in power grids or the control of chemical reactions [208]. The chapter reviews the definitions of system and controller, the difference between open and closed-loop, the mathematical definition of stability in the sense of Lyapunov, the LaSalle invariance theorem and the basics of linear state feedback.

9.1 Systems and Controllers

A system is a set of element(s), interacting or independent that form a whole [207]. This definition includes the employees in a company as it does the parts in a mechanism. Every system has a structure and exhibits a behaviour. Systems are differentiated according to their structure and/or behaviour and one defines categories of systems. Every system also has interconnections defining the relations between the elements in terms of structure and behaviour. A system's state characterises the interconnections between the different elements at a given instant. In general, the state of a system changes over time and the system is said to be dynamic or exhibit dynamic behaviour.

A dynamical system is a concept from mathematics where, the time dependence of a system's state or dynamic behaviour is described using a fixed rule. The rule is a mathematical model or dynamic model of the system's dynamic behaviour. The model is characterised by its state but also by its inputs and outputs. A dynamical system's inputs model how a system's behaviour can be changed by an external action. This can be seen in the same way a motor changes the speed of a car. The car is the system,

its state is its speed and the input is the torque given to the car's wheels. A dynamical system's outputs are a measure of its state by an external observer. The measure can be complete or only partial. The speedometer of a car measures the car's speed but does not give the car's direction. Dynamical systems can also contain disturbances that are similar to inputs. The inputs and disturbances are different from each other in that inputs can be actively changed or designed, disturbances are the result of the system's environment. Using the car example, the driver can actively change how much torque the motor produces while the state of the road is a disturbance.

A standard representation of a dynamical system is as a state model. A state model is defined as a set of ordinary differential equations (ODE) characterising the system's dynamic behaviour in terms of the states and inputs. Each equation is the mathematical rule modelling a given state's time dependence. A dynamical system with n states and m inputs is defined by a state model of the form:

$$\begin{aligned}\dot{x}_1 &= f_1(t, x_1, \dots, x_n) + g_1(t, x_1, \dots, x_n, u_1, \dots, u_m) = f_1(t, \vec{x}) + g_1(t, \vec{x}, \vec{u}), \\ &\vdots \\ \dot{x}_i &= f_i(t, x_i, \dots, x_n) + g_i(t, x_1, \dots, x_n, u_1, \dots, u_m) = f_i(t, \vec{x}) + g_i(t, \vec{x}, \vec{u}), \\ &\vdots \\ \dot{x}_n &= f_n(t, x_1, \dots, x_n) + g_n(t, x_1, \dots, x_n, u_1, \dots, u_m) = f_n(t, \vec{x}) + g_n(t, \vec{x}, \vec{u}).\end{aligned}\tag{9.1}$$

The variables $x_i \in \mathbb{R}$ are the state variables and the state vector $\vec{x} \in \mathbb{R}^n$ characterises the dynamic state of the model at any given instant. The variables $u_i \in \mathbb{R}$ are the inputs and the input vector $\vec{u} \in \mathbb{R}^m$ characterises the current state of all the external actuators. The rule of the differential equations is divided into two terms f_i and g_i . The first term contains the model of the system's intrinsic dynamic behaviour. In other words how the system behaves when no external actions are being applied. The second term characterises how the inputs can influence the system's state. Both terms can be linear or nonlinear depending on the system they model and are assumed, in this presentation, to be smooth functions. If time appears explicitly in the equations, the dynamic model is said to be time variant. The mathematical rule changes over time. If time does not appear, the system is time invariant. The outputs of a state model are functions of state variables that can be observed or measured externally. Most state models are therefore completely characterised by a mathematical description of the form:

$$\dot{\vec{x}} = \vec{f}(t, \vec{x}) + \vec{g}(t, \vec{x}, \vec{u}),\tag{9.2}$$

$$\vec{y} = \vec{h}(\vec{x}),\tag{9.3}$$

$$\vec{x} \in \mathbb{R}^n, \quad \vec{u} \in \mathbb{R}^m, \quad \vec{y} \in \mathbb{R}^p.\tag{9.4}$$

The input vector function \vec{g} will be assumed to be of the form $\vec{g}(\vec{x}, \vec{u}) = \vec{g}(\vec{x})\vec{u}$. Such state models are said to be affine in the input and are the most common state models. A free solution of the state model (9.2) is defined as an evolution of the states $\mathcal{X}(\vec{x}_0, t)$ under no input ($\vec{u} = \vec{0}$) given a vector of initial conditions \vec{x}_0 .

As stated previously, to control a system is to manipulate its intrinsic behaviour and thereby impose a desired behaviour. The purpose of control is to impose a specific behaviour on the system. The outputs of a system are a measure of its behaviour. A

controller monitors the outputs of a dynamical system and compares them to a desired set of outputs. The error between the two behaviours is used to actively and continuously change the inputs of the system.

Initially, controllers were physical systems such as the regulator on a steam engine. Today, controllers are computer chips containing mathematical algorithms for generating physical signals via motors or other actuators. The standard representation of the mathematical algorithm or control law is a rule or vector function that defines the system's inputs at every instant.

$$\vec{u} = \vec{K}(t, \vec{e}). \quad (9.5)$$

The inputs of the control law are the errors \vec{e} between the measured behaviour and desired behaviour. The error will be discussed in the following section. Like the dynamic model, the controller's rule can be time variant or time invariant. In the following sections only time invariant systems and controllers are considered.

Given the previous descriptions and definitions of system and controller, the purpose of control theory is first, to analyse the state model's intrinsic dynamic behaviour and second, to construct a controller with a control law \vec{K} that imposes a desired dynamic behaviour on the state model.

9.2 Open-Loop and Closed-Loop

When a controller and system are connected in series (Fig. 9.1), the information always flows from the controller to the system. The system does not send any information back to the controller. This is called open-loop. In this situation, the vector \vec{e} is equal to the desired behaviour \vec{y}_c . The control law can be for instance, the inverse model of the system (if the equations are invertible, which is not always the case).

$$\textbf{Open-Loop: } \vec{e}(t) = \vec{y}_c(t), \quad \vec{u}(t) = \vec{g}^{-1}(\dot{\vec{x}}_c - \vec{f}(\vec{x}_c), \vec{x}_c), \quad \vec{x}_c = h^{-1}(\vec{y}_c) \quad (9.6)$$

The drawback of open-loop control is that the controller does not know if the desired path is being followed because of the unilateral information flow direction. In open-loop, the controller does not monitor the system's output. The controller assumes the system to follow the desired behaviour. In a perfect world, this assumption is acceptable and makes sense, the system is behaving exactly as the model predicts. In the real world, even the smallest error will make the system diverge from the desired behaviour. This occurs also in simulation where a controller can be given a desired path and an exact inverse model of the system. Divergence from the path occurs during simulation simply because the numerical solver is imperfect. For instance, MATLAB's precision is $\epsilon = 10^{-16}$ which is far from perfect. Perfection exists only on paper.

Closed-loop is defined as creating an information loop between the controller and system. In closed-loop, the controller monitors the system's outputs (Fig. 9.2). The outputs are fed back to the controller that compares them to the desired outputs. Given the error, the controller corrects, if necessary, the inputs using the control law. The error

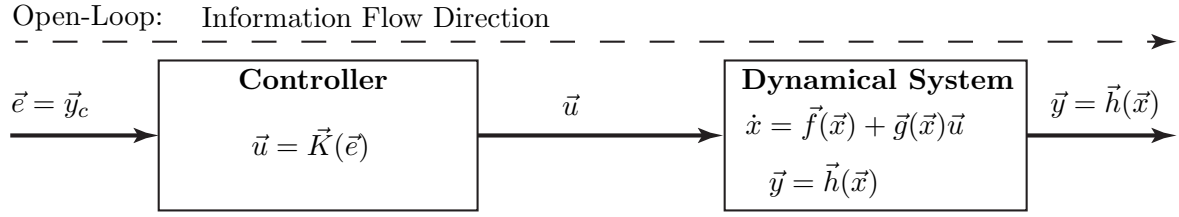


Figure 9.1: *Illustration of the relation between system and controller and the direction of information flow in open-loop as described in section 9.2.*

is always defined as the desired behaviour minus the measured behaviour. This is called negative feedback and is used to reduce the effect of changes in the inputs. The opposite is positive feedback, characterised by exponential growth of the amplitude of the changes in input. As opposed to open-loop, the control law is now a function of this error and not just the desired outputs.

Closed-Loop: $\vec{e}(t) = \vec{y}_c(t) - \vec{y}(t) = \vec{y}_c(t) - \vec{h}(\vec{x}(t)), \quad \vec{u}(t) = \vec{K}(\vec{e}(\vec{y}_c(t), \vec{x}(t))). \quad (9.7)$

The input is function of the states through the measured outputs. The simplest example of closed-loop control is proportional control. The input vector \vec{u} is proportional to the error and the proportionality factor K is called the gain.

Proportional Control: $\vec{u}(t) = K \cdot (\vec{y}_c(t) - \vec{y}(\vec{x})). \quad (9.8)$

The key idea behind closed-loop control is to make the inputs function of the system's dynamic state. If the function is inserted into the the state model, a new system is defined:

$$\dot{x} = \vec{f}(\vec{x}) + \vec{g}(\vec{x})\vec{K}(\vec{y}_c, \vec{x}) = \vec{f}^*(\vec{x}, \vec{y}_c). \quad (9.9)$$

The new model is called the closed-loop state model and has the desired characteristics imposed by the control law. Applied to a real system, closed-loop control defines a new system called the closed-loop dynamical system.

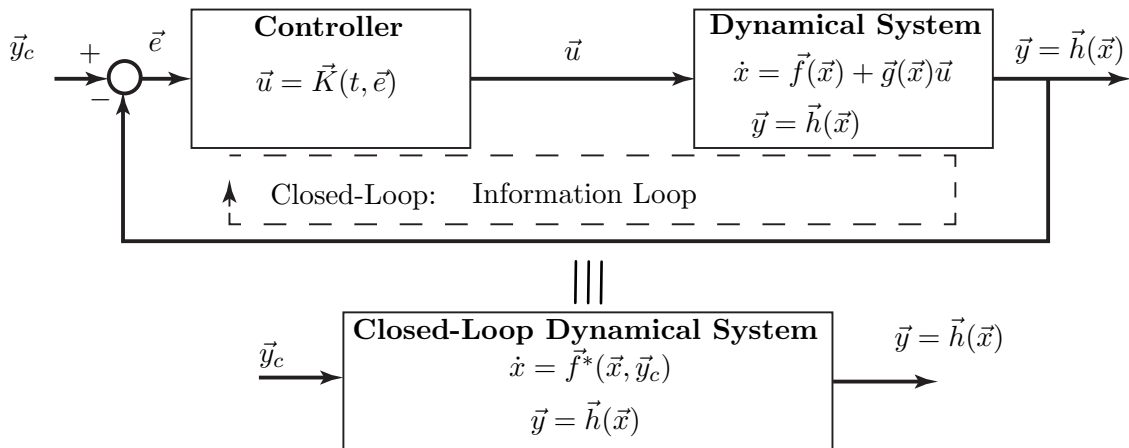


Figure 9.2: *Illustration of the relation between system and controller and the direction of information flow in closed-loop as described in section 9.2.*

The purpose of closed-loop control is to construct a control law that generates the necessary inputs to manipulate the system. The closed-loop behaviour must be as near as possible to the desired behaviour. In simulation, the desired behaviour is generally imposed. Applied to a real system, there remains a difference due to the presence of effects not included in the model. The desired behaviour can be a specific fixed state, in which case the control law is designed for disturbance rejection. The desired behaviour can also be a time-dependent evolution of the state, in which case the control law is designed for trajectory tracking.

A system can also be controlled using multiple feedback loops (Fig. 9.3). This type of control is used for instance to reject disturbances while following a trajectory. The high-level tasks of trajectory planning and tracking are done by an outer feedback loop. The low-level task of disturbance rejection around the trajectory is done by an inner feedback loop. The outer feedback loop generates the corrected trajectory for the inner loop to use as reference. The inner loop corrects the effects of disturbances being applied to the system around the trajectory generated by the outer loop.

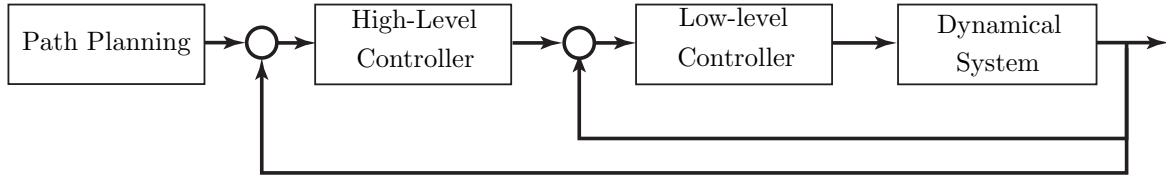


Figure 9.3: Illustration of the multi-feedback loop strategy as described in section 9.2.

9.3 Stability

For any type of closed-loop control, the most indispensable characteristic is stability. *The closed-loop system must be stable.* Stability is in general defined with respect to a certain state called the equilibrium point. For every state model, there are equilibrium states or equilibrium points. These points correspond to dynamic states where the system stops moving. Equilibrium points are fixed points of the state model's mathematical rule and have the following definition.

Definition 25 (Equilibrium Point [153]). *Given a dynamic time invariant system of the form*

$$\dot{x} = \vec{f}(\vec{x}), \quad \vec{x} \in \mathbb{R}^n. \quad (9.10)$$

The equilibrium points are points $\tilde{\vec{x}}$ for which the following holds:

$$0 = \vec{f}(\tilde{\vec{x}}). \quad (9.11)$$

Equilibrium points can be stable or unstable. From a general perspective, an equilibrium point is stable if the system naturally tends to go to that point from any neighbouring point. Oppositely, a system is unstable if it moves away from the point. A system remains at an unstable point, if and only if, it is exactly at the point. If a beam is put upright, it stays upright. However, even the smallest perturbation will make it fall. Stability and instability can be understood in the same way a ball is stable with respect to the bottom of a valley and unstable with respect to the top of a hill (Fig. 9.4). This metaphor applies to almost any problem but is too unspecific to be used directly. For instance, does the ball roll to the bottom of the valley from any arbitrary point? How fast does the ball roll to the bottom of the valley? Thus, stability requires a formal mathematical definition to eliminate any ambiguity.

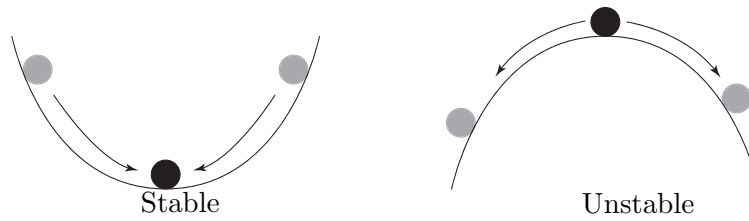


Figure 9.4: *Illustration of stability and instability using the ball metaphor as described in section 9.3.*

The formal definition of stability is called Lyapunov stability (Lyapunov 1892 [136]).

Definition 26 (Lyapunov Stability [153]). *Given a dynamic time invariant system of the form $\dot{x} = \vec{f}(\vec{x})$, an equilibrium point $\tilde{x} = \vec{0}$ and a solution $\mathcal{X}(\vec{x}_0, t)$ starting from \vec{x}_0 . The equilibrium point $\tilde{x} = \vec{0}$ is Lyapunov stable if for any choice of $R > 0$, there exists at least one $r > 0$ such that all solutions starting in the ball of radius r around $\tilde{x} = \vec{0}$, remain in the ball of radius R .*

$$\|\mathcal{X}(\vec{x}_0, t)\|_2, \quad \forall t > 0. \quad (9.12)$$

This definition is specific in that it uses the 2-norm to define the balls of radius r and R . Other norms can also be used. It also clearly defines the notion of neighbourhood around an equilibrium point as a ball defined by a norm.

The above definition of stability is the fundamental definition but is not the most practical definition. To prove a system is stable, one generally uses one of the following theorems that are some of the central theorems of stability in control theory. Both theorems involve a function V called a Lyapunov function.

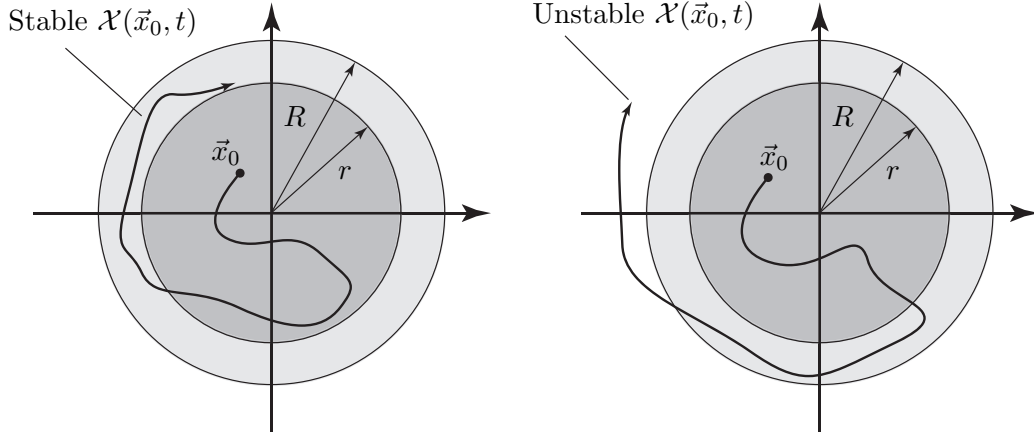


Figure 9.5: Illustration of Lyapunov stability and instability according to definition 26, stated in section 9.3.

Theorem 19 (Local Asymptotic Stability [153]). *If there exists a ball \mathcal{B}_{R_0} such that*

1. $V(\vec{x}) > 0, \forall \vec{x} \in \mathcal{B}_{R_0}, \vec{x} \neq 0$, and $V(\vec{0}) = 0$,
2. $(\frac{d}{dt})V(\vec{x}) < 0, \forall \vec{x} \in \mathcal{B}_{R_0}$,

then $\vec{x} = 0$ is stable. If in addition $(\frac{d}{dt})V(\vec{x}) < 0, \forall \vec{x} \neq 0$ in \mathcal{B}_{R_0} then $\vec{x} = 0$ is asymptotically stable. The function V is called a Lyapunov function.

Theorem 20 (Global Asymptotic Stability [153]). *If there exists a function V such that*

1. $V(\vec{x}) > 0, \forall \vec{x} \neq 0$, and $V(\vec{0}) = 0$,
2. $\|\vec{x}\| \rightarrow \infty, \Rightarrow V(\vec{x}) \rightarrow \infty$,
3. $(\frac{d}{dt})V(\vec{x}) < 0, \forall \vec{x} \neq \vec{0}$,

then $\vec{x} = 0$ is globally asymptotically stable. The function V is called a Lyapunov function.

The strongest form of asymptotic stability is exponential stability. Meaning the asymptotic convergence can be described using a decreasing exponential function of time.

This form of stability is difficult to achieve, especially for systems with nonlinear behaviours.

These theorems are very powerful but are hard to prove. They reduce the proof of stability to finding a single scalar function of the states V . Any candidate for the Lyapunov function is required to satisfy all the points of either theorem 1 or 2. Theorem 2 is harder to prove because it requires the properties to be valid for all $\vec{x} \in \mathbb{R}^n$. The primary difficulty with the Lyapunov function, is that there exists no well defined method for constructing V . Trial and error and intuition are often the only tools.

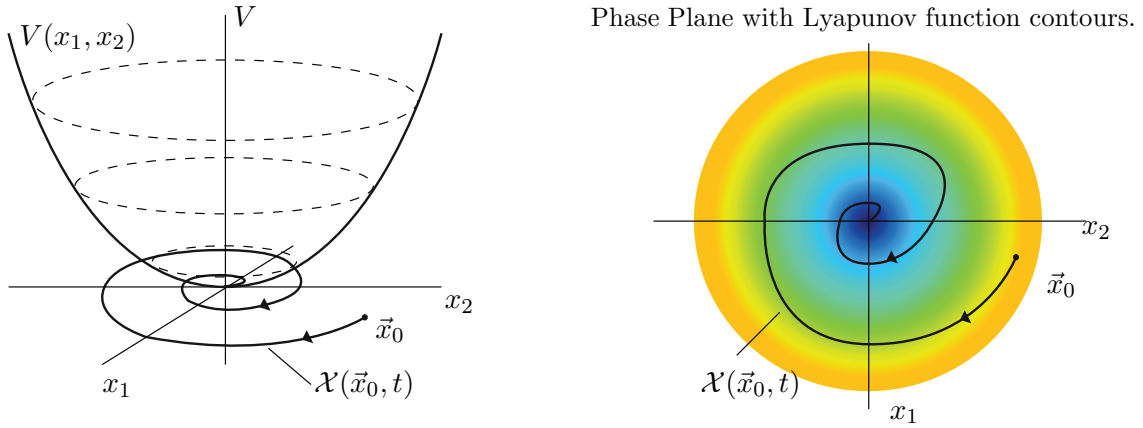


Figure 9.6: Illustration of the Lyapunov function as positive definite function according to theorem 19, stated in section 9.3.

Associated to theorems 1 and 2 is the LaSalle invariance theorem which can be used to identify a region where the system is stable and does not require global stability.

Theorem 21 (LaSalle Invariance Theorem [153]). *Given a function $V(\vec{x}) : \mathbb{R}^n \rightarrow \mathbb{R}$ and a dynamic system $\dot{x} = \vec{f}(\vec{x})$. If it is possible to determine three sets Ω , \mathcal{V} and \mathcal{I} such that:*

- Ω a compact set (closed & bounded) is invariant :

$$\vec{x}_0 \in \Omega \quad \Rightarrow \quad \mathcal{X}(\vec{x}_0, t) \in \Omega, \quad \forall t \geq 0.$$

- In all Ω , the derivative of the function V is less than or equal to zero,

$$\forall \vec{x} \in \Omega \quad \Rightarrow \quad \dot{V}(\vec{x}) := \frac{\partial V}{\partial \vec{x}} \vec{f} \leq 0.$$

- The set \mathcal{V} is a subset containing points in Ω for which the derivative of V is equal to zero.

$$\mathcal{V} = \{\vec{x} \in \mathbb{R}^n | \text{s.t. } \vec{x} \in \Omega, \dot{V}(\vec{x}) = 0\}.$$

- The set \mathcal{I} is the largest invariant set, subset of \mathcal{V}

$$\mathcal{I} \subseteq \mathcal{V}, \quad \forall \vec{x} \in \mathcal{I} \quad \Rightarrow \quad \mathcal{X}(\vec{x}_0, t) \in \mathcal{I}, \quad \forall t \geq 0.$$

Thus, for any given initial condition $\vec{x}_0 \in \Omega$, the solution asymptotically converges to \mathcal{I} ,

$$\vec{x}_0 \in \Omega \quad \Rightarrow \quad \mathcal{X}(\vec{x}_0, t) \rightarrow \mathcal{I}, \quad t \rightarrow \infty.$$

The invariant set \mathcal{I} in this theorem can be a single point, a finite collection of points or an infinite set of points in which case the invariant set is called a limit cycle. The size of the region in which a system is stable is called the domain of attraction.

There are a number of other results related to stability including bounded-input, bounded-output stability (BIBO stability) and Nyquist's stability theorem. These points are not discussed because they are not used in this dissertation.

9.4 Linear State Feedback Control

State feedback control is defined for systems where all the states are observed and used by the controller. In this type of control, the goal is to stabilise the system at the equilibrium point $\tilde{\vec{x}} = \vec{0}$, $\tilde{\vec{u}} = \vec{0}$ ($\vec{0}$ is always an equilibrium under the appropriate coordinate change).

$$\begin{aligned} \dot{\vec{x}} &= \vec{f}(\vec{x}) + \vec{g}(\vec{x})\vec{u}, \\ \vec{y} &= \vec{x}. \end{aligned} \tag{9.13}$$

The control law is a smooth vector function of the system's states.

$$\vec{u} = \vec{K}(\vec{x}) \tag{9.14}$$

The most well known example of state feedback control is linear state feedback. The dynamic state model is linear and is defined by:

$$\begin{aligned} \dot{\vec{x}} &= \mathbf{A}\vec{x} + \mathbf{B}\vec{u}, \\ \vec{y} &= \vec{x}, \\ \vec{x} \in \mathbb{R}^n, \quad \vec{u} \in \mathbb{R}^m, \quad \mathbf{A} \in \mathbb{M}_{n \times n}(\mathbb{R}), \quad \mathbf{B} \in \mathbb{M}_{n \times m}(\mathbb{R}) \end{aligned} \tag{9.15}$$

A linear system ($\dot{\vec{x}} = \mathbf{A}\vec{x}$) is stable without control if the eigenvalues of the matrix \mathbf{A} have negative real parts. The matrix \mathbf{A} is said to be Hurwitz [40].

$$\mathbf{A}\vec{x} = \lambda\vec{x}, \quad \text{with} \quad \Re(\lambda) < 0. \tag{9.16}$$

In linear state feedback, the control law is defined by a linear function of the form:

$$\vec{u} = -\mathbf{K}\vec{x}, \quad \text{where} \quad \mathbf{K} \in \mathbb{M}_{m \times n}(\mathbb{R}). \tag{9.17}$$

The closed-loop state model is defined by:

$$\dot{\vec{x}} = \mathbf{A}\vec{x} + \mathbf{B}\mathbf{K}\vec{x} = \tilde{\mathbf{A}}\vec{x}. \quad (9.18)$$

The values of the gain matrix \mathbf{K} are found such that the closed-loop matrix $\tilde{\mathbf{A}}$ is Hurwitz. The appeal of this type of control is that there exists a wide range of methods for computing the gain matrix [1, 115, 134, 150, 198]. The method can even be applied to non linear systems using the first order Taylor expansion around the equilibrium point $\vec{x} = \vec{0}$.

$$\vec{f}(\vec{x}) = \underbrace{\vec{f}(\tilde{\vec{x}})}_{=0} + \left. \frac{\partial \vec{f}}{\partial \vec{x}} \right|_{\vec{x}=\tilde{\vec{x}}} (\vec{x} - \tilde{\vec{x}}) + \text{higher order terms}, \quad (9.19)$$

Given a nonlinear system and an equilibrium point $\tilde{\vec{x}} = \vec{0}$, $\tilde{\vec{u}} = \vec{0}$. The model is linearised around the equilibrium point using the Taylor expansion. The matrices \mathbf{A} and \mathbf{B} of the linearised model are defined by:

$$\mathbf{A} = \left(\frac{\partial \vec{f}}{\partial \vec{x}} + \frac{\partial \vec{g}}{\partial \vec{x}} \tilde{\vec{u}} \right) \bigg|_{\vec{x}=\tilde{\vec{x}}}, \quad \mathbf{B} = \vec{g}(\tilde{\vec{x}}) \quad (9.20)$$

Once the linearised model is obtained, the gain matrix \mathbf{K} is obtained using any one of the possible methods. The drawback is that the controller is only valid locally around the equilibrium point because the linear model is itself a local model. With regards to the LaSalle invariance theorem the set Ω is relatively small. However, this method does work well on a large number of systems and is therefore very popular. Furthermore, one can compute gain matrices for linearised forms of the model around different points. This method is used in aircraft control and is called gain scheduling.

There are two important properties related to state feedback in general. They are most easily stated in the context of linear state feedback. The first is controllability which is the property that all the states can be modified using the inputs. The second property is observability which is the property that all the states can be observed given the outputs. For state feedback to work, the system must be controllable and observable.

Definition 27 (Controllability). *The state model (9.15) or the pair (\mathbf{A}, \mathbf{B}) is said to be controllable if for any initial condition \vec{x}_0 and any final state \vec{x}_1 , there exists an input that transfers \vec{x}_0 to \vec{x}_1 in a finite time. Otherwise (9.15) or (\mathbf{A}, \mathbf{B}) is said to be uncontrollable.*

Definition 28 (Observability). *The state model (9.15) is said to be observable if for any unknown initial state \vec{x}_0 , there exists a finite time $t_1 > 0$, such that the knowledge of the input \vec{u} and the output \vec{y} over $[0, t_1]$ suffices to determine uniquely the initial state \vec{x}_0 . Otherwise (9.15) is said to be unobservable.*

It is not always necessary for a system to be controllable or observable for a control strategy to successfully stabilise the system. A system that is only partially controllable is stable if the uncontrollable part is stable. To determine if a system is controllable or observable, it is sufficient to compute the ranks of the controllability \mathbf{G} and observability \mathbf{O} matrices, constructed using the pairs (\mathbf{A}, \mathbf{B}) and (\mathbf{A}, \mathbf{C}) respectively [40]. The controllability and observability matrices of a system with n states are defined by:

$$\mathbf{G} = (\mathbf{B} \quad \mathbf{AB} \quad \dots \quad \mathbf{A}^{n-1}\mathbf{B}), \quad \mathbf{O} = \begin{pmatrix} \mathbf{C} \\ \mathbf{CA} \\ \vdots \\ \mathbf{CA}^{n-1} \end{pmatrix} \quad (9.21)$$

A system with n states is controllable if $\text{rank}(\mathbf{G}) = n$. A system is observable if $\text{rank}(\mathbf{O}) = n$. For systems with many states, these conditions can be difficult to evaluate due to numerical instability. Both the controllability and observability matrices use the system matrix at the power of $n - 1$. This can quickly lead to numerical problems.

A final remark concerning control is the notion of observer. If the full state vector cannot be measured, an observer is used to reconstruct the missing states from the measured states. The model of the system and the measured states are used to dynamically reconstruct the missing states and build an observed state vector $\hat{\vec{x}}$. The symbol \wedge indicates observed state vector. This procedure works as long as the states are observable through the measured outputs \vec{y} . The simplest form of observer is called a Luenberger observer. The observed output $\mathbf{C}\hat{\vec{x}}$ is compared to the measured output \vec{y} . The error is used to make the observed states converge to the values of the exact states. The convergence is imposed through the following dynamic equation.

$$\dot{\hat{\vec{x}}} = \mathbf{A}\hat{\vec{x}} + \mathbf{BK}\hat{\vec{x}} + \mathbf{L}(\vec{y} - \mathbf{C}\hat{\vec{x}}), \quad \mathbf{L} \in \mathbb{M}_{n \times p}(\mathbb{R}). \quad (9.22)$$

The observer matrix \mathbf{L} is defined such that the error between the exact states and observed states satisfies the dynamics:

$$\dot{\vec{e}} = (\mathbf{A} - \mathbf{LC})\vec{e}, \quad \vec{e} = \hat{\vec{x}} - \vec{x}. \quad (9.23)$$

For an observer to successfully provide the missing information on the system's state, the matrix $(\mathbf{A} - \mathbf{LC})$ must be Hurwitz and have faster converging dynamics than the control law.

This chapter presented a very brief, very condensed introduction to control theory. The concepts that are used in chapter 10 are primarily Lyapunov stability, observability and the idea of closed-loop control.

Chapter 10

Musculoskeletal Stability through Joint Stiffness Control

10.1 Introduction

The previous chapters of the dissertation have presented a musculoskeletal model of the shoulder and two methods used to deal with its kinematic redundancy and overactuation. The model is being developed for the purpose of studying osteoarthritis, the most common form of arthritis that causes frequent excessive loading of the articulations leading to their premature deterioration [27]. The model has been implemented and used to estimate the force in the glenohumeral articulation, the most affected articulation of the shoulder. Excessive stress is the observed cause of osteoarthritis. However, it has been hypothesised that excessive stress is the result of an underlying neuromuscular dysfunction. Proving or disproving this hypothesis represents the following challenge. Given the complexity of neuromuscular control, where does one begin to search for a cause?

To understand the magnitude of the challenge, consider the following points. The human nervous system is the result of tens of thousands of years of evolution. It has developed into a complex, versatile and highly efficient system capable of managing every process in our body, including the control of our musculoskeletal system [93, 177]. It is only recently that technology has provided us with the tools to analyse in detail certain aspects of the brain's function. The nervous system is of such complexity that the amount of information required to analyse only a portion of its function is already more than a personal computer can handle. With the almost exponential growth of computing power over the last decade, we have constructed more complex and more accurate models that explain the nervous system's functions down to the molecular level [41]. However, at present any analysis of the nervous system still constitutes a challenging task.

A first observation is that any neuromuscular dysfunction creating a deterioration of the musculoskeletal system will most likely be found in the part of the nervous system controlling the musculoskeletal system. This particular task of our nervous system is called human motor control.

Human motor control is achieved in part through proprioception and coordination [177]. Proprioception is the process where the nervous system integrates signals sent by the body's sensors. The signals include information regarding the body's state. The nervous system then coordinates the body's movements by sending activation signals to the muscles to produce force. Thus, human motor control can be understood as control in the sense of modern control theory (cf. chapter 9). There is an information loop between the body's musculoskeletal system and the motor controller (nervous system).

The current leading paradigm for explaining and modelling human motor control is the modern control algorithm known as model predictive control (MPC) [112, 119, 193]. Surprisingly human motor control achieves stability through a number of mechanisms than do the current algorithms developed in control theory [133, 177]. Implementations of modern control theory generally use fast computers communicating with fast reacting actuators at nearly the speed of light (speed at which an electrical signal travels down a wire). The goal being to achieve a near continuous process given that the dynamic behaviour of many dynamical systems is continuous and fast reacting. In contrast, the human nervous system communicates with the body at nearly the speed of sound and involves continuous and discrete processes in its function. Muscles are slow reacting actuators although the dynamics of the musculoskeletal system are faster than the nervous system's reaction time [177]. The subject of how stability of the musculoskeletal system is maintained, in the sense of modern control theory, remains open to controversy [133].

To focus the search for a possible neuromuscular dysfunction, this chapter investigates a particular mechanism that is known to be used in human motor control. The mechanism is called joint stiffness control through antagonistic muscle co-contraction [97, 98, 160]. The topology of the musculature is such that certain muscles act as opposites to other muscles. The muscles are said to be antagonistic. When one muscle contracts, the other muscle is distended and vice versa. It is known that stability of the musculoskeletal system is partly achieved by continuously activating or co-contracting antagonistic muscles or muscle groups [177]. The co-contraction confers more or less stiffness the body's joints, contributing to their stability and thereby to the stability of the entire system. This mechanism is of particular relevance to the investigation of osteoarthritis given that it involves the joints directly.

The goal of this chapter is therefore the investigation of joint stiffness control by antagonistic muscle co-contraction using the model of a cable-driven pendulum. The use of such a model is relevant because in chapter 4, the mathematical structure of models of musculoskeletal systems and cable-driven systems are shown to be almost identical. The investigation uses a simple description of human motor control that defines a certain number of elements regarding the signals exchanged by the nervous and musculoskeletal systems [196]. A more detailed comparison of human motor control and modern control of a pendulum is presented followed by a quick overview of the different mechanisms used by human motor control. The model of the cable-driven pendulum is then presented. Joint stiffness control by antagonistic muscle co-contraction is defined in a formal mathematical context and proven to be a stabilising mechanism in the sense of Lyapunov stability. A control strategy based on joint stiffness control is then formulated and implemented on a physical system. A hypothesis regarding the cause of osteoarthritis is proposed and discussed using the results of the implementation.

10.2 Stability by Antagonistic Muscle Co-contraction

10.2.1 Human Motor Control

The following paragraphs give a brief, simplified overview of the nervous system's anatomy and the physiology of human motor control. The presentation is based on the descriptions found in the following references [85, 107, 141, 177, 196]. Complete presentations can be found in closed-form in the literature [15, 45, 110].

The primary elements of human motor control are the central nervous system (CNS), consisting of the brain and spinal cord, and the peripheral nervous system (PNS) consisting of the nerve cells or neurones emanating from the spinal cord towards other parts of the body (Fig. 10.1). The CNS is responsible for integration and processing of the signals received from the PNS and the coordination of the entire body's activity. The PNS is responsible for proprioception and transmitting signals between the CNS and the other parts of the body. The somatic nervous system (SNS) is the part of the PNS connecting the CNS to the musculoskeletal system. The brachial plexus is the SNS nerve bundle exiting the spinal cord and traveling down the upper limbs. The lumbar plexus is the SNS nerve bundle existing the spinal cord and traveling down the lower limbs.

The building block of the nervous system is the neuron that acts as a signal transmitter and processor. The two main functions of a neuron are to transmit and receive information from other types of cells through sensory receptors and to transmit and receive information from other neurons. The connection between two nerve cells is called a synapse (Fig. 10.1). If a neuron is compared to a tree, then the synapses are found both at the tip of the branches as well as at the tip of the roots. The cell body containing the nucleus would be between the trunk and the roots. The axon is the trunk emanating from the cell body. At the end of the axon are dendrites consisting of smaller branches with the synapses at the tip. Axons are what allow neurons to be extremely long and connect different parts of the body using a single cell.

The transmission of signals within the nervous system is achieved by an action potential. A chemical process creates a potential difference traveling down the axon like a wave. The direction in which the wave travel's depends on the signal's origin. The axons of a neuron are surrounded by a layer of myelin, designed to improve conductivity of the axon given the resistive nature of the axons environment. Neurons can be classified into three groups, based on the direction in which they transmit signals.

- afferent neurons: transmit signals from parts of the body to the spinal cord.
- efferent neurons: transmit signals from the spinal cord to other parts of the body.
- interneurons: found in the entire CNS and do all the integrating and processing.

The nervous system is such that the signals decussate. Meaning that signals coming from the left side of the body cross over to the right side of the CNS and vice versa.

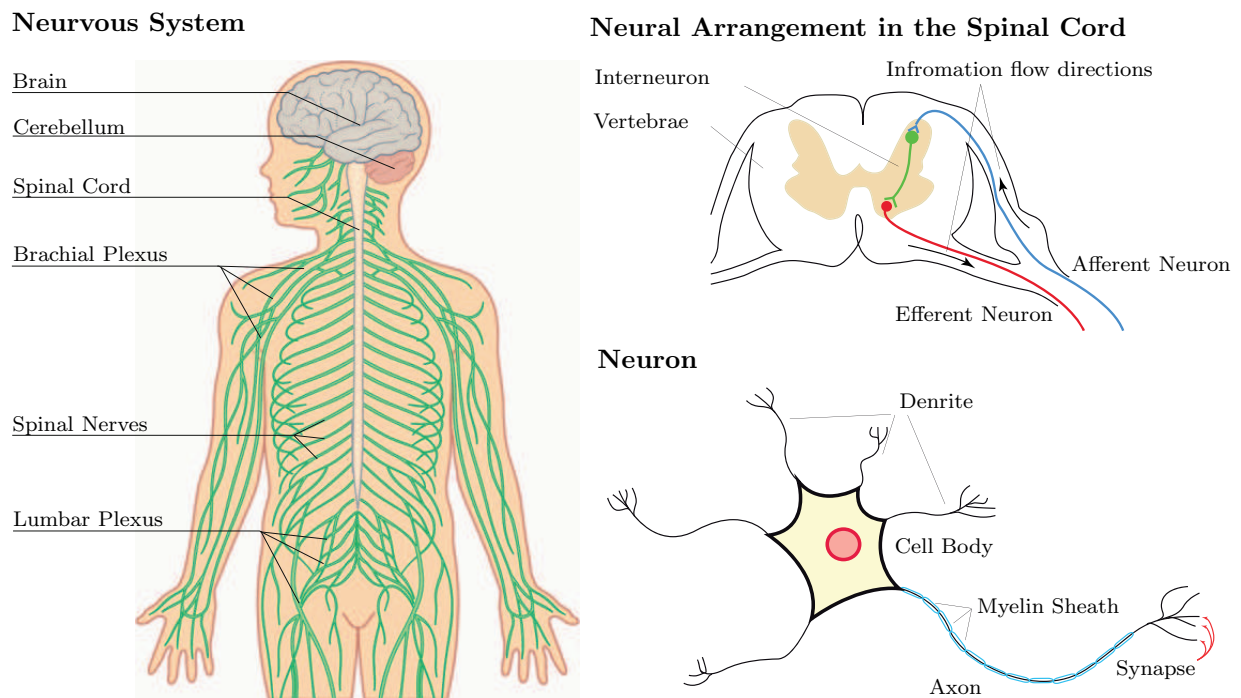


Figure 10.1: *Illustration of the nervous system. The arrangement of interneurons, afferent neurons and efferent neurons at the spinal cord level and the structure of a neuron as described in section 10.2.1.*

The brachial plexus stems from the C5 vertebrae to the T1 vertebrae of the spinal cord. Each muscle is innervated by a group of motor neurons known as motor pools. A motor neuron together with the muscle fibre it innervates is called a motor unit. Each muscle fibre is innervated by a single motor neuron but a motor neuron can connect to multiple muscle fibres. There exist two types of motor neurons. There are alpha-motor neurons (α -motor neurons) that connect to extrafusal muscle fibres and there are gamma-motor neurons (γ -motor neurons) that connect to intrafusal motor fibres (Figure 10.2). The extrafusal fibres are more numerous and give the muscle its strength. Intrafusal muscle fibres are more sensitive to changes in a muscle's length. There is a third type of neuron called a sensory neuron relaying information on a muscle's state back to the spinal cord. Sensory neurons connect to intrafusal muscle fibres by wrapping around them creating muscle spindles. They also connect to the tendon part of the muscle through the golgi tendon organs (GTO).

Human motor control is achieved in part through the use of α -motor neurons, γ -motor neurons and sensory neurons (Fig. 10.3). α -motor neurons transmit activation level signals from the CNS to the extrafusal muscle fibres telling the fibres to generate a certain amount of force within the muscle's strength limits (cf. chapter 2). This defines the muscle fibre's activation level a between 0 and 1. Sensory neurons attached to the golgi tendon organs measure the muscle's tension f which is also an indirect measure of its activity. Given that intrafusal muscle fibres are sensitive to their length, the sensory neurons measure the muscle's length l through the muscle spindles. Furthermore, γ -motor neurons transmit sensitivity level signals s from the CNS to the intrafusal muscle

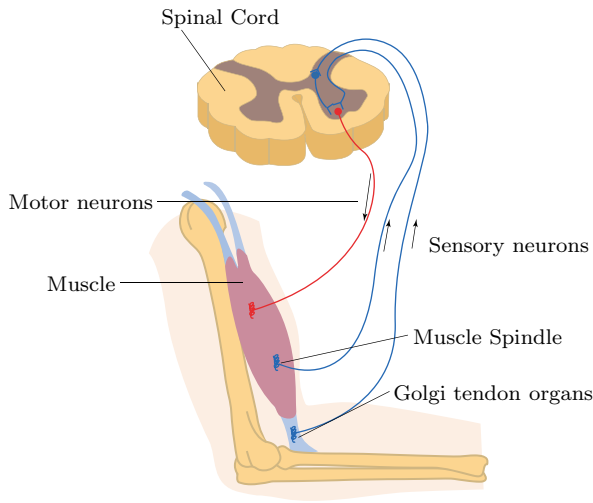
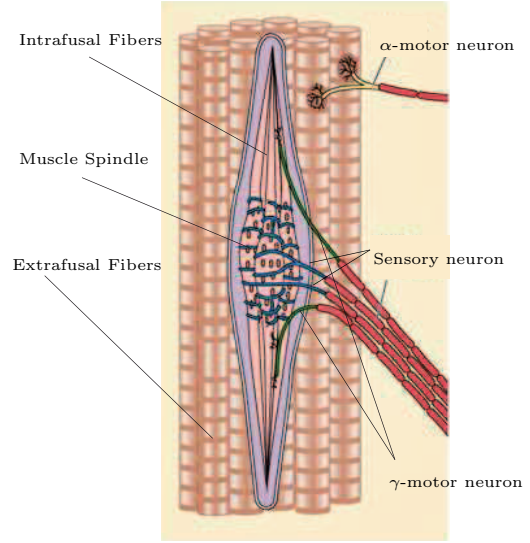
Motor Units**Muscle Spindles**

Figure 10.2: *Illustration of the neuromuscular communication system. Extrafusal & intrafusal muscle fibers with innervation & muscle spindles as described in section 10.2.1.*

fibres. By modulating the sensitivity of the intrafusal muscle fibres, the sensory neurons also measure the rate of change in muscle length \dot{l} . Thus, it is assumed that the CNS measures each skeletal muscle's state in terms of tension, length and rate of change in length. These three states are only part of what the CNS measures. This chapter only considers the muscle's state in terms of (a, l, \dot{l}) because they are the most relevant from a musculoskeletal modelling perspective.

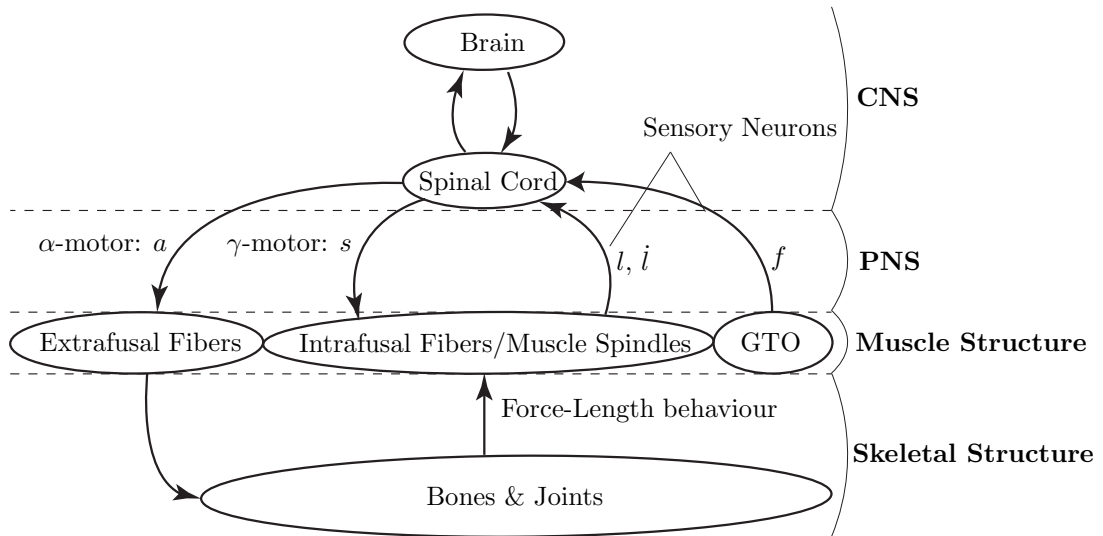


Figure 10.3: *Illustration of the human nervous system and motor control as described in section 10.2.1.*

10.2.2 Stability in Human Motor Control

Human control does agree with modern control theory as defined in chapter 9. There is feedback between the musculoskeletal system and the nervous system. The nervous system monitors the outputs of the musculoskeletal system (f, l, \dot{l}) and changes the input signals (a, s) to manipulate the musculoskeletal system. Furthermore, the musculoskeletal system can be represented by a state model. In chapter 4, the dynamic behaviour of a musculoskeletal shoulder model is presented in terms of the equations of motion. These equations can be used to construct a state model. However, the nervous system does not control our bodies in the way computer chips control physical systems [133, 177]. There is no control law that is a function of the error between desired behaviour and measured behaviour.

To illustrate the differences between human motor control and conventional control, consider the example of a pendulum which is a long body rotating with one degree of freedom around an axis through a revolute joint. This metaphor is relevant because the human body, when upright, can be seen as a pendulum with the rotation axis at our ankles [72, 132, 212]. The pendulum's states are its angle and angular velocity and it is actuated by applying a torque to the pendulum's rotation axis (Fig 10.4). We use our muscles of the entire lower limb to stabilise our bodies. The pendulum's state model is defined by:

$$\begin{aligned} \dot{x}_1 &= x_2, & x_1 &= \vartheta, & x_2 &= \dot{\vartheta} \\ \dot{x}_2 &= -\frac{g_e}{l} \sin(x_1) + cu_1, & c &= cte. \end{aligned} \quad (10.1)$$

A measure of the pendulum's dynamic behaviour is its length. The pendulum's length appears in a parameter called the time constant τ . This value defines the speed at which the pendulum reacts to changes in input and is defined by:

$$\tau = 2\pi\sqrt{l/g_e}, \quad (10.2)$$

where l is the pendulum's length and g_e is the earth's gravitational constant.

For a human being the time constant is between 2.5 and 3 seconds. If a computer is used to control a pendulum with such a time constant, the sampling rate (rate at which the pendulum's state is measured and at which the input signals are updated) needs to be 50 Hz or higher. The time constant of the electric motor being used is approximately 0.002 seconds and the rate at which the signals travel down the wires is near the speed of light. Our nervous system does the same job with a sampling rate between 10 and 30 Hz. A muscle's time constant is roughly 0.04 seconds and the information travels at the speed of sound (~ 80000 times slower). Muscles and electric motors are controlled in a similar way. In human motor control, information is transmitted through the nervous system in waves and the signal is binary. Muscles receive the activation level signals as on/off signals at different frequencies. This is very similar to pulse width modulation (PWM), used to control electric motors. Furthermore, the dynamic behaviour of both muscles and motors can be represented using first order dynamic models. The difference between a muscle and motor is that muscle's react 10 times slower to a step input (step response)(Fig. 10.4).

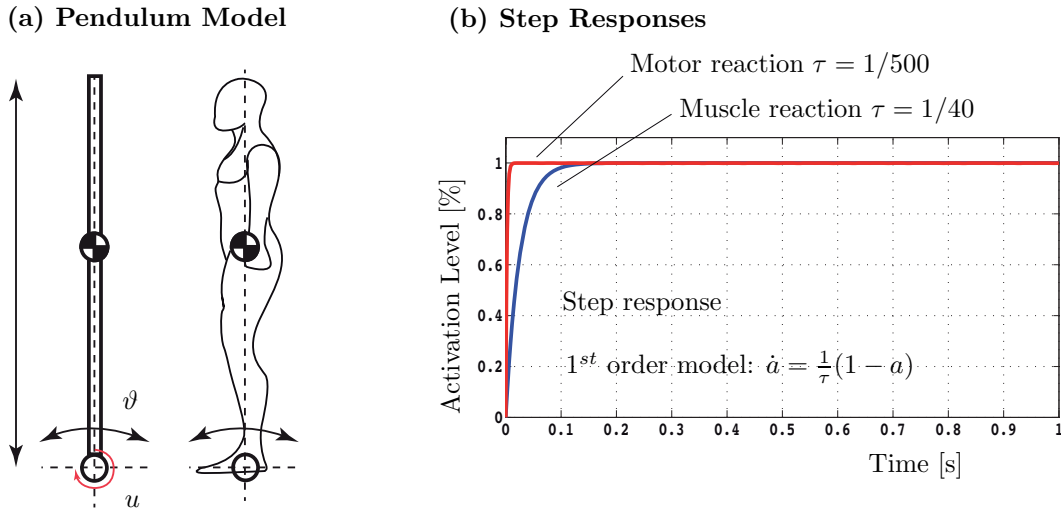


Figure 10.4: (a) Illustration of the pendulum metaphor for human postural control. (b) Example of muscle and electric motor reaction times. Graph obtained using 1st order model with two time constants (Section 10.2.2).

To stabilise our body, human motor control uses multiple mechanisms. This presentation distinguishes between mechanisms that are actively controlled from mechanisms that are passive. For instance, muscle activation is actively controlled while the force-length behaviour of muscles is a passive property helping to stabilise the system (cf. chapter 2). A first mechanism is the use of multiple control loops called reflex loops [177]. These loops, once set in place, never change and are the fastest reacting elements in human motor control. Reflex loops are used to compensate for small perturbations around the current set point and ensure that motion occurs smoothly. There are two reflex loops or reflex pathways. Long-loop reflex pathways traveling into the brain and can be actively regulated. Short-loop reflex pathways traveling to the spinal cord. Short-loop reflexes are passive in that they are not regulated.

A second mechanism is the use of synergies that are groups of neurons that share the same task. An individual neuron processes information slowly. Millions of neurons put together process the same information much faster. Thus, the brain has been called the "most powerful computer in the world" because of its ability to parallel compute on a massive scale. This mechanism can be actively changed to deal with new situations. It can be viewed as a low level or unconscious form of learning and has been modelled using artificial neural nets (ANN) [19, 176, 187].

A third mechanism is motor programs that are neurons designed to activate muscles according to specific patterns. In terms of control, motor programs are executed in open-loop. Once set in place, these patterns never change and produce ballistic movements [133]. Ballistic movements are in general fast movements over a short period of time. The term ballistic is understood as once the movement is initiated by the pattern it will follow a known trajectory similar to a bullet being fired from a gun.

A fourth mechanism is the use of models [177]. The information collected by the sensory neurons is processed by the brain and is used in either forward or inverse models of parts of the body. This mechanism is much slower but gives human motor control the ability

to predict the future inputs. In modern control theory, this is known as a priori control. A model of the system is used to compute the input producing the desired behaviour. Thus, the controller need only correct around the desired input.

The mechanism that will be discussed throughout this chapter is joint stiffness control through antagonistic muscle co-contraction [177, 196]. The human nervous system changes the stiffness of the joints to adapt to its environment using the muscles. This mechanism is observed in hopping or when running over uneven terrain. The stiffness is changed through the control of an antagonist muscle structure. The muscles work against each other. By contracting muscles at different activity levels, the joint stiffness can be varied.

10.2.3 Model of a Cable-Driven Pendulum

This section presents the model of a cable-driven pendulum. The model is relevant to the present discussion, given the use of a pendulum model in the previous section to discuss human motor control. Furthermore, the model constitutes a very simplified model of a shoulder. The pendulum can be seen as the humerus rotating around the glenohumeral joint in the sagittal plane. Lastly, models of cable-driven mechanisms are almost identical to models of musculoskeletal systems. Thus, the results obtained from the cable-driven system can be transposed to musculoskeletal systems.

The system is a pendulum of length l (Fig. 10.5). The pendulum rotates around an axis, normal to the xy plane, placed at the origin O_0 . The pendulum is body \mathcal{B}_1 and the frame is the carrier body \mathcal{B}_0 . The rotation is defined by the angle ψ . The position of any point $S_{0,1}$ on the pendulum is defined by:

$$S_{0,1} : \vec{s}_{0,1} = \mathbf{R}_{1,0}\vec{s}_1, \quad \mathbf{R}_{1,0} = \begin{pmatrix} \cos(\psi) & -\sin(\psi) \\ \sin(\psi) & \cos(\psi) \end{pmatrix}. \quad (10.3)$$

There are four cables attached to the pendulum at four points $S_{1,i}$ on a rectangular plate mounted on the pendulum. The plate is mounted at a distance l_p from the rotation axis and has dimensions $w \times b$. At the opposite end, the cables are attached to four pulleys, centred at $C_{0,i}$. The rotation of each pulley is defined by an angle ϑ_i . The pulleys are of radius r_p . The pulley attachment points $P_{0,i}$ are located on the top of each pulley. There is a disk of radius r centred at the origin, to keep the cables from intersecting the pendulum's rotation axis. The rotation of each pulley is defined by an angle ϑ_i . For the pendulum angle and pulley angles, positive rotation is counterclockwise.

At this point, only the dynamic behaviour of the pendulum is considered. The cables are considered to be taught, massless, frictionless cables wrapping over the pulleys and central disk. The pendulum has a mass M_p and an inertia \mathcal{I}_p (Fig. 10.8). The pendulum's centre of gravity is located at a distance l_g from the rotation axis. The pendulum is considered to be subject to a viscous friction b_p . The dynamic model is built using the Euler-Lagrange equation. The generalised coordinates of the model are the pendulum angle ψ and angular velocity $\dot{\psi}$ with respect to the vertical axis. The equation of motion

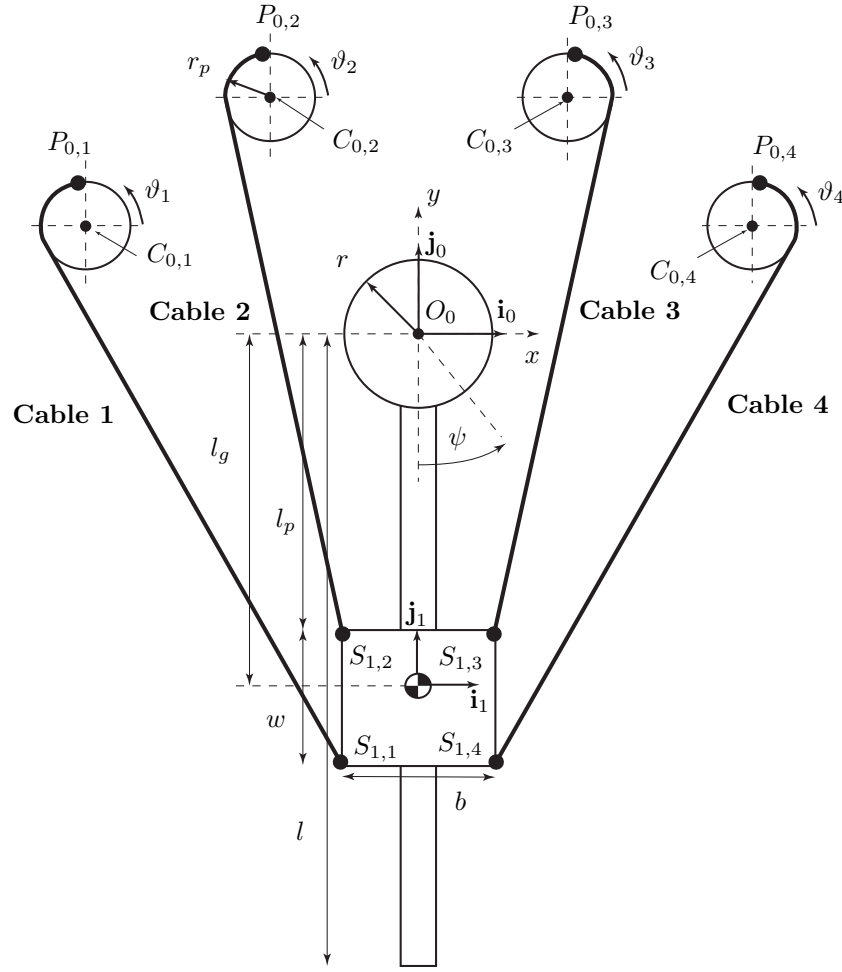


Figure 10.5: *Illustration of the geometry of the cable-driven pendulum system as described in section 10.2.3.*

associated to the model is defined by;

$$\ddot{\psi} = \frac{\left(-b_p \dot{\psi} - M_p g_e l_p \sin(\psi) + \mathbf{W}(\psi) \vec{f}\right)}{(\mathcal{I}_p + M_p l_p^2)} = -A \sin(\psi) - B \dot{\psi} + C \mathbf{W}(\psi) \vec{f}, \quad (10.4)$$

where the vector \vec{f} is the vector of cable tensions. The constants A , B and C are all strictly positive. The matrix $\mathbf{W}(\psi)$ is the 4×1 cable moment-arms matrix. The moment-arms of each cable are defined with respect to the pendulum's axis of rotation. There is a single degree of freedom and therefore, there is a single moment-arm per cable. The moment arm is a vector along the z -axis parallel to the pendulum's rotation axis.

The geometry of the cables is defined by the configuration of the pendulum. The cables are assumed to always be taught. Depending on the configuration of the pendulum, a cable can have two configurations (Fig. 10.6).

- Configuration I: the cable wraps only around the pulley.
- Configuration II: the cable wraps around the pulley and around the central disk.

The geometric configuration \mathcal{C}_i of a cable is defined by a set of points. The first point is the origin $P_{0,i}$, the second point $G_{0,i}$ is when the cable leaves the pulley. For configuration I, there is a third point $S_{1,i}$ where the cable attaches to the pendulum. For configuration II, there are three additional points $H_{0,i}$, $T_{0,i}$ and $S_{1,i}$. The points $H_{0,i}$ and $T_{0,i}$ define the initial and final contact points between the cable and central disk. The location of all the points are computed using planar geometry and a cable's geometry is defined by one of the following set of points:

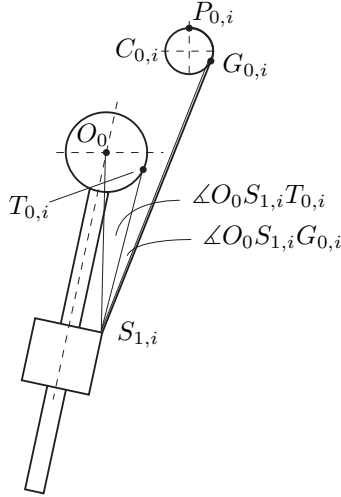
$$\mathcal{C}_{i,I} : \{P_{0,i}, G_{0,i}, S_{1,i}\}, \quad \text{or} \quad \mathcal{C}_{i,II} : \{P_{0,i}, G_{0,i}, H_{0,i}, T_{0,i}, S_{1,i}\}.$$

The two configurations can be identified based on an angle criteria. For any given configuration of the pendulum, the lines $S_{1,i}O_0$, $S_{1,i}G_{0,i}$ and $S_{1,i}T_{0,i}$ are defined, regardless of the wrapping configuration. The following condition on the angles between these lines differentiates between the two cases.

$$\begin{aligned} \text{Configuration I: } & \angle OS_{1,i}T_{0,i} < \angle OS_{1,i}G_{0,i}, \\ \text{Configuration II: } & \angle OS_{1,i}T_{0,i} \geq \angle OS_{1,i}G_{0,i}, \end{aligned} \tag{10.5}$$

This condition differentiates between the two configurations as long as the pendulum remains within the bounds $\psi \in [-\frac{\pi}{2}, \frac{\pi}{2}]$. The pendulum's work space is $|\psi| < 75^\circ$. The configuration of the pulleys physically blocks the pendulum. At an angle $\psi = \pm 75^\circ$ the pendulum touches the pulleys.

Configuration I: Not wrapped



Configuration II: Wrapped

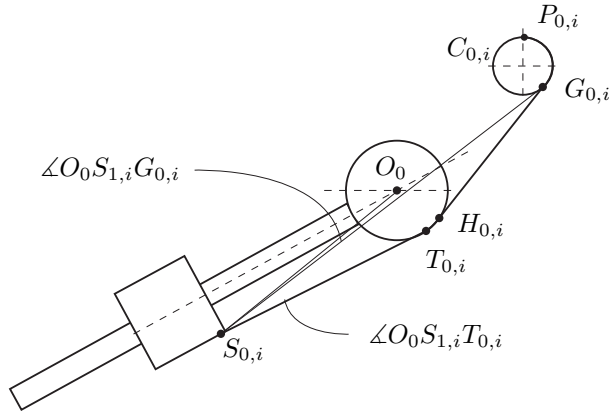


Figure 10.6: *Illustration of the two wrapping configurations and the angular differentiation criterion as described by (10.5).*

The attachment points $P_{0,i}$ are considered to be fixed. The length of each cable is dependent on the angle of the pendulum ψ : $L_i = L_i(\psi)$. The length is computed explicitly using the pendulum's angle. The geometry of the cable is computed, knowing the configuration $\mathcal{C}_{i,I}/\mathcal{C}_{i,II}$ and the length is obtained by adding the length of the segments. For instance:

$$L_i = \|S_{1,i}T_{0,i}\| + l_a(T_{0,i}H_{0,i}) + \|H_{0,i}G_{0,i}\| + r_p l_b(G_{0,i}P_{0,i}). \tag{10.6}$$

The functions $l_a(\cdot)$ and $l_b(\cdot)$ are the lengths of the circular arcs. The action of each cable on the pendulum is defined by its moment-arm (Fig. 10.7). For configurations I and II, the moment-arm vector of a cable is defined by (only the z -axis component is non-zero):

$$\mathcal{C}_{i,I} : \vec{c}_{0,i} = \vec{r}_{0,I,i} \times \vec{b}_{0,I,i}, \quad \mathcal{C}_{i,II} : \vec{c}_{0,i} = \vec{r}_{0,II,i} \times \vec{b}_{0,II,i}. \quad (10.7)$$

The vector $\vec{r}_{0,I,i}$ is the vector from O_0 to $S_{1,i}$. The vector $\vec{r}_{0,II,i}$ is the vector from O_0 to $H_{0,i}$. The vector $\vec{b}_{0,I,i}$ is the unit vector parallel to the line from $S_{1,i}$ to $G_{0,i}$. The vector $\vec{b}_{0,II,i}$ is the unit vector parallel to the line from $H_{0,i}$ to $G_{0,i}$. For the two centre cables attached to pulleys two and three, the moment-arm becomes constant when the cable wraps around the centre disk.

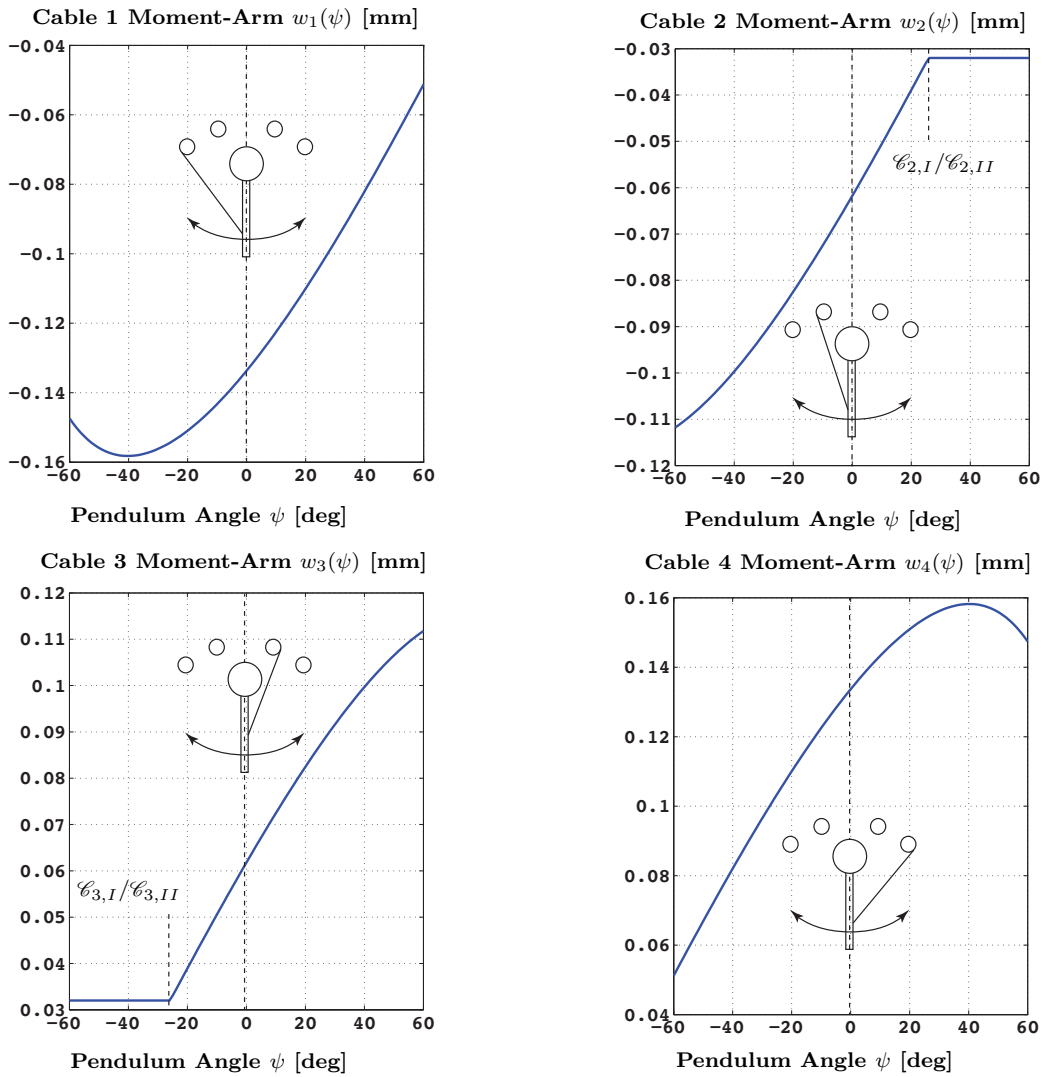


Figure 10.7: The z -axis cable moment-arms $w_i(\psi)$ for $\psi \in [-60^\circ, 60^\circ]$ computed using (10.7).

10.2.4 Stability by Antagonistic Cable Co-contraction

In the human musculoskeletal system, muscles can only pull. Therefore, at least two muscles are required to fully actuate a single degree of freedom. One muscle to pull in one direction and another muscle to pull in the other direction. The two muscles are said to be antagonistic. They work against each other in opposite directions. If antagonistic muscles are activated simultaneously or co-contracted, the degree of freedom reaches an equilibrium point where the effects of both muscles compensate for each other [78, 97]. The equilibrium point depends on the ratio of the muscle co-activation. For higher activation levels at constant ratio, the stiffness of the equilibrium point is increased. It becomes harder for a disturbance to push the system away from the equilibrium point. Thus, antagonistic muscle co-contraction creates stiffness.

Joint stiffness control by antagonistic muscle co-contraction raises a question with respect to its stability. Is it a naturally stabilising mechanism? If two antagonistic muscles are activated, is the system stable without additional help. The following paragraphs investigate and proves stability of antagonistic muscle co-contraction, using the pendulum model. The proof will use the cable-driven pendulum's state model without cables 2 and 3. The pendulum's state model is defined by setting the states: $x_1 = \psi$, $x_2 = \dot{\psi}$. The pendulum's dynamic behaviour is defined by the following state model:

$$\begin{aligned} \dot{x}_1 &= x_2, \\ \dot{x}_2 &= -A \sin(x_1) - Bx_2 + Cw_1(x_1)f_1 + Cw_4(x_1)f_4, \end{aligned} \quad A > 0, B > 0, C > 0. \quad (10.8)$$

The functions $w_1(x_1)$ and $w_4(x_1)$ are the cable moment-arms (third coordinate of (10.7)) (Fig. 10.7). To prove the stability of antagonistic muscle co-contraction, the following theorem must first be proven.

Theorem 22 (Pendulum With Constant Torque). *The state model defined by:*

$$\begin{aligned} \dot{x}_1 &= x_2, \\ \dot{x}_2 &= -A \sin(x_1) - Bx_2 + C \tau, \end{aligned} \quad A > 0, B > 0, C > 0. \quad (10.9)$$

is asymptotically stable to an equilibrium point $(\bar{x}_1, 0)$, $|\bar{x}_1| < \pi/2$ from within the set

$$\Omega := \{\vec{x} \in \mathbb{R}^2 \mid |x_1| < \pi\}, \quad (10.10)$$

if the torque T is constant.

Proof. The equilibrium point $(\bar{x}_1, 0)$ must satisfy the following relation:

$$0 = -A \sin(\bar{x}_1) + C \tau, \quad \Rightarrow \quad \tau = \frac{A}{C} \sin(\bar{x}_1). \quad (10.11)$$

Given that $|\bar{x}_1| < \pi/2$, the torque is bounded by:

$$-\frac{A}{C} < \tau < \frac{A}{C}. \quad (10.12)$$

For a value of τ satisfying this equation, there are two solutions to $\tau = \frac{A}{C} \sin(\bar{x}_1)$: $(|\bar{x}_{1,1}| < \pi/2, 0)$ and $(\pi/2 < |\bar{x}_{1,2}| < \pi, 0)$. By assumption $|\bar{x}_1| < \pi/2$, and therefore only the first solution is considered.

Consider the following lyapunov candidate for this system:

$$V(x_1, x_2) = \frac{1}{2}x_2^2 + A(1 - \cos(x_1)), \quad (10.13)$$

$$\dot{V}(x_1, x_2) = (C\tau - Bx_2)x_2, \quad (10.14)$$

The lyapunov candidate satisfies the condition $\dot{V}(\vec{x}) < -\delta$, $\delta > 0$ outside the following neighbourhood of the origin:

$$\bar{\Omega} := \{\vec{x} \in \mathbb{R}^2 \mid |x_1| > \pi, |x_2| > \frac{C|\tau|}{B}\}. \quad (10.15)$$

The maximum value of $V(\vec{x})$ on the boundary $\partial\bar{\Omega}$ is:

$$V_{\max}(\partial\bar{\Omega}) = \frac{1}{2} \left(\frac{C\tau}{B} \right)^2 + 2A. \quad (10.16)$$

The lyapunov candidate satisfies the condition of uniform boundedness [117]. Thus, system will eventually enter the domain $\bar{\Omega}$ and remain inside the domain. Furthermore, as stated previously, there are at most two fixed points inside Ω , given a value of τ satisfying (10.12). The point $(|\bar{x}_1| < \pi/2, 0) \in \bar{\Omega}$ is a stable centre.

The state model defined by (10.9) is asymptotically stable to an equilibrium point $(\bar{x}_1, 0)$, $|\bar{x}_1| < \pi/2$ from within the set Ω . \square

This theorem is used to prove the stability of muscle co-contraction.

Theorem 23 (Antagonistic Cable Co-contraction Stability). *The pendulum's state model (10.8) is locally asymptotically stable to the point $(\bar{x}_1, 0)$, $|\bar{x}_1| < \frac{\pi}{3}$, within the set*

$$\Omega^* := \{\vec{x} \in \mathbb{R}^2 \mid |x_1| < \frac{\pi}{2}\}, \quad (10.17)$$

by imposing the cable tensions f_1 and f_4 to be fixed at constant values

$$f_1 = \bar{f}_1 = cte \geq 0, \quad f_4 = \bar{f}_4 = cte \geq 0, \quad (10.18)$$

such that $-A\sin(\bar{x}_1) + Cw_1(\bar{x}_1)\bar{f}_1 + Cw_4(\bar{x}_1)\bar{f}_4 = 0$. Furthermore, the moment-arm functions are assumed to have opposite signs (Antagonist muscles).

$$w_1(x_1) < 0, \quad \text{and} \quad w_4(x_1) > 0, \quad \forall x_1 \in]-\frac{\pi}{2}, \frac{\pi}{2}[. \quad (10.19)$$

Proof. The first point to observe is that given the geometry of the system the moment-arm functions $w_1(x_1)$ and $w_4(x_1)$ are bounded functions. The cable attachment points are defined such that in the pendulum frame \mathcal{R}_1 , $\forall x_1 \in]-\frac{\pi}{2}, \frac{\pi}{2}[$, cable 1's force direction vector $\vec{b}_{1,1}$ is always in quadrant II of the pendulum's xy plane. Cable 2's force direction

vector $\vec{b}_{1,2}$ is always in quadrant I (Fig. 10.8). Cable 1's moment-arm function is bounded by:

$$\begin{aligned} \mathbf{R}_{1,0}(x_1) \begin{pmatrix} S_{1,x} \\ S_{1,y} \\ 0 \end{pmatrix} \times \mathbf{R}_{1,0}(x_1) \begin{pmatrix} -1 \\ 0 \\ 0 \end{pmatrix} < w_1(x_1) < 0, \\ \begin{pmatrix} S_{1,x} \cos(x_1) - S_{1,y} \sin(x_1) \\ S_{1,x} \sin(x_1) + S_{1,y} \cos(x_1) \\ 0 \end{pmatrix} \times \begin{pmatrix} -\cos(x_1) \\ -\sin(x_1) \\ 0 \end{pmatrix} < w_1(x_1) < 0, \quad S_{1,y} < 0, \\ -|S_{1,y}| < w_1(x_1) < 0. \end{aligned} \quad (10.20)$$

Cable 4's moment-arm function is bounded by:

$$\begin{aligned} 0 < w_4(x_1) < \mathbf{R}_{1,0}(x_1) \begin{pmatrix} S_{4,x} \\ S_{4,y} \\ 0 \end{pmatrix} \times \mathbf{R}_{1,0}(x_1) \begin{pmatrix} 1 \\ 0 \\ 0 \end{pmatrix}, \\ 0 < w_4(x_1) < \begin{pmatrix} S_{4,x} \cos(x_1) - S_{4,y} \sin(x_1) \\ S_{4,x} \sin(x_1) + S_{4,y} \cos(x_1) \\ 0 \end{pmatrix} \times \begin{pmatrix} \cos(x_1) \\ \sin(x_1) \\ 0 \end{pmatrix}, \quad S_{4,y} < 0, \\ 0 < w_4(x_1) < |S_{4,y}|, \end{aligned} \quad (10.21)$$

where $S_{i,x}$ and $S_{i,y}$ are the x - and y -coordinates of the cable insertion points in the pendulum frame \mathcal{R}_1 . $\mathbf{R}_{1,0}(x_1)$ is the rotation matrix from the pendulum frame to the inertial frame (10.3).

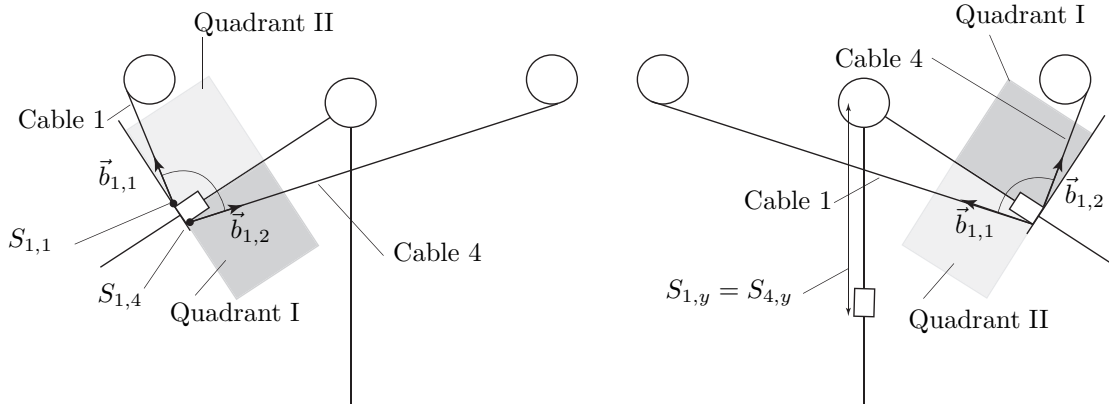


Figure 10.8: *Illustration of the bounding of the moment-arm functions w_1 and w_4 as described in the proof of theorem 4 10.2.4.*

The bounds on the moment-arm functions define bounds on the actuations:

$$-C\bar{f}_1|S_{1,y}| < Cw_1(x_1)\bar{f}_1 < 0, \quad (10.22)$$

$$0 < Cw_4(x_1)\bar{f}_4 < C\bar{f}_4|S_{4,y}|, \quad (10.23)$$

Thus, the state model's dynamics are also bounded:

$$\begin{aligned} \dot{x}_{2,\inf} &= -A \sin(x_1) - Bx_2 - C\bar{f}_1|S_{1,y}| < \dot{x}_2 < \dot{x}_{2,\sup} = -A \sin(x_1) - Bx_2 + C\bar{f}_4|S_{4,y}|, \\ \text{with } \dot{x}_2 &= -A \sin(x_1) - Bx_2 + Cw_1(x_1)\bar{f}_1 + Cw_4(x_1)\bar{f}_4. \end{aligned} \quad (10.24)$$

By theorem 4, the bounding dynamics are stable. The lower bound is asymptotically stable to the equilibrium point $(\bar{x}_{1,\text{inf}}, 0)$ with $-\pi/2 < \bar{x}_{1,\text{inf}} \leq 0$ from within $\Omega = \{\vec{x} \in \mathbb{R}^2 \mid |x_1| < \pi\}$. The upper bound is asymptotically stable to the equilibrium point $(\bar{x}_{1,\text{sup}}, 0)$ with $0 \leq \bar{x}_{1,\text{sup}} \leq \pi/2$ from within $\Omega = \{\vec{x} \in \mathbb{R}^2 \mid |x_1| < \pi\}$.

The stability of the bounding dynamics imposes the following on the cable tensions:

$$0 \leq \bar{f}_1 < \frac{A}{C|S_{1,y}|}, \quad S_{1,y} \neq 0, \quad 0 \leq \bar{f}_4 < \frac{A}{C|S_{4,y}|}, \quad S_{4,y} \neq 0. \quad (10.25)$$

The insertion points $S_{1,1}$ and $S_{1,4}$ of the cables are such that $S_{1,y} = S_{4,y}$ (symmetry).

Furthermore, relations (10.22), (10.23) and (10.25) define:

$$-A < Cw_1(x_1)\bar{f}_1 < 0, \quad 0 < Cw_4(x_1)\bar{f}_4 < A. \quad (10.26)$$

For equilibrium points $(\bar{x}_1, 0)$, $|\bar{x}_1| < \pi/2$, the following relation is defined:

$$\begin{aligned} & -A \sin(\bar{x}_1) + Cw_1(\bar{x}_1)\bar{f}_1 + Cw_4(\bar{x}_1)\bar{f}_4 = 0, \\ \Rightarrow & Cw_1(\bar{x}_1)\bar{f}_1 + Cw_4(\bar{x}_1)\bar{f}_4 = A \sin(\bar{x}_1), \\ \Rightarrow & -A < Cw_1(\bar{x}_1)\bar{f}_1 + Cw_4(\bar{x}_1)\bar{f}_4 < A, \quad \forall \bar{x}_1 \in]-\frac{\pi}{2}, \frac{\pi}{2}[\end{aligned} \quad (10.27)$$

Relations (10.26) and (10.27) agree with each other and impose:

$$-A < Cw_1(x_1)\bar{f}_1 + Cw_4(x_1)\bar{f}_4 < A. \quad (10.28)$$

The actuation generated by the co-contraction is bounded. Through theorem 4, the system is stable to the equilibrium point $(\bar{x}_1, 0)$ with $-\pi/2 < \bar{x}_1 \leq \pi/2$ from within $\Omega = \{\vec{x} \in \mathbb{R}^2 \mid |x_1| < \pi\}$. Therefore, the system is asymptotically stable to the equilibrium point $(\bar{x}_1, 0)$ with $-\pi/3 < \bar{x}_1 \leq \pi/3$ from within $\Omega^* = \{\vec{x} \in \mathbb{R}^2 \mid |x_1| < \pi/2\}$. \square

The previous theorem proves that by activating antagonistic cables, the system is stabilised to an equilibrium point. The value of the equilibrium point depends on the ratio between the cable tensions and the tensions are limited to a maximum value. The cable tensions can be changed without changing the equilibrium point if the ratio between cable tensions remains constant (Fig. 10.9).

10.2.5 Joint Stiffness Control

Thus far, the term "stiffness" has been used without a formal definition. Stiffness generally defines the relation between force and displacement applied to an object. In a spring, it characterises the amount of force Δf required to stretch or compress the spring by Δl . In structural engineering it characterises the change in geometry or deflection (angle $\Delta \vartheta$ or length Δd) of the structure under an applied force Δf . In material science it characterises the amount of deformation $\Delta \epsilon$ of the material under a given load $\Delta \sigma$. The common point between all of these different definitions of stiffness is that when the

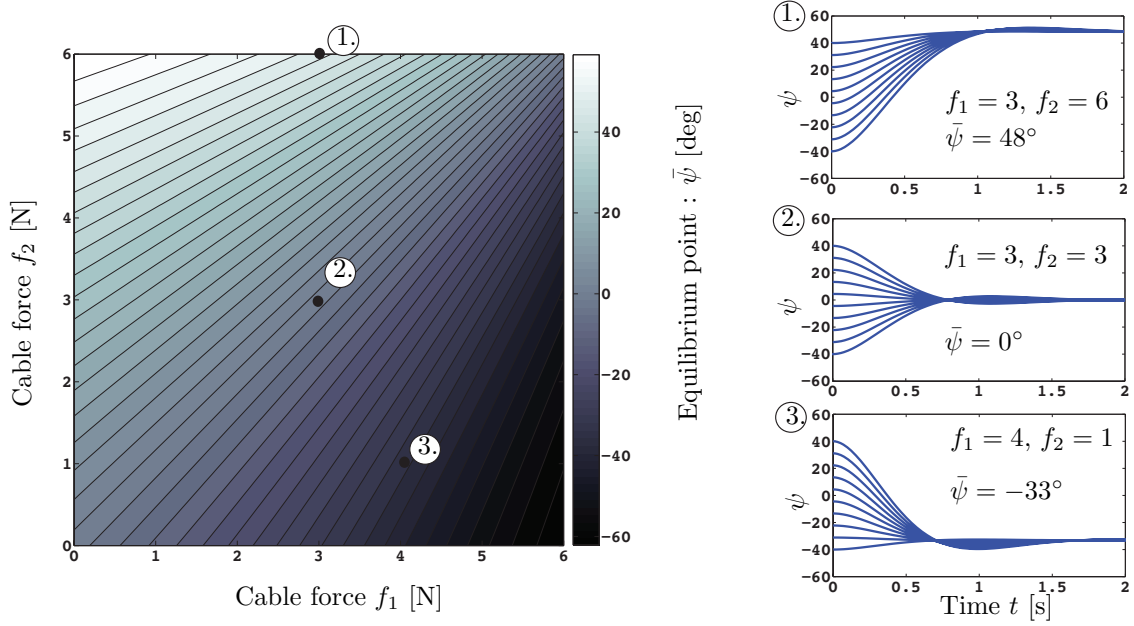


Figure 10.9: *Illustration of the equilibrium point achieved by antagonistic cable co-contraction as described by theorem 5, section 10.2.4.*

force or load is removed, the spring, structure or material returns to its original state. Stiffness characterises a behaviour that is reversible or elastic. Stiffness is mathematically defined as the infinitesimal change in external action over the infinitesimal change in internal reaction.

$$K = \frac{\partial \chi}{\partial q}, \quad \begin{array}{l} \chi : \text{force } f / \text{load } \sigma, \\ q : \text{displacement } l / \text{deflection } d / \text{deformation } \epsilon. \end{array} \quad (10.29)$$

In this chapter, joint stiffness is defined as the required infinitesimal change in joint torque τ to impose an infinitesimal change in joint configuration ψ .

$$K = \frac{\partial \tau}{\partial \psi}, \quad \begin{array}{l} \tau : \text{torque on pendulum axis,} \\ \psi : \text{pendulum angle.} \end{array} \quad (10.30)$$

For the complete cable-driven mechanism (all four cables), the stiffness normalised by the inertia, is defined by:

$$K(x_1) = \frac{\partial \dot{x}_2}{\partial x_1} = -A \cos(x_1) + C \frac{\partial \mathbf{W}(x_1)}{\partial x_1} \vec{f}. \quad (10.31)$$

The stiffness around an equilibrium point \bar{x}_1 is $K(\bar{x}_1)$. For a given muscle activation level, the stiffness is governed by moment-arms. The first term in the previous relation is from the system's dynamics. The second term is from the cable structure. Once the force activation levels are set, the stiffness depends on the internal dynamics and moment-arms. For there to be stability, the moment-arms must be the governing term. The muscle co-contraction must control the stiffness and not the system's dynamics.

Human motor control uses the muscle activation levels to actively change the properties of the joint in terms of stiffness and configuration. Joint stiffness control by antagonistic muscle co-contraction changes the activation levels of the muscles to achieve a

desired characteristic.

There are two distinct methods of using the antagonistic muscles. At constant ratio, the muscle forces can be changed to produce more or less stiffness without changing the equilibrium point. This is called iso-equilibrium stiffness control (Fig. 10.10). The musculature can actively control the stiffness to deal with the external perturbations. At constant stiffness, the equilibrium point can be changed. The activation ratio is changed such that the equilibrium point changes but not the stiffness. This is called iso-stiffness equilibrium control. In general situations, the stiffness and equilibrium point are continuously changed.

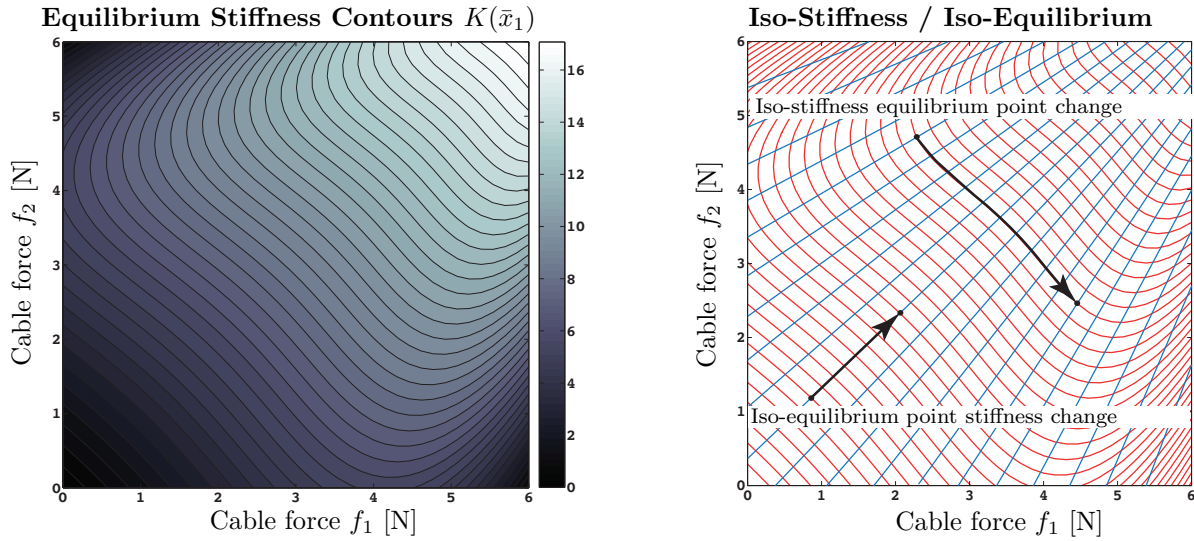


Figure 10.10: *Illustration of the equilibrium stiffness and the relation between iso-stiffness and iso-equilibrium lines 10.2.4.*

10.2.6 Observability of Pendulum States

Joint stiffness control relies on knowledge of the joint's position. In section 10.2.1, it is stated that the nervous system measures primarily each muscle's length, rate of change and activation level. There is another type of nerve cell that measures information regarding the joints, called mechanoreceptor. Mechanoreceptors are known to measure mechanical deformation. There are other types of mechanoreceptors in our skin that give us a sense of touch. Golgi tendon organs are also a type of mechanoreceptor. However, it is unclear if joint mechanoreceptors relay information regarding each joint's current configuration [177]. Therefore, this section shows that the joint's position can be measured or observed through the measure of muscle length and rate of change.

As stated in section 10.2.1, the nervous system measures the muscle lengths L_i and the rates of changes in each length \dot{L}_i . Therefore, are the pendulum states x_1 and x_2 observable through the cable lengths L_i and rates \dot{L}_i ? The short answer is yes, but the observability will be formally proven.

Theorem 24 (Observability of Pendulum States). *The states of the following dynamic system*

$$\dot{x}_1 = x_2, \quad (10.32)$$

$$\dot{x}_2 = -A \sin(x_1) - Bx_2 + C \mathbf{W}(x_1) \vec{f}, \quad (10.33)$$

are observable through the output function defined by:

$$\vec{y}(x_1, x_2) = (L_1 \quad L_2 \quad L_3 \quad L_4 \quad \dot{L}_1 \quad \dot{L}_2 \quad \dot{L}_3 \quad \dot{L}_4)^T, \quad (10.34)$$

Proof. The proof involves showing the observability matrix is full column rank. The matrix is constructed from a linearisation around an arbitrary equilibrium point $\vec{y}_c = (\bar{x}_1, 0)$, $|\bar{x}_1| \leq \frac{\pi}{3}$. The vector \vec{f} is the cable force distribution at the equilibrium point.

$$-A \sin(\bar{x}_1) + C \mathbf{W}(\bar{x}_1) \vec{f} = 0. \quad (10.35)$$

The linearised pendulum model is defined by:

$$\dot{x}_1 \approx x_2, \quad (10.36)$$

$$\dot{x}_2 \approx \left(-A \cos(\bar{x}_1) + C \left. \frac{\partial \mathbf{W}}{\partial x_1} \right|_{x_1=\bar{x}_1} \vec{f} \right) x_1 - Bx_2 + C \mathbf{W}(\bar{x}_1) \vec{f}, \quad (10.37)$$

The state matrices \mathbf{A} and \mathbf{B} are defined by:

$$\mathbf{A} = \begin{pmatrix} 0 & 1 \\ \left(-A \cos(\bar{x}_1) + C \left. \frac{\partial \mathbf{W}}{\partial x_1} \right|_{x_1=\bar{x}_1} \vec{f} \right) & -B \end{pmatrix}, \quad \mathbf{B} = \begin{pmatrix} 0 \\ C \mathbf{W}(\bar{x}_1) \end{pmatrix} \quad (10.38)$$

The output function $\vec{y}(x_1, x_2)$ is also linearised around the equilibrium point:

$$\vec{y}(x_1, x_2) \approx \begin{pmatrix} \bar{L}_1 \\ \vdots \\ \bar{L}_4 \\ \dot{\bar{L}}_1 \\ \vdots \\ \dot{\bar{L}}_4 \end{pmatrix} + \begin{pmatrix} \left. \frac{\partial L_1}{\partial x_1} \right|_{\bar{x}_1, 0} & 0 \\ \vdots & \vdots \\ \left. \frac{\partial L_4}{\partial x_1} \right|_{\bar{x}_1, 0} & 0 \\ \left. \frac{\partial \dot{L}_1}{\partial x_1} \right|_{\bar{x}_1, 0} & \left. \frac{\partial \dot{L}_1}{\partial x_2} \right|_{\bar{x}_1, 0} \\ \vdots & \vdots \\ \left. \frac{\partial \dot{L}_4}{\partial x_1} \right|_{\bar{x}_1, 0} & \left. \frac{\partial \dot{L}_4}{\partial x_2} \right|_{\bar{x}_1, 0} \end{pmatrix} \begin{pmatrix} x_1 \\ x_2 \end{pmatrix} = \vec{y}(\bar{x}_1, 0) + \mathbf{C} \begin{pmatrix} x_1 \\ x_2 \end{pmatrix}. \quad (10.39)$$

The states x_1 and x_2 are locally observable if and only if the observability matrix \mathbf{O} has

full column rank. The observability matrix is defined for this particular model by:

$$\mathbf{O} = \begin{pmatrix} \mathbf{C} \\ \mathbf{CA} \end{pmatrix} = \begin{pmatrix} \frac{\partial L_1}{\partial x_1} \Big|_{\bar{x}_{1,0}} & 0 & \vdots & \vdots & \vdots & \vdots & \vdots & \vdots & \vdots & \vdots & \vdots & \vdots \\ \vdots & \vdots & \frac{\partial L_4}{\partial x_1} \Big|_{\bar{x}_{1,0}} & 0 & \vdots & \vdots & \vdots & \vdots & \vdots & \vdots & \vdots & \vdots \\ \vdots & \vdots & \vdots & \vdots & \frac{\partial \dot{L}_1}{\partial x_2} \Big|_{\bar{x}_{1,0}} & \vdots & \vdots & \vdots & \vdots & \vdots & \vdots & \vdots \\ \frac{\partial \dot{L}_1}{\partial x_1} \Big|_{\bar{x}_{1,0}} & \frac{\partial \dot{L}_1}{\partial x_2} \Big|_{\bar{x}_{1,0}} & \vdots & \vdots & \vdots & \vdots & \vdots & \vdots & \vdots & \vdots & \vdots & \vdots \\ \vdots & \vdots & \frac{\partial \dot{L}_4}{\partial x_1} \Big|_{\bar{x}_{1,0}} & \frac{\partial \dot{L}_4}{\partial x_2} \Big|_{\bar{x}_{1,0}} & \vdots & \vdots & \vdots & \vdots & \vdots & \vdots & \vdots & \vdots \\ 0 & \frac{\partial L_1}{\partial x_1} \Big|_{\bar{x}_{1,0}} & \vdots & \vdots & \vdots & \vdots & \vdots & \vdots & \vdots & \vdots & \vdots & \vdots \\ \vdots & \vdots & \vdots & \vdots & \vdots & \vdots & \vdots & \vdots & \vdots & \vdots & \vdots & \vdots \\ 0 & \frac{\partial L_4}{\partial x_1} \Big|_{\bar{x}_{1,0}} & \vdots & \vdots & \vdots & \vdots & \vdots & \vdots & \vdots & \vdots & \vdots & \vdots \\ \frac{\partial \dot{L}_1}{\partial x_2} \Big|_{\bar{x}_{1,0}} A_{2,1}, \frac{\partial \dot{L}_1}{\partial x_1} \Big|_{\bar{x}_{1,0}} + \frac{\partial \dot{L}_1}{\partial x_2} \Big|_{\bar{x}_{1,0}} A_{2,2} & \vdots & \vdots & \vdots & \vdots & \vdots & \vdots & \vdots & \vdots & \vdots & \vdots & \vdots \\ \vdots & \vdots & \vdots & \vdots & \vdots & \vdots & \vdots & \vdots & \vdots & \vdots & \vdots & \vdots \\ \frac{\partial \dot{L}_4}{\partial x_2} \Big|_{\bar{x}_{1,0}} A_{2,1}, \frac{\partial \dot{L}_4}{\partial x_1} \Big|_{\bar{x}_{1,0}} + \frac{\partial \dot{L}_4}{\partial x_2} \Big|_{\bar{x}_{1,0}} A_{2,2} & \vdots & \vdots & \vdots & \vdots & \vdots & \vdots & \vdots & \vdots & \vdots & \vdots & \vdots \end{pmatrix} \equiv \begin{pmatrix} \times_1 & 0 \\ \times_2 & 0 \\ \times_3 & 0 \\ \times_4 & 0 \\ \times & \times \\ \times & \times \\ \times & \times \\ \times & \times \\ 0 & \star_1 \\ 0 & \star_2 \\ 0 & \star_3 \\ 0 & \star_4 \\ \times & \times \\ \times & \times \\ \times & \times \\ \times & \times \end{pmatrix}. \quad (10.40)$$

The observability matrix is full column rank (rank = 2) for any equilibrium point $\vec{y}_c = (\bar{x}_1, 0)$, $|\bar{x}_1| \leq \frac{\pi}{3}$. Indeed, the first four rows have a single non-zero element (\times_i). Rows 9 to 12 also have a single non-zero element (\star_i). The non-zero elements are in different columns. Furthermore, the elements are equal to each other in pairs of two ($\times_i = \star_i$, $i = 1, 2, 3, 4$). These elements are never zero on the interval $x_1 \in]-\pi/3, \pi/3[$ (Fig. 10.7). Thus, as long as at least one of these elements is non-zero, the matrix is guaranteed to have full column rank. Therefore, the states x_1 and x_2 or ψ and $\dot{\psi}$ are observable through the cable lengths L_i and rates \dot{L}_i . \square

This theorem proves that the state of the pendulum can be known through the lengths and rates of change in length of each cable. It is therefore hypothesised that the nervous system does know the state of each joint using the measured muscle states and the information from the mechanoreceptors [169].

10.3 A Joint Stiffness Control Strategy

Thus far, the general function of human motor control has been presented and the mechanism of joint stiffness control through antagonistic muscle co-contraction has been presented and analysed. The findings are that antagonistic muscle co-contraction produces more or less stiffness around an equilibrium point and the equilibrium point depends on the muscle activation levels. Furthermore, muscle co-contraction yields a stabilising effect around the equilibrium point. The equilibrium point is stable. Meaning, if the skeletal system is pushed away from the equilibrium point by a disturbance, the muscle co-contraction pushes it back to the equilibrium in the same way a spring would.

It was also shown that muscle moment-arms govern the stability around the equilibrium

point. Once the muscle activation levels are set, the moment-arms govern the actuation. Muscle moment-arms play an important role in that they relate skeletal dynamics to muscle forces. In musculoskeletal modelling, moment-arms are used to estimate the muscle forces, given desired skeletal dynamics. Thus, the hypothesis put fourth by this chapter concerning a possible neuromuscular dysfunction causing osteoarthritis is the following. A deterioration in the nervous system's knowledge of the moment-arms can lead to excessive muscle forces. This in turn causes excessive joint forces. There is some form of mismatch between the actual system and the nervous system's perception of the system.

The following sections present and discuss how a mismatch between the system's moment-arms and the moment-arms perceived by the controller can induce excessive joint loading through joint stiffness control. If a mismatch is inserted into the joint stiffness control mechanism, excessive muscle forces are generated and therefore excessive joint forces are generated. To illustrate this point, a joint stiffness control strategy is first proposed for the cable-driven pendulum. The strategy is then implemented onto the real system and tests are run using biased and unbiased moment-arms.

The reason for investigating moment-arms is that they are the primary quantity describing the musculature's ability to actuate the skeletal system. If the moment-arms are not computed correctly, the coordination strategy will yield inappropriate muscle forces. This point was previously illustrated in chapter 8. A poor definition of the shoulder model's muscle wrapping yielded inappropriate muscle activation patterns and overestimated joint reaction forces. There is another less obvious reason for investigating the effect of biased moment-arms. In control in general, there are a number of reasons why a controller can generate inappropriate input patterns. However, in many situations the result is instability. Therefore, the fact that biased moment-arms leads to inappropriate moment-arms without loss of stability is relevant because osteoarthritis is a dysfunction without loss of stability.

10.3.1 Control Algorithm

This section proposes a strategy of using muscle co-contraction to actively control and stabilise the cable-driven pendulum. The general concept of the strategy is to impose a stiffness and compute the required forces by solving the cable-force coordination problem presented in chapter 7. In the previous section only two cables were considered. The proposed strategy uses all four cables for more flexibility. The required torque on the pendulum's axis is produced by four cables thereby reducing the intensity in each cable. To impose a stiffness on the system, around an equilibrium point $(\bar{x}_1, 0)$, is to impose the following behaviour on the pendulum's dynamics.

$$\ddot{x}_2 = -A \sin(x_1) - Bx_2 + C\mathbf{W}(x_1)\vec{f} = -A \sin(x_1) - Bx_2 + K_s(\bar{x}_1 - x_1) + A \sin(\bar{x}_1), \quad (10.41)$$

where $K_s > 0$ is the imposed stiffness. The stiffness around any equilibrium point $(\bar{x}_1, 0)$ is defined by:

$$K(\bar{x}_1) = \left. \frac{\partial \ddot{x}_2}{\partial x_1} \right|_{x_1=\bar{x}_1} = \left(-A \cos(x_1) + C \frac{\partial \mathbf{W}(x_1)}{\partial x_1} \vec{f} \right) \Big|_{x_1=\bar{x}_1} = -A \cos(\bar{x}_1) + K_s. \quad (10.42)$$

where \vec{f} is the vector of muscle forces associated to the equilibrium point.

The proposed strategy is an iso-stiffness strategy. The stiffness coefficient is selected and remains constant. The following theorem proves that such a strategy is stable for the pendulum system.

Theorem 25. *The dynamical system defined by the following state model:*

$$\begin{aligned} \dot{x}_1 &= x_2, \\ \dot{x}_2 &= -A \sin(x_1) - Bx_2 + Cu, \end{aligned} \quad A > 0, \quad B > 0, \quad C > 0, \quad (10.43)$$

is locally asymptotically stable to the point $\vec{x} = (\hat{x}_1, 0)$, $|\bar{x}_1| < \pi$, within the set

$$\Omega := \{\vec{x} \in \mathbb{R}^2 \mid |x_1| < \pi\}, \quad (10.44)$$

using the control law

$$u = K_s(\bar{x}_1 - x_1) + \frac{A}{C} \sin(\bar{x}_1), \quad K_s > B > 0. \quad (10.45)$$

Proof. The proof involves showing that a suitable lyapunov candidate satisfies the conditions of theorem 1 in chapter 9. To prove asymptotic stability of the system within the domain Ω , the following variable change is defined

$$\begin{cases} y_1 = x_1 - \bar{x}_1 - \frac{A}{CK_s} \sin(\bar{x}_1) = x_1 - x_1^*, \\ y_2 = x_2, \end{cases} \Rightarrow \begin{cases} \dot{y}_1 = y_2, \\ \dot{y}_2 = -A \sin(y_1 + x_1^*) - C(K_s y_1 + B y_2). \end{cases} \quad (10.46)$$

Consider the lyapunov candidate

$$V(\vec{y}) = \frac{1}{2} \vec{y}^T \mathbf{P} \vec{y} + A(1 - \cos(y_1 + x_1^*)), \quad (10.47)$$

where the matrix \mathbf{P} is symmetric positive definite [117].

$$\mathbf{P} = \begin{pmatrix} p_{11} & p_{12} \\ p_{12} & p_{22} \end{pmatrix}, \quad p_{12} > 0, \quad p_{11}p_{22} - p_{12}^2 > 0. \quad (10.48)$$

Given that $A > 0$ by assumption and \mathbf{P} is symmetric positive definite, the function $V(\vec{y}) > 0$, $\forall \vec{y} \in \mathbb{R}^2$. The time derivative of the function is defined by:

$$\begin{aligned} \dot{V}(\vec{y}) &= \vec{y}^T \mathbf{P} \dot{\vec{y}} + Ay_2 \sin(y_1 + x_1^*), \\ &= 2(p_{12} - K_d p_{22}) y_2^2 - 2K_s p_{12} y_1^2 + 2(p_{11} - K_d p_{12} - K_s p_{22}) y_1 y_2 + \\ &\quad (y_2 - 2p_{12} y_1 - 2p_{22} y_2) \sin(y_1 + x_1^*). \end{aligned} \quad (10.49)$$

By selecting $p_{11} = \frac{CK_s}{2} + \frac{(CB)^2}{4}$, $p_{12} = \frac{CB}{4}$ and $p_{22} = \frac{1}{2}$, the expression of \dot{V} reduces to

$$\dot{V}(\vec{y}) = -\frac{1}{2} (C^2 K_s B y_1^2 + C B y_2^2 + A C B y_1 \sin(y_1 + x_1^*)). \quad (10.50)$$

This function is negative definite within the set:

$$\Omega_y := \{\vec{y} \in \mathbb{R}^2 \mid |y_1 + x_1^*| < \pi\}, \quad (10.51)$$

The interval is valid because the term $x_1^* = \bar{x}_1 + \frac{A}{CK_s} \sin(\bar{x}_1)$ has the same sign as \bar{x}_1 over the interval $|\bar{x}_1| < \pi$. Furthermore, the derivative is equal to zero for $\vec{y} = (0, 0)$. Thus, (10.46) is asymptotically stable to $\vec{0}$ in Ω_y and therefore (10.43) is asymptotically stable to $(\bar{x}_1, 0)$ in Ω using the control law (10.45). \square

Given a stiffness K_S and equilibrium point \bar{x}_1 the cable tensions must produce the desired input. The desired behaviour is $\vec{y}_c = (\bar{x}_1, 0)$. The outputs of the system are the states $\vec{y} = (x_1, x_2)$. The cable-tension must satisfy the following relation which is the primary task:

$$u = K(\vec{y}_c - \vec{y}) = \left(K_s(\bar{x}_1 - x_1) + \frac{A}{C} \sin(\bar{x}_1) \right) = \mathbf{W}\vec{f} \quad (10.52)$$

Furthermore, the desired behaviour must be within the wrench feasibility space imposed by the strength limits of each cable. The cable tensions are obtained using the same strategy as chapter 7. The coordination strategy is defined as an optimisation problem to find a solution minimising the cable tensions. This is the secondary task. The cost function is the sum of cable forces squared. The primary task is defined as an equality constraint. Bounds are also set on the tensions. Cables can only pull and have a maximum tensile strength. The coordination strategy is thus defined by:

$$\min_{\vec{f}} \quad \Gamma(\vec{f}) = \frac{1}{2} \vec{f}^T \vec{f}, \quad \text{Secondary Task,} \quad (10.53)$$

$$\text{s.t.} \quad \left(K_s(\bar{x}_1 - x_1) + \frac{A}{C} \sin(\bar{x}_1) \right) = \mathbf{W}\vec{f}, \quad \text{Control Law, Primary Task,} \quad (10.54)$$

$$\vec{0} \leq \vec{f} \leq \vec{f}_{\max}, \quad \text{Min/Max Tensions Bounds.} \quad (10.55)$$

This coordination strategy can be solved using the same null-space optimisation approach as defined in chapter 7. A pseudo-inverse of the moment-arms matrix yields a solution minimising the cable tensions while satisfying the control law constraint.

$$\vec{f}^* = \mathbf{W}^T (\mathbf{W}\mathbf{W}^T)^{-1} \left(K_s(\bar{x}_1 - x_1) + \frac{A}{C} \sin(\bar{x}_1) \right). \quad (10.56)$$

The solution is then corrected using the null-space of the moment-arm matrix to satisfy the bounds on the cable-tensions.

$$\vec{f} = \vec{f}^* + \mathbf{N}\vec{v}, \quad \mathbf{W}\mathbf{N} = \mathbf{0}. \quad (10.57)$$

This parameterisation of the problem yields a quadratic program (cf. chapter 7).

$$\min_{\vec{v}} \quad \Gamma(\vec{v}) = \frac{1}{2} \vec{v}^T \mathbf{N}^T \mathbf{N} \vec{v} + \frac{1}{2} (\vec{f}^*)^T \mathbf{N} \vec{v}, \quad (10.58)$$

$$\text{s.t.} \quad \mathbf{N}\vec{v} \leq \vec{f}_{\max} - \vec{f}^*, \quad (10.59)$$

$$-\mathbf{N}\vec{v} \leq \vec{f}^*. \quad (10.60)$$

Thus, the control algorithm is stated in the form of a theorem. A damping factor K_d is included into the control law to have more flexibility. This does not change the stability as long as $K_S > K_d + B > 0$ and $K_d > 0$. There is no proof, given that the previous theorems and proofs have already defined its stability. Lastly, wrench-feasibility is assumed.

Theorem 26 (Joint Stiffness Control Algorithm). *The following dynamic system:*

$$\dot{x}_1 = x_2, \quad (10.61)$$

$$\dot{x}_2 = -A \sin(x_1) - Bx_2 + C \mathbf{W}(x_1) \vec{f}, \quad (10.62)$$

$$\vec{y} = (x_1, x_2)^T, \quad (10.63)$$

is locally asymptotically stable to the point $\vec{y}_c = (\bar{x}_1, 0)$, $|\bar{x}_1| \leq \frac{\pi}{3}$, within the set

$$\Omega := \{\vec{x} \in \mathbb{R}^2 \mid |x_1| < \pi\}, \quad (10.64)$$

using the control law

$$u = K(\vec{y}_c - \vec{y}) = \left(K_s(\bar{x}_1 - x_1) - K_d x_2 + \frac{A}{C} \sin(\bar{x}_1) \right) = \mathbf{W} \vec{f} \quad (10.65)$$

where \vec{f} is defined by

$$\vec{f} = \vec{f}^* + \mathbf{N} \vec{v}, \quad \vec{f}^* = \mathbf{W}^T (\mathbf{W} \mathbf{W}^T)^{-1} \left(K_s(\bar{x}_1 - x_1) - K_d x_2 + \frac{A}{C} \sin(\bar{x}_1) \right). \quad (10.66)$$

The vector \vec{f} is found through the quadratic program

$$\min_{\vec{v}} \quad \Gamma(\vec{v}) = \frac{1}{2} \vec{v}^T \mathbf{N}^T \mathbf{N} \vec{v} + \frac{1}{2} (\vec{f}^*)^T \mathbf{N} \vec{v}, \quad (10.67)$$

$$s.t. \quad \mathbf{N} \vec{v} \leq \vec{f}_{max} - \vec{f}^*, \quad (10.68)$$

$$- \mathbf{N} \vec{v} \leq \vec{f}^*. \quad (10.69)$$

10.3.2 Implementation

The stiffness control strategy was implemented on a physical system (Fig. 10.11). The physical system is exactly like the model presented in section 10.2.3. The pulleys are driven by brushless EC motors through a planetary gear head with a gear of ratio N_g (Fig. 10.8). The electric motors are driven in current I_i and can be viewed as ideal torque sources. The pulleys have an inertia \mathcal{J}_p . The motor's have inertia's \mathcal{J}_m and there is friction $T(\dot{\vartheta}_i)$. The friction on the real system is hypothesised to behave according to the kinetic friction model [4].

$$\tau(\dot{\vartheta}_i) = \sigma_2 \dot{\vartheta}_i + \sigma_0 g(\dot{\vartheta}_i) \text{sign}(\dot{\vartheta}_i) + \left(1 - |\text{sign}(\dot{\vartheta}_i)| \right) \text{sat}(N_g k I_i, \tau_s), \quad (10.70)$$

$$\sigma_0 g(\dot{\vartheta}_i) = \tau_s \exp(-\dot{\vartheta}_i^2 / \nu_s) + \tau_c \left(1 - \exp(-\dot{\vartheta}_i^2 / \nu_s) \right). \quad (10.71)$$

where τ_s is the static friction torque, τ_c is the kinetic friction, ν_s the Stribeck curve coefficient. $\text{sign}(\dot{\theta}_i)$ is the sign usual sign function. $\text{sat}(I_i, T_s)$ is a saturation function that switches between the current input being applied and the static friction force. All the coefficients were identified on the real system using the appropriate techniques [4].

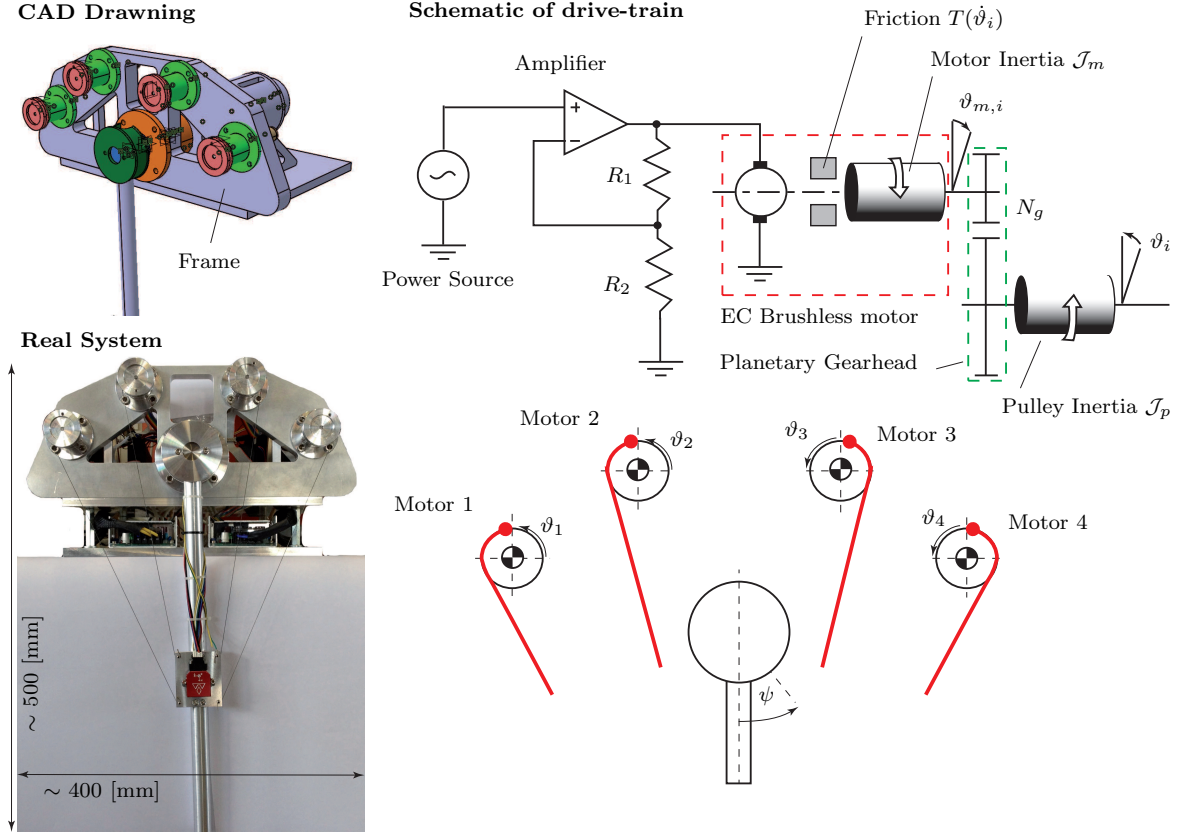


Figure 10.11: Illustration of the physical system and schematic of the drive train as described in section 10.3.3.

The motors are used to generate tension f_i within each cable and actuate the system. A dynamic state model is constructed for each pulley. The states are defined as the angle $x_{1,i} = \vartheta_i$ and angular velocity $x_{2,i} = \dot{\vartheta}_i$. The inputs are the motor currents $u_i = I_i$.

$$\dot{x}_{1,i} = x_{2,i}, \quad (10.72)$$

$$\dot{x}_{2,i} = \frac{1}{(N_g^2 \mathcal{J}_m + \mathcal{J}_p)} (-N_g^2 \tau(\dot{x}_{2,i}) + N_g k I_i - r f_i), \quad i = 1, 2, 3, 4, \quad (10.73)$$

The parameter k is the ideal torque source proportionality constant. A state model is built for the entire system by selecting the states and inputs as follows.

$$\begin{aligned} \vec{x} &: \{x_1 = \psi, x_{1,1} = \vartheta_1, \dots, x_{1,4} = \vartheta_4, x_2 = \dot{\psi}, x_{2,1} = \dot{\vartheta}_1, \dots, x_{2,4} = \dot{\vartheta}_4\}, \\ \vec{u} &: \{u_1 = I_1, u_2 = I_2, u_3 = I_3, u_4 = I_4\}. \end{aligned}$$

All states are measured on the real system using angular encoders. The motor currents are also measured. The resulting model is a non-linear affine in the input state model:

$$\dot{\vec{x}} = \vec{f}(\vec{x}) + \vec{g}(\vec{x})\vec{u}.$$

$$\dot{\vec{x}} = \begin{cases} \dot{x}_1 = x_2 \\ \dot{x}_{1,1} = x_{2,1} \\ \dot{x}_{1,2} = x_{2,2} \\ \dot{x}_{1,3} = x_{2,3} \\ \dot{x}_{1,4} = x_{2,4} \\ \dot{x}_2 = -A \sin(x_1) - Bx_2 + C\mathbf{W}(x_1)\vec{f} \\ \dot{x}_{2,1} = D \cdot \tau(x_{2,1}) + F \cdot f_1 + G \cdot u_1 \\ \dot{x}_{2,2} = D \cdot \tau(x_{2,2}) + F \cdot f_2 + G \cdot u_2 \\ \dot{x}_{2,3} = D \cdot \tau(x_{2,3}) + F \cdot f_3 + G \cdot u_3 \\ \dot{x}_{2,4} = D \cdot \tau(x_{2,4}) + F \cdot f_4 + G \cdot u_4 \end{cases} \quad \begin{cases} A = 4 \frac{M_p g l_p}{\mathcal{I}_p + M l_p^2} \\ B = 4 \frac{b_p}{\mathcal{I}_p + M l_p^2} \\ C = 4 \frac{1}{\mathcal{I}_p + M l_p^2} \\ D = -\frac{1}{N_g^2 \mathcal{J}_m + \mathcal{J}_p} \\ F = -\frac{r}{N_g^2 \mathcal{J}_m + \mathcal{J}_p} \\ G = \frac{N_g k}{N_g^2 \mathcal{J}_m + \mathcal{J}_p} \end{cases} \quad (10.74)$$

Given that each motor is equipped with an encoder, the length of each cable can be computed using the pulley angles ϑ_i . The pendulum is initially at an angle ψ_0 ($= 0$ by default). The initial length $L_i(\psi_0)$ of each cable is known using method the geometric method described in section 10.2.3. The pulley angles are all initially zero and the cables are assumed to always remain taught. Once the pendulum begins to move, the length of each cable is computed using the following relation.

$$\mathcal{L}_i = \mathcal{L}_i(\psi_0) + r\vartheta_i, i = 1, 2, \quad \mathcal{L}_i = \mathcal{L}_i(\psi_0) - r\vartheta_i, i = 3, 4. \quad (10.75)$$

The sign is different for cables three and four because the pulley angle is positive when the cable's length is decreasing.

The joint stiffness control algorithm presented in the previous section is implemented for tracking a reference behaviour $\vec{y}_c = (\bar{x}_1, 0)$. The control algorithm yields the necessary cable tensions f_i that each motor must produce. The motor currents were obtained by assuming that the pulley accelerations $\dot{x}_{2,i}$ are equal to the desired accelerations $\dot{x}_{2,i,c}$. This assumption allows one to define the motor inputs as:

$$u_i = \frac{1}{G} (\dot{x}_{2,i,c} - \alpha D \cdot \tau(x_{2,i}) - F \cdot f_i), \quad i = 1, 2, 3, 4. \quad (10.76)$$

The friction term is incorporated into the control law. This is called friction compensation by positive feedback. The coefficient $0 < \alpha < 1$ is such that the friction term does not destabilise the system and is tuned by hand. Friction compensation is essential because planetary gear heads are prone to large amounts of friction.

The control algorithm was implemented using the assumption that the pendulum states are known and need not be observed. An Luenberger observer was designed and implemented but the observer states were not used for control (cf. chapter 9). The observer was designed for illustration purposes with respect to the discussion of section 10.2.6 on the observability of joint states through the muscle states. The observer is not performant enough to use in a control strategy.

The state variables on the physical system are measured using angular encoders. There is an angular encoder on each motor with a precision of 0.7° (512 counts per turn). On the pendulum itself there is an angular encoder with a precision of 0.08° . The inputs are

also measured. Each motor is controlled by an operational amplifier that also measures the amount of current being applied to each motor. The implantation is done using a sampling rate of 80Hz (Measurements are taken 80 times a second and inputs are sent to the system 80 times a second). Finally, the control algorithm was implemented by imposing a minimum tension $\vec{f}_{\min} > 0$. This ensures that the cables remain taught.

10.3.3 Methods

To analyse the effect of biased moment-arms on the joint reaction force in the joint stiffness control strategy, the system was programmed to track a reference signal that switches between constant values at regular intervals. Each switch is defined using a transition function that smoothly changes the reference value. This avoids any sudden jump in motor current that would yank on the cables and cause damage to the mechanism. The transition function $\xi(t, \psi_A, \psi_B)$ is defined by the following polynomial function. The initial time is always defined as $t_0 = 0$ and the final time T can be modulated to impose more or less dynamics.

$$\xi(t, x_{1,A}, x_{1,B}) = x_{1,A} + \sum_{i=1}^5 p_i (x_{1,B} - x_{1,A}) \left(\frac{t - t_0}{T - t_0} \right)^i. \quad (10.77)$$

The coefficients p_i of the polynomial are obtained by imposing the following initial and final conditions:

$$\begin{aligned} \xi(t_0, x_{1,A}, x_{1,B}) &= x_{1,A}, & \dot{\xi}(t_0, x_{1,A}, x_{1,B}) &= 0, & \ddot{\xi}(t_0, x_{1,A}, x_{1,B}) &= 0, \\ \xi(T, x_{1,A}, x_{1,B}) &= x_{1,B}, & \dot{\xi}(T, x_{1,A}, x_{1,B}) &= 0, & \ddot{\xi}(T, x_{1,A}, x_{1,B}) &= 0. \end{aligned} \quad (10.78)$$

The order of the polynomial function is set at five but other orders can be used. Higher orders allow one to have greater control over the behaviour. The order five is selected because it yields a sufficiently smooth behaviour.

The reference signal uses most of the pendulum's angular space. In section 10.2.3 it was stated that the pendulum can swing in the interval $\pm 75^\circ$. The reference signal is defined with an amplitude range of $\pm 60^\circ$. The constant values are defined at 0° , $\pm 30^\circ$ and 60° .

During one cycle of the reference trajectory, the pendulum's states are measured through an encoder. The states of each motor and the amount of current being applied to each motor are measured. The currents are proportional to the forces within each cable and are used to compute the reaction force in the pendulum's axis.

To analyse the effect of stiffness control on the joint reaction force, the system was set to track the desired path using three settings of the moment arms. First, the path was tracked using nominal values of the moment-arms. Second, the path was tracked using moment-arms that were underestimated by 20%. Third, and last, the path was tracked using moment-arms that were 20% overestimated.

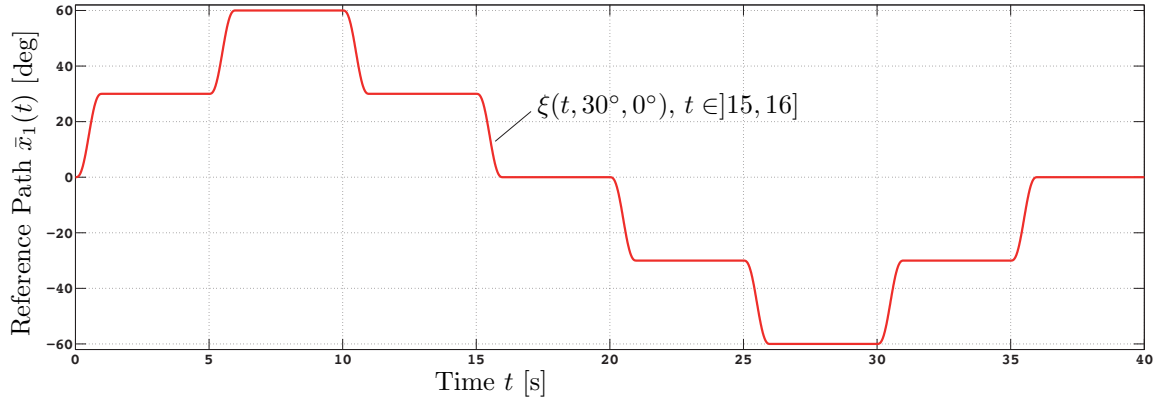


Figure 10.12: Illustration of the reference signal that the system was programmed to track.

10.4 Results

The cable-driven pendulum's ability to follow the desired path $\bar{x}_1 = \psi_c(t)$, using the joint stiffness control strategy is presented in terms of the measured joint angles ψ and velocity $\dot{\psi}$ (Fig. 10.13). A large stiffness value $K_s = 60$ and a long transition time $T = 4$ yield very good tracking of the reference signal. Once the stationary value is achieved, the static error $\psi_c - \psi$ is less than 0.2° at the maximum angle of 60° . A smaller stiffness value $K_s = 20$ and a shorter transition time ($T = 1$) yield poor tracking of the reference signal. The static error around the stationary value is less than 5° at the maximum angle of 60° .

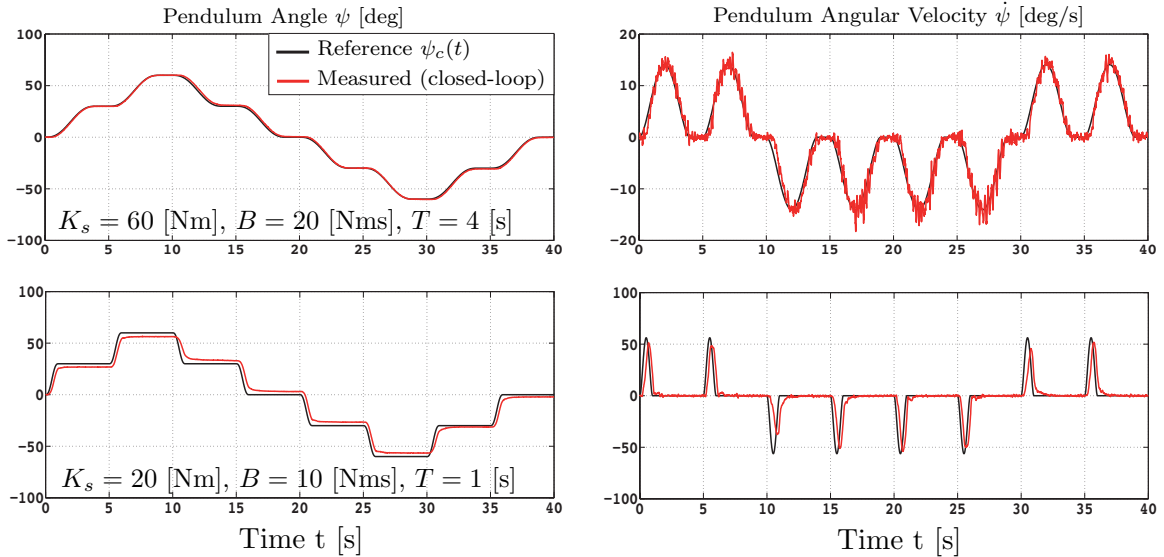


Figure 10.13: Measured behaviour for trajectory tracking using stiffness and damping values $(K_s, B) = (60, 20), (20, 10)$ and transition times $T = 4 [s], 1 [s]$. 10.2.4.

The system's ability to observe the pendulum's state is presented in terms of the observed states (Fig. 10.14). The test was run for a small stiffness value $K_s = 20$ and a

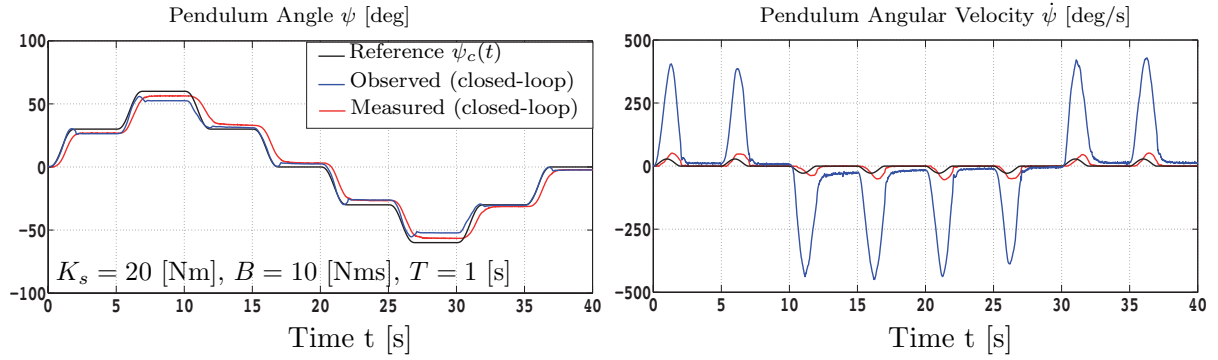


Figure 10.14: *Observed pendulum states over one cycle of the path $\psi_c(t)$ with stiffness and damping values: $K_s = 20$ [Nm], $B = 10$ [Nms]. The transition time was set at $T = 1$ [s].*

short transition time. The observed pendulum angle follows the measured angle quite well considering the nature of the observer. At every change in static angle, there is a small overshoot of the observed angle. There is a static error of less than 4° at the maximum angle of 60° between the measured angle and the observed angle. The observed velocity has an extremely large overshoot and does not converge to a steady state before the next step. The observed velocity does tend towards the measured value but convergence to a static value is not observed.

The required tensions within the cables were observed through the currents in the motors (Fig. 10.15). The maximum cable tensions were observed when the right/left cables had to pull the pendulum towards them at $\pm 60^\circ$ ($t = 10$ and $t = 30$ [s]). The two outer cables were observed to pull harder than the two inner cables. Larger cable tensions were required for faster transition times and higher stiffness values.

The effect of using over or underestimated moments-arms is a decrease or increase in joint reaction force by the same amount (Fig. 10.16). It was observed that a 20% increase in moment-arms lead to a 20% decrease in joint reaction force. Vice-versa, a 20% decrease in moment-arms results in a 20% increase in joint reaction force. This affect was most prominently observed when the cables had to pull the hardest.

10.5 Discussion

In the introduction, it was stated that osteoarthritis could be caused by an underlying neuromuscular dysfunction. The observed cause is frequent excessive loading of the articular cartilage leading to premature deterioration. However, the source of the excessive loading has not been identified [16]. The neuromuscular dysfunction hypothesis results from the following reasoning. A musculoskeletal system is a tensegrity system [188]. The muscles are in tension and the bones are in compression. The compression results from the muscles contracting. The contraction results from neural stimuli. Thus, the neuromuscular dysfunction hypothesis is that the neural stimuli are causing inappropriate

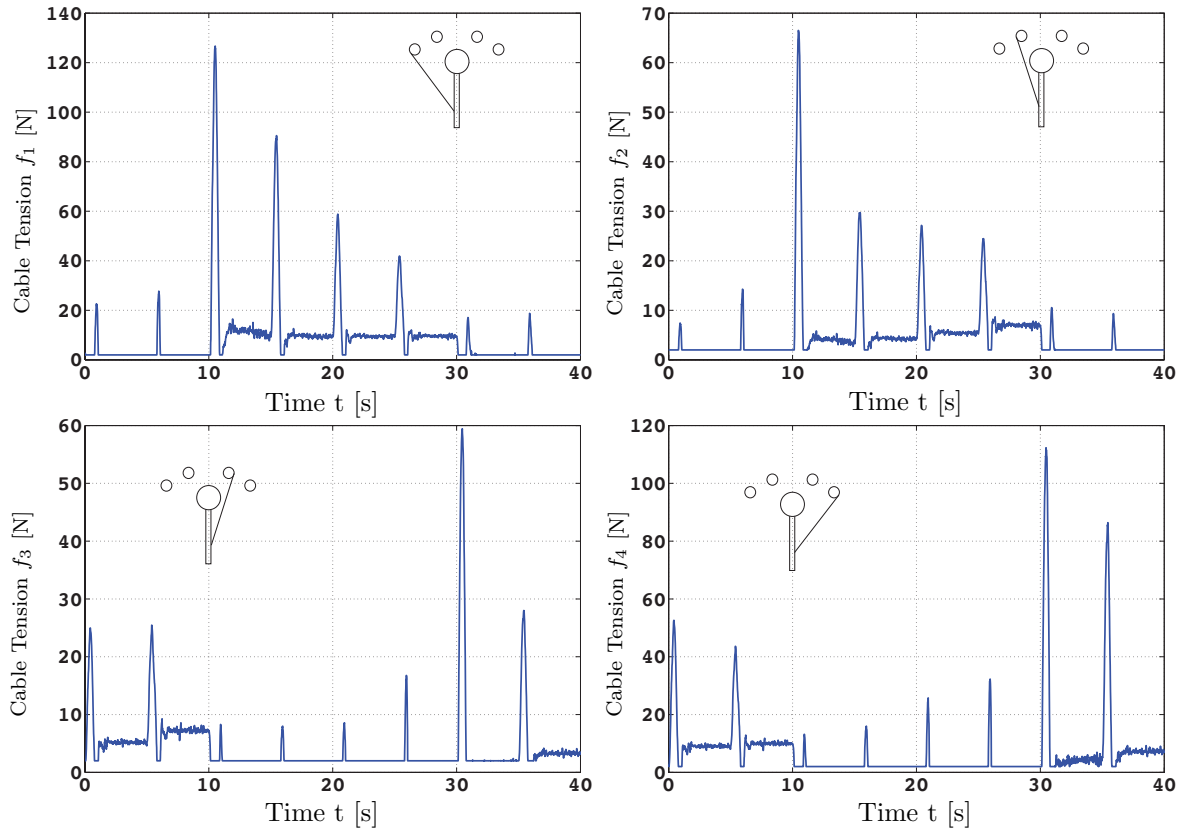


Figure 10.15: *Estimated cable tensions during one cycle of the path $\psi_c(t)$. These tensions are for a stiffness of $K_s = 20$ [Nm], a damping factor of $B = 10$ [Nms]. The transition time was set at $T = 1$ [s].*

muscle contraction leading to excessive loads in the joints. Osteoarthritis is a neural control problem.

The part of our nervous system controlling our musculoskeletal system is called human motor control. Within human motor control is a mechanism called joint stiffness control through antagonistic muscle co-contraction. Our musculature is setup such that certain muscles act as opposites. The nervous system activates or co-contracts these muscles to give the joints variable stiffness. The findings of this chapter show that such a mechanism can contribute to excessive loads in the joints. The findings of this chapter are obtained using a model of a cable-driven pendulum. Although the model is not that of a musculoskeletal system, the results are relevant. Indeed, the model is mathematically identical to a model of a musculoskeletal system. Models of cable-driven mechanisms and models of musculoskeletal systems are based on the same set of principles.

The chapter used a simplified model of neuromuscular interactions where the nervous system measures each muscle's length, rate of change in length and muscle activation level. This information was also shown to contain the state of the joints using the concept of observability from control theory. Therefore, the nervous system is assumed to have full knowledge of the dynamic state of the skeletal system [169]. Furthermore, it is believed that the nervous system has a model of the musculoskeletal system [177]. It

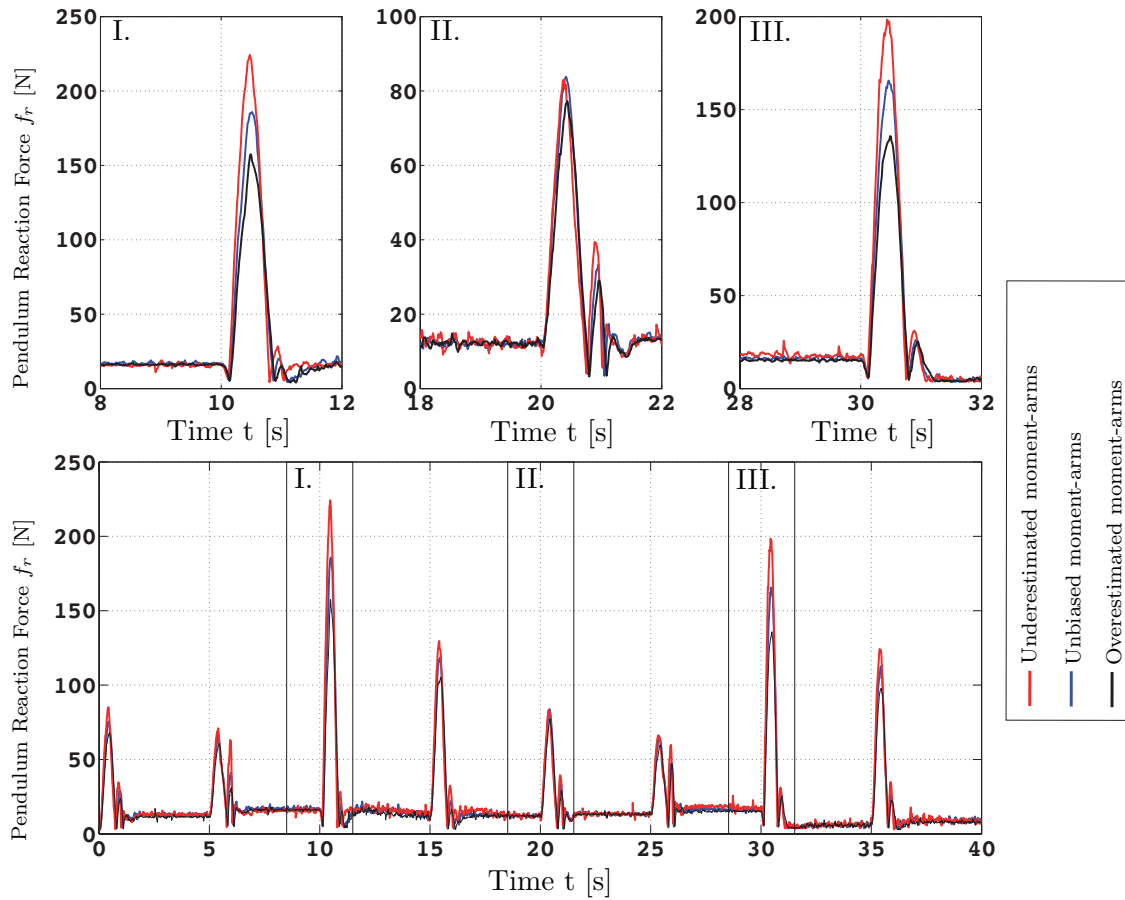


Figure 10.16: *Reaction force in the pendulum rotation axis using nominal, overestimated and underestimated moment-arms.*

uses the model to predict required muscle activation levels.

Throughout this dissertation, muscle moment-arms are shown to govern the prediction of muscle activation levels (cf. chapter 7). The moment-arms can be obtained using the tendon excursion method. The moment-arms are defined as the variation in muscle length over the variation in joint configuration. Given that both quantities are measured by the musculoskeletal system, it is highly probable that the nervous system has a measure of the moment-arms. Indeed, this information characterises the musculature's ability to actuate the skeletal system and produce movement.

Based on the hypothesis that moment-arms are measured by the nervous system, excessive joint loads are produced if the moment-arms are biased. Predicted muscle activation levels computed from biased moment-arms yield altered joint loads. Underestimated moment-arms lead to excessive joint loads. This point was illustrated through an implementation of a joint stiffness control strategy onto a physical cable-driven pendulum system. There are many possible dysfunctions of the system that could disturb human motor control. Biased moment-arms were selected because they yielded altered joint loads without compromising stability. Loss of stability is not on the list of symptoms of osteoarthritis. The insertion of delay into the control loop was tested but quickly lead to instability.

Finally, the results showed that the use of underestimated moment-arms produces excessive loads without producing instability. This point is important because osteoarthritis does not destabilise the musculoskeletal system. Thus, a contributing factor of osteoarthritis could be biased information regarding the musculoskeletal system, leading to underestimated muscle moment-arms, leading to excessive muscle forces, leading to excessive joint forces. This point remains however an unproven conjecture.

10.6 Conclusions

The goal of this chapter was to initiate the investigation of a possible neuromuscular dysfunction as the underlying cause of osteoarthritis. The investigation was carried out using a model of a cable-driven pendulum that is mathematically identical to a model of a musculoskeletal system. The presentation was set in the context of modern control theory, using a simple model of the interactions between the musculoskeletal and nervous systems. The investigation focused on the mechanism of joint stiffness control through antagonistic muscle co-contraction. The results showed that joint stiffness control is a naturally stabilising mechanism. By activating the antagonistic cables, the pendulum is stabilised to an equilibrium point. The equilibrium point is defined by the ratio of the activation levels. The investigation also showed that the joint's dynamic state can be observed through the dynamic states of the muscles. An implementation of a joint stiffness control strategy onto a physical cable-driven pendulum showed that if the controller uses biased information regarding the cable's ability to actuate the system, the reaction force in the joint is increased by a factor proportional to the bias. The use of biased information did not however lead to instability. Therefore, joint stiffness control can contribute to excessive joint loads through antagonistic muscle co-contraction.

The results are relevant to the subject of osteoarthritis and open the discussion on the possible causes but does not provide a definitive answer. The next step of the investigation should be to use a model of a musculoskeletal system such as the shoulder model presented in this dissertation. Also an internal muscle model should be added to the shoulder model to give it more realism.

Chapter 11

Conclusions

Modelling musculoskeletal systems constitutes a necessary tool for understanding musculoskeletal diseases and developing appropriate treatments. Models provide information on the behaviour of musculoskeletal systems that cannot be directly observed. The development of such models is a challenging task because of the complexity of the musculoskeletal systems and because there is no standard validation method.

This dissertation presented a musculoskeletal model of the human shoulder. The model is being developed for the study of osteoarthritis, the most common form of arthritis. Osteoarthritis can be defined as a premature deterioration of the articular cartilage due to frequent excessive loading. The development of proper treatments for osteoarthritis requires identifying and estimating the forces in the affected articulations. Given that the glenohumeral joint is the shoulder articulation that is most affected by osteoarthritis, the model is being specifically designed to compute the reaction force intensity in the shoulder joint, during quasi-static and dynamic movements of the upper limb.

Two main conclusions can be made from the work presented in this dissertation. The first conclusion is that the reaction force in an articulation is dependent on the movement of the articulation itself *and* on the movement of other articulations. The parameterisation of the shoulder's kinematics constitutes the first critical point in estimating the force in the glenohumeral joint. Muscle forces and joint reaction forces are related through the laws of motion from classical mechanics. A muscle activation pattern generates a movement of the skeletal structure and creates a reaction force in the joints. In this dissertation, the kinematics are imposed and the corresponding muscle forces are estimated by inverting the laws of rotation motion. The estimated muscle forces are used to obtain the reaction force in the glenohumeral joint through the translational laws of motion. To sum up, for a musculoskeletal model to successfully predict the joint reaction forces, the kinematic model must be able to accurately reproduce the systems movement.

The second conclusion is that geometry of the muscle model must be designed by considering all the muscles together. In the real shoulder, muscles are coordinated by the nervous system and produce together the overall result of movement and strength of our musculoskeletal system. There have been few analysis of how to use the cable model for representing the musculature. The one most referred to in the literature analyses

muscles individually and describes how to represent muscles with large attachment sites [197]. This constitutes the first step in constructing the model of the musculature. As a second step, this dissertation proposes to analyse the model's wrench-feasibility through the moment-arms. In the model, the relation between muscle forces and movement is defined by muscle moment-arms. The muscles are geometrically modelled by cables defining moment-arms around each joint. The force of a cable multiplied by its moment-arm creates a torque at each joint that contributes with the other cable forces to the movement of the system. A model is wrench feasible if it can generate the same set of movements as the real system.

This leads to the third and final conclusion. The articulations of the real system are stable. Stability in this context is understood as keeping the joint reaction force directed at the surface of the joint. In the real system the muscle-force activation patterns produce stable joint force patterns. In the model, the estimated muscle forces should also produce stable joint reaction forces, without using constraints. For a musculoskeletal model to successfully predict the joint reaction force pattern, the geometric muscle model must be able to accurately reproduce the relation between muscle-forces and movement. To achieve stable reaction force patterns, the geometric muscle model should be designed as a collective, considering each muscle's contribution in relation to the others. A good musculoskeletal model should naturally produce stable joint reaction force patterns.

11.1 Contributions

The motivation of this thesis was the construction of a musculoskeletal model of the human shoulder. The model is based on other shoulder models found in the literature [76, 101, 170]. The main contributions of this thesis are the development of a parameterisation of the shoulder model's kinematics to facilitate motion planning, and the improvement of a geometric model of the shoulder's musculature.

- The model is constructed using classical mechanics on the hypothesis that bones are rigid bodies, articulations are ideal mechanical joints, and muscles are massless, frictionless cables wrapping over the bones. The model is similar to the model constructed from the Virtual Human Project (VHP) dataset [74, 76], but uses a modified model of the scapulothoracic contact. Two ellipsoids are used to constraint the motion of the scapula with respect to the ribcage. The cable model representing the muscles is built using the same framework as the VHP model. The same set of wrapping objects are used but the number of cables can be changed. The final point regarding the model in general is that null-space optimisation is used to estimate the muscle forces rather than the conventional methods.
- The shoulder model is shown to be kinematically redundant. There are more internal degrees of freedom than the number of degrees of freedom of the elbow. The shoulder model's kinematic redundancy was solved using the modified scapulothoracic contact model directly. The modified contact model leads to a redefinition of the shoulder girdle's kinematics as a 2-3 parallel platform. Based on the parallel

definition of the model's kinematics, three different kinematic parameterisations of the parallel model were defined and used to extract a set of seven independent minimal coordinates. The coordinates considerably simplify the kinematic motion planning procedure given their independence. Indeed, abduction in the scapular plane was planned manually using the minimal coordinates and shown to be very similar to the same motion measured on a real shoulder. Furthermore, the coordinates are shown to be a promising new method of developing a regression model of shoulder kinematics that could be used on other models.

- The human shoulder is overactuated. There is an infinite number of muscle activation patterns that generate the same motion. The problem of overactuation was solved in this thesis using null-space optimisation [3, 190]. The method solves the problem by computing an initial muscle activation pattern using a pseudo inverse of the moment-arms matrix. The solution is then corrected to satisfy constraints using the null-space of the moment-arm matrix. Null-space optimisation allowed the detection of faults in the geometric muscle model. For instance, the model never activates the anterior deltoid because the torque generated by the muscle cannot be compensate for by the other muscles. This leads to the following conclusion: it is insufficient to design a cable model of the shoulder's musculature where each muscle is considered independently. The guidelines on how to model each muscle should be used to construct an initial cable model [197]. Once the initial model is defined, it should be optimised to obtain the largest torque-feasible space and thereby guarantee wrench feasibility.
- The purpose of the model is to help improve the understanding of osteoarthritis. The general question driving the research behind the model, is whether or not a neuromuscular disfunction is the underlying cause of osteoarthritis. This dissertation initiates the discussion of neuromuscular control as a possible cause of osteoarthritis. The mechanism of joint stiffness control through antagonistic muscle co-contraction is investigated using a cable-driven pendulum. Human motor control uses this mechanism to help stabilise our musculoskeletal system. Stability is understood here in the sense of Lyapunov stability from modern control theory. The use of a cable-driven pendulum is relevant to the issue in that its mathematical modelling is identical to modelling a musculoskeletal system. The investigation showed that the mechanism is a stabilising mechanism. It also showed that our nervous system measures the length and the rate of change in length of each muscle. Through the measurements, the nervous system can observe the joint's configuration. This point was proven using the concept of observability from control theory. Finally, the implementation of stiffness control onto a physical system showed that bias in the moment-arms, leads to changes in the joint reaction force without loss of stability. The evidence presented in this thesis is not fully conclusive but does open the discussion of the possibility that osteoarthritis is caused by change in the information regarding the muscle's ability to actuate the system. As our bodies age, our nervous system's observation of the musculoskeletal system could become biased causing excessive joint force.
- The final contribution of this thesis is the presentation of musculoskeletal shoul-

der modelling from a technical perspective. Throughout the dissertation, elements from theoretical robotics are used in an effort to mathematically formalise the musculoskeletal modelling of the shoulder. The formalisation helped to construct the minimal set of coordinates and helped improve the geometric muscle model. Finally, the technical details of the model are presented throughout the dissertation in an a way to facilitate the model's reconstruction, improvement, and testing as part of future research work.

11.2 Future Research Directions

At present, the musculoskeletal shoulder model does not activate the anterior deltoid muscle segment due to the moment-arm coupling; the superior part of the trapezius cannot compensate for the moment of force created by the anterior deltoid around the sternoclavicular joint. This issue should be addressed by reviewing the muscle wrapping definitions for each muscle. Furthermore, the joint reaction force is currently being overestimated because the wrapping constraints of certain muscles are defined as being attached to the scapula when anatomy says they should be part of the humerus.

After improving the geometric muscle model as part of future research work, the model should be validated. Thus far, the model has been tested for abduction in the scapular plane. Other movements should be tested to ensure that the muscle wrappings remain coherent, and that the model remains wrench-feasible.

In addition to addressing the current problems, future research can also work on improving the model by adding new elements. For instance, the DSEM model considers internal muscle behaviour and the upper limb [156]. The AnyBody model considers the upper limb and internal muscle dynamics [49]. The AnyBody software also allows one to include humeral head translation using force-dependent kinematics (FDK) [9].

An initial improvement should be to consider the internal behaviour of the muscles. There are a number of models which already exist [77, 95, 177, 186]. These models are mostly for general skeletal muscles and require adaptation for each muscle in the shoulder. Including an internal muscle model will make the bounds on the muscle forces dependent on the configuration of the bones through the force-length behaviour. This will have the effect of reducing the wrench-feasible space. A suggestion for future work would be to combine the development of the internal muscle model with the development of the geometric muscle model.

Another improvement is to include humeral head translation (HHT). Given that HHT adds a certain complexity to the model, strategies should initially be developed on models with reduced complexity. This will allow a more focused approach on the model of humeral head translation. Also it will determine the importance of considering HHT in the model. A foreseeable challenge to including HHT, is the definition of humeral head movement. There are accurate in-vivo studies of humeral head translation but these studies can only consider static positions due to the available measurement techniques such as X-ray, MRI or fluoroscopy [82, 124, 140, 175]. Furthermore, mathematically keeping the humeral head in the glenoid and obtaining movement for the model that is

consistent with the in-vivo data will also be challenging.

Another useful future contribution would consist of including the entire upper limb into the model. The biceps brachii has been shown to have an effect on the glenohumeral joint [216]. Integrating the entire upper limb will also provide a model, capable of analysing shoulder movements that are associated to more complex upper limb movements. At present the model considers an outstretched arm.

An important direction of future research consists of using a forward dynamics approach. The forward dynamics approach has been used but is not as popular as the inverse approach due to its complexity [144, 145, 162]. Using inverse models to estimate the joint reaction force is restrictive in that the movement is completely imposed. The kinematics are stiff. The only freedom is the muscle activation pattern. Also, the inverse model approach is not ideal for incorporating elements such as HHT. As stated previously, HHT can be included into an inverse model approach using FDK. FDK has been proven successful in modelling joints with translation [9]. However, the drawback of using FDK is that it is based on a number of simplifying assumptions such as small movements and slow variation of the translational degrees of freedom. FDK also neglects friction and uses numerical artefacts to create stiffness. These coefficients have to be set empirically. A forward dynamics approach would require some form of run-to-run optimisation. Current methods for such problems include real time optimisation (RTO) [34] and machine learning [151], but one could also develop an entirely new strategy, specifically adapted for the shoulder and non-conforming joints in general. The general idea of these approaches is to run forward simulations and correct the activation patterns before each simulation using an algorithm. The forward approach would include HHT but would not require imposing a specific movement of the humeral head. Translation of the humeral head would result from the activation pattern and be unknown a priori. Finally, a number of such algorithms have been developed in robotics to deal with systems of high complexity where part of the behaviour is unknown [109]. This approach was used for instance to control the Kenshiro humanoid robot which includes a cable-driven shoulder with floating scapula [122].

Appendix A

Technical Details

A.1 Uniform Dilation of an Ellipsoid

In chapter 4, it is stated that the scapulothoracic contact is modelled by constraining two points to remain on the surface of two ellipsoids with common centres. This model is almost equivalent to the model where the two points are constrained to remain at a constant distance from the surface of a single ellipsoid. The single ellipsoid has the same centre as the two ellipsoids but has smaller dimensions. This section proves the statement that using a uniformly dilated ellipsoid is almost equivalent to constraining a point to remain at a constant distance from its surface.

The single ellipsoid with smaller dimensions is assumed to be at the origin of a reference frame and aligned with its axes. The surface is defined by a quadric equation and is parameterised by spherical coordinates (α, β) .

$$\frac{x^2}{A^2} + \frac{y^2}{B^2} + \frac{z^2}{C^2} - 1 = 0, \quad X(\alpha, \beta) := \begin{cases} x = A \cos(\alpha) \sin(\beta), \\ y = B \sin(\alpha) \sin(\beta), \\ z = C \cos(\beta). \end{cases} \quad (\text{A.1})$$

This ellipsoid is referred to as the original ellipsoid. The uniform dilation of an ellipsoid by a factor D is defined by:

$$\frac{x^2}{(A+D)^2} + \frac{y^2}{(B+D)^2} + \frac{z^2}{(C+D)^2} - 1 = 0, \quad \tilde{X}_D(\alpha, \beta) := \begin{cases} x = (A+D) \cos(\alpha) \sin(\beta), \\ y = (B+D) \sin(\alpha) \sin(\beta), \\ z = (C+D) \cos(\beta). \end{cases} \quad (\text{A.2})$$

A point is constrained to remain at a constant distance D from the original ellipsoid. The distance is defined along the normal to the original ellipsoid's surface. The normal to an ellipsoid's surface is defined by:

$$\vec{n}(\alpha, \beta) := \begin{cases} \frac{1}{A} \cos(\alpha) \sin(\beta), \\ \frac{1}{B} \sin(\alpha) \sin(\beta), \\ \frac{1}{C} \cos(\beta), \end{cases} \quad \|\vec{n}\| = \sqrt{\left(\left(\frac{\cos(\alpha)}{A} \right)^2 + \left(\frac{\sin(\alpha)}{B} \right)^2 \right) (\sin(\beta))^2 + \left(\frac{\cos(\beta)}{C} \right)^2} \quad (\text{A.3})$$

The point is constrained to remain at a distance D and is defined by:

$$\bar{X}_D(\alpha, \beta) := \begin{cases} A \cos(\alpha) \sin(\beta) + \frac{D}{\|\vec{n}\|} \cos(\alpha) \sin(\beta), \\ B \sin(\alpha) \sin(\beta) + \frac{D}{\|\vec{n}\|} \sin(\alpha) \sin(\beta), \\ C \cos(\beta) + \frac{D}{\|\vec{n}\|} \cos(\beta). \end{cases} \quad (\text{A.4})$$

The statement is that the error between $\tilde{X}_D(\alpha, \beta)$ and $\bar{X}_D(\alpha, \beta)$ is negligible. The difference vector between the two is defined by:

$$\tilde{X}_D(\alpha, \beta) - \bar{X}_D(\alpha, \beta) := \begin{cases} D \cos(\alpha) \sin(\beta) - \frac{D}{A\|\vec{n}\|} \cos(\alpha) \sin(\beta), \\ D \sin(\alpha) \sin(\beta) - \frac{D}{B\|\vec{n}\|} \sin(\alpha) \sin(\beta), \\ D \cos(\beta) - \frac{D}{C\|\vec{n}\|} \cos(\beta). \end{cases} \quad (\text{A.5})$$

The norm of this vector is defined by:

$$\|\tilde{X}_D(\alpha, \beta) - \bar{X}_D(\alpha, \beta)\| := \frac{D}{\|\vec{n}\|} \sqrt{2\|\vec{n}\|^2 - 2\|\vec{n}\|g(\alpha, \beta)}, \quad (\text{A.6})$$

where the function $g(\alpha, \beta)$ is defined by:

$$g(\alpha, \beta) = \left(\left(\frac{\cos(\alpha)}{\sqrt{A}} \right)^2 + \left(\frac{\sin(\alpha)}{\sqrt{B}} \right)^2 \right) (\sin(\beta))^2 + \left(\frac{\cos(\beta)}{\sqrt{C}} \right)^2. \quad (\text{A.7})$$

It can be shown that this function is bounded by:

$$0 < g(\alpha, \beta) \leq \|\vec{n}\|. \quad (\text{A.8})$$

This inequality can be shown using the following:

$$0 \leq (\cos(\alpha))^2 < |\cos(\alpha)| \leq 1, \quad 0 \leq (\sin(\alpha))^2 < |\sin(\alpha)| \leq 1. \quad (\text{A.9})$$

The error function is bounded by:

$$0 \leq \|\tilde{X}_D(\alpha, \beta) - \bar{X}_D(\alpha, \beta)\| = \sqrt{2(1 - \zeta)}D < \sqrt{2}D. \quad (\text{A.10})$$

In the shoulder model, the values of A , B , C and D are such that:

$$\max(\|\tilde{X}_D(\alpha, \beta) - \bar{X}_D(\alpha, \beta)\|) \approx 1\% \min(A, B, C). \quad (\text{A.11})$$

The difference of using two uniformly dilated ellipsoids rather than a single ellipsoid and fixed distances is negligible (Fig. A.1).

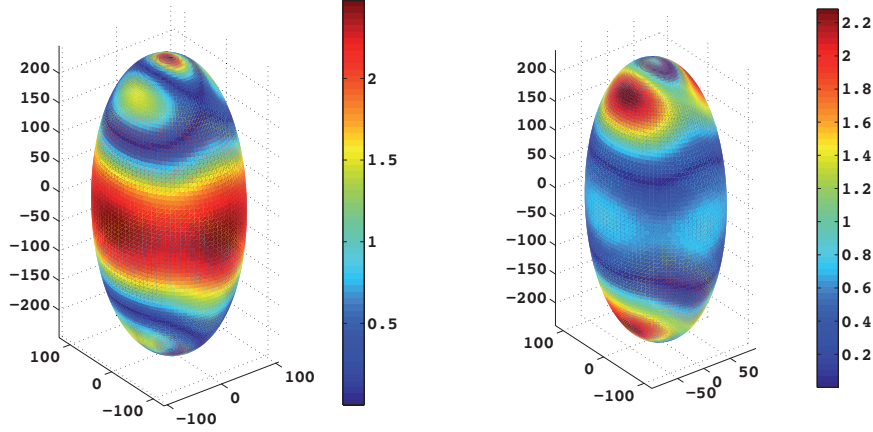


Figure A.1: *Illustration of the error between the two scapulothoracic models. The error is plotted on the original ribcage ellipsoid and defined relative to the original ellipsoid's smallest dimension. The error is plotted in %.*

A.2 Sphere-Ellipsoid Intersection

A.2.1 Quadric Surfaces

Quadrics are surfaces resulting from a locus of zeros of a polynomial equation. More specifically, a quadric is an n -dimensional hyper surface in an $n+1$ -dimensional space. Representing any point in space by a vector $\vec{x} = (x_1, \dots, x_{n+1})^T$, every point on the surface is solution to an equation of the form

$$\vec{x}^T \mathbf{C} \vec{x} + 2\vec{c}^T \vec{x} + r = 0, \quad (\text{A.12})$$

where \mathbf{C} is a $n+1 \times n+1$ matrix, \vec{c} a $n+1 \times 1$ vector and r a constant. This section focuses on quadrics which are two-dimensional surfaces in three-dimensional Euclidean space.

A generalised two-dimensional quadric surface \mathcal{S} is defined by the following equation

$$\begin{aligned} \mathcal{S} : \quad & \alpha_1 x_1^2 + \alpha_2 x_2^2 + \alpha_3 x_3^2 + 2\alpha_4 x_1 x_2 + 2\alpha_5 x_1 x_3 + \dots \\ & 2\alpha_6 x_2 x_3 + 2\alpha_7 x_1 + 2\alpha_8 x_2 + 2\alpha_9 x_3 + \alpha_{10} = 0. \end{aligned} \quad (\text{A.13})$$

In homogeneous coordinates $\vec{x}_h = (\vec{x}^T, w)^T = (x_1, x_2, x_3, w)^T$, the same equation is expressed by:

$$\begin{aligned} \mathcal{S} : \quad & \alpha_1 x_1^2 + \alpha_2 x_2^2 + \alpha_3 x_3^2 + 2\alpha_4 x_1 x_2 + \dots \\ & 2\alpha_5 x_1 x_3 + 2\alpha_6 x_2 x_3 + 2\alpha_7 x_1 w + 2\alpha_8 x_2 w + 2\alpha_9 x_3 w + \alpha_{10} w^2 = 0. \end{aligned} \quad (\text{A.14})$$

where $w = 1$. In matrix form, the quadric surface equation has the form:

$$\mathcal{S} : \vec{x}_h^T \mathbf{C} \vec{x}_h = \begin{pmatrix} x_1 & x_2 & x_3 & 1 \end{pmatrix}^T \begin{pmatrix} \alpha_1 & \alpha_4 & \alpha_5 & \alpha_7 \\ \alpha_4 & \alpha_2 & \alpha_6 & \alpha_8 \\ \alpha_5 & \alpha_6 & \alpha_3 & \alpha_9 \\ \alpha_7 & \alpha_8 & \alpha_9 & \alpha_{10} \end{pmatrix} \begin{pmatrix} x_1 & x_2 & x_3 & 1 \end{pmatrix} = 0. \quad (\text{A.15})$$

The matrix \mathbf{C} is a 4×4 *symmetric* matrix having the following structure

$$\mathbf{C} = \left(\begin{array}{c|c} \mathbf{C}_q & \vec{c}_q \\ \hline - & - \\ \vec{c}_q^T & \alpha_{10} \end{array} \right), \quad (\text{A.16})$$

where \mathbf{C}_q is a 3×3 matrix and \vec{c}_q a 3×1 vector.

The generalised form of a quadric is not always simple to work with. If the quadric is real (eigenvalues of \mathbf{C}_q are all real), it is preferable to have the quadric in canonical form (Tab. A.1). In canonical form, the equation of a real quadric can in general be written by:

$$\mathcal{S}_c : \tilde{\alpha}_1 y_1^2 + \tilde{\alpha}_2 y_2^2 + \tilde{\alpha}_3 y_3^2 + 2\tilde{\alpha}_9 y_3 + \tilde{\alpha}_{10} = 0. \quad (\text{A.17})$$

The canonical coordinate vector is $\vec{y}_h = (\vec{y}^T, 1)^T = (y_1, y_2, y_3, 1)^T$. To pass from this frame to the frame in which the general quadric is defined, a homogeneous transformation is used.

$$\vec{x}_h = \mathbf{H} \vec{y}_h = \left(\begin{array}{c|c} \mathbf{R} & \vec{d} \\ \hline - & - \\ \vec{0}^T & 1 \end{array} \right) \vec{y}_h, \quad (\text{A.18})$$

where \mathbf{R} is the 3×3 rotation matrix and \vec{d} the 3×1 translation vector. Inserting this equation into (A.4) leads to:

$$\vec{x}_h^T \mathbf{C} \vec{x}_h = \vec{y}_h^T \mathbf{H}^T \mathbf{C} \mathbf{H} \vec{y}_h = \vec{y}_h^T \left(\begin{array}{c|c} \mathbf{R}^T \mathbf{C}_q \mathbf{R} & \mathbf{R}^T \mathbf{C}_q \vec{d} + \mathbf{R}^T \vec{c}_q \\ \hline \vec{d}^T \mathbf{C}_q \mathbf{R} + \vec{c}_q^T \mathbf{R} & \vec{d}^T \mathbf{C}_q \vec{d} + 2\vec{d}^T \vec{c}_q + \alpha_{10} \end{array} \right) \vec{y}_h = \vec{y}_h^T \left(\begin{array}{c|c} \tilde{\mathbf{C}}_q & \begin{smallmatrix} 0 \\ 0 \\ \tilde{\alpha}_9 \end{smallmatrix} \\ \hline 0 & \tilde{\alpha}_{10} \end{array} \right) \vec{y}_h, \quad (\text{A.19})$$

where $\tilde{\mathbf{C}}_q$ is *diagonal* with the coefficients $\tilde{\alpha}_1$, $\tilde{\alpha}_2$ and $\tilde{\alpha}_3$ along the diagonal. The coefficients $\tilde{\alpha}_i$ ($i = 1, 2, 3$) are the eigenvalues of the matrix \mathbf{C}_q and $\tilde{\mathbf{C}}_q$. The columns of the rotation matrix \mathbf{R} are the eigenvectors associated to the eigenvalues.

To find the coefficient $\tilde{\alpha}_9$ and the translation vector \vec{d} one can solve the following problem

$$\left(\begin{array}{c} \mathbf{R}^T \mathbf{C}_q \vec{d} + \mathbf{R}^T \vec{c}_q - \begin{pmatrix} 0 \\ 0 \\ \tilde{\alpha}_9 \end{pmatrix} \\ \vec{d}^T \mathbf{C}_q \vec{d} + 2\vec{d}^T \vec{c}_q + \alpha_{10} - \tilde{\alpha}_{10} \end{array} \right) = \mathbf{0}. \quad (\text{A.20})$$

Given an initial estimate $\mu_0 = (\vec{d}_0^T, (\tilde{\alpha}_9)_0)^T$ the solution to the problem is given by the following recursion

$$\vec{\mu}_{k+1} = \vec{\mu}_k - \left(\begin{array}{c|c} \mathbf{R}^T \mathbf{C}_q & \begin{smallmatrix} 0 \\ 0 \\ -1 \end{smallmatrix} \\ \hline - & - \\ 2\mathbf{C}_q \vec{d}_k + 2\vec{c}_q & 0 \end{array} \right)^{-1} \left(\begin{array}{c} \mathbf{R}^T \mathbf{C}_q \vec{d}_k + \mathbf{R}^T \vec{c}_q - \begin{pmatrix} 0 \\ 0 \\ (\tilde{\alpha}_9)_k \end{pmatrix} \\ \vec{d}_k^T \mathbf{C}_q \vec{d}_k + 2\vec{d}_k^T \vec{c}_q + \alpha_{10} - \tilde{\alpha}_{10} \end{array} \right). \quad (\text{A.21})$$

The value of $\tilde{\alpha}_{10}$ is linked to the type of quadric. The type can be determined using the following three scalars.

$$s_1 = \det(\mathbf{C}_q) \quad s_2 = \det(\mathbf{C}) \quad s_3 = |p - n|, \quad \begin{cases} p = N^\circ \text{ positive eigenvalues of } \mathbf{C}_q \\ n = N^\circ \text{ negative eigenvalues of } \mathbf{C}_q \end{cases}. \quad (\text{A.22})$$

An exhaustive list is given in [127]. The quadric can also be normalised with respect to $|\tilde{\alpha}_{10}|$. The normalised canonical form is defined as

$$\bar{\mathcal{J}}_c : \frac{\tilde{\alpha}_1}{|\tilde{\alpha}_{10}|} y_1^2 + \frac{\tilde{\alpha}_2}{|\tilde{\alpha}_{10}|} y_2^2 + \frac{\tilde{\alpha}_3}{|\tilde{\alpha}_{10}|} y_3^2 + 2 \frac{\tilde{\alpha}_9}{|\tilde{\alpha}_{10}|} y_3 \pm 1 = 0, \quad \tilde{\alpha}_{10} \neq 0. \quad (\text{A.23})$$

Table A.1: *List of non-degenerate and degenerate (d) real quadric surfaces in normalised canonical form.*

Non-degenerate	Intrinsic Equations	Degenerate	Intrinsic Equations
Ellipsoid	$x^2/a^2 + y^2/b^2 + z^2/c^2 = 1$	Cone (d)(r)	$x^2/a^2 + y^2/b^2 - z^2/c^2 = 0$
Elliptic Spheroid	$x^2/a^2 + y^2/a^2 + z^2/c^2 = 1$	Circular Cone (d)(r)	$x^2/a^2 + y^2/a^2 - z^2/c^2 = 0$
Sphere	$x^2/a^2 + y^2/a^2 + z^2/a^2 = 1$	Elliptic Cylinder (d)(r)	$x^2/a^2 + y^2/b^2 = 1$
Elliptic paraboloid	$x^2/a^2 + y^2/b^2 - z/c^2 = 0$	Circular Cylinder (d)(r)	$x^2/a^2 + y^2/a^2 = 1$
Circular paraboloid	$x^2/a^2 + y^2/a^2 - z/c^2 = 0$	Hyperbolic Cylinder (d)(r)	$x^2/a^2 - y^2/b^2 = 1$
Hyperbolic paraboloid (r)	$x^2/a^2 - y^2/b^2 - z/c^2 = 0$	Parabolic Cylinder (d)(r)	$x^2 + 2ay = 0$
Hyperboloid (1-sheet) (r)	$x^2/a^2 + y^2/b^2 - z^2/c^2 = 1$		
Hyperboloid (2-sheet)	$x^2/a^2 + y^2/b^2 - z^2/c^2 = -1$		

A.2.2 Ruled Surfaces

A ruled surface \mathcal{S}_r is a surface for which at every point S on the surface, there is a line l passing through S which lies entirely on \mathcal{S}_r . Such surfaces can be described parametrically in terms of two parameters u and v . Any point S on the surface is defined using the general form

$$S(u, v) : \vec{s} = \vec{p}(u) + v\vec{q}(u), \quad (\text{A.24})$$

where $\vec{p}(u)$ and $\vec{q}(u)$ are 3×1 vector functions of u . If the ruled surface is a quadric, it is easier to find the vectors $\vec{p}(u)$ and $\vec{q}(u)$ for the canonical form and then to transform using (A.8). The quadrics that are also ruled surfaces are denoted with an (r) in table A.1. The two most fundamental ruled quadrics are the *hyperbolic paraboloid* and the *hyperbolic cylinder*. These two surfaces are fundamental because they also parameterise the intersection between two quadrics.

The hyperbolic paraboloid described in the previous section (Tab. A.1) has the following parameterisation

$$S(u, v) : \vec{s} = \begin{pmatrix} \frac{a}{c}(u+v) \\ \frac{b}{c}(u-v) \\ 4uv \end{pmatrix} = \begin{pmatrix} \frac{a}{c}u \\ \frac{b}{c}u \\ 0 \end{pmatrix} + v \begin{pmatrix} \frac{a}{c} \\ -\frac{b}{c} \\ 4u \end{pmatrix}. \quad (\text{A.25})$$

This parameterisation comes from the change of variable

$$y_1 = Y_1 + Y_2, \quad y_2 = Y_1 - Y_2, \quad y_3 = 4Y_1Y_2, \quad \text{with} \quad Y_1 = u, \quad Y_2 = v. \quad (\text{A.26})$$

The hyperbolic cylinder, described in the previous section (Tab. A.1), has the parameterisation

$$S(u, v) : \vec{s} = \begin{pmatrix} a \sinh(u) \\ b \cosh(u) \\ v \end{pmatrix} = \begin{pmatrix} a \sinh(u) \\ b \cosh(u) \\ 0 \end{pmatrix} + v \begin{pmatrix} 0 \\ 0 \\ 1 \end{pmatrix}. \quad (\text{A.27})$$

Note that both parameterisations correspond to the normalised canonical forms of the quadric surfaces to which they correspond, respectively:

$$\frac{y_1^2}{a^2} - \frac{y_2^2}{b^2} - \frac{y_3}{c^2} = 0, \quad \frac{y_1^2}{a^2} - \frac{y_2^2}{b^2} - 1 = 0. \quad (\text{A.28})$$

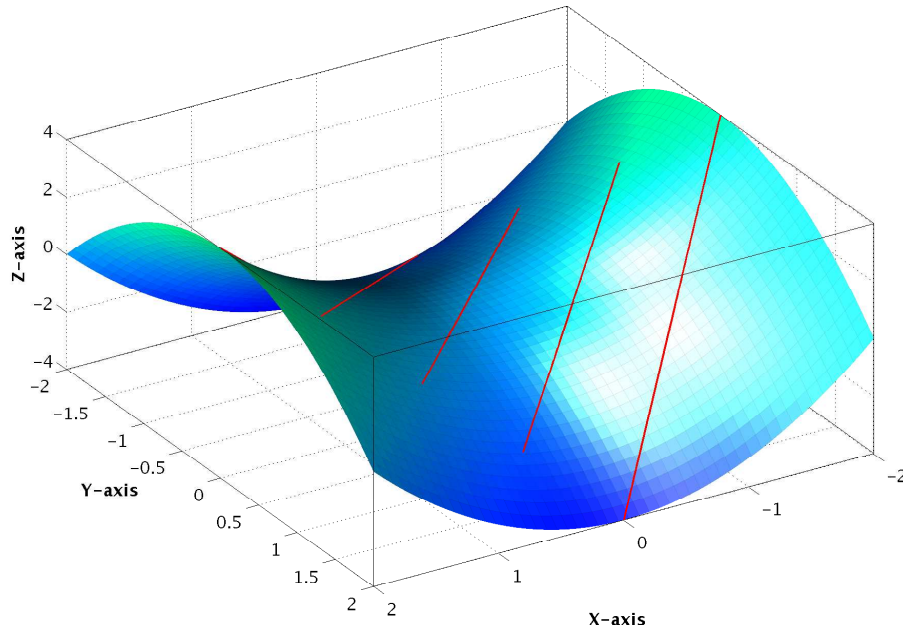


Figure A.2: *Example of the hyperbolic paraboloid with lines representing the ruled surface parameterisation.*

A.2.3 Quadric-Quadric Intersections

The intersection between two quadrics defines a locus of points. The locus in question is one-dimensional, i.e. parameterised by a single variable. There exists an algorithm for constructing the intersection between two quadrics based on the following fundamental theorem [128].

Theorem 27. *Given two real quadric surfaces \mathcal{S} and \mathcal{T} defined by the matrices \mathbf{S} and \mathbf{T} . There exists a real ruled quadric surface \mathcal{Q} belonging to the pencil $\mathbf{E} = \mathbf{S} + \lambda \mathbf{T}$. Where the quadric matrices are define by:*

$$\mathbf{S} = \begin{pmatrix} \alpha_1 & \alpha_4 & \alpha_5 & \alpha_7 \\ \alpha_4 & \alpha_2 & \alpha_6 & \alpha_8 \\ \alpha_5 & \alpha_6 & \alpha_3 & \alpha_9 \\ \alpha_7 & \alpha_8 & \alpha_9 & \alpha_{10} \end{pmatrix} = \left(\begin{array}{c|c} \mathbf{S}_q & \vec{s}_q \\ \hline \vec{s}_q^T & \alpha_{10} \end{array} \right), \quad \mathbf{T} = \begin{pmatrix} \beta_1 & \beta_4 & \beta_5 & \beta_7 \\ \beta_4 & \beta_2 & \beta_6 & \beta_8 \\ \beta_5 & \beta_6 & \beta_3 & \beta_9 \\ \beta_7 & \beta_8 & \beta_9 & \beta_{10} \end{pmatrix} = \left(\begin{array}{c|c} \mathbf{T}_q & \vec{t}_q \\ \hline \vec{t}_q^T & \beta_{10} \end{array} \right), \quad (\text{A.29})$$

The intersection between the two quadrics is defined by:

$$I(u) : \vec{i} = \tilde{p}(u) \pm \sqrt{\sigma(u)} \tilde{q}(u), \quad (\text{A.30})$$

where u is the same parameter used to define the ruled quadric. The ruled quadric is called the parameterisation surface. The ruled surface in question can be found by searching for the quadric with the following property

$$\det(\mathbf{S}_q + \lambda \mathbf{T}_q) = \det(\mathbf{E}_q) = 0. \quad (\text{A.31})$$

The solutions to (A.20) are given as the roots of the following polynomial

$$\mathcal{P}(\lambda) = p_3 \lambda^3 + p_2 \lambda^2 + p_1 \lambda + p_0 = 0, \quad (\text{A.32})$$

$$p_3 = \beta_1 \beta_2 \beta_3 + 2\beta_4 \beta_6 \beta_5 - \beta_5^2 \beta_2 - \beta_4^2 \beta_3 - \beta_1 \beta_6^2,$$

$$p_2 = \alpha_1(\beta_2 \beta_3 - \beta_6^2) + \alpha_2(\beta_1 \beta_3 - \beta_5^2) + \alpha_3(\beta_1 \beta_2 - \beta_4^2) + 2\alpha_4(\beta_5 \beta_6 - \beta_3 \beta_4) + 2\alpha_5(\beta_4 \beta_6 - \beta_2 \beta_5) + 2\alpha_6(\beta_4 \beta_5 - \beta_1 \beta_6),$$

$$p_1 = \beta_1(\alpha_2 \alpha_3 - \alpha_6^2) + \beta_2(\alpha_1 \alpha_3 - \alpha_5^2) + \beta_3(\alpha_1 \alpha_2 - \alpha_4^2) + 2\beta_4(\alpha_5 \alpha_6 - \alpha_3 \alpha_4) + 2\beta_5(\alpha_4 \alpha_6 - \alpha_2 \alpha_5) + 2\beta_6(\alpha_4 \alpha_5 - \alpha_1 \alpha_6),$$

$$p_0 = \alpha_1 \alpha_2 \alpha_3 + 2\alpha_4 \alpha_6 \alpha_5 - \alpha_2 \alpha_5^2 - \alpha_1 \alpha_6^2 - \alpha_4^2 \alpha_3.$$

The solution $\bar{\lambda}$ of interest is identified by testing the conditions set fourth in [127].

$$s_1 = \det(\mathbf{E}_u) = 0, \quad s_2 = \det(\mathbf{E}) > 0, \quad s_3 = |p - n| = 0. \quad (\text{A.33})$$

Once the parameterisation quadric is found, it is identified as either a hyperbolic paraboloid or a hyperbolic cylinder based on the structure of the matrix \mathbf{E} . The intersection in particular is computed by the following procedure.

The ruled quadric is defined by:

$$E(u, v) : \vec{e} = \tilde{p}(u) + v \tilde{q}(u) = \mathbf{R}(\tilde{p}(u) + v \tilde{q}(u)) + \vec{d}, \quad \tilde{p}(u) = \mathbf{R} \tilde{p}(u) + \vec{d}, \quad \tilde{q}(u) = \mathbf{R} \tilde{q}(u). \quad (\text{A.34})$$

This parameterisation must also satisfy the quadric equation for the surface \mathcal{S} , for certain values of u and v . Inserting (A.23) into the quadric equation associated to \mathcal{S} leads to the following expression:

$$\begin{aligned} & (\tilde{p}_h(u) + v \tilde{q}_h(u))^T \cdot \mathbf{S} \cdot (\tilde{p}_h(u) + v \tilde{q}_h(u)) = 0, \\ \Rightarrow & \left(\tilde{q}_h^T(u) \cdot \mathbf{S} \cdot \tilde{q}_h(u) \right) v^2 + 2 \left(\tilde{q}_h^T(u) \cdot \mathbf{S} \cdot \tilde{p}_h(u) \right) v + \tilde{p}_h^T(u) \cdot \mathbf{S} \cdot \tilde{p}_h(u) = 0. \end{aligned} \quad (\text{A.35})$$

This equation gives the expression for $v(u)$:

$$v = \frac{-(\tilde{\mathbf{q}}_h^T(u) \cdot \mathbf{S} \cdot \tilde{\mathbf{p}}_h(u)) \pm \sqrt{(\tilde{\mathbf{q}}_h^T(u) \cdot \mathbf{S} \cdot \tilde{\mathbf{p}}_h(u))^2 - (\tilde{\mathbf{q}}_h^T(u) \cdot \mathbf{S} \cdot \tilde{\mathbf{q}}_h(u)) \tilde{\mathbf{p}}_h^T(u) \cdot \mathbf{S} \cdot \tilde{\mathbf{p}}_h(u)}}{(\tilde{\mathbf{q}}_h^T(u) \cdot \mathbf{S} \cdot \tilde{\mathbf{q}}_h(u))}. \quad (\text{A.36})$$

This equation also defines the interval for u . The possible values for u , must be such that:

$$s(u) = \left(\tilde{\mathbf{q}}_h^T(u) \cdot \mathbf{S} \cdot \tilde{\mathbf{p}}_h(u) \right)^2 - \left(\tilde{\mathbf{q}}_h^T(u) \cdot \mathbf{S} \cdot \tilde{\mathbf{q}}_h(u) \right) \tilde{\mathbf{p}}_h^T(u) \cdot \mathbf{S} \cdot \tilde{\mathbf{p}}_h(u) \geq 0. \quad (\text{A.37})$$

Thus, the bounds on u are obtained by finding the zeros of $s(u)$. Finally, the parameterisation of the intersection is defined by:

$$I(u) : \vec{i} = \tilde{\mathbf{p}}(u) - \frac{\left(\tilde{\mathbf{q}}_h^T(u) \cdot \mathbf{S} \cdot \tilde{\mathbf{p}}_h(u) \right)}{\left(\tilde{\mathbf{q}}_h^T(u) \cdot \mathbf{S} \cdot \tilde{\mathbf{q}}_h(u) \right)} \tilde{\mathbf{q}}(u) \pm \frac{\sqrt{s(u)}}{\left(\tilde{\mathbf{q}}_h^T(u) \cdot \mathbf{S} \cdot \tilde{\mathbf{q}}_h(u) \right)} \tilde{\mathbf{q}}^T(u), \quad u \in [u_-; u_+]. \quad (\text{A.38})$$

The parameter u is parameterised by a normalised coordinate $\mu \in [0, 1]$. The parameterisation is defined by

$$u(\mu) = \begin{cases} u_- + 2\mu(u_+ - u_-) & \text{if } 0 \leq \mu < 0.5 \\ u_+ - 2(\mu - 0.5)(u_+ - u_-) & \text{if } 0.5 \leq \mu \leq 1 \end{cases} \quad (\text{A.39})$$

This presentation of the quadric-quadric intersection problem is general and does not consider a number of important cases which can arise. For a more complete presentation, the reader is referred to [210].

A.2.4 Sphere-Ellipsoid Intersection

This section presents the particular case of the intersection between a sphere \mathbb{S}^2 and an ellipsoid \mathbb{E}^2 . The intersection between a sphere centred at C_s of radius ρ_s and an ellipsoid centred at C_e with axial dimensions e_x , e_y and e_z is a simple example of the quadric-quadric intersection problem. The quadric matrices \mathbf{S} and \mathbf{T} are partially diagonal and can be written by:

$$\mathbf{S} = \begin{pmatrix} \alpha_1 & 0 & 0 & \alpha_7 \\ 0 & \alpha_2 & 0 & \alpha_8 \\ 0 & 0 & \alpha_3 & \alpha_9 \\ \alpha_7 & \alpha_8 & \alpha_9 & \alpha_{10} \end{pmatrix}, \quad \mathbf{T} = \begin{pmatrix} \beta_1 & 0 & 0 & \beta_7 \\ 0 & \beta_2 & 0 & \beta_8 \\ 0 & 0 & \beta_3 & \beta_9 \\ \beta_7 & \beta_8 & \beta_9 & \beta_{10} \end{pmatrix}, \quad (\text{A.40})$$

Thus, the polynomial of λ is given by

$$\mathcal{P}(\lambda) = (\beta_1\beta_2\beta_3)\lambda^3 + (\alpha_1\beta_2\beta_3 + \alpha_2\beta_1\beta_3 + \alpha_3\beta_1\beta_2)\lambda^2 + (\beta_1\alpha_2\alpha_3 + \beta_2\alpha_1\alpha_3 + \beta_3\alpha_1\alpha_2)\lambda + (\alpha_1\alpha_2\alpha_3) = 0. \quad (\text{A.41})$$

Because the sphere is independent of the orientation, the problem can always be solved in the ellipsoid reference frame and thus $\mathbf{R} = \mathbf{I}$. The ruled quadric is given by

$$E(u, v) : \vec{e} = \vec{p}(u) + v\vec{q}(u) + \vec{d}. \quad (\text{A.42})$$

The coordinates can always be arranged such that the implicit equations have the form given by (A.17) for the hyperbolic paraboloid and hyperbolic cylinder. The ruled quadric surface is defined by:

$$\mathbf{E} = \mathbf{S} + \bar{\lambda}\mathbf{T} = \begin{pmatrix} \gamma_1 & 0 & 0 & \gamma_7 \\ 0 & \gamma_2 & 0 & \gamma_8 \\ 0 & 0 & \gamma_3 & \gamma_9 \\ \gamma_7 & \gamma_8 & \gamma_9 & \gamma_{10} \end{pmatrix} = \begin{pmatrix} \alpha_1 + \bar{\lambda}\beta_1 & 0 & 0 & \alpha_7 + \bar{\lambda}\beta_7 \\ 0 & \alpha_2 + \bar{\lambda}\beta_2 & 0 & \alpha_8 + \bar{\lambda}\beta_8 \\ 0 & 0 & \alpha_3 + \bar{\lambda}\beta_3 & \alpha_9 + \bar{\lambda}\beta_9 \\ \alpha_7 + \bar{\lambda}\beta_7 & \alpha_8 + \bar{\lambda}\beta_8 & \alpha_9 + \bar{\lambda}\beta_9 & \alpha_{10} + \bar{\lambda}\beta_{10} \end{pmatrix}. \quad (\text{A.43})$$

If the ruled surface is a hyperbolic cylinder: $\gamma_3 = \gamma_9 = 0$. If the ruled surface is a hyperbolic paraboloid: $\gamma_3 = 0$. Once the type of ruled surface is known, the coefficients are identified and the translation vector \vec{d} is defined.

For the hyperbolic cylinder, the following relation is defined :

$$\gamma_1 x^2 + \gamma_2 y^2 + 2\gamma_7 x + 2\gamma_8 y + \gamma_{10} = \tilde{\alpha}_1 (x - x_0)^2 + \tilde{\alpha}_2 (y - y_0)^2 + \tilde{\alpha}_4 = 0. \quad (\text{A.44})$$

Where the coefficients are

$$\begin{aligned} \tilde{\alpha}_1 &= \gamma_1, & \tilde{\alpha}_2 &= \gamma_2, \\ 2\gamma_7 &= -2\tilde{\alpha}_1 x_0 & 2\gamma_8 &= -2\tilde{\alpha}_2 y_0, \\ \gamma_{10} &= \tilde{\alpha}_1 x_0^2 + \tilde{\alpha}_2 y_0^2 + \tilde{\alpha}_4 \end{aligned}$$

For the hyperbolic paraboloid, the following relation is defined :

$$\gamma_1 x^2 + \gamma_2 y^2 + 2\gamma_7 x + 2\gamma_8 y + 2\gamma_9 z + \gamma_{10} = \tilde{\alpha}_1 (x - x_0)^2 + \tilde{\alpha}_2 (y - y_0)^2 + \tilde{\alpha}_3 (z - z_0) = 0. \quad (\text{A.45})$$

Where the coefficients are

$$\begin{aligned} \tilde{\alpha}_1 &= \gamma_1, & \tilde{\alpha}_2 &= \gamma_2, & \tilde{\alpha}_3 &= 2\gamma_9 \\ 2\gamma_7 &= -2\tilde{\alpha}_1 x_0 & 2\gamma_8 &= -2\tilde{\alpha}_2 y_0, \\ \gamma_{10} &= \tilde{\alpha}_1 x_0^2 + \tilde{\alpha}_2 y_0^2 - \tilde{\alpha}_3 z_0 \end{aligned}$$

These expressions are used to build the intersection.

Appendix B

Shoulder Model Numerical Dataset

B.1 Bony Landmarks and Rotation Matrices

This appendix provides the numerical dataset necessary to construct the musculoskeletal shoulder model described in chapter 4. The dataset was obtained from MRI scans of an adult male's right shoulder. The numerical data was extracted using the Amira 3D Software for Life Sciences.

The MATLAB/ISG reference frame is defined by the following vectors. These vectors are parallel to the unit vectors of the inertial frame \mathcal{R}_0 , but are defined in the Amira frame \mathcal{R}_a .

$$\begin{aligned}\mathbf{k}_{a,0} &= \frac{1}{2} \left(\vec{C7} + \vec{IJ} \right) - \frac{1}{2} \left(\vec{T8} + \vec{PX} \right), \\ \mathbf{i}_{a,0} &= \left(\vec{C7} - \vec{IJ} \right) \times \frac{1}{2} \left(\left(\vec{T8} + \vec{PX} \right) - \vec{IJ} \right), \\ \mathbf{j}_{a,0} &= \mathbf{k}_{a,0} \times \mathbf{i}_{a,0}.\end{aligned}\tag{B.1}$$

The rotation matrix to transform points in the Amira frame into points in the MATLAB/ISG frame is defined by:

$$\mathbf{R}_{a,0} = \left(\frac{\mathbf{i}_{a,0}}{\|\mathbf{i}_{a,0}\|}, \frac{\mathbf{j}_{a,0}}{\|\mathbf{j}_{a,0}\|}, \frac{\mathbf{k}_{a,0}}{\|\mathbf{k}_{a,0}\|} \right).\tag{B.2}$$

The homogeneous transformation from the Amira frame into the MATLAB/ISG inertial frame is defined by:

$$\mathbf{H}_{a,0} = \begin{pmatrix} \mathbf{R}_{a,0} & -\mathbf{R}_{a,0} \cdot \vec{IJ} \\ 0 & 0 & 0 & 1 \end{pmatrix}.\tag{B.3}$$

Using the transformed points, the clavicle, scapula and humerus reference frames are constructed using the following definitions. The unit vectors are in the inertial frame. The clavicle frame vectors in the inertial frame are defined by:

$$\begin{aligned}\mathbf{i}_{0,1} &= \vec{AC}_0 - \vec{SC}_0, \\ \mathbf{j}_{0,1} &= (0 \ 0 \ 1)^T \times \mathbf{i}_{0,1}, \\ \mathbf{k}_{0,1} &= \mathbf{i}_{0,1} \times \mathbf{j}_{0,1}.\end{aligned}\tag{B.4}$$

The rotation matrix to transform points in the clavicle frame \mathcal{R}_1 into points in the inertial frame \mathcal{R}_0 is defined by:

$$\mathbf{R}_{1,0} = \left(\frac{\mathbf{i}_{0,1}}{\|\mathbf{i}_{0,1}\|}, \frac{\mathbf{j}_{0,1}}{\|\mathbf{j}_{0,1}\|}, \frac{\mathbf{k}_{0,1}}{\|\mathbf{k}_{0,1}\|} \right). \quad (\text{B.5})$$

The scapula frame vectors in the inertial frame are defined by:

$$\begin{aligned} \mathbf{i}_{0,2} &= \vec{A}A_0 - T\vec{S}_0 \\ \mathbf{j}_{0,2} &= \mathbf{i}_{0,2} \times \left(\vec{A}I_0 - T\vec{S}_0 \right)^T \\ \mathbf{k}_{0,2} &= \mathbf{i}_{0,2} \times \mathbf{j}_{0,2} \end{aligned} \quad (\text{B.6})$$

The rotation matrix to transform points in the clavicle frame \mathcal{R}_2 into points in the inertial frame \mathcal{R}_0 is defined by:

$$\mathbf{R}_{2,0} = \left(\frac{\mathbf{i}_{0,2}}{\|\mathbf{i}_{0,2}\|}, \frac{\mathbf{j}_{0,2}}{\|\mathbf{j}_{0,2}\|}, \frac{\mathbf{k}_{0,2}}{\|\mathbf{k}_{0,2}\|} \right). \quad (\text{B.7})$$

The humerus frame vectors in the inertial frame are defined by:

$$\begin{aligned} \mathbf{k}_{0,3} &= G\vec{H}_0 - \frac{1}{2} \left(E\vec{M}_0 + E\vec{L}_0 \right), \\ \mathbf{j}_{0,3} &= \left(G\vec{H}_0 - E\vec{L}_0 \right) \times \left(E\vec{L}_0 - E\vec{M}_0 \right), \\ \mathbf{i}_{0,3} &= \mathbf{j}_{0,3} \times \mathbf{k}_{0,3}. \end{aligned} \quad (\text{B.8})$$

The rotation matrix to transform points in the humerus frame \mathcal{R}_3 into points in the inertial frame \mathcal{R}_0 is defined by:

$$\mathbf{R}_{3,0} = \left(\frac{\mathbf{i}_{0,3}}{\|\mathbf{i}_{0,3}\|}, \frac{\mathbf{j}_{0,3}}{\|\mathbf{j}_{0,3}\|}, \frac{\mathbf{k}_{0,3}}{\|\mathbf{k}_{0,3}\|} \right). \quad (\text{B.9})$$

Table B.1: *List of bony landmarks for constructing the shoulder kinematic model. Data provided in the Amira 3D Software for Life Sciences frame.*

Bony Landmark	Initials	X [mm]	Y [mm]	Z [mm]
Jugular Incision	IJ	74.1129	-74.8060	68.9446
Xyphoid Process	PX	82.5171	-133.1130	-76.9724
T8 vertebrae	T8	78.9481	-24.5985	-40.6273
C7 vertebrae	C7	70.5729	-35.7244	150.7640
Sternoclavicular Joint	SC	52.0511	-79.0859	75.0302
Acromioclavicular Joint	AC	-82.1051	-30.7575	145.4510
Glenohumeral Joint	GH	-86.1456	-31.7209	107.6860
Humeroulnar Joint	HU	-103.7780	-33.3235	-205.8640
Trigonum Spinae	TS	-0.9241	52.0670	121.3280
Angulus Inferior	AI	-6.7869	50.3866	-4.7008
Angulus Acromialis	AA	-104.3290	-1.0350	133.7840
Lateral Epicondyle	EL	-127.2850	-54.8861	-208.4960
Medial Epicondyle	EM	-80.2709	-11.7610	-203.2320
Ellipsoid Centre	E	34.06	-10.23	-60.63
Ellipsoid Dimension	AE	106.39	111.48	152.00

B.2 Mass, Intertia and Glendoid Stability

The dynamic model was constructed using the inertial data from [28] (Table B.2). The centre of gravity of each bone is defined by:

$$CG_{0,1} : \vec{x}_{0,1} = \vec{SC}_0 + \frac{1}{2}\mathbf{R}_{1,0} \left(\vec{AC}_1 \right), \quad (\text{B.10})$$

$$CG_{0,2} : \vec{x}_{0,2} = \vec{SC}_0 + \mathbf{R}_{1,0} \left(\vec{AC}_1 \right) + \frac{1}{3}\mathbf{R}_{2,0} \left(\vec{AI}_2 \right), \quad (\text{B.11})$$

$$CG_{0,3} : \vec{x}_{0,3} = \vec{SC}_0 + \mathbf{R}_{1,0} \left(\vec{AC}_1 \right) + \mathbf{R}_{2,0} \left(\vec{GH}_2 \right) + \mathbf{R}_{3,0} \left(\vec{HU}_2 \right). \quad (\text{B.12})$$

The humeral data is also the data for the outstretched arm.

Table B.2: *List of inertial data to construct dynamic model. The data taken from [28]. The humerus data includes the arm.*

Data Type	Clavicle	Scapula	Humerus (Arm)
Mass [kg]	0.156	0.704	3.67
Transverse Inertia [kgm ²]	0.001	0.007	1.996
Longitudinal Inertia [kgm ²]	0.003	0.007	0.309

The glenoid stability constraint is defined using the data collected from the MRI scans. The data contains the dimensions of the glenoid ellipse (H_y, H_z), the centre of the glenoid ellipse GC in the inertial frame but with respect to the centre of the glenohumeral joint. The cone reference frame axes are defined by:

$$\begin{aligned} \mathbf{i}_{0,5} &= G\vec{H}_0 - \vec{GC}_0, \\ \mathbf{k}_{0,5} &= (0, 0, 1)^T, \\ \mathbf{j}_{0,5} &= \mathbf{k}_{0,5} \times \mathbf{i}_{0,5}, \\ \mathbf{k}_{0,5} &= \mathbf{i}_{0,5} \times \mathbf{j}_{0,5}. \end{aligned} \quad (\text{B.13})$$

The rotation matrix to transform a point in the glenoid frame into a point in the inertial frame is defined by:

$$\mathbf{R}_{5,0} = \left(\frac{\mathbf{i}_{0,5}}{\|\mathbf{i}_{0,5}\|}, \frac{\mathbf{j}_{0,5}}{\|\mathbf{j}_{0,5}\|}, \frac{\mathbf{k}_{0,5}}{\|\mathbf{k}_{0,5}\|} \right). \quad (\text{B.14})$$

Table B.3: *The data is provided in the thorax/inertial reference system.*

Data Type	X [mm]	Y [mm]	Z [mm]
Centre of Glenoid GC	-13.80	-15.50	-2.46
Superior/Inferior Dimension H_z , [mm]			17.5
Posterior/Anterior Dimension H_y , [mm]			12.8

B.3 Muscle Geometry and Wrapping

This section provides the geometric data necessary to construct the muscle wrapping. The data contains the origin, the insertion and any via points of each muscle. Each muscle has been given a trio of anchor points to construct the third order splines of the muscle origins, insertions and via points. In the local bone frame, the spline construction is defined by:

$$P_{i,k}(\mu) : \vec{p}_{i,k}(\mu) = \begin{cases} (\mu^3 \ \mu^2 \ \mu \ 1) \mathbf{S} \begin{pmatrix} \vec{p}_{i,s} \\ \vec{p}_{i,s} \\ \vec{p}_{i,m} \\ \vec{p}_{i,f} \end{pmatrix} & \text{if } 0 \leq \mu < 0.5 \\ (\mu^3 \ \mu^2 \ \mu \ 1) \mathbf{S} \begin{pmatrix} \vec{p}_{i,s} \\ \vec{p}_{i,m} \\ \vec{p}_{i,f} \\ \vec{p}_{i,f} \end{pmatrix} & \text{if } 0.5 \leq \mu \leq 1 \end{cases}, \mathbf{S} = \begin{pmatrix} -\frac{1}{2} & \frac{3}{2} & -\frac{3}{2} & \frac{1}{2} \\ 1 & \frac{5}{2} & 2 & -\frac{1}{2} \\ -\frac{1}{2} & 0 & \frac{1}{2} & 0 \\ 0 & 1 & 0 & 0 \end{pmatrix}. \quad (\text{B.15})$$

where μ is the spline parameterisation variable. Each point is defined in terms of its x -, y -, and z -coordinates in the Amira frame. The bone reference frame \mathcal{R}_i ($i = 0, 1, 2, 3$) to which the point is attached is also given.

The data contains the wrapping constraints, modelling the anatomical constraints of the real shoulder which are either other muscles or bony structures. The constraints are of the same type as the ones defined in [76]. The constraints are one of the following:

- None: The muscle has no wrapping constraints,
- Single: The muscle has single cylinder wrapping constraint,
- Double: The muscle has a double wrapping constraint,
- Stub: The muscle has a sphere capped cylinder wrapping constraint.

Each of the constraint types is a smooth surface. The surfaces are characterised by a point, an orientation and a dimension. The point fixes the location of the constraint surface with respect to the bone which it represents. The point is designated by $O_{i,w}$. The subindex i is the index of the bone to which the constraint is attached. The orientation is parameterised by a single vector $\vec{z}_{i,w}$. The constraint surfaces are cylinders, the vector $\vec{z}_{i,w}$ is the cylinder axes direction vector with respect to same bone as $O_{i,w}$. The dimension D_w is the diameter of the cylinder. For sphere capped cylinders, the half sphere is situated in the positive z -axis direction. All the data is provided in the MATLAB frame. The wrappings are constructed using the geometric algorithms from [75]. The D_w values have a sign which indicates which path the muscle segment takes around the cylinder.

Table B.4: *Muscle wrapping data for constructing the muscle geometric model. Data is provided in the Amira 3D Software for Life Sciences frame.*

Subclavius	Origin \mathcal{R}_0			Insertion \mathcal{R}_1		
Point Id	X [mm]	Y [mm]	Z [mm]	X [mm]	Y [mm]	Z [mm]
$\vec{p}_{i,s}$	47.3022	-21.8898	21.4841	124.6826	-8.302	8.677
$\vec{p}_{i,m}$	40.1071	-16.5496	14.6819	106.0602	-0.31249	6.6497
$\vec{p}_{i,f}$	32.8671	-11.9641	8.885	89.4372	5.0201	2.5492
Type: None						
Serratus Anterior Sup.	Origin \mathcal{R}_0			Insertion \mathcal{R}_2		
Point Id	X [mm]	Y [mm]	Z [mm]	X [mm]	Y [mm]	Z [mm]
$\vec{p}_{i,s}$	94.7792	-28.9257	5.9179	-121.029	2.772	-7.7555
$\vec{p}_{i,m}$	78.1183	-33.3803	35.5112	-119.0805	8.5437	6.9199
$\vec{p}_{i,f}$	65.8219	-41.8242	48.2433	-113.547	21.9331	21.7063
Type: Single	Centre \mathcal{R}_0			Axis \mathcal{R}_0		
Radius: 62.4636 [mm]	78.9075	-68.7859	10.967	0.70426	0.099214	-0.70297
Serratus Anterior Mid.	Origin \mathcal{R}_0			Insertion \mathcal{R}_2		
Point Id	X [mm]	Y [mm]	Z [mm]	X [mm]	Y [mm]	Z [mm]
$\vec{p}_{i,s}$	100.5324	-8.6176	-52.4343	-124.7227	0.035524	-48.6225
$\vec{p}_{i,m}$	95.1886	-15.1122	-25.1971	-122.906	-0.065892	-32.328
$\vec{p}_{i,f}$	92.3368	-19.8318	-4.0179	-121.6444	2.3897	-13.4542
Type: Single	Centre \mathcal{R}_0			Axis \mathcal{R}_0		
Radius: 83.3324 [mm]	90.9775	-58.6028	-37.1678	0.43024	0.096155	-0.89758
Serratus Anterior Inf.	Origin \mathcal{R}_0			Insertion \mathcal{R}_2		
Point Id	X [mm]	Y [mm]	Z [mm]	X [mm]	Y [mm]	Z [mm]
$\vec{p}_{i,s}$	114.3886	-82.1116	-165.5598	-129.361	7.5023	-124.0556
$\vec{p}_{i,m}$	126.4075	-24.6966	-110.3313	-131.0031	0.9116	-88.1316
$\vec{p}_{i,f}$	104.6699	-7.7682	-54.275	-126.5523	0.86269	-55.1583
Type: Single	Centre \mathcal{R}_0			Axis \mathcal{R}_0		
Radius: 114.0104 [mm]	66.9717	-55.2411	-75.9889	-0.019976	-0.01175	-0.99973
Trapezius C1-C6	Origin \mathcal{R}_0			Insertion \mathcal{R}_1		
Point Id	X [mm]	Y [mm]	Z [mm]	X [mm]	Y [mm]	Z [mm]
$\vec{p}_{i,s}$	17.933	-40.1305	144.999	110.4728	2.4786	12.9065
$\vec{p}_{i,m}$	6.9117	-54.655	130.1448	142.5331	-4.7352	13.0363
$\vec{p}_{i,f}$	4.4143	-69.5781	116.992	157.5417	-5.5202	7.9516
Type: Single	Centre \mathcal{R}_0			Axis \mathcal{R}_0		
Radius: 65.23 [mm]	63.4174	-48.0171	130.8476	0.17043	-0.90071	0.39959
Trapezius C7	Origin \mathcal{R}_0			Insertion \mathcal{R}_2		
Point Id	X [mm]	Y [mm]	Z [mm]	X [mm]	Y [mm]	Z [mm]
$\vec{p}_{i,s}$	9.3247	-95.6367	80.1995	-45.7456	0.8996	13.1699
$\vec{p}_{i,m}$	9.7249	-86.2045	101.2646	-28.0669	7.2086	14.5804
$\vec{p}_{i,f}$	3.4617	-72.0971	113.1491	-13.8296	18.7389	12.4691
Type: Single	Centre \mathcal{R}_0			Axis \mathcal{R}_0		
Radius: 76.1526 [mm]	48.4107	-55.7942	80.0767	-0.11248	0.89622	0.42911

Trapezius T1	Origin \mathcal{R}_0			Insertion \mathcal{R}_2		
Point Id	<i>X</i> [mm]	<i>Y</i> [mm]	<i>Z</i> [mm]	<i>X</i> [mm]	<i>Y</i> [mm]	<i>Z</i> [mm]
$\vec{p}_{i,s}$	9.5704	-111.3463	35.6335	-79.9134	-11.4331	7.743
$\vec{p}_{i,m}$	7.7586	-106.525	56.8341	-62.1015	-6.056	11.0343
$\vec{p}_{i,f}$	5.5539	-97.0621	78.3253	-50.1784	-0.97814	13.5338
Type: Single	Centre \mathcal{R}_0			Axis \mathcal{R}_0		
Radius: 95.6832 [mm]	63.7866	-84.4989	52.4261	-0.025594	0.53043	0.84734
Trapezius T2-T7	Origin \mathcal{R}_0			Insertion \mathcal{R}_2		
Point Id	<i>X</i> [mm]	<i>Y</i> [mm]	<i>Z</i> [mm]	<i>X</i> [mm]	<i>Y</i> [mm]	<i>Z</i> [mm]
$\vec{p}_{i,s}$	4.3375	-114.3685	-203.4799	-86.013	-12.1708	6.5964
$\vec{p}_{i,m}$	6.1887	-125.1353	-91.0941	-95.9787	-8.495	-2.1346
$\vec{p}_{i,f}$	7.4436	-117.4578	32.2477	-113.4155	-3.393	-0.42729
Type: Single	Centre \mathcal{R}_0			Axis \mathcal{R}_0		
Radius: 121.5968 [mm]	50.3929	-74.9743	-70.7722	0.012283	0.012307	0.99985
Levator Scapulae	Origin \mathcal{R}_0			Insertion \mathcal{R}_2		
Point Id	<i>X</i> [mm]	<i>Y</i> [mm]	<i>Z</i> [mm]	<i>X</i> [mm]	<i>Y</i> [mm]	<i>Z</i> [mm]
$\vec{p}_{i,s}$	16.0717	-42.3965	166.4632	-112.9184	17.2979	23.1744
$\vec{p}_{i,m}$	15.824	-50.0719	154.5936	-117.6254	10.792	15.6349
$\vec{p}_{i,f}$	16.8122	-56.7843	141.4639	-117.2106	4.8568	8.3213
Type: None						
Rhomboid Minor	Origin \mathcal{R}_0			Insertion \mathcal{R}_2		
Point Id	<i>X</i> [mm]	<i>Y</i> [mm]	<i>Z</i> [mm]	<i>X</i> [mm]	<i>Y</i> [mm]	<i>Z</i> [mm]
$\vec{p}_{i,s}$	10.1598	-85.1539	101.1227	-119.332	7.178	7.618
$\vec{p}_{i,m}$	9.7589	-91.293	90.9366	-119.7223	0.62991	-2.048
$\vec{p}_{i,f}$	9.6095	-96.2044	79.1984	-121.3933	-0.48993	-11.5158
Type: None						
Rhomboid Major T1-T2	Origin \mathcal{R}_0			Insertion \mathcal{R}_2		
Point Id	<i>X</i> [mm]	<i>Y</i> [mm]	<i>Z</i> [mm]	<i>X</i> [mm]	<i>Y</i> [mm]	<i>Z</i> [mm]
$\vec{p}_{i,s}$	7.7951	-100.6494	72.6624	-122.0314	-1.3421	-16.8202
$\vec{p}_{i,m}$	12.0043	-108.3404	54.4455	-124.3712	-2.7343	-38.3552
$\vec{p}_{i,f}$	13.2638	-114.3854	32.1064	-127.6047	-1.1541	-65.5843
Type: Single	Centre \mathcal{R}_0			Axis \mathcal{R}_0		
Radius: 90.2222 [mm]	49.2891	-79.2561	39.7921	-0.077561	0.21154	0.97429
Rhomboid Major T3-T4	Origin \mathcal{R}_0			Insertion \mathcal{R}_2		
Point Id	<i>X</i> [mm]	<i>Y</i> [mm]	<i>Z</i> [mm]	<i>X</i> [mm]	<i>Y</i> [mm]	<i>Z</i> [mm]
$\vec{p}_{i,s}$	16.0253	-120.6784	-20.5786	-132.9776	2.8646	-122.1601
$\vec{p}_{i,m}$	14.735	-119.6945	5.0805	-132.0646	-0.99899	-94.523
$\vec{p}_{i,f}$	13.6637	-117.1852	25.4825	-129.3213	-1.4088	-70.663
Type: Single	Centre \mathcal{R}_0			Axis \mathcal{R}_0		
Radius: 90.2222 [mm]	52.2229	-88.3502	-9.6992	-0.052258	0.054114	0.99717

Pectoralis Minor	Origin \mathcal{R}_0			Insertion \mathcal{R}_2		
Point Id	X [mm]	Y [mm]	Z [mm]	X [mm]	Y [mm]	Z [mm]
$\vec{p}_{i,s}$	112.4553	1.9047	-114.5028	-33.6689	66.8144	-12.1784
$\vec{p}_{i,m}$	108.3519	-2.7766	-85.7049	-36.7303	63.7507	-9.9863
$\vec{p}_{i,f}$	104.19	-11.663	-48.3304	-40.1253	60.8655	-7.3816
Type: None						
Pectoralis Major Sup.	Origin \mathcal{R}_1			Insertion \mathcal{R}_3		
Point Id	X [mm]	Y [mm]	Z [mm]	X [mm]	Y [mm]	Z [mm]
$\vec{p}_{i,s}$	6.5281	6.8431	-6.0261	6.0428	10.2123	-81.5794
$\vec{p}_{i,m}$	30.0086	13.1245	-4.589	5.0411	9.4042	-89.0349
$\vec{p}_{i,f}$	53.5354	17.2967	-3.6244	3.8217	8.5626	-94.5638
Type: Single	Centre \mathcal{R}_0			Axis \mathcal{R}_0		
Radius: 78.733 [mm]	89.7779	-32.6979	-17.2779	-0.31284	0.31596	-0.89571
Pectoralis Major Mid.	Origin \mathcal{R}_0			Insertion \mathcal{R}_3		
Point Id	X [mm]	Y [mm]	Z [mm]	X [mm]	Y [mm]	Z [mm]
$\vec{p}_{i,s}$	8.527	24.306	-78.8645	6.7832	10.2222	-68.0628
$\vec{p}_{i,m}$	9.7158	16.0647	-50.3474	5.727	10.3971	-75.4138
$\vec{p}_{i,f}$	24.1675	-2.6064	-12.786	5.7225	10.2745	-83.3312
Type: Single	Centre \mathcal{R}_0			Axis \mathcal{R}_0		
Radius: 103.5784 [mm]	72.1919	-31.2906	-52.9492	-0.0025661	0.32076	-0.94716
Pectoralis Major Inf.	Origin \mathcal{R}_0			Insertion \mathcal{R}_3		
Point Id	X [mm]	Y [mm]	Z [mm]	X [mm]	Y [mm]	Z [mm]
$\vec{p}_{i,s}$	45.934	39.1666	-157.381	7.5278	12.1484	-52.3811
$\vec{p}_{i,m}$	10.9816	34.5373	-117.0259	7.0048	11.1011	-62.0383
$\vec{p}_{i,f}$	8.7838	25.2681	-85.1756	6.6532	10.5044	-70.9866
Type: Single	Centre \mathcal{R}_0			Axis \mathcal{R}_0		
Radius: 119.8136 [mm]	65.2042	-25.25	-103.5016	0.36618	0.15146	-0.91814
Latisimuss Dorsi Thoracic	Origin \mathcal{R}_0			Insertion \mathcal{R}_3		
Point Id	X [mm]	Y [mm]	Z [mm]	X [mm]	Y [mm]	Z [mm]
$\vec{p}_{i,s}$	10.6486	-127.1927	-59.9564	6.2547	10.1442	-81.9018
$\vec{p}_{i,m}$	8.025	-125.1166	-121.7227	6.1941	10.4861	-77.1875
$\vec{p}_{i,f}$	5.3463	-122.0054	-173.2486	5.6998	10.404	-70.9403
Type: Double	Centre \mathcal{R}_0			Axis \mathcal{R}_0		
Radius: 126.8796 [mm]	66.287	-75.6991	-117.425	0.064623	-0.03431	0.99732
	Centre \mathcal{R}_3			Axis \mathcal{R}_3		
Radius: 27.2296 [mm]	-5.1088	-2.0566	-75.6967	0.019975	0.067257	-0.99754
Latisimuss Dorsi Lumbar	Origin \mathcal{R}_0			Insertion \mathcal{R}_3		
Point Id	X [mm]	Y [mm]	Z [mm]	X [mm]	Y [mm]	Z [mm]
$\vec{p}_{i,s}$	16.6142	-92.133	-303.7379	7.1407	11.6001	-56.8227
$\vec{p}_{i,m}$	12.0451	-107.6165	-240.7004	6.2475	11.0229	-62.8968
$\vec{p}_{i,f}$	5.1454	-121.5951	-186.0512	5.6569	10.0836	-68.0006
Type: Double	Centre \mathcal{R}_0			Axis \mathcal{R}_0		
Radius: 144.3066 [mm]	78.1611	-42.8298	-240.6841	-0.075133	-0.11952	0.98999
	Centre \mathcal{R}_3			Axis \mathcal{R}_3		
Radius: 27.2296 [mm]	-6.9135	-2.3851	-63.8543	0.1204	-0.0078034	-0.99269

Latisimuss Dorsi Iliac	Origin \mathcal{R}_0			Insertion \mathcal{R}_3		
Point Id	X [mm]	Y [mm]	Z [mm]	X [mm]	Y [mm]	Z [mm]
$\vec{p}_{i,s}$	29.3382	-114.9391	-371.6228	7.2496	10.6415	-43.4864
$\vec{p}_{i,m}$	21.7063	-96.3715	-338.6665	6.9115	10.7837	-49.0554
$\vec{p}_{i,f}$	17.3063	-89.5	-308.8827	7.2819	11.9251	-53.6699
Type: Double	Centre \mathcal{R}_0			Axis \mathcal{R}_0		
Radius: 168.1542 [mm]	78.0742	-36.8231	-202.3643	-0.14768	-0.10953	0.98295
	Centre \mathcal{R}_3			Axis \mathcal{R}_3		
Radius: 27.2296 [mm]	-5.7337	1.1047	-52.4145	0.038747	-0.11434	-0.99269
Anterior Deltoid	Origin \mathcal{R}_1			Insertion \mathcal{R}_3		
Point Id	X [mm]	Y [mm]	Z [mm]	X [mm]	Y [mm]	Z [mm]
$\vec{p}_{i,s}$	126.6803	-0.87531	10.275	9.4509	4.0979	-129.2376
$\vec{p}_{i,m}$	143.604	-0.39192	7.1363	9.56	5.2246	-139.2259
$\vec{p}_{i,f}$	160.8002	6.0558	0.40596	9.3273	5.3664	-148.3023
Point Id	Via A			Via B \mathcal{R}_3		
$\vec{p}_{i,s}$				23.0056	13.9745	-102.6272
$\vec{p}_{i,m}$				23.4855	10.2534	-102.7768
$\vec{p}_{i,f}$				23.3426	5.9889	-102.9171
Type: Single	Centre \mathcal{R}_2			Axis \mathcal{R}_2		
Radius: -73.1998 [mm]	-14.6895	44.6045	-32.5017	0.73986	-0.50467	0.44489
Middle Deltoid	Origin \mathcal{R}_2			Insertion \mathcal{R}_3		
Point Id	X [mm]	Y [mm]	Z [mm]	X [mm]	Y [mm]	Z [mm]
$\vec{p}_{i,s}$	-0.20406	-0.074248	0.13482	10.2435	-0.36749	-129.4244
$\vec{p}_{i,m}$	11.8236	27.4926	1.9362	10.8922	0.59153	-139.4917
$\vec{p}_{i,f}$	1.0065	39.9286	9.0799	10.3543	1.1799	-147.7047
Point Id	Via A \mathcal{R}_2			Via B \mathcal{R}_3		
$\vec{p}_{i,s}$	20.1262	5.4089	-0.075243	21.9272	-7.8303	-103.3292
$\vec{p}_{i,m}$	19.672	32.11	0.066403	22.6176	-3.6131	-103.215
$\vec{p}_{i,f}$	8.8135	52.8413	2.7152	23.3555	1.4133	-103.0751
Type: Stub	Centre \mathcal{R}_3			Axis \mathcal{R}_3		
Radius: 55.3988 [mm]	6.9099	-3.21	0.56374	0.28815	-0.024237	0.95728
Posterior Deltoid	Origin \mathcal{R}_2			Insertion \mathcal{R}_3		
Point Id	X [mm]	Y [mm]	Z [mm]	X [mm]	Y [mm]	Z [mm]
$\vec{p}_{i,s}$	-69.6536	-10.1689	2.1174	9.7675	-4.5744	-129.1426
$\vec{p}_{i,m}$	-29.2521	-3.4775	7.3322	11.1254	-3.3937	-138.7676
$\vec{p}_{i,f}$	-3.5772	-0.92811	-0.30127	10.6649	-3.3442	-147.7837
Point Id	Via A \mathcal{R}_2			Via B \mathcal{R}_3		
$\vec{p}_{i,s}$	-38.2118	-13.8338	-13.9952	14.3382	-20.1916	-103.4148
$\vec{p}_{i,m}$	-14.3091	-11.162	-6.1601	18.0168	-16.2487	-103.4438
$\vec{p}_{i,f}$	9.0994	-1.4206	-8.9833	20.6761	-11.6495	-103.4046
Type: Stub	Centre \mathcal{R}_2			Axis \mathcal{R}_2		
Radius: 58.0972 [mm]	3.4356	31.7188	-25.3069	0.2912	-0.17793	0.93997

Supraspinatus	Origin \mathcal{R}_2			Insertion \mathcal{R}_3		
Point Id	X [mm]	Y [mm]	Z [mm]	X [mm]	Y [mm]	Z [mm]
$\vec{p}_{i,s}$	-92.7644	31.4612	22.0077	23.834	9.767	6.4975
$\vec{p}_{i,m}$	-101.1358	22.9552	13.4189	25.7241	2.5645	5.9216
$\vec{p}_{i,f}$	-104.8622	10.9751	5.223	24.4828	-5.4397	3.8368
Point Id	Via A \mathcal{R}_2			Via B		
$\vec{p}_{i,s}$	-54.4191	40.7818	5.6817			
$\vec{p}_{i,m}$	-56.2815	27.0486	4.2737			
$\vec{p}_{i,f}$	-58.7211	13.4467	-2.6139			
Type: Single	Centre \mathcal{R}_3			Axis \mathcal{R}_3		
Radius: 41.9158 [mm]	1.167	2.3044	2.4789	0.0013802	0.99991	0.013388
Infraspinatus	Origin \mathcal{R}_2			Insertion \mathcal{R}_3		
Point Id	X [mm]	Y [mm]	Z [mm]	X [mm]	Y [mm]	Z [mm]
$\vec{p}_{i,s}$	-124.0628	-1.9184	-105.6435	9.8596	-17.645	-7.6911
$\vec{p}_{i,m}$	-115.8308	-3.1223	-58.2159	17.373	-16.6175	0.37414
$\vec{p}_{i,f}$	-107.9192	0.17217	-13.055	23.5991	-10.3027	3.044
Point Id	Via A \mathcal{R}_2			Via B		
$\vec{p}_{i,s}$	-38.4143	9.8302	-57.7836			
$\vec{p}_{i,m}$	-38.6937	3.2995	-30.2236			
$\vec{p}_{i,f}$	-35.5198	3.7126	-3.7866			
Type: Stub	Centre \mathcal{R}_3			Axis \mathcal{R}_3		
Radius: 41.9158 [mm]	1.0394	-0.96844	1.8502	-0.0013809	-0.99991	-0.013387
Subscapularis	Origin \mathcal{R}_2			Insertion \mathcal{R}_3		
Point Id	X [mm]	Y [mm]	Z [mm]	X [mm]	Y [mm]	Z [mm]
$\vec{p}_{i,s}$	-123.4762	7.3923	-122.5987	-3.3505	20.0523	-13.5801
$\vec{p}_{i,m}$	-116.0687	1.189	-29.0969	-4.1732	23.0766	-6.468
$\vec{p}_{i,f}$	-103.6795	22.1996	7.8449	-0.21938	24.4173	-0.067492
Point Id	Via A \mathcal{R}_2			Via B		
$\vec{p}_{i,s}$	-66.6935	26.507	-53.8117			
$\vec{p}_{i,m}$	-65.0629	28.4745	-31.1974			
$\vec{p}_{i,f}$	-66.4803	35.0349	-13.4779			
Type: Stub	Centre \mathcal{R}_3			Axis \mathcal{R}_3		
Radius: 41.9158 [mm]	-19.6158	0.39544	-5.8439	0.0013825	0.99991	0.013387
Teres Minor	Origin \mathcal{R}_2			Insertion \mathcal{R}_3		
Point Id	X [mm]	Y [mm]	Z [mm]	X [mm]	Y [mm]	Z [mm]
$\vec{p}_{i,s}$	-87.0304	2.9277	-98.9601	9.5286	-8.4224	-24.7259
$\vec{p}_{i,m}$	-69.9267	6.3263	-71.0541	8.6471	-11.0262	-17.2425
$\vec{p}_{i,f}$	-53.4579	11.6022	-54.0939	9.0415	-15.3647	-11.0582
Point Id	Via A \mathcal{R}_2			Via B		
$\vec{p}_{i,s}$	-39.943	3.277	-82.3658			
$\vec{p}_{i,m}$	-33.9335	3.9595	-69.5523			
$\vec{p}_{i,f}$	-32.2664	3.7599	-57.2188			
Type: Stub	Centre \mathcal{R}_3			Axis \mathcal{R}_3		
Radius: 41.9158 [mm]	-12.696	-1.8977	-28.0528	-0.0013809	-0.99991	-0.013387

Teres Major	Origin \mathcal{R}_2			Insertion \mathcal{R}_3		
Point Id	<i>X</i> [mm]	<i>Y</i> [mm]	<i>Z</i> [mm]	<i>X</i> [mm]	<i>Y</i> [mm]	<i>Z</i> [mm]
$\vec{p}_{i,s}$	-119.7216	-0.086785	-124.673	-7.7406	-7.1199	-64.2176
$\vec{p}_{i,m}$	-103.8587	1.3343	-113.6005	-5.8226	-7.5546	-52.9684
$\vec{p}_{i,f}$	-89.3545	2.2673	-96.8496	-4.0775	-7.4641	-42.6903
Type: Single	Centre \mathcal{R}_2			Axis \mathcal{R}_2		
Radius: -88.1642 [mm]	-70.3344	41.235	-69.2185	0.15794	0.11704	-0.98049

Coracobrachialis	Origin \mathcal{R}_2			Insertion \mathcal{R}_3		
Point Id	<i>X</i> [mm]	<i>Y</i> [mm]	<i>Z</i> [mm]	<i>X</i> [mm]	<i>Y</i> [mm]	<i>Z</i> [mm]
$\vec{p}_{i,s}$	-28.9214	69.2424	-15.8828	-1.7615	6.0047	-128.974
$\vec{p}_{i,m}$	-23.783	69.1095	-16.4699	-0.75833	7.6193	-116.4488
$\vec{p}_{i,f}$	-20.0873	65.7181	-17.1945	-0.23017	8.135	-104.5418
Point Id	Via A			Via B \mathcal{R}_3		
$\vec{p}_{i,s}$				-6.9501	14.5571	-99.8291
$\vec{p}_{i,m}$				-4.7246	11.4883	-92.895
$\vec{p}_{i,f}$				-2.9801	8.9123	-87.2432
Type: None						

Bibliography

- [1] J. Ackermann. Der Entwurf Regelungssyteme im Zustandsraum. *Regelungstechnik und Prozessdatenverarbeitung*, 7:297–300, 1972.
- [2] D.C. Ackland, P. Pak, M. Richardson, and M.G. Pandy. Moment arms of the muscles crossing the anatomical shoulder. *Journal of Anatomy*, 213(4):383–390, 2008.
- [3] M. Aeberhard, Y. Michellod, P. Mullhaupt, A. Terrier, D.P. Pioletti, and D. Gillet. Dynamical biomechanical model of the shoulder: Null space based optimization of the overactuated system. In *Robotics and Biomimetics, 2008. ROBIO 2008. IEEE International Conference on*, pages 67 –73, feb. 2009.
- [4] F. Altpeter. *Friction Modeling, Identification and Compensation*. PhD thesis, EPFL, Lausanne, 1999.
- [5] K.N. An, Y. Ueba, E.Y. Chao, W.P. Cooney, and R.L. Linscheid. Tendon excursion and moment arm of index finger muscles. *Journal of Biomechanics*, 16(6):419 – 425, 1983.
- [6] K.N. An, B.M. Kwak, E.Y. Chao, and B.F. Morrey. Determination of muscle and joint forces: a new technique to solve the indeterminate problem. *Journal of Biomechanical Engineering*, 106:364–367, 1984.
- [7] K.N. An, K. Takahashi, T.P. Harrigan, and E.Y. Chao. Determination of muscle orientations and moment arms. *Journal of Biomechanical Engineering*, 106(3): 280–282, 1984.
- [8] M.S. Andersen, M. Damsgaard, and J. Rasmussen. Kinematic analysis of over-determinate biomechanical systems. *Computer Methods in Biomechanics and Biomedical Engineering*, 12(4):371–384, 2009.
- [9] M.S. Andersen, M. Damsgaard, and J. Rasmussen. Force-dependent kinematics: a new analysis method for non-conforming joints. In *XIII International Symposium on Computer Simulation in Biomechanics*, 2011.
- [10] M. Apreleva, I.M. IV Parsons, J.P. Warner, F.H. Fu, and S.L.-Y. Woo. Experimental investigation of reaction forces at the glenohumeral joint during active abduction. *Journal of Shoulder and Elbow Surgery*, 9(5):409 – 417, 2000.

-
- [11] Xueling Bai, Gaofeng Wei, Ming Ye, Dongmei Wang, Yan Hu, Zongliang Liu, Wenzhong Nie, Linlin Zhang, Wenting Ji, Yunting Li, and Chengtao Wang. Finite element musculoskeletal modeling of mechanical virtual human of china. In *Bioinformatics and Biomedical Engineering, 2008. ICBBE 2008. The 2nd International Conference on*, pages 1847–1850, May 2008.
 - [12] Sir R.S. Ball. *Theory of Screws: a study in the dynamics of a rigid body*. Hodges Publication, Dublin, 1876.
 - [13] J.W. Baumgarte. A new method of stabilization for holonomic constraints. *Journal of Applied Mechanics*, 50:869–870, 1983.
 - [14] M.S. Bazaraa, H.D. Sherali, and Shetty C. M. *Nonlinear Programming: Theory and Algorithms*. John Wiley and Sons, New York, 2 edition, 1993.
 - [15] M.F. Bear, B.W. Connors, and M.A. Paradiso. *Neuroscience: Exploring the brain*. Lippincott, Williams & Wilkins, 3rd edition, 2000.
 - [16] R. Becker, A. Berth, M. Nehring, and F. Awiszus. Neuromuscular quadriceps dysfunction prior to osteoarthritis of the knee. *Journal of Orthopaedic Research*, 22(4):768–773, 2004.
 - [17] G. Bergmann, F. Graichen, A. Bender, A. Rohlmann, A. Halder, A. Beier, and P. Westerhoff. In vivo gleno-humeral joint loads during forward flexion and abduction. *Journal of Biomechanics*, 44(8):1543 – 1552, 2011.
 - [18] J.M. Berthelot. *Mechanics of Rigid Bodies*. Springer, New-York, 1999.
 - [19] D. Blana and E.K. Kirsch R.F. Chadwick. Combined feedforward and feedback control of a redundant, nonlinear, dynamic musculoskeletal system. *Med. Biol. Eng. Comput.*, 47:533–542, 2009.
 - [20] B. Bolsterlee, H.E. Veeger, and F.C.T. van der Helm. Modelling clavicular and scapular kinematics: from measurement to simulation. *Medical & Biological Engineering & Computing*, 52(3):283–291, 2014.
 - [21] P. Bosscher, A.T. Riechel, and I. Ebert-Uphoff. Wrench-feasible workspace generation for cable-driven robots. *Robotics, IEEE Transactions on*, 22(5):890–902, 2006.
 - [22] J. Botsis and M. Deville. *Mécanique des Milieux Continus: Une Introduction*. Lausanne: Presses Polytechniques et Universitaires Romandes, 2006.
 - [23] O. Bottema and Roth B. *Theoretical Kinematics*. Dover Publications, 2012.
 - [24] S. Boyd and L. Vandenberghe. *Convex Optimization*. Cambridge University Press, 2004.
 - [25] P.W. Brand, Cranor K.C., and J.C. Ellis. Tendon and pulleys at the metacarpophalangeal joint of a finger. *The Journal of Bone & Joint Surgery*, 57(6):779–784, 1975.
-

-
- [26] R.A. Brand, D.R. Pedersen, and J.A. Friederich. The sensitivity of muscle force predictions to changes in physiologic cross-sectional area. *Journal of Biomechanics*, 19:589–596, 1986.
 - [27] K.D. Brandt, P. Dieppe, and E.L. Randin. Etiopathogenesis of osteoarthritis. *Journal of the American Osteopathic Association*, 34:531–559, 2008.
 - [28] M.D.K. Breteler, C.W. Spoor, and F.C.T. van der Helm. Measuring muscle and joint geometry parameters of a shoulder for modeling purposes. *Journal of Biomechanics*, 32(11):1191 – 1197, 1999.
 - [29] T. Bruckmann and A. Pott. *Cable-driven parallel robots*. Springer Science & Business Media, 2013.
 - [30] J.A. Buckwalter, W.D. Stanish, R.N. Rosier, R.C. Schenck, D.A. Dennis, and R.D. Coutts. The increasing need for nonoperative treatment of patients with osteoarthritis. *Clinical Orthopaedics and Related Research*, 385:36–45, 2001.
 - [31] J. Burdick. *Kinematic analysis and design of redundant robot manipulators*. PhD thesis, Stanford University, Stanford, 1988.
 - [32] R. Cailliet. *The Illustrated Guide to Functional Anatomy of the Musculoskeletal System*. American Medical Association, 2004.
 - [33] S. Carbes. Shoulder rhythm report: Anyscript support wiki, 2011.
 - [34] B. Chachuat, B. Srinivasan, and D. Bonvin. Adaptation strategies for real-time optimization. *Computers & Chemical Engineering*, 33:1557–1567, 2009.
 - [35] B.C. Chachuat. Nonlinear and dynamic optimisation, from theory to practice, 2006.
 - [36] E.K.J. Chadwick and F.C.T. van der Helm. Musculoskeletal modelling of the shoulder, 2003.
 - [37] I.W. Charlton and G.R. Johnson. A model for the prediction of the forces at the glenohumeral joint. In *Proc. Inst. Mech. Eng. [H]*, volume 220, page 801–812, 2006.
 - [38] W.I. Charlton and G.R. Johnson. Application of spherical and cylindrical wrapping algorithms in a musculoskeletal model of the upper limb. *Journal of Biomechanics*, 34(9):1209 – 1216, 2001.
 - [39] M. Chasles. Note sur les propriétés générales du système de deux corps semblables entr’eux et placés d’une manière quelconque dans l’espace; et sur le déplacement fini ou infiniment petit d’un corps solide libre. *Bulletin des Sciences Mathématiques, Astronomiques, Physiques et Chimiques*, 14:321–326, 1830.
 - [40] C.-T. Chen. *Linear System Theory and Design*. Oxford University Press, New York Oxford, 3 edition, 1999.
 - [41] W. Chen and E. De Schutter. Python-based geometry preparation and simulation visualization toolkits for steps. *Frontiers in Neuroinformatics*, 2014.
-

-
- [42] L. Chéze, B.J. Fregly, and J. Dimnet. A solidification procedure to facilitate kinematic analyses based on video system data. *Journal of Biomechanics*, 28(7):879 – 884, 1995.
 - [43] E.A. Codman. *The Shoulder: Rupture of the Supraspinatus Tendon and Other Lesions In or About the Subacromial Bursa*. Boston: Thomas Todd Co., 1934.
 - [44] E. Conkur and R. Buckingham. Clarifying the definition of redundancy as used in robotics. *Robotica*, 15:583 – 586, 1997.
 - [45] A.R. Crossman and D. Neary. *Neuroanatomy, An illustrated colour text*. Chuchill Livingstone Elsevier, 4rd edition, 2010.
 - [46] A. Curnier. *Mécanique des Solides Déformables*. Lausanne: Presses Polytechniques et Universitaires Romandes, 2005.
 - [47] A.G. Cutti and E.K. Chadwick. Shoulder biomechanics and the success of translational research. *Medical & Biological Engineering & Computing*, 52:205–210, 2014.
 - [48] A.G. Cutti and H.E.J. (DirkJan) Veeger. Shoulder biomechanics: today’s consensus and tomorrow’s perspectives. *Medical & Biological Engineering & Computing*, 47: 463–466, 2009.
 - [49] M. Damsgaard, J. Rasmussen, S.T. Christensen, E. Surma, and M. de Zee. Analysis of musculoskeletal systems in the anybody modeling system. *Simulation Modelling Practice and Theory*, 14(8):1100 – 1111, 2006.
 - [50] J. H. deGroot and R. Brand. A three-dimension regression model of the shoulder rhythm. *Clinical biomechanics*, 16:735–743, 2001.
 - [51] S.L. Delp and J.P. Loan. A graphics-based software system to develop and analyze models of musculoskeletal structures. *Computers in Biology and Medicine*, 25(1): 21 – 34, 1995.
 - [52] S.L. Delp, F.C. Anderson, A.S. Arnold, P. Loan, A. Habib, C.T. John, E. Guendelman, and D.G. Thelen. Opensim: Open-source software to create and analyse dynamic simulations of movement. *IEEE Transactions on Biomedical Engineering*, 54(11):1940–1950, 2007.
 - [53] W. T. Dempster. Mechanism of shoulder movement. *Archives of Physical Medicine and Rehabilitation*, 46(1):49–69, 1965.
 - [54] C.R. Dickerson, D.B. Chaffin, and R.E. Hughes. A mathematical musculoskeletal shoulder model for proactive ergonomic analysis. *Computer Methods in Biomechanics and Biomedical Engineering*, 10:389–400, 2007.
 - [55] B.F. Dulin and C.F. Martin. *Introduction to differential geometry for engineers*. New York: Marcel Dekker, 1990.
 - [56] R. Dumas and L. Cheze. Soft tissue artifact compensation by linear 3d interpolation and approximation methods. *Journal of Biomechanics*, 42(13):2214 – 2217, 2009.
-

-
- [57] I. Ebert-Uphoff and P.A. Voglewede. On the connections between cable-driven robots, parallel manipulators and grasping. In *Robotics and Automation, 2004. Proceedings. ICRA '04. 2004 IEEE International Conference on*, volume 5, pages 4521–4526, April 2004.
- [58] A. El Habachi, S. Duprey, L. Cheze, and R. Dumas. A parallel mechanism of the shoulder—application to multi-body optimisation. *Multibody System Dynamics*, pages 1–13, 2014.
- [59] C. Engelhardt, D. Ingram, P. Muellhaupt, E. Pralong, A. Farron, D. Pioletti, and A. Terrier. Solving overconstrained kinematic in numerical shoulder model using nullspace optimization. In *10th International Symposium on Computer Methods in Biomechanics and Biomedical Engineering, CMBBE 2012 Berlin*, april 2012.
- [60] Ch. Engelhardt, V.M. Camine, D. Ingram, Ph. Mullhaupt, A. Farron, D. Pioletti, and A. Terrier. Comparison of an emg-based and a stress-based method to predict shoulder muscle forces. *Computer Methods in Biomechanics and Biomedical Engineering*, 0(0):1–8, 2014.
- [61] A. E. Engin and S. M. Chen. Statistical data base for the biomechanical properties of the human shoulder complex-part i : Kinematics of the shoulder complex. *Journal of biomechanical engineering*, 108:215–221, 1986.
- [62] A. E. Engin and S. M. Chen. Statistical data base for the biomechanical properties of the human shoulder complex-part ii : Passive resistive properties beyond the shoulder complex sinus. *Journal of biomechanical engineering*, 108:222–227, 1986.
- [63] A. E. Engin and S. T. Tumer. Three-dimensional kinematic modeling of the human shoulder complex—part i: Physical model and determination of joint sinus cones. *Journal of biomechanical engineering*, 111(2):107–112, 1989.
- [64] A. E. Engin and S. T. Tumer. Three-dimensional kinematic modeling of the human shoulder complex—part ii: Mathematical modeling and solution via optimization. *Journal of biomechanical engineering*, 111(2):113–221, 1989.
- [65] A.E. Engin. On the biomechanics of the shoulder complex. *Journal of Biomechanics*, 13(7):575 – 590, 1980.
- [66] A. Erdemir, S. McLean, W. Herzog, and A.J. van den Bogert. Model-based estimation of muscle forces exerted during movements. *Clinical Biomechanics*, 22: 131–154, 2007.
- [67] L. Euler. Quacunque corporum rigidorum. *Novi Commentarii academiae scientiarum Petropolitanae*, 20:189–207, 1776.
- [68] P. Favre, J.G. Snedeker, and C. Gerber. Numerical modelling of the shoulder for clinical applications. *Philosophical transactions. Series A, Mathematical, physical, and engineering sciences*, 367:2095–2118., 2009.
-

-
- [69] Ph. Favre. *A model to study active shoulder motion and stability*. PhD thesis, ETHZ, Zurich, 2011.
- [70] Ph. Favre, R. Sheikh, S.F. Fucentese, and H.A.C. Jacob. An algorithm for estimation of shoulder muscle forces for clinical use. *Clinical Biomechanics*, 20(8):822 – 833, 2005.
- [71] Ph. Favre, M. Senteler, J. Hipp, S. Scherrer, C. Gerber, and J.G. Snedeker. An integrated model of active glenohumeral stability. *Journal of Biomechanics*, 45(13): 2248 – 2255, 2012.
- [72] R.C. Fitzpatrick, J.L. Taylor, and D.I. McCloskey. Ankle stiffness of standing humans in response to imperceptible perturbation: reflex and task-dependent components. *Journal of Physiology*, 454:533–547, 1992.
- [73] L.D. Freedman and R.R. Munro. Abduction of the arm in the scapular plane: Scapular and glenohumeral movements. a roentgenographic study. *The Journal of Bone & Joint Surgery*, 48(8):1503–1510, 1966.
- [74] B.A. Garner and M.G. Pandy. Musculoskeletal model of the upper limb based on the visible human male dataset. *Computer Methods in Biomechanics and Biomedical Engineering*, 4(2):107–124, 1999.
- [75] B.A. Garner and M.G. Pandy. The obstacle-set method for representing muscle paths in musculoskeletal models. *Computer Methods in Biomechanics and Biomedical Engineering*, 3(1):1–30, 2000.
- [76] B.A. Garner and M.G. Pandy. A kinematic model of the upper limb based on the visible human project (vhp) image dataset. *Computer Methods in Biomechanics and Biomedical Engineering*, 2(2):93–126, 2001.
- [77] B.A. Garner and M.G. Pandy. Estimation of musculotendon properties in the human upper limb. *Annals of Biomedical Engineering*, 31:207–220, 2003.
- [78] A. Goodwin, B.-H. Zhou, R.V. Baratta, M. Solomonow, and A. P. Keegan. The influence of antagonist muscle control strategies on the isometric frequency response of the cat’s ankle joint. *Biomedical Engineering, IEEE Transactions on*, 44(7):634–639, 1997.
- [79] V.E. Gough and S.G. Whitehall. Universal tyre test machine. In *Proceedings of 9th. Int. Congress of F.I.S.I.T.A*, 117, page 117–135, 1962.
- [80] M. Gouttefarde and C.M. Gosselin. Analysis of the wrench-closure workspace of planar parallel cable-driven mechanisms. *Robotics, IEEE Transactions on*, 22(3): 434–445, 2006.
- [81] M. Gouttefarde, J.-P. Merlet, and D. Daney. Wrench-feasible workspace of parallel cable-driven mechanisms. In *Robotics and Automation, 2007 IEEE International Conference on*, pages 1492–1497, 2007.
-

-
- [82] H. Graichen, T. Stammberger, H. Bonel, K.-H. Englmeier, M. Reiser, and F. Eckstein. Glenohumeral translation during active and passive elevation of the shoulder * a 3d open-mri study. *Journal of Biomechanics*, 33:609–613, 2000.
- [83] H. Gray. *Anatomy of the Human Body Gray*. Philadelphia: Lea & Febiger, 1918.
- [84] T.-J. Grewal. *Quantifying the Shoulder Rhythm and Comparing Non-Invasive Methods of Scapular Tracking for Overhead and Axially Rotated Humeral Postures*. PhD thesis, University of Waterloo, Waterloo, 2011.
- [85] M.J. Grey. *Proprioceptive Sensory Feedback, Encyclopedia of Life Sciences*. John Wiley & Sons, 2010.
- [86] C. Gruber and W. Benoit. *Mécanique Générale*. Lausanne: Presses Polytechniques et Universitaires Romandes, 1998.
- [87] B. Grunbaum. *Convex Polytopes*. Spinrger-Verlag, New York, 2 edition, 2003.
- [88] S. Gupta, F.C.T. van der Helm, J.C. Sterk, F. van Keulen, and B.L. Kaptein. Development and experimental validation of a three-dimensional finite element model of the human scapula. *Proc. Inst Mech Eng H.*, 218(2):127–142, 2004.
- [89] L.N. Hand and J.D. Finch. *Analytical Mechanics*. Cambridge University Press, New York, 1998.
- [90] R. Happee. Inverse dynamic optimization including muscular dynamics, a new simulation method applied to goal directed movements. *Journal of Biomechanics*, 27(5):953 – 960, 1994.
- [91] R.S. Hartenberg and J. Denavit. *Kinematic synthesis of linkages*. New York: McGraw-Hill, 1964.
- [92] M. Hassan and A. Khajepour. Optimization of actuator forces in cable-based parallel manipulators using convex analysis. *Robotics, IEEE Transactions on*, 24(3): 736–740, 2008.
- [93] J. Hawkins. *On Intelligence*. Times Books, 2004.
- [94] W. Herzog and P. Binding. Predictions of antagonistic muscular activity using nonlinear optimization. *Mathematical Biosciences*, 111(2):217 – 229, 1992.
- [95] A.V. Hill. The heat of shortening and the dynamic constants of muscle. *Proceedings of the Royal Society of London. Series B, Biological Sciences*, 126(843):pp. 136–195, 1938.
- [96] K. Hoffman and R. Kunze. *Linear Algebra*. PHI Learning Private Limited, New Delhi, 2 edition, 2010.
- [97] N. Hogan. Adaptive control of mechanical impedance by coactivation of antagonistic muscles. *IEEE Transactions on Automatic Control*, 29(8):681–690, 1984.
-

-
- [98] N. Hogan. The mechanics of multi-joint posture and movement control. *Biological Cybernetics*, 52(5):315–331, 1985.
 - [99] D. Holm. Geometric mechanics, part i: Dynamics and symmetry. Imperial College course material, 2012.
 - [100] D. Holm. Geometric mechanics, part ii: Rotating, translating and rolling. Imperial College course material, 2012.
 - [101] K. R. S. Holzbaur, W. M. Murray, and S. L. Delp. A model of the upper extremity for simulating musculoskeletal surgery and analyzing neuromuscular control. *Annals of Biomedical Engineering*, 33:829–840, 2005.
 - [102] R.E. Hughes, G. Niebur, J. Liu, and K.N. An. Comparison of two methods for computing abduction moment arms of the rotator cuff. *Journal of Biomechanics*, 31(2):157 – 160, 1998.
 - [103] C. Högfors, B. Peterson, and P. Herberts. Biomechanical model of the human shoulder-i. elements. *Journal of biomechanics*, 20(2):157–166, 1987.
 - [104] C. Högfors, B. Peterson, G. Sigholm, and P. Herberts. Biomechanical model of the human shoulder-ii. the shoulder ryrthm. *Journal of biomechanics*, 24(8):699–709, 1991.
 - [105] V.T. Inman, M. Saunders, and L.C. and Abbott. The role of the scapula in athletic shoulder function. 1944. *Clinical Orthopaedics Related Research*, 330:3–12, 1996.
 - [106] Abhinandan Jain. Minimal coordinates formulation of contact dynamics. In *Multibody Dynamics 2013, ECCOMAS Thematic Conference*, pages 153–160, 2013.
 - [107] Houk J.C. and W. Zevrymer. Handbook of physiology, the nervous system ii, chapter 8, neural control of muscle length and tension, 1981.
 - [108] R.H. Jensen and D.T. Davy. An investigation of muscle lines of action about the hip: A centroid line approach vs the straight line approach. *Journal of Biomechanics*, 8(2):103 – 110, 1975.
 - [109] M. Jäntschi. *Non-linear Control Strategies for Musculoskeletal robots*. PhD thesis, Technische Universität München, 2013.
 - [110] E.R. Kandel, J.H. Schwartz, and T.M. Jessell. *Principles of Neural Science*. McGraw-Hill Medical, 3rd edition, 2000.
 - [111] T.R. Kane and A. son. *Dynamics, Theory and Applications*. McGraw-Hill, New York, 2005.
 - [112] M.L. Kaplan and J.H. Heegaard. Predictive algorithms for neuromuscular control of human locomotion. *Journal of Biomechanics*, 34(8):1077–1083, 2001.
 - [113] A.R. Karduna, P.W. McClure, L.A. Michener, and B. Sennett. Dynamic measurements of three-dimensional scapular kinematics: A validation study. *Journal of Biomechanical Engineering*, 123(2):184–190, 2001.
-

-
- [114] D. Karlsson and B. Peterson. Towards a model for force predictions in the human shoulder. *Journal of biomechanics*, 25(2):189–199, 1992.
- [115] J. Kautsky, N. K. Nichols, and P. Van Dooren. Robust pole assignment in linear state feedback. *Int. Journal of Control*, 41(5):1129–1155, 1985.
- [116] A.B. Kempe. *How to Draw a Straight Line*. London: Macmillan and Co., 1877.
- [117] H.K. Khalil. *Nonlinear Systems*. Prentice Hall, Upper Saddle River, NJ, 3 edition, 2000.
- [118] W.B. Kibler. The role of the scapula in athletic shoulder function. *American Journal of Sports medicine*, 26(2):325–337, 1998.
- [119] T. Kiemel, A.J. Elahi, and J.J. Jeka. Identification of the plant for upright stance in humans: multiple movement patterns from a single neural strategy. *Journal of Neurophysiology*, 100:3394–3406, 2008.
- [120] A. Kontaxis and G.R. Johnson. Gleohumeral contact force after total shoulder replacement. *Journal of Bone and Joint Surgery*, 90(Supp II):212–213, 2008.
- [121] J.H. Koolstra and T.M. van Eijden. Combined finite-element and rigid-body analysis of human jaw joint dynamics. *Journal of Biomechanics*, 38:2431–2439, 2005.
- [122] T. Kozuki, Y. Motegi, T. Shirai, Y. Asano, J. Urata, Y. Nakanishi, K. Okada, and M. Inaba. Design of upper limb by adhesion of muscles and bones - detail human mimetic musculoskeletal humanoid kenshiro. In *Intelligent Robots and Systems (IROS), 2013 IEEE/RSJ International Conference on*, pages 935–940, Nov 2013.
- [123] G.A. Kramer. *Solving Geometric Constraint Systems: a case study in kinematics*. MIT Press, Boston Massachusetts, 1992.
- [124] P.-Y. Lagacé, F. Billuart, X. Ohl, W. Skalli, P. Tétreault, J. de Guise, and N. Hagemeister. Analysis of humeral head displacements from sequences of biplanar x-rays: repeatability study and preliminary results in healthy subjects. *Computer Methods in Biomechanics and Biomedical Engineering*, 15(3):221–229, 2014.
- [125] A. Leick. *GPS satellite surveying, 3rd Edition*. Wiley, 1990.
- [126] J. Lenarcic, T. Bajd, and M.M. Stanisic. *Robot Mechanisms*. Springer Science+Buisness Media, Dordrecht, 2013.
- [127] J.Z. Levin. A parametric algorithm for drawing pictures of solid objects composed of quadric surfaces. *Commun. ACM*, 19(10):555–563, 1976.
- [128] J.Z. Levin. Mathematical models for determining the intersections of quadric surfaces. *Computer Graphics and Image Processing*, 11(1):73 – 87, 1979.
- [129] N. Lindsay. Modelling of the shoulder mechanism. a report describing the development of a three-dimensional biomechanical model of the human shoulder complex. Technical Report 106, Institute of Mechanical Engineering, Aalborg University, Denmark, ISSN 0905-4219, 2001.
-

-
- [130] J. Liu, R.E. Hughes, W.P. Smutz, G. Niebur, and K. N. An. Roles of deltoid and rotator cuff muscles in shoulder elevation. *Clinical Biomechanics*, 12(1):32 – 38, 1997.
- [131] R. Longchamp. *Commande Numérique de Systèmes Dynamiques*. Presses Polytechniques et Universitaires Romandes, 3 edition, 2006.
- [132] I.D. Loram and M. Lakie. Human balancing of an inverted pendulum: position control by small, ballistic-like, throw and catch movements? *Journal of Physiology*, 504(3):1111–1124, 2002.
- [133] I.D. Loram, H. Gollee, M. Lakie, and P.J. Gawthrop. Human control of an inverted pendulum: Is continuous control necessary? is intermittent control effective? is intermittent control physiological? *Journal of Physiology*, 589(2):307–324, 2011.
- [134] D. G. Luenberger. Canonical forms for linear multivariable systems. *Automatic Control, IEEE Transactions on*, 12(3):290–293, 1967.
- [135] M.E. Lund, M. de Zee, M.S. Andersen, and J. Rasmussen. On validation of multi-body musculoskeletal models. *Journal of Engineering in Medicine*, 226(2):82 – 94, 2012.
- [136] A. M. Lyapunov. *The General Problem of the Stability of Motion*, (A. T. Fuller trans.). Taylor & Francis, London, 1992.
- [137] D. Mackenzie. The poincaré conjecture-proved. *Science (American Association for the Advancement of Science)*, 314:1848–1849, 2006.
- [138] M. Makhsous, C. Högfors, A. Siemien’ski, and B. Peterson. Total shoulder and relative muscle strength in the scapular plane. *Journal of Biomechanics*, 32(11): 1213 – 1220, 1999.
- [139] S.P. Marsden, D.C. Swailes, and G.R. Johnson. Algorithms for exact multi-object muscle wrapping and application to the deltoid muscle wrapping around the humerus. *Journal of Engineering in Medicine in Proc. Inst. Mech. Eng. H.*, 7: 1081–1095, 2008.
- [140] D.F. Massimini, P.J. Boyer, R. Papannagari, T.J. Gill, J.P. Warner, and G. Li. In-vivo glenohumeral translation and ligament elongation during abduction and abduction with internal and external rotation. *Journal of Orthopaedic surgery and research*, 7, 2012.
- [141] P.B.C. Mathews. Handbook of physiology, the nervous system ii, chapter 6, muscle spindles: their messages and their fusimotor supply, 1981.
- [142] W. Maurel. *3D modeling of the human upper limb including the biomechanics of joints, muscles and soft tissues*. PhD thesis, EPFL, Lausanne, 1998.
- [143] P.W. McClure, L.A. Michener, B.J. Sennett, and A.R. Karduna. Direct 3-dimensional measurement of scapular kinematics during dynamic movements in vivo. *Journal of Shoulder and Elbow Surgery*, 10(3):269 – 277, 2001.
-

-
- [144] S.G. McLean, A. Su, and A.J. van den Bogert. Development and validation of a 3-d model to predict knee joint loading during dynamic movement. *J. Biomech. Eng.*, 125:864–874, 2003.
- [145] S.G. McLean, X. Huang, A. Su, and A.J. van den Bogert. Sagittal plane biomechanics cannot injure the acl during sidestep cutting. *Clin. Biomech.*, 19:828–838, 2004.
- [146] J.-P. Merlet. The kinematics of the redundant n -1 wire driven parallel robot. In *Robotics and Automation (ICRA), 2012 IEEE International Conference on*, pages 2313–2318, 2012.
- [147] Carel G.M. Meskers, Michiel A.J. van de Sande, and Jurriaan H. de Groot. Comparison between tripod and skin-fixed recording of scapular motion. *Journal of Biomechanics*, 40(4):941 – 946, 2007.
- [148] Y. Michellod. *Overactuated systems coordination*. PhD thesis, EPFL, Lausanne, 2009.
- [149] I. Michiels and J. Grevenstein. Kinematics of shoulder abduction in the scapular plane: On the influence of abduction velocity and external load. *Clinical Biomechanics*, 10(3):137 – 143, 1995.
- [150] G. S. Miminis and C. C. Paige. A direct algorithm for pole assignment of time-invariant multi-input linear systems using state feedback. *Automatica*, 24(3):343–356, 1988.
- [151] T. Mitchell. *Machine Learning*. New York, NY: McGraw-Hill, 1997.
- [152] S. Mollier. Über die statik und mechanik des menschlichen schultergürtels unter normalen und pathologischen verhältnissen. *Festschrift zum 70. Geburtstag von Carl von Kupffer. G. Fischer.*, pages 487–567, 1899.
- [153] Ph. Müllhaupt. *Introduction à l’analyse et à la commande des systèmes non linéaires*. Presses Polytechniques et Universitaires Romandes, 1 edition, 2009.
- [154] R.R. Neptune and M.L. Hull. A theoretical analysis of preferred pedaling rate selection in endurance cycling. *Journal of Biomechanics*, 32:409–41, 1999.
- [155] A. Nikooyan, H. Veeger, E. Chadwick, M. Praagman, and F. van der Helm. Development of a comprehensive musculoskeletal model of the shoulder and elbow. *Journal of Biomechanics*, 43(25):3007 – 3014, 2011.
- [156] A.A. Nikooyan, H.E.J. Veeger, P. Westerhoff, F. Graichen, G. Bergmann, and F.C.T. van der Helm. Validation of the delft shoulder and elbow model using in-vivo glenohumeral joint contact forces. *Journal of Biomechanics*, 43(15):3007 – 3014, 2010.
- [157] P.E. Nikravesh. *Computer aided analysis of mechanical systems*. Prentice-Hall International Inc., 1988.
-

-
- [158] A. Nolte, P. Augat, and J. Rasmussen. Analysis of the muscle and joint forces in the shoulder joint using the anybody simulation model. *Journal of Biomechanics: 16th ESB Congress*, 41, 2008.
- [159] A Noshadi, M. Mailah, and A Zolfagharian. Active force control of 3-rrr planar parallel manipulator. In *Mechanical and Electrical Technology (ICMET), 2010 2nd International Conference on*, pages 77–81, Sept 2010.
- [160] J.L. Oliver and P.M. Smith. Neural control of leg stiffness during hopping in boys and men. *Journal of Electromyography and Kinesiology*, 20(5):973–979, 2010.
- [161] J.C. Otis, C.-C. Jiang, T.L. Wickiewicz, M.G.E. Peterson, R.F. Warren, and T.J. Santner. Changes in the moment arms of the rotator cuff and deltoid muscles with abduction and rotation. *The Journal of Bone & Joint Surgery*, 76(5):667–676, 1994.
- [162] M.G. Pandy. Computer modeling and simulation of human movement. *Annual Review of Biomedical Engineering*, 3:245–273, 2001.
- [163] M.G. Pandy, B.A. Garner, and F.C. Anderson. Optimal control of non-ballistic muscular movements: a constraint-based performance criterion for rising from a chair. *Journal of Biomechanics*, 117:15–26, 1995.
- [164] M. L. Poinso. *The Elements of Statics (Translated from french)*. Cambridge University Press (1848), 1848.
- [165] L.S. Pontryagin. *L.S. Pontryagin Selected Works, Volume 4: Mathematical Theory of Optimal Processes*. CRC Press, 1987.
- [166] N.K. Poppen and P.S. Walker. Forces at the glenohumeral joint in abduction. *Journal of Clinical Orthopedics*, 135:165–170, 1978.
- [167] M. Praagman, E.K.J. Chadwick, F.C.T. van der Helm, and H.E.J. Veeger. The relationship between two different mechanical cost functions and muscle oxygen consumption. *Journal of Biomechanics*, 39(4):758 – 765, 2006.
- [168] J.A. Prinold, M. Masjedi, G.R. Johnson, and A.M.J. Bull. Musculoskeletal shoulder models: A technical review and proposals for research foci, proceedings of the institution of mechanical engineers, part h. *Journal of Engineering in Medicine*, 227:1041–1057, 2013.
- [169] D. Purves, G.J. Augustine, D. Fitzpatrick, L.C. Katz, A.-S. LaMantia, J.O. McNamara, and S.M. Williams. *Neuroscience*. Sinauer Associates, 5 edition, 2012.
- [170] C. Quental, J. Folgado, J. Ambrósio, and J. Monteiro. A multibody biomechanical model of the upper limb including the shoulder girdle. *Multibody System Dynamics*, 28:83–108, 2012.
- [171] N.A. Ramaniraka, A. Terrier, N. Theumann, and O. Siegrist. Effects of the posterior cruciate ligament reconstruction on the biomechanics of the knee joint: a finite element analysis. *Clinical Biomechanics*, 20(4):434 – 442, 2005.
-

-
- [172] J. Rasmussen, Damsgaard M., and M. Voigt. Muscle recruitment by the min/max criterion – a comparative numerical study. *Journal of Biomechanics*, 34(3):409–415, 2001.
- [173] F. Reuleaux. *The Kinematics of Machinery*. Dover, New York (1963), 1876.
- [174] P.J. Rundquist, D.D. Anderson, C.A. Guanche, and P.M. Ludewig. Shoulder kinematics in subjects with frozen shoulder. *Archives of Physical Medicine and Rehabilitation*, 84(10):1473 – 1479, 2003.
- [175] J.G. San Juan and A.R. Karduna. Analysis of humeral head displacements from sequences of biplanar x-rays: repeatability study and preliminary results in healthy subjects. *Journal of Biomechanics*, 43:771–774, 2010.
- [176] R.M. Sanner and M. Kosha. A mathematical model of the adaptive control of human arm motions. *Biological Cybernetics*, 80:369–382, 1999.
- [177] R. Shadmehr and S.P. Wise. *The Computational Neurobiology of Reaching and Pointing*. MIT-Press, 3rd edition, 2005.
- [178] Y. Shen, H. Osumi, and T. Arai. Set of manipulating forces in wire driven systems. In *Intelligent Robots and Systems '94. 'Advanced Robotic Systems and the Real World', IROS '94. Proceedings of the IEEE/RSJ/GI International Conference on*, volume 3, pages 1626–1631 vol.3, 1994.
- [179] M. Sherman, A. Seth, and Delp S. How to compute muscle moment arm using generalized coordinates, 2010.
- [180] K. Shiino. Schultergelenkbewegungen und schultermuskularbeit. *Arch. Anat. Physiol., Suppl. Anat.*, pages 1–88, 1913.
- [181] B. Siciliano and O. Khatib. *Springer Handbood of Robotics*. Srpinger Handbooks., 2008.
- [182] F. Steenbrink, C.G.M. Meskers, B. van Vliet, J. Slaman, H.E.J. (DirkJan) Veejer, and J.H. De Groot. Arm load magnitude affects selective shoulder muscle activation. *Medical & Biological Engineering & Computing*, 47:565–572, 2009.
- [183] D. Sternad. *Progress in Motor Control: A Multidisciplinary Perspective*. Springer Science & Business Media, 2008.
- [184] D. Stewart. A platform with six degrees of freedom. In *Proceedings of the Institute of Mechanical Engineering, London, UK*, volume 180, page 371–386, 1965.
- [185] J. Stillwell. *Mathematics and Its History*. Springer Science+Business Media, 3 edition, 2010.
- [186] Sybert Stroeve. Impedance characteristics of a neuromusculoskeletal model of the human arm i. posture control. *Biological Cybernetics*, 81:475–494, 1999.
-

-
- [187] Sybert Stroeve. Impedance characteristics of a neuromusculoskeletal model of the human arm ii. movement control. *Biological Cybernetics*, 81:495–504, 1999.
- [188] R.L. 2nd Swanson. Biotensegrity: a unifying theory of biological architecture with applications to osteopathic practice, education, and research—a review and analysis. *Rheumatic Diseases Clinics of North America*, 113:34–52, 2013.
- [189] A. Terrier, A. Reist, F. Merlini, and A. Farron. Simulated joint and muscle forces in reversed and anatomic shoulder prostheses. *Journal of Bone and Joint Surgery*, 90:751–756, 2008.
- [190] A. Terrier, M. Aeberhard, Y. Michellod, Ph. Mullhaupt, D. Gillet, A. Farron, and D.P. Pioletti. A musculoskeletal shoulder model based on pseudo-inverse and null-space optimization. *Medical Engineering and Physics*, 32(9):1050–1056, 2010.
- [191] D. Tsirakos, V. Baltzopoulos, and Bartlett R. Inverse optimization: functional and physiological considerations related to the force-sharing problem. *Crit Rev Biomed Eng.*, 25(4-5):371–407, 1997.
- [192] J.J. Uicker, G.R. Pennock, and J.E. Shigley. *Theory of Machines and Mechanisms*. Oxford University Press, New York, 2003.
- [193] F.J. Valero-Cuevas, H. Hoffmann, M.U. Kurse, J.J. Kutch, and E.A. Theodorou. Computational models for neuromuscular function. *IEEE Rev. Biomed. Eng.*, 2: 110–135, 2009.
- [194] F.C.T. van der Helm. A finite element musculoskeletal model of the shoulder mechanism. *Journal of Biomechanics*, 27(5):551 – 553, 555–569, 1994.
- [195] F.C.T. van der Helm. Analysis of the kinematic and dynamic behaviour of the shoulder mechanism. *Journal of Biomechanics*, 27(5):527 – 550, 1994.
- [196] F.C.T. van der Helm and L.A. Rozendaal. Musculoskeletal systems with intrinsic and proprioceptive feedback. In *Biomechanics and Neural Control of Posture and Movement*, pages 164–174, 2000.
- [197] F.C.T. van der Helm and R. Veenbaas. Modeling the mechanical effect of muscles with large attachment sites: Application to the shoulder mechanism. *Journal of Biomechanics*, 24(12):1151 – 1163, 1991.
- [198] A. Varga. Robust pole assignment via sylvester equation based state feedback parametrization. In *Computer-Aided Control System Design, 2000. CACSD 2000. IEEE International Symposium on*, pages 13–18, 2000.
- [199] Miroslav Šenk and Laurence Chèze. A new method for motion capture of the scapula using an optoelectronic tracking device: a feasibility study. *Computer Methods in Biomechanics and Biomedical Engineering*, 13(3):397–401, 2010.
- [200] J.D.W. Webb. *Contributions of the deltoid and rotator cuff to shoulder mobility and stability: A 3D Finite Element Analysis*. PhD thesis, Stanford University, 2011.
-

-
- [201] P. Westerhoff, F. Graichen, A. Bender, and G. Rohlmann, A. and Bergmann. An instrumented implant for in vivo measurement of contact forces and contact moments in the shoulder joint. *Medical Engineering & Physics*, 31(2):207–213, 2009.
- [202] L. Westerlund. *The Extended Arm of Man - A History of the Industrial Robot*. Informationsförlaget, 2000.
- [203] D.E. Whitney. Resolved motion rate control of manipulators and human prostheses. *Man-Machine Systems, IEEE Transactions on*, 10(2):47–53, june 1969.
- [204] T.E. Whittaker. *A treatise on the analytical dynamics of particles and rigid bodies. Analytical dynamics, 3rd ed.* Cambridge Universtiy Press, Cambridge, 1927.
- [205] H. A. Wieland, M. Michaelis, B. J. Kirschbaum, and K. A. Rudolphi. Osteoarthritis - an untreatable disease? *Nature Review Drug Discovery*, 4:331–344, 2005.
- [206] Wikipedia. Osteoarthritis, 2014. URL <http://en.wikipedia.org/wiki/Osteoarthritis>. [Online; accessed 23-October-2014].
- [207] Wikipedia. System, 2014. URL <http://en.wikipedia.org/wiki/System>. [Online; accessed 15-October-2014].
- [208] Wikipedia. Control theory, 2014. URL http://en.wikipedia.org/wiki/Control_theory. [Online; accessed 15-October-2014].
- [209] Wikipedia. Double pendulum, 2014. URL http://http://en.wikipedia.org/wiki/Double_pendulum. [Online; accessed 13-October-2014].
- [210] I. Wilf and Y. Manor. Quadric-surface intersection curves: shape and structure. *Computer-Aided Design*, 25(10):633 – 643, 1993.
- [211] D.A. Winter. *Biomechanics and Motor Control of Human Movement*. John Wiley & Sons, Hoboken, New Jersey, 4 edition, 2009.
- [212] D.A. Winter, A.E. Patal, F. Prince, M. Ishac, and K. Gielo-Perczak. Stiffness control of balance in quiet standing. *Journal of Neurophysiology*, 80:1211–1221, 1998.
- [213] J. Wittenburg. *Dynamics of Multibody Systems*. Springer-Verlag, 1977.
- [214] G. Wu, F.C.T. van der Helm, H.E.J. Veeger, M. Makhssous, P. Van Roy, C. Anglin, J. Nagels, A.R. Karduna, K. McQuade, X. Wang, F.W. Werner, and B. Buchholz. Isb recommendation on definitions of joint coordinate systems of various joints for the reporting of human joint motion—part ii: shoulder, elbow, wrist and hand. *Journal of Biomechanics*, 38(5):981 – 992, 2005.
- [215] Xu Xu, Jia-hua Lin, and Raymond W. McGorry. A regression-based 3-d shoulder rhythm. *Journal of Biomechanics*, In Press:–, 2014.
-

-
- [216] T. Yanagawa, C.J. Goodwin, K.B. Shelburne, J.E. Giphart, M.R. Torry, and M.G. Pandy. Contributions of the individual muscles of the shoulder to glenohumeral joint stability during abduction. *Journal of Biomechinal Engineering*, 130(2):–, 2008.
 - [217] G. Yang, W. Lin, M.S. Kurbanhusen, Cong Bang Pham, and Song Huat Yeo. Kinematic design of a 7-dof cable-driven humanoid arm: a solution-in-nature approach. In *Advanced Intelligent Mechatronics. Proceedings, 2005 IEEE/ASME International Conference on*, pages 444–449, 2005.
 - [218] J. Yang, X. Feng, Y. Xiang, J.H. Kim, and S. Rajulu. Determining the three-dimensional relation between the skeletal elements of the human shoulder complex. *Journal of Biomechanics*, 42:1762–1767, 2009.
 - [219] J. Yang, X. Feng, J.H. Kim, and S. Rajulu. Review of biomechanical models for human shoulder complex. *Int. J. Human Factors and Simulation*, 1:271–293, 2010.
 - [220] L. Zollo, B. Siciliano, C. Laschi, G. Teti, and P. Dario. Compliant control for a cable-actuated anthropomorphic robot arm: an experimental validation of different solutions. In *Robotics and Automation, 2002. Proceedings. ICRA '02. IEEE International Conference on*, volume 2, pages 1836–1841 vol.2, 2002.
-

Glossary

abduction Abduction refers to a motion that pulls a structure or part away from the midline of the body. 17

acromioclavicular articulation The acromioclavicular articulation is the articulation between the acromion process of the scapula and the lateral end of the clavicle (All anatomical definitions are from Wikipedia). 12

acromion The acromion is a bony process on the scapula (shoulder blade). 11

actin Actin is a globular multi-functional protein that forms microfilaments. 15

adduction Adduction refers to a motion that pulls a structure or part toward the midline of the body, or towards the midline of a limb. 17

afferent In the nervous system, afferent neurons carry nerve impulses from receptors or sense organs toward the central nervous system. 201

alpha-motor neurons Alpha motor neurons (also called alpha motoneurons), are large lower motor neurons of the brainstem and spinal cord. 202

articular cartilage Articular or hyaline cartilage is cartilage that is transparent. It is found on many joint surfaces. It is pearly bluish in color with firm consistency and has a considerable amount of collagen. 12

axon An axon, also known as a nerve fibre, is a long, slender projection of a nerve cell, or neuron, that typically conducts electrical impulses away from the neuron's cell body. 201

brachial plexus The brachial plexus is a network of nerve, running from the spine, formed by the ventral rami of the lower four cervical nerves and first thoracic nerve roots (C5-C8, T1). 201

central nervous system The central nervous system is the part of the nervous system consisting of the brain and spinal cord. 201

clavicle The clavicle or collarbone is a long bone that serves as a strut between the scapula and the sternum. It makes up the anterior part of the shoulder girdle. 11

connectin Connectin, is a giant protein, greater than 1 μm in length, that functions as a molecular spring which is responsible for the passive elasticity of muscle. 15

conoid ligament The conoidLigament, the posterior and medial fasciculus, is a dense band of fibers, conical in form, with its base directed upward. 13

coracobrachialis The coracobrachialis is the smallest of the three muscles that attach to the coracoid process of the scapula. 15

coracohumeral ligament The coracohumeral ligament is a broad ligament which strengthens the upper part of the capsule of the shoulder joint. 13

coracoid process The coracoid process is a small hook-like structure on the lateral edge of the superior anterior portion of the scapula. 11

coronal plane The coronal plane (also known as the frontal plane) is any vertical plane that divides the body into ventral and dorsal (belly and back) sections. 16

deltoid The deltoid muscle is the muscle forming the rounded contour of the shoulder. Anatomically, it appears to be made up of three distinct sets of fibres though electromyography suggests that it consists of at least seven groups that can be independently coordinated by the central nervous system. 15

dendrites Dendrites are the branched projections of a neuron that act to propagate the electrochemical stimulation received from other neural cells to the cell body, or soma, of the neuron from which the dendrites project. 201

depression Depression refers to movement in an inferior direction, the opposite of elevation. 17

efferent In the nervous system, efferent nerves carry nerve impulses away from the central nervous system to effectors such as muscles or glands. 201

elevation Elevation refers to movement in a superior direction. 17

extension Extension is the opposite of flexion, describing a straightening movement that increases the angle between body parts. 17

extrafusal muscle fibres Extrafusal muscle fibres are the skeletal standard muscle fibres that are innervated by alpha motor neurons and generate tension by contracting, thereby allowing for skeletal movement. They make up large mass of skeletal (striated) muscle and are attached to bone by fibrous tissue extensions (tendons). 15

flexion Flexion describes a bending movement that decreases the angle between two parts. 17

gamma-motor neurons Gamma motor neurons, also called gamma motoneurons, are a type of lower motor neuron that take part in the process of muscle contraction, and represent about 30% of fibres going to the muscle. 202

glenohumeral articulation The glenohumeral articulation is the articulation between the head of the humerus and the glenoid cavity of the scapula. 12

glenoid cavity The glenoid cavity is a part of the shoulder. It is a shallow pyriform, articular surface, which is located on the lateral angle of the scapula. 11

glenoid labrum The glenoid labrum is a fibrocartilaginous rim attached around the margin of the glenoid cavity in the shoulder blade. 12

golgi tendon organs The Golgi organ senses changes in muscle tension. It is a proprioceptive sensory receptor organ that is at the origins and insertion of skeletal muscle fibres into the tendons of skeletal muscle. It provides the sensory component of the Golgi tendon reflex. 202

humeral head The upper extremity of the humerus or humeral head consists of the bone's large rounded head joined to the body by a constricted portion called the neck, and two eminences, the greater and lesser tubercles. 12

humerolulnar articulation The humerolulnar joint is part of the elbow-joint. It composed of two bones, the humerus and ulna, and is the junction between the trochlear notch of ulna and the trochlea of humerus. 12

humerus The humerus is a long bone in the arm or forelimb that runs from the shoulder to the elbow. 11

infraspinatus The infraspinatus muscle is a thick triangular muscle, which occupies the chief part of the infraspinatous fossa. 15

interneurons An interneuron is a neuron that forms a connection between other neurons. Interneurons are neither motor nor sensory. 201

intrafusar muscle fibres Intrafusar muscle fibers are skeletal muscle fibers that serve as specialized sensory organs (proprioceptors) that detect the amount and rate of change in length of a muscle.[1] They constitute the muscle spindle and are innervated by two axons, one sensory and one motor. 15

lateral border The lateral border is the thickest of the three. It begins above at the lower margin of the glenoid cavity, and inclines obliquely downward and backward to the inferior angle. 11

lateral epicondyle The lateral epicondyle of the humerus is a small, tuberculated eminence, curved a little forward, and giving attachment to the radial collateral ligament of the elbow-joint, and to a tendon common to the origin of the supinator and some of the extensor muscles. 12

latissimus dorsi The latissimus dorsi is the larger, flat, dorso-lateral muscle on the trunk, posterior to the arm, and partly covered by the trapezius on its median dorsal region. 15

levator scapulae The levator scapulae is a skeletal muscle situated at the back and side of the neck. Its main function is to lift the scapula. 14

ligaments Band of fibrous tissue connecting bones or cartilages, serving to support and strengthen joints. 13

lumbar plexus The lumbar plexus is a nervous plexus in the lumbar region of the body which forms part of the lumbosacral plexus. It is formed by the divisions of the first four lumbar nerves (L1-L4) and from contributions of the subcostal nerve (T12), which is the last thoracic nerve. 201

medial border The medial border of the scapula (vertebral border, medial margin) is the longest of the three borders, and extends from the superior to the inferior angle. 11

medial epicondyle The medial epicondyle of the humerus in humans is larger and more prominent than the lateral epicondyle and is directed slightly more posteriorly in the anatomical position. 12

motor neurons A motor neuron (or motoneuron) is a nerve cell (neuron) that originates in the motor region of the cerebral cortex or the brain stem, whose cell body is located in the spinal cord and whose fibre (axon) projects outside the spinal cord to directly or indirectly control muscles. 202

muscle fascicle In anatomy, a fascicle is a bundle of skeletal muscle fibres surrounded by perimysium, a type of connective tissue. 15

muscle spindles Muscle spindles are sensory receptors within the belly of a muscle that primarily detect changes in the length of this muscle. They convey length information to the central nervous system via sensory neurons. 202

myelin Myelin is a dielectric (electrically insulating) material that forms a layer, the myelin sheath, usually around only the axon of a neuron. 201

myofibrils A myofibril is a basic rod-like unit of a muscle. Muscles are composed of tubular cells called myocytes, also known as muscle fibres, and these cells in turn contain many chains of myofibrils. 15

myosin Myosins comprise a family of ATP-dependent motor proteins and are best known for their role in muscle contraction and their involvement in a wide range of other eukaryotic motility processes. 15

neuron A neuron is an electrically excitable cell that processes and transmits information through electrical and chemical signals. 201

pectoralis major The pectoralis major is a thick, fan-shaped muscle, situated at the chest (anterior) of the human body. 15

pectoralis minor The pectoralis minor is a thin, triangular muscle, situated at the upper part of the chest, beneath the pectoralis major in the human body. 14

peripheral nervous system The peripheral nervous system (or PNS), is composed of nerves leading to and from the central nervous system. 201

proprioception Proprioception is the sense of the relative position of neighbouring parts of the body and strength of effort being employed in movement. 201

rhomboid major The rhomboid major is a skeletal muscle on the back that connects the scapula with the vertebrae of the spinal column. 14

rhomboid minor The rhomboid minor is a small skeletal muscle on the back that connects the scapula with the vertebrae of the spinal column. 14

sagittal plane The sagittal plane is a vertical plane which passes from anterior to posterior, dividing the body into right and left halves. 16

scapula The scapula or shoulder blade, is the bone that connects the humerus with the clavicle. The scapula forms the posterior located part of the shoulder girdle. 11

scapulo-humeral rhythm Coordinated rotational movement of the scapula that accompanies abduction, adduction, internal and external rotation, extension, and flexion of the humerus; roughly a 2:1 ratio. 18

scapulothoracic joint The scapulocostal joint (also known as the scapulothoracic joint) is a physiological joint formed by an articulation of the anterior scapula and the posterior thoracic rib cage. 13

sensory neuron Sensory neurons are nerve cells that transmit sensory information (sight, sound, feeling, etc.). They are activated by sensory input, and send projections to other elements of the nervous system, ultimately conveying sensory information to the brain or spinal cord. 202

serratus anterior The serratus anterior is a muscle that originates on the surface of the 1st to 8th ribs at the side of the chest and inserts along the entire anterior length of the medial border of the scapula. 14

shoulder girdle The pectoral girdle or shoulder girdle is the set of bones which connects the upper limb to the axial skeleton on each side. It consists of the clavicle and scapula. 11

skeletal muscles Skeletal muscle is a form of striated muscle tissue which is under the control of the somatic nervous system; that is to say, it is voluntarily controlled. 14

somatic nervous system The somatic nervous system is the part of the peripheral nervous system associated with the voluntary control of body movements via skeletal muscles. 201

sternoclavicular articulation The sternoclavicular articulation is the articulation of the manubrium of the sternum and the first costal cartilage with the medial end of the clavicle. 12

sternum The sternum or breastbone is a long flat bony plate shaped like a capital "T" located anteriorly to the heart in the centre of the thorax (chest). 11

subclavius The subclavius is a small triangular muscle, placed between the clavicle and the first rib. 15

subscapularis The subscapularis is a large triangular muscle which fills the subscapular fossa and inserts into the lesser tubercle of the humerus and the front of the capsule of the shoulder-joint. 15

supraspinatus The supraspinatus is a relatively small muscle of the upper back that runs from the supraspinatous fossa superior of the scapula to the greater tubercle of the humerus. 15

synapse In the nervous system, a synapse is a structure that permits a neuron (or nerve cell) to pass an electrical or chemical signal to another cell. 201

synovial articulations A synovial joint, also known as a diarthrosis, is the most common and most movable type of joint in the body of a mammal. As with most other joints, synovial joints achieve movement at the point of contact of the articulating bones. 12

tendons A tendon (or sinew) is a tough band of fibrous connective tissue that usually connects muscle to bone and is capable of withstanding tension. 14

teres major The teres major muscle is a muscle of the upper limb and one of seven scapulohumeral muscles. 15

teres minor The teres minor is a narrow, elongated muscle of the rotator cuff. 15

thorax The thorax or chest is a part of the anatomy of humans, located between the neck and the abdomen. In terms of the bones it is comprised of the ribs, sternum and vertebrae. 11

transverse plane The transverse plane (also called the horizontal plane, axial plane, or transaxial plane) is an imaginary plane that divides the body into superior and inferior parts. It is perpendicular to the coronal and sagittal planes. 16

trapezius The trapezius is a large superficial muscle that extends longitudinally from the occipital bone to the lower thoracic vertebrae and laterally to the spine of the scapula. 14

ulna The ulna is one of the two long bones in the forearm, the other being the radius. 12

Z-disks A dark thin protein band to which actin filaments are attached in a striated muscle fibre, marking the boundaries between adjacent sarcomeres. 15

Index

- acromioclavicular articulation, 12
- augmented Lagrange function, 70
- carrier link, 52
- centre of mass, 43
- Chasles' theorem, 35
- clavicle, 11
- closed-loop, 187
- control law, 187
- controllability, 194
- controller, 187
- coordinate system, 22
- degrees of freedom, 59
- differentiable manifold, 106
- dynamic shoulder model, 82
- end-effector, 52
- equations of motion, 47
- equilibrium point, 189
- Euclidean displacements, 24
- Euler's laws of motion, 39
- Euler-Lagrange Equation, 69
- force, 39
- forward kinematic map, 61
- fundamental transport theorem, 33
- generalised coordinates, 62
- geometric configuration, 23
- glenohumeral articulation, 12
- higher kinematic pairs, 55
- holonomic-skleronomic, 60
- homogeneous transformation, 58
- humerus, 11
- inputs, 186
- instability, 190
- instantaneous screw axis, 37
- kinematic chain, 54
- kinematic constraint, 60
- kinematic pair, 54
- kinematic redundancy, 94
- kinematic shoulder model, 75
- kinetic energy, 48
- Lagrange function, 68
- lever arm, 40
- lower kinematic pairs, 55
- Lyapunov function, 190
- Lyapunov stability, 190
- machine, 52
- mass, 43
- mechanism, 52
- minimal coordinates, 122
- mobility, 59
- moment of force, 40
- moment of inertia, 43
- muscle cable model, 87
- muscle forces, 85
- muscle moment-arms, 143
- musculoskeletal modelling, 74
- Newton's laws of motion, 38
- observability, 194
- observer, 195
- open-loop, 187
- outputs, 186
- overactuation, 95
- parallel mechanism, 52
- Poinsot's theorem, 42
- Poisson formula, 31
- power, 48
- principle of transmissibility, 40
- principle of virtual power, 65
- principle of virtual work, 66
- quaternion, 30

rotation matrix, 26

scapula, 11

scapulothoracic, 13

scapulothoracic contact model, 79

screw motion, 35

shoulder girdle, 14

space, 22

special orthogonal group, 27

spherical pair, 55

spherical slider pair, 55

stability, 190

state model, 186

states, 186

sternoclavicular articulation, 12

system, 185

Tait-Bryan angles, 27

tendon excursion method, 149

torque, 41

universal pair, 55

virtual displacement, 64

work, 48

wrench, 41

wrench feasibility, 153

David Ryan Ingram

Chemin de Longet 68b, CH-1926 Fully, Switzerland

Nationality: American **Date of Birth:** 16-Mai-1983

Email: david.ingram@epfl.ch **Phone:** +41(0)78 923 31 35

EDUCATION

PhD École Polytechnique Fédérale de Lausanne Lausanne (EPFL), Laboratoire d'Automatique, Switzerland, 2009–2014

Master of Science MSc *en Génie Mécanique avec Mineur en Science des Matériaux*, EPFL, School of Mechanical Engineering, 2007–2009

Bachelor *en Génie Mécanique*, EPFL, School of Mechanical Engineering, 2004–2007

WORK EXPERIENCE

2009–2014 Teaching and research duties at the Laboratoire d'Automatique

- Supervision more than 25 semester projects in dynamics and control
- Teaching assistant for various courses

2003–2008 Summer job at MANOR SA, Vevey Switzerland

2006 One month internship at RUAG Space SA, Nyon Switzerland

2002 Summer job at Henri Badoux SA, Aigle Switzerland

2001 Summer job at Aiglon College, Villars-sur-Ollon Switzerland

TECHNICAL SKILLS

- Advanced mathematics
- Modeling and analysis of dynamical systems
- Design of control strategies
- Machine design
- Electronics
- Finite elements analysis
- Programming Languages: Matlab, LabView, C et C++

PUBLICATIONS

- D. Ingram, C. Engelhardt, A. Farron, A. Terrier and P. Muellhaupt. Moment Arms : A Key Element In Muscle Force Estimation. *Journal of Computer Methods in Biomechanics and Biomedical Engineering*, 2013
- D. Ingram, C. Engelhardt, A. Farron, A. Terrier and P. Muellhaupt. A Minimal Set of Coordinates for Describing Humanoid Shoulder Motion. *IEEE/RSJ International Conference on Intelligent Robots and Systems (IROS)*, Tokyo, JAPAN, 2013
- D. Ingram, Philippe, M. Alexandre T., Pralong E., and Farron A. Dynamical biomechanical model of the shoulder for muscle-force estimation. *Proceedings of the IEEE RAS-EMBS International Conference on Biomedical Robotics and Biomechatronics*, 2012
- D. Ingram, S. S. Willson, P. Müllhaupt and D. Bonvin. Stabilization of the cart-pendulum system through approximate manifold decomposition. *IFAC*, Milano, Italy 2011, 2011

LANGUAGES

- French
 - English
 - German
-